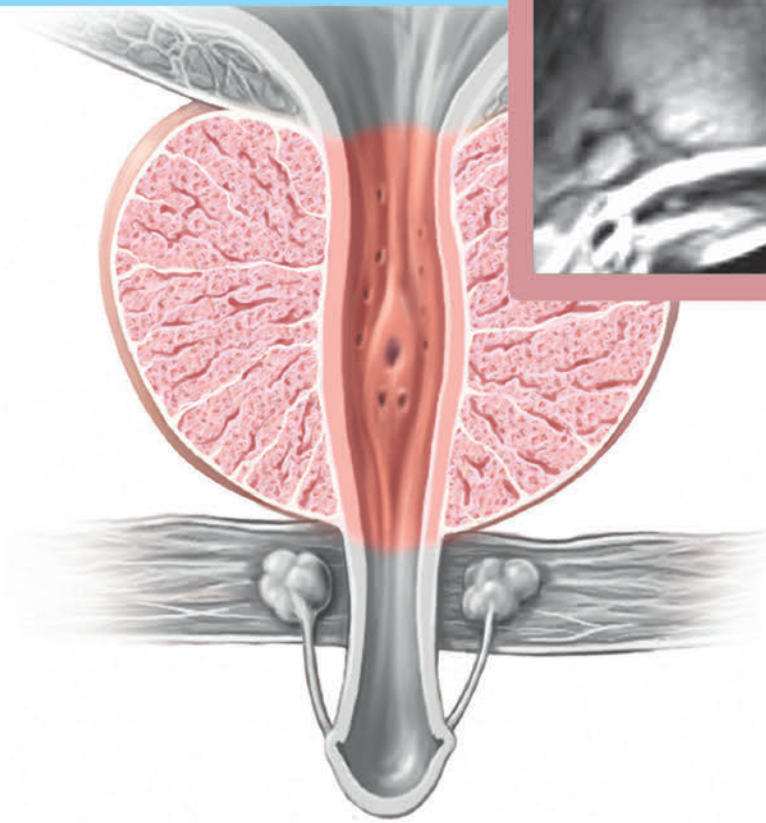
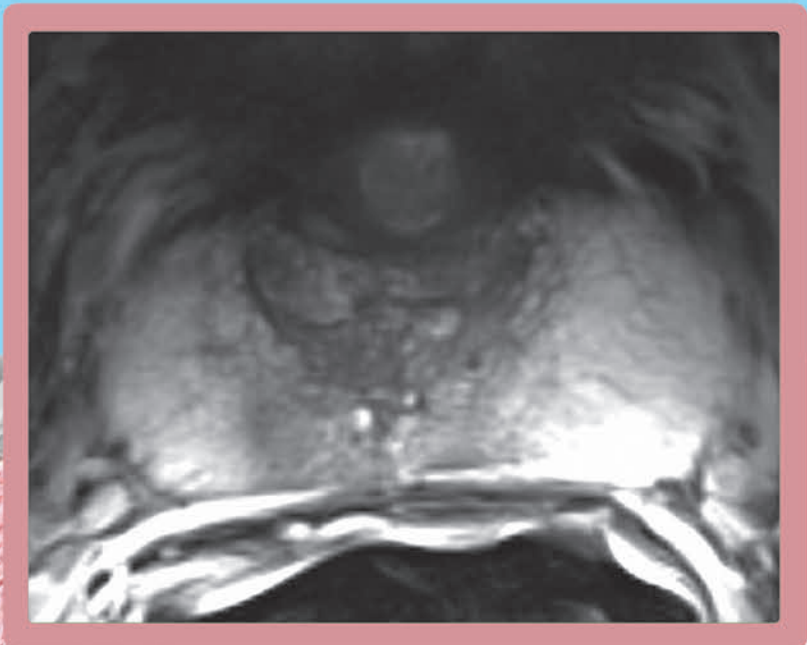


MRI of the Prostate

A Practical Approach

Andrew B. Rosenkrantz



MRI of the Prostate

A Practical Approach

Andrew B. Rosenkrantz, MD

Associate Professor of Radiology and Urology

Department of Radiology

NYU Langone Medical Center

New York University School of Medicine

New York, New York

Thieme

New York • Stuttgart • Delhi • Rio de Janeiro

Thieme Medical Publishers, Inc.
333 Seventh Avenue
New York, New York 10001

Executive Editor: William Lamsback
Managing Editor: J. Owen Zurhellen IV
Editorial Assistant: Mary B. Wilson
Director, Editorial Services: Mary Jo Casey
Production Editor: Sean Woznicki
International Production Director: Andreas Schabert
Vice President, Editorial and E-Product Development: Vera Spillner
International Marketing Director: Fiona Henderson
International Sales Director: Louisa Turrell
Director of Sales, North America: Mike Roseman
Senior Vice President and Chief Operating Officer: Sarah Vanderbilt
President: Brian D. Scanlan

Library of Congress Cataloging-in-Publication Data

Names: Rosenkrantz, Andrew B., author.
Title: MRI of the prostate : a practical approach / Andrew B. Rosenkrantz.
Description: New York : Thieme, [2017] | Includes bibliographical references.
Identifiers: LCCN 2015051099 (print) | LCCN 2016001134 (ebook) | ISBN 9781626232686 (hardcover) | ISBN 9781626232693 (eISBN)
Subjects: | MESH: Prostatic Neoplasms--diagnosis | Magnetic Resonance Imaging
Classification: LCC RC280.P7 (print) | LCC RC280.P7 (ebook) | NLM WJ 762 | DDC 616.99/463--dc23
LC record available at <http://lccn.loc.gov/2015051099>

Copyright © 2017 by Thieme Medical Publishers, Inc.

Thieme Publishers New York
333 Seventh Avenue, New York, NY 10001 USA
+1 800 782 3488, customerservice@thieme.com

Thieme Publishers Stuttgart
Rüdigerstrasse 14, 70469 Stuttgart, Germany
+49 [0]711 8931 421, customerservice@thieme.de

Thieme Publishers Delhi
A-12, Second Floor, Sector-2, Noida-201301
Uttar Pradesh, India
+91 120 45 566 00, customerservice@thieme.in

Thieme Publishers Rio de Janeiro,
Thieme Publicações Ltda.
Edifício Rodolpho de Paoli, 25º andar
Av. Nilo Peçanha, 50 – Sala 2508
Rio de Janeiro 20020-906 Brasil
+55 21 3172 2297

Cover design: Thieme Publishing Group
Typesetting by DiTech Process Solutions

Printed in China by Everbest Printing Co.

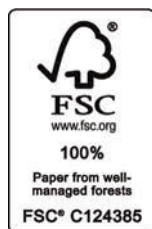
ISBN 978-1-62623-268-6

Also available as an e-book:
eISBN 978-1-62623-269-3

Important note: Medicine is an ever-changing science undergoing continual development. Research and clinical experience are continually expanding our knowledge, in particular our knowledge of proper treatment and drug therapy. Insofar as this book mentions any dosage or application, readers may rest assured that the authors, editors, and publisher have made every effort to ensure that such references are in accordance with **the state of knowledge at the time of production of the book.**

Nevertheless, this does not involve, imply, or express any guarantee or responsibility on the part of the publisher in respect to any dosage instructions and forms of applications stated in the book. **Every user is requested to examine carefully** the manufacturers' leaflets accompanying each drug and to check, if necessary in consultation with a physician or specialist, whether the dosage schedules mentioned therein or the contraindications stated by the manufacturers differ from the statements made in the present book. Such examination is particularly important with drugs that are either rarely used or have been newly released on the market. Every dosage schedule or every form of application used is entirely at the user's own risk and responsibility. The authors and publisher request every user to report to the publisher any discrepancies or inaccuracies noticed. If errors in this work are found after publication, errata will be posted at www.thieme.com on the product description page.

Some of the product names, patents, and registered designs referred to in this book are in fact registered trademarks or proprietary names even though specific reference to this fact is not always made in the text. Therefore, the appearance of a name without designation as proprietary is not to be construed as a representation by the publisher that it is in the public domain.



This book, including all parts thereof, is legally protected by copyright. Any use, exploitation, or commercialization outside the narrow limits set by copyright legislation without the publisher's consent is illegal and liable to prosecution. This applies in particular to photostat reproduction, copying, mimeographing or duplication of any kind, translating, preparation of microfilms, and electronic data processing and storage.

5 4 3 2 1

Dedicated to my parents, Carole and Dan, and to my future wife, Andrea, for all of their love and support.

Contents

Foreword by Peter L. Choyke	viii
Foreword by Samir S. Taneja	x
Preface	xii
Contributors	xiv
1 Introduction to Prostate Cancer: Clinical Considerations	1
<i>Marc A. Bjurlin, Samir S. Taneja, and Andrew B. Rosenkrantz</i>	
2 Prostate Cancer Pathology	11
<i>Fang-Ming Deng, Jianhong Li, Max X. Kong, Jonathan Melamed, and Ming Zhou</i>	
3 Introduction to Prostate MRI Protocols: Hardware, T2-Weighted Imaging and MR Spectroscopy	23
<i>John Conklin and Masoom A. Haider</i>	
4 Diffusion-Weighted Imaging of the Prostate	41
<i>François Cornud</i>	
5 Dynamic Contrast-Enhanced MRI of the Prostate	60
<i>Ismail Baris Turkbey, Sandeep Sankineni, and Peter L. Choyke</i>	
6 Prostate Imaging–Reporting and Data System (PI-RADS)	70
<i>Michael Spektor and Jeffrey C. Weinreb</i>	
7 Prostate Cancer Staging and Surgical Planning	81
<i>Jurgen J. Fütterer</i>	
8 Post-Treatment Follow-Up and Assessment for Recurrence	94
<i>Adam T. Froemming, Lyndsay Viers, Eric May, and Akira Kawashima</i>	
9 Prebiopsy MRI and MRI-Targeted Biopsy	113
<i>Karoly Viragh and Daniel J. A. Margolis</i>	
10 MRI and Active Surveillance	127
<i>Max Kates, H. Ballentine Carter, and Katarzyna J. Macura</i>	
11 PET/CT and PET/MR Imaging Evaluation of Prostate Cancer	140
<i>Hossein Jadvar</i>	
12 Teaching Atlas of Instructional and Interesting Cases	152
<i>Ankur M. Doshi and Andrew B. Rosenkrantz</i>	
Index	204

Foreword

It may be hard to believe today, but it wasn't long ago that imaging played a negligible role in the diagnosis of prostate cancer. Transrectal ultrasound (TRUS), introduced in the mid-1980s as a screening tool for identifying prostate cancer, proved inadequate and hence was relegated to guiding needles into the prostate for random biopsies. The advent of prostate specific antigen (PSA) testing in the late 1980s and TRUS "guided" biopsies led to an explosion of diagnoses of prostate cancer, rocketing prostate cancer into the top rank of non-skin malignancies in men. Screening for prostate cancer became a routine part of a physical examination, and public service announcements urged men to improve their "prostate awareness". At the same time, the epidemiology community was warning (although the warnings fell on deaf ears) that the policy of screening the general population with a blood test with a high false positive rate followed by random biopsy was a recipe for disaster. Soon the United States experienced a massive overdiagnosis of occult, indolent low-grade cancers even while physicians were missing potentially significant lesions located in regions not sampled by the normal biopsy template. By 2012 the United States Preventive Services Task Force examined the unimpressive results of screening and declared PSA screening to be of dubious value, thereby casting a pall on the very concept of early diagnosis of prostate cancer.

But into this story came a bright light, prostate MRI, which was introduced as a method of detecting prostate cancer in the mid-2000s. Many of the distinguished early advocates of prostate MRI are authors in this book and have worked relentlessly to improve the usefulness of prostate MRI to its current state. Prostate MRI promised to actually localize tumors instead of relying on the guesswork of the random biopsy. Early on it was recognized, however, that there was no "magic bullet" MR sequence for prostate cancer detection and characterization. Rather, the combination of T2-weighted imaging (with its anatomical precision), diffusion-weighted imaging (with its ability to detect water motion in tissue), dynamic contrast-enhanced imaging, (with its ability to identify leaky vessels), and MR spectroscopy (which detects changes in the relative proportions of the metabolites choline and citrate) proved that a multiparametric approach is needed for diagnosing prostate cancer. Each of these methods is detailed in this book by experts who had much to do with our current understanding of the role of MRI. Prostate MRI is not easy to perform or

interpret, and the collective experience of these authors will provide the reader with practical advice on how to acquire and report MRI properly. Once tumors can be detected, they can then be accurately biopsied using any of several methods, also detailed herein. The ability to use imaging to guide biopsy has increased the detection rate of clinically significant cancers while reducing the diagnoses of inconsequential tumors. This has revolutionized the field of prostate cancer diagnosis. No longer does a diagnosis have to depend on luck and chance but rather it relies on a rational sequence of events beginning with accurate localization and characterization of a prostate lesion on MRI. Like most major paradigm shifts in medicine, this one has met with resistance. For instance, there was no uniformity among early pioneers regarding diagnostic criteria for biopsy resulting in criticism of the entire field. The need to standardize the lexicon and the criteria for an MR positive lesion that required biopsy was clear. Thus was born the PI-RADS classification, which is already in its second version, the chapter on which is written by one of the leaders of the effort to gather a worldwide consensus on diagnosing prostate cancer with MRI.

Beyond diagnosis, prostate MRI can be used for staging and surgical planning as well as for detecting recurrence after radical prostatectomy or radiation therapy, topics well covered in this book. At the same time, there has been greater recognition of the value of active surveillance in the management of patients with low-grade cancers; prostate MRI will play a major role here as well.

Medicine is an everchanging rebalancing act as knowledge is gained and old concepts are abandoned. Even while MRI has advanced the field, there have also been changes in our understanding of and terminology for the pathology of prostate cancer, improved understanding regarding driver mutations and molecular pathways, and improved surgical procedures with decreased morbidity. This results in an everchanging recalibration of the best way to diagnose and manage patients with prostate cancer. As we look to the future in the later chapters of this book, we see a potentially important new role for positron emission tomography (PET) combined with MRI or CT. New, highly specific PET probes that target prostate cancer with high affinity and specificity could represent the next phase of the story.

Dr. Andrew Rosenkrantz and his team of expert contributors have compiled a considerable body of knowledge regarding this fast-changing field in *MRI of the Prostate: A*

Practical Approach. The advances of the last decade are summarized succinctly for the busy reader, with an emphasis on pragmatic hints to improve image acquisition and interpretation. Yet the true value of this book is in enabling readers with some prior skill in imaging to help their own patients get the best imaging possible and then undergo a targeted biopsy of the right lesion, so the patient may receive the right treatment thus deriving the maximum benefit from their diagnosis while suffering a minimum of

side effects. If this book accomplishes that for you, as I expect, then it has done quite a bit.

*Peter L. Choyke, MD, FACR
Program Director
Molecular Imaging Program
Center for Cancer Research
National Cancer Institute
Bethesda, Maryland*

Foreword

The discipline of prostate cancer management has greatly evolved over the past 25 years since the clinical inception of prostate-specific antigen (PSA) testing. Aggressive screening and detection of early stage prostate cancer has resulted in an incremental reduction in prostate cancer mortality over the past decades, but reduced mortality and improved oncologic outcomes have come at the cost of detecting and treating a huge number of indolent cancers that may never have harmed the patient due to the prolonged lead time of the disease. As urologists have become aware of the indolent nature of most early stage prostate cancers, and realized the perils of unnecessary treatment, the goals of prostate cancer detection have changed. Whereas we previously sought to identify every cancer we could find, we now wish to selectively identify only those cancers that cause harm, avoiding the detection and treatment of those that do not. An effective reduction in prostate cancer detection, without increase in prostate cancer mortality, is a goal unique in cancer medicine, but one that requires better tools.

While improved risk assessment in prostate cancer will require, in part, better understanding of disease biology through genetic and molecular evaluation, it also would benefit from better characterization of the cancer, and this is what multiparametric magnetic resonance imaging (mpMRI) has provided us. The use of mpMRI in prostate cancer detection and risk assessment has empowered a change in thinking at every level of the disease management paradigm. Initially conceived as a method of disease localization for biopsy and staging, mpMRI has evolved into a non-invasive risk assessment tool.

Historically, the overtreatment of prostate cancer can be, in part, attributed to poor characterization of the disease at diagnostic biopsy. When conducting a nontargeted biopsy, or systematic sampling, diagnosis is limited by sampling error resulting in false-negatives, incorrect risk assessment, and false-positives, defined as the detection of indolent disease unlikely to harm the patient. As such, the biopsy itself may be a major contributor to the significant over-detection of indolent cancer observed in the PSA era. When linked to biopsy, mpMRI has the potential to improve the prostate cancer diagnostic and therapeutic paradigm through provision of more accurate diagnostic data.

The rationale behind mpMRI of the prostate in the pre-biopsy setting is relatively simple. Through localization, and

sampling of the most suspicious regions noted on MRI, the rate of false-negatives should decline. Additionally, upon directly sampling suspicious regions, more accurate characterization of cancer should be feasible, thus allowing better decision making in regard to the necessity for therapy. Finally, if applied in a prebiopsy setting for risk stratification, upon establishing thresholds for biopsy, the detection of indolent disease might be greatly reduced by avoiding biopsy altogether.

Similarly, in men with known low-risk prostate cancer diagnosed on a systematic biopsy, mpMRI offers the ability to determine the risk of occult high-grade cancer missed by the baseline biopsy. In this way it offers the ability to overcome sampling error through localization rather than additional sampling. More accurate risk stratification of these men has allowed an improved ability to select candidates for active surveillance, and to safely maintain them on surveillance without an excessive number of biopsies in follow-up. For those requiring therapy, knowledge of disease location and extent may improve the outcomes of conventional therapy and offer inroads to novel targeted therapeutic approaches.

The implementation of mpMRI in clinical practice is currently undergoing an exponential growth, but many hurdles to successful wide adoption remain. Efforts to establish reproducibility in study quality through standardization of study protocol, reporting standards, and interpretation are underway, and, in this regard, education is essential. Additional refinement is needed in technologies integrating biopsy targeting with MRI findings to ensure standardization of biopsy approach. Finally, cost must be evaluated to determine if the increased cost of imaging is offset by the reduction in downstream costs of over-detection and overtreatment.

In this book, my colleague and collaborator, Dr. Andrew Rosenkrantz, has constructed a valuable resource for both practicing radiologists and urologists engaged in the care of prostate cancer patients. In a series of wonderfully orchestrated chapters, the book outlines the critical elements of prostate imaging in the contemporary era, ranging from imaging protocol to reporting to image-interpretation and clinical application. Unlike conventional anatomical imaging, interpretation of the integration of functional and anatomical imaging requires knowledge of the subtle nuances influencing outcome. This book provides a

comprehensive discussion of these nuances and potentially enables the radiologist and urologist to adapt mpMRI of the prostate in their own practice.

Multiparametric MRI of the prostate has already dramatically changed the way we think about prostate cancer detection, risk assessment, and therapy. In my own career and practice, mpMRI has arguably had the greatest impact on the care of my patients of any advance over the past 20 years. In the future, mpMRI will continue to influence our thought as technological advance and increased experience further expand the capabilities of mpMRI and its applications. We are undergoing a renaissance in cancer diagnos-

tics and therapy, and imaging will be at the heart of the revolution.

Samir S. Taneja, MD

*The James M. Neissa and Janet Riha Neissa Professor of
Urologic Oncology
Professor of Urology and Radiology
Director, Division of Urologic Oncology
Co-Director, Smilow Comprehensive Prostate Cancer Center
Department of Urology, NYU Langone Medical Center
New York University School of Medicine
New York, New York*

Preface

When describing the contemporary management of prostate cancer, perhaps Bob Dylan's 1964 song "The Times They Are A-Changing" aptly applies. Awareness is increasing of the generally indolent nature of prostate cancer, recognizing that most patients will not be harmed by their disease if left untreated. On this basis, closely monitoring appropriately selected patients through active surveillance, without immediate treatment, is becoming a more commonly applied management strategy. For those patients who do undergo treatment, previously applied therapies continue to undergo refinements to allow for more precise intervention, as evidenced by nerve-sparing surgery and targeted radiation strategies. In addition, minimally invasive intervention involving an expanding array of focal ablative therapies (including cryoablation, high-intensity focused ultrasound, photodynamic therapy, laser ablation, and radiofrequency ablation) continue to gain in clinical implementation. These trends have propelled a critical need to develop more precise biopsy strategies, in comparison with the traditional standard systematic biopsy scheme used in the past, for more reliably determining patients' level of risk, as well as for more reliably localizing their disease to enable targeted treatment.

State-of-the-art prostate MRI provides a technology for meeting these needs. Although first described in the 1980s, its use remained fairly limited outside of academic centers until undergoing a surge in interest during the early 2000s. A combination of factors accounted for this expansion. First, in response to the previously noted evolution in the clinical management of prostate cancer, patients and referring physicians were more strongly seeking a new tool to facilitate tumor localization and characterization in new diagnoses. Also, this time period witnessed important technological advancements in MRI, in terms of both hardware (relating to the main magnet itself and receiver coil design) and software (relating to emergence of diffusion-weighted imaging and dynamic contrast-enhanced imaging for prostate cancer evaluation). In addition, the radiologic community's experience and expertise in prostate MRI interpretation grew, aided by a series of high-quality radiologic-pathologic investigations published during this time. Two additional key developments that have further promoted the clinical integration of prostate MRI are the advent of advanced technologies for performing MRI-targeted prostate biopsies (namely, direct in-bore systems and real-time MRI/ultrasound fusion systems) and the dissemination of the Prostate Imaging-Reporting and Data System (PI-RADS) for prostate MRI interpretation and reporting, as developed by an international expert panel.

Within this context, many radiology practices are currently experiencing a growing demand for prostate MRI

services, and their radiologists are being called upon to provide high-quality interpretations. However, prostate MRI remains challenging. Given the recent rapid developments in the area, radiologists in practice may have had little exposure to the interpretation of prostate MRI during their training. In addition, individual examinations frequently present a diagnostic dilemma in view of the often heterogeneous appearance of the prostate, as well as the wide spectrum of both normal anatomical findings and benign processes that can mimic or mask a tumor and lead to an equivocal result. Furthermore, prostate MRI interpretation is greatly enhanced by having a rich understanding of the many clinical and histologic aspects of the disease. These considerations contribute to the variability in interpretation among centers and the potential challenges in applying prostate MRI clinically in a consistent fashion.

This book seeks to help address these issues. Rather than providing a comprehensive review of the topic, it aims to deliver a practical overview of the fundamentals of prostate MRI acquisition, interpretation, and reporting. Key aspects that are most important for offering a high-quality prostate MRI in routine practice are emphasized. The focus is clinical, intending to reflect how prostate MRI is optimally performed and interpreted in daily practice.

An outstanding collection of experts in the field have prepared chapters for this textbook. I am incredibly grateful to these individuals for their contributions, without which this work would not have been possible. Given the truly multidisciplinary nature of the topic, the initial chapters provide a basic overview of the disease's clinical (Chapter 1) and pathologic (Chapter 2) aspects. Additional chapters cover the gamut from MRI acquisition [including hardware and T2-weighted imaging (Chapter 3), diffusion-weighted imaging (Chapter 4), and dynamic contrast-enhanced imaging (Chapter 5)], to interpretation using PI-RADS (Chapter 6), and various clinical applications of prostate MRI [including disease staging (Chapter 7), recurrent disease (Chapter 8), MRI-targeted biopsy (Chapter 9), and active surveillance (Chapter 10)]. Also, in view of the emerging number of PET radiotracers that complement MRI findings for prostate cancer evaluation, as well as continued advancement of both PET/MRI systems and technologies for performing PET and MRI fusion, an additional chapter explores PET and PET/MRI for primary prostate cancer evaluation (Chapter 11). The final chapter is entirely image-based and provides a collection of annotated cases that depict a mixture of classic findings as well as diagnostic pitfalls and challenges (Chapter 12).

In addition to radiologists currently in practice, other audiences may find this textbook to be of value as well. Radiology trainees, MRI technologists, as well as other

specialists who manage prostate cancer patients (including urologists as well as radiation and medical oncologists), may also benefit from this work. Also, it must be emphasized that this textbook, by itself, is not sufficient for learning the material. Readers are encouraged to immerse themselves in this exciting topic and to integrate their reading of the text with further educational opportunities and, of course, direct first-hand experience in prostate MRI interpretation. Such experiences optimally occur in a multidisciplinary setting in which the radiologist maintains robust communication with urologists and other referring physicians. In addition, a system for obtaining feedback from

one's interpretations based on subsequent pathologic assessment is immensely beneficial for fostering continued improvement. Ultimately, this textbook is hoped to provide a valuable resource for radiologists and other practitioners involved in prostate MRI interpretation and thereby make a meaningful contribution to improving the care of patients undergoing evaluation for this disease.

*Andrew B. Rosenkrantz
New York, New York
July 2016*

Contributors

H. Ballentine Carter, MD

Professor of Urology and Oncology
Director, Division of Adult Urology
The James Buchanan Brady Urological Institute
The Johns Hopkins University School of Medicine
Baltimore, Maryland

Marc A. Bjurlin, DO, MSc

Assistant Professor of Urology
Director of Urologic Oncology
NYU Lutheran Medical Center
NYU Langone Health System
New York University School of Medicine
New York, New York

Peter L. Choyke, MD, FACR

Program Director
Molecular Imaging Program
Center for Cancer Research
National Cancer Institute
Bethesda, Maryland

John Conklin, MD, MSc

Diagnostic Radiology Resident
Department of Medical Imaging
Faculty of Medicine
University of Toronto
Toronto, Ontario, Canada

François Cornud, MD

Consultant Radiologist
Department of Radiology
Hôpital Cochin
Paris-Descartes University
Paris, France

Fang-Ming Deng, MD, PhD

Assistant Professor of Pathology
Department of Pathology
NYU Langone Medical Center
New York University School of Medicine
New York, New York

Ankur M. Doshi, MD

Assistant Professor
Department of Radiology
NYU Langone Medical Center
New York University School of Medicine
New York, New York

Adam T. Froemming, MD

Assistant Professor
Department of Radiology
Mayo Clinic
Rochester, Minnesota

Jurgen J. Fütterer, MD, PhD

Professor
Department of Radiology and Nuclear Medicine
Radboud University Medical Center
Nijmegen, Netherlands
Department of Robotics and Mechatronics
University Twente
Enschede, Netherlands

Masoom A. Haider, MD, FRCPC

Professor of Radiology
University of Toronto
Senior Scientist
Sunnybrook Research Institute & Sunnybrook Health
Sciences Center
Toronto, Ontario, Canada

Hossein Jadvar, MD, PhD, MPH, MBA

Associate Professor of Radiology and Biomedical
Engineering
Department of Radiology
University of Southern California Keck School of Medicine
Los Angeles, California

Max Kates, MD

Resident, Urological Surgery
James Buchanan Brady Urological Institute
The Johns Hopkins Medical Institutions
Baltimore, Maryland

Akira Kawashima, MD, PhD

Professor
Department of Radiology
Mayo Clinic
Rochester, Minnesota

Max X. Kong, MD

Staff Pathologist
Pathology Consultants of New Mexico
Roswell, New Mexico

Jianhong Li, MD, PhD

Urological Pathology Fellow
Department of Pathology
NYU Langone Medical Center
New York University School of Medicine
New York, New York

Katarzyna J. Macura, MD, PhD, FACR

Professor of Radiology, Urology, and Oncology
The Russell H. Morgan Department of Radiology and
Radiological Science
The Johns Hopkins University School of Medicine
Baltimore, Maryland

Daniel J. A. Margolis, MD

Associate Professor of Radiology
UCLA David Geffen School of Medicine
Los Angeles, California

Eric May, MD

Department of Radiology
Mayo Clinic
Rochester, Minnesota

Jonathan Melamed, MD

Professor
Department of Pathology
NYU Langone Medical Center
New York University School of Medicine
New York, New York

Andrew B. Rosenkrantz, MD

Associate Professor of Radiology and Urology
Department of Radiology
NYU Langone Medical Center
New York University School of Medicine
New York, New York

Sandeep Sankineni, MD

Molecular Imaging Program
National Cancer Institute
National Institutes of Health
Bethesda, Maryland

Michael Spektor, MD

Assistant Professor
Department of Radiology
Yale University School of Medicine
New Haven, Connecticut

Samir S. Taneja, MD

The James M. Neissa and Janet Riha Neissa Professor of
Urologic Oncology
Professor of Urology and Radiology
Director, Division of Urologic Oncology
Co-Director, Smilow Comprehensive Prostate Cancer
Center
Department of Urology
NYU Langone Medical Center
New York University School of Medicine
New York, New York

Baris Turkbey, MD

Molecular Imaging Program
National Cancer Institute
National Institutes of Health
Bethesda, Maryland

Lyndsay Viers, MD

Department of Radiology
Mayo Clinic
Rochester, Minnesota

Karoly Viragh, MD

Assistant Professor
Department of Radiology
Columbia University Medical Center
Lawrence Hospital
Bronxville, New York

Jeffrey C. Weinreb, MD, FACR, FISMRM

Professor of Radiology and Biomedical Sciences
Vice Chair of Strategic Planning and Innovation
Yale University School of Medicine
Yale-New Haven Medical Center
New Haven, Connecticut

Ming Zhou, MD, PhD

Professor
Department of Pathology
NYU Langone Medical Center
New York University School of Medicine
New York, New York

1 Introduction to Prostate Cancer: Clinical Considerations

Marc A. Bjurlin, Samir S. Taneja, and Andrew B. Rosenkrantz

1.1 Incidence, Demographics, and Survival

Prostate cancer is the second most common cancer in men in the United States, after only skin cancer. After lung cancer, prostate cancer is the second leading cause of cancer death in American men. It is estimated that there are nearly 3 million American men currently living with prostate cancer.¹ Prostate cancer alone accounted for about one-quarter of new cancer diagnoses in men, with 220,800 new diagnoses and 27,540 estimated deaths in 2015 alone.² Approximately 14% of men (1 in 7) will be diagnosed with prostate cancer at some point during their lifetime, with a median age at diagnosis of 66 years, and about 1 in 38 men will die of prostate cancer.¹ For men with prostate cancer, 80.4% are diagnosed at the local stage.¹ Although the 5-year relative survival rate for men diagnosed in the United States from 2001 to 2007 with local or regional disease was 100%, the rate for distant disease was 28%.¹

1.2 Public Health Burden

Prostate cancer is a major public health concern and is associated with significant health-care costs. With an estimated increase in the elderly population from 400 million individuals >65 years in 2000 to approximately 1.5 billion by 2050³ coupled with an increase in the 10-year relative survival rate of those diagnosed with prostate cancer, the economic burden of prostate cancer is predicted to increase markedly.⁴ Earlier detection through prostate-specific-antigen (PSA) screening has been successful in identifying men who might benefit from treatment. As a result, many men are now diagnosed earlier and with lower-stage cancer than was previously the case effectively increasing the economic burden of this disease.^{4,5,6} In the United States, the total estimated expenditure on prostate cancer was nearly \$10 billion in 2006, approximately \$12 billion in 2010, and projected to reach almost \$20 billion by 2020.⁷ The mean annual costs per patient were \$10,612 in the initial phase after diagnosis, \$2,134 for continuing care, and \$33,691 in the last year of life.⁸ Patterns of costs vary widely based on initial treatment. Watchful waiting is reported to have the lowest initial treatment cost (\$4,270). In comparison, initial treatment costs are highest for combined hormonal and radiation therapy (\$17,474), as well as for surgery (\$15,197). Five-year total costs are highest for hormonal therapy alone (\$26,896), followed by combined hormonal and radiation therapy (\$25,097), and then by surgery (\$19,214).⁹ However, improved paradigms for the clinical management of prostate cancer could greatly decrease these costs, specifically for men with low-risk indolent disease whose life expectancy will be not be affected by prostate cancer. For instance, the cumulative annual cost attributable to the “overtreatment” of prostate cancer in the United States has reached nearly \$60 billion. Furthermore, the ability to not treat the 80% of men with low-grade disease who will never die of prostate cancer is estimated would save \$1.32 billion per year nationally.¹⁰

1.3 Risk Factors

Improved identification of risk factors could help guide risk-adapted screening and preventive interventions. Both modifiable lifestyle factors and preventive therapies exist that might reduce the risk of developing prostate cancer. Age is the most important nonmodifiable factor. In unscreened populations, prostate cancer has the steepest age-incidence curve of all cancers, showing a rapid increase in the seventh decade. Racial variation is also significant. In the United States, compared with white men of European ancestry, black men of African ancestry have 58% greater incidence of prostate cancer and 144% greater mortality, whereas Hispanic men have 14% lower incidence and 17% lower mortality.¹¹ The relative risk of developing prostate cancer is approximately 2.5 times greater in men who have a first-degree relative with prostate cancer. Family history is important, although only 35% of the familial risk is explained by known genes.¹²

Exposure to a variety of external agents may also play a role in the development of prostate cancer. First, smoking is associated with a moderately increased risk for prostate cancer.¹³ The association between prostate cancer and smoking is much stronger, especially for aggressive cancers, in heavy smokers.¹⁴ In addition, obesity is associated with a significantly increased risk for both low- and high-risk prostate cancer in black men.¹⁵ However, among white men, the link between obesity and prostate cancer is less clear. Although no links with specific dietary factors have been definitively established, red meat, dairy protein, dietary fat, and coffee have all been postulated to serve as risk factors.¹⁶ Finally, although the role of inflammation in prostate cancer carcinogenesis remains controversial, the risk for prostate cancer may be increased in men with a history of urinary tract infections¹⁷ as a result of chronic intraprostatic inflammation.¹⁸

1.4 Symptoms

In most cases, prostate cancer symptoms are not apparent in the early stages of the disease. Prostate cancer that is more advanced may cause signs and symptoms such as decreased force in the stream of urine, blood in the semen, discomfort in the pelvic area, bone pain, and erectile dysfunction. However, such urinary symptoms are often similar in benign prostatic hyperplasia, and these signs and symptoms cannot reliably differentiate benign prostatic disease from cancer.

1.5 Prostate-Specific-Antigen Screening for the Early Detection of Prostate Cancer

Prostate-specific antigen is a well-established tumor marker that aids in the diagnosis, staging, and follow-up of prostate cancer. Biochemically, PSA is a serine protease, also known as human kallikrein 3 (hK3). The majority of PSA produced by the prostate is excreted in the semen, but a small proportion

“leaks” into the systemic circulation and can be measured as serum PSA. Studies by Stamey et al showed that, on a weight for weight basis, prostate cancer tissue released 30 times more PSA into the circulation than normal prostate tissue, perhaps because of loss of normal tissue architecture.¹⁹ Although PSA has been employed for screening for the early detection of prostate cancer, its use remains controversial. Randomized data shows that PSA screening results in diagnosis at earlier stages, improved oncologic outcomes after treatment, and lower prostate cancer mortality. However, important shortcomings of PSA screening include unnecessary biopsies due to false-positive PSA tests, overdiagnosis of some clinically insignificant cancers, and potential side effects from prostate biopsy and/or prostate cancer treatment.²⁰ Autopsy studies have demonstrated a high prevalence of asymptomatic localized prostate cancer among men who die from other causes. This observation has led to the criticism that prostate cancer screening leads to unnecessarily aggressive intervention in many men who would not develop symptomatic disease within their lifetimes. The prevalence of prostate cancer has been reported to be 0.5%, 23%, 35%, and 46% among men in the <50, 50 to 59, 60 to 69, and ≥70 age groups, respectively, with the majority being low-risk disease.²¹ One randomized prospective trial of PSA screening for prostate cancer showed a relative reduction in mortality from prostate cancer of 21% at 13 years of follow-up. However, a total of 781 men needed to be invited to screening and 27 to be diagnosed with prostate cancer to avert 1 death from the disease, highlighting

the concept that not all cancers have lethal potential within a man’s natural longevity. Despite showing a clear prostate cancer mortality reduction, these findings may not be sufficient to justify population-based screening. This ongoing controversy is highlighted by the divergent recommendations on screening from multiple professional organizations (► Table 1.1).

The American Urological Association (AUA) guidelines from 2013 recommend individualized decisions about screening for higher risk men aged <55 years, such as those with a positive family history and African-American men, while the National Comprehensive Cancer Network (NCCN) recommends starting the risks and benefits discussion of PSA screening at age 45.^{22,23} For men ages 55 to 69, the AUA recommends shared decision making about screening. Although this group has the strongest evidence for screening benefit, there remains potential for harm. For this reason, the AUA emphasizes the importance of a bilateral discussion about screening between the patient and physician that incorporates the benefits, risks, uncertainties, and patient’s values and preferences. Finally, the AUA recommends against routine PSA screening in men of age >70 years, while acknowledging that some men of age >70 years in excellent health may still benefit from screening. In comparison, the United States Preventative Services Task Force (USPSTF) recommendations from 2012 advised against routine PSA screening, given concerns related to uncertain mortality reduction, overdiagnosis of indolent disease, as well as costs.²⁴

Table 1.1 Professional organizations’ recommendations for PSA screening

Guideline group	Recommendation (2012–2014)	Year	Reference
United States Preventative Services Task Force	Against	2012	Moyer et al <i>Annals of Int Med</i> 2012 ²⁴
Melbourne (expert panel)	For patients in good health, baseline PSA at 40–50 PSA screening as part of a multivariable approach	2013	Murphy et al <i>BJU Int</i> 2014 ⁷⁸
European Association of Urology	Baseline PSA at 40–45 years	2013	Heidenreich et al <i>Eur Urol</i> 2014 ⁷⁹
National Comprehensive Cancer Network	Baseline PSA at 45 years	2014	Carroll et al <i>J Natl Cancer Inst</i> 2014 ²³
American Cancer Society	Shared decision making in patients ≥ 50 years	2014	Smith et al <i>CA Cancer J Clin</i> 2014 ⁸⁰
American College of Physicians	Shared decision making in patients 50–69 years	2013	Qaseem et al <i>Ann Intern Med</i> 2013 ⁸¹
European Society of Medical Oncology (expert opinion)	PSA screening suitable for well-informed men at 50–75 years	2012	Horwich et al <i>Ann Onc</i> 2013 ⁸²
American Urological Association	Shared decision making in patients 55–69 years	2013	Carter et al <i>J Urol</i> 2013 ²²
American Society of Clinical Oncology	Shared decision making in patients with > 10 years life expectancy	2012	Basch et al <i>J Clin Oncol</i> 2012 ⁸³

Abbreviation: PSA, prostate-specific antigen.

1.5.1 PSA Derivatives and Emerging Prostate Cancer Biomarkers

Various PSA metrics in addition to total PSA, such as PSA velocity, PSA density, free PSA, and PSA doubling time, have been incorporated into PSA screening to improve prostate cancer screening sensitivity and specificity. The rate of change in PSA over time (PSA velocity [PSAV]) is associated with both prostate cancer risk and aggressiveness. PSA velocity may increase the specificity of screening for clinically significant prostate cancer, but its ability to increase the predictive value beyond that of PSA alone is controversial.²⁵ PSA density (PSAD), defined as the PSA level divided by prostate volume, at the time of diagnosis has been shown to be a significant predictor of progression to treatment, along with age and PSA slope.²⁶ PSAD may be useful in the selection of potential candidates for active surveillance and for monitoring for subsequent disease progression in men being managed by active surveillance. In addition, PSA circulates through the blood in two ways: either bound to other proteins or unbound, referred to as free PSA (fPSA). The fPSA test measures the percentage of unbound PSA, whereas the conventional PSA test measures the total of both free and bound PSA. In men with prostate cancer, there appears to be a lower proportion of free PSA, expressed as a decrease in the ratio of free to total (f/t) PSA. In a study using an f/t PSA ratio of >25% to determine the need for a prostate biopsy, 95% of cancers were detected and 20% of unnecessary biopsies avoided.²⁷ These findings resulted in the Food and Drug Administration approving the f/t PSA ratio for helping guide decisions to perform a biopsy in men with a PSA of 4 to 10 ng/mL. However, the free fraction is the most labile with rapid degradation even at 4°C, which may impact the utility of the ratio in clinical practice. Finally, the PSA doubling time, defined as the time required for the PSA level to double, has been applied as an indicator of clinical progression in patients with prostate cancer.²⁸ For example, a short PSA doubling time (<3 months) appears to be significantly associated with the onset of recurrence and the risk of death from prostate cancer. A longer PSA doubling time is associated with a longer time to metastasis, to prostate cancer-specific death, and to death from all causes.²⁹

In addition to these conventional PSA derivatives to enhance PSA-based prostate cancer screening, a generation of prostate cancer biomarkers has emerged, consisting of serum-, urine-, and tissue-based assays that may supplement PSA testing. These biomarkers are being explored for various purposes, including (1) to help clinicians determine whom to biopsy, such as PCA3,³⁰ the Prostate Health Index (phi),³¹ and 4K score³⁰ (with the latter two representing advanced ratios based on PSA isoforms); (2) to help clinicians determine when to perform a repeat biopsy following a prior negative biopsy, such as ConfirmMDx,³² Prostate Core Mitomic Test, TMPRSS2-ERG,³² and the phosphatase and tensin homolog (PTEN) gene;³² (3) to help clinicians determine which men with a positive biopsy to treat or not treat, such as Oncotype DX³² and Prolaris^{®32} and (4) to help clinicians predict the probability of metastasis after radical prostatectomy, such as Decipher.³² Although these biomarkers hold promise for assisting clinicians in improving risk assessment, reducing overtreatment, and providing more selective therapy for patients with high-risk disease, further understanding is needed to appreciate their potential benefits and

limitations. Additional outcomes data and standardization in clinical usage are ultimately needed to guide practice.

1.6 Systematic Transrectal Ultrasound-Guided Prostate Biopsy

Biopsy of the prostate to diagnose or exclude cancer is performed nearly 1 million times annually in the United States, most frequently as a result of an elevated PSA.³³ Most biopsies are conducted under ultrasound guidance by a transrectal approach (► Fig. 1.1). Using this technique, tissue cores are obtained systematically throughout the prostate, most commonly using a 12-core biopsy template, matching the approach supported by the American Urological Association (► Fig. 1.2).³⁴ A variety of techniques have emerged for optimizing this biopsy scheme, including computerized and image-guided techniques, although conventional systematic sampling employing a variable number of cores remains the standard in practice. The use of a 12-core systematic biopsy that incorporates apical and lateral cores of the prostate increases cancer detection rates compared to traditional sextant sampling methods, reduces the likelihood that patients will require a repeat biopsy given improved negative predictive value, ultimately allows more accurate risk



Fig. 1.1 Schematic of standard transrectal ultrasound-guided prostate biopsy being performed.

stratification, and does not appear to increase the likelihood of detecting insignificant cancers as compared to the 6-core sextant sampling.^{34,35} However, only limited evidence supports the use of initial biopsy schemes involving more than 12 cores.

Currently, both endfire and sidefire configurations of the biopsy probe are used for prostate sampling (► Fig. 1.3). While endfire and sidefire ultrasound probes are generally viewed as having similar cancer detection rates and complications, and are thus both used in clinical practice, some recent literature suggests slightly higher detection rates with an endfire probe.^{36,37} The sidefire transrectal probe has been associated with a better patient tolerance profile.^{37,38}

Improvements in anesthesia techniques have allowed urologists to obtain a greater number of cores as well as cores from

different locations in the gland, such that urologists may potentially perform a “saturation” biopsy procedure within an office setting that incorporates a very large number of transrectal cores.³⁹ A periprostatic nerve block is commonly used during transrectal ultrasound (TRUS) guided biopsy in which the optimal injection site seems to be the angle between the prostate and the seminal vesicles, which can be easily identified as a hypoechoic area on TRUS. A concentration of 1% lidocaine (5 mL per side) is sufficient to provide pain relief. Despite lack of a standardized dose or optimal technique, periprostatic nerve block remains the clinical gold standard.⁴⁰

1.6.1 Complications of Prostate Biopsy

According to the AUA clinical guidelines on the incidence, prevention, and complications related to prostate needle biopsy, the most common urological side effects of a prostate needle biopsy include hematuria, rectal bleeding, hematospermia, urinary tract infection, and acute urinary retention.^{41,42} Erectile dysfunction and vasovagal response also may occur following prostate biopsy, although they are generally self-limiting and well tolerated (► Table 1.2). Most infectious complications after

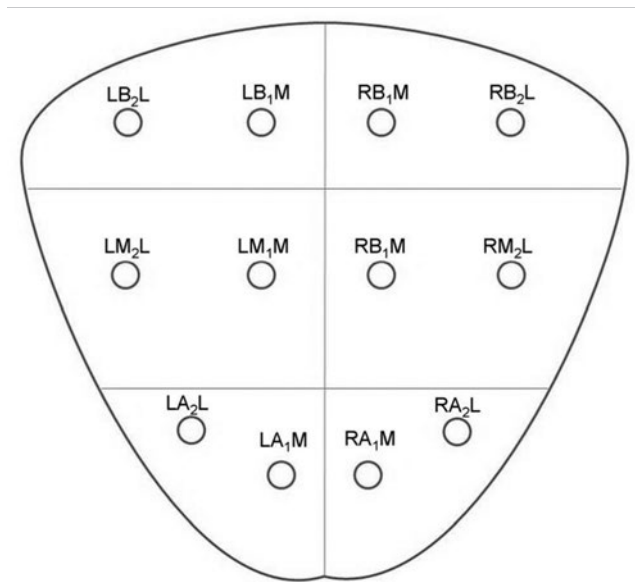


Fig. 1.2 12-core extended systematic prostate biopsy template with lateral cores. LBL, left base lateral; LBM, left base medial; RBM, right base medial; RBL, right base lateral; LML, left mid lateral; LMM, left mid medial; RMM, right mid medial; RML, right mid lateral; LAL, left apex lateral; LAM, left apex medial; RAM, right apex medial; RAL, right apex lateral.

Complication	Incidence
Hematuria	23–84% ^{84,85,86,87}
Rectal bleeding	17–45% ^{84,85,86,87}
Hematospermia	12–93% ^{84,85,86,87}
Urinary tract infection	2–6% ⁸⁸
Bacteremia	0.1–2.2% ⁴⁶
Hospitalization	0.6–4.1% ⁴⁴
Erectile dysfunction	2.2% ⁸⁹
Urinary retention	1% ^{87,90,91}
Vasovagal response	1.4–5.3% ^{92,93}

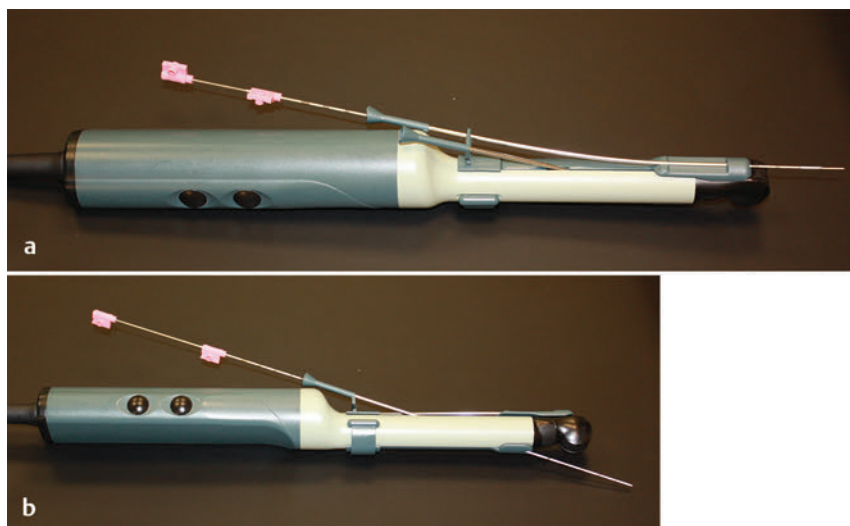


Fig. 1.3 (a) Endfire and (b) sidefire configurations of the biopsy probe used for prostate sampling.

prostate biopsy are limited to symptomatic urinary tract infection and low-grade febrile illness, which can be readily treated with oral or intravenous antibiotics. However, postbiopsy sepsis has also emerged as a risk of this procedure. The incidence of infectious complications following prostate biopsy in large multi-institutional studies ranges from 0.1 to 7% depending upon the antimicrobial prophylactic regimen used,^{43,44,45} with approximately 30 to 50% of these patients having accompanying bacteremia.^{46,47} In a meta-analysis and review of prostate biopsy results, Shen et al determined that there were no significant differences in the incidence of major or minor complications between the transperineal and transrectal technique.⁴⁸ However, the nature of the complications is different, with infection being more common with the transrectal route.

1.6.2 Prevention of Prostate Biopsy Complications

Current considerations for the prevention of bleeding complications after prostate biopsy include withholding anticoagulants, including warfarin, nonsteroidal anti-inflammatory drugs, herbal supplements, and clopidogrel, for 7 to 10 days prior to the biopsy when it is possible to do so. Fluoroquinolones or cephalosporins remain the recommended prophylactic antibiotics, although the frequency of quinolone-resistant infections is increasing. Prebiopsy screening with rectal swabs may allow identification of those men harboring antibiotic-resistant organisms in their endogenous gastrointestinal flora and for whom fluoroquinolone prophylaxis may not be appropriate. Prebiopsy rectal swabs have identified fluoroquinolone-resistant isolates in up to 22% of patients and are considered to have contributed to the decrease in postbiopsy infection.^{43,49}

1.7 Limitations of Contemporary Systematic Biopsy Technique

The contemporary random 12-core systematic biopsy strategy relies on sampling efficiency for cancer detection and is consequently subject to sampling error (► Fig. 1.4).⁵⁰ Cancers are often small, intermingled with benign stroma, and not uniformly distributed within the gland. As a result, clinically significant cancers frequently go undetected. Undersampling of the prostate during ultrasound-guided biopsy also leads

to incorrect risk stratification in a subset of men, given the potential to erroneously categorize clinically significant tumors as low volume or low grade. Random nontargeted prostate biopsies risk inadequate sampling of a cancer lesion, often at its periphery. For instance, the biopsy may only demonstrate a small length of the tumor having a low Gleason score, when in fact, a clinically significant portion with a higher Gleason score may exist adjacent to the site of the positive biopsy core.

Approximately 30 to 50% of men over age 50 years harbor clinically insignificant prostate cancer at autopsy. These clinically insignificant cancers are often identified by chance during a systematic biopsy approach, contributing, in part, to the problem of overdiagnosis and overtreatment of indolent prostate cancer. Repeat biopsies in patients with persistent clinical suspicion for prostate cancer serves to further increase detection of clinically insignificant prostate cancer. The recent trend of trying to overcome sampling error by increasing the number of cores obtained during a single biopsy session, or by repeated biopsy sessions, further escalates the risk of identifying small, indolent cancers, which may have little relationship with the patient's PSA elevation and also escalates the overall costs.³⁴

1.8 Treatment Options for Localized Prostate Cancer

Selection of a particular option for prostate cancer treatment depends on the assessment of several factors, including the patient's life expectancy, overall health status, and tumor characteristics.

1.8.1 Active Surveillance

For men diagnosed with early-stage lower-risk prostate cancer (low Gleason score, low PSA level, and localized), definitive treatment may not be beneficial. Autopsy studies have shown that up to 60% of older men have some areas of cancer within the prostate.⁵¹ Men who choose not to undergo immediate therapy may opt for continued follow-up under a program of active surveillance. Active surveillance for men with prostate cancer involves closely monitoring the course of the disease with the expectation of intervening with potentially curative therapy should there be any evidence of cancer progression.

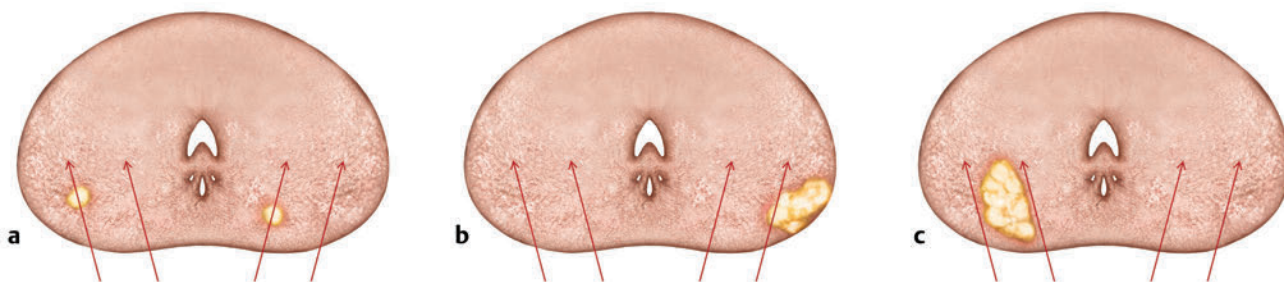


Fig. 1.4 Current limitations of prostate biopsy. (a) Clinically insignificant cancers are often identified by chance during a systematic biopsy (oversampling). (b) Systematic biopsies may lead to incorrect risk stratification categorizing clinically significant tumors as low volume or low grade (undersampling). (c) Systematic deployment of needle biopsies may lead to clinically significant tumors being missed on initial biopsy (undersampling).

The NCCN's recommended active surveillance protocol includes obtaining a PSA level no more often than every 6 months and a digital rectal examination and repeat prostate biopsy no more often than every 12 months unless clinically indicated.⁵² Several studies have shown that patients with lower-grade, localized prostate cancer have a very low risk for clinical progression within the first 10 to 15 years after the diagnosis.^{53,54} Through appropriate surveillance, patients can be reclassified following the initial low-risk disease as in fact being at a higher risk for disease progression and thus receive definitive therapy, an approach that is believed to not substantially decrease the chance of cure. Generally, patients with high-grade tumors at diagnosis have a relatively higher risk of adverse pathology, progression, metastasis, and mortality if not treated; they are not suitable for active surveillance. The AUA considers active surveillance, interstitial brachytherapy, external beam radiation therapy, and radical prostatectomy to be appropriate treatment options for patients diagnosed with low- and intermediate-risk prostate cancer.⁵⁵ However, the NCCN guidelines define a very low-risk group: clinical stage T1c, fewer than 3 positive biopsy cores, with $\leq 50\%$ of cancer in each core, and a PSA density < 0.15 ng/mL.⁵² For this very low-risk group, the NCCN recommends active surveillance as the preferred management option for those patients having a life expectancy of less than 20 years. In comparison, for the low-risk group (stage T1-T2a, Gleason score ≤ 6 , T1-T2a, PSA < 10 ng/mL), the NCCN recommends active surveillance for those patients having a life expectancy of less than 10 years, while considering active surveillance, radiation therapy, and radical prostatectomy as options for those patients having a longer life expectancy.⁵²

1.8.2 Interstitial Prostate Brachytherapy

Patients with clinically localized prostate cancer are considered candidates for interstitial prostate brachytherapy, but no guidelines exist with respect to which risk groups should be offered this approach. Some practitioners will use this treatment option for low-risk disease only, while others will treat both low- and intermediate-risk patients using this approach. The radioactive needles are implanted via a transperineal approach under guidance of transrectal ultrasound or magnetic resonance imaging. Common regimens employ 120 grays (Gy) (palladium) or 140 Gy (iodine-125), with dosimetry performed following implantation in order to assess the satisfactory dose distribution of the implanted radioactive seeds throughout the prostate. One of the most important factors in predicting the effectiveness of an implant is implant quality. An excellent implant is defined as one in which 90% or more of the prostate gland volume receives at least 100% of the prescription dose.⁵⁶

1.8.3 External-Beam Radiation Therapy

External-beam radiation therapy may be used as a curative treatment option for prostate cancer in men who do not have a history of inflammatory bowel disease or a history of prior pelvic radiation therapy. The manner in which external-beam radiation therapy is applied varies based on the patient's level of risk. For low-risk patients, randomized controlled trials in which higher radiation doses led to improved biochemical recurrence-free survival outcomes suggest a benefit of dose

escalation.^{57,58} For patients with locally advanced or high-grade disease (Gleason score > 7), randomized controlled trials have shown that 2 to 3 years of androgen-deprivation therapy in conjunction with a standard radiation dose (~ 70 Gy) improve survival.⁵⁹ Follow-up at 6-month intervals for 5 years and annually thereafter is common for the assessment of the oncologic outcome. For patients in the intermediate-risk category, randomized controlled trials have shown that either short-course hormonal therapy (~ 6 months) administered concurrently with standard-dose external-beam radiation therapy, or external-beam radiation therapy with dose escalation (78–79 Gy) are options.^{60,61,62}

1.8.4 Radical Prostatectomy

Radical prostatectomy is a surgical procedure in which the entire prostate gland and attached seminal vesicles plus the ampulla of the vas deferens are removed. Radical prostatectomy may be performed using a retropubic or perineal incision or by using a conventional laparoscopic or robot-assisted technique. The objective of a radical prostatectomy is to optimize not only the oncologic efficiency by removing all cancer (without a positive surgical margin) but also to balance the functional aspect including continence and potency recovery. During a nerve-sparing procedure, an attempt is made to spare the two cavernous nerve sheaths (lying slightly underneath and to the sides of the prostate gland) that produce erections. This technique has been associated with improved rates of postoperative sexual and urinary function.^{63,64,65,66} Incontinence rates are approximately 20% during the first year of follow-up. In addition, 70–75% of men experience erectile dysfunction in the same time period.⁶⁷ However, depending on tumor characteristics and the patient's baseline sexual function, a non-nerve-sparing approach may be performed on one or both sides.⁶³ Pelvic lymphadenectomy can be performed concurrently with radical prostatectomy and is generally reserved for patients with a higher risk of nodal involvement.⁶⁸

1.8.5 Cryosurgery

Cryosurgery (also called cryotherapy) is the use of extreme cold, often in the form of liquid nitrogen or argon gas, to destroy abnormal tissue. Cryoprobes are placed percutaneously through the perineum into the prostate under ultrasound or MRI guidance and monitoring of the freezing of the cells occurs, thus limiting damage to adjacent healthy tissue. The AUA consensus opinion is that primary cryosurgery is an option for men who have clinically organ-confined disease of any grade and a negative metastatic evaluation. Cryosurgery offers the benefit that it is a minimally invasive procedure, the procedure can be repeated if needed, and it may be used to treat men who cannot have surgery or radiation therapy because of their age or other medical problems. Outcomes after cryosurgery seem to compare favorably with those reported in contemporary series of patients who receive radiation therapy, particularly with respect to late failure rates.^{69,70} High-risk patients may require a multimodal approach when undergoing cryosurgery. Data are limited regarding the outcomes for clinical stage T3 disease undergoing cryosurgery, and the role of cryosurgery in this setting is currently undetermined.⁷¹

More recently, an array of ablative therapies have emerged, including cyroablation, high-intensity focused ultrasound, electroporation, radiofrequency ablation, and vascular-targeted photodynamic therapy. These may be applied to varying extents in a focal manner, targeting areas of tumor without treating the entire prostate. While focal therapy remains an area of active investigation at the time of this writing, long-term follow-up data regarding its oncologic efficacy is currently lacking.

1.9 Tumor Grade

Tumor aggressiveness is determined by the pathologist via examination of the microscopic pattern of the cancer cells. Overwhelmingly, the most commonly used grading system for prostate cancer is the Gleason grading system, first described in 1966.^{72,73,74} This system assigns a grade ranging from 1 (least aggressive) to 5 (most aggressive) based on the architectural pattern of the tumor at histologic evaluation, with a higher grade indicating lesser differentiation. In 2005, the International Society of Urological Pathology modified the Gleason grading system such that Gleason patterns 1 and 2 no longer exist in contemporary readings, leaving Gleason pattern 3 as the lowest assigned pattern. Tumors often show multiple grade patterns within the prostate or even within a single biopsy core. To account for this variability, the Gleason score is obtained by assigning both primary and secondary Gleason grades for the dominant and second most dominant patterns that are identified, respectively. The Gleason score is then generally displayed, for example, as 3+4, with 3 and 4 representing these two most common patterns. Typically, pathologists do not assign Gleason grades below 3, such that the overall Gleason score is not below 3+3. Furthermore, tumor aggressiveness increases with subsequent stepwise increases in the Gleason score (namely, from 3+3, to 3+4, 4+3, 4+4, 4+5, 5+4, and 5+5), and is in turn associated with increasing mortality. Tumors with Gleason score 3+3 are generally considered to be low grade, and those with a Gleason score of 4+4 or higher are considered to be high grade. Those with Gleason scores of 3+4 or 4+3 have variably been considered as intermediate or as high grade in various contexts.

1.10 Prostate Cancer Staging

Tumor stage refers to the degree to which the tumor involves the prostate gland or has spread beyond the prostate. The American Joint Committee on Cancer (AJCC) has established a system for tumor staging that is widely applied in clinical practice.⁷⁵ This system categorizes the local extent of prostate cancer within the pelvis as follows: T1: tumor cannot be felt on digital rectal examination or visualized on imaging; T1a/b: incidental histologic tumor in $\leq 5\%$ or $> 5\%$ of tissue, respectively; T1c: tumor identified by needle biopsy (because of PSA level); T2: tumor is large enough to be felt on digital rectal examination or visualized on imaging, although remains confined to the prostate; T3: tumor extends beyond the confines of the gland and possibly to the seminal vesicles (T3); T4: tumor invades adjacent structures (other than the seminal vesicles). Patient outcomes after treatment are progressively worse as the T stage increases. Nonetheless, patients with spread of tumor to lymph

nodes or to the bones or other distant metastatic sites have the poorest outcomes.

Schemes have been developed to stratify patients' level of risk, which is intended to help guide treatment selection. These schemes are based on the PSA level, biopsy Gleason score, and AJCC clinical T category, all of which have been associated with the risk of prostate cancer-specific mortality following radical prostatectomy, external-beam radiation therapy, or interstitial prostate brachytherapy.⁷⁶ While variations on this system exist, the AUA supports the following risk categories: low risk: PSA < 10 ng/mL and a Gleason score of ≤ 6 and clinical stage T1c or T2a; intermediate risk: PSA > 10 to 20 ng/mL or a Gleason score of 7 or clinical stage T2b but not qualifying for high risk; high risk: PSA ≥ 20 ng/mL or a Gleason score of ≥ 8 or clinical stage $\geq T2c$.⁵⁵

1.11 Overview of Clinical Diagnosis and Management Pathway of Prostate Cancer

Men who have an abnormal PSA, digital rectal examination, or adjunct biomarker at the time of screening for the early detection of prostate cancer are frequently recommended to undergo a prostate biopsy. As previously noted, systematic prostate biopsy is typically performed in a transrectal fashion with guidance by transrectal ultrasound to localize the prostate. Men who are diagnosed with prostate cancer are counseled on treatment options based on their risk stratification. Men whose biopsy does not reveal prostate cancer frequently endure continued monitoring, often with the taking of serial PSA levels. However, this current paradigm leaves ample opportunities for improvement. PSA as well as other clinical biomarkers still lack sufficient specificity for prostate cancer, leading to many negative biopsies. In addition, the risk of missing cancer on the initial prostate biopsy due to sampling error is substantial, often resulting in the need for one or more repeat biopsies in the common situation of persistent clinical suspicion for prostate cancer.⁷⁷ Moreover, systematic biopsy frequently diagnoses indolent tumors unlikely to harm the patient. Current strategies for risk stratification may erroneously classify patients with significant tumor as being low risk, leading to uncertainty that may result in patients with indolent tumors selecting aggressive intervention. For those patients undergoing treatment, intervention is largely performed in a nontargeted fashion that has substantial risks of side effects impacting quality of life. Also, traditional approaches for following patients who have had one or more negative biopsies, are on active surveillance, or have undergone treatment for prostate cancer, lack sensitivity and specificity for progression of the disease. Clearly, an improved method for reliably localizing tumors within the prostate as well as for establishing their level of aggressiveness and patient risk could greatly benefit patients with known or suspected prostate cancer.

State-of-the-art multiparametric MRI of the prostate addresses all of these challenges and is a central component of an ongoing major shift in prostate cancer management. Prostate MRI was first performed clinically in the 1980s, largely to assist local staging in patients with known prostate cancer, for

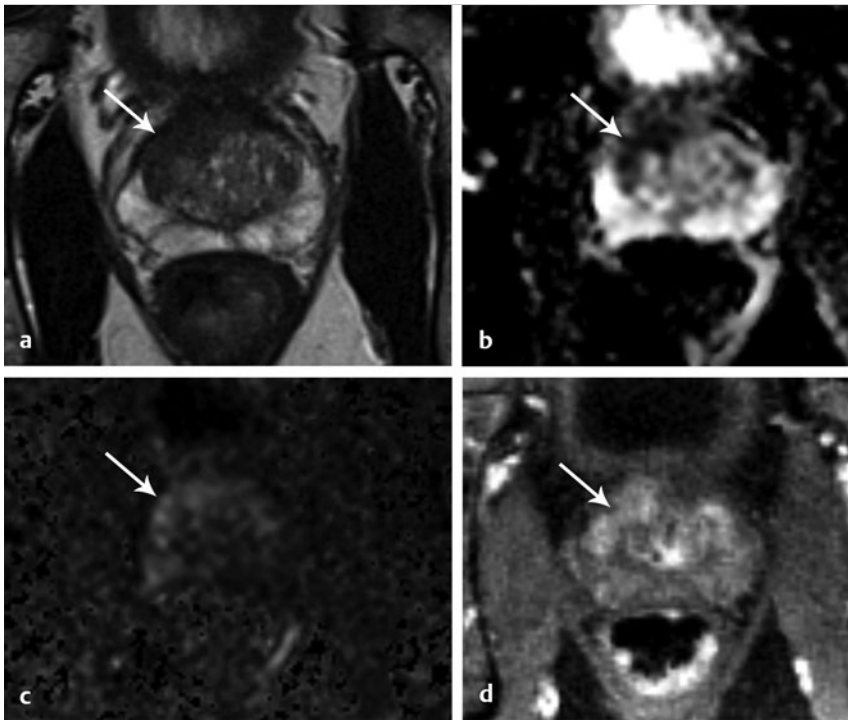


Fig. 1.5 75-year-old man with prostate-specific antigen of 8.2 ng/mL and a prior negative prostate biopsy. Magnetic resonance imaging was performed to help identify a target for repeat biopsy. (a) Axial T2-weighted image shows elliptical poorly marginated lesion in right anterior transition zone (arrow). (b) Apparent diffusion coefficient (ADC) map shows low ADC in lesion (arrow). (c) High b-value diffusion-weighted imaging (1,500 s/mm²) shows increased signal intensity (arrow). (d) Early dynamic post-contrast T1-weighted image shows early enhancement (arrow). Targeted biopsy of lesion using an MRI-ultrasound fusion system demonstrated Gleason score 4 + 5 tumor.

instance, by identifying gross extraprostatic extension, seminal vesicle invasion, and abnormal pelvic lymph nodes. However, early implementations of prostate MRI had notably limited performance in detecting and localizing tumor within the prostate. Nonetheless, a convergence of factors has combined to greatly alter the role of prostate MRI in clinical practice. Development of additional sequences to complement standard anatomical imaging (most importantly, diffusion-weighted imaging and dynamic contrast-enhanced imaging), improvements in scanner and receiver coil technology, and continual optimization of radiologists' interpretations have enhanced the performance of MRI in localizing tumors within the prostate, as evidenced by a number of studies showing strong performance in this regard. Moreover, multiparametric prostate MRI appears to have a particularly high sensitivity for high-risk clinically significant tumors, although relatively low sensitivity for low-risk, potentially indolent tumors, thereby facilitating selective diagnosis of clinically important tumors and appropriate risk stratification. It is this ability to reliably localize significant tumors within the prostate that may be at the crux of prostate MRI's impact on patient management (► Fig. 1.5), in turn assisting the decision to biopsy, the decision to treat, disease staging, surveillance regimens, and image-guided interventions. Through optimal integration of state-of-the-art prostate MRI into clinical practice, it is anticipated that physicians will be able to reliably diagnose and treat men with significant tumors that warrant therapy, while also reducing the frequency of prostate cancer overdiagnosis and overtreatment. This book provides an overview of prostate MRI, focusing on acquisition, interpretation, staging, image-guided biopsy, surveillance, and post-treatment monitoring to help the reader achieve and maintain a high-quality prostate MRI program within his or her own clinical practice.

References

- [1] Stat Fact Sheets SEER. Prostate Cancer. <http://seer.cancer.gov/statfacts/html/prost.html>.
- [2] Siegel RL, Miller KD, Jemal A. Cancer statistics, 2015. *CA Cancer J Clin* 2015; 65(1):5–29
- [3] Lunenfeld B. The ageing male: demographics and challenges. *World J Urol* 2002; 20(1):11–16
- [4] Helgesen F, Holmberg L, Johansson JE, Bergström R, Adami HO. Trends in prostate cancer survival in Sweden, 1960 through 1988: evidence of increasing diagnosis of nonlethal tumors. *J Natl Cancer Inst* 1996; 88(17):1216–1221
- [5] Sedjo RL, Byers T, Barrera E Jr. et al. ACS Cancer Incidence & Mortality Ends Committee. A midpoint assessment of the American Cancer Society challenge goal to decrease cancer incidence by 25% between 1992 and 2015. *CA Cancer J Clin* 2007; 57(6):326–340
- [6] Taichman RS, Loberg RD, Mehra R, Pienta KJ. The evolving biology and treatment of prostate cancer. *J Clin Invest* 2007; 117(9):2351–2361
- [7] Mariotto AB, Yabroff KR, Shao Y, Feuer EJ, Brown ML. Projections of the cost of cancer care in the United States: 2010–2020. *J Natl Cancer Inst* 2011; 103(2):117–128
- [8] Roehrborn CG, Black LK. The economic burden of prostate cancer. *BJU Int* 2011; 108(6):806–813
- [9] Snyder CF, Frick KD, Blackford AL et al. How does initial treatment choice affect short-term and long-term costs for clinically localized prostate cancer? *Cancer* 2010; 116(23):5391–5399
- [10] Aizer AA, Gu X, Chen MH et al. Cost implications and complications of overtreatment of low-risk prostate cancer in the United States. *J Natl Compr Canc Netw* 2015; 13(1):61–68
- [11] Merrill RM, Sloan A. Risk-adjusted incidence rates for prostate cancer in the United States. *Prostate* 2012; 72(2):181–185
- [12] Lichtenstein P, Holm NV, Verkasalo PK et al. Environmental and heritable factors in the causation of cancer—analyses of cohorts of twins from Sweden, Denmark, and Finland. *N Engl J Med* 2000; 343(2):78–85
- [13] Huncharek M, Haddock KS, Reid R, Kupelnick B. Smoking as a risk factor for prostate cancer: a meta-analysis of 24 prospective cohort studies. *Am J Public Health* 2010; 100(4):693–701
- [14] Zu K, Giovannucci E. Smoking and aggressive prostate cancer: a review of the epidemiologic evidence. *Cancer Causes Control* 2009; 20(10):1799–1810
- [15] Barrington WE, Schenk JM, Etzioni R et al. Difference in Association of Obesity With Prostate Cancer Risk Between US African American and Non-Hispanic White Men in the Selenium and Vitamin E Cancer Prevention Trial (SELECT). *JAMA Oncol* 2015; 1(3):342–349

- [16] Cuzick J, Thorat MA, Andriole G et al. Prevention and early detection of prostate cancer. *Lancet Oncol* 2014; 15(11):e484–e492
- [17] Sutcliffe S, Platz EA. Inflammation and prostate cancer: a focus on infections. *Curr Urol Rep* 2008; 9(3):243–249
- [18] De Marzo AM, Platz EA, Sutcliffe S et al. Inflammation in prostate carcinogenesis. *Nat Rev Cancer* 2007; 7(4):256–269
- [19] Stamey TA, Yang N, Hay AR, McNeal JE, Freiha FS, Redwine E. Prostate-specific antigen as a serum marker for adenocarcinoma of the prostate. *N Engl J Med* 1987; 317(15):909–916
- [20] Loeb S, Bjurlin MA, Nicholson J et al. Overdiagnosis and overtreatment of prostate cancer. *Eur Urol* 2014; 65(6):1046–1055
- [21] Yin M, Bastacky S, Chandran U, Becich MJ, Dhir R. Prevalence of incidental prostate cancer in the general population: a study of healthy organ donors. *J Urol* 2008; 179(3):892–895, discussion 895
- [22] Carter HB, Albertsen PC, Barry MJ et al. Early detection of prostate cancer: AUA Guideline. *J Urol* 2013; 190(2):419–426
- [23] Carroll PR, Parsons JK, Andriole G et al. National comprehensive cancer network. Prostate cancer early detection, version 1.2014. Featured updates to the NCCN Guidelines. *J Natl Compr Canc Netw* 2014; 12(9):1211–1219, quiz 1219
- [24] Moyer VA, LeFevre ML, Siu AL; U.S. Preventive Services Task Force. Screening for prostate cancer: U.S. Preventive Services Task Force recommendation statement. *Ann Intern Med* 2012; 157(2):120–134
- [25] Vickers AJ, Till C, Tangen CM, Lilja H, Thompson IM. An empirical evaluation of guidelines on prostate-specific antigen velocity in prostate cancer detection. *J Natl Cancer Inst* 2011; 103(6):462–469
- [26] Carter HB, Kettermann A, Warlick C et al. Expectant management of prostate cancer with curative intent: an update of the Johns Hopkins experience. *J Urol* 2007; 178(6):2359–2364, discussion 2364–2365
- [27] Catalona WJ, Partin AW, Slawin KM et al. Use of the percentage of free prostate-specific antigen to enhance differentiation of prostate cancer from benign prostatic disease: a prospective multicenter clinical trial. *JAMA* 1998; 279(19):1542–1547
- [28] Pound CR, Partin AW, Eisenberger MA, Chan DW, Pearson JD, Walsh PC. Natural history of progression after PSA elevation following radical prostatectomy. *JAMA* 1999; 281(17):1591–1597
- [29] D'Amico AV, Chen MH, Roehl KA, Catalona WJ. Preoperative PSA velocity and the risk of death from prostate cancer after radical prostatectomy. *N Engl J Med* 2004; 351(2):125–135
- [30] Vedder MM, de Bekker-Grob EW, Lilja HG et al. The added value of percentage of free to total prostate-specific antigen, PCA3, and a kallikrein panel to the ERSPC risk calculator for prostate cancer in prescreened men. *Eur Urol* 2014; 66(6):1109–1115
- [31] Stephan C, Vincendeau S, Houlgatte A, Cammann H, Jung K, Semjonow A. Multicenter evaluation of [-2]prostate-specific antigen and the prostate health index for detecting prostate cancer. *Clin Chem* 2013; 59(1):306–314
- [32] Boström PJ, Bjartell AS, Catto JW et al. Genomic Predictors of Outcome in Prostate Cancer. *Eur Urol* 2015; 68(6):1033–1044
- [33] Welch HG, Fisher ES, Gottlieb DJ, Barry MJ. Detection of prostate cancer via biopsy in the Medicare-SEER population during the PSA era. *J Natl Cancer Inst* 2007; 99(18):1395–1400
- [34] Bjurlin MA, Carter HB, Schellhammer P et al. Optimization of initial prostate biopsy in clinical practice: sampling, labeling and specimen processing. *J Urol* 2013; 189(6):2039–2046
- [35] Eichler K, Hempel S, Wilby J, Myers L, Bachmann LM, Kleijnen J. Diagnostic value of systematic biopsy methods in the investigation of prostate cancer: a systematic review. *J Urol* 2006; 175(5):1605–1612
- [36] Rom M, Pycha A, Wiunig C et al. Prospective randomized multicenter study comparing prostate cancer detection rates of end-fire and side-fire transrectal ultrasound probe configuration. *Urology* 2012; 80(1):15–18
- [37] Raber M, Scattoni V, Gallina A et al. Does the transrectal ultrasound probe influence prostate cancer detection in patients undergoing an extended prostate biopsy scheme? Results of a large retrospective study. *BJU Int* 2012; 109(5):672–677
- [38] Moussa AS, El-Shafei A, Diaz E et al. Identification of the variables associated with pain during transrectal ultrasonography-guided prostate biopsy in the era of periprostatic nerve block: the role of transrectal probe configuration. *BJU Int* 2013; 111(8):1281–1286
- [39] Zaytoun OM, Moussa AS, Gao T, Fared K, Jones JS. Office based transrectal saturation biopsy improves prostate cancer detection compared to extended biopsy in the repeat biopsy population. *J Urol* 2011; 186(3):850–854
- [40] Autorino R, De Sio M, Di Lorenzo G et al. How to decrease pain during transrectal ultrasound guided prostate biopsy: a look at the literature. *J Urol* 2005; 174(6):2091–2097
- [41] American Urological Association. AUA/SUNA White Paper on the Incidence, Prevention and Treatment of Complications Related to Prostate Needle Biopsy. Available at: <http://www.auanet.org/common/pdf/education/clinical-guidance/AUA-SUNA-PNB-White-Paper.pdf>.
- [42] Loeb S, Vellekoop A, Ahmed HU et al. Systematic review of complications of prostate biopsy. *Eur Urol* 2013; 64(6):876–892
- [43] Liss MA, Chang A, Santos R et al. Prevalence and significance of fluoroquinolone resistant *Escherichia coli* in patients undergoing transrectal ultrasound guided prostate needle biopsy. *J Urol* 2011; 185(4):1283–1288
- [44] Nam RK, Saskin R, Lee Y et al. Increasing hospital admission rates for urological complications after transrectal ultrasound guided prostate biopsy. *J Urol* 2010; 183(3):963–968
- [45] Loeb S, Carter HB, Berndt SI, Ricker W, Schaeffer EM. Complications after prostate biopsy: data from SEER-Medicare. *J Urol* 2011; 186(5):1830–1834
- [46] Otrrock ZK, Oghlakan GO, Salamoun MM, Haddad M, Bizri AR. Incidence of urinary tract infection following transrectal ultrasound guided prostate biopsy at a tertiary-care medical center in Lebanon. *Infect Control Hosp Epidemiol* 2004; 25(10):873–877
- [47] Zaytoun OM, Vargo EH, Rajan R, Berglund R, Gordon S, Jones JS. Emergence of fluoroquinolone-resistant *Escherichia coli* as cause of postprostate biopsy infection: implications for prophylaxis and treatment. *Urology* 2011; 77(5):1035–1041
- [48] Shen PF, Zhu YC, Wei WR et al. The results of transperineal versus transrectal prostate biopsy: a systematic review and meta-analysis. *Asian J Androl* 2012; 14(2):310–315
- [49] Steensels D, Slabbaert K, De Wever L, Vermeersch P, Van Poppel H, Verhaegen J. Fluoroquinolone-resistant *E. coli* in intestinal flora of patients undergoing transrectal ultrasound-guided prostate biopsy—should we reassess our practices for antibiotic prophylaxis? *Clin Microbiol Infect* 2012; 18(6):575–581
- [50] Bjurlin MA, Meng X, Le Nobin J et al. Optimization of prostate biopsy: the role of magnetic resonance imaging targeted biopsy in detection, localization and risk assessment. *J Urol* 2014; 192(3):648–658
- [51] Zlotta AR, Egawa S, Pushkar D et al. Prevalence of prostate cancer on autopsy: cross-sectional study on unscreened Caucasian and Asian men. *J Natl Cancer Inst* 2013; 105(14):1050–1058
- [52] NCCN Guidelines. http://www.nccn.org/professionals/physician_gls/f_guidelines.asp.
- [53] Klotz L. Active surveillance with selective delayed intervention for favorable risk prostate cancer. *Urol Oncol* 2006; 24(1):46–50
- [54] Johansson JE, Andrén O, Andersson SO et al. Natural history of early, localized prostate cancer. *JAMA* 2004; 291(22):2713–2719
- [55] Thompson I, Thrasher JB, Aus G et al. AUA Prostate Cancer Clinical Guideline Update Panel. Guideline for the management of clinically localized prostate cancer: 2007 update. *J Urol* 2007; 177(6):2106–2131
- [56] D'Souza WD, Thames HD, Kuban DA. Dose-volume conundrum for response of prostate cancer to brachytherapy: summary dosimetric measures and their relationship to tumor control probability. *Int J Radiat Oncol Biol Phys* 2004; 58(5):1540–1548
- [57] Zietman AL, DeSilvio ML, Slater JD et al. Comparison of conventional-dose vs high-dose conformal radiation therapy in clinically localized adenocarcinoma of the prostate: a randomized controlled trial. *JAMA* 2005; 294(10):1233–1239
- [58] Dearnaley DP, Sydes MR, Graham JD et al. RT01 collaborators. Escalated-dose versus standard-dose conformal radiotherapy in prostate cancer: first results from the MRC RT01 randomised controlled trial. *Lancet Oncol* 2007; 8(6):475–487
- [59] Bolla M, Collette L, Blank L et al. Long-term results with immediate androgen suppression and external irradiation in patients with locally advanced prostate cancer (an EORTC study): a phase III randomised trial. *Lancet* 2002; 360(9327):103–106
- [60] Jones CU, Hunt D, McGowan DG et al. Radiotherapy and short-term androgen deprivation for localized prostate cancer. *N Engl J Med* 2011; 365(2):107–118
- [61] Denham JW, Steigler A, Lamb DS et al. Short-term neoadjuvant androgen deprivation and radiotherapy for locally advanced prostate cancer: 10-year data from the TROG 96.01 randomised trial. *Lancet Oncol* 2011; 12(5):451–459
- [62] D'Amico AV, Manola J, Loffredo M, Renshaw AA, DellaCroce A, Kantoff PW. 6-month androgen suppression plus radiation therapy vs radiation therapy alone for patients with clinically localized prostate cancer: a randomized controlled trial. *JAMA* 2004; 292(7):821–827

- [63] Walsh PC. Patient-reported impotence and incontinence after nerve-sparing radical prostatectomy. *J Urol* 1998; 159(1):308–309
- [64] Steineck G, Bjartell A, Hugosson J et al. LAPPRO steering committee. Degree of preservation of the neurovascular bundles during radical prostatectomy and urinary continence 1 year after surgery. *Eur Urol* 2015; 67(3):559–568
- [65] Reeves F, Preece P, Kapoor J et al. Preservation of the neurovascular bundles is associated with improved time to continence after radical prostatectomy but not long-term continence rates: results of a systematic review and meta-analysis. *Eur Urol* 2015; 68(4):692–704
- [66] Michl U, Tennstedt P, Feldmeier L et al. Nerve-sparing Surgery Technique, Not the Preservation of the Neurovascular Bundles, Leads to Improved Long-term Continence Rates After Radical Prostatectomy. *Eur Urol* 2015
- [67] Haglind E, Carlsson S, Stranne J et al. LAPPRO steering committee. Urinary Incontinence and Erectile Dysfunction After Robotic Versus Open Radical Prostatectomy: A Prospective, Controlled, Nonrandomised Trial. *Eur Urol* 2015; 68(2):216–225
- [68] Carroll P, Coley C, McLeod D et al. Prostate-specific antigen best practice policy—part II: prostate cancer staging and post-treatment follow-up. *Urology* 2001; 57(2):225–229
- [69] Hubosky SG, Fabrizio MD, Schellhammer PF, Barone BB, Tepera CM, Given RW. Single center experience with third-generation cryosurgery for management of organ-confined prostate cancer: critical evaluation of short-term outcomes, complications, and patient quality of life. *J Endourol* 2007; 21(12):1521–1531
- [70] Bahn DK, Lee F, Badalament R, Kumar A, Gresnik J, Chernick M. Targeted cryoablation of the prostate: 7-year outcomes in the primary treatment of prostate cancer. *Urology* 2002; 60(2) Suppl 1:3–11
- [71] Best practice policy statement on cryosurgery for the treatment of prostate cancer. <http://www.auanet.org/education/guidelines/cryosurgery.cfm>.
- [72] National Cancer Institute. Prostate Cancer Treatment (PDQ)—For Health Professionals. <http://www.cancer.gov/types/prostate/hp/prostate-treatment-pdq>.
- [73] Gleason DF. The Veteran's Administration Cooperative Urologic Research Group: histologic grading and clinical staging of prostatic carcinoma. In: Tannenbaum M ed. *Urologic Pathology: The Prostate*. Lea and Febiger, Philadelphia, 1977; 171–198
- [74] Gleason DF. Classification of prostatic carcinomas. *Cancer Chemother, —"In: Tannenbaum M, ed. Urologic..." Rep* 1966; 50(3):125–128
- [75] American Joint Committee on Cancer. Cancer staging references. <https://cancerstaging.org/references-tools/quickreferences/Pages/default.aspx>.
- [76] D'Amico AV, Whittington R, Malkowicz SB et al. Biochemical outcome after radical prostatectomy, external beam radiation therapy, or interstitial radiation therapy for clinically localized prostate cancer. *JAMA* 1998; 280(11):969–974
- [77] Abraham NE, Mendhiratta N, Taneja SS. Patterns of repeat prostate biopsy in contemporary clinical practice. *J Urol* 2015; 193(4):1178–1184
- [78] Murphy DG, Ahlering T, Catalona WJ et al. The Melbourne Consensus Statement on the early detection of prostate cancer. *BJU Int* 2014; 113(2):186–188
- [79] Heidenreich A, Bastian PJ, Bellmunt J et al. European Association of Urology. EAU guidelines on prostate cancer. part 1: screening, diagnosis, and local treatment with curative intent—update 2013. *Eur Urol* 2014; 65(1):124–137
- [80] Smith RA, Manassaram-Baptiste D, Brooks D et al. Cancer screening in the United States, 2014: a review of current American Cancer Society guidelines and current issues in cancer screening. *CA Cancer J Clin* 2014; 64(1):30–51
- [81] Qaseem A, Barry MJ, Denberg TD, Owens DK, Shekelle P Clinical Guidelines Committee of the American College of Physicians. Screening for prostate cancer: a guidance statement from the Clinical Guidelines Committee of the American College of Physicians. *Ann Intern Med* 2013; 158(10):761–769
- [82] Horwich A, Hugosson J, de Reijke T, Wiegel T, Fizazi K, Kataja V Panel Members. European Society for Medical Oncology. Prostate cancer: ESMO Consensus Conference Guidelines 2012. *Ann Oncol* 2013; 24(5):1141–1162
- [83] Basch E, Oliver TK, Vickers A et al. Screening for prostate cancer with prostate-specific antigen testing: American Society of Clinical Oncology Provisional Clinical Opinion. *J Clin Oncol* 2012; 30(24):3020–3025
- [84] Rosario DJ, Lane JA, Metcalfe C et al. Short term outcomes of prostate biopsy in men tested for cancer by prostate specific antigen: prospective evaluation within ProtecT study. *BMJ* 2012; 344:d7894
- [85] de la Taille A, Antiphon P, Salomon L et al. Prospective evaluation of a 21-sample needle biopsy procedure designed to improve the prostate cancer detection rate. *Urology* 2003; 61(6):1181–1186
- [86] Ghani KR, Dundas D, Patel U. Bleeding after transrectal ultrasonography-guided prostate biopsy: a study of 7-day morbidity after a six-, eight- and 12-core biopsy protocol. *BJU Int* 2004; 94(7):1014–1020
- [87] Raaijmakers R, Kirkels WJ, Roobol MJ, Wildhagen MF, Schrder FH. Complication rates and risk factors of 5802 transrectal ultrasound-guided sextant biopsies of the prostate within a population-based screening program. *Urology* 2002; 60(5):826–830
- [88] Williamson DA, Barrett LK, Rogers BA, Freeman JT, Hadway P, Paterson DL. Infectious complications following transrectal ultrasound-guided prostate biopsy: new challenges in the era of multidrug-resistant *Escherichia coli*. *Clin Infect Dis* 2013; 57(2):267–274
- [89] Akyol I, Adayener C. Transient impotence after transrectal ultrasound-guided prostate biopsy. *J Clin Ultrasound* 2008; 36(1):33–34
- [90] Berger AP, Gozzi C, Steiner H et al. Complication rate of transrectal ultrasound guided prostate biopsy: a comparison among 3 protocols with 6, 10 and 15 cores. *J Urol* 2004; 171(4):1478–1480, discussion 1480–1481
- [91] Zaytoun OM, Anil T, Moussa AS, Jianbo L, Fareed K, Jones JS. Morbidity of prostate biopsy after simplified versus complex preparation protocols: assessment of risk factors. *Urology* 2011; 77(4):910–914
- [92] Djavan B, Waldert M, Zlotta A et al. Safety and morbidity of first and repeat transrectal ultrasound guided prostate needle biopsies: results of a prospective European prostate cancer detection study. *J Urol* 2001; 166(3):856–860
- [93] Rodríguez LV, Terris MK. Risks and complications of transrectal ultrasound guided prostate needle biopsy: a prospective study and review of the literature. *J Urol* 1998; 160(6 Pt 1):2115–2120

2 Prostate Cancer Pathology

Fang-Ming Deng, Jianhong Li, Max X. Kong, Jonathan Melamed, and Ming Zhou

2.1 Anatomy and Histology of Normal Prostate and Prostate Cancer

2.1.1 Anatomy and Histology of Normal Prostate

In an adult male without significant hyperplasia, the average weight of the prostate gland is approximately 20 to 30 g. It is shaped as an inverted cone, with the base at the bladder neck and the apex at the urogenital diaphragm. Anatomically and biologically, the prostate can be divided into three glandular zones (peripheral, central, and transition zones) and a fourth nonglandular region, termed the anterior fibromuscular stroma. The central zone (~ 25% of the prostate volume) is an inverted cone structure with ducts branching from the verumontanum to the prostate base and surrounding the ejaculatory ducts. The transition zone (5% of the prostate volume) lies in the bilateral base to midregion of the gland and is composed of ducts that extend laterally from the urethral wall and curve anteromedially. It typically enlarges in older men due to benign prostatic hyperplasia. The peripheral zone (70% of the prostate volume) extends posterolaterally around the central zone and distal prostatic urethra.^{1,2}

Histologically, the prostate consists of epithelial and stromal cells. Epithelial cells are arranged in tubuloalveolar glands that consist of ducts that branch out from the urethra and terminate in acini. The glands have an irregular contour with luminal undulation and papillary infolding. The glands comprise mainly two cell types: luminal secretory cells and basal cells. Secretory cells have a columnar or cuboidal shape with clear to pale cytoplasm and pseudostratified nuclei. Basal cells are small, flat, and situated at the periphery of the glands beneath the secretory cells (► Fig. 2.1). Central zone glands are larger than peripheral and transition zone glands and more complex, with intraluminal ridges, papillary infolding, and occasional epithelial arches and cribriform glands that mimic prostatic intraepithelial neoplasm. The acini are mainly lined by luminal secretory cells and basal cells. The proximal portion of the prostatic duct is lined by urothelial cells. The distal portion of the prostatic ducts, as well as some acini, may exhibit cuboidal and columnar epithelium admixed with urothelium.

Benign prostatic hyperplasia (BPH), also known as nodular hyperplasia, is a common urologic condition related to overgrowth of the epithelium and fibromuscular tissue of the transition zone and periurethral area. Grossly, nodular hyperplasia consists of variably sized nodules that are rubbery, firm or soft, and yellow-gray, with a bulging surface. Nodular hyperplasia is composed of varying proportions of epithelium and stroma (smooth muscle and fibroconnective tissue). The glandular component of BPH is made up of hyperplastic small and large acini and often shows cystic change (► Fig. 2.2 a; ► Fig. 2.2 b). The luminal secretory epithelium consists of tall columnar cells with pale-staining cytoplasm. The basal cells are variably seen, ranging from barely detectable to hyperplastic.

2.1.2 Anatomy and Histology of Prostate Cancer

Prostate cancer is the most common noncutaneous cancer in American man, with increasing incidence in older age groups. The American Cancer Society estimates about 220,800 new cases of prostate cancer and about 27,540 deaths from prostate cancer in 2015. While about 6 cases in 10 are diagnosed in men aged 65 or older, it is rare before age 40. The average age at the time of diagnosis is 66. Prostate cancer is the second leading cause of cancer death in American men, behind only lung cancer. About 1 man in 38 will die of prostate cancer.³

Most prostate cancers arise in the peripheral zone, and some can result in abnormal findings on digital rectal examination. Histologically, prostate carcinoma has a constellation of architectural, cytoplasmic, nuclear, and intraluminal features. Architecturally, the glands of gland-forming prostate carcinomas are more crowded than normal and typically exhibit a haphazard growth pattern, with these malignant glands oriented perpendicular to each other and irregularly separated by fibromuscular bundles. They also display infiltrated growth pattern, with malignant glands situated between or flanking benign glands (► Fig. 2.3). When prostate carcinoma becomes less differentiated, it partially or totally loses glandular differentiation and forms cribriform structures, fused glands, poorly delineated glands, solid sheets or cords, and even single cells (► Fig. 2.4). Prostate carcinoma typically displays enlarged nuclei with prominent nucleoli. Mitoses and apoptotic bodies are not frequently seen in prostate adenocarcinoma but are more common in this setting than in benign glands.

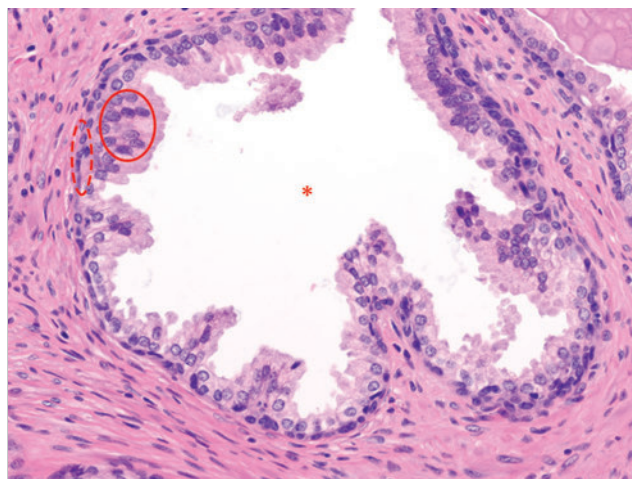


Fig. 2.1 A normal prostate gland exhibiting irregular contour with luminal papillary folding. It comprises mainly two cell types: luminal secretory cells (solid oval) and basal cells (dashed oval). Secretory cells are columnar or cuboidal shaped with clear to pale cytoplasm and pseudostratified nuclei. Basal cells are small, flat, and situated at the periphery of the gland beneath the secretory cells. Asterisk, glandular lumen.

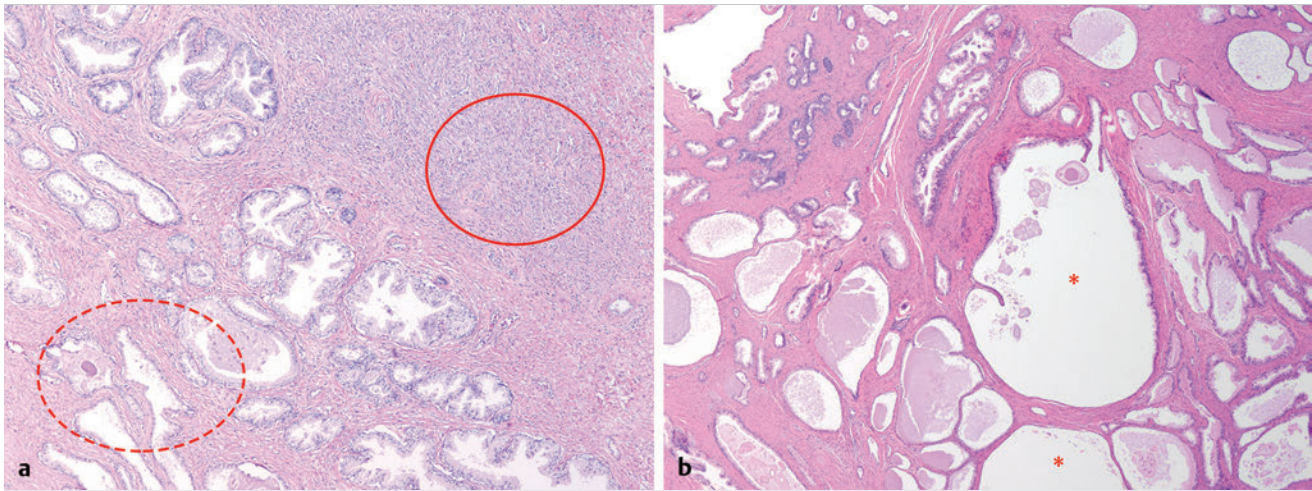


Fig. 2.2 Benign prostatic hyperplasia (BPH) (a), Stromal (right upper solid circle) and glandular proliferation (left lower dashed circle). (b), Cystic dilated glands (asterisk) in a BPH nodule.

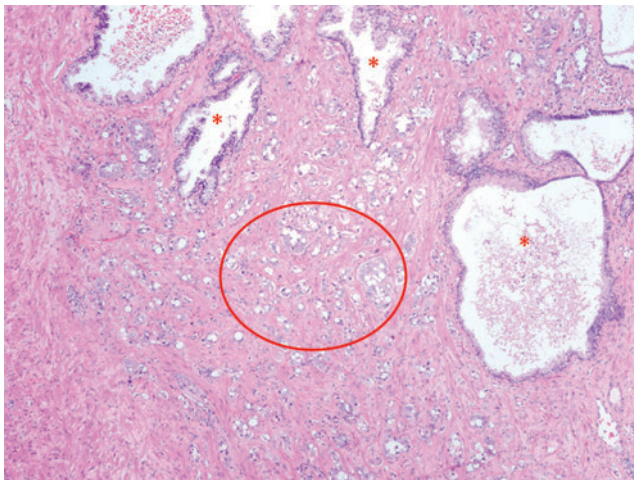


Fig. 2.3 Prostate adenocarcinoma glands display infiltrative growth pattern, with malignant glands (for example, circle) situated between or flanking benign glands (asterisks).

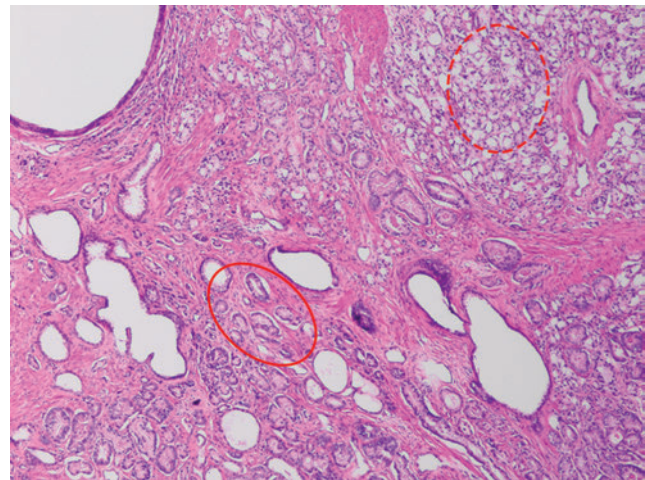


Fig. 2.4 Well-differentiated prostate adenocarcinoma is gland-forming. The malignant glands display more crowded architecture than normal glands, and typically exhibit a haphazard growth pattern (solid circle, lower half). Poorly differentiated prostate adenocarcinoma partially or totally loses glandular differentiation and forms cribriform structures, fused glands, poorly delineated glands, solid sheets or cords, and even single cells (dashed circle, upper half).

2.1.3 Multifocality and Dominant Nodule in Radical Prostatectomy

It is well documented that prostate cancer (PCa) presents as a multifocal disease, with two or more tumor nodules present within the prostate gland, in the majority of cases.^{4,5,6,7} Prostate cancer also demonstrates heterogeneity among different tumor nodules in the same prostate gland. Histologically, different tumor nodules in the same prostatectomy specimen often show different Gleason scores.^{5,8} Arora et al showed multifocal cancer was present in 87% of radical prostatectomy (RP) specimens. However, in only 9% of the cases of multifocal cancer did all tumor nodules have the same primary and secondary Gleason grades as the overall Gleason grades assigned to the RP specimen.⁵ At molecular and genetic levels, Cheng et al studied the pattern of allelic loss in prostate cancer from patients who had two or more

separate cancer foci and observed that the pattern of allelic loss was distinct between different foci in 15 of 18 cases, supporting an independent clonal origin of the multiple tumor foci in a single patient.⁹ A recent study on *TMPRSS2* gene rearrangements in multifocal PCa demonstrated differing gene arrangement status and class between different tumor foci, providing further molecular evidence of independent clonal origin of multifocal cancer foci.¹⁰ The morphological and genetic heterogeneity of multifocal PCa suggests that different cancer foci may be biologically distinct, with the presumption that some tumor foci are more aggressive than others within the same prostate gland.

The concept of the dominant nodule (DN) was first introduced by McNeal et al¹¹ to refer to the tumor nodule that most

likely harbors the most aggressive biological behavior among the multifocal tumor nodules within the prostate and therefore presumably dictates the tumor's overall biological behavior. In 2005, the International Society of Urological Pathology (ISUP) consensus recommended use of the DN for tumor grading and tissue banking for research on RP specimens.¹² The DN concept has also garnered considerable interest recently in focal therapy for PCa, as the DN is naturally the ideal target for therapeutic intervention. However, the definition of the DN is ambiguous in terms of which of the pathologic parameters (tumor size, Gleason grade [GG], or staging parameter) should be used to in fact determine which nodule is the DN. At the 2009 ISUP consensus meeting, the urologic pathology experts did not reach a consensus on the pathologic parameters that define the DN in RP specimens.¹³ Currently, the DN is generally defined as the tumor nodule of the largest size in the setting of multifocal disease.^{5,6,7,11,12} However, the largest tumor volume, highest GS, and staging parameters (i.e., extraprostatic extension) do not always occur in the same tumor nodule.^{5,7}

Our group's study¹⁴ showed that prognostically important pathologic parameters (largest tumor volume, highest GS, and staging parameters) occur in the same tumor nodule in the majority of multifocal prostate cancer (88.7%), such that the concept of the DN is valid in these patients. In these cases, the DN can be used to assign an overall GS and procure tissue for research. However, adverse pathologic parameters (largest tumor volume, highest GS, and staging parameters) did not occur in the same tumor nodule in 11.3% of cases. In these cases, pathologists may deemphasize the DN concept and instead report the multifocality and pathologic features of all independent tumor foci.

2.1.4 Pathologically Insignificant and Significant Prostate Cancer

The notion of insignificant PCa has progressively emerged in the last two decades. The clinical relevance of such a definition was based on previous studies that suggested that low-grade, small volume, and organ-confined PCa may be indolent and unlikely to progress to biological significance in the absence of treatment.^{15,16} An accurate definition of insignificant disease may be important for the clinician to better manage patients after radical treatment and propose alternative therapies (active surveillance) more confidently. To date, the most commonly used criteria for defining insignificant PCa are based on the pathologic assessment of the RP specimen and include three well-established prognostic factors: (1) Gleason score (GS) no more than 6 without any Gleason pattern 4 or 5, even as a tertiary Gleason pattern; (2) organ-confined disease (no extraprostatic extension [EPE], seminal vesicle invasion [SVI], and lymph node invasion [LNI]); and (3) tumor volume <0.5 cm³. The pathologic criteria for insignificant PCa might be improved by incorporating factors other than the pathologic features alone, such as age, prostate-specific antigen level (PSA) level, and comorbidities.¹⁷

The differentiation of patients with significant versus insignificant PCa based on prostate biopsy may be more important. Men harboring insignificant PCa can be selected for active surveillance, while those with significant PCa usually require definitive treatment such as prostatectomy.

The most commonly used biopsy pathology criteria for insignificant PCa is the Epstein criteria: no Gleason pattern 4 or 5, less than 3 cores from a sextant biopsy positive for tumor, and no core with >50% tumor involvement.¹⁸ However, minimal disease on biopsy does not reliably predict minimal disease in the subsequent prostatectomy specimen in terms of the size and grade of tumor, extraprostatic extension, or positive margins. Thus, reasoned accounting should be made of other data, particularly prostate-specific-antigen kinetics and potential molecular markers, before undertaking a course of active surveillance or radiation therapy as monotherapy.^{19,20}

2.2 Prostate Cancer

2.2.1 Prostate Cancer and Histologic Variants

Prostate cancer is typically composed of usual acinar adenocarcinoma with a minority of acinar carcinoma and non-acinar carcinoma variants or types. Variants of usual acinar adenocarcinoma defined in 2004 by the World Health Organization (WHO) include atrophic, pseudohyperplastic, foamy, mucinous (colloid), signet ring, oncocytic, and lymphoepithelioma-like carcinomas (► Table 2.1). Adenocarcinomas of atrophic, pseudohyperplastic, and foamy variants do not appear to be different from usual acinar adenocarcinoma and typically behave as conventional low-grade acinar Gleason score 6 prostate cancers in terms of patient outcome after radical prostatectomy.^{21,22,23} Mucinous (colloid) adenocarcinoma used to be thought to confer a worse prognosis. However, recent reports indicate that mucinous adenocarcinoma treated by radical prostatectomy is not more aggressive than usual acinar adenocarcinoma and may even be less aggressive.²⁴ Prostate adenocarcinomas of signet ring-cell or lymphoepithelioma-like variants are rare and usually have very poor clinical outcomes.

Non-acinar carcinoma variants of prostatic carcinoma account for about 5 to 10% of primary prostate carcinomas. These histologic variants or types include, according to the

Table 2.1 Histologic variants of prostate carcinoma

Histologic variants
Foamy gland carcinoma
Pseudohyperplastic carcinoma
Adenocarcinoma with atrophic features
Adenocarcinoma with glomeruloid features
Large duct carcinoma
Mucinous (colloid) carcinoma
Small cell neuroendocrine carcinoma
Sarcomatoid carcinoma (carcinosarcoma)
Signet ring-cell carcinoma
Squamous and adenosquamous carcinoma
Adenoid cystic-type basaloid carcinoma
Urothelial carcinoma

WHO, sarcomatoid carcinoma, ductal adenocarcinoma, urothelial carcinoma, squamous and adenosquamous carcinoma, basal cell carcinoma, neuroendocrine tumors, including small cell carcinoma, and clear cell adenocarcinoma. Ductal adenocarcinoma is the most common histologic variant of prostatic carcinoma. The incidence of ductal adenocarcinoma including both pure ductal adenocarcinoma and mixed ductal–acinar adenocarcinoma is about 3% of all prostatic carcinomas, with mixed ductal–acinar adenocarcinoma being more common than pure ductal adenocarcinoma. In radical prostatectomy specimens, the ductal adenocarcinoma is composed of confluent masses of papillary and/or cribriform adenocarcinoma. The ductal adenocarcinoma is almost always intimately admixed with acinar adenocarcinoma. Microscopically, prostatic duct adenocarcinoma is characterized by pseudostratified columnar epithelium, and therefore, it has also been termed endometrioid, endometrial, papillary, or papillary ductal adenocarcinoma. The outcome for men with prostatic ductal adenocarcinoma is, in most studies, worse than that for men with usual prostatic acinar adenocarcinoma, probably because of higher stage and grade. Some patients with this variant respond to radical prostatectomy, hormonal therapy, and radiation therapy.²⁵

Recently, several PCa histologic types with distinct clinicopathologic features have been redefined. These include intraductal carcinoma and prostate cancer with neuroendocrine differentiation.

Intraductal Carcinoma of the Prostate

Intraductal carcinoma of the prostate (IDC-P) represents spread of invasive carcinoma into preexisting benign ducts and acini and is strongly associated with high-grade (Gleason grades 4 or 5), large-volume, invasive prostate cancers.²⁶

The glands of intraductal carcinoma of the prostate are larger than normal peripheral zone glands and exhibit markedly irregular and branching contours. In addition to the presence of malignant epithelial cells filling large acini and prostatic ducts with preservation of basal cells, the diagnosis of IDC-P requires

the presence of a solid or dense cribriform pattern (► Fig. 2.5 a; ► Fig. 2.5 b). If these features are not present, a diagnosis of IDC-P can be made if there is nonfocal comedonecrosis involving > 2 glands¹, or marked nuclear atypia², whereby the nuclei are at least 6 times larger than adjacent benign nuclei.^{26,27}

Studies have established that IDC-P represents an aggressive form of PCa and is an adverse pathologic parameter in both radical prostatectomy and needle biopsy specimens. The presence of IDC-P is associated with other adverse pathologic features in radical prostatectomy specimens, including higher Gleason scores, larger tumor volumes, and greater probability of extraprostatic extension, seminal vesicle invasion, and pelvic lymph node metastasis. It is also associated with decreased biochemical progression-free survival and with postsurgical biochemical recurrence. Epstein et al reported cases of IDC-P in prostate biopsies without invasive carcinoma.²⁸ They found that the presence of IDC-P, even in the absence of documented invasive carcinoma, was associated with an aggressive clinical course and adverse pathologic findings in subsequent radical prostatectomy specimens. Based on their studies of needle biopsy with IDC-P and previous studies in the literature that demonstrated consistent association of IDC-P at radical prostatectomy with multiple adverse prognostic factors, definitive therapy was recommended in men with IDC-P on needle biopsy, even in the absence of pathologically documented invasive PCa.

Prostate Cancer with Neuroendocrine Differentiation

Neuroendocrine (NE) differentiation can occur de novo with or without concurrent PCa, or as a transformed phenotype emerging from prior treatment for prostate cancer. Neuroendocrine phenotype generally confers a more aggressive clinical behavior and less favorable prognosis than that of conventional PCa. To standardize the diagnosis and facilitate further study, a morphological classification of NE differentiation in PCa was proposed recently²⁹ and consists of 6 categories: (1) usual prostate adenocarcinoma with NE differentiation, (2) adenocarcinoma

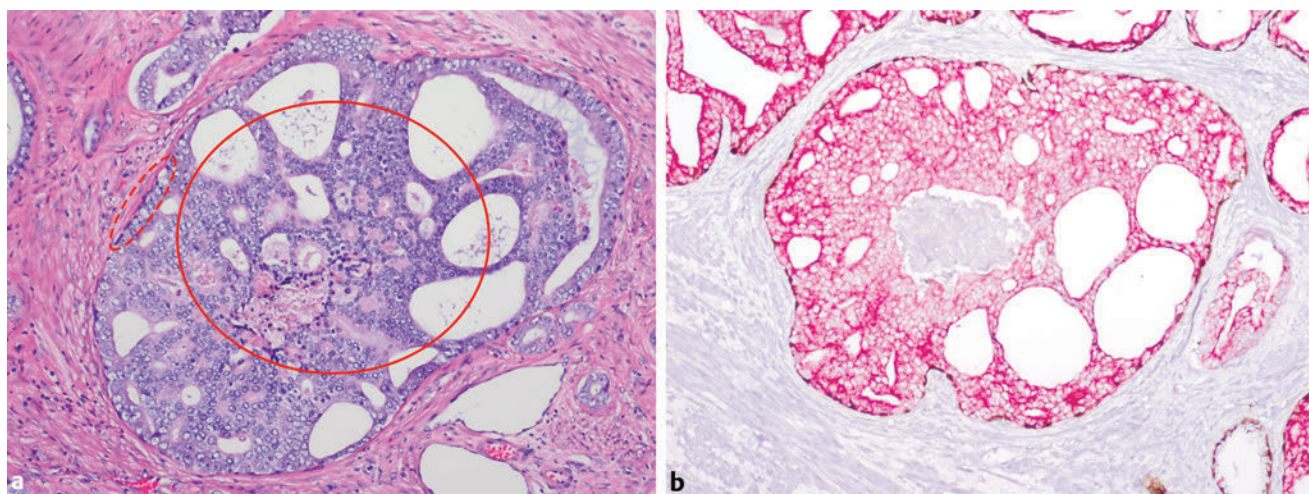


Fig. 2.5 (a) Intraductal carcinoma of the prostate displays a cribriform proliferation of malignant cells that distend the lumen of the large prostatic duct (solid circle) with preservation of benign basal cells (dashed oval). (b) Immunostains highlight the malignant cells (AMACR, red) and the preserved basal cells (high molecular weight keratin and P63, brown).

with Paneth-cell-like NE differentiation, (3) carcinoid tumor, (4) small cell carcinoma, (5) large cell NE carcinoma, and (6) mixed NE carcinoma-acinar adenocarcinoma.

Usual PCa with NE differentiation refers to typical acinar or ductal PCa in which NE differentiation is demonstrated only by immunohistochemical positivity (synaptophysin, chromogranin A, and CD 56). The clinical significance of NE differentiation in these tumors is uncertain and most of the studies have shown no effect on outcomes. Prostate cancer with Paneth-cell-like differentiation is typical PCa containing changes resembling Paneth-cells (i.e., prominent eosinophilic cytoplasmic granules on light microscopy and neurosecretory granules on electron microscopy). The clinical significance of PCa with Paneth-cell-like differentiation is not completely understood, although studies have shown that seemingly poorly differentiated PCa with Paneth-cell-like differentiation has a favorable prognosis.

Prostate carcinoid tumor is a well-differentiated NE tumor with the classical morphology of carcinoid tumor arising in the prostatic parenchyma. It expresses NE markers, but not PSA. It is exceedingly rare, and strict diagnostic criteria should be used. Small cell carcinoma is an aggressive NE tumor recognized by its typical morphology and immunoprofiles similar to small cell carcinoma of the lung. Large cell NE carcinoma is a high-grade NE tumor with both morphological NE features (large nests of tumor cells with peripheral palisading, non-small cell nuclear features) and extensive NE marker expression. The majority of cases represent progression from a prior typical PCa following long-standing androgen ablation. Mixed NE carcinoma and acinar PCa comprise distinct components of NE (small cell or large cell) carcinoma and typical acinar PCa with abrupt transition. Most, if not all, cases of mixed small cell carcinoma and PCa represent NE transformation after androgen-deprivation therapy, and are hormone resistant with a poor prognosis.

2.2.2 Clinically Significant Cancer Gleason Grading System

The Gleason grading system, developed by Dr. Donald Gleason in 1967, remains the cornerstone for the management of prostate cancer. The system is relatively simple and reasonably reproducible. It may be considered the key parameter for planning treatment, as well as the most important prognostic factor in predicting pathologic findings at radical prostatectomy, biochemical failure (rise in PSA after treatment), local and distant metastasis after therapy, and PCa specific mortality. The system assigns histologic patterns 1 through 5, with 1 being the most differentiated and 5 the least differentiated. The *Gleason score* is defined as the sum of the most and second-most common Gleason patterns and ranges from 2 to 10.³⁰ It has undergone continuous modification in response to changes in the clinical practice of diagnosis and treatment of prostate cancer since its inception.^{31,32} The most significant changes were introduced in 2005 at the auspices of the International Society of Urological Pathology (ISUP), although further modifications also ensued.³¹ The resulting contemporary grading system is referred to as the *2005 ISUP modified Gleason grading system* (► Fig. 2.6). However, it is important to stress that the changes put forth by ISUP in 2005 simply codified what had already been used in practice by many pathologists.

Important Changes in the 2005 Modified Gleason Grading System

Some of the changes are definitional, including precise definitions of each Gleason grade and grading criteria for PCa morphological variants. Others are operational, that is, how to report a Gleason grade in special circumstances, including reporting of a secondary pattern of lower or higher grade when present to a limited extent, a tertiary pattern in both biopsy and prostatectomy specimens, etc.

The most important change is perhaps the strict definition of each grade. A Gleason score of 1+1=2 should not be assigned, with only rare exceptions, regardless of the specimen type. Gleason scores of 2 to 4 should rarely be assigned in needle biopsies, if ever. They should rarely be used in transurethral-resection (TURP) and radical-prostatectomy (RP) specimens. Indeed, the Gleason grade starts at 3 and the Gleason score starts at 6 in prostate biopsy specimens and most TURP and RP specimens.

Gleason grade 3 is strictly defined as discrete, well-formed cancer glands. Ill-defined glands with poorly formed glandular lumens are considered grade 4, together with other grade 4 patterns such as fused, cribriform, and hypernephroid glands. However, grade 4 poorly formed glands should be differentiated from small glands resulting from tangential sectioning. The latter typically encompasses only a few poorly formed glands that are adjacent to or intermingle with other well-formed small glands. A few poorly formed glands adjacent to other small

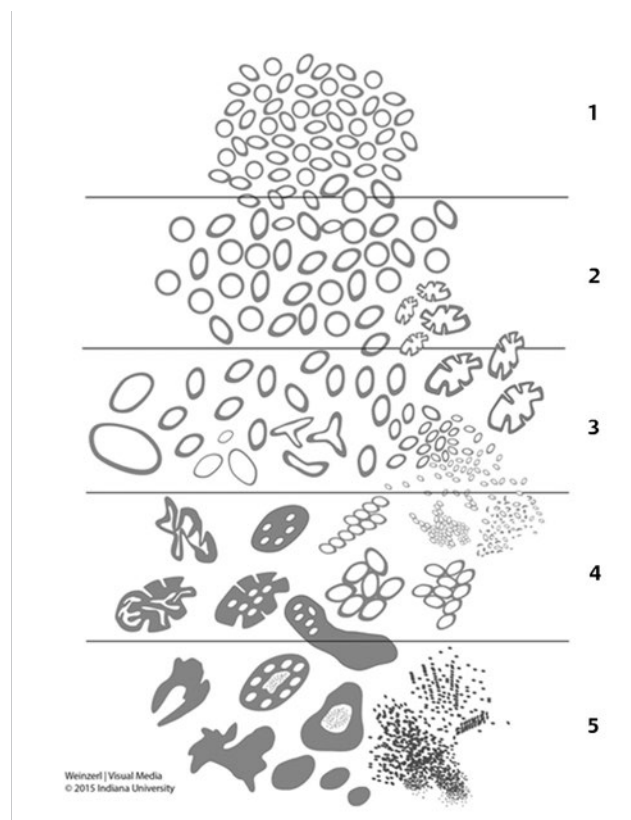


Fig. 2.6 The 2005 International Society of Urological Pathology (ISUP) modified classification of Gleason grading, showing the characteristic architecture of Gleason patterns 1 through 5. Used with permission from The Trustees of Indiana University; illustration by Thomas Weizerl.

grade 3 glands are not considered grade 4. Most cribriform patterns, if not all, are diagnosed as grade 4.

Grading of PCa with histologic patterns such as glomerulation and mucinous fibroplasia, as well as with one of the histologic variants, is based on the underlying glandular architecture. The peculiar namesake of the histologic pattern or variation should be ignored.

Implications of Modified Gleason Grading System

Gleason score 6 prostate cancer has become a homogeneous group with uniformly excellent prognosis

The 2005 modified Gleason grading system's strict definition of Gleason grade 3 and its inclusion of any high-grade (grade 4 and 5) tertiary pattern in the final Gleason score in prostate biopsy specimens have led to reassigning many prior GS 6 cancers to GS 7. One immediate effect of this change is that GS 6 cancers have become more homogeneous in their clinical behavior and now more uniformly exhibit excellent prognosis when diagnosed in both radical prostatectomy and biopsy specimens. Eggener et al studied the 15-year cancer specific mortality following radical prostatectomy from 1987 to 2005. Of 9557 patients with organ-confined GS 6 PCa, only 3 (0.03%) died of cancer.³³ Similar reports demonstrated that in patients with pathologically organ-confined Gleason score ≤ 6 PCa, biochemical recurrence and local recurrence following radical prostatectomy were extremely rare and no patients experienced distant metastasis or prostate cancer-specific death.^{34,35} Gleason score 6 PCa diagnosed on biopsy also has an excellent prognosis despite sampling error and potential upgrade to GS ≥ 7 at radical prostatectomy. Pierorazio et al studied 5205 patients with GS 6 PCa diagnosed on biopsy.³⁶ Almost a third (31.7%) of cases were upgraded to GS ≥ 7 on radical prostatectomy. However, the 5-year biochemical-recurrence-free survival was 94.7% (vs. 82.7% for GS 7 on biopsy). The excellent prognosis of GS 6 PCa sparked a debate whether GS 6 PCa on radical-prostatectomy specimens should be labeled as cancer. Our opinion is that the cancer label should be retained for GS 6 tumors, as these lesions are morphologically and genetically similar to higher grade PCa and can invade extraprostatic tissue. Furthermore, GS 6 PCa in prostate-biopsy specimens is upgraded to a higher Gleason score on radical prostatectomy in a substantial fraction of cases.

Is the modified Gleason grading system better than the original system?

To claim the modified Gleason system is better than the original one, it has to be shown that it can improve the interobserver reproducibility among pathologists who use it as well as the concordance in Gleason scores between biopsy and radical-prostatectomy specimens. Ultimately, it must also demonstrate a better association with clinical outcomes.

Studies have shown that the interobserver reproducibility increases from approximately 60% with the original system to approximately 80% with the modified system.^{37,38,39} The improvement has been particularly impressive for GS 7 PCa. The inter-observer reproducibility for this GS increased from

27% in a study conducted in 1997 to 68% in a study conducted in 2008.^{37,39}

The modified Gleason grading system has also improved the concordance between the Gleason scores of the biopsy and radical-prostatectomy (RP) specimens. Before the 2005 modifications, Gleason scores were concordant between biopsy and RP specimens in 28 to 68% of cases.³⁹ The discordance was mainly due to biopsy undergrading and accounted for 24 to 60% of the discordant cases. Biopsy over-grading was less of a problem and accounted for 5 to 32% of the discordant cases. In general, there was a better concordance in high-grade PCa. After the modified Gleason grading system was implemented, there was a 12 to 15% increase in overall exact concordance between biopsy and RP specimens.^{37,40} However, biopsy undergrading is still responsible for the majority of the discordance.

The most important question is how the modified Gleason grading system affects the prediction of clinical outcomes. To date, only a very few studies have addressed this question. Several studies have shown that the correlation between biopsy GS and the risk of biochemical recurrence or PCa-specific survival was significantly better using the modified grading scheme. A study by Delahunt et al, however, reported that the original system outperformed the modified one in predicting PSA nadir following external-beam radiation therapy and hormone therapy.⁴¹ Hence, more studies are needed before a definitive conclusion can be reached.

Impact of modified Gleason grading system on patient management

Biopsy GS plays a pivotal role in treatment decision making. For example, the U.S. National Cancer Center Network Practical Guidelines (<http://www.nccn.org/>) stratify PCa patients into 6 recurrence risk groups based on several clinicopathologic parameters including the biopsy GS and extent, clinical stage, serum PSA, and PSA density (PSAD). Patients within the different risk groups are offered different therapeutic modalities. Therefore, it is expected that an upward shift in GS resulting from the modified grading system will impact how patients are managed.

An increasing number of patients are choosing active surveillance (AS) in which patients are monitored closely and definitive treatment such as surgery, radiation, or hormonal ablation is withheld until there is sign of progression. Active-surveillance criteria vary from institution to institution,⁴² although traditionally a GS ≤ 6 is required in most criteria. With a modified Gleason grading system, fewer cases are graded as GS 6 and more cases as GS 7. Therefore, fewer patients would qualify for AS, which may worsen the issue of overtreatment for PCa. However, as a GS 6 PCa diagnosed according to the modified Gleason grading system constitutes a more homogeneous group with excellent prognosis, patients on AS may be safer with less likelihood to progress to definitive treatment.

With this modified ISUP Gleason grading system, many GS 6 cancers by the old grading system are upgraded to GS 7 cancers on biopsy, even with minimal quantity ($\leq 5\%$) of Gleason pattern 4 (GP 4) component. Recently, we analyzed the pathologic features of 256 consecutive needle biopsies and their corresponding RP specimens.⁴³ Of 107 biopsies with GS 3+4=7, 22

(20.6%) exhibited minimal quantity ($\leq 5\%$) of GP 4. Ten of these 22 cases (45%) had pathologically insignificant tumor in the RP specimen. The quantity of GP 4 in the GS 7 biopsy was significantly associated with GS, pathologic stage, and total tumor volume in the corresponding RP specimen. The GS, pathologic stage, total tumor volume, and insignificant tumor rate in RP specimens were not significantly different between the biopsy groups of GS 6 and GS 7 with minimal GP 4, whereas those parameters were significantly different between biopsy groups of GS 3+3 and GS 3+4 with 6 to 50% of GP 4 and between biopsy groups of GS 7 with minimal GP 4 and GS 7 with 6 to 50% of GP 4. These findings demonstrate that pathologic parameters in the RP specimen are similar between the biopsy groups of GS 6 and GS 7 with minimal ($< 5\%$) GP 4, such that cases of GS 7 with minimal GP 4 on biopsy are often downgraded in RP specimens. Furthermore, recent studies have shown that GS 3+4 PCa diagnosed on biopsy is associated with a more favorable prognosis than GS 4+3 PCa,⁴⁴ raising the possibility that AS may be a reasonable management option for intermediate-risk PCa. Bul et al followed patients with low risk (T1/T2, PSA < 10 ng/mL, PSAD < 0.2 ng/mL/mL, GS < 6 , positive cores < 2) and intermediate-risk PCa (PSA 10–20 ng/mL, GS = 7) and found that the 10-year metastasis-free survival and disease-specific survival are similar between low-risk and intermediate-risk patients, suggesting that AS is a safe approach for intermediate-risk PCa.⁴⁵ Therefore, the reduced enrollment of patients into AS due to the upward grade shift caused by the modified Gleason grading system may become effectively counterbalanced through a reduced rate of progression to definitive treatment among patients already on AS, as well as by more patients with intermediate risk being managed by AS.

Limitations of modified Gleason grading system

There have been such substantial changes to the Gleason grading system that the modified system is essentially a different system from the original one. It is therefore difficult to compare the outcome data in contemporary series with that in historical ones. Another issue is the artificial improvement of prognosis due to score migration (the so-called Will Rogers phenomenon). The modified Gleason system has practically eliminated GS 2 to 5. Furthermore, some PCAs that were graded as GG 3 in the original system are now graded as GG 4 due to the strict definition of GG 3. As the result, some PCa cases in the lower-grade group (GS 6), which have better prognoses, are moved into a higher-grade group (\geq GS 7), thereby improving the overall prognosis of the higher-grade group.

Further modification of Gleason grading system

A very important limitation of the Gleason grading system, both the original and modified systems, is that the numerical scale of Gleason scores does not accurately reflect the biological aggressiveness of the disease. The Gleason scores range from 2 to 10, with 7 further divided into 3+4 and 4+3. However, the modified Gleason grading system has practically eliminated GS 2 to 5 in biopsy specimens, as well as in the majority of radical-prostatectomy specimens. Therefore, the lowest GS in both biopsy and radical prostatectomy is generally 6. Since 6 is in the middle of the 2 to 10 numerical scale, patients may reason that they have

a moderately aggressive cancer despite the fact that GS 6 PCa is the least aggressive tumor assigned in modern practice. To avoid such confusion, Epstein and his associates proposed a new prognostic grouping of prostate cancers by Gleason scores.³⁶ They broke prostate cancers into 5 prognostic groups: group I for GS 6, II for GS 3+4, III for GS 4+3=7, IV for GS 8 and V for GS 9/10. It was previously shown that these categories predicted prognosis in 7,869 men undergoing radical prostatectomy at the Johns Hopkins Hospital.³⁶ The 5-year rates of biochemical-progression-free survival were 94.6%, 82.7%, 65.1%, 63.1%, and 34.5%, respectively, for men assigned to prognostic groups 1 to 5 on biopsy, and 96.6%, 88.1%, 69.7%, 63.7%, and 34.5%, respectively, for men assigned to prognostic groups 1 to 5 on radical prostatectomy ($p < 0.001$). At an ISUP consensus conference on prostate cancer grading, new pooled data on more than 20,000 surgical cases and more than 16,000 biopsies showed similar highly prognostic stratification for the five proposed prognostic groups (unpublished data). Although this change in terminology awaits ratification and validation (via long-term use), it seems logical and welcome for both pathologists and urologists.

Correlation of biopsy Gleason score with radical prostatectomy Gleason score

Several recent studies have compared needle-biopsy Gleason scores with those observed on radical-prostatectomy specimens. In a large study performed at the Johns Hopkins Hospital, a Gleason score of 5 to 6 on biopsy corresponded to the same score on radical prostatectomy in 64% of cases.⁴⁴ With a Gleason score ≥ 7 on biopsy, the radical prostatectomy score was the same in 87.5% of cases. In general, adverse findings on needle biopsy accurately predict adverse findings on radical prostatectomy, while favorable findings on needle biopsy do not necessarily predict favorable findings on radical prostatectomy.

Three major factors account for the discrepancy between biopsy and radical prostatectomy score. The first major source of discrepancy is interobserver variability among pathologists evaluating biopsy specimens. As discussed above, there is a marked tendency for pathologists to undergrade prostate cancer of limited extent on needle biopsy. Another source of discrepancy between biopsy and radical prostatectomy Gleason scores is the presence of tumors that are on the borderline between two grades. The final major source of discrepancy reflects the heterogeneous nature of prostate cancer and the inherent limitation of prostate needle biopsy, which samples only a very small fraction of the prostate gland. When there is a high-grade component present within the radical-prostatectomy specimen that is not sampled by needle biopsy, a discrepancy results. This typically occurs when a tumor on needle biopsy is graded as Gleason score 3+3, but the corresponding radical-prostatectomy specimen also has Gleason pattern 4, which was not sampled on the biopsy, and this results in an undergrading of the biopsy (3+3) compared to the prostatectomy specimen (3+4). Extended needle biopsy schemes, entailing taking more than 10 to 12 cores per biopsy session, as opposed to the conventional 6-cores sextant biopsy scheme, improve the associations between biopsy and radical-prostatectomy Gleason scores.

Quantification of Amount of Cancer on Radical Prostatectomy and Needle Biopsy

Quantification of the amount of cancer on radical prostatectomy is a significant predictor of biochemical recurrence in patients with prostate cancer. There are many methods of quantifying the amount of cancer in radical prostatectomy specimens, including the maximum tumor diameter, percentage of gland involved by tumor, and tumor volume. Tumor volume has often been measured using the grid method. Briefly, a transparent film with a 2×2 mm grid is overlaid on the slides. Each square in the grid represents a tumor volume of 0.013 cm³ (area [0.04 cm²] × thickness of tissue section [3 mm] × correction factor for fixation-induced tissue shrinkage [1.12]).⁴⁶ The tumor volume of a traced focus is obtained by multiplying the total number of squares within the traced lesion by 0.013.

Multiple methods of quantifying the amount of cancer found on needle biopsy have been developed and studied, including measurement of the: (1) number of positive cores; (2) total millimeters of cancer among all cores; (3) percentage of each core occupied by cancer; (4) greatest percentage of tumor involving a single core; and (5) total percentage of cancer in the entire specimen. There are multiple studies claiming superiority of one technique over the other, although no one method has been shown to be clearly superior to the others. The other widely used method of quantifying the amount of cancer on needle biopsy is measurement of the percentage of each biopsy core containing cancer, which has been associated with the likelihood of extraprostatic extension, seminal vesicle invasion, and positive surgical margins. Nonetheless, a limited total extent (<3 mm) of cancer on all biopsy cores in a set does not necessarily predict “insignificant” amounts of tumor in the entire prostate. One feasible and rationale approach may be for pathologists to report the number of cores containing cancer along with one other parameter quantifying tumor extent. Several recent studies found that both the number of cores positive for cancer and the total percentage of core length involved by cancer independently predicted extraprostatic extension and positive surgical margins. At our institution, the number of cores containing cancer is reported along with the tumor length and percentage of cancer present on each involved core.

Staging of Prostate Cancer

Documenting and reporting pathologic staging parameters in radical prostatectomy specimens are key components in providing optimal management for patients with prostate cancer. In the seventh edition of the *AJCC Cancer Staging Manual* (2009), the pathologic stages for prostate cancer include pT2, pT3, and pT4 subgroups. T2 tumors are organ confined and subclassified as: T2a (less than one-half of one lobe involved); T2b (more than one-half of one lobe involved); and T2c (bilateral involvement). T3 tumors are non-organ confined and subclassified as T3a (extraprostatic extension or microscopic invasion of the bladder neck) and T3b (seminal vesical invasion). T4 tumors are fixed or have invasion of the external sphincter, rectum, bladder (except the bladder neck), levator muscle, and/or pelvic wall.

Although staging is only applied to radical-prostatectomy specimens, findings in biopsy specimens may predict non-organ-confined tumor and need to be reported.

Extraprostatic extension and seminal vesicle invasion

The presence of cancer glands in extraprostatic tissue and seminal vesicles indicates non-organ-confined disease. Prostatic biopsy may occasionally contain, and urologists may also target, seminal vesicles or extraprostatic tissue. Since the presence of fat within the prostate gland is exceedingly rare, observing cancer cells within fat on prostate needle biopsy can be safely interpreted as extraprostatic extension (► Fig. 2.7). On the other hand, the distinction between seminal vesicle and the ejaculatory duct, an intraprostatic structure, is not always possible. Therefore, the diagnostic term *prostate cancer involving seminal vesicle/ejaculatory duct* structure may be used. The invasion by cancer cells of the seminal vesicle/ejaculatory duct structure is an adverse pathologic feature.

Perineural Invasion

Perineural invasion is defined as the presence of prostate cancer tracking along or around a nerve. Since perineural invasion has been demonstrated to be one of the major mechanisms of extension of prostate cancer from the prostatic parenchyma to the periprostatic soft tissue, perineural invasion that is extensive enough to be sampled on needle biopsy may signal an increased risk of extraprostatic extension of the cancer. The absence of perineural invasion on biopsy, however, does not indicate organ-confined disease at radical prostatectomy.

The reported positive predictive value of perineural invasion at biopsy for extraprostatic extension at radical prostatectomy ranges from 38 to 93%.⁴⁷ No clear consensus exists regarding whether perineural invasion on needle biopsy has independent predictive value for extraprostatic extension beyond that provided by the biopsy Gleason score and preoperative serum PSA level. However, the presence of perineural invasion on needle biopsy independently predicts lymph node metastases and postoperative cancer progression. When perineural invasion is seen on biopsy, the urologists should consider excising the neurovascular bundle on that side. Some radiation oncology studies have reported that perineural invasion is an independent risk factor for adverse outcome after external-beam radiation therapy, and in patients with

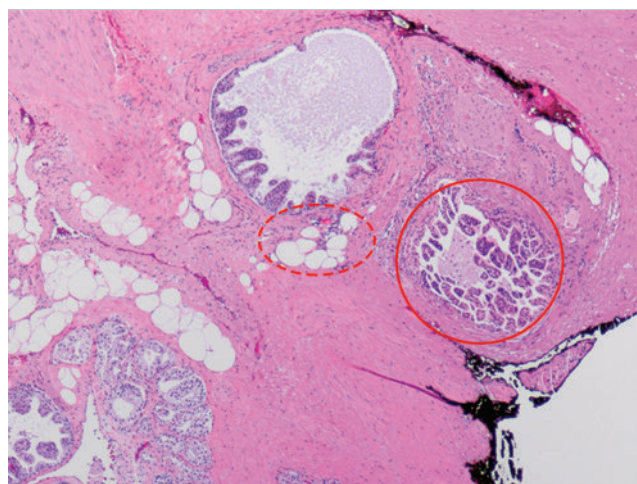


Fig. 2.7 Extraprostatic extension characterized by cancer glands (solid circle) admixed with periprostatic adipose tissue (dashed oval).

a high Gleason score and perineural invasion, adjuvant hormonal therapy or dose escalation (brachytherapy) have been advocated.⁴⁸ However, our study suggested that perineural invasion on needle biopsy does not predict biochemical failure following low dose brachytherapy.⁴⁹ Other pathologic features of perineural invasion, including multifocality and largest diameter of perineural invasion, may help improve the prognostic significance of perineural invasion.⁵⁰

2.3 Prostatic Intraepithelial Neoplasia

This entity was first described by McNeal in 1960 and has been labeled “intraductal dysplasia,” “carcinoma in situ,” and “intraductal carcinoma.” Prostatic intraepithelial neoplasia (PIN) is the current preferred diagnostic term for a putative premalignant proliferation of atypical epithelial cells within the preexisting prostatic ducts and acini.⁵¹ In other words, prostatic intraepithelial neoplasia glands architecturally resemble benign glands but are lined with cytologically malignant cells. Prostatic intraepithelial neoplasia can only be definitively diagnosed by histologic examination of prostatic tissue, as there are no specific clinical or radiologic findings. Nor does it increase serum PSA level.

Based on the severity of architectural and cytologic atypia, PIN can be categorized as low grade or high grade, with much more pronounced atypia in the latter category (► Fig. 2.8). Low-grade PIN (LGPIN) should not be diagnosed on prostate biopsy. Finding low-grade PIN on needle biopsy is not associated with an increased risk for detecting cancer on subsequent biopsies, as is the case for high-grade PIN. Specifically, prostate cancer is found in approximately 18% of repeat biopsy cases, whether the initial biopsy shows low-grade PIN or solely normal prostate tissue. In addition, there is poor diagnostic reproducibility for low-grade PIN even among expert urologic pathologists.

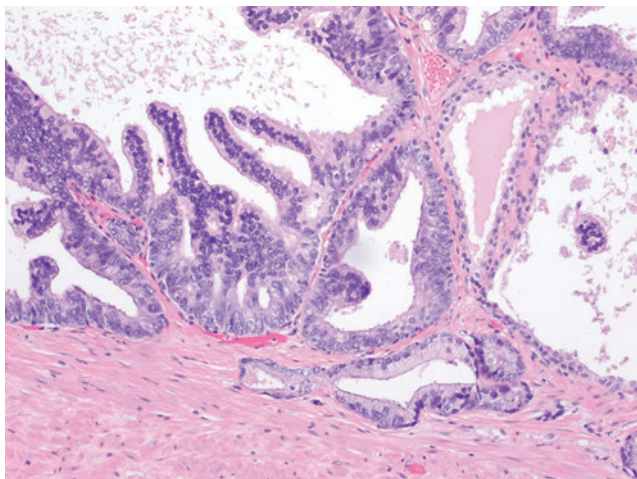


Fig. 2.8 High-grade prostatic intraepithelial neoplasia showing involvement of atypical/neoplastic cells (inner luminal cells) in prostate glands with partially preserved basal layers (peripheral small, flat cells). The neoplastic cells display nucleomegaly, prominent nucleoli, and hyperchromatic and clumpy chromatin

The incidence of high-grade PIN (HGPIN) on prostate needle biopsies varies remarkably in the literature from 0 to 24.6% with a mean of 7.7%.⁵² There seems to be no association between the incidence of HGPIN and the setting of the pathology practice or the timing or extent of prostate sampling. Rather, such variation in incidence is likely the result of a lack of clearly defined diagnostic criteria and technical factors in prostate biopsy processing.

The importance of recognizing HGPIN on needle biopsy is its association with prostate cancer on subsequent repeat biopsy.⁵² In the early 1990s, the average risk of cancer associated with HGPIN was estimated to be nearly 50%. Such risk, however, has decreased dramatically in recent studies.⁵³ In studies published since 2000, the mean cancer risk is 23.5%, similar to an eventual cancer risk of 22.7% following an initial benign diagnosis without HGPIN that has been published in the studies during the same time period. A possible explanation is that the extended biopsy scheme that has been increasingly used in recent years improves cancer detection on the initial biopsy, thereby potentially reducing cancer detection on subsequent biopsies. These findings seem to cast doubt on the previously held notion that HGPIN is a significant risk factor for cancer detected on subsequent biopsy and that patients with such a diagnosis should undergo repeat biopsy. However, this conclusion remains controversial, as additional recent studies continue to report that the cancer risk after an initial HGPIN diagnosis remains significantly higher than after a benign diagnosis. Our group's recommendation is that HGPIN should still be considered as a risk factor for detecting cancer on subsequent prostate biopsies, and therefore should be diagnosed and reported by pathologists until new data and consensus emerge.

There has also been a large amount of interest in whether clinical and other histologic factors may help predict which men are at higher risk for cancer following a biopsy diagnosis of HGPIN. However, no laboratory parameters, including serum PSA level, PSA velocity, PSA density, or free to total PSA ratio, nor DRE and TRUS findings predict which men will have cancer after an initial HGPIN diagnosis.⁵² It is controversial whether the number of cores with HGPIN predicts the risk of cancer. Most studies found no association, although a few studies observed that the cancer risk was significantly higher when at least two cores were involved with HGPIN compared to when only one core was involved. In general, different architectural patterns of HGPIN do not differ significantly in cancer risk. In addition, investigations have failed to demonstrate the value of molecular markers in stratifying the cancer risk associated with HGPIN.

There is no consensus regarding when and how often repeat biopsy should be performed following a HGPIN diagnosis. Most studies recommend repeat biopsy at 3 to 6 months or 6 to 12 months, or even at 36 months. Without a clear guideline, such recommendations should be individualized and based on clinical parameters and the patient's and physician's preference. Since the prostate lobe contralateral to the site in which the initial HGPIN was diagnosed also carries considerable risk for cancer, albeit not as high as the side in which HGPIN was diagnosed, the rebiopsy should sample the entire gland with an emphasis on the area in which HGPIN was initially found.

2.4 Atypical Glands Suspicious for Cancer (ATYP)

Atypical glands suspicious for cancer (ATYP) is a diagnostic term used by pathologists to describe a gland or a focus of glands suspicious for prostate cancer, although lacking sufficient architectural and/or cytologic atypia to establish a definitive diagnosis. Unlike prostate cancer or HGPIN, ATYP is not a distinct biological entity. Rather, it encompasses a range of benign lesions that exhibit architectural and cytologic atypia as well as undersampled small foci of cancer. Many terms have been applied to such entities in the past, including atypia, atypical hyperplasia, borderline lesion, lesion of uncertain significance, or atypical small acinar proliferation (ASAP). However, many of these terms have been used to describe other morphological entities as well. For example, atypical hyperplasia has been applied to HGPIN. Atypical small acinar proliferation in particular has been widely used, although it is not an accurate term as many atypical glands are not small. In addition, some urologists mistake ASAP for HGPIN. For these reasons, we advocate the use of the descriptive terminology atypical glands suspicious for prostate cancer, or ATYP.

The incidence of ATYP on prostate biopsies varies depending on the patient population and pathologist's experience. With improved diagnostic criteria for the presence of limited cancer in prostate biopsy specimens as well as improved immunohistochemical markers, one may expect a greater fraction of ATYP to be resolved as being benign or in fact cancer, leading to a reduction of the incidence of diagnosed ATYP. On average, ATYP is found in 4.4% (range 0.7–23.4%) of prostate biopsies.⁵²

Similar to HGPIN, the clinical significance of recognizing ATYP on needle biopsies is its association with a higher risk of prostate cancer on repeat biopsies. Unlike HGPIN, the increased cancer risk associated with ATYP has held steady in reports from early 1990 to present.⁵⁴ On average, 40% (17–70%) of men with ATYP on initial biopsy are found to

have cancer on subsequent biopsies. Similar to HGPIN, no clinical parameters, including serum PSA, TRUS, or DRE, predict which patients with an ATYP diagnosis will be found to have cancer on repeat biopsy.⁵²

Several studies observed that following an initial ATYP diagnosis, cancer was detected at the same site as the initial ATYP diagnosis in approximately 50% of cases, and at the same site or in an adjacent sextant in 71 to 85% of cases, but in the contralateral lobe in only in 17 to 27% of cases.^{55,56,57} Based on these data, a rational approach for performing rebiopsy following an initial ATYP diagnosis may include collection of 3 cores from the site of the initial ATYP biopsy, 2 cores from each adjacent site, and 1 core from each site elsewhere.⁵⁵ Because of the high risk of cancer on rebiopsy following an ATYP diagnosis, patients should be advised to undergo prompt rebiopsy, typically within 3 to 6 months after the initial biopsy.

2.5 Benign Mimickers of Prostatic Adenocarcinoma

Before making a diagnosis of carcinoma, especially when cancer is present in small amounts, it is prudent for the pathologist to consider the various benign patterns and processes that can simulate prostatic adenocarcinoma. Many disease processes and normal tissues can mimic prostate carcinoma. Whereas seminal vesicle tissue had in the distant past been considered one of the most common mimickers of prostate cancer, partial atrophy and benign crowded glands are considered the most common benign lesions that currently cause difficulty for pathologists. Morphological features are the key in differentiating benign mimickers from adenocarcinoma. Special immunostains using AMACR and basal markers (high molecular weight keratin and P63) are very useful in difficult cases (► Fig. 2.9). In comparison, the value of the immunostain for ERG is minimal. It is crucial for pathologists to be familiar with the histologic features of these benign cancer mimickers. Urologists and radiologists should also be aware of these entities, even if detailed

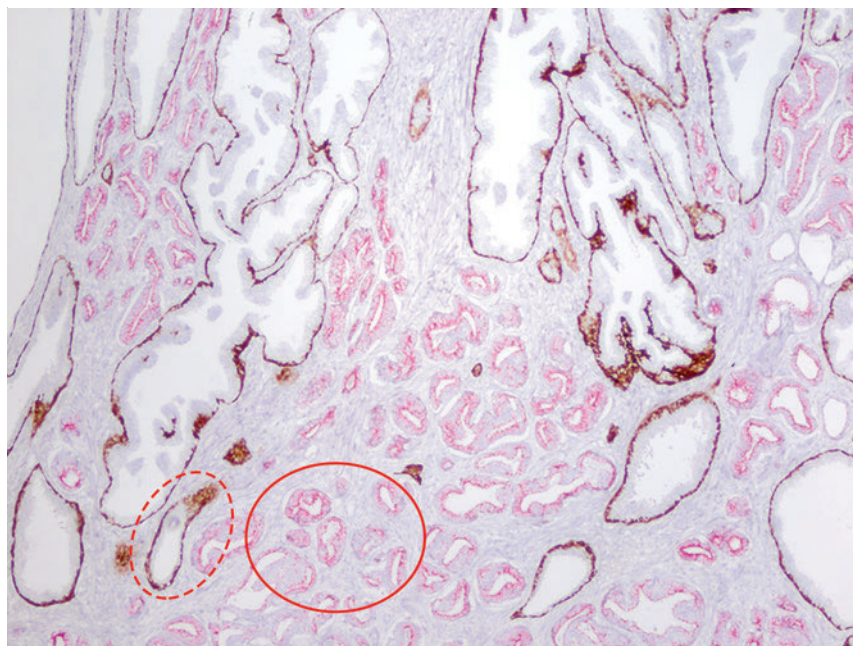


Fig. 2.9 Immunohistochemistry (PIN4, also called triple stain) commonly used in prostate carcinoma diagnosis. Tumor glands (*circle*) overexpress AMACR (red) and lose basal layers, with cytoplasm labeled by high molecular weight keratin and nuclei labeled by P63). The adjacent benign gland (*dashed oval*) has a preserved basal layer (brown, with cytoplasm labeled by high molecular weight keratin and nucleus labeled by P63) and no AMACR overexpression (red).

Table 2.2 Benign mimickers of prostatic adenocarcinoma.

Normal anatomical structures	Hyperplasia	Inflammatory lesions	Metaplasia	Atrophy
Central zone glands	Benign prostatic hyperplasia (BPH), small gland pattern	Reactive atypia	Mucinous metaplasia	Simple lobular atrophy
Seminal vesicles	Basal cell hyperplasia	Non-specific granulomatous prostatitis	Nephrogenic metaplasia	Cystic atrophy
Cowper's gland	Adenoid cysticlike basal cell hyperplasia	Xanthoma		Partial atrophy
Verumontanum mucosal gland hyperplasia	Atypical adenomatous hyperplasia	Malakoplakia		Postatrophic hyperplasia
Mesonephric gland hyperplasia	Sclerosing adenosis	Usual prostatitis with crush artifacts		
Paraganglia	Clear-cell cribriform hyperplasia	Signet ring-like change in lymphocytes and stromal cells		

Table 2.3 Histologic features suggestive of a benign diagnosis

Architectural features	Cytoplasmic features	Nuclear features	Intraluminal contents	Stroma
Lobulated growth	Pale to clear cytoplasm	Lacking nuclear atypia	Corpora amyloacea	Hyalinized stroma
Small and large glands intermingled without cytologic difference	Atrophy	Random nuclear atypia	Microcalcification	Cellular stroma
Large glands with branching and papillary infolding	Lipofuscin pigment			

knowledge of their histologic features may not be of practical importance for them. We list these benign mimickers of prostatic adenocarcinoma in ► Table 2.2, and the histologic features that suggest a benign diagnosis in ► Table 2.3.

References

- [1] McNeal JE. Regional morphology and pathology of the prostate. *Am J Clin Pathol* 1968; 49(3):347–357
- [2] Fine SW, Reuter VE. Anatomy of the prostate revisited: implications for prostate biopsy and zonal origins of prostate cancer. *Histopathology* 2012; 60(1):142–152
- [3] American Cancer Society. <http://www.cancer.org/cancer/prostatecancer/detailedguide/prostate-cancer-key-statistics/>. Last Revised: 03/12/2015
- [4] Villers A, McNeal JE, Freiha FS, Stamey TA. Multiple cancers in the prostate. Morphologic features of clinically recognized versus incidental tumors. *Cancer* 1992; 70(9):2313–2318
- [5] Arora R, Koch MO, Eble JN, Ulbright TM, Li L, Cheng L. Heterogeneity of Gleason grade in multifocal adenocarcinoma of the prostate. *Cancer* 2004; 100(11):2362–2366
- [6] Wise AM, Stamey TA, McNeal JE, Clayton JL. Morphologic and clinical significance of multifocal prostate cancers in radical prostatectomy specimens. *Urology* 2002; 60(2):264–269
- [7] Andreou M, Cheng L. Multifocal prostate cancer: biologic, prognostic, and therapeutic implications. *Hum Pathol* 2010; 41(6):781–793
- [8] Ruijter ET, van de Kaa CA, Schalken JA, Debruyne FM, Ruiters DJ. Histological grade heterogeneity in multifocal prostate cancer. Biological and clinical implications. *J Pathol* 1996; 180(3):295–299
- [9] Cheng L, Song SY, Pretlow TG et al. Evidence of independent origin of multiple tumors from patients with prostate cancer. *J Natl Cancer Inst* 1998; 90(3):233–237
- [10] Mehra R, Han B, Tomlins SA et al. Heterogeneity of TMPRSS2 gene rearrangements in multifocal prostate adenocarcinoma: molecular evidence for an independent group of diseases. *Cancer Res* 2007; 67(17):7991–7995
- [11] McNeal JE, Price HM, Redwine EA, Freiha FS, Stamey TA. Stage A versus stage B adenocarcinoma of the prostate: morphological comparison and biological significance. *J Urol* 1988; 139(1):61–65
- [12] Epstein JI, Allsbrook WC Jr, Amin MB, Egevad LL. ISUP Grading Committee. The 2005 International Society of Urological Pathology (ISUP) Consensus Conference on Gleason Grading of Prostatic Carcinoma. *Am J Surg Pathol* 2005; 29(9):1228–1242
- [13] van der Kwast TH, Amin MB, Billis A et al. ISUP Prostate Cancer Group. International Society of Urological Pathology (ISUP) Consensus Conference on Handling and Staging of Radical Prostatectomy Specimens. Working group 2: T2 substaging and prostate cancer volume. *Mod Pathol* 2011; 24(1):16–25
- [14] Huang CC, Deng FM, Kong MX, Ren Q, Melamed J, Zhou M. Re-evaluating the concept of “dominant/index tumor nodule” in multifocal prostate cancer. *Virchows Arch* 2014; 464(5):589–594
- [15] Epstein JI, Walsh PC, Carmichael M, Brendler CB. Pathologic and clinical findings to predict tumor extent of nonpalpable (stage T1c) prostate cancer. *JAMA* 1994; 271(5):368–374
- [16] Trpkov K, Yilmaz A, Bismar TA, Montironi R. ‘Insignificant’ prostate cancer on prostatectomy and cystoprostatectomy: variation on a theme ‘low-volume/low-grade’ prostate cancer? *BJU Int* 2010; 106(3):304–315
- [17] Ploussard G, Epstein JI, Montironi R et al. The contemporary concept of significant versus insignificant prostate cancer. *Eur Urol* 2011; 60(2):291–303
- [18] Bastian PJ, Mangold LA, Epstein JI, Partin AW. Characteristics of insignificant clinical T1c prostate tumors. A contemporary analysis. *Cancer* 2004; 101(9):2001–2005
- [19] Johnstone PAS, Rossi PJ, Jani AB, Master V. ‘Insignificant’ prostate cancer on biopsy: pathologic results from subsequent radical prostatectomy. *Prostate Cancer Prostatic Dis* 2007; 10(3):237–241
- [20] Shaw GL, Thomas BC, Dawson SN et al. Identification of pathologically insignificant prostate cancer is not accurate in unscreened men. *Br J Cancer* 2014; 110(10):2405–2411

- [21] Kaleem Z, Swanson PE, Vollmer RT, Humphrey PA. Prostatic adenocarcinoma with atrophic features: a study of 202 consecutive completely embedded radical prostatectomy specimens. *Am J Clin Pathol* 1998; 109(6):695-703
- [22] Humphrey PA, Kaleem Z, Swanson PE, Vollmer RT. Pseudohyperplastic prostatic adenocarcinoma. *Am J Surg Pathol* 1998; 22(10):1239-1246
- [23] Hudson J, Cao D, Vollmer R, Kibel AS, Grewal S, Humphrey PA. Foamy gland adenocarcinoma of the prostate: incidence, Gleason grade, and early clinical outcome. *Hum Pathol* 2012; 43(7):974-979
- [24] Osunkoya AO, Nielsen ME, Epstein JI. Prognosis of mucinous adenocarcinoma of the prostate treated by radical prostatectomy: a study of 47 cases. *Am J Surg Pathol* 2008; 32(3):468-472
- [25] Morgan TM, Welty CJ, Vakar-Lopez F, Lin DW, Wright JL. Ductal adenocarcinoma of the prostate: increased mortality risk and decreased serum prostate specific antigen. *J Urol* 2010; 184(6):2303-2307
- [26] Zhou M. Intraductal carcinoma of the prostate: the whole story. *Pathology* 2013; 45(6):533-539
- [27] Guo CC, Epstein JI. Intraductal carcinoma of the prostate on needle biopsy: Histologic features and clinical significance. *Mod Pathol* 2006; 19(12):1528-1535
- [28] Robinson BD, Epstein JI. Intraductal carcinoma of the prostate without invasive carcinoma on needle biopsy: emphasis on radical prostatectomy findings. *J Urol* 2010; 184(4):1328-1333
- [29] Epstein JI, Amin MB, Beltran H et al. Proposed morphologic classification of prostate cancer with neuroendocrine differentiation. *Am J Surg Pathol* 2014; 38(6):756-767
- [30] Gleason DF. Histologic grading of prostate cancer: a perspective. *Hum Pathol* 1992; 23(3):273-279
- [31] Epstein JI. An update of the Gleason grading system. *J Urol* 2010; 183(2):433-440
- [32] Egevad L, Mazzucchelli R, Montironi R. Implications of the International Society of Urological Pathology modified Gleason grading system. *Arch Pathol Lab Med* 2012; 136(4):426-434
- [33] Eggener SE, Scardino PT, Walsh PC et al. Predicting 15-year prostate cancer specific mortality after radical prostatectomy. *J Urol* 2011; 185(3):869-875
- [34] Hernandez DJ, Nielsen ME, Han M et al. Natural history of pathologically organ-confined (pT2), Gleason score 6 or less, prostate cancer after radical prostatectomy. *Urology* 2008; 72(1):172-176
- [35] Donin NM, Laze J, Zhou M, Ren Q, Lepor H. Gleason 6 prostate tumors diagnosed in the PSA era do not demonstrate the capacity for metastatic spread at the time of radical prostatectomy. *Urology* 2013; 82(1):148-152
- [36] Pierorazio PM, Walsh PC, Partin AW, Epstein JI. Prognostic Gleason grade grouping: data based on the modified Gleason scoring system. *BJU Int* 2013; 111(5):753-760
- [37] Fine SW, Epstein JI. A contemporary study correlating prostate needle biopsy and radical prostatectomy Gleason score. *J Urol* 2008; 179(4):1335-1338, discussion 1338-1339
- [38] Helpap B, Egevad L. The significance of modified Gleason grading of prostatic carcinoma in biopsy and radical prostatectomy specimens. *Virchows Arch* 2006; 449(6):622-627
- [39] Steinberg DM, Sauvageot J, Piantadosi S, Epstein JI. Correlation of prostate needle biopsy and radical prostatectomy Gleason grade in academic and community settings. *Am J Surg Pathol* 1997; 21(5):566-576
- [40] Ozok HU, Sagnak L, Tuygun C et al. Will the modification of the Gleason grading system affect the urology practice? *Int J Surg Pathol* 2010; 18(4):248-254
- [41] Delahunt B, Lamb DS, Srigley JR et al. Gleason scoring: a comparison of classical and modified (international society of urological pathology) criteria using nadir PSA as a clinical end point. *Pathology* 2010; 42(4):339-343
- [42] Iremashvili V, Pelaez L, Manoharan M, Jorda M, Rosenberg DL, Soloway MS. Pathologic prostate cancer characteristics in patients eligible for active surveillance: a head-to-head comparison of contemporary protocols. *Eur Urol* 2012; 62(3):462-468
- [43] Huang CC, Kong MX, Zhou M et al. Gleason score 3 + 4 = 7 prostate cancer with minimal quantity of gleason pattern 4 on needle biopsy is associated with low-risk tumor in radical prostatectomy specimen. *Am J Surg Pathol* 2014; 38(8):1096-1101
- [44] Stark JR, Perner S, Stampfer MJ et al. Gleason score and lethal prostate cancer: does 3 + 4 = 4 + 3? *J Clin Oncol* 2009; 27(21):3459-3464
- [45] Bul M, van den Bergh RC, Zhu X et al. Outcomes of initially expectantly managed patients with low or intermediate risk screen-detected localized prostate cancer. *BJU Int* 2012; 110(11):1672-1677
- [46] Billis A, Freitas LL, Magna LA, Samara AB, Ferreira U. Prostate cancer with bladder neck involvement: pathologic findings with application of a new practical method for tumor extent evaluation and recurrence-free survival after radical prostatectomy. *Int Urol Nephrol* 2004; 36(3):363-368
- [47] Zhou M, Epstein JI. The reporting of prostate cancer on needle biopsy: prognostic and therapeutic implications and the utility of diagnostic markers. *Pathology* 2003; 35(6):472-479
- [48] Bonin SR, Hanlon AL, Lee WR, Movsas B, al-Saleem TI, Hanks GE. Evidence of increased failure in the treatment of prostate carcinoma patients who have perineural invasion treated with three-dimensional conformal radiation therapy. *Cancer* 1997; 79(1):75-80
- [49] Weight CJ, Ciezki JP, Reddy CA, Zhou M, Klein EA. Perineural invasion on prostate needle biopsy does not predict biochemical failure following brachytherapy for prostate cancer. *Int J Radiat Oncol Biol Phys* 2006; 65(2):347-350
- [50] Maru N, Ohori M, Kattan MW, Scardino PT, Wheeler TM. Prognostic significance of the diameter of perineural invasion in radical prostatectomy specimens. *Hum Pathol* 2001; 32(8):828-833
- [51] Bostwick DG, Qian J. High-grade prostatic intraepithelial neoplasia. *Mod Pathol* 2004; 17(3):360-379
- [52] Epstein JI, Herawi M. Prostate needle biopsies containing prostatic intraepithelial neoplasia or atypical foci suspicious for carcinoma: implications for patient care. *J Urol* 2006; 175(3 Pt 1):820-834
- [53] O'dowd GJ, Miller MC, Orozco R, Veltri RW. Analysis of repeated biopsy results within 1 year after a noncancer diagnosis. *Urology* 2000; 55(4):553-559
- [54] Schlesinger C, Bostwick DG, Iczkowski KA. High-grade prostatic intraepithelial neoplasia and atypical small acinar proliferation: predictive value for cancer in current practice. *Am J Surg Pathol* 2005; 29(9):1201-1207
- [55] Allen EA, Kahane H, Epstein JI. Repeat biopsy strategies for men with atypical diagnoses on initial prostate needle biopsy. *Urology* 1998; 52(5):803-807
- [56] Iczkowski KA, Bassler TJ, Schwob VS et al. Diagnosis of "suspicious for malignancy" in prostate biopsies: predictive value for cancer. *Urology* 1998; 51(5):749-757, discussion 757-758
- [57] Park S, Shinohara K, Grossfeld GD, Carroll PR. Prostate cancer detection in men with prior high grade prostatic intraepithelial neoplasia or atypical prostate biopsy. *J Urol* 2001; 165(5):1409-1414

3 Introduction to Prostate MRI Protocols: Hardware, T2-Weighted Imaging, and MR Spectroscopy

John Conklin and Masoom A. Haider

3.1 Introduction

Prostate magnetic resonance imaging (MRI) protocols are built around the fundamental concept of multiparametric MRI (mpMRI). Multiparametric MRI involves the combination of high-resolution anatomical imaging (T2-weighted images) with functional imaging techniques such as diffusion-weighted imaging (DWI), dynamic contrast-enhanced MRI (DCE-MRI), and magnetic resonance spectroscopic imaging (MRSI) to improve the sensitivity and specificity for prostate cancer detection and staging. In addition to the selection of imaging sequences, many factors contribute to image quality in prostate MRI. These include hardware considerations such as field strength and receiver coil design, timing of examination with respect to previous biopsy, and patient preparation. This chapter provides a review of the technical considerations relevant to prostate MRI prototyping with a focus on hardware considerations, T2WI weighted imaging, and MRSI. DWI and DCE-MRI acquisitions are covered in detail in Chapter 4 and Chapter 5, respectively.

3.2 Hardware Requirements

3.2.1 Field Strength

Though initially established at 1.5T,¹ mpMRI of the prostate is increasingly performed at 3.0T in both clinical and research settings.^{2,3} The primary benefit of imaging at 3.0T over 1.5T is the increase in signal-to-noise ratio (SNR), which scales approximately linearly with field strength,⁴ providing a theoretical doubling of the available SNR. In practical terms, the SNR gain is less than 100% at 3.0T due in part to safety considerations. The SNR increase at 3.0T may be exploited to improve the image quality in sequences with intrinsically low SNR such as DWI and MRSI. Alternately, increased SNR can be used to improve spatial resolution in anatomical (T2-weighted) images, allowing for a decrease in voxel volume and providing more precise delineation of prostate anatomy and pathology. Increased SNR can also be used to decrease scan time and improve temporal resolution in DCE-MRI, and improve spectral resolution in MRSI.

However, the move to 3.0T is associated with a number of technical challenges. Radio-frequency (RF) power deposition, as quantified by the specific absorption rate (SAR), increases with the square of the main magnetic field strength, resulting in a theoretical quadrupling of power deposition at 3.0T. Thus, some sequences may require alteration to their conventional parameters to stay within power deposition limits set by the U.S. Food and Drug Administration and European Union. For example, T2-weighted fast spin-echo (FSE) sequences may be modified to employ a partial rather than a complete refocusing pulse, or utilize a variable flip angle 3.4.2 Artifacts and Pitfalls to reduce SAR.^{5,6} These changes are usually sufficient to meet current safety regulations for prostate examinations at 3.0T.²

Small changes in tissue T2 values occur with the transition from 1.5T to 3.0T.^{7,8} However, these changes are not very pronounced and generally do not require much alteration in the optimal TE (echo time).^{3,9,10} Susceptibility effects are also more severe at high field strengths, which is particularly relevant for MRSI and DWI acquisitions (see 3.4.2 Artifacts and Pitfalls). Lower field strength (1.5 T) is therefore preferred in the presence of metallic implants such as hip prostheses in order to minimize susceptibility artifacts. Homogeneity of the main field is also more difficult to maintain at 3.0T, which may lead to signal variability across the image.

The above limitations can be minimized using modern MRI systems. When properly optimized, both 1.5T and 3.0T magnets can provide adequate diagnostic quality for prostate MRI in clinical practice. However, there is a general consensus that the advantages of imaging at 3.0T over 1.5T when this option is available outweigh the disadvantages in most settings.

For example, staging accuracy of biopsy-proven local prostate cancer was shown to be improved at 3.0T compared to 1.5T at a single institution.^{11,12} However, there remains a paucity of large studies comparing the same patients at both field strengths using otherwise equivalent hardware and acquisition techniques. Until such studies are available, it is reasonable to assume that the improvements in image quality at 3.0T, particularly the improved spatial resolution in T2-weighted anatomical imaging, could result in improved staging performance.

Prostate MR imaging at field strengths less than 1.5T is not recommended.

3.2.2 Endorectal Coils

Introduced in the late 1980s, the principle behind the endorectal coil (ERC) is to minimize the distance between the prostate and the receiver coil and to maximize the signal obtained from the gland and adjacent anatomy. Similar to imaging at higher field strengths, the primary benefit of using an ERC is improved SNR. When compared to conventional pelvic phased-array surface coils, the increase in SNR provided by an ERC is approximately tenfold.¹³

Conventional ERC designs include a single RF coil element contained within a balloon which is inflated to tightly approximate the coil with the adjacent prostate (eCoil; Medrad Inc, Warrendale, PA). However, if the balloon is filled with air, significant susceptibility artifacts may result (see 3.4.2 Artifacts and Pitfalls). To minimize these artifacts, the balloon should be filled with a susceptibility-matched fluid such as perfluorocarbon or barium.¹⁴ The proper positioning of an inflatable ERC is illustrated in ► Fig. 3.1.

Noninflatable rigid endorectal coils have been developed (Endo Coil Array; Hologic Inc, Bedford, MA) (► Fig. 3.2). Rigid coils are associated with reduced geometric distortion of the gland and provide increased SNR compared to inflatable coils.^{15,16} Recently, a multichannel rigid ERC was shown to provide even greater SNR improvement.¹⁷ Disadvantages of the

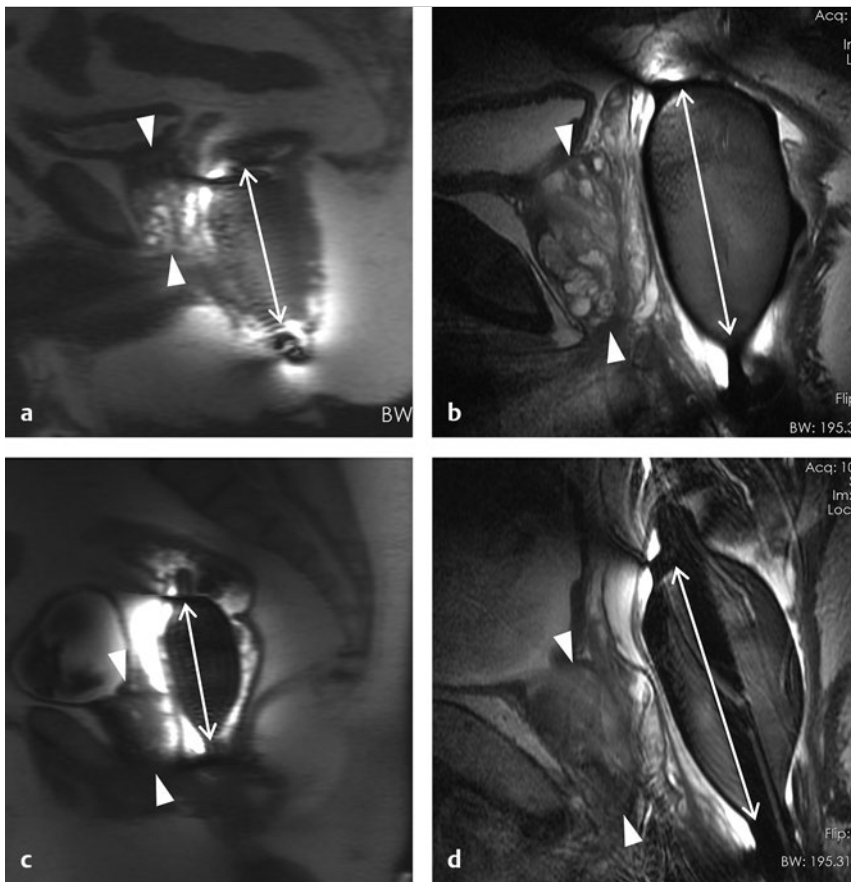


Fig. 3.1 Proper positioning of an inflatable endorectal coil (ERC) filled with barium. *Top row:* Scout image (a) shows malpositioning of the ERC with the sensitive portion of the coil (double-headed arrow) positioned inferiorly and incompletely covering the prostate gland (arrowheads). (b) Sagittal T2-weighted image following advancement of the coil shows correct positioning, with the entire gland located within the sensitive portion of the coil. *Bottom row:* Scout image (c) shows malpositioning of the ERC with the sensitive portion of the coil positioned superiorly and incompletely covering the prostate gland. (d) Sagittal T2-weighted image following partial withdrawal of the coil shows correct positioning, with the entire gland located within the sensitive portion of the coil. Note the presence of motion ghosts in image (d), which occur along the phase-encoding (in this case, superior–inferior) direction. (Used with permission from Haider MA, Krieger A, Elliott C, et al. Prostate imaging: Evaluation of a reusable two-channel endorectal receiver coil for MR imaging at 1.5T. *Radiology* 2014;270:556-565.)

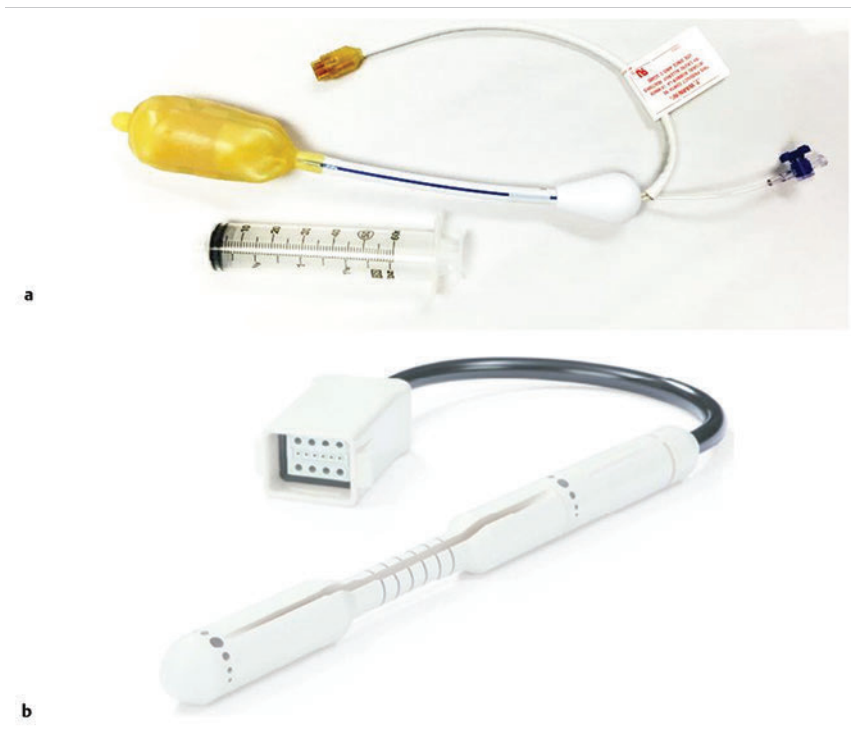


Fig. 3.2 Examples of balloon-inflatable and rigid endorectal coils. (a) A typical single-channel balloon-inflatable endorectal receiver coil (eCoil, Medrad Inc, Warrendale, PA), and a 60-cm³ syringe used for balloon inflation. The blue stripe indicates the anterior (sensitive) direction of the coil. (b) A two-channel solid reusable phased-array endorectal receiver coil (Endo Coil Array, Hologic Inc., Bedford, MA). The rigid coil design includes two overlapping coil elements spanning the 8.5-cm long coil head. The maximum diameter is 2.5 cm, significantly narrower at the level of the anus when properly positioned. (b reproduced with permission from Haider et al, 2014¹⁷.)

rigid ERC design include increased motion artifacts (the inflated balloon is thought to reduce movement of the rectal wall) and the need for disinfection between patients due to the nondisposable nature of the currently approved device.

The ERC is typically employed in combination with a pelvic phased-array (PPA) coil in order to maximize SNR, although the ERC can also be employed independently. Combined use of ERC and PPA coils harnesses the high SNR of ERC and the wide field

of view (FOV) of PPA coil designs. When combined with a PPA coil, the signal within the prostate gland is typically dominated by the contribution from the ERC rather than the PPA (>90%).¹⁸ Endorectal coils are particularly advantageous for larger patients, where PPA coils may be limited by the greater distance from the body surface to the prostate. Use of an ERC has been shown to improve staging accuracy for prostate cancer compared to PPA coils alone at both 1.5 T and 3.0T.^{11,19} However, ERC use is not without its disadvantages, which are summarized in ► Table 3.1. Contraindications to ERC are provided in ► Table 3.2.¹⁹

Using 1.5T without an endorectal coil for staging is controversial and considered suboptimal by many. However, other factors contribute to overall SNR beyond field strength and ERC use, for example, receiver bandwidth, coil design, and RF chain efficiency. While the improved image quality of 3.0T and ERC are desirable, factors such as cost, equipment availability, and patient acceptance must also be taken into account.

3.2.3 Surface Coils

Clinical prostate MRI is performed with multichannel PPA receiver coils, either independently or in combination with an ERC. Many centers use a multichannel cardiac surface coil, as this provides increased central pelvic SNR in thinner patients. Current recommendations stipulate use of at least an 8- or 16-channel array, and at least a 16-channel array if used independently of an ERC.²⁰ While some authors have advocated ERC use at 1.5 T in order to obtain diagnostic-quality images in a reasonable time frame,^{19,21,22} current guidelines accept the use of PPA coils alone at 1.5T, provided a modern 16-channel coil is used.²⁰ An ERC is strongly recommended for MRSI at 1.5 T.²

Table 3.1 Advantages and disadvantages of using an endorectal coil

Advantages	Disadvantages
Increased spatial resolution for T2-weighted anatomical imaging	Increased artifacts (phase ghosts)
Increased temporal resolution for DCE-MRI	Geometric distortion of the prostate gland
Increased SNR for intrinsically low SNR sequences (DWI, MRSI)	Increased cost of examination
	Increased procedure time
	Patient preference/discomfort
	Signal dropoff in anterior gland

Abbreviations: DCE, dynamic contrast-enhanced; SNR, signal-to-noise ratio; DWI, diffusion-weighted imaging; MRSI, magnetic resonance spectroscopic imaging.

Table 3.2 Contraindications to endorectal coil (ERC) use for prostate MRI

Contraindications
Anal fissures and strictures
Previous anorectal surgery, including rectal surgery with end-to-end anastomoses
Inflammatory bowel disease
High anal sphincter tone preventing ERC insertion
Large hemorrhoids

Several studies indicate that 3.0-T imaging with a PPA coil provides similar image quality to 1.5-T imaging with an ERC and similar accuracy for local staging of prostate cancer,^{23,24,25,26} suggesting that 3.0-T imaging with PPA coils may provide an alternative for patients in whom an ERC is unacceptable, contraindicated, or unavailable. However, there is also evidence that imaging at 3.0T with an ERC improves prostate cancer detection²⁷ and staging accuracy¹¹ compared to imaging at 3.0T with surface coils alone. Thus, while 3.0-T prostate MRI performed without an ERC may be an attractive option from both the patient's and the physician's perspective, it is important to understand the trade-offs involved in forgoing the use of the ERC. A recent study of 51 tumors in 20 patients who underwent 3.0-T MRI with and without an ERC showed higher sensitivity and positive predictive value for tumor detection with ERC, in part due to improved detection of small tumors.²⁷ Comparative images obtained at 1.5 and 3.0T with and without an ERC are shown in ► Fig. 3.3.

In summary, the need for the endorectal coil is controversial. Many experts believe that staging accuracy is maximized with the use of an ERC at 3.0T. However, for cancer localization, many groups are performing MRI at 3.0T without an ERC. The most challenging hardware combination is an older 1.5-T MRI system without an ERC. Such systems may be more limited in the detection of smaller cancers and minimal extraprostatic extension. The use of such a hardware configuration should be undertaken with caution.

3.3 Pulse Sequences

Prostate MRI protocols should be tailored to the specific patient, clinical setting, and available equipment. At a minimum, high-resolution T2-weighted anatomical images and diffusion-weighted images (DWI) should be included in all prostate MRI protocols. While routine acquisition of dynamic contrast-enhanced (DCE) images is also advised, the additive value of this sequence is currently an area of controversy (as discussed in Chapter 5). Additional anatomical sequences (e.g., T1-weighted images) and functional sequences (e.g., MRSI) may be included depending on the clinical scenario, as discussed below. However, unnecessary sequences should be avoided, as this prolongs the duration of the study, increases patient discomfort, and may decrease patient compliance.

3.3.1 T2-Weighted Imaging

T2-weighted imaging forms the backbone of any prostate MRI examination, due to its ability to delineate zonal anatomy and to detect, localize, and stage cancer, including assessment for extraprostatic extension (EPE) and seminal vesicle invasion (SVI).

Imaging Technique

Two-dimensional multiplanar T2-weighted images should be acquired in the axial plane and in at least one other orthogonal plane (coronal or sagittal), and preferably in all three planes, using a fast spin-echo sequence (also called turbo spin-echo or rapid acquisition with relaxation enhancement). Axial images should be in a plane orthogonal to the rectum with complete coverage of the prostate gland and seminal vesicles. Adequate coverage is typically obtained with 20 to 30 slices using a 3- to 4-mm slice thickness and no slice gap.

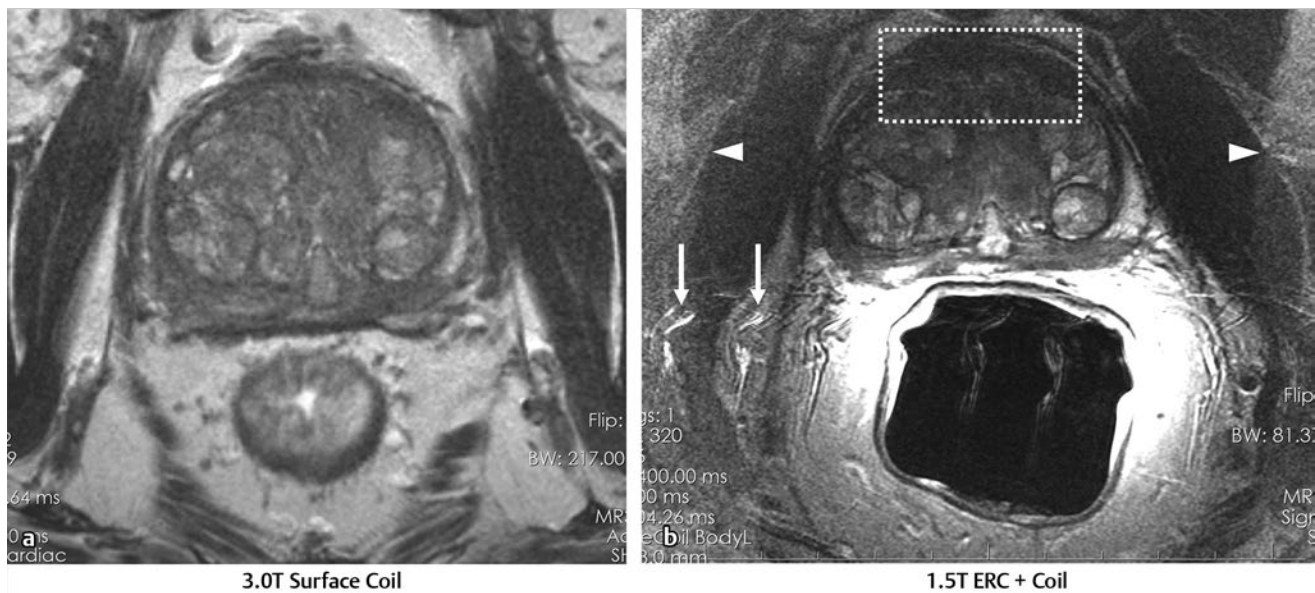


Fig. 3.3 Influence of field strength and receiver coil design on image quality. (a) Axial T2-weighted image acquired with a cardiac phased-array surface coil at 3.0 T (voxel volume = 0.5 × 0.5 × 3.0 mm, number of excitations (NEX) = 2, acquisition time 305 s). (b) Axial T2-weighted image in the same patient acquired using the same surface coil in combination with an endorectal coil (ERC) at 1.5 T (voxel volume = 0.27 × 0.43 × 3.0 mm, NEX = 1, acquisition time 136 s). Despite the shorter acquisition time, lower field strength, and decreased voxel volume, the image obtained with an ERC provides improved soft tissue detail within the posterior gland due to the large signal-to-noise ratio (SNR) gain provided by the ERC. The improvement related to the ERC is less apparent in the anterior gland, where signal drop-off and increased noise (graininess) are observed (dotted box in image b). Note the presence of phase ghosts (arrows) typically seen with ERC use. Aliasing is also apparent (arrowheads), which is attributable to the surface coil rather than the ERC itself.

The echo time (TE) should be chosen to maximize contrast between the peripheral and transition zones and between prostate cancer and normal glandular tissue based on their intrinsic T2 values. At 1.5 T, the T2 values of cancerous tissue, the transition zone, and the peripheral zone are reported as 82 ms, 88 ms, and 122 ms, respectively.²⁸ A TE of approximately 100 to 130 ms is typically used to achieve optimal image contrast between these tissues, with a TR of 2 to 5 s.

The phase-encoding direction should be set to left–right and the frequency-encoding direction to anterior–posterior in order to prevent phase ghosting artifacts related to rectal motion from obscuring the prostate gland.

High spatial resolution is required to precisely delineate prostatic anatomy and assess for extraprostatic extension. Long echo trains (greater than ~ 35) should be avoided to reduce associated image blurring and loss of spatial resolution. Recommended minimum T2-weighted imaging parameters according to the PI-RADS version 1.0 consensus statement guidelines are provided in ► Table 3.3.²⁰

In addition, three-dimensional (3D) T2-weighted fast spin-echo sequences may be employed as an adjunct to conventional two-dimensional (2D) multiplanar images, for example 3D VISTA (Philips Medical Systems, Best, The Netherlands), 3D SPACE (Siemens Healthcare, Erlangen, Germany), and 3D FSE-Cube (GE Healthcare, Milwaukee, WI). These sequences use prolonged echo trains with variable flip angles to efficiently obtain high-resolution isotropic 3D images. Isotropic acquisition may be particularly useful in delineating fine anatomical details and in discriminating between true lesions and partial volume averaging. For example, 3D T2-weighted images have been shown to improve the delineation of the neurovascular bundles in

Table 3.3 Recommended T2-weighted imaging parameters and protocol considerations.

Protocol considerations / imaging parameters	Recommendation
Field strength	1.5 T or 3.0 T
Receiver coils	8- or 16-channel pelvic phased-array coil ± endorectal coil (optional but desirable)
Antiperistaltic agent	Buscopan or glucagon
Planar orientation	Axial and sagittal 2D T2-weighted images ± coronal images
Slice thickness	4 mm at 1.5 T, 3 mm at 3.0 T
Slice gap	None
In-plane resolution	0.5 × 0.5 to 0.7 × 0.7 mm
Field of view	Must encompass entire prostate gland and seminal vesicles (approximately 12–20 cm).

Source: Adapted from PI-RADS consensus statement, cancer detection protocol, Barentz et al, 2012²⁰.

patients with previous nerve-sparing radical prostatectomy.²⁹ Because 3D acquisitions can be reformatted in arbitrary planar orientations, these sequences may one day replace 2D multiplanar T2-weighted images in clinical practice, which would provide significant time savings (in one study, 3 min 52 s for 3D isotropic SPACE acquisition vs. 11 min for 2D FSE images in three orthogonal planes).³⁰ However, tissue contrast is not identical between 2D and 3D T2-weighted images,³¹ and in some cases contrast in 3D images may be inferior for prostate

cancer detection. Further, 3D MR imaging is generally more motion sensitive than 2D multislice imaging and cannot at present match the high (submillimeter) in-plane resolution of 2D imaging sequences. Because of these limitations, multiplanar 2D imaging remains the standard for clinical practice.

Anatomy on T2-Weighted Imaging

The anatomical divisions of the prostate as reported by McNeal³² are well demonstrated on T2-weighted imaging (► Fig. 3.4; ► Fig. 3.5). In the craniocaudal direction, the gland is divided into the base (below the bladder), midgland, and apex. Histologically, the gland is divided into four zones: the anterior fibromuscular stroma, which is partially continuous with the detrusor muscle of the bladder wall; the transition zone (TZ) surrounding the urethra; the central zone (CZ) surrounding the ejaculatory ducts; and the peripheral zone (PZ). The TZ makes up an inconsequential portion of the gland in young men but accounts for an increasing proportion with advancing age and development of benign prostatic hyperplasia (BPH) and gives rise to about 20% of prostate cancers. The PZ contains the majority of the glandular tissue (~ 70%) and gives rise to about 70% of prostate cancers.³³

On axial T2-weighted images, the PZ appears as a homogeneously hyperintense crescent of tissue along the posterior and lateral gland. In older studies, the CZ and TZ were often grouped together as the “central gland,” described as having a heterogeneously intermediate- to low-signal on T2-weighted images. More recently, it has been shown that the TZ and CZ can be accurately differentiated on MRI, with the CZ appearing as a region of more homogeneously low T2 signal in the majority of patients.³⁴ Hence, the term “central gland” should be avoided.

The prostate is separated from adjacent soft tissues by the prostate capsule, which appears as a thin hypointense rim surrounding the gland (► Fig. 3.6). This serves as an important marker for extraprostatic extension. Note that the prostate lacks a true capsule, and the so-called prostate capsule histopathologically represents a thin band of concentric fibromuscular tissue, which is incomplete anteriorly and apically. The neurovascular bundles are located posterolateral to the gland in the 5 o'clock and 7 o'clock positions and serve as an important route of extraprostatic extension.

Pathology on T2-Weighted Imaging

In general, PZ pathology on T2-weighted imaging appears hypointense on a bright background of normal glandular tissue. Prostate cancers within the PZ appear as round or ill-defined hypointense focal lesions (► Fig. 3.7). However, this appearance is nonspecific, and benign entities such as prostatitis, atrophy, hemorrhage, scars, and post-treatment changes may mimic PZ cancer (► Fig. 3.8).³⁵ Cancers within the TZ pose a greater challenge in detection, as the signal characteristics of cancer and the transition zone may overlap.³⁶ These lesions typically appear as a homogeneous mass with ill-defined margins (“erased charcoal” or “smudgy fingerprint” sign), and may have a lenticular, water-drop, or spiculated shape (► Fig. 3.9). Higher-grade malignancies tend to have lower T2 signal intensity than lower-grade tumors.³⁷

Prostate cancers may exhibit invasive behavior within the gland or outside the gland (extraprostatic extension), where common paths of spread include seminal vesicle invasion (SVI) and neurovascular bundle invasion (NVBI). The sharp demarcation of the prostatic capsule on T2-weighted images is crucial

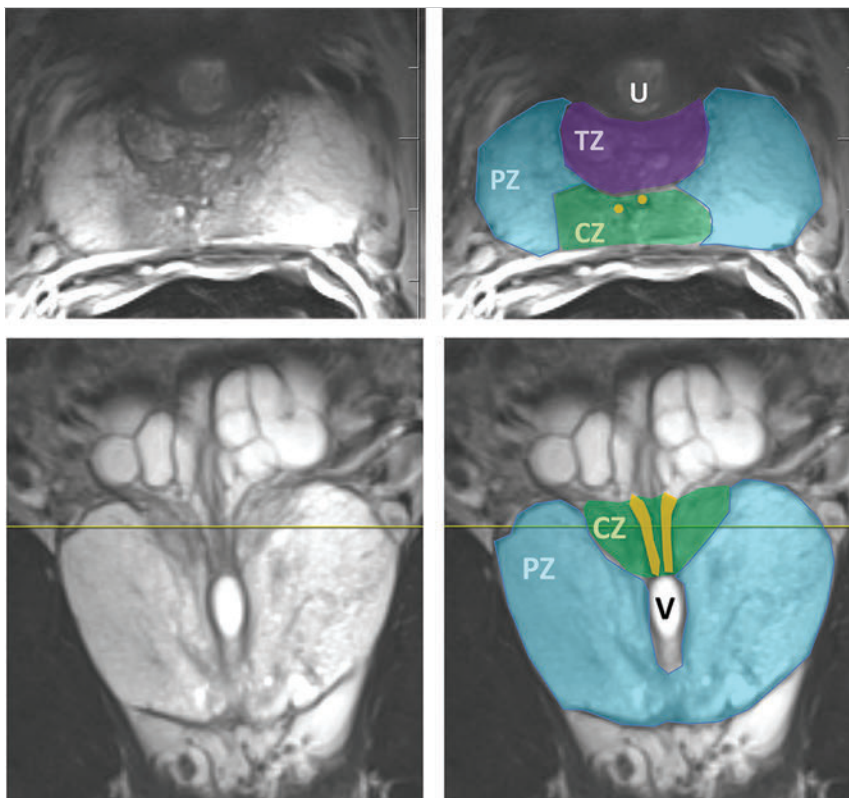


Fig. 3.4 Color-coded zonal anatomy of the prostate on T2-weighted MRI. *Top row:* Axial images. *Bottom row:* Coronal images. *Left column:* Unmarked images. *Right column:* Color-coded overlay delineating anatomical zones of the prostate. The central zone (CZ, green) is a vertical wedge of tissue lateral to the ejaculatory ducts (yellow) with its base cephalad to the gland capsule. The transition zone (TZ, purple) is located adjacent to the urethra (U) proximal to the level of the verumontanum and is the site of benign prostatic hyperplasia (BPH) nodules. The peripheral zone (PZ, blue) appears as a homogeneously hyperintense crescent along the posterior and lateral aspects of the gland. See text for further discussion. A prostatic utricle cyst is noted (V). The horizontal line on the coronal images indicates the slice location for the corresponding axial images.

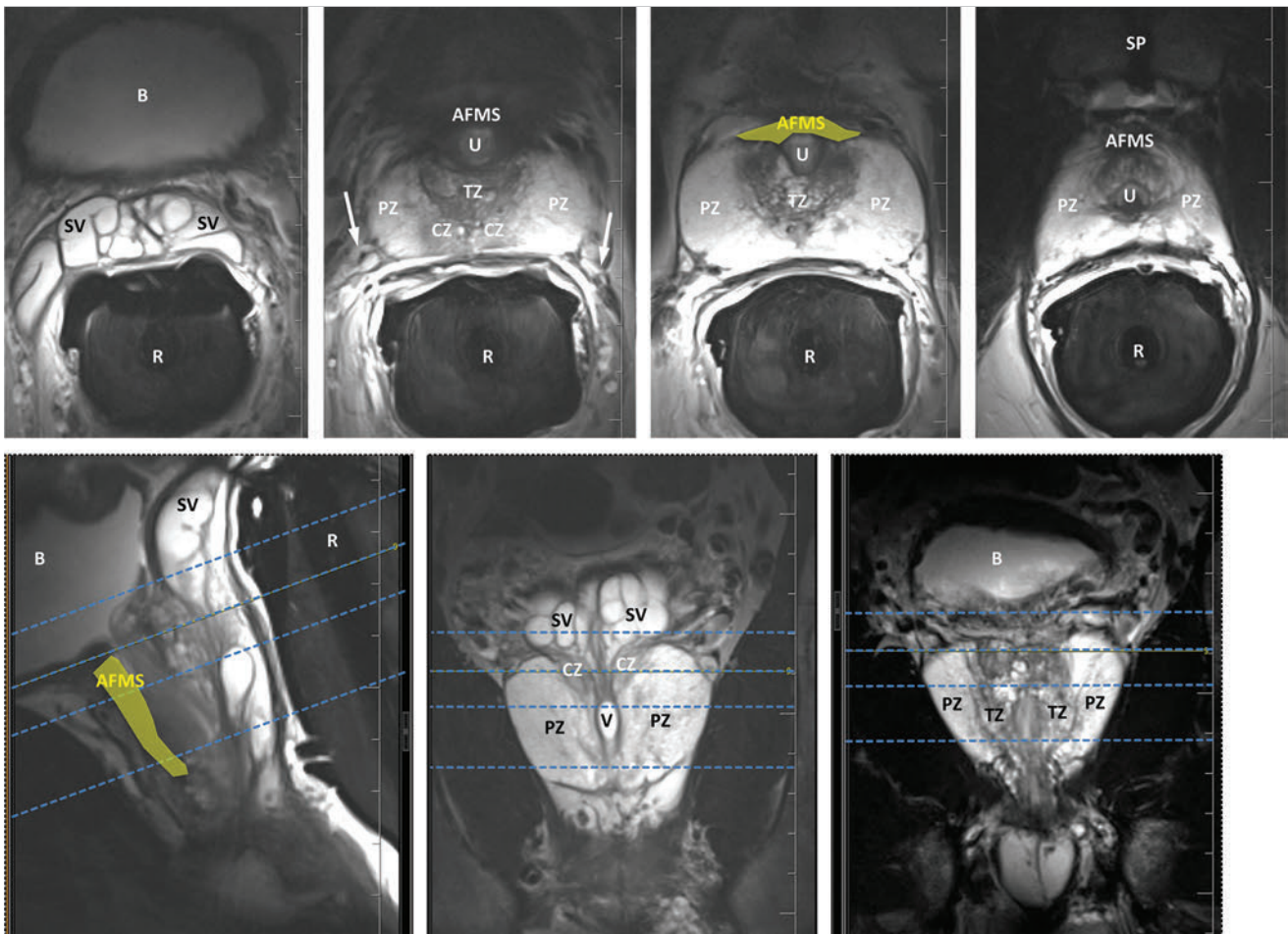


Fig. 3.5 Normal prostate anatomy on T2-weighted MRI, continued. *Top row:* Sequential axial images from above the level of the base to the level of the apex of the prostate. *Bottom row:* One sagittal and two coronal images (middle image is more posterior, right image is more anterior) with dashed lines indicating the slice locations for the sequential axial images. B, bladder; SV, seminal vesicles; R, rectum; AFMS, anterior fibromuscular stroma (highlighted in yellow on selected images); U, urethra; TZ, transition zone; PZ, peripheral zone; CZ, central zone.

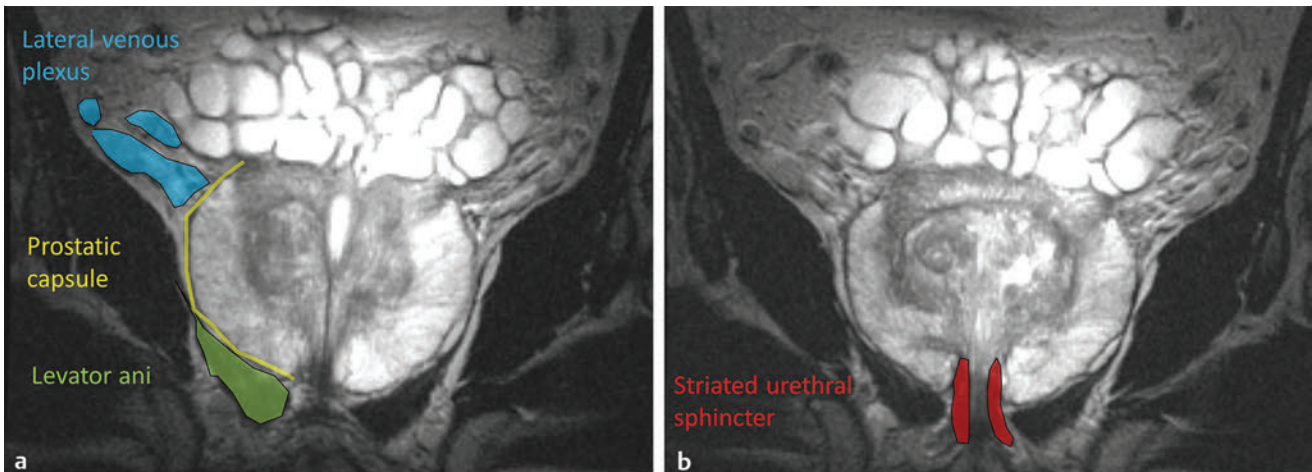


Fig. 3.6 Normal periprostatic anatomy on coronal T2-weighted MRI. The lateral venous plexus (blue overlay) consists of serpiginous vascular structures extending along either side of the prostate gland lateral to the seminal vesicles, with associated chemical shift artifact due to the multiple interfaces created between the serpiginous veins and adjacent periprostatic fat. The prostatic pseudocapsule (yellow overlay) appears as a thin hypointense line surrounding the prostate gland, serving as an important marker for extraprostatic extension. The normal appearance and orientation of the levator ani muscle (green overlay) and striated urethral sphincter (red overlay) is also depicted.

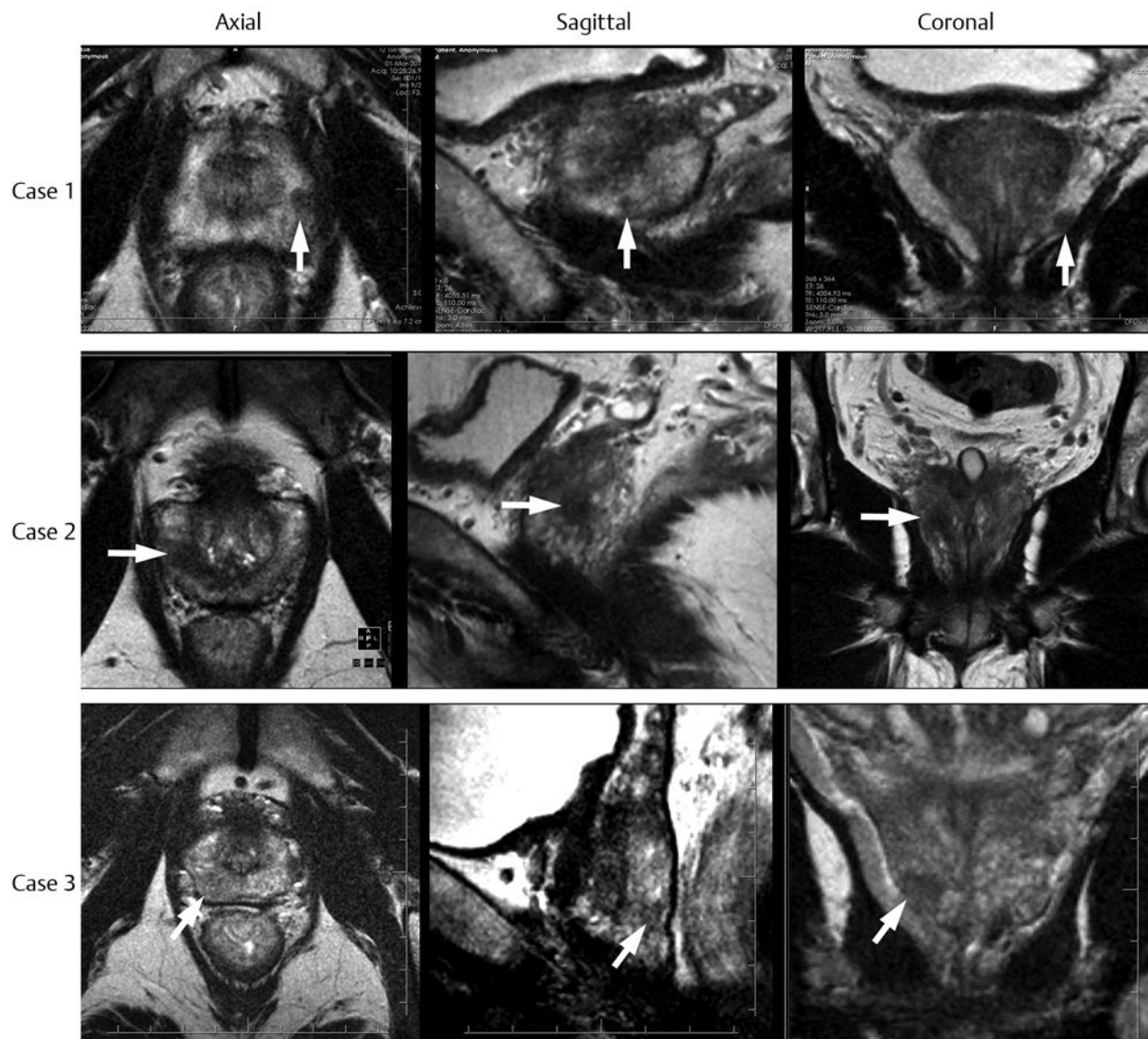


Fig. 3.7 Peripheral zone cancer on orthogonal multislice T2-weighted images. Axial (*left*), sagittal (*middle*), and coronal (*right*) images demonstrate typical appearance of peripheral zone cancer. **Case 1** (*top row*): Images from a 69-year-old man with prostate-specific antigen (PSA) of 7.95 ng/dL demonstrate a circumscribed hypointense nodule within the left lateral peripheral zone at the apex (confirmed Gleason score [GS] 7 cancer). **Case 2** (*middle row*): Images from a 74-year-old man under active surveillance with rising PSA demonstrate a homogeneously hypointense nodule in the right lateral peripheral zone at the level of the midgland (confirmed GS 9 cancer). **Case 3** (*bottom row*): Images from a 56-year-old man with rising PSA of 2.2 ng/dL demonstrate a more subtly hypointense nodule in the right posterior lateral peripheral zone at the apex (confirmed GS 7 cancer), which was better demonstrated with diffusion-weighted imaging. This case illustrates the importance of separate orthogonal planar acquisitions for identification and characterization of prostate tumors, particularly near the base and apex. The lesions in all cases are diagnosed with more confidence when the nodular appearance is confirmed on sagittal and coronal images.

for this assessment in which the most important question is whether the tumor is contained within the gland (T stage ≤ 2) or extends outside the gland (T stage ≥ 3). Features of EPE on T2-weighted images are asymmetry, thickening or irregularity of the neurovascular bundles, bulge of the prostatic capsule, irregular or spiculated margins, obliteration of the rectoprostatic angle, tumor-capsule interface > 1 cm, and capsular breach with measurable extraprostatic disease or bladder wall invasion²⁰ (► Fig. 3.10). Features of SVI on T2-weighted images are focal or diffuse T2 hypointensity within the seminal vesicle,

loss of the normal angle between the base of the prostate and the seminal vesicle, and direct tumor extension from the base of the prostate into and surrounding the seminal vesicle²⁰ (► Fig. 3.11).

The assessment of EPE on T2-weighted images plays an important role in surgical planning. For example, MRI has proven utility in evaluating patients for possible nerve-sparing surgery, which carries a lower risk of impotence and incontinence. In patients undergoing conventional open prostatectomy, MRI has been shown to improve the

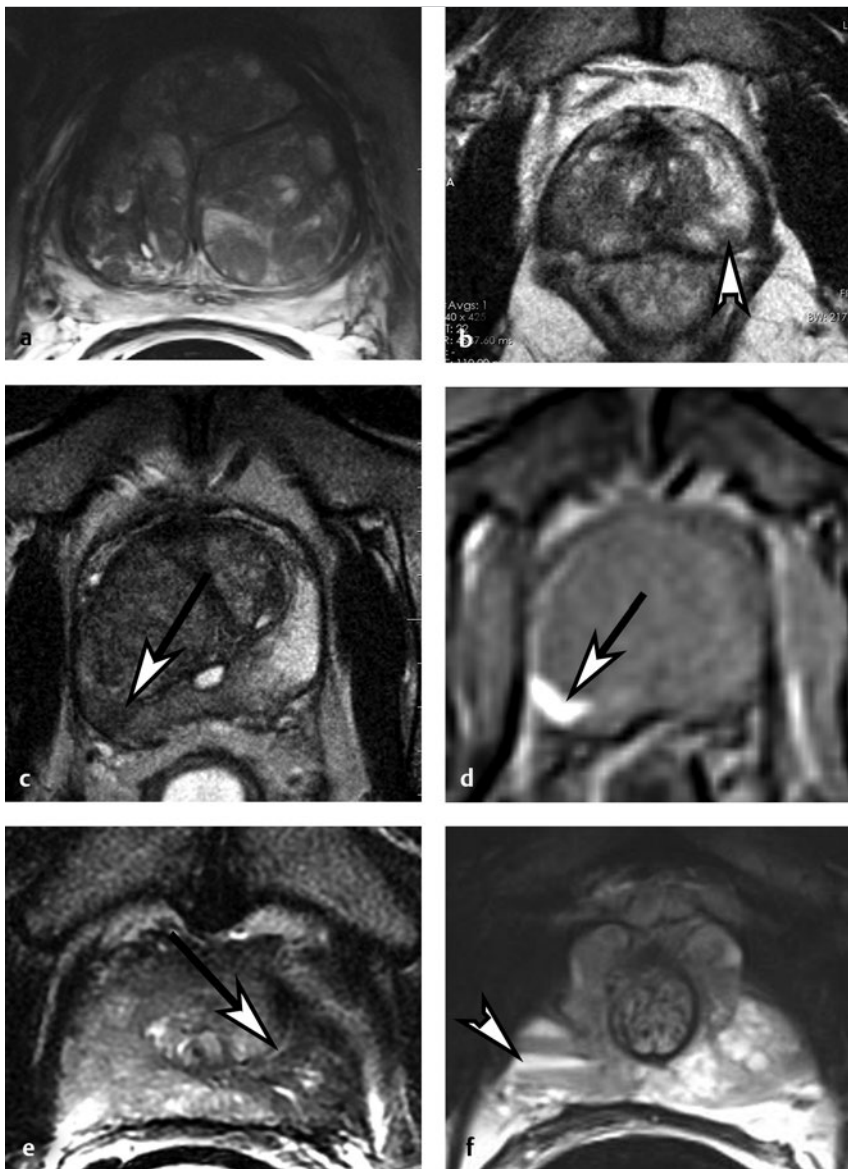


Fig. 3.8 Benign prostate pathology and cancer mimics on T2-weighted imaging. (a) Benign prostatic hyperplasia (BPH), appearing as encapsulated nodules with circumscribed margins within the transition zone (TZ). Nodules containing more stromal elements are typically T2 hypointense, whereas those containing more glandular elements are T2 hyperintense. Areas of cystic atrophy in BPH in the TZ also appear T2 hyperintense. (b) Prostatitis, seen as bandlike or wedge-shaped areas of T2 hypointensity within the peripheral zone (PZ, *arrowhead*). Prostatitis may also appear as diffuse hypointensity on T2-weighted images. (c) Hemorrhage, seen as an area of T2 hypointensity within the PZ (*arrow*) could mimic malignancy. Corresponding T1-weighted image (d) shows characteristic hyperintensity confirming the diagnosis of hemorrhage (*arrow*). (e) Fibrosis and granulomatous inflammation, appearing as a large area of low signal intensity within the left peripheral zone (*arrow*), which could mimic a peripheral zone cancer with extraprostatic extension. This case highlights the need for correlation of T2-weighted images with additional functional imaging sequences to improve specificity for cancer detection. (f) Dilated periprostatic veins, which can mimic peripheral zone cancer on other sequences (e.g., diffusion-weighted or dynamic contrast-enhanced images), but can be clearly identified as veins with fluid hematocrit levels on high-resolution T2-weighted images. Note the presence of a hematocrit level (*arrowhead*), confirming the diagnosis.

surgeon's accuracy in deciding whether to resect or spare the neurovascular bundles³⁸ (► Fig. 3.12). More recently, MRI has been shown to improve decision making regarding nerve sparing in robot-assisted laparoscopic prostatectomy (RALP),³⁹ where the operator lacks the tactile feedback they relied on in open surgery to determine the extent of tumor invasion.

3.3.2 T1-Weighted Imaging

T1-weighted images are typically acquired in the axial plane using either 2D or 3D spoiled gradient-echo sequences. These images are particularly useful for identification of postbiopsy intraprostatic hemorrhage, which manifests as hyperintensity on T1-weighted images, typically within the PZ and seminal vesicles (► Fig. 3.8d). Hemorrhage will also cause T2 shortening (► Fig. 3.8c) and can result in false positive interpretation of malignancy on T2-weighted images. A “hemorrhage exclusion” sign has been described, where hemorrhage-associated T1

shortening is seen to spare regions of tumor. This is hypothesized to relate to increased citrate in noncancerous areas resulting in a longer half-life of hemorrhage in normal prostatic tissue.⁴⁰

The presence of hemorrhage may limit interpretation of mpMRI. Therefore, if hemorrhage is detected on a preliminary T1-weighted sequence and if the clinical situation allows, the examination may be rescheduled in 3 to 4 weeks time to allow for resolution of the hemorrhage.²⁰ However, this approach remains controversial (see 3.4.1 Timing of MRI in the Setting of a Recent Biopsy).

T1-weighted images are also used for assessment of local nodal and bony metastases, particularly when a wide FOV is used. Lower spatial resolution for T1-weighted images compared to T2-weighted images is acceptable in order to increase anatomical coverage and decrease acquisition time. Note that most low- to intermediate-risk patients undergoing MRI for prostate cancer detection or local staging do not require dedicated wide FOV T1-weighted imaging.²⁰

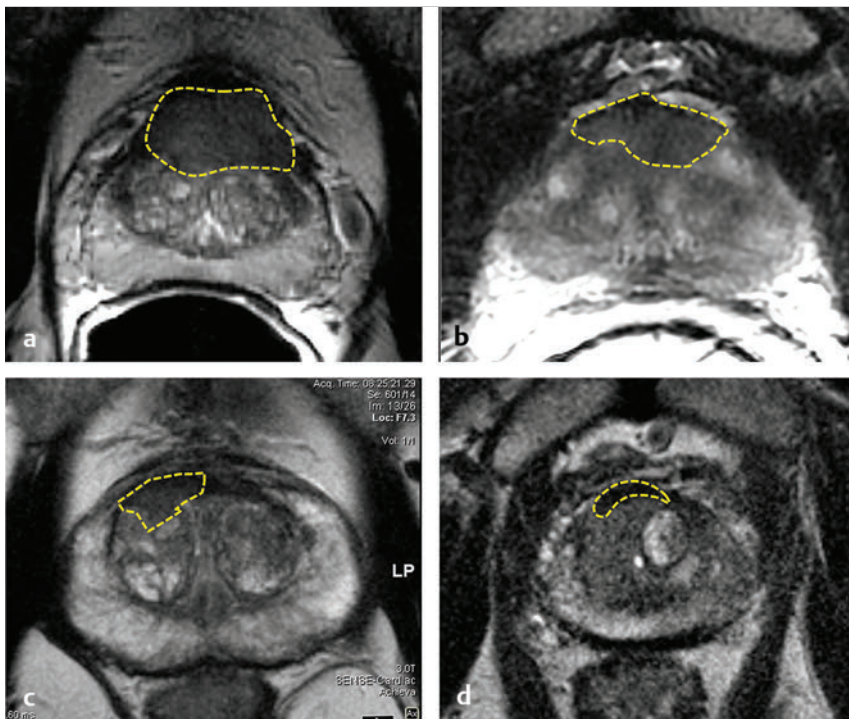


Fig. 3.9 Cancers of transition zone (TZ) and the anterior fibromuscular stroma (AFMS) on T2-weighted images. Margins of the tumor (which are often less well circumscribed by peripheral zone cancers) are delineated by the dashed yellow lines. (a) Large irregularly shaped homogeneously hypointense tumor involving the AFMS and anterior TZ at the level of the midgland in a patient with prostate-specific antigen (PSA) > 10 ng/mL. (b) Lenticular poorly circumscribed hypointense lesion centered within the AFMS at the base, with ill-defined smudgy margins (“erased charcoal” or “smudgy fingerprint” sign) particularly along the right lateral border. This patient, undergoing active surveillance, had confirmed Gleason score [GS] 7 cancer on targeted biopsy. (c) Lenticular hypointense nodule in the right AFMS and right anterior TZ in a patient under active surveillance with PSA rising from 2.6 to 4.0 ng/dL over prior 2 years (confirmed GS 7 cancer). (d) Homogeneously hypointense teardrop-shaped nodule in the posterior TZ at the level of the midgland in a patient with a PSA rise to 11.0 ng/mL (confirmed GS 7 cancer on core biopsy).

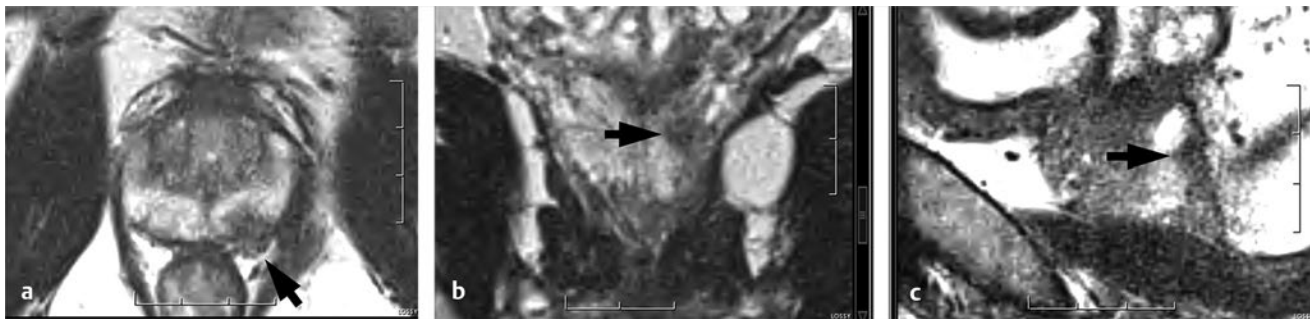


Fig. 3.10 Extraprostatic extension on T2-weighted images. (a) Axial, (b) coronal, and (c) sagittal images in a 51-year-old with prostate-specific antigen of 9.9 ng/dL demonstrate a circumscribed hypointense tumor in the left posterior medial peripheral zone (arrows). There is capsular breach and obliteration of the left rectoprostatic angle in comparison to the normal rectoprostatic angle on the right, consistent with stage T3a disease (see Chapter 7 for full details regarding prostate cancer staging). As illustrated in this case, extraprostatic extension can be detected on T2-weighted imaging even at 1.5 T without the use of an endorectal coil, although in this case there is a large amount of extraprostatic tumor, which facilitates the diagnosis.

3.3.3 Magnetic Resonance Spectroscopy

Magnetic resonance spectroscopic imaging (MRSI) is a functional imaging technique that allows estimation of the concentration of metabolites within a given biological tissue by means of MR imaging. As in other MR techniques, the signal in MRSI is obtained from ^1H . However, a spectrum (rather than a single intensity value) is sampled at each voxel, and the concentrations of metabolites are estimated by the relative size of peaks at characteristic frequencies within the spectrum.

The concentrations of certain metabolites are altered in prostate cancer and can serve as a biomarker for the presence of malignancy. The most relevant metabolites for prostate MRSI are citrate (present as a doublet at 2.6 ppm), creatine (3.0 ppm), and choline (3.2 ppm). Normal prostate tissue is high in citrate, which

is synthesized and secreted in large amounts by prostatic epithelial cells, and low in choline⁴¹ (► Fig. 3.13b). In prostate cancer, the level of citrate is reduced due to alterations in cell function^{42, 43} and loss of the characteristic ductal morphology,^{44,45} while the level of choline is increased due to changes in cell membrane synthesis and degradation within cancer cells,^{46,47} resulting in an elevated choline-to-citrate ratio (► Fig. 3.13a; ► Fig. 3.13c).

While creatine is less altered between healthy and malignant tissue, it is difficult to separate from the choline peak. Thus, the choline and creatine-to-citrate (CC/C) ratio is often employed. Prostate tissue is also high in polyamines, particularly spermine, which has a peak between and usually overlapping that of choline and creatine. As such, the choline, spermine, and creatine-to-citrate ratio (CSC/C) is also sometimes used due to the inability to spectrally resolve these three peaks.⁴⁸ Importantly, the spectral appearance of the strongly coupled citrate and

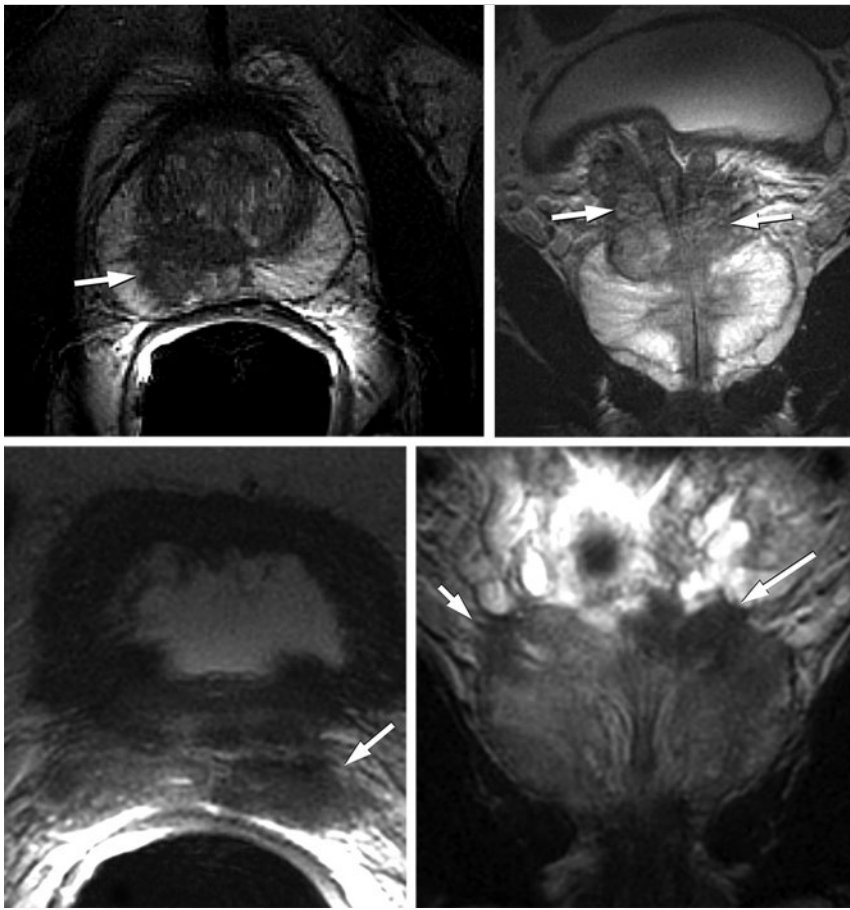


Fig. 3.11 Seminal vesicle invasion (SVI) on axial (*left*) and coronal (*right*) T2-weighted images. **Case 1** (*top row*): Axial image shows an irregular hypointense tumor involving the right posterior medial peripheral zone and right posterior transition zone (*arrow*). Coronal image demonstrates hypointense tumor involving the seminal vesicles bilaterally (*arrows*) with obliteration of the normal angle between the prostatic base and the seminal vesicles. **Case 2** (*bottom row*): Hypointense nodules in the left posterior medial and right posterior lateral peripheral zone (*arrows*) with SVI on the left (*long arrow*) and bilateral extraprostatic extension at the prostatic base.

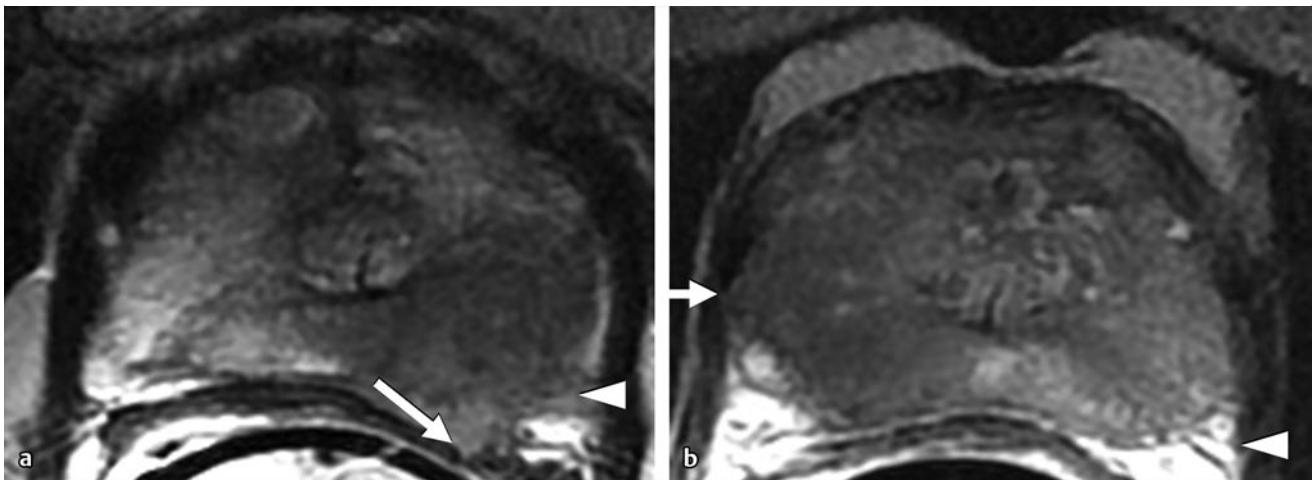


Fig. 3.12 T2-weighted imaging for planning of nerve-sparing surgery. **(a)** Axial image in a patient with prostate-specific antigen (PSA) of 4.5 ng/dL and a palpable nodule on digital rectal examination shows a large low-signal tumor within the left peripheral zone (confirmed Gleason score 9 cancer) with obliteration of the rectoprostatic angle and invasion of the left neurovascular bundle (*arrowhead*) and invasion of the left anterior rectal wall (*arrow*). The tumor was thus deemed too extensive for surgical treatment, and the patient underwent external-beam radiation therapy. **(b)** Axial image in a patient with PSA of 3.7 ng/dL and a negative digital rectal examination demonstrates a large poorly defined area of hypointensity within the right peripheral zone (confirmed Gleason score 8 cancer). The right posterolateral margin of the tumor demonstrates spiculation and clear extraprostatic extension (*arrow*), therefore the right neurovascular bundle was sacrificed at surgery. Note the normal appearance of the left neurovascular bundle and left rectoprostatic angle (*arrowhead*), which allowed the surgeons to proceed confidently with nerve-sparing surgery on the left.

spermine spin systems depends on the pulse sequence parameters and field strength of the acquisition. When this dependence is properly accounted for, the CSC/C ratio provides a

quantitative marker of prostate cancer metabolism that can be compared across different field strengths, vendors, and institutions.⁴⁹

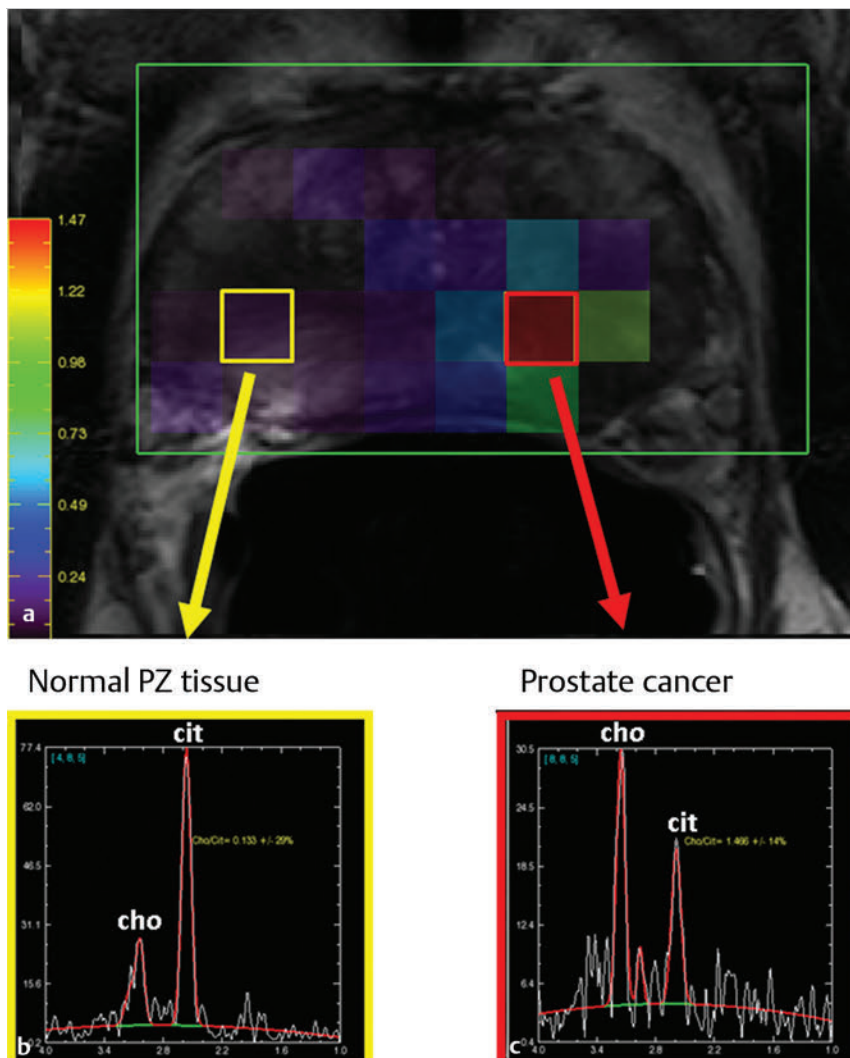


Fig. 3.13 MR spectra of normal prostatic tissue and prostate cancer. (a) MR spectroscopic image acquisition showing a color map of the choline-to-citrate ratio overlaid on an axial T2-weighted image of the prostate. (b) Sample MR spectrum from a voxel containing normal peripheral zone glandular tissue, showing the low ratio of choline to citrate (as discussed in the text, the choline peak often overlaps with the adjacent peaks for creatine and polyamines, particularly spermine). (c) Sample MR spectrum for a voxel containing tumor, showing an increase in choline relative to citrate. This is one of the characteristic features of prostate cancer. (Images courtesy of Dr. Baris Turkbey, Center for Cancer Research, National Institutes of Health, Bethesda, MD.)

In comparison to other MRI methods such as DCE-MRI and DWI, MRSI is technically more challenging, requiring specialized expertise in acquisition, postprocessing, and interpretation to be successful. While a comprehensive description of MRSI methodology is beyond the scope of this text, the major technical considerations are summarized here, and the reader is referred to any of several recent review articles for further detail.^{48,50,51}

The metabolites detected by MRSI are present in much lower concentration than water and lipid protons making this an inherently low SNR technique, with implications for both hardware and pulse sequence design. An ERC is therefore recommended to perform MRSI at 1.5T in a reasonable time frame, while the ERC is optional (though still desirable) at 3.0T. In addition to the increased SNR, performing MRSI at 3.0T also provides improved spectral resolution, as the spacing (or dispersion) of peaks along the spectra increases linearly with field strength.² Because MRSI is highly sensitive to alterations in susceptibility, it is particularly important to use a susceptibility-matched fluid in the ERC balloon and to avoid imaging in the setting of postbiopsy hemorrhage.

In contrast to single voxel or 2D techniques, MRSI of the prostate is performed using 3D chemical shift imaging and point-resolved spectroscopy (PRESS) volume localization. The volume

of interest (or PRESS box) from which the MRSI data is acquired must be carefully selected with reference to the T2-weighted anatomical images and should be adjusted to maximize inclusion of the prostate gland and exclusion of extraprostatic tissues. This “box” is defined by successive application of three slab-selective excitation pulses one along each of the *x*, *y*, and *z* directions. Because the rectangular PRESS box does not conform to the smooth contour of the prostate, oblique saturation bands are then applied along the corners of the box to eliminate signal from extraprostatic tissue (particularly extraprostatic fat, seminal vesicles, and the anterior rectal wall) and to provide a better match to the shape of the gland (► Fig. 3.14).

Optimal shimming is critical to the acquisition of high-quality spectra because the linewidths of metabolites are broadened by any inhomogeneities in the main field. This is particularly true at 3.0T, where increased susceptibility effects make the homogeneity of the main field more difficult to maintain.² At present, shimming is performed using a combination of the standard manufacturer-provided autoshim, with additional manual adjustments along the three primary axes as necessary. Homogeneity of the main field is also required for good water and lipid suppression, which is obtained using specialized excitation pulses,^{52,53,54,55} allowing detection of spectra from metabolites present in much lower abundance than water and fat.

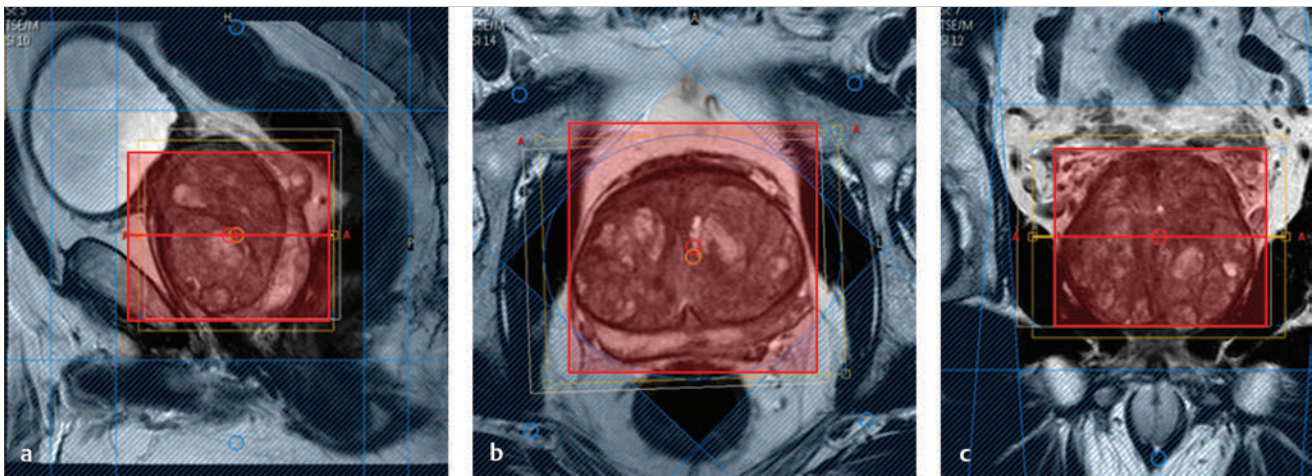


Fig. 3.14 Prescription of the PRESS (point-resolved spectroscopy) volume-of-interest box (red rectangle) and oblique saturation bands (cross-hatched blue rectangles) overlaid on T2-weighted images in the sagittal (a), axial (b) and coronal (c) planes. (Images courtesy of Dr. Baris Turkbey, Center for Cancer Research, National Institutes of Health, Bethesda, MD.)

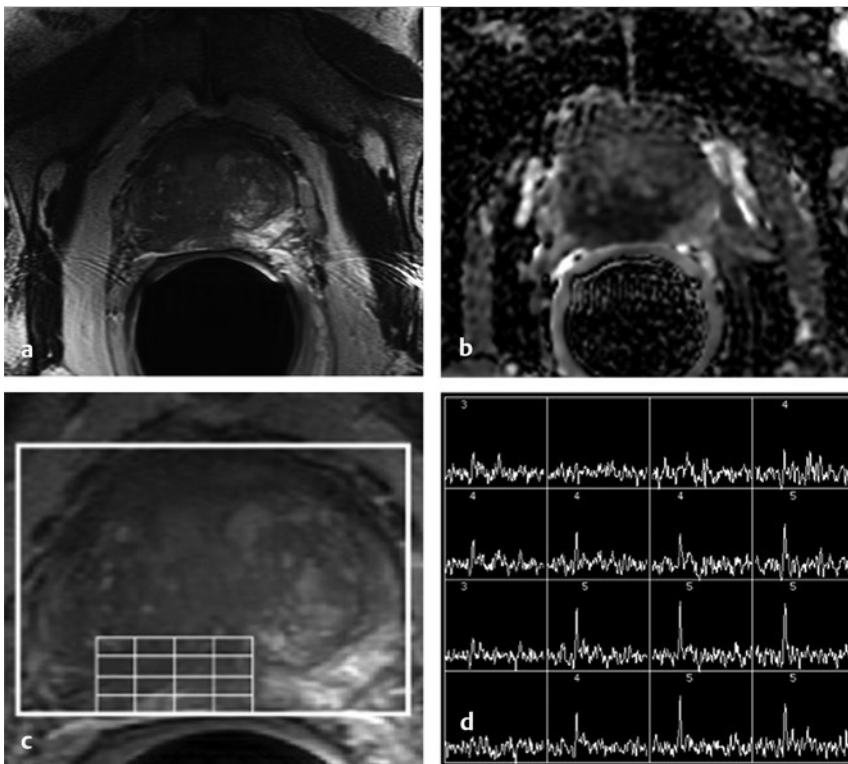


Fig. 3.15 Magnetic resonance spectroscopy in a 64-year-old man with prostate-specific antigen of 12 ng/dL and confirmed Gleason score 9 cancer. (a) Axial T2-weighted image and (b) apparent diffusion coefficient map demonstrate a hypointense tumor with restricted diffusion in the posterior medial peripheral zone and the posterior transition zone. (d) Magnetic resonance spectra corresponding to (c) the 4×4 grid of voxels overlying the tumor demonstrate an increased choline peak and decreased citrate peak in keeping with prostate cancer. Spectra are automatically graded on a scale of 1 to 5, with high scores indicated increasing likelihood of malignancy. (Images courtesy of Dr. Antonio Westphalen, University of California San Francisco School of Medicine.)

Another technical challenge for MRSI is achieving clinically palatable acquisition times. Because spectra must be acquired in the absence of a readout gradient, 3D spatial encoding requires a series of three nested phase-encoding loops, leading to long acquisition times for even relatively small matrix sizes. For example, at 1.5T using a 0.7-cm³ effective voxel size, one study required 17 minutes to obtain a MRSI data set,⁵⁶ although this can be reduced with use of weighted k-space acquisition and filtering.⁵⁷ At 3.0T using an ERC, MRSI with 0.6-cm³ effective voxels can be obtained in a more reasonable 9 minutes.⁵⁸ The larger voxel size (0.5 to 1 cm³) in MRSI is required in order to maintain an adequate SNR and reasonable acquisition time given the above technical considerations. This has clinical implications, as

tumors less than 0.5 cm³ may be missed on MRSI due to partial volume averaging with adjacent normal tissue.

Once the MRSI acquisition is complete, a number of manual and automated postprocessing steps are required, which are performed through vendor-specific-MRSI software analysis packages. These include the combination of data from different coil elements, Fourier transformation to recover the spatial localization of the data, frequency and phase corrections to account for B₀ field inhomogeneity across the prostate, baseline correction for residual unsuppressed water and lipid signals, model fitting of the spectral data, and integration of the area under each metabolite peak to determine the relative concentrations of each metabolite.⁴⁸

The choice of an appropriate model for spectral fitting must take into account the hardware and pulse sequence used in the acquisition due to the aforementioned dependence of the strongly coupled citrate and spermine spin systems on the field strength and pulse sequence parameters.^{48,59} The MRSI data can then be displayed as a contiguous array of spectra and metabolite ratios covering the majority of the prostate gland. Because they are obtained during the same examination, spectral data from MRSI can be directly overlaid on high-resolution T2-weighted images, allowing correlation between areas of anatomical abnormality (hypointensity on T2-weighted images) and areas of metabolic abnormality (elevated CC/C ratio), as shown in ► Fig. 3.15.

Interpretation of spectra requires knowledge of the zonal anatomy of the prostate. For example, the normal CZ and TZ contain significantly lower levels of citrate than the PZ, and the tissues adjacent to the urethra, seminal vesicles, and ejaculatory ducts may contain high levels of choline due to the presence of glycerophosphocholine within these structures.⁵¹ After exclusion of voxels which are uninterpretable (e.g., due to insufficient water or lipid suppression or contamination with glycerophosphocholine), standardized scoring systems are applied and a score on a 5-point scale is assigned for each MRSI voxel, with higher scores indicating greater probability of malignancy.^{60,61} In the PZ, where the majority of MRSI work has been focused, voxels with a CC/C ratio greater than 2 standard deviations above the mean are generally considered “possibly malignant,” while those with CC/C ratios 3 standard deviations or more above the mean are considered “probably malignant,” although there is no absolute threshold and these ratios are influenced by technical considerations such as field strength and quality of the spectra.⁵¹ To diagnose prostate cancer, there should be at least 2 adjacent voxels with CC/C ratios greater than 2 and 3 standard deviations above the mean, respectively.²⁰

Although MRSI is capable of differentiating prostate cancer from noncancerous tissue,⁶² a well-designed prospective multicenter study failed to demonstrate any incremental benefit of MRSI over conventional T2-weighted imaging for the detection and localization of prostate cancer.⁶³ It should be noted that this was performed on older 1.5T MRI systems and there have been improvements in MRSI quality since that time (e.g., proper accounting for strongly coupled spermine and citrate spin systems in the model fitting, as discussed above).

Metabolic abnormalities detected using MRSI may be useful in tumor grading, as they have been shown to correlate with tumor aggressiveness (Gleason score [GS])⁶⁴ although similar correlations exist with diffusion parameters⁶⁵ and signal intensity on T2-weighted images.⁶⁶ There are also clinical limitations to the use of MRSI, which is vulnerable to increased susceptibility effects in the setting of postbiopsy hemorrhage (requiring an interval of at least 8 weeks between biopsy and MR examination),⁶⁷ and limited ability to differentiate prostate cancer from benign entities such as acute prostatitis and stromal BPH.⁵¹ These limitations have led to the downgrading of MRSI to an optional technique in most centers, and it has not been included in the most recent guidelines for clinical prostate mpMRI (PI-RADS version 2.0).

In summary, MRSI is a potentially useful tool in prostate cancer characterization in experienced hands. However, the technical challenges and time required have limited its widespread

application. As the quality and SNR of MRI systems have improved over time, there is renewed interest in the application of MRSI for characterization of high-grade cancer and potentially obviating the need for a contrast injection by replacing DCE-MRI with MRSI.

3.3.4 Diffusion-Weighted Imaging and Dynamic Contrast-Enhanced MRI

Despite the high sensitivity of T2-weighted imaging for prostate cancer,^{68,69} the low specificity of T2 signal abnormalities has motivated the augmentation of T2-weighted images with additional functional imaging techniques. Diffusion-weighted imaging (DWI) and dynamic contrast-enhanced (DCE-MRI) have emerged as powerful imaging tools to increase the accuracy of mpMRI in prostate cancer detection, localization, and staging. DWI and DCE-MRI are discussed in detail in Chapters 4 and 5.

3.4 Maximizing Image Quality/Artifacts/Pitfalls

3.4.1 Timing of MRI in the Setting of a Recent Biopsy

Hemorrhage is commonly observed in the PZ and seminal vesicles following transrectal ultrasound-guided biopsy, and has been reported in up to 81% of patient's within 3 weeks of biopsy and 49% of patients more than 3 weeks from time of biopsy.⁷⁰ Blood products can disseminate throughout the ductal system to involve a greater portion of the PZ than would be expected based on the number and trajectory of the biopsy cores and, in some cases, may involve the entire PZ.⁷⁰ While it is has been shown that postbiopsy hemorrhage may adversely affect the interpretation of T2-weighted images,⁷⁰ the optimal timing of MRI examination postbiopsy has been controversial. Because postbiopsy changes should diminish over time, delays ranging from 3 to 10 weeks have been recommended between the time of biopsy and performance of a staging MRI.^{20,67} However, these delays are not always feasible, may be unacceptable to patients and referring clinicians, and may breach time-to-treatment guidelines. In fact, multiple studies now suggest that postbiopsy delay may not be required when using modern mpMRI protocols.^{71,72,73} For example, while one recent study found a trend toward decreased sensitivity in the presence of hemorrhage for T2-weighted imaging alone, there was no significant decrease in performance for DWI or DCE-MRI, and most importantly no decrease in performance for the overall accuracy of the combined mpMRI protocol.⁷²

As a precaution, current guidelines recommend a delay of 6 weeks between the time of biopsy and staging MRI where possible, with the acknowledgement that this may not always be feasible or necessary.²⁰

3.4.2 Artifacts and Pitfalls

Prostate MRI is subject to a number of artifacts the radiologist should be aware of, some of which are specific to use of an ERC. First, the sensitivity profile of the coil often creates a “signal flare” artifact,¹⁸ seen as a band of high signal at the

interface between the ERC and the soft tissue of the posterior rectal wall (► Fig. 3.16). This occurs due to the high SNR immediately adjacent to the coil and may produce a strong signal gradient across the PZ, making this area more difficult to assess. A related artifact is loss of signal within the anterior gland, particularly in the setting of BPH, which may limit assessment of the anterior TZ. A variety of post-processing strategies can be employed to take into account the sensitivity profile of the ERC and produce a more uniform signal across the image.⁷⁴ However, this correction comes at the cost of increased noise with distance from the coil, which may also limit assessment of the anterior gland (► Fig. 3.17).

As in other organ systems, motion is a significant source of artifacts in prostate MRI. Motion artifact comes in two forms, phase ghosting and blurring. Blurring is more intuitive and occurs due to motion between the time of RF excitation and echo formation (i.e., within a single phase-encoding step), resulting in a loss of sharpness in the appearance of the moving structure. Phase ghosting occurs due to movement between phase-encoding steps. The inconsistent location of spins as the phase-encoding data is acquired leads to accrual of phase error. If the motion has a periodic component, replications or “ghosts” of the moving tissue are cast across the full width of the image, but only in the phase-encoding direction, regardless of the direction of motion. For this reason, the phase-encoding

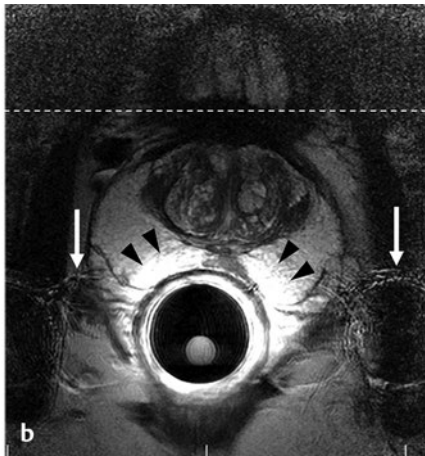
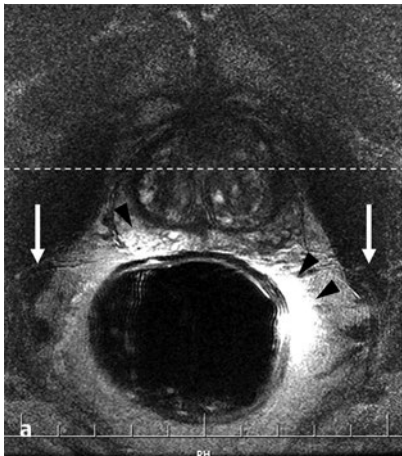


Fig. 3.16 MRI artifacts related to use of an endorectal coil (ERC) demonstrated on an axial T2-weighted images obtained at 1.5 T. (a) Image obtained using a single-channel balloon-inflatable endorectal receiver coil (eCoil, Medrad Inc, Warrendale, PA). (b) Image obtained using a dual-channel solid reusable phased-array endorectal receiver coil (Endo Coil Array, Hologic Inc., Bedford, MA). Both images demonstrate characteristic “signal flare” artifact, seen as a band of high signal at the interface between the ERC and the adjacent soft tissues of the posterior rectal wall and posterior peripheral zone (*arrowheads*). Also note the anterior signal drop-off in both images, visible as a “noise band” (dashed line) that results from the decreasing signal-to-noise ratio (SNR) with distance from the rectum. These artifacts are a direct result of the coil sensitivity profile and are unique to ERC use. Typical phase artifact (*arrows*) is seen as replications, or “ghosts,” of the high signal interface between the ERC and adjacent soft tissues, which are cast along the phase-encoding (left-right) direction. As seen here, these artifacts may limit assessment of the posterior peripheral zone and neurovascular bundles. Although phase ghosts can occur with and without an ERC, they are more common when an ERC is used, and more severe with rigid rather than balloon-inflatable ERC designs. Both images were obtained using a 512 × 320 matrix, 14-cm field-of-view, and 3-mm slice thickness.

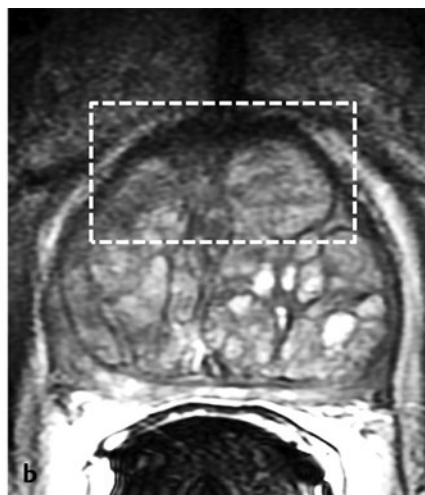


Fig. 3.17 Decreased anterior signal-to-noise ratio (SNR) in the setting of benign prostatic hyperplasia (BPH). Axial T2-weighted images obtained at 1.5 T using an endorectal coil (ERC) in patients with an anteroposterior diameter of the prostate measuring (a) 3.2 cm, and (b) 5.1 cm. Note the decreased SNR (“graininess”) in the anterior gland of the patient with more severe prostatic enlargement (*dashed box* in image (b)). This effect can be partially compensated for by employing a combination of ERC and surface phased-array coils to boost SNR in the anterior gland. However, even the combined approach may provide poor image quality in the setting of excess body habitus, which increases the distance between the anterior gland and the surface coil array.

direction should always be assigned as left–right so that ghosting does not obscure assessment of the prostate gland. While motion artifacts are observed in both endorectal and non–endorectal coil MRI studies, they are more frequent,¹⁸ and rated as more significant,¹⁹ when using an ERC. Specifically, phase ghosts related to the anterior aspect of the ERC and anterior rectal wall may obscure assessment of the neurovascular bundles (► Fig. 3.16).^{14,17,18} In a recent study, phase artifacts were worse with a rigid compared to balloon-inflatable ERC design.¹⁷ For this rigid coil, the negative impact of phase ghosts can be reduced by adjusting the angle of the coil to direct artifacts away from the prostate and neurovascular bundles and by positioning the ERC so it applies less pressure on the prostate, as excess pressure compresses the gland in anteroposterior (AP) dimension and brings the phase ghosts into closer proximity. Alternative k-space sampling strategies such as periodically rotated overlapping parallel lines with enhanced reconstruction (PROPELLER; General Electric Medical Systems) or BLADE (Siemens Healthcare) have been shown to reduce motion artifacts in T2-weighted MRI, though at a cost of reduced image contrast.⁷⁵

Another category of artifacts relevant to prostate MRI are those related to magnetic susceptibility. Susceptibility is a property of all materials and represents the degree to which a material becomes magnetized when placed in an external magnetic field. When two adjacent materials with differing susceptibility are placed side by side, they become magnetized to different degrees, creating a localized gradient or inhomogeneity in the main magnetic field. This leads to characteristic artifacts at the interfaces between tissues with different susceptibilities, for example between air, bone, soft tissue, and certain blood products (e.g., hemosiderin).

In prostate imaging, susceptibility artifacts may be seen in association with rectal gas, metallic implants, postbiopsy hemorrhage, or from the ERC itself. These artifacts take the form of geometric distortion, signal dropout, and signal “pile-up,” and are most apparent in single-shot echo-planar imaging (EPI) acquisitions (i.e., DWI) due to intrinsically low bandwidth along the phase-encoded direction.^{2,76} Susceptibility artifacts increase with magnetic field strength⁷⁷ and may result in apparent displacement of tissues up to several voxels. Though often obvious, susceptibility artifacts may be subtle and can mimic peripheral zone malignancy (► Fig. 3.18), a pitfall which can be avoided through close correlation with multiplanar T2-weighted images. Susceptibility effects are also detrimental to MRSI acquisitions, resulting in broadening of linewidths and loss of spectral resolution. For these reasons, a susceptibility-matched fluid such as perfluorocarbon or barium should be used when performing prostate MRI with a balloon-inflatable ERC. Most inflatable ERCs use a dual-balloon design, and care must be taken to avoid underfilling of the inner balloon with the susceptibility-matched fluid. Underfilling leaves a thin air gap between the inner and outer balloons, resulting in susceptibility artifacts and negating any benefit of the barium suspension (► Fig. 3.19). Susceptibility artifacts can be also be minimized by imaging at a lower field strength (1.5 T), though this is not always desirable or possible. When performing DWI at 3.0T, susceptibility artifacts can be reduced by combining single-shot EPI sequences with parallel imaging and short echo-train lengths to reduce the accrual of phase errors.²

In addition to the above artifacts, the positioning of the ERC itself has an important impact on image quality. It is crucial to assess the ERC position on scout images in order to confirm that

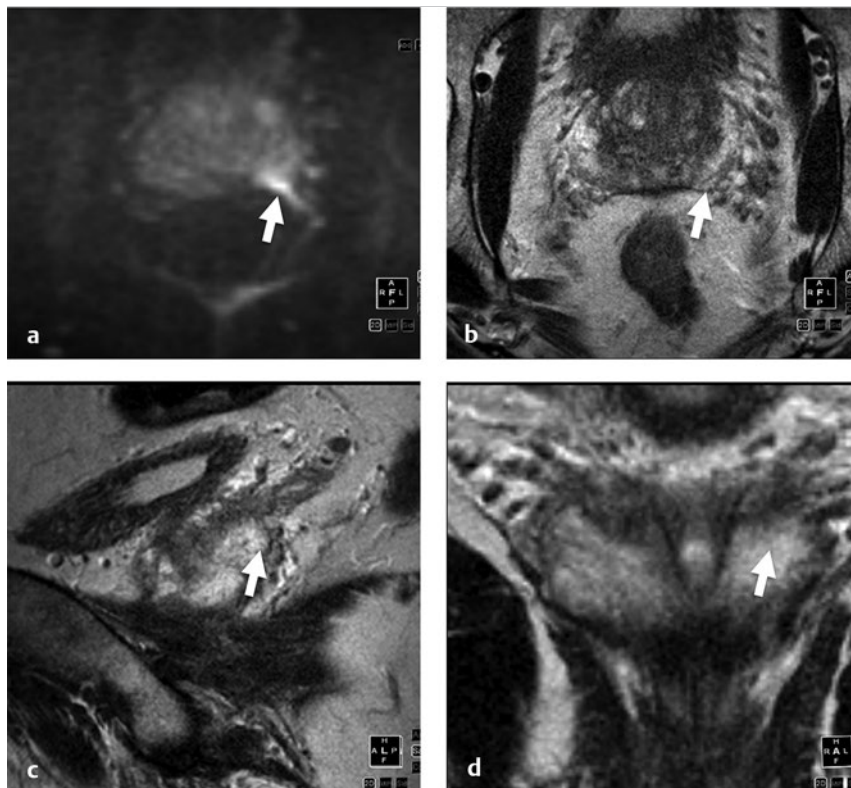


Fig. 3.18 Susceptibility-artifact-mimicking prostate cancer. (a) Axial diffusion-weighted image shows geometric distortion and signal “pile up” at the rectoprostatic interface, creating apparent hyperintensity within the left lateral posterior peripheral zone (arrow). Axial (b), sagittal (c), and coronal (d) T2-weighted images through this level demonstrate no corresponding nodule (arrows), confirming this to be an artifactual distortion rather than a true lesion.

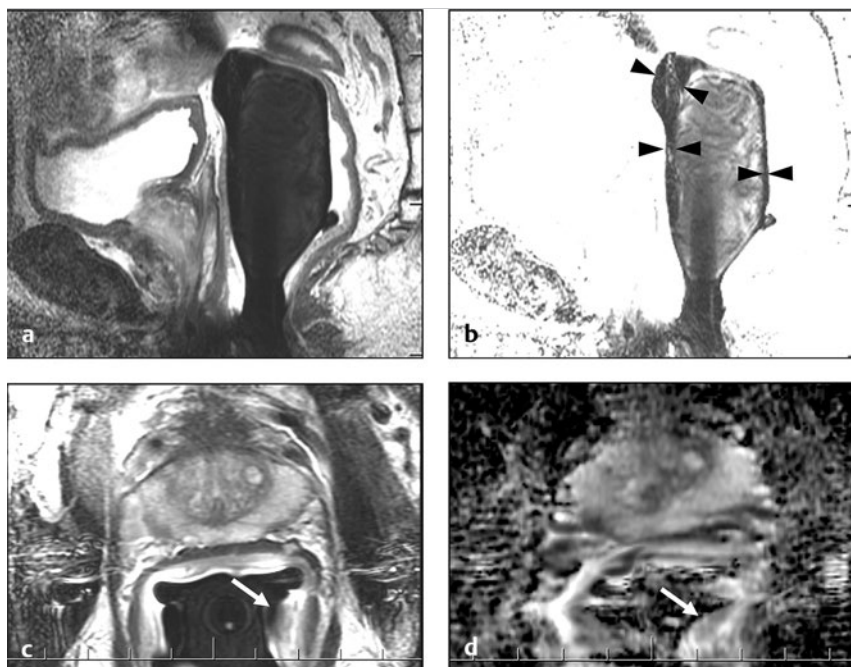


Fig. 3.19 Susceptibility artifact related to air gap when using a balloon-inflatable endorectal coil (ERC) and susceptibility-matched barium suspension. (a) Sagittal T2-weighted image through the prostate obtained using a balloon-inflatable ERC filled with susceptibility-matched barium suspension. (b) Same image as in (a) but with more aggressive windowing shows a thin hypointense air gap (arrowheads) between the barium-filled inner balloon and the outer balloon that abuts the rectal wall. This occurs due to under-filling of the inner balloon with barium and is one potential pitfall when using a double-balloon design and susceptibility-matched barium suspension. Axial T2-weighted image (c) and apparent diffusion coefficient (ADC) map (d) demonstrate susceptibility artifacts due to the air gap, for example geometric distortion along the left rectal wall (arrow). The artifacts are more severe on the ADC map, due to the greater sensitivity of diffusion-weighted images to corruption by susceptibility artifacts.

the prostate is centered within the sensitive volume of the coil in the sagittal plane (► Fig. 3.1), and that there is not an excessive rotation ($>20^\circ$) of the coil relative to the prostate in the axial plane. Malrotation of the ERC may result in the sensitive volume of the coil being directed laterally, or even posteriorly, toward the sacrum. Therefore, coil insertion and assessment of correct positioning should only be performed by appropriately trained personnel (radiologist or radiologist-trained assistant).

3.5 Patient Preparation

To minimize motion artifacts related to bowel peristalsis, use of a spasmolytic agent prior to prostate MRI has been recommended²⁰ and is often performed.⁷⁸ The two most commonly used agents are butylscopolamine (Buscopan) and glucagon. While these agents may be beneficial in some patients, recent studies have shown little systematic improvement in image quality with Buscopan in comparison to MRI performed without a spasmolytic agent,^{78,79} and the incremental cost and possibility of adverse reactions should be taken into account when considering routine use of these drugs.

To minimize susceptibility artifacts, efforts should be made to eliminate gas and stool from the rectum prior to MRI. Stool may be eliminated by a self-administered fleet enema performed the day of the examination, at least 2 hours prior to imaging. However, in some patients an enema may stimulate peristalsis and result in increased motion artifact.

To eliminate air from the rectum, decompression using suction via a small catheter may be performed. If there is rectal air present during a study performed without use of an ERC, imaging the patient in the prone position may be helpful in moving the air to an antedependent position away from the prostate.

Some investigators recommend that patients refrain from ejaculation for at least 3 days prior to prostate MRI.⁸⁰ This recommendation is supported by the finding that quantitative changes in the apparent diffusion coefficient (ADC) and T2

within the PZ are observed immediately after ejaculation, with potential implications for prostate cancer detection.⁸¹ Note, however, that this finding was observed in healthy young men, and requires validation in older subjects with and without prostate cancer. Nonetheless, refraining from ejaculation is generally recommended as a precautionary measure.

3.6 Summary

In summary, there are numerous hardware and pulse sequence options available for mpMRI of the prostate. The use of 3.0T systems with and without an endorectal coil is acceptable for most clinical situations, as is the use of 1.5T with an endorectal coil. Use of 1.5T systems without an endorectal coil may be problematic for cancer localization, particularly on older systems, and is not advocated for local staging. High-resolution T2-weighted imaging forms the backbone of any mpMRI protocol, and is essential for tumor localization and local staging including assessment of extraprostatic extension. DWI and DCE-MRI are functional imaging techniques that play an important role in improving the sensitivity and specificity of T2-weighted imaging, and are covered in detail in Chapters 4 and 5. Although MRSI is not part of the currently recommended mpMRI exam, spectroscopy may gain wider adoption in the future as a substitute for DCE-MRI due to concerns regarding the cost and safety of gadolinium-based contrast agents. To accomplish this, improvements in the robustness of the MRSI acquisition will be required.

References

- [1] Mazaheri Y, Shukla-Dave A, Muellner A, Hricak H. MRI of the prostate: clinical relevance and emerging applications. *J Magn Reson Imaging* 2011; 33(2):258–274
- [2] Lagemaat MW, Scheenen TW. Role of high-field MR in studies of localized prostate cancer. *NMR Biomed* 2014; 27(1):67–79
- [3] Rouvière O, Hartman RP, Lyonnet D. Prostate MR imaging at high-field strength: evolution or revolution? *Eur Radiol* 2006; 16(2):276–284

- [4] Kuhl CK, Träber F, Schild HH. Whole-body high-field-strength (3.0-T) MR Imaging in Clinical Practice. Part I. Technical considerations and clinical applications. *Radiology* 2008; 246(3):675–696
- [5] Hennig J, Scheffler K. Hyperchoes. *Magn Reson Med* 2001; 46(1):6–12
- [6] Hennig J, Weigel M, Scheffler K. Multiecho sequences with variable refocusing flip angles: optimization of signal behavior using smooth transitions between pseudo steady states (TRAPS). *Magn Reson Med* 2003; 49(3):527–535
- [7] de Bazelaire CM, Duhamel GD, Rofsky NM, Alsop DC. MR imaging relaxation times of abdominal and pelvic tissues measured in vivo at 3.0 T: preliminary results. *Radiology* 2004; 230(3):652–659
- [8] Gibbs P, Liney GP, Pickles MD, Zelhof B, Rodrigues G, Turnbull LW. Correlation of ADC and T2 measurements with cell density in prostate cancer at 3.0 Tesla. *Invest Radiol* 2009; 44(9):572–576
- [9] Fütterer JJ, Scheenen TW, Huisman HJ, Klomp DW, van Dorsten FA, Hulsbergen-van de Kaa CA et al. Initial experience of 3 tesla endorectal coil magnetic resonance imaging and 1H-spectroscopic imaging of the prostate. *Investigative Radiology* 2004; 39(11):671–680
- [10] Torricelli P, Barberini A, Cinquantini F, Sighinolfi M, Cesinaro AM. 3-T MRI with phased-array coil in local staging of prostatic cancer. *Acad Radiol* 2008; 15(9):1118–1125
- [11] Fütterer JJ, Engelbrecht MR, Jäger GJ, Hartman RP, King BF, Hulsbergen-Van de Kaa CA et al. Prostate cancer: comparison of local staging accuracy of pelvic phased-array coil alone versus integrated endorectal-pelvic phased-array coils. Local staging accuracy of prostate cancer using endorectal coil MR imaging. *Eur Radiol* 2007; 17(4):1055–1065
- [12] Fütterer JJ, Heijmink SW, Scheenen TW, Jäger GJ, Hulsbergen-Van de Kaa CA, Witjes JA et al. Prostate cancer: local staging at 3-T endorectal MR imaging—early experience. *Radiology* 2006; 238(1):184–191
- [13] Bittencourt LK, Hausmann D, Sabaneef N, Gasparetto EL, Barentsz JO. Multiparametric magnetic resonance imaging of the prostate: current concepts. *Radiol Bras* 2014; 47(5):292–300
- [14] Noworolski SM, Crane JC, Vigneron DB, Kurhanewicz J. A clinical comparison of rigid and inflatable endorectal-coil probes for MRI and 3D MR spectroscopic imaging (MRSI) of the prostate. *J Magn Reson Imaging* 2008; 27(5):1077–1082
- [15] deSouza NM, Gilderdale DJ, Puni R, Coutts GA, Young IR. A solid reusable endorectal receiver coil for magnetic resonance imaging of the prostate: design, use, and comparison with an inflatable endorectal coil. *J Magn Reson Imaging* 1996; 6(5):801–804
- [16] Noworolski SM, Reed GD, Kurhanewicz J, Vigneron DB. Post-processing correction of the endorectal coil reception effects in MR spectroscopic imaging of the prostate. *J Magn Reson Imaging* 2010; 32(3):654–662
- [17] Haider MA, Krieger A, Elliott C, Da Rosa MR, Milot L. Prostate imaging: evaluation of a reusable two-channel endorectal receiver coil for MR imaging at 1.5 T. *Radiology* 2014; 270(2):556–565
- [18] Shah ZK, Elias SN, Abaza R, Zynger DL, DeRenne LA, Knopp MV et al. Performance comparison of 1.5-T endorectal coil MRI with 3.0-T nonendorectal coil MRI in patients with prostate cancer. *Acad Radiol* 2015; 22(4):467–474
- [19] Heijmink SW, Fütterer JJ, Hambroek T, Takahashi S, Scheenen TW, Huisman HJ et al. Prostate cancer: body-array versus endorectal coil MR imaging at 3 T—comparison of image quality, localization, and staging performance. *Radiology* 2007; 244(1):184–195
- [20] Barentsz JO, Richenberg J, Clements R, Choyke P, Verma S, Villeirs G et al. European Society of Urogenital Radiology. ESUR prostate MR guidelines 2012. *Eur Radiol* 2012; 22(4):746–757
- [21] Hricak H, Choyke PL, Eberhardt SC, Leibel SA, Scardino PT. Imaging prostate cancer: a multidisciplinary perspective. *Radiology* 2007; 243(1):28–53
- [22] Schnall MD, Lenkinski RE, Pollack HM, Imai Y, Kressel HY. Prostate: MR imaging with an endorectal surface coil. *Radiology* 1989; 172(2):570–574
- [23] Beyersdorff D, Taymoorian K, Knösel T, Schnorr D, Felix R, Hamm B et al. MRI of prostate cancer at 1.5 and 3.0 T: comparison of image quality in tumor detection and staging. *AJR. Am J Roentgenol* 2005; 185(5):1214–1220
- [24] Park BK, Kim B, Kim CK, Lee HM, Kwon GY. Comparison of phased-array 3.0-T and endorectal 1.5-T magnetic resonance imaging in the evaluation of local staging accuracy for prostate cancer. *J Comput Assist Tomog* 2007; 31(4):534–538
- [25] Sosna J, Pedrosa I, Dewolf WC, Mahallati H, Lenkinski RE, Rofsky NM. MR imaging of the prostate at 3 Tesla: comparison of an external phased-array coil to imaging with an endorectal coil at 1.5 Tesla. *Acad Radiol* 2004; 11(8):857–862
- [26] Torricelli P, Cinquantini F, Ligabue G, Bianchi G, Sighinolfi P, Romagnoli R. Comparative evaluation between external phased array coil at 3T and endorectal coil at 1.5 T: preliminary results. *J Comput Assist Tomog* 2006; 30(3):355–361
- [27] Turkbey B, Merino MJ, Gallardo EC, Shah V, Aras O, Bernardo M et al. Comparison of endorectal coil and nonendorectal coil T2 W and diffusion-weighted MRI at 3 Tesla for localizing prostate cancer: correlation with whole-mount histopathology. *J Magn Reson Imaging* 2014; 39(6):1443–1448
- [28] Gibbs P, Tozer DJ, Liney GP, Turnbull LW. Comparison of quantitative T2 mapping and diffusion-weighted imaging in the normal and pathologic prostate. *Magnetic Magn Reson Med* 2001; 46(6):1054–1058
- [29] Panebianco V, Sciarra A, Osimani M, Lisi D, Ciccariello M, Saliccia S et al. 2D and 3D T2-weighted MR sequences for the assessment of neurovascular bundle changes after nerve-sparing radical retropubic prostatectomy with erectile function correlation. *Eur Radiol* 2009; 19(1):220–229
- [30] Rosenkrantz AB, Neil J, Kong X, Melamed J, Babb JS, Taneja SS et al. Prostate cancer: Comparison of 3D T2-weighted with conventional 2D T2-weighted imaging for image quality and tumor detection. *AJR. Am J Roentgenol* 2010; 194(2):446–452
- [31] Lichy MP, Wietek BM, Mugler JP III, Horger W, Menzel MI, Anastasiadis A et al. Magnetic resonance imaging of the body trunk using a single-slab, 3-dimensional, T2-weighted turbo-spin-echo sequence with high sampling efficiency (SPACE) for high spatial resolution imaging: initial clinical experiences. *Investigative Radiology* 2005; 40(12):754–760
- [32] McNeal JE. The zonal anatomy of the prostate. *The Prostate* 1981; 2(1):35–49
- [33] Claus FG, Hricak H, Hattery RR. Pretreatment evaluation of prostate cancer: role of MR imaging and 1 H MR spectroscopy. *Radiographics* 2004; 24 Suppl 1:S167–S180
- [34] Vargas HA, Akin O, Franiel T, Goldman DA, Udo K, Touijer KA et al. Normal central zone of the prostate and central zone involvement by prostate cancer: clinical and MR imaging implications. *Radiology* 2012; 262(3):894–902
- [35] Murphy G, Haider M, Chai S, Sreeharsha B. The expanding role of MRI in prostate cancer. *AJR. Am J Roentgenol* 2013; 201(6):1229–1238
- [36] Puech P, Betrouni N, Makni N, Dewalle AS, Villers A, Lemaitre L. Computer-assisted diagnosis of prostate cancer using DCE-MRI data: design, implementation and preliminary results. *Int J Comput Assist Radiol surg* 2009; 4(1):1–10
- [37] Sung YS, Kwon HJ, Park BW, Cho G, Lee CK, Cho KS et al. Prostate cancer detection on dynamic contrast-enhanced MRI: computer-aided diagnosis versus single perfusion parameter maps. *AJR. Am J Roentgenol* 2011; 197(5):1122–1129
- [38] Hricak H, Wang L, Wei DC, Coakley FV, Akin O, Reuter VE et al. The role of preoperative endorectal magnetic resonance imaging in the decision regarding whether to preserve or resect neurovascular bundles during radical retropubic prostatectomy. *Cancer* 2004; 100(12):2655–2663
- [39] McClure TD, Margolis DJ, Reiter RE, Sayre JW, Thomas MA, Nagarajan R et al. Use of MR imaging to determine preservation of the neurovascular bundles at robotic-assisted laparoscopic prostatectomy. *Radiology* 2012; 262(3):874–883
- [40] Barrett T, Vargas HA, Akin O, Goldman DA, Hricak H. Value of the hemorrhage exclusion sign on T1-weighted prostate MR images for the detection of prostate cancer. *Radiology* 2012; 263(3):751–757
- [41] Kurhanewicz J, Swanson MG, Nelson SJ, Vigneron DB. Combined magnetic resonance imaging and spectroscopic imaging approach to molecular imaging of prostate cancer. *J Magn Reson Imaging* 2002; 16(4):451–463
- [42] Costello LC, Franklin RB. Concepts of citrate production and secretion by prostate. 1. Metabolic relationships. *Prostate* 1991; 18(1):25–46
- [43] Costello LC, Franklin RB. Concepts of citrate production and secretion by prostate: 2. Hormonal relationships in normal and neoplastic prostate. *Prostate* 1991; 19(3):181–205
- [44] Kahn T, Bürrig K, Schmitz-Dräger B, Lewin JS, Fürst G, Mödder U. Prostatic carcinoma and benign prostatic hyperplasia: MR imaging with histopathologic correlation. *Radiology* 1989; 173(3):847–851
- [45] Schiebler ML, Tomaszewski JE, Bezzi M, Pollack HM, Kressel HY, Cohen EK et al. Prostatic carcinoma and benign prostatic hyperplasia: correlation of high-resolution MR and histopathologic findings. *Radiology* 1989; 172(1):131–137
- [46] Aboagye EO, Bhujwala ZM. Malignant transformation alters membrane choline phospholipid metabolism of human mammary epithelial cells. *Cancer Res* 1999; 59(1):80–84
- [47] Daly PF, Lyon RC, Faustino PJ, Cohen JS. Phospholipid metabolism in cancer cells monitored by 31P NMR spectroscopy. *J Biol Chem* 1987; 262(31):14875–14878

- [48] Kobus T, Wright AJ, Scheenen TW, Heerschap A. Mapping of prostate cancer by 1 H MRSI. *NMR Biomed* 2014; 27(1):39–52
- [49] Kobus T, Wright AJ, Weiland E, Heerschap A, Scheenen TW. Metabolite ratios in 1 H MR spectroscopic imaging of the prostate. *Magn Reson Med* 2015; 73(1):1–12
- [50] Posse S, Otazo R, Dager SR, Alger J. MR spectroscopic imaging: principles and recent advances. *J Magn Reson Imaging* 2013; 37(6):1301–1325
- [51] Verma S, Rajesh A, Fütterer JJ, Turkbey B, Scheenen TW, Pang Y et al. Prostate MRI and 3D MR spectroscopy: how we do it. *AJR. Am J Roentgenol* 2010; 194(6):1414–1426
- [52] Cunningham CH, Vigneron DB, Chen AP, Xu D, Hurd RE, Sailasuta N et al. Design of symmetric-sweep spectral-spatial RF pulses for spectral editing. *Magn Reson Med* 2004; 52(1):147–153
- [53] Mescher M, Merkle H, Kirsch J, Garwood M, Gruetter R. Simultaneous in vivo spectral editing and water suppression. *NMR Biomed* 1998; 11(6):266–272
- [54] Schrickler AA, Pauly JM, Kurhanewicz J, Swanson MG, Vigneron DB. Dualband spectral-spatial RF pulses for prostate MR spectroscopic imaging. *Magn Reson Med* 2001; 46(6):1079–1087
- [55] Star-Lack J, Nelson SJ, Kurhanewicz J, Huang LR, Vigneron DB. Improved water and lipid suppression for 3D PRESS CSI using RF band selective inversion with gradient dephasing (BASING). *Magn Reson Med* 1997; 38(2):311–321
- [56] Weinreb JC, Blume JD, Coakley FV, Wheeler TM, Cormack JB, Sotko CK et al. Prostate cancer: sextant localization at MR imaging and MR spectroscopic imaging before prostatectomy—results of ACRIN prospective multi-institutional clinicopathologic study. *Radiology* 2009; 251(1):122–133
- [57] Heerschap A, Jager GJ, van der Graaf M, Barentsz JO, Ruijs SH. Proton MR spectroscopy of the normal human prostate with an endorectal coil and a double spin-echo pulse sequence. *Magn Reson Med* 1997; 37(2):204–213
- [58] Yakar D, Heijmink SW, Hulsbergen-van de Kaa CA, Huisman H, Barentsz JO, Fütterer JJ et al. Initial results of 3-dimensional 1H-magnetic resonance spectroscopic imaging in the localization of prostate cancer at 3 Tesla: should we use an endorectal coil? *Invest Radiol* 2011; 46(5):301–306
- [59] Hegde JV, Mulkern RV, Panych LP, Fennessy FM, Fedorov A, Maier SE et al. Multiparametric MRI of prostate cancer: an update on state-of-the-art techniques and their performance in detecting and localizing prostate cancer. *J Magn Reson Imaging* 2013; 37(5):1035–1054
- [60] Fütterer JJ, Scheenen TW, Heijmink SW, Huisman HJ, Hulsbergen-Van de Kaa CA, Witjes JA et al. Standardized threshold approach using three-dimensional proton magnetic resonance spectroscopic imaging in prostate cancer localization of the entire prostate. *Invest Radiol* 2007; 42(2):116–122
- [61] Jung JA, Coakley FV, Vigneron DB, Swanson MG, Qayyum A, Weinberg V et al. Prostate depiction at endorectal MR spectroscopic imaging: investigation of a standardized evaluation system. *Radiology* 2004; 233(3):701–708
- [62] Scheenen TW, Fütterer J, Weiland E, van Hecke P, Lemort M, Zechmann C et al. Discriminating cancer from noncancer tissue in the prostate by 3-dimensional proton magnetic resonance spectroscopic imaging: a prospective multicenter validation study. *Investigative Radiology* 2011; 46(1):25–33
- [63] Beyersdorff D, Taupitz M, Winkelmann B, Fischer T, Lenk S, Loening SA et al. Patients with a history of elevated prostate-specific antigen levels and negative transrectal US-guided quadrant or sextant biopsy results: value of MR imaging. *Radiology* 2002; 224(3):701–706
- [64] Haider MA, van der Kwast TH, Tanguay J, Evans AJ, Hashmi AT, Lockwood G et al. Combined T2-weighted and diffusion-weighted MRI for localization of prostate cancer. *AJR. Am J Roentgenol* 2007; 189(2):323–328
- [65] Kim CK, Park BK, Lee HM, Kwon GY. Value of diffusion-weighted imaging for the prediction of prostate cancer location at 3 T using a phased-array coil: preliminary results. *Invest Radiol* 2007; 42(12):842–847
- [66] Lim HK, Kim JK, Kim KA, Cho KS. Prostate cancer: apparent diffusion coefficient map with T2-weighted images for detection—a multireader study. *Radiology* 2009; 250(1):145–151
- [67] Qayyum A, Coakley FV, Lu Y, Olpin JD, Wu L, Yeh BM et al. Organ-confined prostate cancer: effect of prior transrectal biopsy on endorectal MRI and MR spectroscopic imaging. *AJR. Am J Roentgenol* 2004; 183(4):1079–1083
- [68] Kim JK, Hong SS, Choi YJ, Park SH, Ahn H, Kim CS et al. Wash-in rate on the basis of dynamic contrast-enhanced MRI: usefulness for prostate cancer detection and localization. *J Magn Reson Imaging* 2005; 22(5):639–646
- [69] Ocak I, Bernardo M, Metzger G, Barrett T, Pinto P, Albert PS et al. Dynamic contrast-enhanced MRI of prostate cancer at 3 T: a study of pharmacokinetic parameters. *AJR. Am J Roentgenol* 2007; 189(4):849
- [70] White S, Hricak H, Forstner R, Kurhanewicz J, Vigneron DB, Zaloudek CJ et al. Prostate cancer: effect of postbiopsy hemorrhage on interpretation of MR images. *Radiology* 1995; 195(2):385–390
- [71] Park KK, Lee SH, Lim BJ, Kim JH, Chung BH. The effects of the period between biopsy and diffusion-weighted magnetic resonance imaging on cancer staging in localized prostate cancer. *BJU Int* 2010; 106(8):1148–1151
- [72] Rosenkrantz AB, Mussi TC, Hindman N, Lim RP, Kong MX, Babb JS et al. Impact of delay after biopsy and post-biopsy haemorrhage on prostate cancer tumour detection using multi-parametric MRI: a multi-reader study. *Clin Radiol* 2012; 67(12):e83–e90
- [73] Tamada T, Sone T, Jo Y, Yamamoto A, Yamashita T, Egashira N et al. Prostate cancer: relationships between postbiopsy hemorrhage and tumor detectability at MR diagnosis. *Radiology* 2008; 248(2):531–539
- [74] Belaroussi B, Milles J, Carme S, Zhu YM, Benoit-Cattin H. Intensity non-uniformity correction in MRI: existing methods and their validation. *Med Image Anal* 2006; 10(2):234–246
- [75] Rosenkrantz AB, Bennett GL, Doshi A, Deng FM, Babb JS, Taneja SS. . . T2-weighted imaging of the prostate: Impact of the BLADE technique on image quality and tumor assessment. *Abdom Imaging* 2015; 40(3):552–559
- [76] Mazaheri Y, Vargas HA, Nyman G, Akin O, Hricak H. Image artifacts on prostate diffusion-weighted magnetic resonance imaging: trade-offs at 1.5 Tesla and 3.0 Tesla. *Acad Radiol* 2013; 20(8):1041–1047
- [77] Kuhl CK, Gieseke J, von Falkenhausen M, Textor J, Gernert S, Sonntag C et al. Sensitivity encoding for diffusion-weighted MR imaging at 3.0 T: intraindividual comparative study. *Radiology* 2005; 234(2):517–526
- [78] Wagner M, Rief M, Busch J, Scheurig C, Taupitz M, Hamm B et al. Effect of butylscopolamine on image quality in MRI of the prostate. *Clin Radiol* 2010; 65(6):460–464
- [79] Roethke MC, Kuru TH, Radbruch A, Hadaschik B, Schlemmer HP. Prostate magnetic resonance imaging at 3 Tesla: Is administration of hyoscine-N-butyl-bromide mandatory? *World J Radiol* 2013; 5(7):259–263
- [80] Sankineni S, Osman M, Choyke PL. Functional MRI in prostate cancer detection. *Biomed Res Int* 2014; 2014:590638
- [81] Medved M, Sammet S, Yousuf A, Oto A. MR imaging of the prostate and adjacent anatomic structures before, during, and after ejaculation: qualitative and quantitative evaluation. *Radiology* 2014; 271(2):452–460

4 Diffusion-Weighted Imaging of the Prostate

François Cornud

4.1 Introduction

Historically, conventional T2-weighted MRI was applied clinically largely for local staging of prostate cancer in order to assess whether the tumor was organ confined. However, more recently, additional sequences including dynamic contrast-enhanced MRI (DCE-MRI), magnetic resonance spectroscopic imaging (MRSI), and diffusion-weighted MRI (DWI) have emerged, leading to the concept of multiparametric MRI that is now routinely applied in the management of prostate cancer (PCa).¹ Among these, DWI is the sequence that currently has gained the widest acceptance, owing to its high accuracy in localization of tumor foci in the prostate. Specifically, the loss of luminal and ductal spaces as well as the increased cellular density, that occur in prostate cancer contribute to “free” diffusion of water molecules, as is assessed by diffusion-weighted imaging (DWI).² Furthermore, DWI has a potential role as a noninvasive biomarker for tumor aggressiveness.³ This chapter reviews the technical aspects of DWI and the clinical impact of DWI on the management of prostate cancer.

4.2 Technical Aspects

Conventional MRI is based on the ^1H signal from water ($^1\text{H}_2\text{O}$). Water molecules of the body have constant random brownian motion, a property that is explored by DWI. The high concentration of $^1\text{H}_2\text{O}$ provides a strong signal from which an image can be generated. Nonetheless, the contrast mechanism of DWI is distinct from that of conventional MRI.⁴ DWI studies the

displacement of water molecules during the interval between the application of two diffusion-sensitizing gradients. In simple fluids, $^1\text{H}_2\text{O}$ diffusion is “free”. However, in biologic tissues, diffusion is restricted given the impedance to the displacement of water molecules, largely by cell membranes. The extent of restriction to motion of water molecules is in proportion to the cellular density (► Fig. 4.1).

In tissues with less dense cellularity, $^1\text{H}_2\text{O}$ can move relatively freely in the extracellular space.² However, cellularity, and thus the presence of cell membranes, generally increases in tumor tissues. Cell membranes are hydrophobic and act as obstacles to molecular motion of water within the extracellular space, thereby resulting in diffusion restriction.

To measure water motion using DWI, the most common sequence used is a single-shot echo-planar-imaging spin-echo pulse sequence (► Fig. 4.2), in which rectangular gradient pulses of equal strength are applied before and after the 180-degree refocusing pulse.⁴ The first gradient pulse causes an initial dephasing of the water molecules. Water molecules that are static will be completely rephased by the second gradient pulse, without any significant change in the measured signal intensity.² In comparison, water molecules that are moving will not be completely rephased by the second gradient pulse due to the displacement, thus leading to a signal loss on the acquired DWI (► Fig. 4.2). The strength of these gradient pulses, in part determined by the gradient’s amplitude, is reflected by the b value of the DWI sequence. Use of stronger gradient pulses (indicated by a greater b value) increases the sensitivity of the DWI sequence to water motion.

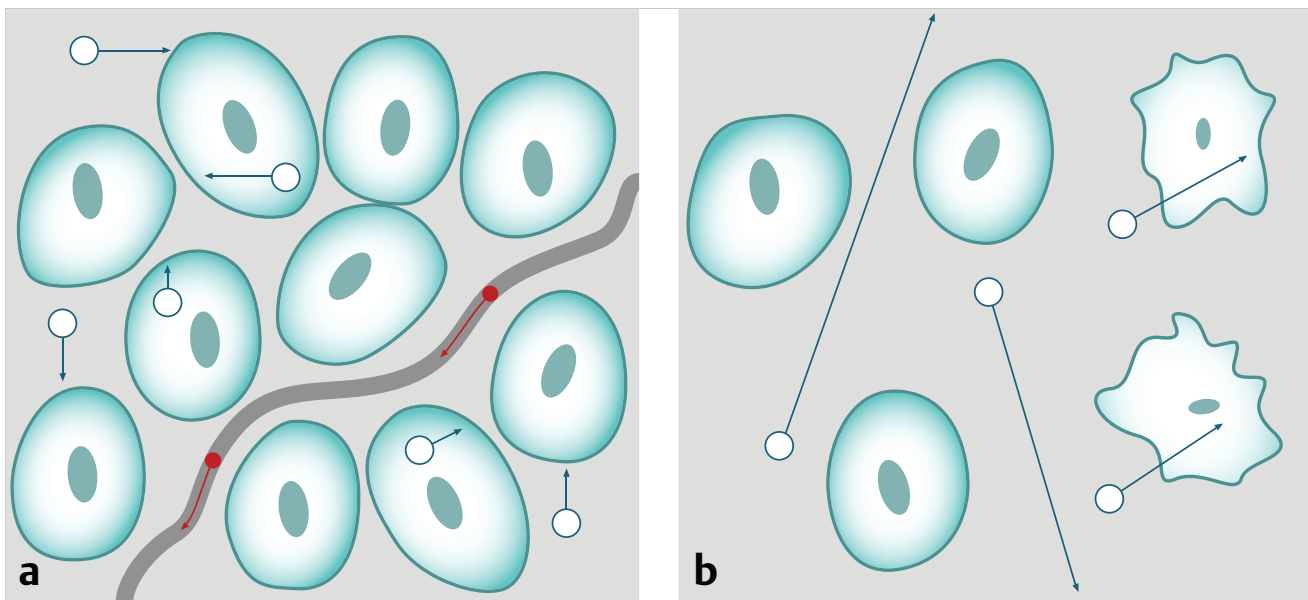


Fig. 4.1 Diffusion of water molecules. (a) Tissue with a high cellular density and intact cell membranes. Water molecules within the extracellular space (white arrows) have impeded diffusion because the extracellular space is small, and cell membranes present a barrier to “free” diffusion of the water molecules. Water molecules of the capillary network (red arrows), which are also evaluated by diffusion-weighted imaging (DWI), move faster, thereby impacting diffusion metrics. (b) Tissue with a low (or absent) cellular density and/or defective cell membranes. The extracellular space is increased and “free” diffusion of water molecules, particularly between the extracellular and intracellular spaces, is greater.

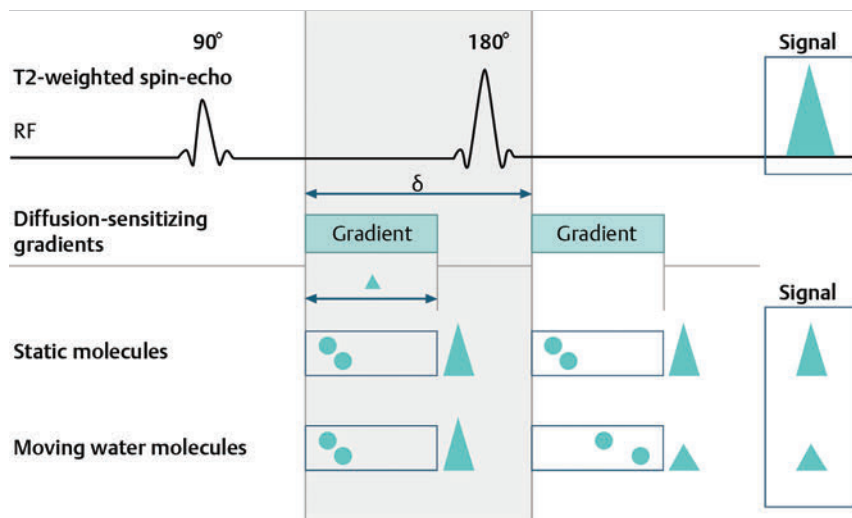


Fig. 4.2 Water diffusion metrics. Two rectangular gradient pulses of equal strength are applied before and after the 180-degree refocusing pulse of the fast spin-echo sequence. δ (diffusion time) is the time interval between the two gradient lobes, and Δ (gradient duration) is the overall time interval during which the gradients are applied. Static water molecules will be completely rephased by the second gradient pulse without any significant change in the measured signal intensity (signal). Moving water molecules will not be completely rephased by the second gradient pulse due to the displacement, thus leading to a signal loss on the diffusion-weighted imaging sequence.

This paragraph provides sample acquisition parameters for performing DWI. Selection of these parameters must take into consideration the presence of susceptibility and distortion artifacts that are commonly encountered on DW images.⁴ For instance, the echo time (TE) should be set to the minimum value possible to help reduce such artifacts. Parallel imaging with a reduction factor of 2 (or occasionally 3 if there is a very high signal-to-noise ratio [SNR]) also helps reduce distortion artifacts, in part by allowing for a decreased TE, and thus should routinely be used. The field of view (FOV, approximately 220×220 mm) is reduced to fit the prostate. A slice thickness of 3.0 to 3.5 mm and a matrix size of approximately 108×108 are used to provide both sufficient SNR and spatial resolution. Oversampling is applied in order to prevent aliasing artifacts that may occur given the reduced FOV. The resulting resolution (approximately $1.2 \times 1.2 \times 3.5$ mm³) allows for the registration of DWI with T2W images, which may help readers identify suspicious foci.⁵ The receiver bandwidth is set to 1,493 Hz in the readout direction in order to prevent chemical shift artifacts. Multiple slice excitations and signal averages (for instance, 10–20 signal averages) over an extended acquisition duration improve the signal- and contrast-to-noise (CNR) ratios. Using modern systems, it may be possible to obtain different numbers of signal averages for each acquired b value, thereby allowing for obtaining a particularly high number of signal averages for the highest b values in a time-efficient manner. A total acquisition time of 5 to 8 minutes may be reasonable to allow for enough signal averages to attain sufficient SNR.

If a rectal coil is being used, then thinner partitions (2.5 mm) and an even smaller FOV can be acquired, whether at 3T or 1.5T,⁶ in order to improve spatial resolution and decrease artifacts, despite a resulting loss in SNR and CNR. In evaluating this trade-off, Medved et al showed that the higher spatial resolution (voxel size of 3.1 vs 6.7 mm³) outweighed the decrease in CNR and provided significantly better lesion conspicuity and overall image quality.⁶ This sequence adjustment may help improve the detection of small or sparse prostate cancers.

Qualitative assessment of prostate DWI consists of a visual assessment of the extent of signal attenuation within tissues on DW images. This assessment incorporates two data sets: the apparent diffusion coefficient (ADC) map and the high b-value source images.

4.3 High b Value Images

Diffusion-weighted images with a high b value ($b \geq 800$ s/mm²) are routinely acquired in order to increase the conspicuity of tumor foci within the prostate. Higher b values provide greater contrast between tissues based on differences in the extent of signal attenuation of water molecules. At b values less than 800 s/mm², visual detection of tumors using DW images is limited given the strong contributions of T2 weighting to the images at such b values. As a result, the displayed signal intensity reflects both water diffusion and T2 relaxation times. Benign glandular prostate tissue may have a long T2 relaxation time and thus maintains a high signal intensity on DW images that may obscure increased signal intensity within tumors (► Fig. 4.3). This obscuring of tumors relating to T2 shine-through effects may be commonly encountered even when using a high b value of 800 to 1000 s/mm². One study reported that within this b-value range, tumors were visible in fewer than half of cases.⁷

One approach to increase tumor visibility is to use a short TE (≤ 90 ms) in order to decrease the T2 weighting and thus reduce the T2 shine-through effect. A more powerful approach to increase the conspicuity of tumor foci is to select an ultrahigh b value ($b \geq 1400$ s/mm²), which increases diffusion weighting even further, providing greater suppression of the benign prostate (► Fig. 4.4) and thus improving the sensitivity of source DW images for PCa detection compared with standard high b values (► Fig. 4.5).

In a study of 41 patients with biopsy-proven prostate cancer imaged at 3T with 5 b values (0, 1000, 1500, 2000, 2500 s/mm²), Metens et al reported the highest tumor visibility at $b = 1500$ s/mm² and $b = 2000$ s/mm², as well as the best CNR at $b = 1500$ s/mm², thus supporting the use of ultrahigh b values.⁸ Likewise, in a study of 201 patients undergoing radical prostatectomy as the reference standard, Katahira et al showed a significantly higher sensitivity (73.2%), specificity (89.7%), and accuracy (84.2%) using $b = 2000$ -s/mm² images than using $b = 1000$ -s/mm² images (sensitivity: 61.2%, specificity: 82.6%, accuracy: 75.5%), for results pooled among three independent readers.⁹ Such results were confirmed in the study by Rosenkrantz et al, who showed, in a series of 29 patients, also with radical prostatectomy serving as the reference standard, the

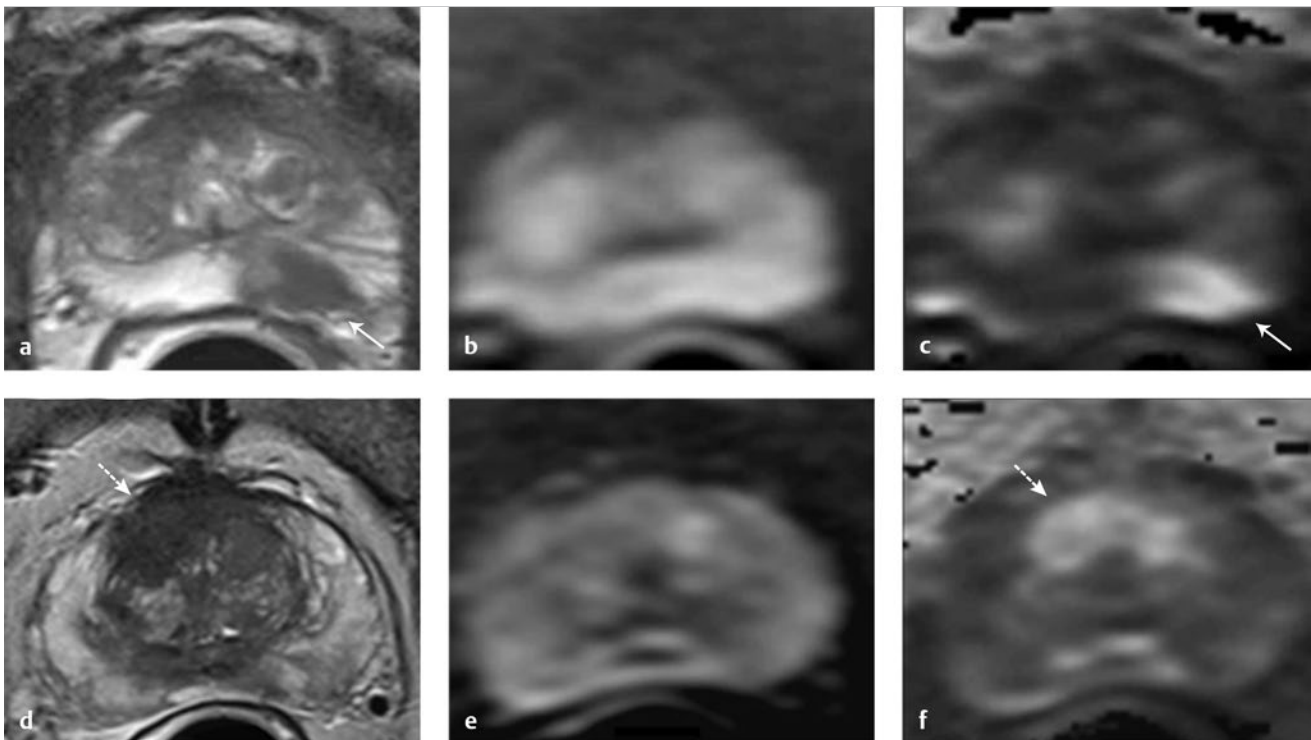


Fig. 4.3 T2 shine-through effect. The left posterior peripheral zone tumor (*solid arrow*) and the right anterior transition zone tumor (*dashed arrow*) are depicted on the T2-weighted image (a,d), although they are not visualized on the $b = 1000 \text{ s/mm}^2$ diffusion-weighted sequence (b,e), in part due to the T2 shine-through effect resulting from the long T2 relaxation time of the benign glandular prostate tissue. However, the lesions are well-visualized on the $b = 1600 \text{ s/mm}^2$ DW image (*arrow*; c,f) given the greater strength of diffusion weighting and decreased T2 shine-through effect.

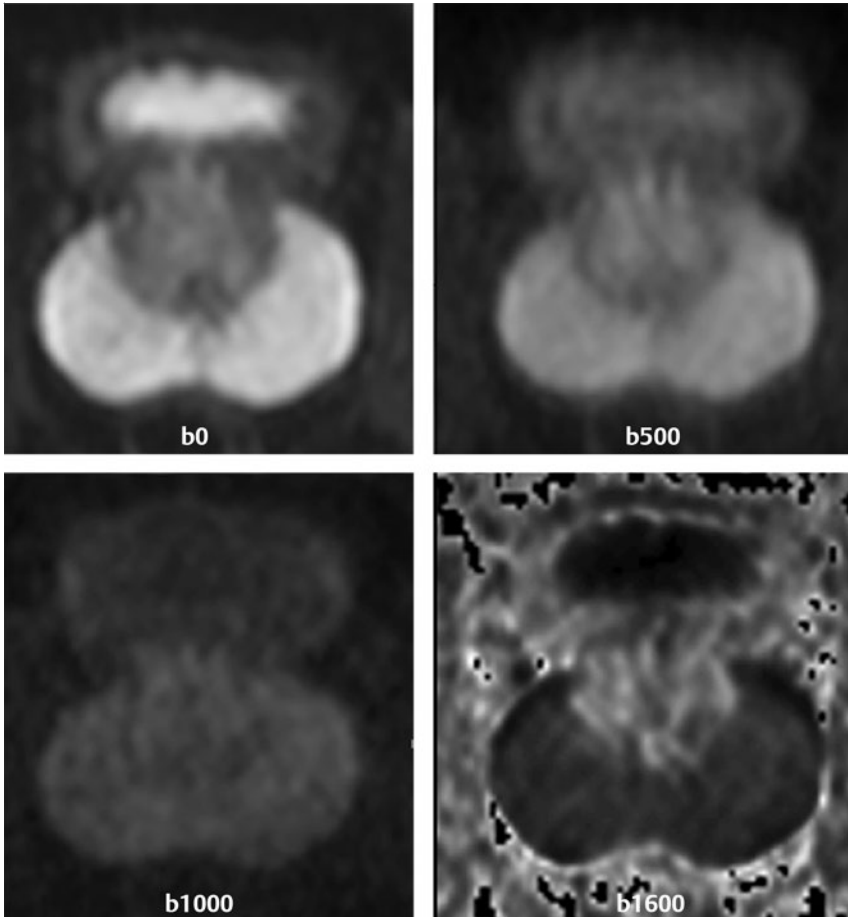


Fig. 4.4 Suppression of the benign prostate increases progressively as the b value increases from 50 s/mm^2 (low) to 500 s/mm^2 (intermediate) to 1000 s/mm^2 (high) and to 1600 s/mm^2 (ultrahigh; a computed DWI in this example), given the increasing strength of diffusion weighting at higher b values.

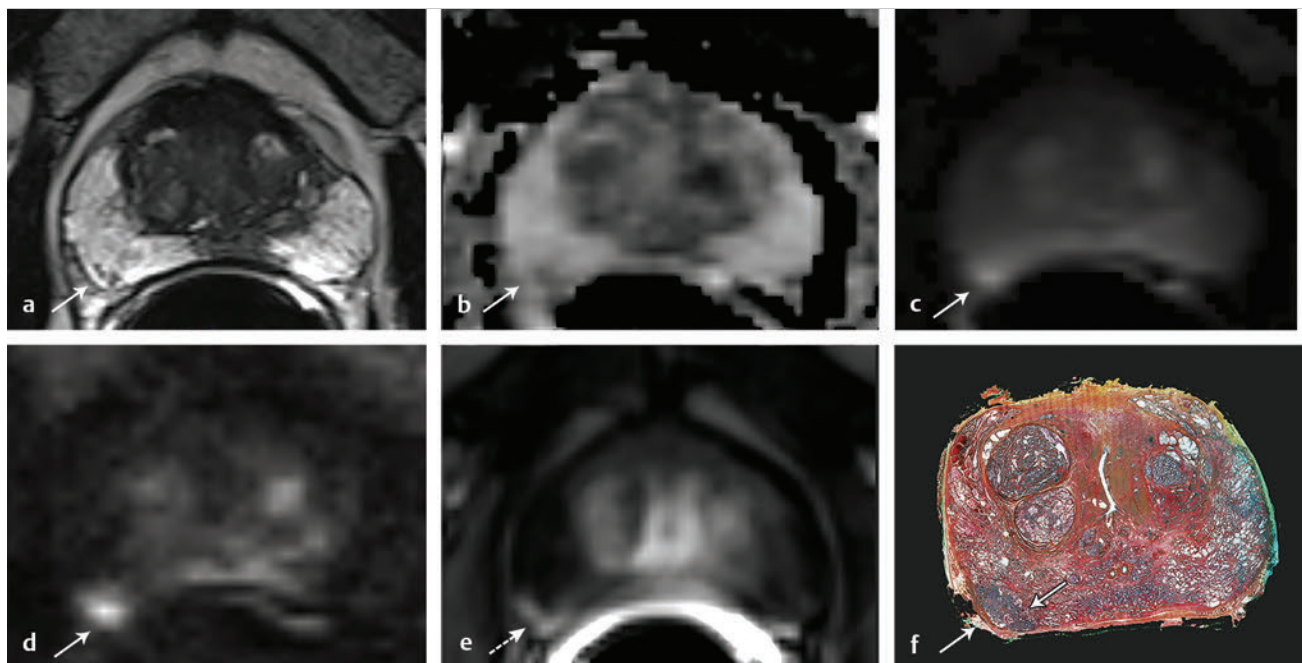


Fig. 4.5 Increased conspicuity of a right posterior peripheral zone tumor (*arrow*) on the $b = 2000 \text{ s/mm}^2$ image (d) compared with the $b = 1000 \text{ s/mm}^2$ image (c). Note that the tumor is barely visible on the T2-weighted image (a) and on the apparent diffusion coefficient map (b). Dynamic contrast-enhanced MRI (e) shows increased periprostatic enhancement (*dashed arrow*) in the region of a vessel but does not clearly show increased enhancement in the tumor. Histopathology from the radical prostatectomy (f) showed a Gleason score 4+3 tumor (*arrows*) with minimal extraprostatic extension.

significantly higher sensitivity of DW images, interpreted by two independent readers, acquired at $b = 2000 \text{ s/mm}^2$ compared to those acquired at $b = 1000 \text{ s/mm}^2$ for detecting tumor foci.¹⁰

Despite the value of ultrahigh b values for tumor detection, the direct acquisition of such b values is challenging. As the b value passes 1000 s/mm^2 , the presence of artifacts increases to potentially very pronounced levels, and the SNR may become very low, thereby degrading image quality. A longer TE may be required in order to acquire ultrahigh b -value DW images on some systems, thereby contributing to the greater distortions artifacts. While more signal averages may be used to help maintain sufficient SNR, this in turn prolongs the overall scan time. Sufficient SNR at ultrahigh b values is optimally provided through use of a 3-T system or use of an endorectal coil at 1.5 T. To circumvent this limitation, an alternative solution is to calculate the ultrahigh b value ($\geq 1400 \text{ s/mm}^2$) images from a set of lower b -value images by extrapolating the signal decay of the DW curve. This approach is already commercially available on some MR platforms (► Fig. 4.6). These computed ultrahigh b -value DW images provide the image contrast of directly acquired ultrahigh b -value images, which helps improve tumor detection, yet without any additional acquisition time in comparison with that needed to acquire standard b -value images. Furthermore, these images avoid the technical challenges inherent in avoiding greater distortion artifacts when directly acquiring the ultrahigh b -value images, for instance, not requiring any adjustment in TE.

Several studies report clinical utility of computed ultrahigh b values, using as a reference standard either biopsy findings¹¹

¹² or histology from radical prostatectomy.¹³ For instance, Maas et al in a series of 42 patients with biopsy-proven PCa, imaged at 3 T using a pelvic phased-array coil, reported that the CNR of acquired and computed DWI at a b value of 1400 s/mm^2 was similar.¹¹ They concluded that calculated DWI could be used in place of acquired DWI at $b = 1400 \text{ s/mm}^2$ as a means of increasing the conspicuity of tumor foci. Moreover, the authors also showed that lesion conspicuity could be improved even further using calculated DW images by increasing the calculated b value up to 5000 s/mm^2 (► Fig. 4.7).

These results were confirmed in the study by Rosenkrantz et al performed at 3 T using a pelvic phased-array coil and acquired b values of 50, 1000, and 1500 s/mm^2 .¹³ The authors reported that the numerous measures of quality and diagnostic performance of the DW sequence (suppression of benign tissue, reduced distortion, absence of artifacts, sensitivity, and positive predictive values for tumor detection and tumor-to-peripheral zone contrast) were equal or superior using computed DW images at $b = 1500 \text{ s/mm}^2$ than using the directly acquired $b = 1000$ - or 1500 - s/mm^2 images for interpretation by two independent readers.

In a third study of 106 patients with PCa proven by MRI-TRUS image fusion biopsy, Grant et al compared acquired and calculated $b = 2000 \text{ s/mm}^2$ images at 3 T.¹² Although image quality was slightly inferior for the calculated images in their study, tumor visibility was similar between the two image sets.

Given these considerations, it currently is recommended to incorporate some implementation of ultrahigh b -value DWI ($b \geq 1400 \text{ s/mm}^2$) within routine clinical protocols. Depending upon the gradient performance, coil design, and software platform, DWI with directly acquired b values greater than

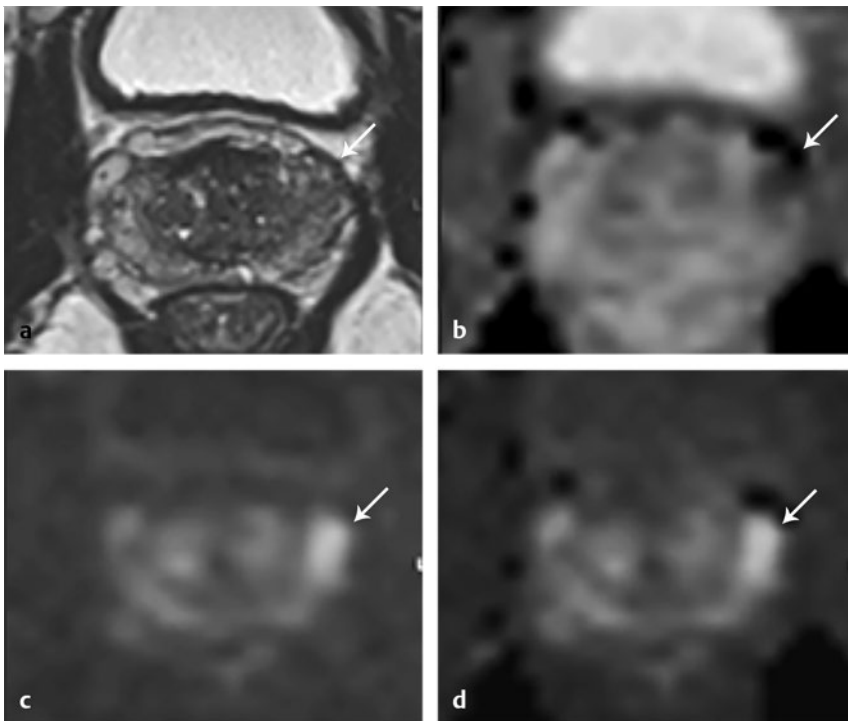


Fig. 4.6 Left anterior peripheral zone tumor (arrow) that is clearly visualized on apparent diffusion coefficient map (b) although not well seen on T2-weighted MRI (a). The lesion has similar conspicuity on an acquired $b = 1600 \text{ s/mm}^2$ diffusion-weighted image (DWI) (c) and a $b = 1600 \text{ s/mm}^2$ DWI computed from data for DWI at b values of 50, 500, and 1000 s/mm^2 (d).

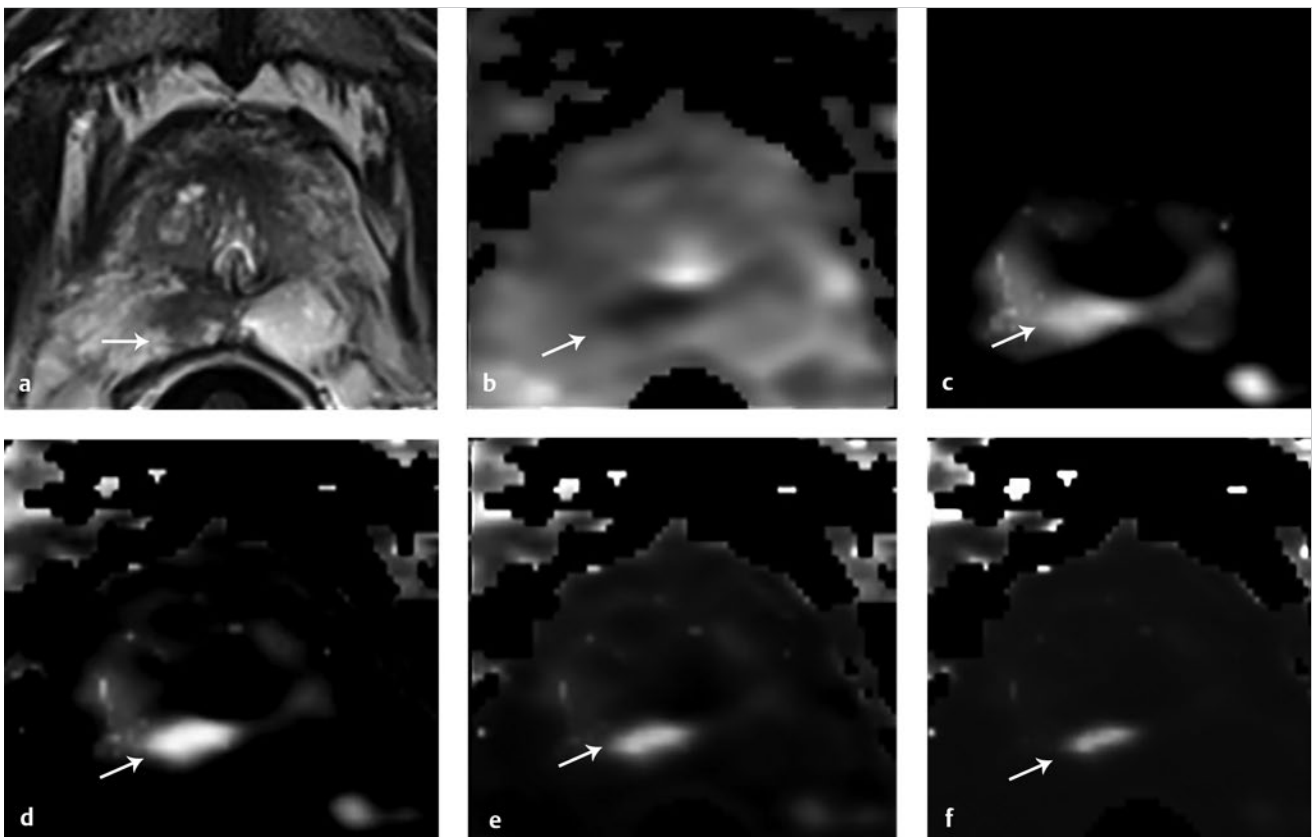


Fig. 4.7 Right posterior peripheral zone lesion (arrow) is visualized on T2-weighted MRI (a), apparent diffusion coefficient map (b), and $b = 1000 \text{ s/mm}^2$ diffusion-weighted image (DWI) (c). On computed b-value DWI, contrast between the lesion and benign peripheral zone increases as the computed b-value increases further to 2000 s/mm^2 (d), 3000 s/mm^2 (e), and 5000 s/mm^2 (f) due to the increasing suppression of the benign prostate. (Computed b value images prepared using Olea Medical Systems, La Ciotat, France.)

1000 s/mm² may be prohibitive in clinical practice. Thus, the feasibility of incorporating ultrahigh b-value DWI is facilitated by computed DWI. However, computed DWI is not currently available for all MR systems. Thus, some practices will still need to acquire these ultrahigh b-value DWI directly, taking all steps possible to reduce associated artifacts. One important measure that helps to decrease distortion artifacts on DWI is ensuring that the rectum is empty of air. If an endorectal coil is used, then it is recommended to inflate the coil with perfluorocarbon or fluids containing manganese, such as pineapple juice, which substantially lessen the signal brightness on T2W and DW sequences. When not using an endorectal coil, technologists should be trained to instruct the patient to evacuate their rectum before starting the examination. Additional approaches that some practices employ to help reduce rectal gas for non-endorectal coil exams include administration of a rectal laxative 1 to 2 hours before the MRI and aspiration of rectal gas using a female bladder catheter just before the examination, once the patient is on the table. Although not standard among all centers, such simple precautions may help ensure a collapsed rectum in most cases.

It is anticipated that continued improvements in MRI hardware and software will improve the quality of acquired DWI and the clinical availability of computed DWI, which in turn will enhance the diagnostic performance of mpMRI. For instance, DWI at $b \geq 1400$ s/mm² may help differentiate prostate cancer from focal prostatitis in the peripheral zone (PZ) (► Fig. 4.8) and possibly from stromal benign prostatic hyperplasia (BPH) nodules in the transition zone (TZ) (► Fig. 4.9).

Whereas prostatitis and stromal BPH often show increased signal on DWI at $b = 1000$ s/mm², this signal (for prostatitis more so than for stromal BPH) is more likely to be suppressed at ultrahigh b values. In comparison, prostate cancer, given its increased degree of impeded diffusion relative to these benign entities, remains hyperintense at the ultrahigh b values. Thus, it is expected that incorporation of DWI at $b \geq 1400$ s/mm² may improve the diagnostic performance of the Prostate Imaging-

Reporting and Data System (PI-RADS) particularly in the characterization of equivocal lesions (PI-RADS assessment category 3).

4.4 The Apparent Diffusion Coefficient Map

Data obtained from DWI performed at different b values allows for a quantitative analysis. Although such an analysis is possible using only two b values, three b values are most commonly obtained in clinical practice: one low (50 or 100 s/mm²), one intermediate (400 or 500 s/mm²), and one high (800 or 1000 s/mm²). A b value of 0 is generally avoided for the low b value in order to avoid the influence of the early capillary component on the measured diffusion signal (see below). By plotting the logarithm of the measured signal intensity on the y-axis against the b values on the x-axis, a line can be traced through the points for each of the acquired b values whose slope characterizes the ADC of the given tissue (► Fig. 4.10).

The ADC is interpreted to represent the net displacement of water molecules over a timescale reflecting the diffusion-sensitizing gradients applied during the DWI acquisition. The use of several b values helps improve the fit of the curve and potentially minimize errors in the ADC calculation. Current MR systems and workstations can automatically calculate the ADC value for each pixel and display the results as a parametric map. The ADC map is not affected by the T2 shine-through effects that impact the source DW images. However, measured ADC values are inversely correlated with the highest b-value used during the acquired sequence. Regions of interest are used to obtain ADC measurements within suspicious focal areas within the prostate. Low ADC values within an area indicate the presence of restricted diffusion. Such areas exhibit a low signal intensity on the ADC map in contrast with their high signal intensity on the source DW images, in both instances reflecting the same underlying phenomenon (► Fig. 4.8; ► Fig. 4.11).

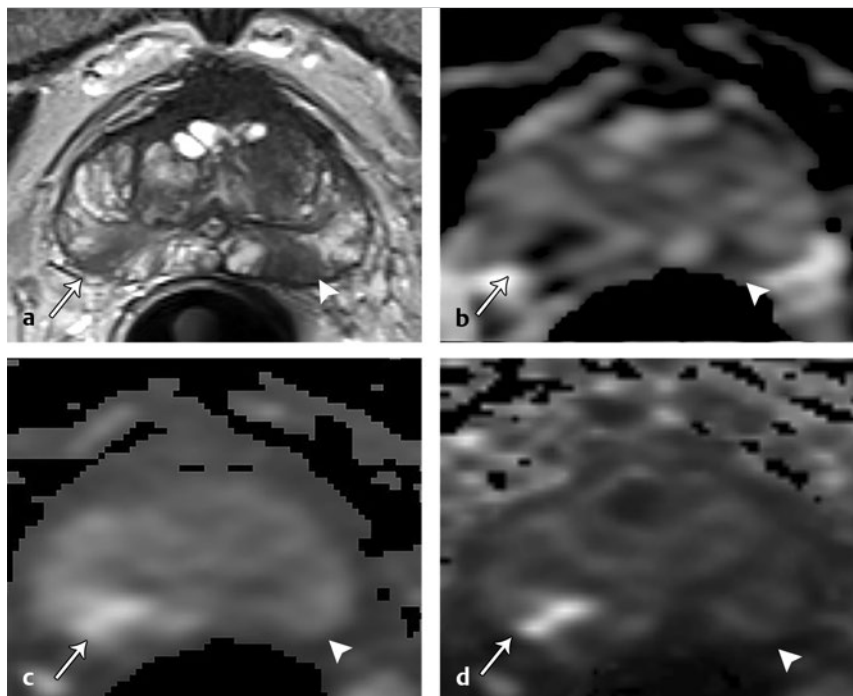


Fig. 4.8 Differentiation of prostate cancer from focal prostatitis in the peripheral zone. Decreased signal is present in the posterior right (arrow) and posterior left (arrowhead) peripheral zones on T2-weighted images (a), with a wedge/linear shape on the right and a more masslike configuration on the left. However, the apparent diffusion coefficient map (b) and $b = 1000$ s/mm² diffusion-weighted image (DWI) (c) show greater diffusion restriction on the right. Computed $b = 1600$ s/mm² DWI (d) shows increased signal only for the lesion on the right. Histologic evaluation revealed a Gleason score 3+4 tumor on the right and prostatitis on the left.

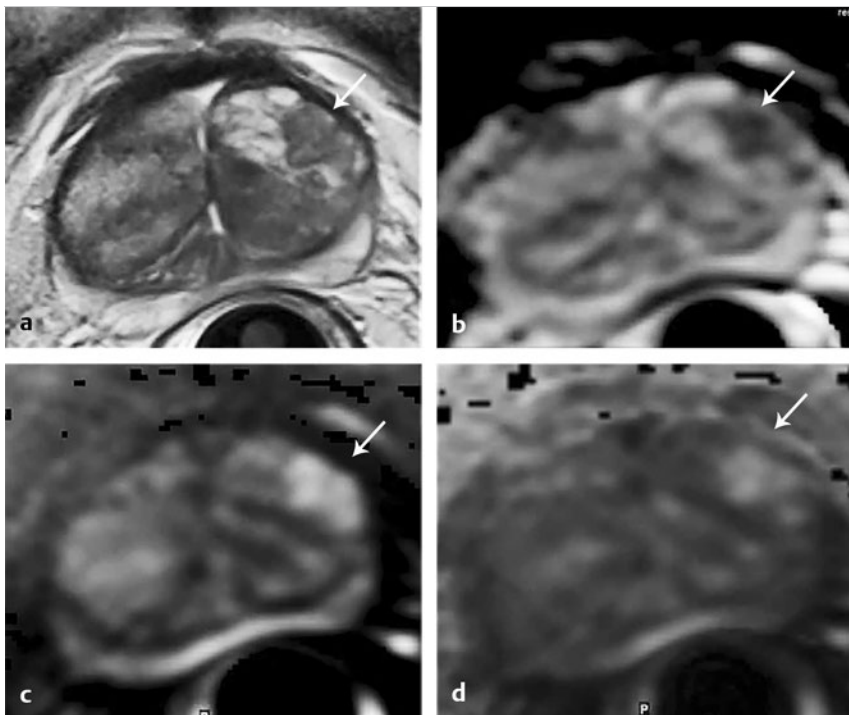


Fig. 4.9 Characterization of a stromal benign prostatic hyperplasia (BPH) nodule in the transition zone. The left anterior transition zone lesion (arrow) is hypointense on diffusion-weighted imaging (a), although only partly encapsulated. The lesion is dark on the apparent diffusion coefficient map (b) and hyperintense on the $b = 1000 \text{ s/mm}^2$ diffusion-weighted image (DWI) (c). The degree of hyperintensity is less pronounced on the $b = 2000 \text{ s/mm}^2$ DWI (d) than on the $b = 1000 \text{ s/mm}^2$ DWI. Targeted biopsies using MRI- transrectal ultrasound fusion demonstrated a BPH nodule.

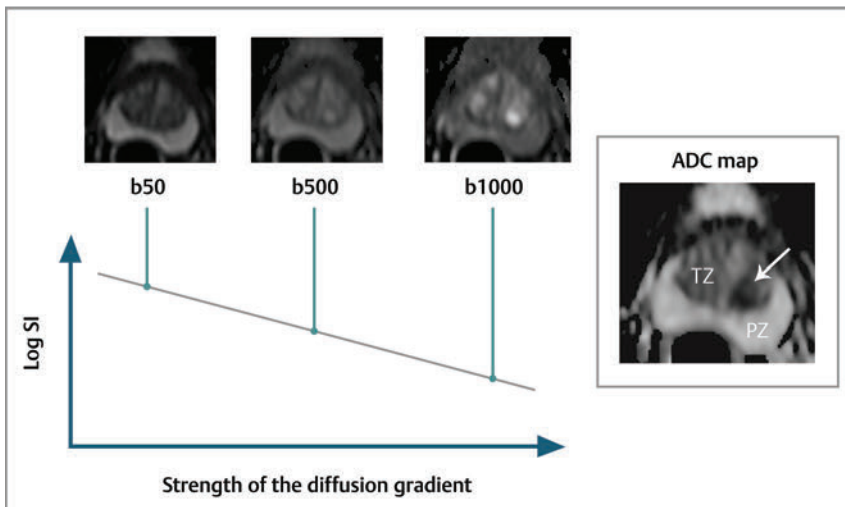


Fig. 4.10 Apparent diffusion coefficient (ADC) calculation by monoexponential diffusion-weighted imaging. Logarithm of signal (Log SI) is plotted against each b value for each image voxel acquired at the same anatomical position. This process is repeated for all voxels, and the results are depicted as a parametric map of ADC values. On the ADC map, the normal peripheral zone (PZ) exhibits high ADC, greater than that of benign prostatic hyperplasia (BPH) within the transition zone (TZ). The left posterior transition zone lesion (arrow), abutting the surgical capsule, is a stromal BPH nodule, although exhibiting increased signal on the $b = 1000 \text{ s/mm}^2$ diffusion-weighted image and decreased ADC.

Several studies have evaluated the b value that optimizes tumor visibility on the ADC map. Kim et al.¹⁴ reported in a series of 48 patients that focal lesions were more conspicuous on the ADC map when constructed from a maximal b value of $1,000 \text{ s/mm}^2$ than from one of $2,000 \text{ s/mm}^2$. Similarly, Kitajima et al.¹⁵ reported that in 26 patients with biopsy-proven PCa, the lesion conspicuity on the ADC map calculated using a maximal b value of 2000 s/mm^2 was not superior to that calculated using a maximum b value of 1000 s/mm^2 . Moreover, Rosenkrantz et al.¹⁰ despite observing a higher diagnostic performance of source $b = 2000 \text{ s/mm}^2$ images than of source $b = 1000 \text{ s/mm}^2$ images, reported no difference in sensitivity from a visual analysis between ADC maps calculated using these two b values ($p \geq 0.309$).

These findings suggest that calculation of the ADC map should not incorporate b values $> 1,000 \text{ s/mm}^2$. Even if using b values up to 1000 s/mm^2 , the optimal selection of b values

within this range remains controversial. Thormer et al.¹⁶ evaluated 41 patients with biopsy-proven PCa at 3 T using an endorectal coil before prostatectomy. Four combinations of b values ($0-800$, $50-800$, $400-800$ and $0-50-400-800 \text{ s/mm}^2$) were used to calculate the ADC map, and tumor conspicuity was visually assessed on each map by three independent radiologists. The best tumor conspicuity was obtained with ADC maps calculated from b values of $50-800 \text{ s/mm}^2$, followed by b values of $0-800 \text{ s/mm}^2$. Currently, the PI-RADS version 2 guidelines recommend acquiring three b values (low, intermediate, and high, as previously noted), avoiding a b value of 0. While incorporation of an ultrahigh b value is also advised, this should not be acquired as part of the multi- b -value DWI acquisition that is used for generating the ADC map. Rather, if the ultrahigh b -value images cannot be computed from the acquired lower b -value data, then it is advised that direct acquisition of the ultrahigh b -value images be accomplished in a second, separate DW

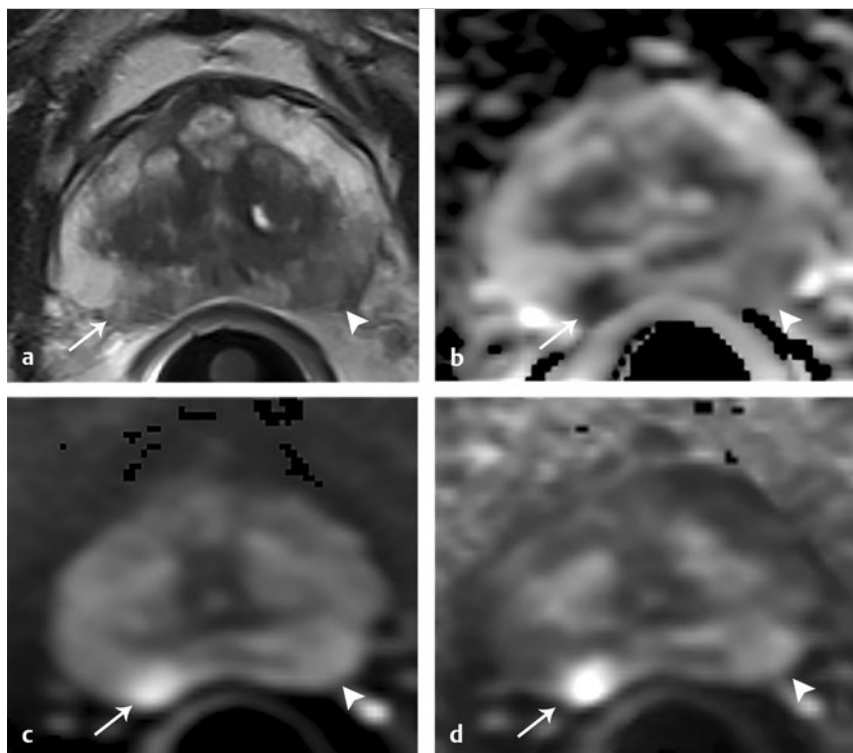


Fig. 4.11 Apparent diffusion coefficient (ADC) map in the peripheral zone. The diffusion-weighted image (DWI) (a) shows decreased signal within the posterior peripheral zone on both the right (arrow) and the left (arrowhead). The ADC map (b) shows marked hypointensity only for the lesion on the right, and the $b = 1000 \text{ s/mm}^2$ DWI (c) shows marked hyperintensity also only for the lesion on the right. Conspicuity of the lesion on the right increases further on the computed $b = 1600 \text{ s/mm}^2$ DWI (d). Targeted biopsies demonstrated Gleason score 3+4 prostate cancer on the right and benign tissue on the left.

acquisition comprising solely the ultrahigh b-value data, thus excluding this data from the ADC map calculation.

4.5 Quantitative Assessment of Prostate Diffusion-Weighted-MRI in the Peripheral Zone

Numerous studies have investigated the potential added value of quantitative ADC metrics to not only improve the diagnostic accuracy of tumor detection and localization compared with a visual assessment but also to determine tumor aggressiveness.

4.5.1 Diagnosis of Prostate Cancer

An initial publication reported that the mean ADC value was significantly lower in PCa than in benign tissue.¹⁷ Subsequently, many articles have confirmed the presence of a significant difference.^{17,18,19,20,21,22,23,24,25,26} However, the reported values of ADC in prostate cancer show great variation, ranging from $0.98 \pm 0.22 \times 10^{-3} \text{ mm}^2/\text{s}$ to $1.39 \pm 0.23 \times 10^{-3} \text{ mm}^2/\text{s}$.^{24,25} One factor contributing to this variation is the selection of b value among the studies, given that ADC values are lower when computed using higher maximum b values. For instance, in the study by Vargas et al,²⁷ ADC values were lower at $b = 1000 \text{ s/mm}^2$ than at $b = 700 \text{ s/mm}^2$, and in the study by Kitajima et al,²⁸ ADC values were lower at $b = 2000 \text{ s/mm}^2$ than at $b = 1000 \text{ s/mm}^2$. Thus, it could be anticipated that two^{20,21} of the three studies performed using a maximum b value up to 600 s/mm^2 ^{19,20,21} show higher ADC values, (1.33 ± 0.32 and $1.43 \pm 0.19 \times 10^{-3} \text{ mm}^2/\text{s}$) in cancer than those studies performed using a maximal b value $> 600 \text{ s/mm}^2$. However, even above 600 s/mm^2 , the ADC values continue to exhibit much variation among protocols using

comparable acquisition parameters. The studies by Kumar et al²⁴ and Desouza et al,²² which used only slightly different protocols (five and four b values, high b values of 1000 and 800 s/mm^2 , respectively), provide a representative example, as the mean ADC values in cancer were substantially lower in the study by Kumar et al than in that of Desouza et al ($0.98 \pm 0.22 \times 10^{-3} \text{ mm}^2/\text{s}$ vs. $1.30 \pm 0.30 \times 10^{-3} \text{ mm}^2/\text{s}$) and the obtained cutoff values for differentiating cancer from benign tissue were substantially different ($1.17 \times 10^{-3} \text{ mm}^2/\text{s}$ vs. $1.36 \times 10^{-3} \text{ mm}^2/\text{s}$, respectively). Another finding shared by essentially all of these studies is that despite the significant difference of ADC values between cancer and benign tissue, an overlap in ADC values exists between benign and malignant tissue in individual patients, with this overlap potentially being substantial. This concern was particularly well illustrated in a study by Nagel et al²⁹ that evaluated 88 consecutive patients having suspicious focal areas on mpMRI (3T, pelvic phased-array coil, b values of 0, 100, 500, and 800 s/mm^2) and in whom 116 biopsy cores were obtained by MR-guided biopsies. The mean ADC value of normal tissue ($1.22 \pm 0.21 \times 10^{-3} \text{ mm}^2/\text{s}$) was higher than that of both benign prostatitis ($1.08 \pm 0.18 \times 10^{-3} \text{ mm}^2/\text{s}$, $p < 0.001$) and of PCa ($0.88 \pm 0.15 \times 10^{-3} \text{ mm}^2/\text{s}$, $p < 0.001$). However, considerable overlap was observed between prostate cancer and prostatitis. No difference in ADC value was demonstrated between low-grade cancer (Gleason score < 7) and high-grade cancer (any percentage of Gleason pattern 4), which may explain, at least in part, the sub-optimal performance of ADC values in identifying prostate cancer.

Given the published studies, reliably differentiating cancer from benign foci purely on the basis of measurements of the absolute ADC value seems difficult if not impossible at present. Thus, detection of prostate cancer continues to largely rely on a visual assessment of both the signal intensity on ultrahigh b-value DW images combined with a visual assessment of the ADC map, as is recommended by PI-RADS version 2.

4.5.2 Apparent Diffusion Coefficient Map and Peripheral Zone Tumor Aggressiveness

Partly related to the very large increase in the number of men undergoing sextant prostate biopsies over the recent decades, many men are currently being diagnosed with indolent or non-significant prostate cancer that will not impact survival or cause harm.³⁰ These tumors do not require radical treatments, which are associated with potential side effects including incontinence and impotence that greatly impact patients' quality of life. Diffusion-weighted magnetic resonance imaging, in addition to clinical, biochemical, and pathologic features, may aid in establishing the aggressiveness of prostate cancer and help predict those tumors most likely to progress rapidly. While tumor grade is the primary determinant of tumor aggressiveness (in particular, presence of a component with a Gleason score of 4 or 5), tumor volume and extraprostatic extension are also important considerations.

4.5.3 Apparent Diffusion Coefficient Map and Gleason Score of Peripheral Zone Tumors

Many studies have investigated the ability of ADC values to predict tumor Gleason score using biopsy results as the reference standard.^{20,21,23,31,32,33,34,35,36,37} However, such studies are suboptimal given that sextant biopsies can miss high Gleason grades in approximately 30% of cases. Magnetic resonance-targeted biopsies (in-bore or using MRI-TRUS image registration³⁴) may provide a more appropriate reference standard but are also limited: small amounts of Gleason pattern 4 (up to 20%) can be missed,³⁸ and in the author's experience,³⁹ Gleason score 3 + 4 tumors on fusion biopsy having a Gleason pattern 4 $\geq 30\%$ are commonly upgraded to Gleason score 4 + 3 at pathologic examination of prostatectomy specimens.

As a result, the most robust way of evaluating the ability of ADC values to estimate the Gleason score as well as the percentage of Gleason pattern 4 is to correlate ADC metrics with findings from the pathologic examination of the radical prostatectomy specimen. Indeed, such an association has been performed in nearly 20 studies as of this writing.^{27,40,41,42,43,44,45,46,47,48,49,50,51,52,53,54,55} While the maximum b value used for DWI acquisition was 800 to 1,000 s/mm² in the majority of these studies, important variation in selection of intermediate b values is apparent. Indeed, many of the studies used only two b values (commonly 0 and 1000 s/mm²). The use of only two b-values is likely to be, at least partly, vendor dependent given the lack of multi-b-value functionality of DWI on many MR platforms at the time of the publication of the articles.

All of the studies agree that there is an inverse relationship between the ADC value and the Gleason score, with a correlation coefficient that varies from 0.32 (weak correlation) to 0.50 (fair correlation). In studies that specifically compare ADC values of Gleason score 6 tumors to those of Gleason score > 7 tumors,^{27,40,43,44,45,51,53,55} the ADC value of Gleason score 6 tumors is significantly higher, measuring above 1.0×10^{-3} mm²/s in all studies but one,⁴⁰ with values ranging from 1.0 to 1.3 x

10^{-3} mm²/s, compared with that of Gleason score > 7 tumors (ADC values ranging from 0.69 to 0.88×10^{-3} mm²/s).

Some of these studies aimed to achieve even greater precision, exploring the ability of ADC values to characterize intermediate-grade tumors (Gleason score 7), which has consistently presented a greater challenge for DWI than separating low- and high-grade tumors. For this purpose, limitations of TRUS-guided biopsies are well known: Gleason score 6 tumors can be upgraded to Gleason score 7 at surgical pathology in at least 25% of cases, and Gleason score 3 + 4 tumors can be upgraded to Gleason score 4 + 3 tumors in 20 to 66% of the cases.⁵⁶ Being able to detect the most aggressive foci within an individual tumor using DWI conceptually should improve the accuracy in differentiating Gleason score 3 + 4 and Gleason score 4 + 3 tumors, which is clinically important given the well-established poorer prognosis of tumors with Gleason score 4 + 3 compared to those with Gleason score 3 + 4.^{57,58,59} Furthermore, the percentage of Gleason pattern 4 (%G4) may also provide a useful marker of tumor aggressiveness as reported by Stamey et al,⁶⁰ who demonstrated that biological progression after radical treatment increased for each 10% increment of %G4. Cheng et al similarly showed that the percentage of Gleason pattern 4 and 5 could predict survival after radical prostatectomy.⁶¹

The accuracy of ADC values in discriminating Gleason scores of intermediate-grade tumors from those of lower- or higher-grade tumors varies across studies. Yoshimitsu et al⁵⁵ failed to find a significant difference in ADC values between tumors with Gleason scores 6 and 7 or between tumors with Gleason scores 7 and 8. While a number of studies^{27,43,45,48,50,53} have compared ADC values between tumors with Gleason scores of 3 + 4 and 4 + 3, results of these studies have been discrepant. Verma et al⁵³ and Rosenkrantz et al⁵⁰ failed to show a significant difference between the two groups, while four studies^{27,43,45,48} found a significant difference. These discrepancies probably relate, at least in part, not only to differences in the MRI protocol across studies but also to varying amounts of Gleason pattern 4 among included patients having a Gleason score of 3 + 4. Intuitively, it may indeed be expected that tumors with small amounts of Gleason pattern 4 (up to 20 to 25%) may have a mean ADC value similar to that of Gleason 6 tumors given potential sparse distribution of the Gleason pattern 4 component, thereby making it virtually impossible to detect by imaging an area within the tumor having more restricted diffusion as a marker of the Gleason pattern 4 component. Moreover, even in studies that did report the ability to differentiate intermediate- from lower- and higher-grade tumors using ADC values, substantial overlap between the subclasses was noted, as supported by reported high standard deviations of ADC values within the groups.

In order to circumvent these limitations, Rosenkrantz et al recently proposed a potentially improved approach to evaluating the ADC map⁵⁰ in a study of 70 patients imaged before prostatectomy at 3T using a pelvic phased-array coil. Instead of measuring the mean ADC value on a single slice, the authors measured the whole-tumor ADC using in-house-developed software that allows placement of three-dimensional volumes of interest (VOIs) incorporating tumor voxels across multiple slices. From these measurements, the number of voxels having a given ADC value can be normalized to the total number of voxels within the VOI, allowing for computation of the so-called ADC entropy, which reflects the textural heterogeneity of the tissue.

In that study, ADC entropy was significantly higher in Gleason score 4+3 tumors than in Gleason score 3+4 tumors, although mean ADC was not significantly different between the groups.

4.5.4 Apparent Diffusion Coefficient Ratio and Gleason Score

The ADC ratio refers to the ratio of the mean ADC value of the tumor itself to the ADC value of a surrounding reference tissue. Computation of the ADC ratio is intended to provide intrapatient normalization of ADC measurements and potentially compensate for equipment-related variations and thereby improve discriminatory performance compared with absolute ADC values. One approach to obtaining the ADC ratio entails placement of a region of interest in the contralateral benign PZ, in mirror position to the tumor.

As with absolute ADC metrics, there is conflicting data regarding the value of ADC ratios. Lebovici et al, in a series of 22 men imaged at 1.5 T using an endorectal coil and transperineal 20-core saturation biopsy protocol serving as the reference standard, showed that the ADC ratio performed better than the ADC value in the PZ to discriminate Gleason score 8–9 from Gleason score 6–7 tumors.⁶² In that study, the mean ADC ratio for high-grade tumors was significantly lower (0.40 ± 0.09) than that of low- and intermediate-grade tumors (0.54 ± 0.09). Furthermore, the area under the curve (AUC) for differentiating these two tumor groups was 0.90 for the ADC ratio, compared with 0.75 for the ADC value. Similarly, Thormer et al,⁵² in a series of 45 patients imaged at 3 T using an endorectal coil (b values: 50–500–800 s/mm²) prior to prostatectomy reported that a cutoff value of the ADC ratio of 0.46 allowed for a correct characterization of 79% of tumors, performing better than TRUS-guided sextant biopsies, which only correctly characterized 75% of tumors. In addition, the AUC of the ADC ratio (0.90) was superior to that of the ADC value (0.79). However, these results were not confirmed by De Cobelli et al,⁶³ who correlated the ADC value and the ADC ratio (b values: 0–800–1600 s/mm²) with the surgical Gleason score at 1.5 T using an endorectal coil in 39 patients. The AUC was 0.92 ($p=0.12$) for the ADC value and 0.86 for the ADC ratio ($p=0.42$), indicating no incremental

value of the ADC ratio compared to that of the ADC value. Finally, in a study by Rosenkrantz et al of 58 patients imaged before radical prostatectomy in which two independent observers performed ADC value and ADC ratio assessments separately in the peripheral zone and transition zone, ADC values significantly outperformed ADC ratios in the PZ for both readers, whereas the two approaches had mixed results among the two readers in the TZ.⁶⁴

In assessing the relevance of ADC metrics for differentiating prostate cancer from benign PZ tissue and for evaluating tumor aggressiveness, Scheenen et al⁶⁵ emphasized that two distinct parameters (► Fig. 4.2) impact the strength of the diffusion-sensitizing gradients applied during a DW sequence: the diffusion time, which is the time interval between the two pulsed field gradient lobes, and the gradient duration, which is the overall time interval during which the gradients are applied. The ADC value is derived from the decay of the MR signal during this interval and thus can be influenced by either of these two parameters. Following a qualitative visual evaluation of the ADC map, further incorporation of quantitative ADC measurements for tumor characterization must therefore be done with caution. The ADC value not only depends linearly on the diffusion time, but also on the square of the gradient duration. Therefore, quantitative measurements of the ADC of prostate cancer and of benign tissue optimally should be compared between patients for which both the diffusion time and gradient duration were *the same*. However, in routine practice, it is difficult to determine when this condition is indeed the case, as these parameters are integrated together via the b value, reflecting a composite of the two parameters, and their separate values are typically not accessible to the radiologist.

Despite these limitations, we suggest that use of two particular threshold values in terms of ADC measurements may remain clinically helpful when employing a standardized DWI protocol, as recommended in PI-RADS version 2 computation of the ADC map from a low (not b=0), intermediate, and high (b=800–1000 s/mm², but not higher) b value. First, above an ADC measurement of approximately 1.1 to 1.2×10^{-3} mm², significant tumor is uncommon (► Fig. 4.12).⁶⁶ Second, below an ADC measurement of approximately 0.850×10^{-3} mm²/s, high-grade cancer with more than 20 to 25% G4 can be suspected

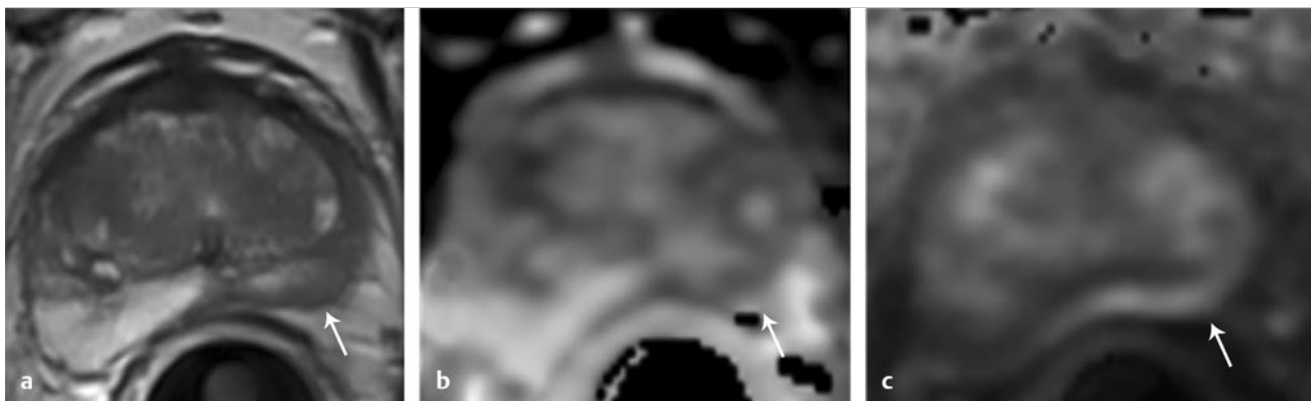


Fig. 4.12 Apparent diffusion coefficient (ADC) metrics for differentiating prostatitis from cancer. T2-weighted image (a) shows a hypointense lesion in the left posterior peripheral zone (arrow). The ADC map (b) shows a mildly reduced ADC value ($ADC = 1.25 \times 10^{-3}$ mm²/s). The computed b = 1600 s/mm² diffusion-weighted image (c) shows mild hyperintensity that is not substantially brighter than other areas within the prostate. Targeted biopsy of this region demonstrated chronic inflammation.



Fig. 4.13 Apparent diffusion coefficient (ADC) metric and tumor aggressiveness. T2-weighted image (a) shows an anterior apical tumor with decreased signal (arrow). The ADC map (b) shows markedly reduced ADC in the lesion, with an ADC value of $0.65 \times 10^{-3} \text{ mm}^2/\text{s}$, determined from a b 50–500–1000 s/mm² diffusion-weighted imaging sequence. Histopathology of the radical prostatectomy specimen (c) demonstrated a corresponding Gleason score 4 + 3 tumor (70% Gleason pattern 4).

(► Fig. 4.13).⁴⁶ These two threshold values may help guide decisions regarding whether to perform biopsy of PI-RADS category 3 lesions as well as may indicate the presence of a high Gleason pattern component that may or may not be identified on the biopsy findings.

4.5.5 Apparent Diffusion Coefficient Map and Tumor Volume

Several studies using the radical prostatectomy specimen as the reference standard have investigated whether DWI can predict the actual pathologic tumor volume. Mazaheri et al⁶⁷ and Isebaert et al,⁶⁸ in series of 42 and 75 patients, respectively, who underwent endorectal coil MR at 1.5 T, reported a significant correlation between findings from DWI and pathologic tumor volumes (0.60 and 0.75, respectively, $p < 0.0001$). In the study by Mazaheri et al, DWI outperformed T2W-MRI, which exhibited a correlation coefficient with pathologic tumor volume of 0.37. Similarly, Turkbey et al,⁶⁹ in a series of 135 patients who underwent 3-T endorectal coil MRI, reported a positive correlation between pathologic tumor volume and mpMRI tumor volume (Pearson correlation coefficient 0.633, $p < 0.0001$). Although the mpMRI protocol included a DW sequence, the authors reported that final regions of interest were drawn on T2W-MRI when assessing tumor volume correlations.

The main limitation of such studies is an overall emphasis on assessing the correlation in tumor volumes between MRI and pathology, as excellent correlation does not exclude systematic bias (tumor volume underestimation or overestimation) in the estimation when paired volumes are compared on an individual basis. Two studies have demonstrated limitations of DWI for estimating tumor volume when using statistical tests to explore potential systematic bias, such as Bland-Altman plots⁷⁰ or residual analysis.⁷¹ First, Le Nobin et al,⁷⁰ in a study of 37 patients who underwent pelvic phased-array coil 3-T mpMRI, compared MRI and histopathologic volumes using software to coregister MRI and three-dimensional digital reconstructions of radical prostatectomy specimens. The software did not use whole mount slides but rather reconstructed pathologic slides from a classical step-section analysis. The authors observed that the ADC maps tended to systematically underestimate tumor volumes, with a mean difference between tumor volume measured on the ADC maps and pathologic volume of -47%

(-143 to +49%), greater than the degree of underestimation of tumor volumes using T2WI (mean difference obtained with T2W-MRI of -32% [-128 to +65%]). Comparable results were obtained by Cornud et al in a series of 84 patients imaged at 1.5 T using a rectal coil.⁷¹ MRI and pathologic tumor volumes were measured by planimetry. Although the study showed that tumor volumes estimated by T2W or ADC maps correlated significantly with pathologic volume ($r^2 = 0.82$ and 0.83 , respectively), ADC maps underestimated pathologic volume in 49% of cases by a mean of 0.56 cm^3 (range 0.005 to 2.84 cm^3).

These two studies indicate that the boundaries of tumors are difficult to detect by DWI. Tumor extension beyond the boundaries of the visible portion of the tumor on MRI is typically sparse with an infiltrative histologic pattern that currently precludes its reliable identification by any imaging modality.^{72,73} As a result, when using the ADC map, T2W-MRI, or both to guide focal tumor ablation, a target volume that incorporates a safety margin around the tumor should be defined rather than aiming to ablate solely the visible tumor volume on MRI.⁷¹

4.6 Advanced Diffusion-Weighted Imaging Techniques to Improve the Accuracy of the Apparent Diffusion Coefficient ADC Map in the Peripheral Zone

4.6.1 Biexponential Diffusion (Intravoxel Incoherent Motion Phenomenon), or How to Separate the Perfusion and the Diffusion Effects in Diffusion-Weighted Imaging

Le Bihan et al developed the intravoxel incoherent motion (IVIM) model to describe a biexponential, instead of a monoexponential, signal decay when diffusion gradients are applied.⁷⁴ In this model (► Fig. 4.14), two compartments are present, the capillary and the tissue compartments. In the capillary compartment, the movement of water molecules mimics a diffusion process (pseudodiffusion), evaluated by a specific pseudodiffusion

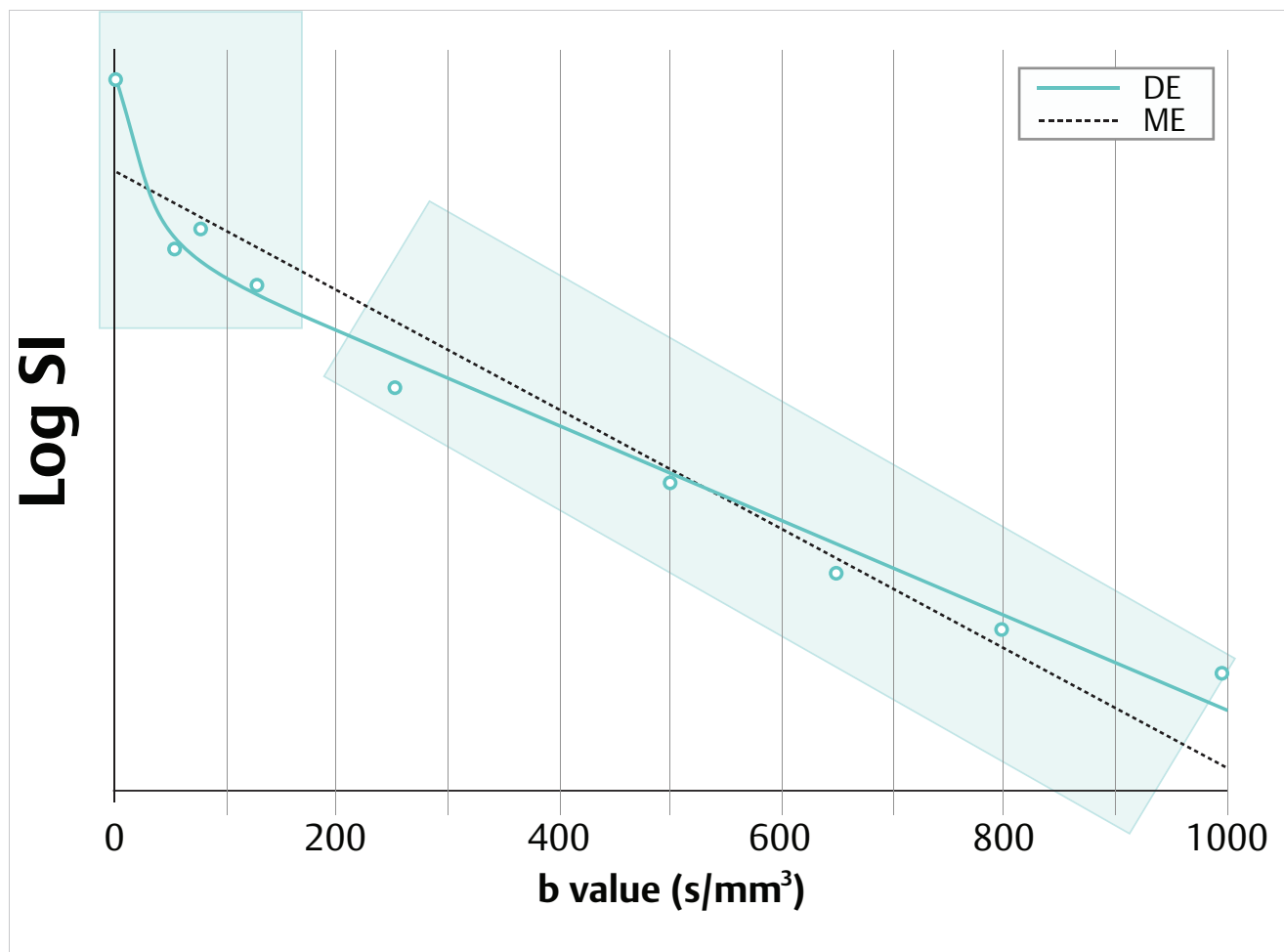


Fig. 4.14 Biexponential diffusion-weighted (DW) signal intensity decay curve (solid green line). At low b values, the curve is steep (within the light green rectangular box on the left). However, at higher b values, the slope is less steep (within the light green rectangular box to the center and right). The hockey-stick shape of the biexponential curve (solid green line) provides a better fit to the acquired DW data (open green points) than the monoexponential model (dotted line) used to generate the ADC map.

coefficient (D^* , or ADC_{fast}) derived from the weighting achieved using low b values ($0\text{--}100\text{ s/mm}^2$). D^* is represented by the initial portion of the signal intensity decay curve, which has a steep slope consistent with the nature of signal intensity attenuation resulting from capillary water motion. The second part of the curve represents water motion at the higher b values. The slope is less steep and reflects tissue diffusion (D , or ADC_{slow}). The term f corresponds to the blood volume derived from water protons flowing through pseudorandomly oriented microcapillaries and has been labelled the perfusion fraction by LeBihan et al.⁷⁴

In comparison with the diffusion metric D from the biexponential model, the conventional metric ADC, which is calculated using a monoexponential model, is influenced by the microcapillary perfusion that is significant at low b values. At high b values, this component becomes insignificant given negligible capillary signal attenuation at such b values. On the other hand, although D^* is perfusion sensitive, it is also affected by true tissue diffusion effects. There is no consensus regarding the number of small b values that should be acquired when applying a biexponential diffusion model, although a compromise between the number of b values and the number of signal averages is needed in order to maintain acceptable measurement

times. In our practice, IVIM is performed using 10 b values ($0, 10, 20, 30, 40, 50, 100, 200, 500, 1000\text{ s/mm}^2$).

Several studies have applied the bi-exponential model for DWI in the prostate. The number of b values ranged from 4 to 16.^{33,75,76,77,78} Among the three IVIM parameters (D , D^* , and f), D has shown the highest accuracy to discriminate prostate cancer from benign tissue. Kuru et al evaluated 50 patients (23 without cancer and 27 with biopsy-proven cancer) at 3T using a pelvic phased-array coil and seven b values ($0, 50, 100, 150, 200, 250, 800\text{ s/mm}^2$). D and ADC values performed similarly in discriminating tumor from benign tissue (AUC = 0.9), although only D was able to discriminate low-grade (Gleason score < 7) and high-grade (Gleason score > 7) prostate cancer.

A single study by Riches et al⁷⁹ used b values < 50 s/mm^2 in a comparison between the monoexponential and biexponential models in 50 patients at 1.5T using an endorectal coil and eleven b values ($0, 1, 2, 4, 10, 20, 50, 100, 200, 400, 800\text{ s/mm}^2$). The authors observed that D was lower than ADC in normal PZ tissue ($1.34 \pm 0.28 \times 10^{-3}\text{mm}^2/\text{s}$ vs. $1.66 \pm 0.34 \times 10^{-3}\text{mm}^2/\text{s}$), respectively) and in prostate cancer ($0.82 \pm 0.45 \times 10^{-3}\text{mm}^2/\text{s}$ vs. $1.33 \pm 0.52\text{mm}^2/\text{s}$, respectively). The study also showed that the

biexponential model using the full b value range offered the best fit to the acquired data, provided that b values $< 20 \text{ s/mm}^2$ were included. When the minimum b value was increased above 20 s/mm^2 in both models, the monoexponential model provided a better description of the acquired data. The other parameters of the biexponential model (D^* and f) showed great variation with large associated standard deviations and were not discriminant between cancer and benign tissue. Nonetheless, the authors suggested that separation of this highly variable perfusion component using the IVIM model may increase the clinical utility of the diffusion coefficient in diagnosis of prostate cancer.

Our experience (unpublished data) at 1.5 T with a reusable endorectal coil (Invivo Corporation; Gainesville, FL) and using a

10 b value sequence ($0-10-20-30-40-50-100-500-1000 \text{ s/mm}^2$) sequence ($TR/TE = 4000/70$) showed that D and ADC values performed equally well ($AUC = 0.89$ and 0.91 , respectively) (► Fig. 4.15). The optimal cutoff value to differentiate cancer from benign foci was $1.07 \times 10^{-3} \text{ mm}^2/\text{s}$ for the ADC value (sensitivity, 84%; specificity 83%) and $1.19 \times 10^{-3} \text{ mm}^2/\text{s}$ for D (sensitivity, 86%; specificity 83%).

Given the findings, although the biexponential model may provide a mathematically improved fitting of the DW signal intensity data when multiple b values are acquired, further studies are required to establish an incremental diagnostic value over that of the monoexponential model in prostate cancer detection.

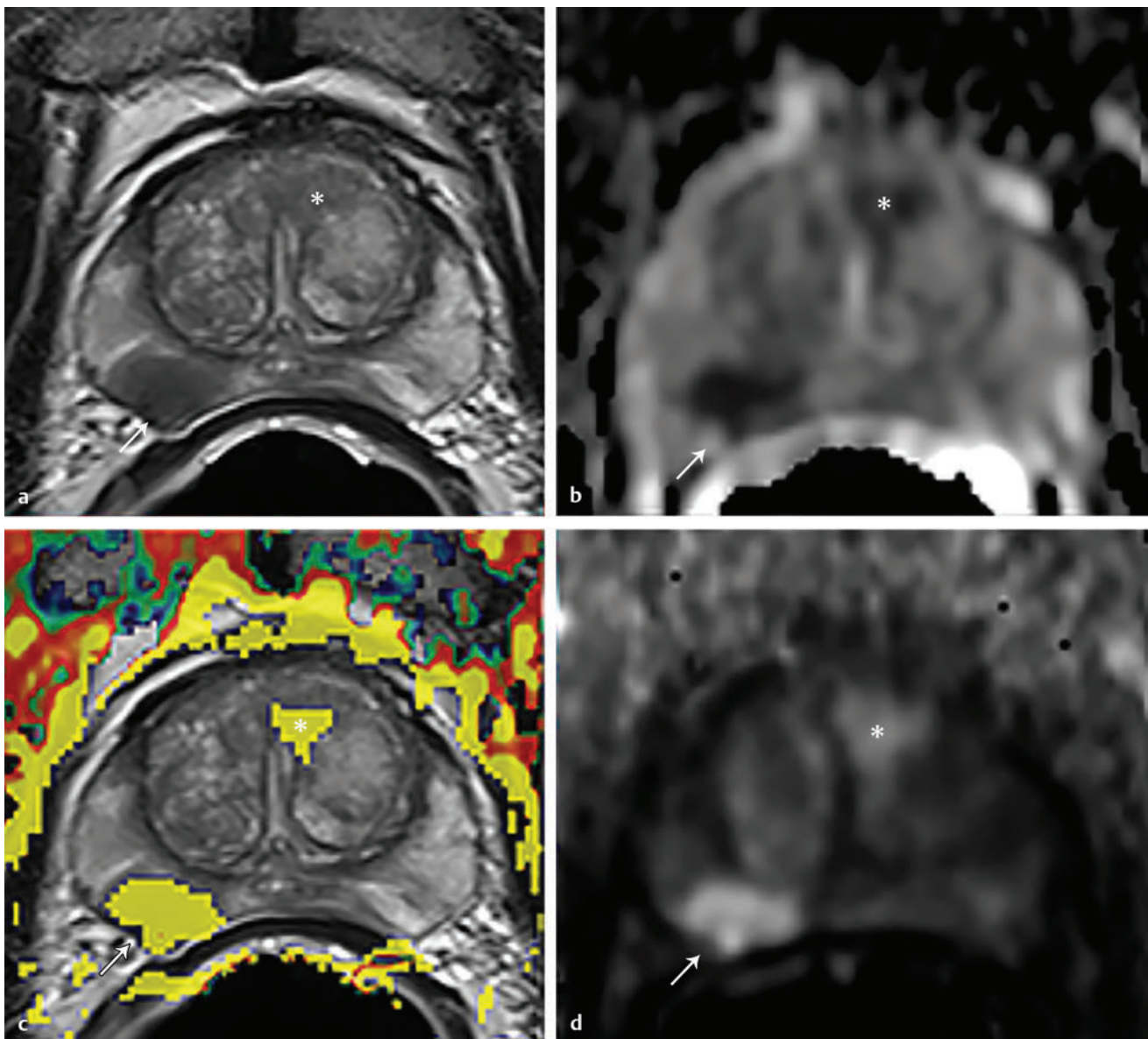


Fig. 4.15 Biexponential diffusion in clinical practice. Typical peripheral zone tumor (*arrow*) visible on the T2-weighted image (a), the apparent diffusion coefficient (ADC) map ($ADC = 0.86 \times 10^{-3} \text{ mm}^2/\text{s}$) (b), and the computed $b = 1600 \text{ s/mm}^2$ diffusion-weighted image (DWI) (c). The color-coded biexponential model (d) shows a low value of D (cutoff of $1.20 \times 10^{-3} \text{ mm}^2/\text{s}$) but adds no additional information to the ADC value or the overall DWI assessment. Targeted biopsy of the lesion showed a Gleason score 4 + 3 tumor. Note as well the nonencapsulated mildly hypointense region in the transition zone (*asterisk*) exhibiting abnormality on all parameters (ADC map, D map, and $b = 1600 \text{ s/mm}^2$ DWI), suggesting a possible secondary tumor, although targeted biopsies were not performed.

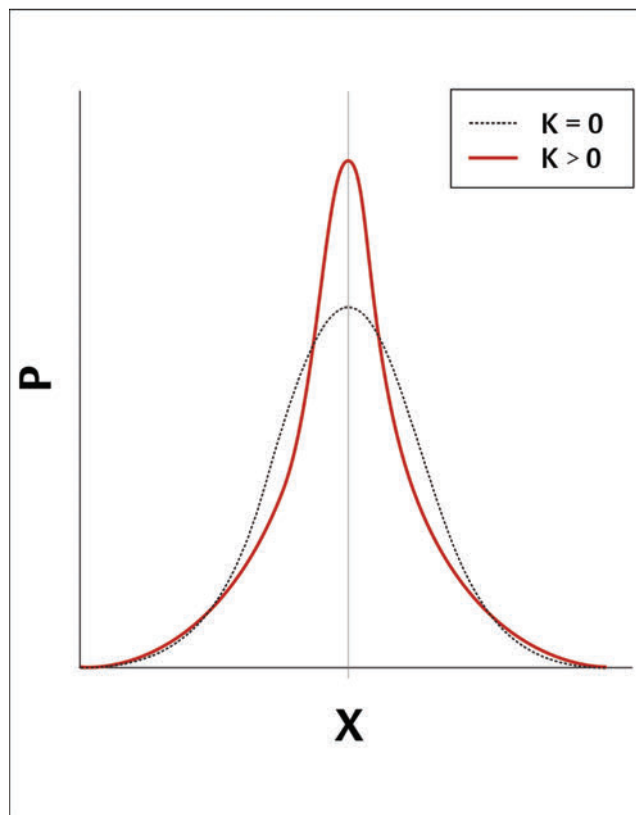


Fig. 4.16 Gaussian and non-gaussian distributions. The dashed line represents a gaussian distribution (kurtosis = 0), as occurs in “free” diffusion. The solid line represents a more peaked non-gaussian distribution (kurtosis > 0), as occurs in more complex tissue environments lacking “free” diffusion.

4.6.2 Diffusion Kurtosis Imaging

The overlap of quantitative ADC values of higher- and lower-grade prostate cancer as well as of benign tissue may also be due to another limitation of the standard monoexponential estimation of ADC, that is, that it assumes a gaussian distribution of the displacements of the water molecules. Rather, as cellularity increases and restricts water diffusion, displacement of water molecules is believed to become non-gaussian (► Fig. 4.16). The term kurtosis describes the deviation of a non-gaussian distribution compared with a gaussian distribution. Using diffusion kurtosis MRI (DKI), it is possible to quantify this deviation. The kurtosis (K) is extracted from DW images acquired using a maximum b value of approximately 2000 s/mm^2 and may provide better differentiation between prostate cancer and benign tissue. Such a very high maximum b value is needed in order for the non-gaussian distribution of water diffusion behavior to manifest itself.

A limited number of studies have explored DK-MRI in the prostate in a clinical setting. The initial study by Rosenkrantz et al⁸⁰ evaluated 47 patients with biopsy-proven prostate cancer imaged at 3T using a pelvic phased-array coil and five b values ranging from 0 to 2000 s/mm^2 . K values were higher (0.96 ± 0.24) in cancer than in benign PZ tissue (0.57 ± 0.07) and also higher in Gleason score >6 tumors (1.05 ± 0.26) than in Gleason score 6 tumors (0.89 ± 0.20 , $p < .001$). Furthermore, K

outperformed ADC in terms of the sensitivity for differentiating cancer from benign PZ tissue (93.3% vs. 78.5%, $p < 0.001$) without any associated loss of specificity (95.7%, $p > 0.99$) and also showed a significantly higher AUC (70% vs. 62%, $p = 0.010$) for differentiating Gleason score 6 tumors from Gleason score >6 tumors.

However, a subsequent study by Roethke et al⁸¹ did not confirm these promising results. The authors evaluated 55 patients at 3T using a 16-channel pelvic phased-array coil and nine b values (0, 50, 250, 500, 750, 1000, 1250, 1500, 2000 s/mm^2) in order to compute K and D metrics (D representing the diffusion coefficient of the DK sequence that is corrected to account for the observed non-gaussian diffusion behavior). Standard ADC values were extracted from a separate DW protocol that included two b values (0, 800). Transperineal biopsy using MRI-TRUS image registration was the reference standard. D and ADC values were significantly lower in cancer than in benign tissue, and K was significantly higher in cancer (1.01 ± 0.21) than in benign tissue (0.76 ± 0.14 , $p < 0.05$). However, contrary to Rosenkrantz et al,⁸⁰ Receiver operating characteristic (ROC) analyses did not reveal a significant difference between K and standard ADC for detection of prostate cancer. With regard to tumor aggressiveness, K and standard ADC showed a comparable significant difference ($p < 0.05$) for discrimination between Gleason score 6 and Gleason score >6 tumors. As a result, no significant difference was established between standard DWI- and DKI-derived metrics.

Roethke et al⁸¹ suggested that the discrepancy compared with the results of Rosenkrantz et al⁸² was related to the nature in which the standard ADC metric was extracted. Namely, in the study by Rosenkrantz et al, ADC was calculated from the DW-kurtosis sequence, which requires an increased echo time (81 ms) in order to acquire the very high b values necessary for this sequence. This longer echo time may decrease the SNR, which may adversely impact the quality of the ADC map in comparison with that which can be obtained if performing a conventional DWI acquisition with standard b values. For instance, the DWI acquisition used in the study by Roethke et al for calculating the ADC map with a monoexponential fit incorporated a substantially shorter echo time (58 ms) in view of the relatively lower acquired b values.⁸¹ These authors concluded that the value of conventional ADC is underestimated when ADC is extracted from a DK acquisition.

In conclusion, preliminary data suggests that DK-MRI has potential to enhance the performance of DWI for diagnosis and assessment of aggressiveness of prostate cancer, although further studies are required to reconcile differences among the results of early studies in this area.

4.6.3 Diffusion Tensor Imaging and Anisotropy

In tissues with a directionally oriented structural organization, the displacement due to diffusion of water molecules depends upon the direction along which the displacement is measured. Water displacements perpendicular to an aligned structure are small given that water must cross or go around the structure in order to move in this direction. In contrast, water moving parallel to the structure moves more easily along the structure (► Fig. 4.17a) and thus exhibits a greater displacement. The

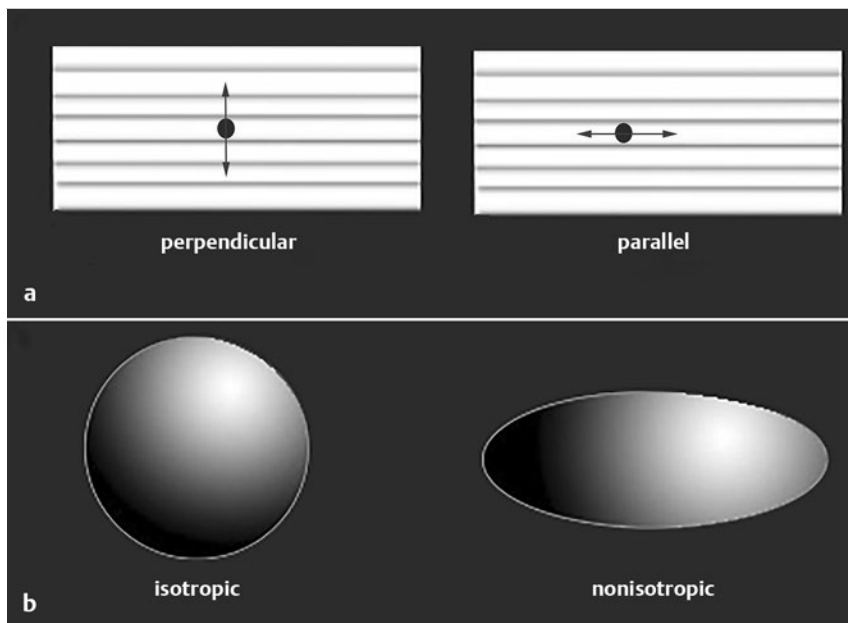


Fig. 4.17 Diffusion tensor imaging (DTI) (a) DTI evaluates the directionality of the displacement of water molecules due to diffusion (represented by black dots with arrows). For tissues with an inherent structural directionality, the restrictions to diffusion will be different perpendicular and parallel to the tissue's structural directionality. (b) Anisotropy. Isotropic diffusion (fractional anisotropy = 0) indicates equivalent water diffusion in all directions, as represented by the sphere. Anisotropic diffusion (fractional anisotropy > 0) indicates variable diffusion in different spatial directions, as represented by the ellipsoid. DTI requires performing diffusion acquisitions in at least six different directions in order to define a diffusion tensor and assess the degree of anisotropy of diffusion of water in a tissue.

prostate gland exhibits this anisotropic effect to at least some extent. This effect—the specific directionality of water displacements—may be evaluated using diffusion tensor imaging (DTI), which acquires a diffusion tensor that captures the unique diffusion orientations. For DTI, diffusion acquisitions must be performed in at least six different directions. The resulting six derived diffusion data sets are used to calculate an ellipsoid representing the spatial orientation of diffusion for each voxel. The calculated fractional anisotropy (FA) represents the degree to which the diffusion ellipsoid deviates from a sphere (► Fig. 4.17b), with greater deviation indicating greater diffusion anisotropy in comparison with the isotropic diffusion represented by a sphere.

The incremental value of DTI over standard DW has not been established for prostate cancer assessment. The FA of normal prostate has been evaluated in several studies and was observed to be higher in the fibromuscular stromal tissue of the TZ than in the epithelium-containing PZ.^{82,83,84} However, FA has also variably been reported to be higher,²⁰ lower,⁸⁵ or unchanged following radiation therapy for prostate cancer,⁸⁶ as well as similar in prostate cancer as compared with normal PZ.^{84,87} Thus, further studies are required to establish a role for DTI in prostate cancer characterization.

4.7 DWI of the Transition Zone

Approximately 30% of prostate cancers originate in the TZ. The diagnosis of TZ tumors remains difficult on the basis of T2W-MRI alone owing to the presence of stromal BPH which is hypointense and can have either an ill-defined or a more nodular morphology. The shape, signal intensity, margins, and location must all be taken into consideration when assessing the likelihood of cancer within TZ lesions.⁸⁸ One study by Chesnais et al⁸⁹ of 117 benign and 20 malignant TZ nodules, using the radical prostatectomy specimen as the reference standard, reported that 20 and 18 of the 20 TZ cancers involved the anterior and apical aspects of the TZ, respectively, indicating important regions of the TZ to inspect closely for suspicious lesions.

4.7.1 Qualitative DWI of the TZ

Studies have explored the incremental value of the ADC map compared to that of T2W-MRI, using the RP specimen as the reference standard. In some studies,^{90,91} T2W images and ADC maps were read simultaneously. Yoshizako et al⁹⁰ evaluated 26 TZ tumors (tumor size > 10 mm) at 1.5 T using an endorectal coil and a $b = 0-1,000$ s/mm² DW sequence and reported a sensitivity of 61% in the detection of TZ cancer for T2W-MRI, which increased, although nonsignificantly, to 81% with the aid of the ADC map. The accuracy and the positive predictive value also increased from 64 and 76% and 83 and 91%, respectively. However, Delongchamp et al,⁹¹ in a series of 57 patients evaluated at 1.5 T using an endorectal coil, reported that the AUC of the combination of T2W-MRI and semiquantitative evaluation of ADC maps (0.88) was not greater than that of T2W-MRI alone (0.84).

In other studies, T2W images were read first, while the combination of T2W images + ADC maps were read in a second session. Again, results were discrepant among such studies. Haider et al⁹² at 1.5 T using an endorectal coil and a $b = 0-600$ s/mm² DW sequence reported that DWI provided no improvement in the diagnosis of TZ cancer, compared to T2W-MRI. The value of the AUC was similar for both sequences (0.79) and the sensitivity was low for both T2W-MRI (36%) and T2W-MRI + DWI (42%). Similar findings were observed by Hoeks et al in a series of 28 patients evaluated at 3 T using an endorectal coil and a $b = 50-500-800$ s/mm² DW sequence in which four radiologists first interpreted T2W images and then performed a combined assessment with DW images.⁹³ Detection accuracy for tumors > 0.5 cm³ did not differ between T2W-MRI and T2W-MRI + ADC maps for all TZ cancers (68% vs. 66%, $p=0.85$), for Gleason pattern 4/5 tumors (79% vs. 72-75%, $p=0.13$), or for Gleason pattern 2/3 tumors (66% vs. 62-65%, $p=0.47$). Sensitivity was 53% for all tumors, 72% for high-grade tumors, and 42% for low-grade tumors.

In comparison, a study by Jung et al⁹⁴ reported that the combination of T2W-MRI and ADC maps performed better than T2W-MRI alone. The authors evaluated 156 patients with TZ tumors at 1.5 T using an endorectal coil and a $b = 0-1000$ s/mm² DW

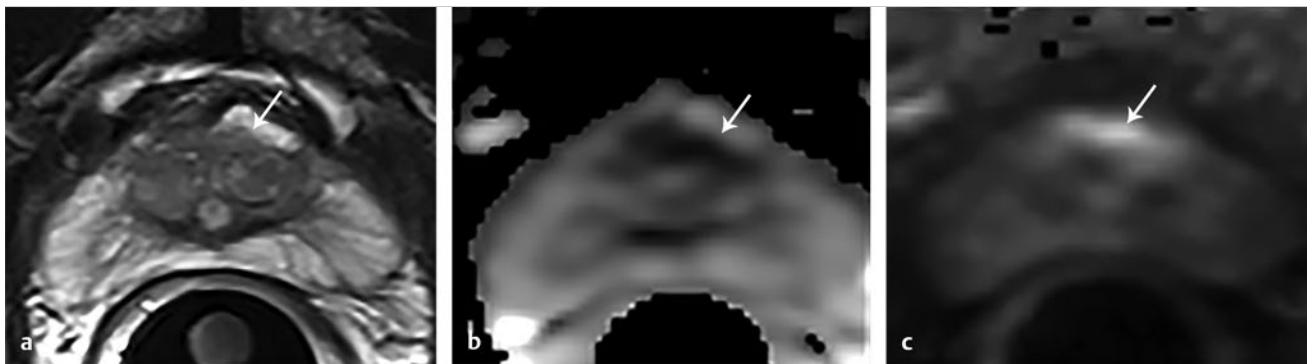


Fig. 4.18 Incremental value of diffusion-weighted image (DWI) for the detection of transition zone prostate cancer. The apparent diffusion coefficient (ADC) map (b) exhibits focal decreased ADC in the left anterior transition zone (arrow). The computed $b = 1600 \text{ s/mm}^2$ DWI (c) shows corresponding hyperintensity. The lesion is not clearly visible on T2-weighted imaging (a). Targeted biopsy demonstrated a Gleason score 3 + 3 tumor in this region (maximum cancer core length of 6 mm).

sequence. Two blinded readers first evaluated the T2W images alone, and then, 4 weeks later, evaluated the ADC maps in addition to the T2W images. Tumor detection was significantly improved for the two readers by the combined approach, with AUC increasing from 0.60 to 0.71 to 0.75 at the patient level. Sensitivity of T2W-MRI was 64% for tumors $> 0.5 \text{ cm}^3$, yet 70 to 74% for tumors $< 0.5 \text{ cm}^3$. In comparison, sensitivity of T2W-MRI + ADC maps was 76 to 96% for tumors $> 0.5 \text{ cm}^3$ and 64 to 91% for tumors $< 0.5 \text{ cm}^3$.

Two studies investigated the potential value of source DW images obtained using an ultrahigh b value ($b = 2000 \text{ s/mm}^2$) to localize TZ cancer. First, Katahira et al evaluated 201 patients before radical prostatectomy at 3T using a pelvic phased-array coil.⁹ Three radiologists independently interpreted three sets of images in a random fashion: the T2W images and two sets of source DW images, one acquired using a $b = 0\text{--}1000 \text{ s/mm}^2$ sequence and one acquired using a $b = 0\text{--}2000 \text{ s/mm}^2$ sequence. The AUC increased from 0.68 for T2WI to 0.76 for T2WI + DWI at $b = 1000 \text{ s/mm}^2$ and to 0.85 for T2WI + DWI at $b = 2000 \text{ s/mm}^2$. Similarly, Rosenkrantz et al evaluated 106 TZ cancers at 3T using a pelvic phased-array coil before radical prostatectomy.⁹⁵ Three radiologists independently reviewed first T2W images and then incorporated $b = 1000 \text{ s/mm}^2$ DW images with the associated ADC map, followed by incorporating $b = 2000 \text{ s/mm}^2$ DWI images. Sensitivity increased from 19.4 to 33.9% for T2W images to 50 to 54.8% for the combination of T2W images + $b = 2000 \text{ s/mm}^2$ DW images. ($p < 0.011$), and increased further to 62.9 to 74.2% ($p = 0.013$) following incorporation of $b = 2000 \text{ s/mm}^2$ DW images, demonstrating the additional value of ultrahigh b -value DW images in the detection of TZ cancer. These results suggest that even if T2W-MRI remains the dominant sequence in the attribution of the global PI-RADS assessment category, the hyperintensity within tumors at $b = 2000 \text{ s/mm}^2$ may be more conspicuous than the decreased signal within tumors on the ADC map. In clinical practice, visually bright foci, as identified at the ultrahigh b value (► Fig. 4.18), help draw the radiologist's attention to a potential lesion and trigger more detailed analysis of the area using the rest of the MR data sets.⁹⁶ In this sense, initial localization of the suspicious region using the $b = 2000 \text{ s/mm}^2$ images can be useful in raising one's confidence regarding the presence of a lesion, even if the final PI-RADS category is largely determined by T2W-MRI.

4.7.2 Quantitative DWI of the TZ

For the diagnosis of prostate cancer, ADC values of TZ tumors have been found to be significantly lower than those of benign BPH in many studies.^{90,97,98,99} However, most studies compared ADC values of TZ cancer with that of benign nodules in general, including both glandular BPH (typically exhibiting high ADC) and stromal BPH (typically exhibiting low ADC), without specifically comparing ADC values of TZ tumors with that of benign stromal nodules. Such an approach may not provide the most clinically relevant study design, even if one observes lower ADC values in TZ tumors. A more helpful comparison may be with the ADC value of stromal BPH nodules, given the extent to which the homogeneously decreased T2W signal and decreased ADC within such nodules may mimic a tumor. In one study at 1.5T using an endorectal coil and a maximum b value of 1000 s/mm^2 , Oto et al reported significantly lower ADC values in TZ tumors ($1.05 \times 10^{-3} \text{ mm}^2/\text{s}$) than in stromal BPH ($1.27 \times 10^{-3} \text{ mm}^2/\text{s}$).⁹⁷ However, this finding was not confirmed in an alternate study,¹⁰⁰ and differentiation of stromal BPH from TZ tumors continues to be considered a diagnostic challenge based on quantitative ADC assessment, pending further investigation.

A number of studies have investigated associations between ADC values and Gleason scores in the TZ.^{28,53,54,94,101} Studies by Jung et al⁹⁴ and Kitajima et al²⁸ performed at 3T using a pelvic phased-array coil and a $b = 0\text{--}1000 \text{ s/mm}^2$ DW sequence, observed that mean ADCs decreased from 1.10 to $1.23 \times 10^{-3} \text{ mm}^2/\text{s}$ in Gleason score 3 + 3 tumors to 0.98 to $1.12 \times 10^{-3} \text{ mm}^2/\text{s}$ in Gleason score 3 + 4 tumors, 0.87 to $1.01 \times 10^{-3} \text{ mm}^2/\text{s}$ in Gleason score 4 + 3 tumors, and 0.75 to $0.87 \times 10^{-3} \text{ mm}^2/\text{s}$ in Gleason score $> 4 + 3$ tumors. However such trends were not confirmed in several other studies. For instance, Kobus et al¹⁰¹ and Vos et al⁵⁴ in two studies using a combination of DWI and MR spectroscopy (MRS) to determine TZ tumor aggressiveness reported that the ADC values had no incremental value for determination of aggressiveness in TZ tumors compared with MRS. In addition, Verma et al⁵³ at 1.5T using an endorectal coil and a $b = 0\text{--}600 \text{ s/mm}^2$ DW sequence, did not identify a significant difference in ADC values between Gleason score 3 + 3 ($1.00 \times 10^{-3} \text{ mm}^2/\text{s}$) and Gleason score 3 + 4 tumors ($1.07 \times 10^{-3} \text{ mm}^2/\text{s}$), although the latter group showed a significantly higher ADC than Gleason score 4 + 3 tumors ($0.87 \times 10^{-3} \text{ mm}^2/\text{s}$). Among

these studies, even when significant differences in ADC were observed between tumors with different Gleason scores, the standard deviations were large, with substantial overlap between groups in terms of the ADC values.

Based on these studies, ADC values may have some value for estimating aggressiveness of TZ tumors, although more limited in comparison with the role of ADC values in estimating aggressiveness of PZ tumors.

References

- [1] Hoeks CM, Barentsz JO, Hambrock T et al. Prostate cancer: multiparametric MR imaging for detection, localization, and staging. *Radiology* 2011; 261(1):46–66
- [2] Koh DM, Collins DJ. Diffusion-weighted MRI in the body: applications and challenges in oncology. *AJR Am J Roentgenol* 2007; 188(6):1622–1635
- [3] Padhani AR, Liu G, Koh DM et al. Diffusion-weighted magnetic resonance imaging as a cancer biomarker: consensus and recommendations. *Neoplasia* 2009; 11(2):102–125
- [4] Neil JJ. Diffusion imaging concepts for clinicians. *J Magn Reson Imaging* 2008; 27(1):1–7
- [5] Rosenkrantz AB, Mannelli L, Kong X et al. Prostate cancer: utility of fusion of T2-weighted and high b-value diffusion-weighted images for peripheral zone tumor detection and localization. *J Magn Reson Imaging* 2011; 34(1):95–100
- [6] Medved M, Soylu-Boy FN, Karademir I et al. High-resolution diffusion-weighted imaging of the prostate. *AJR Am J Roentgenol* 2014; 203(1):85–90
- [7] Rosenkrantz AB, Kong X, Niver BE et al. Prostate cancer: comparison of tumor visibility on trace diffusion-weighted images and the apparent diffusion coefficient map. *AJR Am J Roentgenol* 2011; 196(1):123–129
- [8] Metens T, Miranda D, Absil J, Matos C. What is the optimal b value in diffusion-weighted MR imaging to depict prostate cancer at 3T? *Eur Radiol* 2012; 22(3):703–709
- [9] Katahira K, Takahara T, Kwee TC et al. Ultra-high-b-value diffusion-weighted MR imaging for the detection of prostate cancer: evaluation in 201 cases with histopathological correlation. *Eur Radiol* 2011; 21(1):188–196
- [10] Rosenkrantz AB, Hindman N, Lim RP et al. Diffusion-weighted imaging of the prostate: Comparison of b1000 and b2000 image sets for index lesion detection. *J Magn Reson Imaging* 2013; 38(3):694–700
- [11] Maas MC, Fütterer JJ, Scheenen TW. Quantitative evaluation of computed high B value diffusion-weighted magnetic resonance imaging of the prostate. *Invest Radiol* 2013; 48(11):779–786
- [12] Grant KB, Agarwal HK, Shih JH et al. Comparison of calculated and acquired high b value diffusion-weighted imaging in prostate cancer. *Abdom Imaging* 2015; 40(3):578–586
- [13] Rosenkrantz AB, Chandarana H, Hindman N et al. Computed diffusion-weighted imaging of the prostate at 3 T: impact on image quality and tumour detection. *Eur Radiol* 2013; 23(11):3170–3177
- [14] Kim CK, Park BK, Lee HM, Kwon GY. Value of diffusion-weighted imaging for the prediction of prostate cancer location at 3 T using a phased-array coil: preliminary results. *Invest Radiol* 2007; 42(12):842–847
- [15] Kitajima K, Kaji Y, Kuroda K, Sugimura K. High b-value diffusion-weighted imaging in normal and malignant peripheral zone tissue of the prostate: effect of signal-to-noise ratio. *Magn Reson Med Sci* 2008; 7(2):93–99
- [16] Thörmer G, Otto J, Reiss-Zimmermann M et al. Diagnostic value of ADC in patients with prostate cancer: influence of the choice of b values. *Eur Radiol* 2012; 22(8):1820–1828
- [17] Issa B. In vivo measurement of the apparent diffusion coefficient in normal and malignant prostatic tissues using echo-planar imaging. *J Magn Reson Imaging* 2002; 16(2):196–200
- [18] Hosseinzadeh K, Schwarz SD. Endorectal diffusion-weighted imaging in prostate cancer to differentiate malignant and benign peripheral zone tissue. *J Magn Reson Imaging* 2004; 20(4):654–661
- [19] Sato C, Naganawa S, Nakamura T et al. Differentiation of noncancerous tissue and cancer lesions by apparent diffusion coefficient values in transition and peripheral zones of the prostate. *J Magn Reson Imaging* 2005; 21(3):258–262
- [20] Gibbs P, Pickles MD, Turnbull LW. Diffusion imaging of the prostate at 3.0 tesla. *Invest Radiol* 2006; 41(2):185–188
- [21] Pickles MD, Gibbs P, Sreenivas M, Turnbull LW. Diffusion-weighted imaging of normal and malignant prostate tissue at 3.0 T. *J Magn Reson Imaging* 2006; 23(2):130–134
- [22] deSouza NM, Reinsberg SA, Scurr ED, Brewster JM, Payne GS. Magnetic resonance imaging in prostate cancer: the value of apparent diffusion coefficients for identifying malignant nodules. *Br J Radiol* 2007; 80(950):90–95
- [23] Kim CK, Park BK, Han JJ, Kang TW, Lee HM. Diffusion-weighted imaging of the prostate at 3 T for differentiation of malignant and benign tissue in transition and peripheral zones: preliminary results. *J Comput Assist Tomogr* 2007; 31(3):449–454
- [24] Kumar V, Jagannathan NR, Kumar R et al. Apparent diffusion coefficient of the prostate in men prior to biopsy: determination of a cut-off value to predict malignancy of the peripheral zone. *NMR Biomed* 2007; 20(5):505–511
- [25] Mazaheri Y, Shukla-Dave A, Hricak H et al. Prostate cancer: identification with combined diffusion-weighted MR imaging and 3D 1H MR spectroscopic imaging—correlation with pathologic findings. *Radiology* 2008; 246(2):480–488
- [26] Tamada T, Sone T, Jo Y et al. Apparent diffusion coefficient values in peripheral and transition zones of the prostate: comparison between normal and malignant prostatic tissues and correlation with histologic grade. *J Magn Reson Imaging* 2008; 28(3):720–726
- [27] Vargas HA, Akin O, Franiel T et al. Diffusion-weighted endorectal MR imaging at 3 T for prostate cancer: tumor detection and assessment of aggressiveness. *Radiology* 2011; 259(3):775–784
- [28] Kitajima K, Takahashi S, Ueno Y et al. Clinical utility of apparent diffusion coefficient values obtained using high b-value when diagnosing prostate cancer using 3 tesla MRI: comparison between ultra-high b-value (2000s/mm²) and standard high b-value (1000s/mm²). *J Magn Reson Imaging* 2012; 36(1):198–205
- [29] Nagel KN, Schouten MG, Hambrock T et al. Differentiation of prostatitis and prostate cancer by using diffusion-weighted MR imaging and MR-guided biopsy at 3 T. *Radiology* 2013; 267(1):164–172
- [30] Schröder FH, Hugosson J, Roobol MJ et al; ERSPC Investigators. Screening and prostate-cancer mortality in a randomized European study. *N Engl J Med* 2009; 360(13):1320–1328
- [31] deSouza NM, Riches SF, Vanas NJ et al. Diffusion-weighted magnetic resonance imaging: a potential non-invasive marker of tumour aggressiveness in localized prostate cancer. *Clin Radiol* 2008; 63(7):774–782
- [32] Giles SL, Morgan VA, Riches SF, Thomas K, Parker C, deSouza NM. Apparent diffusion coefficient as a predictive biomarker of prostate cancer progression: value of fast and slow diffusion components. *AJR Am J Roentgenol* 2011; 196(3):586–591
- [33] Shinmoto H, Oshio K, Tanimoto A et al. Biexponential apparent diffusion coefficients in prostate cancer. *Magn Reson Imaging* 2009; 27(3):355–359
- [34] Turkbey B, Shah VP, Pang Y et al. Is apparent diffusion coefficient associated with clinical risk scores for prostate cancers that are visible on 3-T MR images? *Radiology* 2011; 258(2):488–495
- [35] Van As N, Charles-Edwards E, Jackson A et al. Correlation of diffusion-weighted MRI with whole mount radical prostatectomy specimens. *Br J Radiol* 2008; 81(966):456–462
- [36] Woodfield CA, Tung GA, Grand DJ, Pezzullo JA, Machan JT, Renzulli JF II. Diffusion-weighted MRI of peripheral zone prostate cancer: comparison of tumor apparent diffusion coefficient with Gleason score and percentage of tumor on core biopsy. *AJR Am J Roentgenol* 2010; 194(4):W316–W322
- [37] Yağci AB, Ozari N, Aybek Z, Düzcan E. The value of diffusion-weighted MRI for prostate cancer detection and localization. *Diagn Interv Radiol* 2011; 17(2):130–134
- [38] Delongchamps NB, Lefevre A, Bouazza N, Beuvon F, Legman P, Cornud F. Detection of significant prostate cancer with MR-targeted biopsies: Should TRUS-MRI fusion guided biopsies alone be a standard of care? *J Urol* 2015; 193(4):1198–1204
- [39] Lanz C, Cornud F, Beuvon F et al. Gleason score determination with TRUS-MRI fusion guided prostate biopsies: are we gaining in accuracy? *J Urol* 2016; 195(1):88–93
- [40] Bittencourt LK, Barentsz JO, de Miranda LC, Gasparetto EL. Prostate MRI: diffusion-weighted imaging at 1.5 T correlates better with prostatectomy Gleason Grades than TRUS-guided biopsies in peripheral zone tumours. *Eur Radiol* 2012; 22(2):468–475
- [41] Chamie K, Sonn GA, Finley DS et al. The role of magnetic resonance imaging in delineating clinically significant prostate cancer. *Urology* 2014; 83(2):369–375
- [42] Donati OF, Afaq A, Vargas HA et al. Prostate MRI: evaluating tumor volume and apparent diffusion coefficient as surrogate biomarkers for predicting tumor Gleason score. *Clin Cancer Res* 2014; 20(14):3705–3711

- [43] Hambrock T, Somford DM, Huisman HJ et al. Relationship between apparent diffusion coefficients at 3.0-T MR imaging and Gleason grade in peripheral zone prostate cancer. *Radiology* 2011; 259(2):453–461
- [44] Itatani R, Namimoto T, Kajihara H et al. Triage of low-risk prostate cancer patients with PSA levels 10 ng/ml or less: comparison of apparent diffusion coefficient value and transrectal ultrasound-guided target biopsy. *AJR Am J Roentgenol* 2014; 202(5):1051–1057
- [45] Itou Y, Nakanishi K, Narumi Y, Nishizawa Y, Tsukuma H. Clinical utility of apparent diffusion coefficient (ADC) values in patients with prostate cancer: can ADC values contribute to assess the aggressiveness of prostate cancer? *J Magn Reson Imaging* 2011; 33(1):167–172
- [46] Kim TH, Jeong JY, Lee SW et al. Diffusion-weighted magnetic resonance imaging for prediction of insignificant prostate cancer in potential candidates for active surveillance. *Eur Radiol* 2015; 25(6):1786–1792
- [47] Kitajima K, Takahashi S, Ueno Y et al. Do apparent diffusion coefficient (ADC) values obtained using high b-values with a 3-T MRI correlate better than a transrectal ultrasound (TRUS)-guided biopsy with true Gleason scores obtained from radical prostatectomy specimens for patients with prostate cancer? *Eur J Radiol* 2013; 82(8):1219–1226
- [48] Nagarajan R, Margolis D, Raman S et al. Correlation of Gleason scores with diffusion-weighted imaging findings of prostate cancer. *Adv Urol* 2012; 2012:374805
- [49] Oto A, Yang C, Kayhan A et al. Diffusion-weighted and dynamic contrast-enhanced MRI of prostate cancer: correlation of quantitative MR parameters with Gleason score and tumor angiogenesis. *AJR Am J Roentgenol* 2011; 197(6):1382–1390
- [50] Rosenkrantz AB, Triolo MJ, Melamed J, Rusinek H, Taneja SS, Deng FM. Whole-lesion apparent diffusion coefficient metrics as a marker of percentage Gleason 4 component within Gleason 7 prostate cancer at radical prostatectomy. *J Magn Reson Imaging* 2015; 41(3):708–714
- [51] Somford DM, Hambrock T, Hulsbergen-van de Kaa CA et al. Initial experience with identifying high-grade prostate cancer using diffusion-weighted MR imaging (DWI) in patients with a Gleason score $\leq 3+3=6$ upon schematic TRUS-guided biopsy: a radical prostatectomy correlated series. *Invest Radiol* 2012; 47(3):153–158
- [52] Thörmer G, Otto J, Horn LC et al. Non-invasive estimation of prostate cancer aggressiveness using diffusion-weighted MRI and 3D proton MR spectroscopy at 3.0T. *Acta Radiol* 2015; 56(1):121–128
- [53] Verma S, Rajesh A, Morales H et al. Assessment of aggressiveness of prostate cancer: correlation of apparent diffusion coefficient with histologic grade after radical prostatectomy. *AJR Am J Roentgenol* 2011; 196(2):374–381
- [54] Vos EK, Kobus T, Litjens GJ et al. Multiparametric Magnetic Resonance Imaging for Discriminating Low-Grade From High-Grade Prostate Cancer. *Invest Radiol* 2015; 50(8):490–497
- [55] Yoshimitsu K, Kiyoshima K, Irie H et al. Usefulness of apparent diffusion coefficient map in diagnosing prostate carcinoma: correlation with stepwise histopathology. *J Magn Reson Imaging* 2008; 27(1):132–139
- [56] Corcoran NM, Hong MK, Casey RG et al. Upgrade in Gleason score between prostate biopsies and pathology following radical prostatectomy significantly impacts upon the risk of biochemical recurrence. *BJU Int* 2011; 108(8 Pt 2):E202–E210
- [57] Chan TY, Partin AW, Walsh PC, Epstein JI. Prognostic significance of Gleason score 3+4 versus Gleason score 4+3 tumor at radical prostatectomy. *Urology* 2000; 56(5):823–827
- [58] Chandra RA, Chen MH, Zhang D, Loffredo M, D'Amico AV. Age, Comorbidity, and the Risk of Prostate Cancer-Specific Mortality in Men With Biopsy Gleason Score 4+3: Implications on Patient Selection for Multiparametric MRI. *Clin Genitourin Cancer* 2015; 13(4):400–405
- [59] Merrick GS, Butler WM, Galbreath RW, Lief JH, Adamovich E. Biochemical outcome for hormone-naïve patients with Gleason score 3+4 versus 4+3 prostate cancer undergoing permanent prostate brachytherapy. *Urology* 2002; 60(1):98–103
- [60] Stamey TA, McNeal JE, Yemoto CM, Sigal BM, Johnstone IM. Biological determinants of cancer progression in men with prostate cancer. *JAMA* 1999; 281(15):1395–1400
- [61] Cheng L, Koch MO, Juliar BE et al. The combined percentage of Gleason patterns 4 and 5 is the best predictor of cancer progression after radical prostatectomy. *J Clin Oncol* 2005; 23(13):2911–2917
- [62] Lebovici A, Sfrangeu SA, Feiler D et al. Evaluation of the normal-to-diseased apparent diffusion coefficient ratio as an indicator of prostate cancer aggressiveness. *BMC Med Imaging* 2014; 14:15
- [63] De Cobelli F, Ravelli S, Esposito A et al. Apparent diffusion coefficient value and ratio as noninvasive potential biomarkers to predict prostate cancer grading: comparison with prostate biopsy and radical prostatectomy specimen. *AJR Am J Roentgenol* 2015; 204(3):550–557
- [64] Rosenkrantz AB, Khalef V, Xu W, Babb JS, Taneja SS, Doshi AM. Does normalisation improve the diagnostic performance of apparent diffusion coefficient values for prostate cancer assessment? A blinded independent-observer evaluation. *Clin Radiol* 2015; 70(9):1032–1037
- [65] Scheenen TW, Rosenkrantz AB, Haider MA, Fütterer JJ. Multiparametric Magnetic Resonance Imaging in Prostate Cancer Management: Current Status and Future Perspectives. *Invest Radiol* 2015; 50(9):594–600
- [66] Sonn GA, Chang E, Natarajan S et al. Value of targeted prostate biopsy using magnetic resonance-ultrasound fusion in men with prior negative biopsy and elevated prostate-specific antigen. *Eur Urol* 2014; 65(4):809–815
- [67] Mazaheri Y, Hricak H, Fine SW et al. Prostate tumor volume measurement with combined T2-weighted imaging and diffusion-weighted MR: correlation with pathologic tumor volume. *Radiology* 2009; 252(2):449–457
- [68] Isebaert S, De Keyzer F, Haustermans K et al. Evaluation of semi-quantitative dynamic contrast-enhanced MRI parameters for prostate cancer in correlation to whole-mount histopathology. *Eur J Radiol* 2012; 81(3):e217–e222
- [69] Turkbey B, Mani H, Aras O et al. Correlation of magnetic resonance imaging tumor volume with histopathology. *J Urol* 2012; 188(4):1157–1163
- [70] Le Nobin J, Orczyk C, Deng FM et al. Prostate tumour volumes: evaluation of the agreement between magnetic resonance imaging and histology using novel co-registration software. *BJU Int* 2014; 114 6b:E105–E112
- [71] Cornud F, Khoury G, Bouazza N et al. Tumor target volume for focal therapy of prostate cancer—does multiparametric magnetic resonance imaging allow for a reliable estimation? *J Urol* 2014; 191(5):1272–1279
- [72] Langer DL, van der Kwast TH, Evans AJ et al. Intermixed normal tissue within prostate cancer: effect on MR imaging measurements of apparent diffusion coefficient and T2—sparse versus dense cancers. *Radiology* 2008; 249(3):900–908
- [73] Rosenkrantz AB, Mendrinis S, Babb JS, Taneja SS. Prostate cancer foci detected on multiparametric magnetic resonance imaging are histologically distinct from those not detected. *J Urol* 2012; 187(6):2032–2038
- [74] Le Bihan D, Breton E, Lallemand D, Aubin ML, Vignaud J, Laval-Jeantet M. Separation of diffusion and perfusion in intravoxel incoherent motion MR imaging. *Radiology* 1988; 168(2):497–505
- [75] Döpfert J, Lemke A, Weidner A, Schad LR. Investigation of prostate cancer using diffusion-weighted intravoxel incoherent motion imaging. *Magn Reson Imaging* 2011; 29(8):1053–1058
- [76] Kuru TH, Roethke MC, Stieltjes B et al. Intravoxel incoherent motion (IVIM) diffusion imaging in prostate cancer - what does it add? *J Comput Assist Tomogr* 2014; 38(4):558–564
- [77] Pang Y, Turkbey B, Bernardo M et al. Intravoxel incoherent motion MR imaging for prostate cancer: an evaluation of perfusion fraction and diffusion coefficient derived from different b-value combinations. *Magn Reson Med* 2013; 69(2):553–562
- [78] Quentin M, Blondin D, Klases J et al. Comparison of different mathematical models of diffusion-weighted prostate MR imaging. *Magn Reson Imaging* 2012; 30(10):1468–1474
- [79] Riches SF, Hawtin K, Charles-Edwards EM, de Souza NM. Diffusion-weighted imaging of the prostate and rectal wall: comparison of biexponential and monoexponential modelled diffusion and associated perfusion coefficients. *NMR Biomed* 2009; 22(3):318–325
- [80] Rosenkrantz AB, Sigmund EE, Johnson G et al. Prostate cancer: feasibility and preliminary experience of a diffusional kurtosis model for detection and assessment of aggressiveness of peripheral zone cancer. *Radiology* 2012; 264(1):126–135
- [81] Roethke MC, Kuder TA, Kuru TH et al. Evaluation of Diffusion Kurtosis Imaging Versus Standard Diffusion Imaging for Detection and Grading of Peripheral Zone Prostate Cancer. *Invest Radiol* 2015; 50(8):483–489
- [82] Gürses B, Kabakci N, Kovanlikaya A et al. Diffusion tensor imaging of the normal prostate at 3 Tesla. *Eur Radiol* 2008; 18(4):716–721
- [83] Bourne RM, Kurniawan N, Cowin G, Sved P, Watson G. Microscopic diffusion anisotropy in formalin fixed prostate tissue: preliminary findings. *Magn Reson Med* 2012; 68(6):1943–1948
- [84] Xu J, Humphrey PA, Kibel AS et al. Magnetic resonance diffusion characteristics of histologically defined prostate cancer in humans. *Magn Reson Med* 2009; 61(4):842–850
- [85] Manenti G, Cariani M, Mancino S et al. Diffusion tensor magnetic resonance imaging of prostate cancer. *Invest Radiol* 2007; 42(6):412–419
- [86] Takayama Y, Kishimoto R, Hanaoka S et al. ADC value and diffusion tensor imaging of prostate cancer: changes in carbon-ion radiotherapy. *J Magn Reson Imaging* 2008; 27(6):1331–1335

- [87] Kozlowski P, Chang SD, Meng R et al. Combined prostate diffusion tensor imaging and dynamic contrast enhanced MRI at 3T—quantitative correlation with biopsy. *Magn Reson Imaging* 2010; 28(5):621–628
- [88] Akin O, Sala E, Moskowitz CS et al. Transition zone prostate cancers: features, detection, localization, and staging at endorectal MR imaging. *Radiology* 2006; 239(3):784–792
- [89] Chesnais AL, Niaf E, Bratan F et al. Differentiation of transitional zone prostate cancer from benign hyperplasia nodules: evaluation of discriminant criteria at multiparametric MRI. *Clin Radiol* 2013; 68(6):e323–e330
- [90] Yoshizako T, Wada A, Hayashi T et al. Usefulness of diffusion-weighted imaging and dynamic contrast-enhanced magnetic resonance imaging in the diagnosis of prostate transition-zone cancer. *Acta Radiol* 2008; 49(10):1207–1213
- [91] Delongchamps NB, Rouanne M, Flam T et al. Multiparametric magnetic resonance imaging for the detection and localization of prostate cancer: combination of T2-weighted, dynamic contrast-enhanced and diffusion-weighted imaging. *BJU Int* 2011; 107(9):1411–1418
- [92] Haider MA, van der Kwast TH, Tanguay J et al. Combined T2-weighted and diffusion-weighted MRI for localization of prostate cancer. *AJR Am J Roentgenol* 2007; 189(2):323–328
- [93] Hoeks CMA, Hambroek T, Yakar D et al. Transition zone prostate cancer: detection and localization with 3-T multiparametric MR imaging. *Radiology* 2013; 266(1):207–217
- [94] Jung SI, Donati OF, Vargas HA, Goldman D, Hricak H, Akin O. Transition zone prostate cancer: incremental value of diffusion-weighted endorectal MR imaging in tumor detection and assessment of aggressiveness. *Radiology* 2013; 269(2):493–503
- [95] Rosenkrantz AB, Kim S, Campbell N, Gaing B, Deng FM, Taneja SS. Transition zone prostate cancer: revisiting the role of multiparametric MRI at 3 T. *AJR Am J Roentgenol* 2015; 204(3):W266–W272
- [96] Barral M, Cornud F, Neuzillet Y, et al. Characteristics of undetected prostate cancer on diffusion-weighted MR Imaging at 3-Tesla with a b-value of 2000s/mm: Imaging-pathologic correlation. *Diagn Interv Imaging*. 2015;92:923–929.
- [97] Oto A, Kayhan A, Jiang Y et al. Prostate cancer: differentiation of central gland cancer from benign prostatic hyperplasia by using diffusion-weighted and dynamic contrast-enhanced MR imaging. *Radiology* 2010; 257(3):715–723
- [98] Kim CK, Park BK, Kim B. High-b-value diffusion-weighted imaging at 3 T to detect prostate cancer: comparisons between b values of 1,000 and 2,000 s/mm². *AJR Am J Roentgenol* 2010; 194(1):W33–W37
- [99] Kim JH, Kim JK, Park BW, Kim N, Cho KS. Apparent diffusion coefficient: prostate cancer versus noncancerous tissue according to anatomical region. *J Magn Reson Imaging* 2008; 28(5):1173–1179
- [100] Hoeks CM, Vos EK, Bomers JG, Barentsz JO, Hulsbergen-van de Kaa CA, Scheenen TW. Diffusion-weighted magnetic resonance imaging in the prostate transition zone: histopathological validation using magnetic resonance-guided biopsy specimens. *Invest Radiol* 2013; 48(10):693–701
- [101] Kobus T, Vos PC, Hambroek T et al. Prostate cancer aggressiveness: in vivo assessment of MR spectroscopy and diffusion-weighted imaging at 3 T. *Radiology* 2012; 265(2):457–467

5 Dynamic Contrast-Enhanced MRI of the Prostate

Baris Turkbey, Sandeep Sankineni, and Peter L. Choyke

5.1 Introduction

Dynamic contrast-enhanced MRI (DCE-MRI) is one of the three pulse sequences that comprise a multiparametric MRI for noninvasive evaluation of the prostate gland in patients with either a clinical suspicion or diagnosis of prostate cancer. DCE-MRI has been widely used in oncologic imaging since it offers assessment of the vascularity as well as capillary permeability characteristics within tumors. This chapter discusses the current role of DCE-MRI in prostate cancer, with particular attention to the Prostate Imaging–Reporting and Data System version 2 (PI-RADS v2) guidelines.

5.2 What is Dynamic Contrast-Enhanced MRI?

Angiogenesis is a key step for cancer growth and is characterized by blood vessel proliferation that is induced in response to high needs for oxygen and nutrients. The pattern of vessels in tumor angiogenesis does not follow the classic arteriole–capillary–venule hierarchy. Instead, the vessels are more disorganized, anarchic, permeable, and tortuous than the normal vasculature.¹ DCE-MRI noninvasively evaluates this neoangiogenic process. DCE-MRI consists of T1-weighted (T1W) fast gradient-echo images of the prostate before, during, and after intravenous injection of a low molecular weight gadolinium chelate. During DCE-MRI, the prostate is scanned using serial volumetric acquisitions obtained in continual fashion. Much variability exists among centers in terms of numerous aspects of DCE-MRI acquisition, including both the temporal resolution and total acquisition duration. Variability in the temporal resolution relates to the inherent trade-off in MRI between temporal resolution and spatial resolution. While a temporal resolution of ≤ 15 seconds is advised by PI-RADS v2, many centers prefer to use a more rapid temporal resolution of under 7 seconds. Although not widely used in clinical practice, even faster temporal resolutions of approximately 3 seconds have been successfully implemented as well. In addition, in the past, extended acquisitions for 5 minutes or longer were common.^{2,3} However, given the diminished role of characterizing extended contrast kinetics in PI-RADS v2 (as described in more detail below), PI-RADS v2 now supports a more abbreviated DCE-MRI acquisition, advising a minimum of duration of only 2 minutes.⁴ While maintaining high temporal resolution, the spatial resolution of DCE-MRI should also be adjusted to prevent volume averaging and to enable optimum depiction of suspicious lesions. Novel acquisition schemes, for instance combining DCE-MRI with radial acquisition, compressed sensing, and advanced parallel imaging reconstruction methods, may be able to further optimize the combination of both high spatial resolution and high temporal resolution in the future.⁵ While acquisition of DCE-MRI can vary depending on the MRI scanner and coil elements available, the PI-RADS v2 document summarizes the acceptable ranges for technical specifications (► Table 5.1).

5.3 How to Evaluate and Interpret Dynamic Contrast-Enhanced MRI?

DCE-MRI can be evaluated qualitatively, quantitatively, or semiquantitatively. The qualitative approach is the most commonly used method for interpretation of DCE-MRI. Qualitatively, tumors exhibit early enhancement of the contrast media relative to the surrounding prostate parenchyma due to the leakiness of tumor vessels.³ Qualitative analysis involves scrolling through the serial dynamic time points in order to visually assess for a region of earlier contrast enhancement within lesions. This can be accomplished using a regular Picture Archiving and Communication System (PACS) workstation with a trackwheel mouse without additional software. The qualitative approach is the simplest method and is recommended by PI-RADS v2 guidelines, which summarizes such a qualitative evaluation in the form of a binary assessment (“negative” or “positive”) (► Table 5.2). Negative enhancement refers to the absence of early enhancement as well as to diffuse enhancement that does not correspond to a focal finding identified on T2W-MRI and/or DW-MRI. DCE-MRI is also considered negative when there is focal enhancement in a lesion predicted to represent a benign prostatic hyperplasia nodule based on its characteristic T2W-MRI features (for instance, a well-circumscribed nodule located in the transition zone). Positive enhancement refers to enhancement that is “focal, and earlier than or contemporaneous with enhancement of adjacent normal prostatic tissues, and that corresponds to a suspicious finding on T2W-MRI and/or DW-MRI.” Thus, in qualitative analysis, DCE-MRI is considered positive if there is focal early enhancement in a lesion corresponding to an abnormality identified on T2W-MRI

Table 5.1 DCE-MRI pulse sequence parameters suggested by PI-RADS v2 guidelines

DCE-MRI sequence parameters	2D or 3D T1W gradient-echo images (3D preferred)
TR/TE	< 100 ms / < 5 ms
Slice thickness	3 mm, no gaps
Field of view	Entire prostate gland & seminal vesicles
In plane dimension	≤ 2 mm x ≤ 2 mm
Temporal resolution	≤ 10 s (< 7 s preferred)
Total observation time	≥ 2 min
Contrast dose	0.1 mmol/kg standard GBCA or equivalent high relaxivity GBCA
Contrast injection rate	2–3 cm ³ /s with continuous image acquisition

Abbreviations: DCE-MRI, dynamic contrast-enhanced MRI; 2D, two-dimensional; 3D, three-dimensional; GBCA, gadolinium-based contrast agents; T1W, T1-weighted; TR, relaxation time; TE, echo time.

Source: Adapted from American College of Radiology (ACR) Prostate Imaging–Reporting and Data System (PI-RADS), version 2, 2015. Available at www.acr.org.

Table 5.2 DCE-MRI scoring criteria in PI-RADS v2 guidelines

DCE-MRI score	Criteria
Positive (must meet all 3 criteria)	<ol style="list-style-type: none"> 1. Focal 2. Enhances earlier than or simultaneously with enhancement of adjacent normal tissue 3. Corresponds to suspicious finding on T2WI and/or DWI
Negative (if any criterion holds true)	No early enhancement or Diffuse enhancement, not corresponding to a focal finding on T2WI and /or DWI or Focal enhancement corresponding to a lesion demonstrating features of BPH on T2WI

Abbreviations: BPH, benign prostatic hyperplasia; DWI, diffusion-weighted imaging; DCE-MRI, dynamic contrast-enhanced MRI; T2WI, T2-weighted imaging.

Source: Adapted from American College of Radiology (ACR) Prostate Imaging–Reporting and Data Systems (PI-RADS), version 2, 2015. Available at www.acr.org.

or DW-MRI.⁶ When performing qualitative visual assessment of DCE-MRI, generation of subtracted postcontrast images can be useful to increase conspicuity of enhancing foci, as well as to eliminate increased signal in areas of postbiopsy hemorrhage that is encountered on the baseline T1WI.

Semiquantitative analysis entails analyzing the enhancement kinetics within a given region of interest in the prostate, considering both the washin and washout of the enhancement curve. Semiquantitative assessment may be performed in two different fashions. One approach is to use software to generate time-signal-intensity curves depicting the contrast kinetics within a suspicious region identified either on the source images or on other sequences. Most commonly, such curves are evaluated using a schema based on three curve types. In this schema, type 1 refers to persistently increasing enhancement, which is typically observed in benign prostate tissue; type 2 refers to an initial rapid rise followed by a plateau of enhancement, which is observed in either tumors or benign inflammatory processes; and type 3 refers to a rapid rise and subsequent decline (washout) in enhancement, representing the curve type that is the most suspicious for prostate cancer. Alternatively a voxel-by-voxel parametric map may be constructed from the dynamic image sets in which the voxel values characterize various aspects of the kinetic curve such as the slope of the washin, the slope of the washout, the time to peak, or the peak enhancement. The map is typically displayed in a colored fashion superimposed on the T1- or T2-weighted images and is then evaluated visually for an area of abnormal color, indicating an abnormality of the given semiquantitative perfusion metric. Although semiquantitative methods are also relatively straightforward provided that appropriate software is available, challenges exist in their application. Most notably, all three kinetic patterns (curve types 1, 2, and 3) can be present in either benign or malignant prostate lesions given the increased vascularity of benign processes such as benign prostatic hyperplasia (BPH) nodules and inflammation. Hansford et al evaluated the diagnostic performance and interobserver agreement of curve

type analysis in 120 patients among 3 readers. While similar receiver operating characteristic curves were reported for all readers, mean area under the curves (AUCs) were poor (0.58 ± 0.04 [standard deviation] to 0.63 ± 0.04). Observer agreement in differentiating type 3 curves from either type 1 or type 2 curves was substantial ($0.66 < k < 0.79$), and better in PCa than in healthy tissue. However, the interreader agreement for differentiating type 1 from type 2 curves was only moderate to substantial ($0.49 < k < 0.78$). Based on the findings, the authors concluded that this semiquantitative approach provided an overall poor performance for differentiating prostate cancer from benign tissue.⁷ While the semiquantitative approach was endorsed in PI-RADS v1, concerns regarding its greater complexity compared with a visual qualitative method (including the need for dedicated software) yet questionable reproducibility and accuracy, have hampered its widespread clinical use, and the method was removed from PI-RADS v2.

Quantitative analysis is the most sophisticated DCE-MRI evaluation. This approach entails calculating a set of kinetic parameters by fitting the enhancement curve to one of a number of pharmacokinetic models, most commonly the Tofts model. Parameters derived from the Tofts model include K^{trans} (transendothelial transport of contrast medium from the vascular compartment to the tumor interstitium), k_{ep} (reverse transport parameter of contrast medium back to the vascular space), V_p (plasma volume fraction compared to whole tissue volume), and V_e (extravascular, extracellular volume fraction of the tumor), which collectively are intended to characterize tumor and tissue permeability properties.⁸ These parameters are typically computed on a voxel-by-voxel basis and displayed as a parametric map overlaid on an anatomical image set, as is also possible using the semiquantitative approach. K^{trans} and k_{ep} tend to be higher in cancer foci compared to normal tissue. Nonetheless, as in the semiquantitative approach, these parameters are nonspecific and may also be abnormal in benign processes such as BPH nodules and inflammation.⁹ Furthermore, software required for a quantitative approach is less widely available in clinical practice, and the implementation of this method is more technically demanding, for instance requiring measurement of an arterial input function in order to improve the precision of K^{trans} estimates. Variability in DCE-MRI acquisition parameters, as well as in the algorithms used by software packages for performing the Tofts model, lead to inter- and inpatient variation in the computed perfusion metrics. This method did not appear in either PI-RADS v1 or v2 given insufficient peer-reviewed published data or expert consensus to support routine adoption of quantitative analysis for clinical use (PI-RADS v2 document).

5.4 Dynamic contrast-enhanced MRI in the Detection of Localized Prostate Cancer

For more than a decade, DCE-MRI has been considered an important component of multiparametric MRI protocols for detecting prostate cancer (► Fig. 5.1; ► Fig. 5.2; ► Fig. 5.3; ► Fig. 5.4). Indeed, early studies of this technique showed an incremental benefit compared with T2W-MRI alone. For instance, in a cohort of 70 patients who underwent radical prostatectomy, combined use of

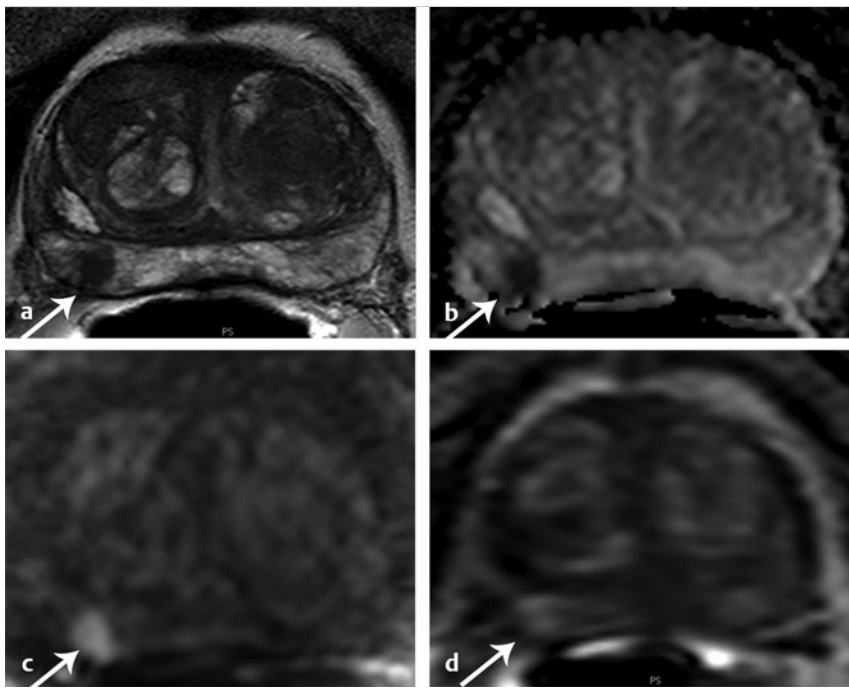


Fig. 5.1 A 55-year-old patient with prostate-specific antigen = 8.98 ng/mL. Axial T2-weighted MRI shows a hypointense lesion in the right mid-peripheral zone (arrow) (a). Apparent diffusion coefficient (ADC) map of from diffusion-weighted MRI (DW-MRI) identify a hypointense lesion in the same location (b), which is further confirmed by a hyperintense signal pattern on the high b-value DW-MRI (c). The lesion shows focal hyperenhancement on dynamic contrast-enhanced MRI (d). The patient underwent MRI-transrectal ultrasound fusion-targeted biopsy which resulted in a Gleason score 4+4 prostate cancer diagnosis. The patient then underwent a robot-assisted radical prostatectomy, for which histopathology revealed Gleason score 3+4 prostate cancer within the lesion.

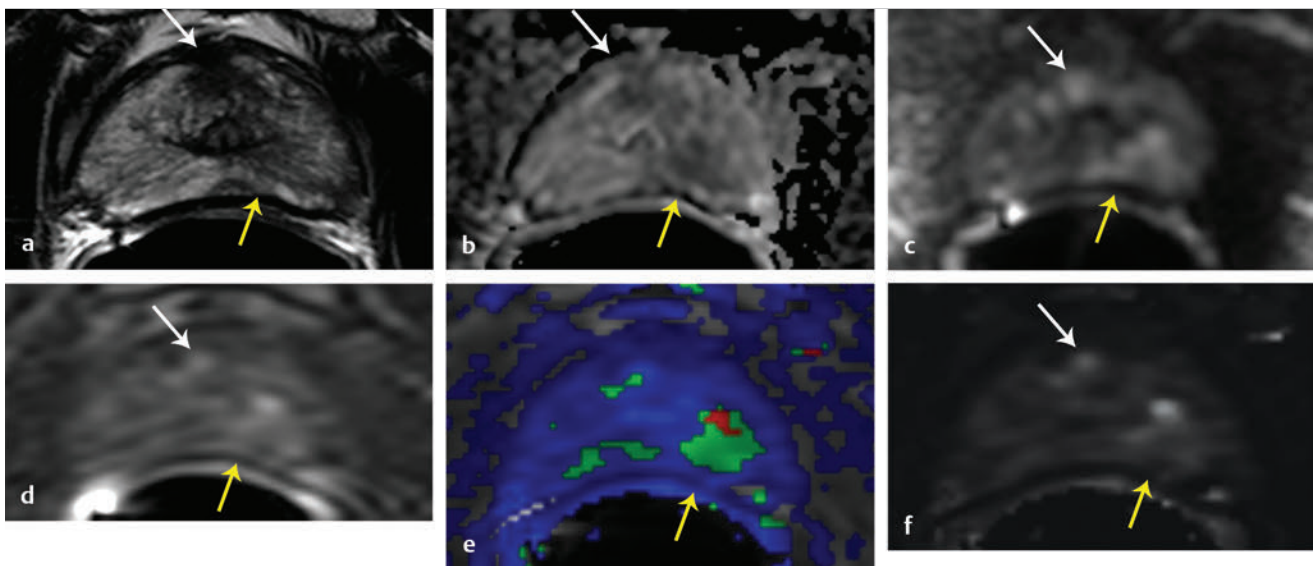


Fig. 5.2 A 65-year-old man with prostate-specific antigen = 7.3 ng/mL. Axial T2-weighted MRI shows a hypointense lesion in the midline anterior transition zone (white arrow) and a slightly hypointense heterogeneous lesion in the left apical peripheral zone (yellow arrow) (a). The apparent diffusion coefficient map from diffusion-weighted MRI (b) and the $b = 2000s/mm^2$ DW-MRI (c) show a hypointense and a hyperintense signal pattern within the midline anterior transition zone lesion (white arrows) and the left apical peripheral zone lesion (yellow arrows), respectively. Dynamic contrast-enhanced MRI demonstrates focal enhancement within both lesions; however, the enhancement is more focal in the midline anterior transition zone lesion (white arrow) compared to the left apical peripheral zone lesion (yellow arrow) (d). The K^{trans} map (e) localizes only the left apical peripheral zone lesion (yellow arrow), whereas the k_{ep} map (f) localizes both lesions (white and yellow arrows). The patient underwent a targeted biopsy via the MRI-transrectal ultrasound fusion approach and histopathology revealed Gleason score 3+4 cancer in both lesions.

DCE-MRI with T2W-MRI was found to have a probability of tumor detection of 0.58 compared to use of T2W-MRI alone, which was approximately 0.43. However, its role has more recently been questioned given a view by some experts that findings from DCE-MRI may enhance tumor detection compared with findings from the combination of T2W-MRI and DW-MRI alone, but in less than 20% of cases. The exact additive role of DCE-MRI relative to T2W- and DW-MRI has not been extensively investigated. Nonetheless,

one meta-analysis aimed to systematically review DCE-MRI for the detection of prostate cancer in comparison with T2W- and DW-MRI. This meta-analysis included 22 high-quality studies. Both DCE-MRI (0.82–0.86) and DW-MRI (0.84–0.88) yielded significantly better AUC than T2W-MRI alone (0.68–0.77).¹⁰ While DCE-MRI improved tumor detection in comparison with T2W-MRI alone, DCE-MRI did not clearly raise performance compared with the combination of T2WI and DWI.¹⁰ Thus, a simpler MRI

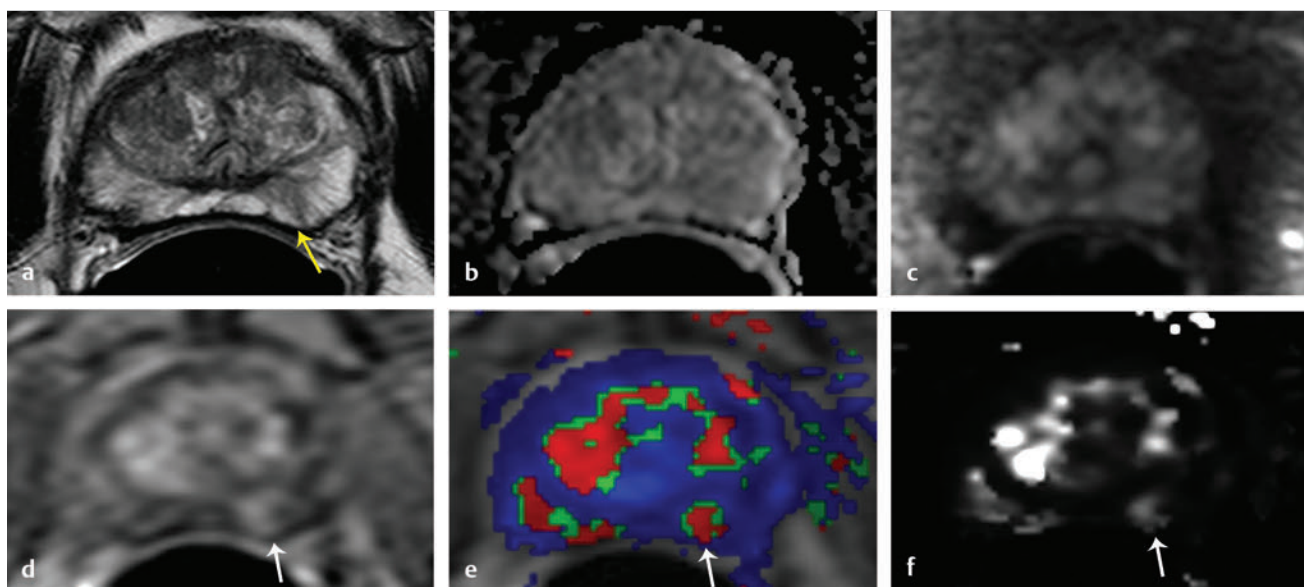


Fig. 5.3 A 69-year-old man with prostate-specific antigen = 9.6 ng/mL. Axial T2-weighted MRI (T2W-MRI) shows a patchy signal pattern in the peripheral zone (more prominent on the left) (a). The apparent diffusion coefficient (ADC) map from diffusion-weighted MRI (DW-MRI) (b) and the $b = 2000 \text{ s/mm}^2$ DW-MRI (c) show no lesion in the peripheral zone. Dynamic contrast-enhanced MRI (DCE-MRI) demonstrates focal enhancement within the left apical mid-peripheral zone lesion (arrow) (d). K^{trans} (e) and k_{ep} (f) maps derived from DCE-MRI also localize the left apical mid-peripheral zone lesion (arrows). The focal enhancing lesion in the left apical mid-peripheral zone is found to correspond to a focal heterogeneous lesion in the left apical mid-peripheral zone on T2W-MRI (yellow arrow) (a). The patient underwent a targeted biopsy via the MRI-transrectal ultrasound fusion approach and histopathology revealed Gleason score 3 + 4 cancer in the left apical mid-peripheral zone lesion. Please note that the entire right peripheral zone is coded false positively on the K^{trans} (e) and k_{ep} (f) maps.

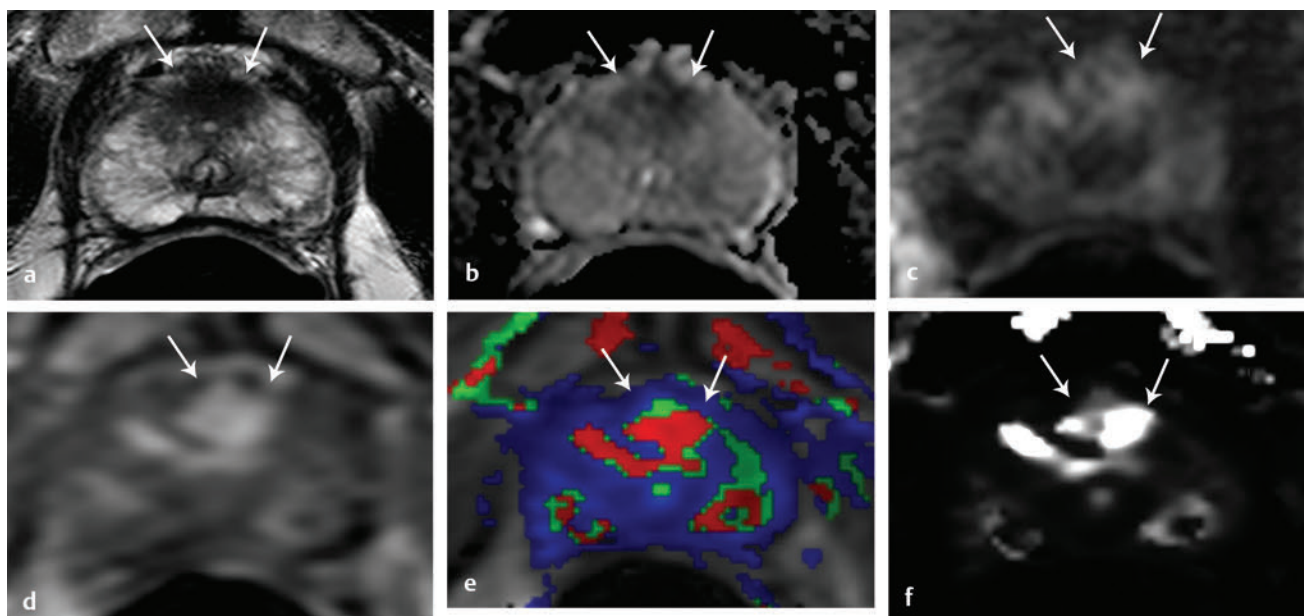


Fig. 5.4 A 69-year-old man with prostate-specific antigen = 9.6 ng/mL. Axial T2-weighted MRI shows a linear hypointense lesion in the midline midanterior transition zone (arrows) (a). The apparent diffusion coefficient map from diffusion-weighted MRI (DW-MRI) (b) and the $b = 2000 \text{ s/mm}^2$ DW-MRI (c) show a diffuse hypointense and a diffuse hyperintense signal pattern within the midline midanterior transition zone lesion, respectively (arrows). Dynamic contrast-enhanced MRI (DCE-MRI) demonstrates focal enhancement within the midline midanterior transition zone lesion (arrows) (d). K^{trans} (e) and k_{ep} (f) maps derived from DCE-MRI also localize the midline midanterior transition zone lesion (arrows). The patient underwent a targeted biopsy via the MRI-transrectal ultrasound fusion approach and histopathology revealed Gleason score 4 + 4 cancer in the midline midanterior transition zone lesion.

protocol including only T2W-MRI and DW-MRI without DCE-MRI may be sufficient for tumor detection.¹⁰ Another meta-analysis compared the diagnostic performance of DW-MRI and DCE-

MRI for prostate cancer detection within the same patient populations. This analysis included only 5 eligible studies (265 patients). The pooled sensitivity was 58.4% (95%

confidence interval [CI], 53.5–63.1%) for DW-MRI and 55.3% (95% CI, 50.4–60.1%) for DCE-MRI, whereas pooled specificity was 89.0% (95% CI, 87.2–90.7%) for DW-MRI and 87.9% (95% CI, 86.0–89.6%) for DCE-MRI. At the summary receiver-operating-characteristic curve analysis, AUC was 0.810 ($p = 0.059$) for DW-MRI and 0.786 ($p = 0.079$) for DCE-MRI. The performance of DW-MRI and DCE-MRI was thus very similar, with both sequences offering greater specificity than sensitivity.¹¹ The findings suggest that DCE-MRI may not offer an advantage over DW-MRI.

Currently, PI-RADS v2 guidelines prepared by the American College of Radiology and the European Society of Urogenital Radiology advise that DCE-MRI only impact the assessment of indeterminate (PI-RADS assessment category 3) lesions in the peripheral zone, elevating the overall assessment category for such lesions to a PI-RADS category 4 when DCE-MRI is positive. While PI-RADS v2 supports reporting the DCE-MRI score for transition zone (TZ) lesions, the DCE-MRI score currently does not in any circumstance influence the overall assessment category in the TZ. This decision was made essentially due to the common hypervascularity within BPH nodules, including both rapid washin and washout, thus limiting the diagnostic value of DCE-MRI findings in this zone. The lack of diagnostic value of DCE-MRI in the TZ is supported by studies (► Fig. 5.5; ► Fig. 5.6).¹²

Nonetheless, PI-RADS v2 also suggests that it is important to carefully evaluate the DCE-MRI for suspicious abnormalities when interpreting T2W-MRI and DW-MRI.⁴ That is, the high-contrast nature of DCE-MRI, as well as better spatial resolution than DWI, may help to initially identify potential abnormalities and to draw the reader's attention to areas to then evaluate more carefully on T2WI and DWI. Although an isolated finding identified solely on DCE-MRI without a correlate on other sequences is considered benign and does not receive a PI-RADS assessment category using

PI-RADS v2, findings on DCE-MRI may help in the evaluation of an equivocal or challenging lesion identified on other sequences and raise the reader's confidence in raising suspicion for a subtle lesion (► Fig. 5.3; ► Fig. 5.7). In particular, findings from DCE-MRI may be useful for possible lesions in regions of the prostate that are anatomically challenging to evaluate, such as the central zone, distal apex, and anterior fibromuscular stroma, as well as the subcapsular crescentic lesions (► Fig. 5.7; ► Fig. 5.8). For instance, one study observed type 1 or type 2 kinetic curves in the normal central zone, suggesting that the presence of a type 3 curve in this region may be useful for differentiating normal central zone tissue and central zone tumor.¹³ In addition, occasionally, a high-grade or infiltrative tumor that is not readily appreciated using DWI and the apparent diffusion coefficient (ADC) ADC may show an abnormality using DCE-MRI. Thus, while further research is required to establish the exact additive value of DCE-MRI within the context of a multiparametric protocol, radiologists may still deem DCE-MRI to be a useful sequence for these practical purposes. Finally, DCE-MRI may be useful as an alternative parameter when the primary sequences are degraded for technical reasons (i.e., motion artifact on T2W-MRI; distortions, susceptibility artifact, or low signal-to-noise ratio on DWI/ADC).

DCE-MRI has also been explored for assessing prostate cancer aggressiveness. However, results have been mixed, with some studies showing strong associations between DCE-MRI metrics and aggressiveness and other studies showing no relationship. For instance, in a cohort of 45 patients with prostate cancer who underwent DCE-MRI, tumors were classified as low-grade (only Gleason grade of 2 or 3), intermediate-grade (secondary or tertiary Gleason grade 4 without grade 5 component), or high-grade (primary Gleason grade of 4 and/or any grade 5 component).¹⁴ DCE-MRI was viewed as a parametric overlay on T2W-MRI, and mean and quartile values from semiquantitative

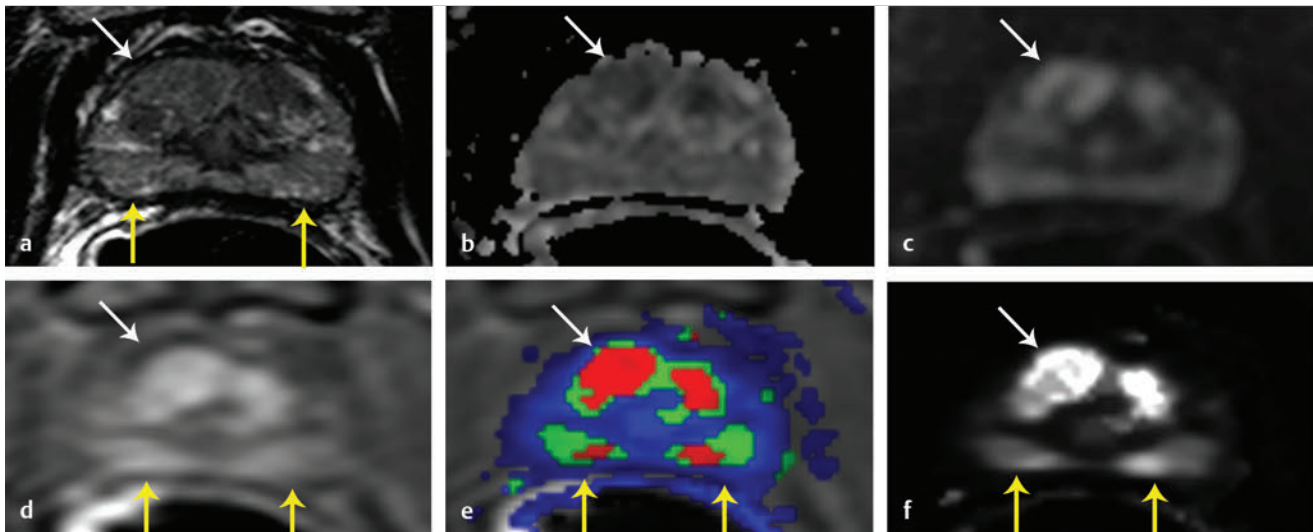


Fig. 5.5 A 63-year-old man with prostate-specific antigen = 11 ng/mL. Axial T2-weighted MRI (T2W-MRI) (a), the apparent diffusion coefficient map from diffusion-weighted MRI (b), and the $b=2000 \text{ s/mm}^2$ DW-MRI (c) show a lesion in the right apical midanterior transition zone (also affecting the left anterior transition zone) (white arrows). Dynamic contrast-enhanced MRI (DCE-MRI) demonstrates focal enhancement within the lesion (white arrow) (d); additionally the K^{trans} (e) and k_{ep} (f) maps derived from DCE-MRI localize the anterior transition zone lesion (white arrows). The patient underwent a targeted biopsy via the MRI–transrectal ultrasound fusion approach and histopathology revealed Gleason score 4 + 4 cancer within the anterior transition zone lesion. Please note that the peripheral zone has a patchy heterogeneous signal pattern on T2W-MRI (consistent with inflammatory changes) (yellow arrows) (a), which demonstrates false-positive hyperenhancement on DCE-MRI (d) and on K^{trans} and k_{ep} maps (e,f; yellow arrows).

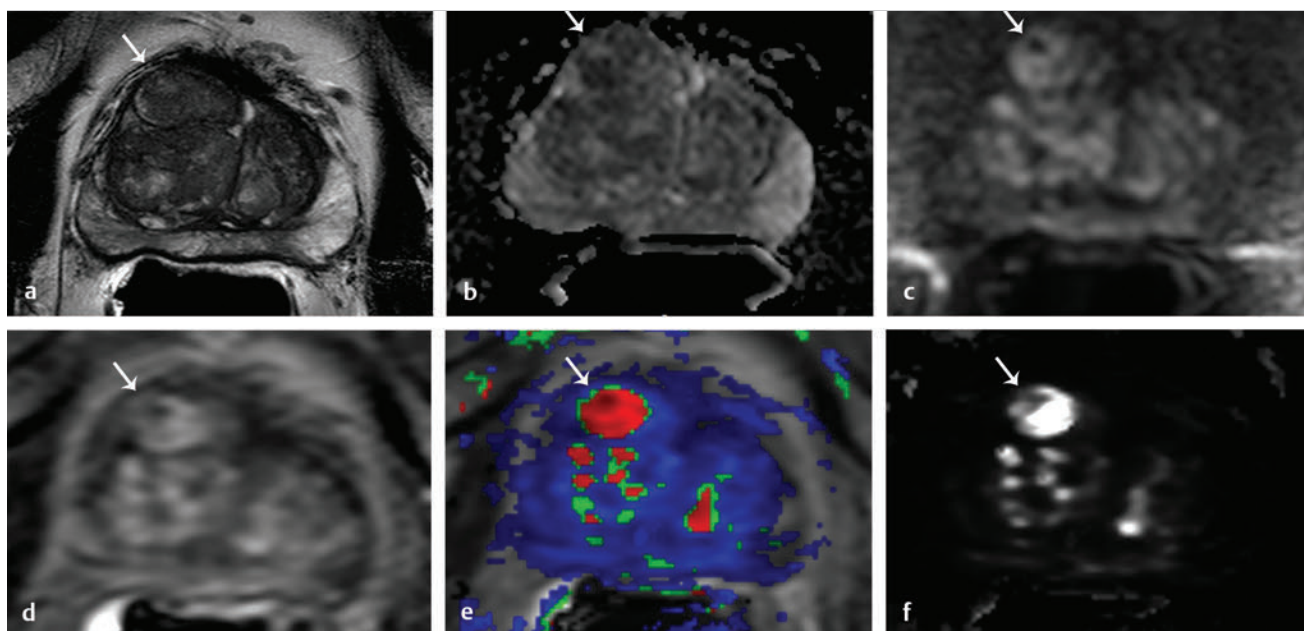


Fig. 5.6 A 65-year-old man with prostate-specific antigen = 16 ng/mL. Axial T2-weighted MRI shows a well-defined hypointense nodule in the right midanterior transition zone (*arrow*) (a). The apparent diffusion coefficient (ADC) map from diffusion-weighted MRI (DW-MRI) (b) and the $b = 2000 \text{ s/mm}^2$ DW-MRI (c) show a diffuse hypointense and a diffuse hyperintense signal pattern within the right midanterior transition zone nodule, respectively (*arrows*). Dynamic contrast-enhanced MRI demonstrates focal enhancement within the right midanterior transition zone nodule (*arrow*) (d). The K^{trans} (e) and k_{ep} (f) maps derived from DCE-MRI also localize the right midanterior zone nodule (*arrows*). This nodule corresponds to a benign prostatic hyperplasia nodule and falsely appears positive for cancer on the raw DCE-MRI and quantitative DCE-MRI maps.

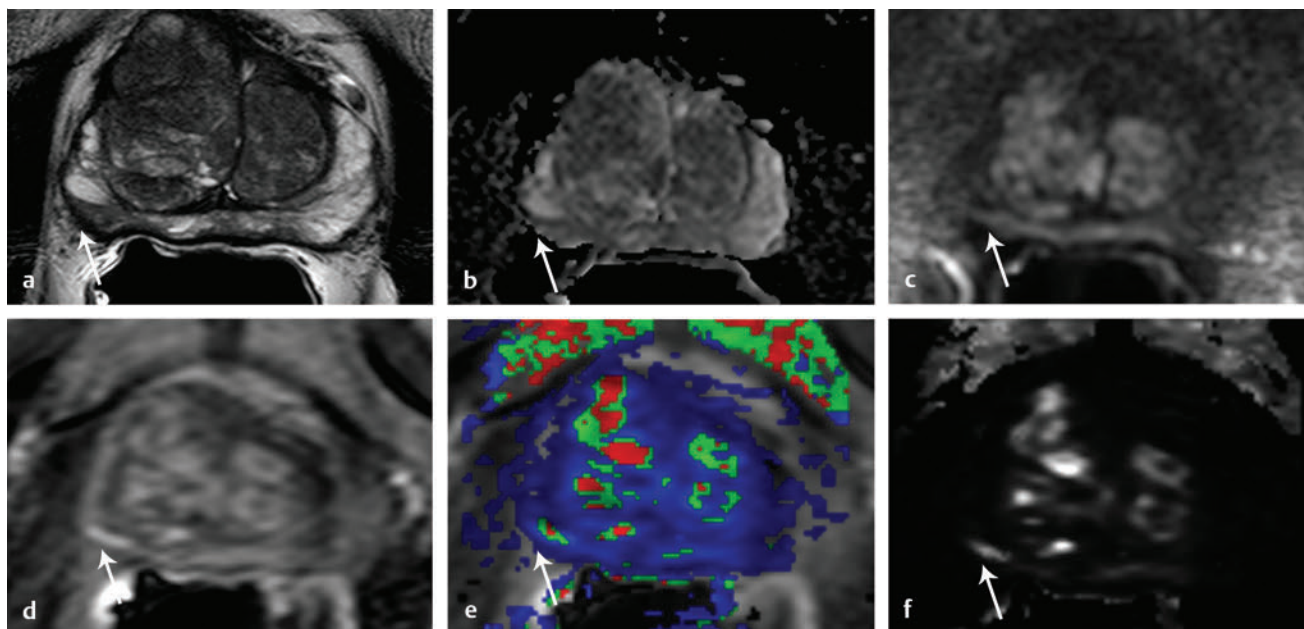


Fig. 5.7 A 65-year-old man with prostate-specific antigen = 16 ng/mL. Axial T2-weighted MRI shows a linear hypointense lesion in the right mid-peripheral zone (*arrow*) (a). The apparent diffusion coefficient map from diffusion-weighted MRI (DW-MRI) (b) and the $b = 2000 \text{ s/mm}^2$ DW-MRI (c) show a diffuse hypointense and a diffuse hyperintense signal pattern within the right mid-peripheral zone, respectively (*arrows*). Dynamic contrast-enhanced MRI (DCE-MRI) demonstrates focal enhancement within the right mid-peripheral zone lesion (*arrow*) (d). K^{trans} (e) and k_{ep} (f) maps derived from DCE-MRI also localize the right mid-peripheral zone lesion (*arrows*). The patient underwent a targeted biopsy via the MRI-transrectal ultrasound fusion approach and histopathology revealed Gleason score 4+4 cancer in the right mid-peripheral zone lesion.

and pharmacokinetic model parameters were extracted from tumor regions. Significant differences were present for the mean and 75th percentile (hereafter, p75) values of washin, the mean

value of the washout, and the p75 of the transfer constant (K^{trans}), as well as between low-grade and high-grade prostate cancer in the peripheral zone. Receiver-operating-characteristic (ROC) curve

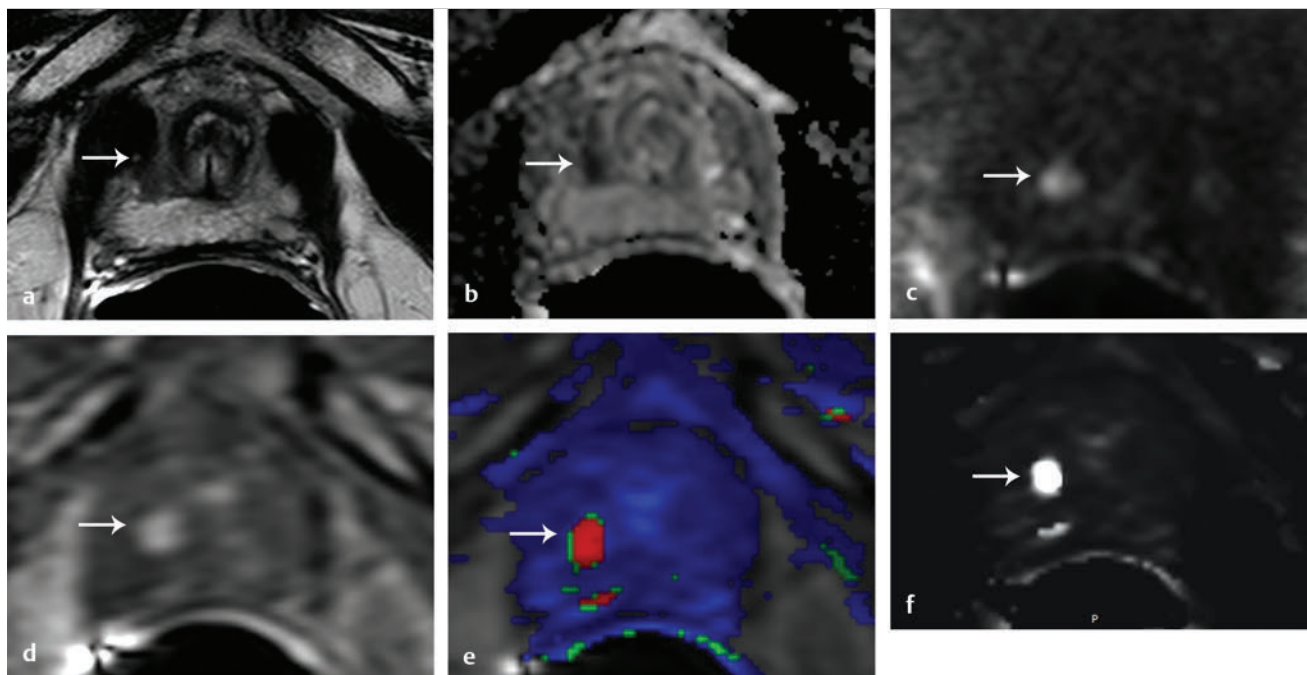


Fig. 5.8 A 70-year-old man with prostate-specific antigen = 4.6 ng/mL. Axial T2-weighted MRI shows a hypointense lesion in the right distal apical anterior peripheral zone (arrow) (a). The apparent diffusion coefficient map from diffusion-weighted MRI (DW-MRI) (b) and the $b = 2000 \text{ s/mm}^2$ DW-MRI (c) show a diffuse hypointense and a diffuse hyperintense signal pattern within the right distal apical anterior peripheral zone lesion, respectively (arrows). Dynamic contrast-enhanced MRI (DCE-MRI) demonstrates focal enhancement within the right distal apical anterior peripheral zone lesion (arrow) (d). K^{trans} (e) and k_{ep} (f) maps derived from DCE-MRI also localize the right distal apical anterior peripheral zone lesion (arrows). The patient underwent a targeted biopsy via MRI-transrectal ultrasound fusion approach and histopathology revealed Gleason score 4 + 3 cancer in the right distal apical anterior peripheral zone lesion.

analysis identified that the best discriminating performance between low-grade prostate cancer and intermediate- plus high-grade prostate cancer in the peripheral zone was the p75 of washin, K^{trans} , and the rate constant (k_{ep}) (AUC=0.72). Their results were only valid for the peripheral zone since this study included only a limited number of tumors in the transition zone. They concluded that quantitative parameters (K^{trans} and k_{ep}) and semiquantitative parameters (washin and washout) derived from DCE-MRI at 3T have the potential to assess the aggressiveness of PCa in the peripheral zone.¹⁴ The same group also aimed to correlate pharmacokinetic DCE-MRI parameters with microvascular and lymphatic histology parameters in 18 patients with localized prostate cancer.¹⁵ They correlated K^{trans} , V_e , and k_{ep} with immunohistochemically depicted microvessel density (MVD), area (MVA), and perimeter (MVP) and lymph vessel density (LVD), area (LVA), and perimeter (LVP). They identified no correlation between absolute values of microvascular parameters and DCE-MRI parameters. In contrast, there is significant correlation between the ratio of k_{ep} in tumor and normal tissue (correcting for individual variations in microvasculature) and both MVD (correlation coefficient = 0.61, $p = 0.007$) and MVP (correlation coefficient = 0.54, $p = 0.022$). Among the lymphovascular parameters, only LVA showed a negative correlation with k_{ep} (correlation coefficient = -0.66, $p = 0.003$).¹⁵ Part of the difficulty in applying quantitative DCE-MRI for determining tumor aggressiveness relates to the variability of the methodologies used to process and interpret DCE-MRI, as well as the challenge in incorporating such methods into a clinical setting. On the other hand, Oto et al studied 73 prostatectomy patients for evaluating the correlation between DW-MRI and DCE-MRI with prostate cancer aggressiveness. They reported a

moderate negative correlation between ADC values and Gleason score ($r = -0.376$, $p = 0.001$), although K^{trans} , V_e , k_{ep} , and V_p from DCE-MRI did not show any correlation between Gleason score or vascular endothelial growth factor (VEGF) expression.¹⁶ Further research is needed to understand the potential of DCE-MRI for assessment of prostate cancer aggressiveness.

5.5 Dynamic contrast-enhanced MRI in the Detection of Local Recurrence in Prostate Cancer Patients with Biochemical Recurrence

Definitive therapy approaches such as radical prostatectomy or radiation therapy result in cure in the majority of prostate cancer patients. However, 15 to 30% of treated men experience biochemical recurrence (BCR) during follow-up.¹⁷ BCR can result in metastatic disease and eventually in death if not detected and treated in a timely manner. The multiparametric MRI features of the treated prostate gland either with surgery or radiation are distinctly different than in the untreated prostate (► Fig. 5.9; ► Fig. 5.10). Normal anatomical features may be completely lost, while surgical clips, brachytherapy seeds, or fiducial markers used for external-beam radiation may result in substantial distortion of DW-MRI. Therefore, DCE-MRI becomes of greater importance in this setting. The most important sign of cancer recurrence is the presence of early enhancement

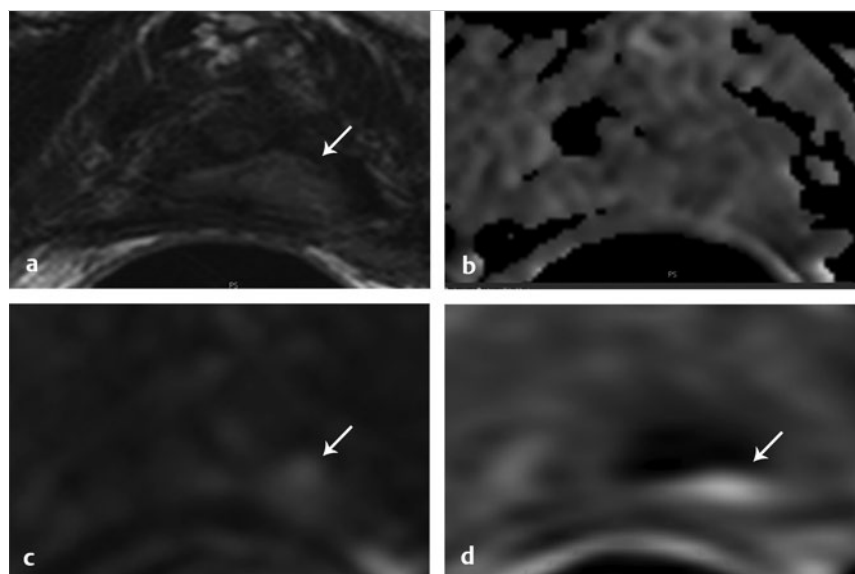


Fig. 5.9 A 74-year-old man with prostate-specific antigen = 0.98 ng/mL (status: post-radical prostatectomy > 20 years). Axial T2-weighted MRI shows intermediate-signal intensity soft tissue in the prostatectomy bed (arrow) (a). This lesion is invisible on apparent diffusion coefficient map from diffusion-weighted MRI (DW-MRI) (b); however, it appears as a hyperintense focus on the $b = 2000 \text{ s/mm}^2$ DW-MRI (arrow) (c). Dynamic contrast-enhanced MRI shows early focal hyper-enhancement in the lesion (arrow) (d). The patient underwent a targeted biopsy via MRI-transrectal ultrasound fusion approach for which histopathology revealed recurrent prostate cancer within the lesion.

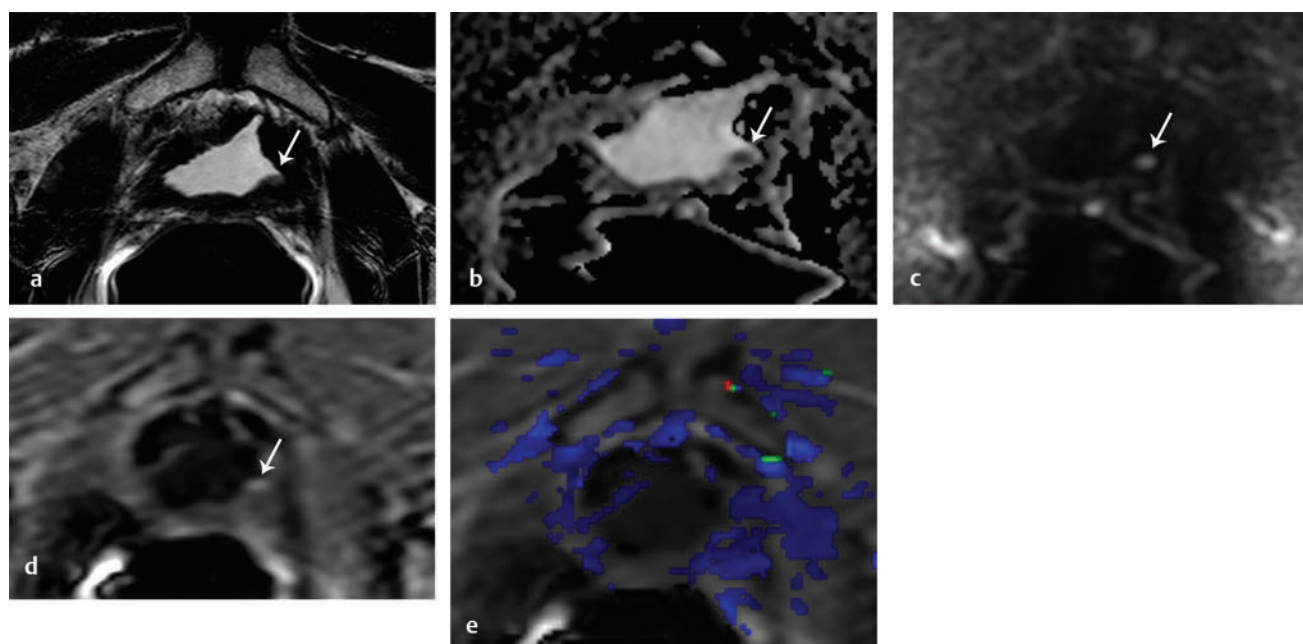


Fig. 5.10 A 71-year-old man with prostate-specific antigen = 0.14 ng/mL following radical prostatectomy for Gleason score 4+4 tumor 2 years previously. Axial T2-weighted MRI shows an intermediate-signal-intensity lesion in the left bladder wall superior to the anastomosis level (arrow) (a). The apparent diffusion coefficient map from DW-MRI (b) and the $b = 2000 \text{ s/mm}^2$ DW-MRI (c) show a diffuse hypointense and a diffuse hyperintense signal pattern within the lesion, respectively (arrows). Dynamic contrast-enhanced MRI (DCE-MRI) demonstrates focal enhancement within the lesion (arrow) (d). K^{trans} map (e) and k_{ep} map (not shown) derived from DCE-MRI do not show any lesion. The patient underwent a targeted biopsy via MRI-transrectal ultrasound fusion approach and histopathology revealed recurrent prostate cancer within the lesion.

within the surgical bed (mainly near the urethral anastomosis) or within the radiated prostate gland. This enhancement is generally perceptible by qualitative assessment, although the other evaluation methods may also be helpful. Panebianco et al validated the role of multiparametric MRI in the detection of local recurrence after prostatectomy in 242 patients.¹⁸ Their validation was PSA reduction after external-beam radiation in 126 patients (mean PSA = 1.3 ng/mL, lesion size range of 4–8 mm) and ultrasound-guided biopsy in 116 patients (mean PSA = 2 ng/mL, lesion size range of 9–15 mm). In the first group of

patients, they reported sensitivity and specificity of 98% and 94%, respectively, for the combination of T2W-MRI and DCE-MRI, whereas in the second group, the sensitivity and specificity of the same combination was 100% and 97%, respectively. They concluded that DCE-MRI was the most reliable pulse sequence to identify foci of recurrence after prostatectomy.¹⁸

One meta-analysis aimed to assess the effectiveness of MRI during the follow-up of patients with prostate cancer after undergoing external-beam radiation therapy (EBRT) or radical prostatectomy.¹⁹ The analysis identified 14 qualifying studies

among 768 existing studies in the literature. Seven studies examining patients after radical prostatectomy had a pooled sensitivity and specificity on the patient level of 82% (95% CI, 78–86%) and 87% (95% CI, 81–92%), respectively for MP-MRI. In the subgroup analysis, compared with T2W MRI, DCE-MRI showed higher pooled sensitivity (85%; 95% CI, 78–90%) and specificity (95%; 95% CI, 88–99%). Nine studies examining men after EBRT had a pooled sensitivity and specificity on the patient level of 82% (95% CI, 75–88%) and 74% (95% CI, 64–82%), respectively. Compared with T2W-MRI, DCE-MRI showed higher pooled sensitivity (90%; 95% CI, 77–97%) and specificity (81%; 95% CI, 64–93%). Although this meta-analysis included only a limited number of studies, its results revealed that DCE-MRI currently stands as the most critical pulse sequence to detect local recurrence in prostate cancer patients who experience BCR after definitive whole-gland therapy.¹⁹

5.6 Challenges of Dynamic Contrast-Enhanced MRI

DCE-MRI has a number of challenges. Among the standard mpMRI pulse sequences, it is relatively more invasive given the requirement for a bolus injection of gadolinium-based contrast media, which entails a low risk of allergic reactions or of inducing nephrogenic systemic fibrosis in patients with severe kidney failure, especially those on dialysis. Moreover, a recent paper reported that intravenous gadolinium exposure may be

associated with neuronal tissue deposition even in patients with normal kidney function.²⁰ DCE-MRI also adds to the cost of the examination, not just in terms of the cost of the contrast agent and associated injection equipment, but also in terms of the prolonged examination time. Another limitation, as previously noted, is the substantial overlap between contrast enhancement patterns of tumors and those of premalignant or benign pathologies such as benign prostatic hyperplasia and prostatitis (► Fig. 5.5; ► Fig. 5.11; ► Fig. 5.12). Finally, there continues to be substantial variability between centers in the methods used for the acquisition, processing, and interpretation of DCE-MRI. PI-RADS v2 has aimed to address such variability and standardize implementation of DCE-MRI through its more straightforward visual assessment and its binary classification of findings.

5.7 Conclusion

In conclusion, DCE-MRI is currently deemed a standard component of multiparametric prostate MRI protocols, according to PI-RADS v2. Although its current role in lesion detection for untreated patients is in question and the exact value of DCE-MRI is a topic of active investigation, DCE-MRI findings do impact the overall PI-RADS assessment category for indeterminate lesions in the peripheral zone and may facilitate initial lesion localization on other sequences. Also, DCE-MRI has a central role in the detection and localization of recurrent cancer in patients who experience BCR after definitive treatment for prostate cancer.

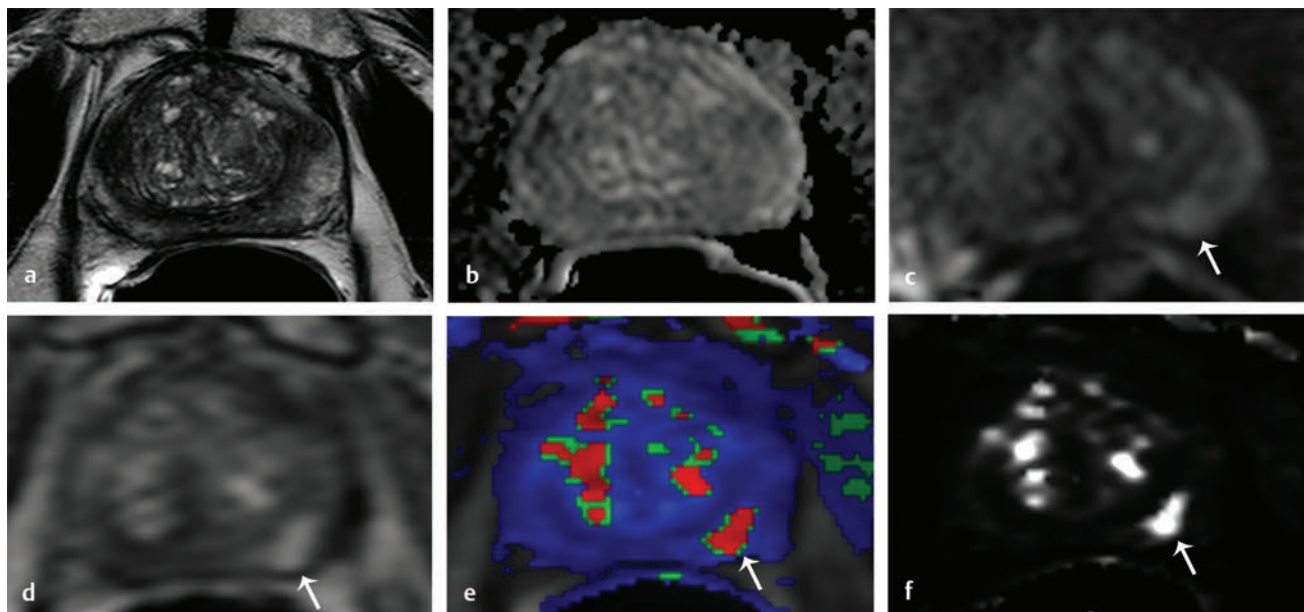


Fig. 5.11 A 70-year-old man with prostate-specific antigen = 4.6 ng/mL. Axial T2-weighted MRI (a) and apparent diffusion coefficient map of diffusion-weighted MRI (DW-MRI) (b) show a heterogeneous peripheral zone bilaterally without evidence of a focal lesion, $b = 2000 \text{ s/mm}^2$ DW-MRI (c) shows a focal slightly hyperintense lesion in the left mid-peripheral zone (arrow). Dynamic contrast-enhanced MRI (DCE-MRI) demonstrates focal enhancement within the left mid-peripheral zone lesion (arrow) (d). K^{trans} (e) and k_{ep} (f) maps derived from DCE-MRI also localize the left mid-peripheral zone lesion (arrows). The patient underwent a targeted biopsy via MRI-TRUS (transrectal ultrasound) fusion approach and histopathology revealed markedly atypical glands highly suspicious for prostate carcinoma in the left mid-peripheral zone lesion.

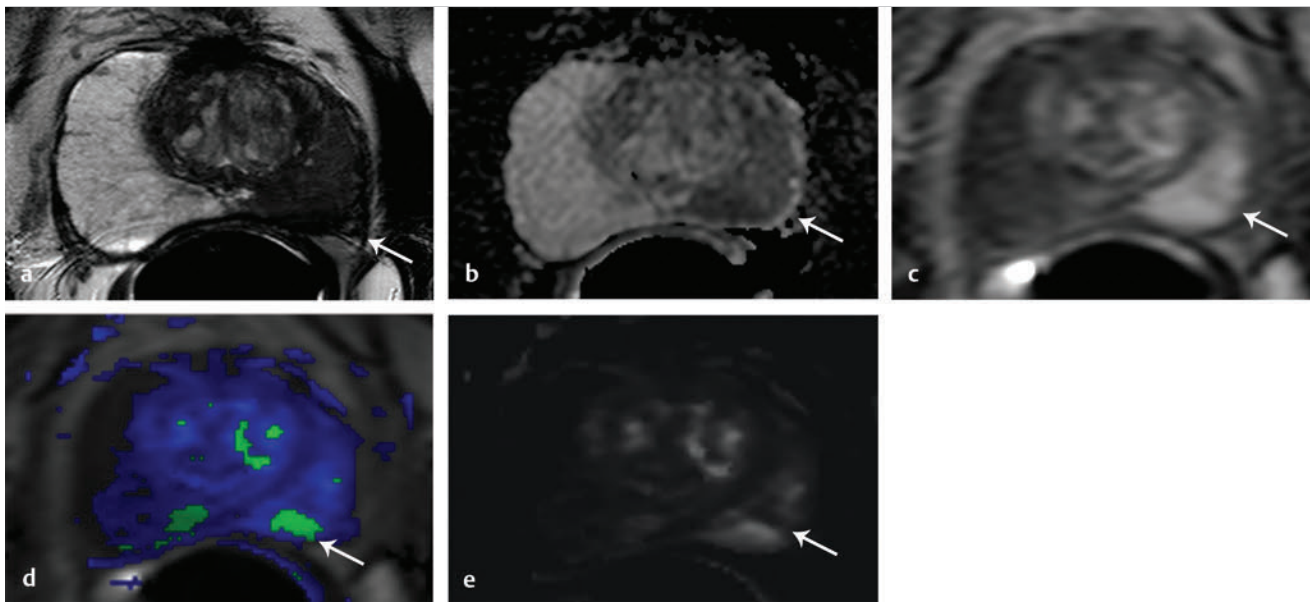


Fig. 5.12 A 61-year-old man with prostate-specific antigen = 4.3 ng/mL. Axial T2-weighted MRI shows a large hypointense lesion in the left hemiprostatic peripheral zone (*arrow*) (a), apparent diffusion coefficient map of diffusion-weighted MRI demonstrates a hypointense signal pattern within the lesion (*arrow*) (b); dynamic contrast-enhanced MRI (DCE-MRI) reveals diffuse enhancement within the lesion (*arrow*) (c), whereas K^{trans} (d) and K_{ep} (e) maps derived from DCE-MRI shows a heterogeneous positive pattern within the left peripheral zone lesion (*arrows*). The patient underwent a targeted biopsy via MRI-TRUS (transrectal ultrasound) fusion approach and histopathology revealed chronic granulomatous prostatitis.

References

- [1] Folkman J. Tumor angiogenesis: therapeutic implications. *N Engl J Med* 1971; 285(21):1182–1186
- [2] Ocak I, Bernardo M, Metzger G et al. Dynamic contrast-enhanced MRI of prostate cancer at 3 T: a study of pharmacokinetic parameters. *AJR Am J Roentgenol* 2007; 189(4):849
- [3] Turkbey B, Pinto PA, Mani H et al. Prostate cancer: value of multiparametric MR imaging at 3 T for detection—histopathologic correlation. *Radiology* 2010; 255(1):89–99
- [4] American College of Radiologists (ACR) Prostate Imaging–Recording and Data Systems, version 2. <http://www.acr.org/~/media/ACR/Documents/PDF/QualitySafety/Resources/PIRADS/PIRADS%20V2.pdf>. Accessed June 30, 2015.
- [5] Rosenkrantz AB, Geppert C, Grimm R et al. Dynamic contrast-enhanced MRI of the prostate with high spatiotemporal resolution using compressed sensing, parallel imaging, and continuous golden-angle radial sampling: preliminary experience. *J Magn Reson Imaging* 2015; 41(5):1365–1373
- [6] Turkbey B, Thomasson D, Pang Y, Bernardo M, Choyke PL. The role of dynamic contrast-enhanced MRI in cancer diagnosis and treatment. *Diagn Interv Radiol* 2010; 16(3):186–192
- [7] Hansford BG, Peng Y, Jiang Y et al. Dynamic Contrast-enhanced MR Imaging Curve-type Analysis: Is It Helpful in the Differentiation of Prostate Cancer from Healthy Peripheral Zone? *Radiology* 2015; 275(2):448–457
- [8] Choyke PL, Dwyer AJ, Knopp MV. Functional tumor imaging with dynamic contrast-enhanced magnetic resonance imaging. *J Magn Reson Imaging* 2003; 17(5):509–520
- [9] Noworolski SM, Vigneron DB, Chen AP, Kurhanewicz J. Dynamic contrast-enhanced MRI and MR diffusion imaging to distinguish between glandular and stromal prostatic tissues. *Magn Reson Imaging* 2008; 26(8):1071–1080
- [10] Tan CH, Hobbs BP, Wei W, Kundra V. Dynamic contrast-enhanced MRI for the detection of prostate cancer: meta-analysis. *AJR Am J Roentgenol* 2015; 204(4):W439–W448
- [11] Haghghi M, Shah S, Taneja SS, Rosenkrantz AB. Prostate cancer: diffusion-weighted imaging versus dynamic-contrast enhanced imaging for tumor localization—a meta-analysis. *J Comput Assist Tomogr* 2013; 37(6):980–988
- [12] Hoeks CM, Hambrock T, Yakar D et al. Transition zone prostate cancer: detection and localization with 3-T multiparametric MR imaging. *Radiology* 2013; 266(1):207–217
- [13] Hansford BG, Karademir I, Peng Y et al. Dynamic contrast-enhanced MR imaging features of the normal central zone of the prostate. *Acad Radiol* 2014; 21(5):569–577
- [14] Vos EK, Litjens GJ, Kobus T et al. Assessment of prostate cancer aggressiveness using dynamic contrast-enhanced magnetic resonance imaging at 3 T. *Eur Urol* 2013; 64(3):448–455
- [15] van Niekerk CG, van der Laak JA, Hambrock T et al. Correlation between dynamic contrast-enhanced MRI and quantitative histopathologic microvascular parameters in organ-confined prostate cancer. *Eur Radiol* 2014; 24(10):2597–2605
- [16] Oto A, Yang C, Kayhan A et al. Diffusion-weighted and dynamic contrast-enhanced MRI of prostate cancer: correlation of quantitative MR parameters with Gleason score and tumor angiogenesis. *AJR Am J Roentgenol* 2011; 197(6):1382–1390
- [17] Cha D, Kim CK, Park SY, Park JJ, Park BK. Evaluation of suspected soft tissue lesion in the prostate bed after radical prostatectomy using 3 T multiparametric magnetic resonance imaging. *Magn Reson Imaging* 2015; 33(4):407–412
- [18] Panebianco V, Barchetti F, Sciarra A et al. Prostate cancer recurrence after radical prostatectomy: the role of 3-T diffusion imaging in multi-parametric magnetic resonance imaging. *Eur Radiol* 2013; 23(6):1745–1752
- [19] Wu LM, Xu JR, Gu HY et al. Role of magnetic resonance imaging in the detection of local prostate cancer recurrence after external beam radiotherapy and radical prostatectomy. *Clin Oncol (R Coll Radiol)* 2013; 25(4):252–264
- [20] McDonald RJ, McDonald JS, Kallmes DF et al. Intracranial Gadolinium Deposition after Contrast-enhanced MR Imaging. *Radiology* 2015; 275(3):772–782

6 Prostate Imaging–Reporting and Data System (PI-RADS)

Michael Spektor and Jeffrey C. Weinreb

6.1 Introduction

Multiparametric magnetic resonance imaging (mpMRI) is considered the most sensitive and specific imaging technique for localizing clinically significant prostate cancer. However, variation in the performance, interpretation, and reporting of prostate mpMRI examinations has been a significant obstacle to its widespread acceptance and use. In order to address this variation, the European Society of Urogenital Radiology (ESUR) published a set of consensus guidelines called Prostate Imaging–Reporting and Data System (PI-RADS).¹

Since its publication in 2012, PI-RADS has been validated in various clinical and research scenarios.^{2,3,4} However, experience has also revealed several limitations, in part due to rapid progress in the field. In an effort to update and improve upon the original version of PI-RADS, the American College of Radiology (ACR), ESUR, and the AdMeTech Foundation collaborated to develop PI-RADS version 2 (PI-RADS v2), which was released in 2015.⁵ PI-RADS v2 includes information about clinical considerations and technical specifications for mpMRI as well as a lexicon of terminology. This chapter will focus on criteria employed in PI-RADS v2 for the assessment of the prostate gland for detection and diagnosis of cancer on mpMRI examinations.

6.2 PI-RADS Assessment

Based on the current uses and capabilities of mpMRI and MRI-targeted procedures, PI-RADS v2 defines clinically significant cancer on pathology as those tumors that have a Gleason score ≥ 7 (including 3+4 with a prominent, but not predominant, Gleason pattern 4 component) and volume $> 0.5 \text{ cm}^3$ or extraprostatic extension (EPE).

PI-RADS v2 has the following 5 assessment categories:

- PI-RADS 1 Very low (clinically significant cancer is highly unlikely to be present)
- PI-RADS 2 – Low (clinically significant cancer is unlikely to be present)
- PI-RADS 3 – Intermediate (the presence of clinically significant cancer is equivocal)
- PI-RADS 4 – High (clinically significant cancer is likely to be present)
- PI-RADS 5 – Very high (clinically significant cancer is highly likely to be present)

The 5-point scale to score the imaging findings is based on the likelihood (probability) that a combination of mpMRI features on T2-weighted imaging (T2WI), diffusion weighted imaging (DWI), and dynamic contrast-enhanced (DCE) imaging represent the presence of a clinically significant cancer for an identified lesion in the prostate gland. To arrive at one of these 5 PI-RADS v2 assessment categories for each suspicious finding in the prostate, T2WI and DWI are each assessed using a 5-point scale, and DCE-MRI is classified as either positive or negative. Then, using the appropriate PI-RADS v2 table for either the peripheral zone (PZ) or the transition zone (TZ), these three parameters (for T2WI, DWI, and

sometimes DCE-MRI) are integrated, and each lesion is assigned a PI-RADS v2 assessment category (PI-RADS 1–5) that indicates the likelihood that it is a clinically significant cancer.

It is important to note that there is a range of both malignant and benign histologies in the prostate gland, and at present there may be some overlap in their mpMRI characteristics. A PI-RADS v2 assessment category of PI-RADS 1 does not exclude the possibility of clinically significant cancer. Rather, it simply indicates that it is highly unlikely. Similarly, assessment category PI-RADS 5 does not provide proof that a lesion is a clinically significant cancer but rather indicates that it is highly likely. Currently, ranges of percent probabilities have not been assigned to each PI-RADS v2 assessment category. As PI-RADS v2 is tested and refined, this may become possible in the future.

Assignment to a specific PI-RADS v2 assessment category is based solely on mpMRI findings. It does not take into account other factors, such as serum prostate-specific antigen (PSA), digital rectal examination, patient history, or choice of treatment. However, these factors, along with local preferences, experience, and clinical history may determine recommendations regarding patient management, including biopsy.

6.3 Diffusion-Weighted Imaging Scoring

A score of 1 to 5 is assigned on DWI by comparing the signal intensity in a lesion to the average signal of normal prostate tissue in the histologic zone in which it is located. Nonetheless, the findings on DWI should always be correlated with findings on T2WI, T1WI, and DCE-MRI. ▶ Table 6.1 provides the criteria for assigning a score from 1 through 5 based on findings from DWI. Note that these criteria take into consideration: (1) lesion shape and margins; (2) signal intensity; (3) size; and (4) observations from both the high b-value images and the apparent

Table 6.1 Scheme for deriving overall PI-RADS assessment category in the peripheral zone

DWI	T2WI	DCE	PI-RADS assessment category
1	Any ^a	Any	1
2	Any	Any	2
3	Any	-	3
		+	4
4	Any	Any	4
5	Any	Any	5

^a “Any” means that any score from 1 to 5 on the 5-point scale can be assigned; “+” or “-” means positive or negative for contrast enhancement. *Abbreviations:* DCE, dynamic contrast-enhanced MRI; DWI, diffusion-weighted imaging; T2WI, T2-weighted imaging; PI-RADS, Prostate Imaging–Reporting and Data System v2.

Source: Adapted from American College of Radiology (ACR) Prostate Imaging–Reporting and Data System, version 2. Available at www.acr.org.

PI-RADS Assessment for Peripheral Zone on DWI

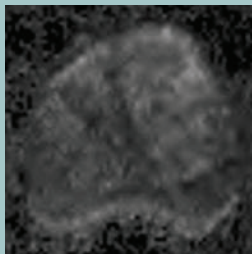
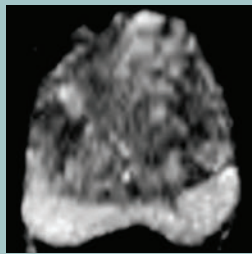

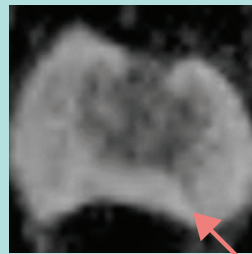
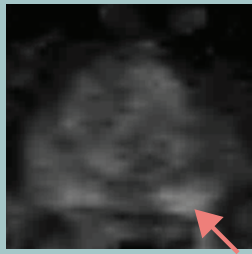
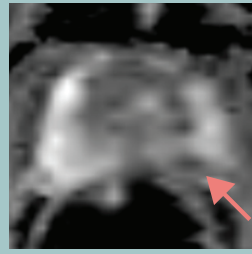
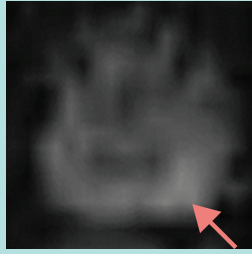
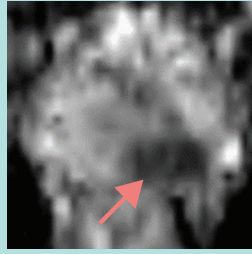
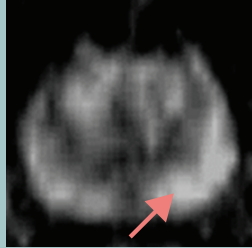
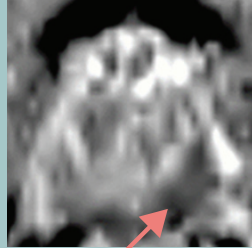
Score	Findings	DWI	ADC
1	No abnormality (i.e., normal) on ADC and high b-value DWI.		
2	Indistinct hypointense on ADC (arrow).		
3	Focal mildly / moderately hypointense on ADC (arrow) and isointense / mildly hyperintense on high b-value DWI.		
4	Focal markedly hypointense on ADC (arrow) and markedly hyperintense on high b-value DWI; <1.5 cm on axial images.		
5	Same as 4 but ≥ 1.5 cm in greatest dimension (arrow) or definite extraprostatic extension / invasive behavior.		

Fig. 6.1 PI-RADS assessment for peripheral zone on diffusion-weighted imaging (DWI). ADC, apparent diffusion coefficient; PI-RADS, Prostate Imaging–Reporting and Data System v2. (Adapted from the American College of Radiology [ACR] Prostate Imaging–Reporting and Data System, version 2. Available at www.acr.org.)

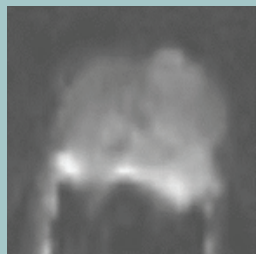
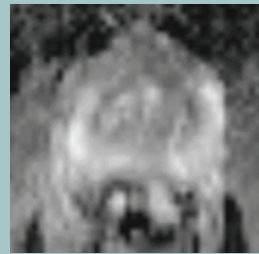

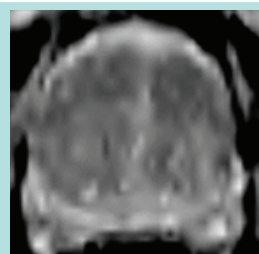

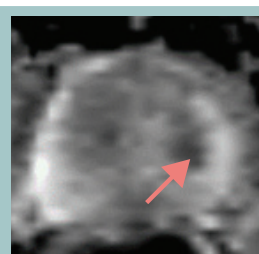
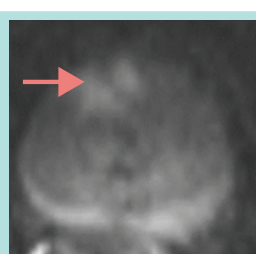
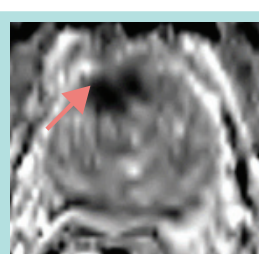

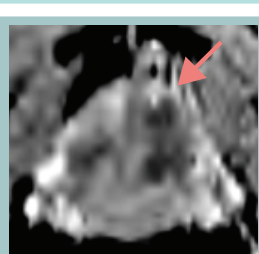
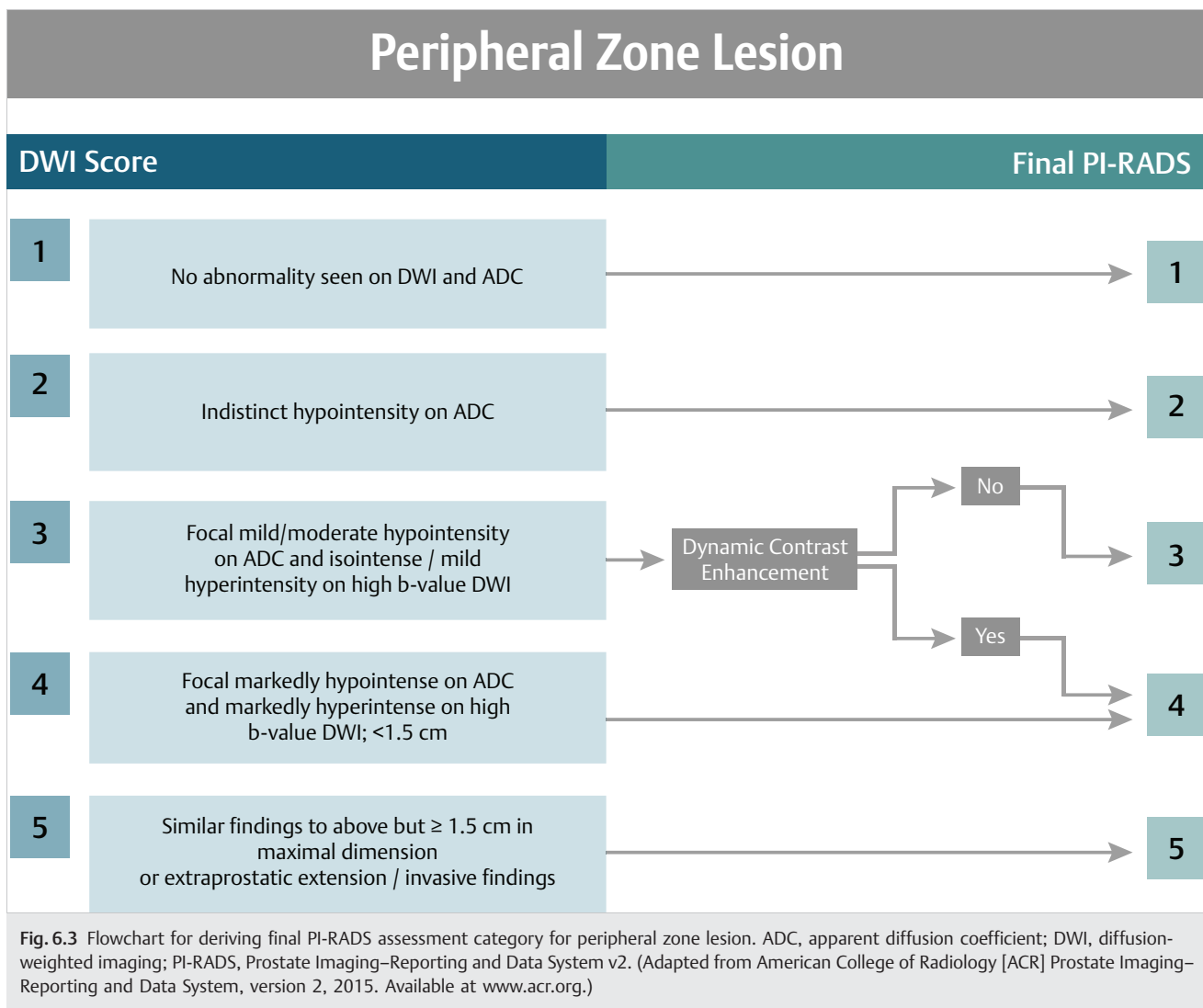
PI-RADS Assessment for Transition Zone on DWI			
Score	Findings	DWI	ADC
1	No abnormality (i.e., normal) on ADC and high b-value DWI.		
2	Indistinct hypointense on ADC.		
3	Focal mildly / moderately hypointense on ADC (arrow) and isointense / mildly hyperintense on high b-value DWI.		
4	Focal markedly hypointense on ADC (arrow) and markedly hyperintense on high b-value DWI; <1.5 cm on axial images.		
5	Same as 4 but ≥ 1.5 cm in greatest dimension (arrow) or definite extraprostatic extension / invasive behavior.		

Fig. 6.2 PI-RADS assessment for transition zone on diffusion-weighted imaging (DWI). ADC, apparent diffusion coefficient; PI-RADS, Prostate Imaging–Reporting and Data System v2. (Adapted from the American College of Radiology [ACR] Prostate Imaging–Reporting and Data System, version 2. Available at www.acr.org.)



diffusion coefficient (ADC) map. See ▶ Fig. 6.1 and ▶ Fig. 6.2 for examples.

In the peripheral zone (PZ), assignment of a PI-RADS v2 assessment category for a lesion is based predominantly on the DWI score (▶ Table 6.1; ▶ Fig. 6.3).

For example, if the DWI score is 4 and the T2WI score is 2, then the PI-RADS assessment category should be 4. The only exception to this direct relationship of the DWI score and PI-RADS assessment category in the PZ is a positive (+) DCE score, which upgrades a DWI score of 3 to the final PI-RADS assessment category of 4 – high (clinically significant cancer is likely to be present). See section 6.5 DCE-MRI scoring for definitions of positive and negative scores for DCE-MRI.

Certain benign conditions display a focal hypointense ADC signal. Familiarity with these conditions and their typical MR appearance is essential for making the appropriate PI-RADS assessment. For example, although fibrosis, calculi, and hemorrhage are hypointense on both T2WI and ADC due to insufficient signal, they will also be markedly hypointense on all DWI images, essentially excluding clinically significant disease. Benign prostatic hypertrophy presents a greater challenge. Encapsulated, circumscribed, and round nodules in the TZ (transition zone) or

PZ generally represent benign prostatic hyperplasia (BPH) or extruded BPH, respectively, regardless of their ADC/DWI signal. However, not uncommonly, BPH nodules may lack some or all of their benign morphological features and demonstrate marked ADC hypointensity, making assessment difficult. This remains a recognized limitation of mpMRI diagnosis and usually requires great expertise and experience on the part of the reader.

6.4 T2-Weighted Image Scoring

Scoring of T2WI also utilizes a 5-point scale, although the definitions of each score slightly differ between the PZ and TZ, as shown in ▶ Fig. 6.4 and ▶ Fig. 6.5.

On T2WI, clinically significant cancers in the PZ usually appear as round or ill-defined hypointense focal lesions. It is important to note that many benign conditions may mimic this appearance, including prostatitis, hemorrhage, glandular atrophy, benign hyperplasia, biopsy-related scars, and post-hormonal therapy or post-ablation changes. Careful inspection of additional sequences may provide clues to the correct diagnosis.

TZ cancers are even more problematic. When benign prostatic hyperplasia (BPH) is present, the TZ is composed of variable

PI-RADS Assessment for Peripheral Zone on T2WI

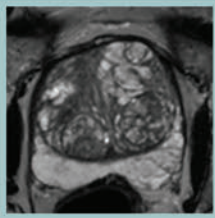
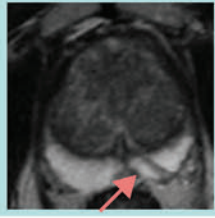



Score	Findings	T2WI
1	Uniform hyperintense signal intensity (normal).	
2	Linear (arrow), wedge-shaped, or diffuse mild hypointensity, usually indistinct margin.	
3	Heterogeneous signal intensity or noncircumscribed, rounded, moderate hypointensity (arrow).	
4	Circumscribed, homogeneous moderate hypointense focus/mass confined to prostate and <1.5 cm in greatest dimension (arrow).	
5	Same as 4 but ≥ 1.5 cm in greatest dimension (arrow) or definite extraprostatic extension / invasive behavior.	

Fig. 6.4 PI-RADS assessment for peripheral zone on T2-weighted imaging (T2WI). PI-RADS, Prostate Imaging–Reporting and Data System v2. (Adapted from American College of Radiology [ACR] Prostate Imaging–Reporting and Data System, version 2, 2015. Available at www.acr.org.)

amounts of glandular (T2-hyperintense) and stromal (T2-hypointense) tissue resulting in heterogeneous signal intensity. Identifying T2 hypointense cancer amongst the regions of benign stromal hyperplasia is challenging. Typical T2W features of TZ tumors that may prove useful include ill-defined moderate hypointensity (“erased charcoal” or “smudgy fingerprint” appearance), spiculated margins, lenticular shape, absence of a complete hypointense capsule, and invasion of the urethral sphincter and anterior fibromuscular stroma. The more features present, the higher the likelihood of a clinically significant TZ cancer.

Just as DWI is the dominant sequence for assigning an assessment category to a PZ lesion, T2WI is the primary determining sequence for a lesion in the TZ (► Table 6.2; ► Fig. 6.6): For example,

if the T2WI score for a TZ lesion is 4 and the DWI score is 2, then the PI-RADS assessment category should be 4. Comparable to in the PZ, the only exception to this direct relationship between the T2WI score and the final PI-RADS assessment category occurs with the T2WI score of 3, in which case the DWI score serves as a tiebreaker (namely, a DWI score of 5 leads to an upgrade of a TZ lesion with a T2WI score of 3 to a PI-RADS assessment category of 4).

Needless to say, determining the correct zonal location of a lesion is critical, as the dominant factors for PI-RADS assessment are T2WI for the TZ and DWI for the PZ. Areas where clear delineation of the zonal origin of a finding may be especially problematic include the interface of the central zone (CZ) and the PZ at the base of the gland, as well as the interface of the anterior horn of the PZ with the TZ

PI-RADS Assessment for Transition Zone on T2WI

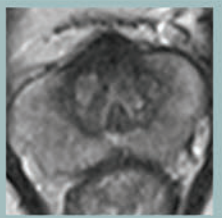
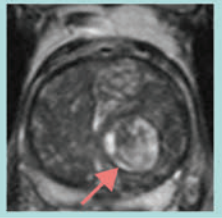

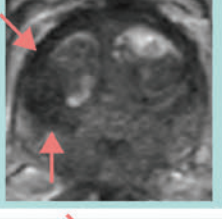
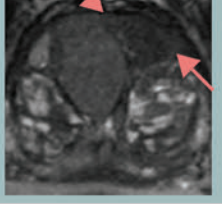
Score	Findings	T2WI
1	Homogeneous intermediate signal intensity (normal).	
2	Circumscribed (arrow) hypointense signal intensity or heterogeneous encapsulated nodule(s) (BPH).	
3	Heterogeneous signal intensity with obscured margins (arrow). Includes others that do not qualify as 2, 4, or 5.	
4	Lenticular (arrows) or noncircumscribed, homogeneous and moderately intense signal intensity, and < 1.5 cm in greatest dimension.	
5	Same as 4 but ≥ 1.5 cm in greatest dimension (arrow) or definite extraprostatic extension / invasive behavior.	

Fig. 6.5 PI-RADS assessment for transition zone on T2-weighted imaging (T2WI). BPH, benign prostatic hyperplasia; PI-RADS, Prostate Imaging–Reporting and Data System v2. (Adapted from American College of Radiology [ACR] Prostate Imaging–Reporting and Data System, version 2, 2015. Available at www.acr.org.)

and associated anterior fibromuscular stroma. In addition, both PZ and TZ cancers may extend across anatomical boundaries (i.e., exhibit invasive behavior), further complicating assessment. Other examples of invasive behavior are extension across regional parts within a zone, extension into the seminal vesicles, or extension outside of the gland (extraprostatic extension).

6.5 Dynamic contrast-enhanced MRI Scoring

Dynamic contrast-enhanced MRI is considered “positive” when there is focal enhancement that occurs before or

contemporaneous with enhancement of adjacent normal prostatic tissue and that corresponds to a signal abnormality on DWI and/or T2WI (► Fig. 6.7). Typically this enhancement occurs within 10 seconds of contrast appearing within the femoral arteries, although it may vary based on the contrast injection rate, cardiac output, temporal resolution used to acquire the images, and other factors. Note that this determination solely considers the presence of focal early enhancement, such that assessment for presence of washout, kinetic curve types (i.e., curve type 1, 2, and 3), or other advanced perfusion metrics derived from pharmacokinetic models (i.e., K^{trans} from a Tofts model) do not influence the DCE-MRI score.

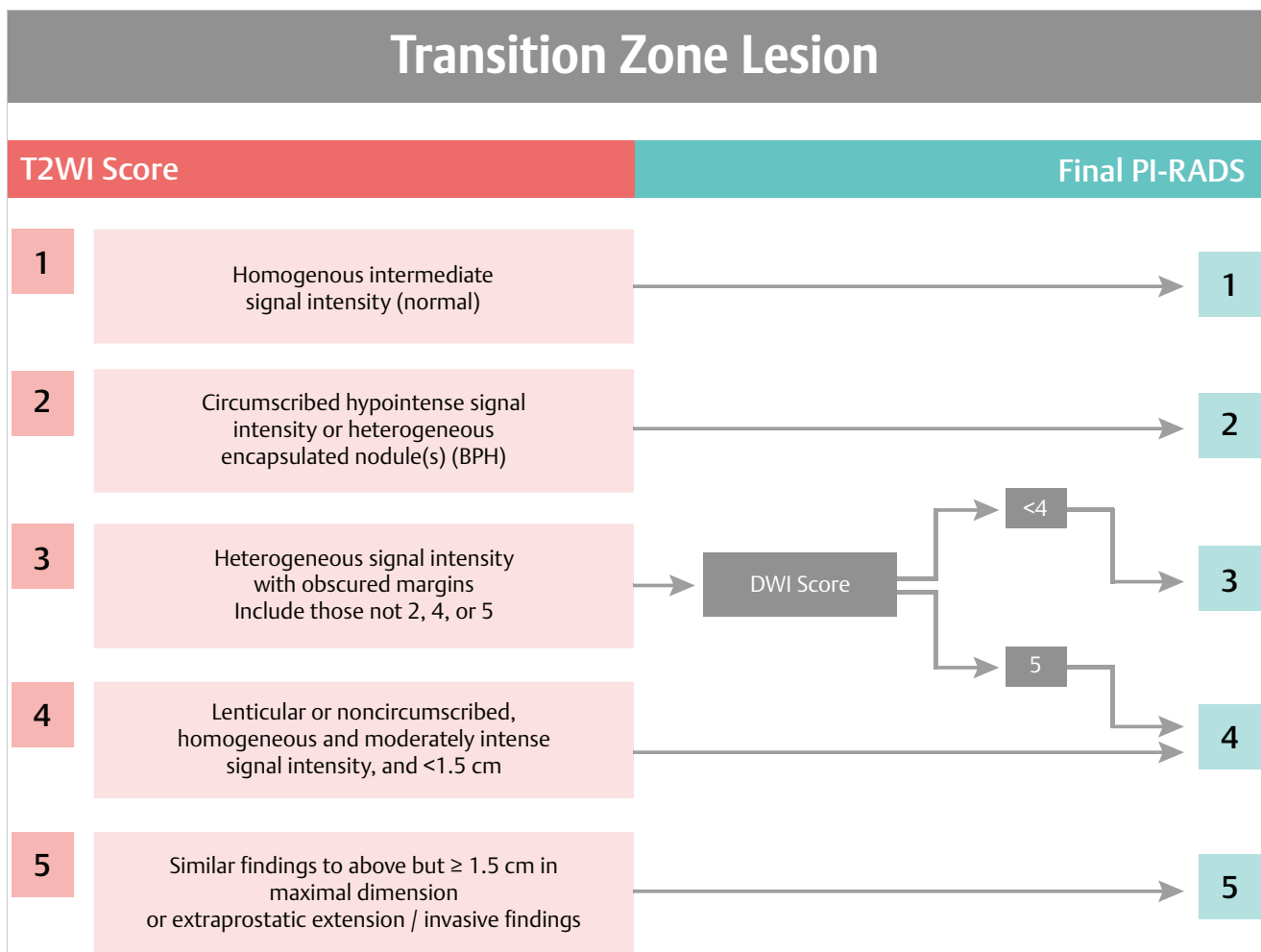


Fig. 6.6 Flowchart for deriving final PI-RADS assessment category for transition zone lesion. BPH, benign prostatic hyperplasia; DWI, diffusion-weighted imaging; PI-RADS, Prostate Imaging–Reporting and Data System; T2WI, T2-weighted imaging. (Adapted from American College of Radiology [ACR] Prostate Imaging–Reporting and Data System, version 2, 2015. Available at www.acr.org.)

Table 6.2 Scheme for deriving overall PI-RADS assessment category in the transition zone

T2WI	DWI	DCE	PI-RADS assessment category
1	Any ^a	+ or -	1
2	Any	+ or -	2
3	≤ 4	+ or -	3
	5	+ or -	4
4	Any	+ or -	4
5	Any	+ or -	5

^a “Any” means that any score from 1 to 5 on the 5-point scale can be assigned; “+” or “-” means positive or negative for contrast enhancement. *Abbreviations:* DCE, dynamic contrast-enhanced MRI; DWI, diffusion-weighted imaging; T2WI, T2-weighted imaging; PI-RADS, Prostate Imaging–Reporting and Data System v2. *Source:* Adapted from American College of Radiology (ACR) Prostate Imaging–Reporting and Data System, version 2. Available at www.acr.org.

Some benign processes are DCE-MRI positive. BPH nodules serve as the most common example of a benign process exhibiting occasional early enhancement, although their benign morphology on T2WI (round shape, circumscribed and encapsulated margins) often suggests the correct diagnosis. Diffuse nonfocal early enhancement not localized to a specific T2WI or DWI abnormality is often seen in the setting of prostatitis and also considered a benign finding on DCE-MRI.

When T2WI and DWI are of diagnostic quality, DCE-MRI plays a minor role in determining the PI-RADS v2 assessment category. Thus, DCE-MRI does not contribute to determination of the assessment category when the finding in the PZ has a low (PI-RADS 1 or 2) or high (PI-RADS 4 or 5) likelihood of clinically significant cancer. However, in the PZ, a positive DCE-MRI score upgrades a DWI score of 3 to the final PI-RADS v2 assessment category of 4. The DCE score does not influence the final PI-RADS v2 assessment category for lesions in the TZ.

PI-RADS Assessment for Dynamic Contrast-Enhanced (DCE) MRI

	Findings	Precontrast	Postcontrast	ADC
Negative	1. No early enhancement, OR 2. Diffuse enhancement not corresponding to a focal finding on T2WI and/or DWI, OR 3. Focal enhancement corresponding to a lesion demonstrating features of BPH on T2WI			
Positive Peripheral Zone	1. Focal, AND 2. Earlier than or contemporaneously with enhancement of adjacent normal prostatic tissues, AND 3. Corresponds to suspicious finding on T2WI and/or DWI			
Positive Transition Zone	Same criteria as peripheral zone			

Fig. 6.7 PI-RADS assessment for dynamic contrast-enhanced (DCE) MRI. ADC, apparent diffusion coefficient; DWI, diffusion-weighted imaging; PI-RADS, Prostate Imaging–Reporting and Data System; T2WI, T2-weighted imaging. (Adapted from American College of Radiology [ACR] Prostate Imaging–Reporting and Data System, version 2, 2015. Available at www.acr.org.)

Table 6.3 Scheme for deriving overall PI-RADS assessment category in the peripheral or transition zone without adequate DWI

T2WI	DWI	DCE	PI-RADS assessment category
1	X ^a	+ or -	1
2	X	+ or -	2
3	X	-	3
		+	4
4	X	+ or -	4
5	X	+ or -	5

^a “X” means the image is inadequate for evaluation; “+” or “-” means positive or negative for contrast enhancement.

Abbreviations: DCE, dynamic contrast-enhanced MRI; DWI, diffusion-weighted imaging; T2WI, T2-weighted imaging; PI-RADS, Prostate Imaging–Reporting and Data System v2.

Source: Adapted from American College of Radiology (ACR) Prostate Imaging–Reporting and Data System, version 2. Available at www.acr.org.

6.6 PI-RADS Assessment Category X

Various technical and/or patient factors may significantly hamper mpMRI examination. One or more of the three components of the mpMRI (T2WI, DWI, DCE-MRI) may be suboptimal or absent, necessitating a different scoring scheme. T2WI is by far the most robust of the three components and is rarely the culprit. Lacking an adequate T2WI is rare and may preclude evaluation altogether. The more common scenario is inadequate DWI and/or DCE-MRI. If both are inadequate or missing, then the assessment should be largely limited to staging for determination of EPE. If one of these two sequences is inadequate or missing, then that component should be assigned a PI-RADS assessment category X, and the lesion should be scored according to the following alternate schemes depending on the imaging component with assessment category X and the location of the lesion: ▶ Table 6.3, ▶ Table 6.4, and ▶ Table 6.5.

6.7 Benign Findings on mpMRI

Many signal abnormalities within the prostate are benign.

Table 6.4 Scheme for deriving overall PI-RADS assessment category in the peripheral zone without adequate DCE-MRI (determined by DWI assessment category)

DWI	T2WI	DCE	PI-RADS assessment category
1	Any ^a	X	1
2	Any	X	2
3	Any	X	3
4	Any	X	4
5	Any	X	5

^a “Any” means that any score on the 5-point scale can be assigned; “X” means the image is inadequate for evaluation.

Abbreviations: DCE, dynamic contrast-enhanced MRI; DWI, diffusion-weighted imaging; T2WI, T2-weighted imaging; PI-RADS, Prostate Imaging–Reporting and Data System v2.

Source: Adapted from American College of Radiology (ACR) Prostate Imaging–Reporting and Data System, version 2. Available at www.acr.org.

Table 6.5 Scheme for Deriving Overall PI-RADS Assessment Category in the transition zone without adequate DCE

T2WI	DWI	DCE	PI-RADS assessment category
1	Any ^a	X	1
2	Any	X	2
3	≤ 4	X	3
	5	X	4
4	Any	X	4
5	Any	X	5

^a “Any” means that any score on the 5-point scale can be assigned; “X” means the image is inadequate for evaluation.

Abbreviations: DCE, dynamic contrast-enhanced MRI; DWI, diffusion-weighted imaging; T2WI, T2-weighted imaging; PI-RADS, Prostate Imaging–Reporting and Data System v2.

Source: Adapted from American College of Radiology (ACR) Prostate Imaging–Reporting and Data System, version 2. Available at www.acr.org.

6.7.1 Benign Prostatic Hyperplasia

BPH arises in the TZ, although exophytic and extruded BPH nodules can be found in the PZ. Benign prostatic hyperplasia may appear as bandlike areas and/or encapsulated round nodules with circumscribed margins. Predominantly glandular BPH nodules and cystic atrophy exhibit moderate-to-marked T2 hyperintensity and are distinguished from malignant tumors by their signal and capsule. Predominantly stromal nodules exhibit T2 hypointensity. Many BPH nodules demonstrate a mixture of signal intensities. BPH nodules may be highly vascular on DCE-MRI and can demonstrate a range of signal intensities on DWI.

6.7.2 Hemorrhage

Hemorrhage appears as a focal or diffuse hyperintense signal on T1WI and an iso-hypointense signal on T2WI. However, chronic blood products may appear hypointense on all MR sequences. Hemorrhage in the PZ and/or seminal vesicles is common, especially after biopsy.

6.7.3 Cysts

Cysts may contain “simple” fluid and appear markedly hyperintense on T2WI and dark on T1WI. However, they can also contain blood products or proteinaceous fluid, which may demonstrate a variety of signal characteristics including hyperintense signal on T1WI.

6.7.4 Calcifications

Calcifications, if visible, appear as markedly hypointense foci on all sequences.

6.7.5 Prostatitis

Prostatitis can result in decreased signal in the PZ on both T2WI and the ADC map. Prostatitis may also increase perfusion, resulting in a false-positive DCE-MRI result. However, the morphology is commonly bandlike, wedge-shaped, indistinct, or

diffuse, rather than focal, round, oval, or irregular, and the decrease in signal on the ADC map is generally not as great nor as focal as in cancer.

6.7.6 Atrophy

Atrophy typically appears as areas of low signal on T2WI and mildly decreased signal on the ADC map from loss of glandular tissue in the PZ. The ADC is generally not as low as in cancer, and there is often contour retraction of the involved prostate.

6.7.7 Fibrosis

Fibrosis may be associated with wedge- or band-shaped areas of low signal on T2WI.

In addition, normal anatomical structures are prone to be misinterpreted as suspicious for tumor, particularly by inexperienced readers of prostate MRI. One such structure of particular note is the CZ, which readers must recognize as a distinct region from the TZ, and a normally encountered finding on prostate MRI. The CZ is a band of tissue surrounding the ejaculatory ducts at the posteromedial base of the prostate that exhibits decreased T2 signal and decreased ADC, thereby potentially mimicking a large lesion in this region.^{6,7} It may be recognized by its location at the posteromedial base, symmetric appearance, conical shape, relationship with the ejaculatory ducts, and lack of rapid enhancement kinetics.⁸ Other anatomical structures that may pose a diagnostic pitfall include periprostatic nerves and vessels that course in proximity to the capsule, as well as the anterior fibromuscular stroma, the fibrous pseudocapsule between the peripheral and transition zones, and the fascia between the two lobes of the prostate at the posterior midline, all of which may exhibit benign thickening and thus mimic a suspicious lesion for some readers.^{6,7} Dedicated reader experience in prostate MRI incorporating follow-up of the pathologic outcomes from examinations that one has interpreted has been shown to improve reader performance and can help avoid such diagnostic pitfalls.^{9,10,11}

6.8 Reporting

The major objectives of PI-RADS v2 are to improve prostate cancer detection, localization, characterization, and risk stratification in patients with suspected tumor. In order to meet these goals, it is imperative to communicate results of an mpMRI examination in a clear, concise, and structured fashion. Lack of standardized terminology and reporting has been considered an impediment to the value and widespread use of MRI. Prostate Imaging–Reporting and Data System v2 contains a number of recommendations to help reduce variability in image interpretation, simplify terminology, and standardize content.

Prostate volume should always be reported, as it may be useful to calculate PSA density (PSA/prostate volume) and influence various management decisions. It can be determined using manual or automated segmentation or calculated using the formula for a prolate ellipse: (maximum AP diameter) x (maximum transverse diameter) x (maximum longitudinal diameter) x 0.52.

The proper method for measuring lesions themselves has been a subject of investigation and debate, and our existing methods underestimate both the tumor volume and extent compared to histology.^{12,13} Nevertheless, standardization of lesion measurements should facilitate MR-pathologic correlation and research. For PI-RADS v2, a lesion in the PZ should be measured on DWI (the “dominant” sequence in the PZ) and a lesion in the TZ should be measured on T2WI (the “dominant” sequence in the TZ). If lesion measurement is difficult or compromised on DWI (for PZ) or T2WI (for TZ), then measurement should be made on the sequence that shows the suspicious

finding best. Regardless, the MRI report should clearly state the image number and sequence used to obtain the measurement.

The minimum requirement is to report the largest dimension of a lesion on an axial image. If the largest dimension of a suspicious finding is on a sagittal or coronal image, then this measurement and the imaging plane should also be reported. If a lesion is not clearly delineated on an axial image, then the measurement on the plane which best depicts the finding should be reported. Alternatively, lesion volume may be documented.

As prostate cancer is usually multifocal, up to four lesions with a PI-RADS assessment category of 3, 4, or 5 may be assigned on the sector map. If there are more than four suspicious lesions, then only the four with the highest likelihood of clinically significant cancer (i.e., highest PI-RADS assessment category) should be reported.

From a clinical perspective, in a patient with multifocal tumors, the index lesion is the tumor focus that will drive any adverse oncologic outcome in the patient.^{14,15,16} On MRI, the lesion designated as the index lesion is anticipated to yield the highest Gleason score, contribute to extraprostatic extension, or produce positive margins at surgery. The lesion with the highest PI-RADS v2 assessment category should be designated as the index lesion. If the highest PI-RADS v2 assessment category is assigned to two or more lesions, then the index lesion should be the one that shows extraprostatic extension. Thus, a smaller lesion with EPE should be defined as the index lesion despite the presence of a larger lesion with the identical PI-RADS assessment category. If none of the lesions demonstrate

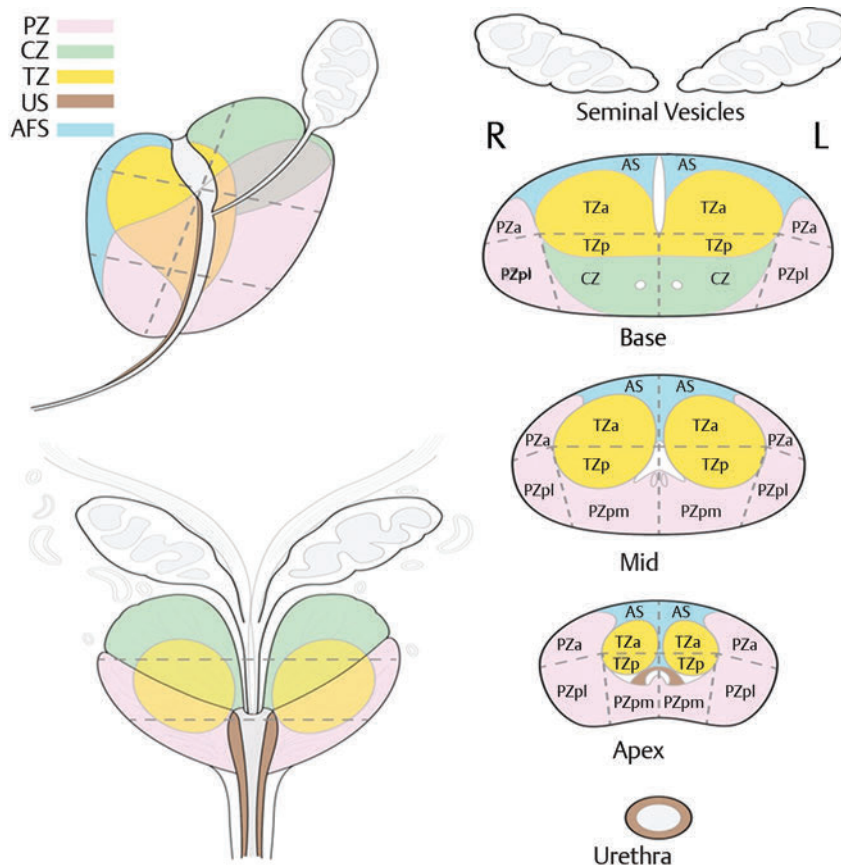


Fig. 6.8 Prostate sector map for indication of location of lesions. AFS, anterior fibromuscular stroma; CZ, central zone; PZ, peripheral zone; TZ, transition zone; US, urethral sphincter. (The prostate sector map, modified courtesy of David A. Rini, Department of Art as Applied to Medicine, Johns Hopkins University, is based on previously published figures by Villers et al [Curr Opin Urol. 2009;19:274–282] and Dickinson et al [Eur Urol. 2011;59:477–494] with anatomical correlation to the normal histology of the prostate by McNeal [Am J Surg Pathol. 1988;12:619–633].)

extraprostatic extension, then the largest of the tumors with the highest PI-RADS v2 assessment category should be considered the index lesion.

Reporting of additional findings with PI-RADS assessment category 2 or definitely benign findings (e.g., cyst) is optional, although may be helpful to use as landmarks to guide subsequent biopsy or for tracking lesions on subsequent mpMRI examinations.

Each reported lesion should be assigned to a prostate sector(s) on a sector map consisting of 39 sectors: 36 for the prostate, 2 for the seminal vesicles, and 1 for the external urethral sphincter (► Fig. 6.8):

- The prostate is divided into right and left halves on axial sections by a vertical line drawn through the center (indicated by the prostatic urethra) and into anterior and posterior halves by a horizontal line through the middle of the gland.
- The right and left PZ at the prostate base, midgland, and apex are each subdivided into three sections: anterior (a), medial posterior (mp), and lateral posterior (lp).
- The right and left TZ at the prostate base, midgland, and apex are each subdivided into two sections: anterior (a) and posterior (p).
- The anterior fibromuscular stroma (AS) is divided into right and left halves at the prostate base, midgland, and apex.
- The seminal vesicles (SV) are divided into right and left halves.

Division of the prostate and associated structures into sectors standardizes reporting and facilitates precise localization for MRI-targeted biopsy and therapy, pathologic correlation, and research. This sector map should be attached to the radiology report (either in electronic or hardcopy format) with identified suspicious findings clearly marked. If a suspicious finding extends beyond the boundaries of one sector, then all involved neighboring sectors should be indicated on the map (as a single lesion). In addition, the term “central gland” should not be used to refer to the location of a suspicious lesion. While this term historically was used to refer collectively to the TZ and CZ on MRI, this term does not represent a distinct anatomical zone or area of the prostate that is referenced by pathologists. In addition, it is now well recognized that the TZ and CZ can be readily distinguished using modern MRI technology, such that the specific zone should be stated.

6.9 Conclusions

The Prostate Imaging–Reporting and Data System v2 was designed to promote global standardization of prostate mpMRI examinations. It is not a comprehensive prostate cancer diagnosis document and should be used in conjunction with other current resources. For example, it does not address the use of MRI for detection of suspected recurrent prostate cancer following therapy, progression during active surveillance, or the use of MRI for evaluation of other parts of the body (e.g., the skeletal system) that may be involved with prostate cancer.

In addition, there are multiple new and emerging imaging techniques for prostate cancer assessment and local staging that

will undoubtedly affect the proposed interpretation scheme in the future. Some of these novel technologies include: *in vivo* MR spectroscopic imaging (MRSI); diffusion tensor imaging (DTI); diffusion kurtosis imaging (DKI); multiple b-value assessment of fractional ADC; intravoxel incoherent motion (IVIM); blood oxygenation level–dependent (BOLD) imaging; intravenous ultrasmall superparamagnetic iron oxide (USPIO) agents; and hybrid magnetic resonance–positron emission tomography (MR-PET). As relevant data and experience become available, these additional techniques may be incorporated into future versions of PI-RADS.

References

- [1] Barentsz JO, Richenberg J, Clements R et al. European Society of Urogenital Radiology. ESUR prostate MR guidelines 2012. *Eur Radiol* 2012; 22(4):746–757
- [2] Rosenkrantz AB, Kim S, Lim RP et al. Prostate cancer localization using multiparametric MR imaging: comparison of Prostate Imaging Reporting and Data System (PI-RADS) and Likert scales. *Radiology* 2013; 269(2):482–492
- [3] de Rooij M, Hamoen EHJ, Fütterer JJ, Barentsz JO, Rovers MM. Accuracy of multiparametric MRI for prostate cancer detection: a meta-analysis. *AJR Am J Roentgenol* 2014; 202(2):343–351
- [4] Arumainayagam N, Ahmed HU, Moore CM et al. Multiparametric MR imaging for detection of clinically significant prostate cancer: a validation cohort study with transperineal template prostate mapping as the reference standard. *Radiology* 2013; 268(3):761–769
- [5] American College of Radiology. MR Prostate Imaging Reporting and Data System version 2.0. Accessed June 2015, from <http://www.acr.org/Quality-Safety/Resources/PI-RADS>.
- [6] Rosenkrantz AB, Verma S, Turkbey B. Prostate cancer: top places where tumors hide on multiparametric MRI. *AJR Am J Roentgenol* 2015; 204(4):W449–56
- [7] Vargas HA, Akin O, Franiel T et al. Normal central zone of the prostate and central zone involvement by prostate cancer: clinical and MR imaging implications. *Radiology* 2012; 262(3):894–902
- [8] Hansford BG, Karademir I, Peng Y et al. Dynamic contrast-enhanced MR imaging features of the normal central zone of the prostate. *Acad Radiol* 2014; 21(5):569–577
- [9] Garcia-Reyes K, Passoni NM, Palmeri ML et al. Detection of prostate cancer with multiparametric MRI (mpMRI): effect of dedicated reader education on accuracy and confidence of index and anterior cancer diagnosis. *Abdom Imaging* 2015; 40(1):134–142
- [10] Akin O, Riedl CC, Ishill NM, Moskowitz CS, Zhang J, Hricak H. Interactive dedicated training curriculum improves accuracy in the interpretation of MR imaging of prostate cancer. *Eur Radiol* 2010; 20(4):995–1002
- [11] Seltzer SE, Getty DJ, Tempany CM et al. Staging prostate cancer with MR imaging: a combined radiologist–computer system. *Radiology* 1997; 202(1):219–226
- [12] Bratan F, Melodelima C, Souchon R et al. How accurate is multiparametric MR imaging in evaluation of prostate cancer volume? *Radiology* 2015; 275(1):144–154
- [13] Le Nobin J, Orczyk C, Deng FM et al. Prostate tumour volumes: evaluation of the agreement between magnetic resonance imaging and histology using novel co-registration software. *BJU Int* 2014; 114 6b:E105–E112
- [14] Ahmed HU. The index lesion and the origin of prostate cancer. *N Engl J Med* 2009; 361(17):1704–1706
- [15] Karavitakis M, Winkler M, Abel P, Livni N, Beckley I, Ahmed HU. Histological characteristics of the index lesion in whole-mount radical prostatectomy specimens: implications for focal therapy. *Prostate Cancer Prostatic Dis* 2011; 14(1):46–52
- [16] Weinreb JC, Barentsz JO, Choyke PL et al. PI-RADS Prostate Imaging - Reporting and Data System: 2015, Version 2. *Eur Urol* 2016; 69(1):16–40

7 Prostate Cancer Staging and Surgical Planning

Jurgen J. Fütterer

7.1 Introduction

The goal of any staging system is to combine available data about malignant disease to assess prognoses and survival characteristics, as well as to stratify appropriate treatment modalities. Cancer staging systems codify the extent of cancer to provide clinicians and patients with the means to quantify prognosis for individual patients and to compare groups of patients across practices worldwide, whether for patients receiving routine care or participating in clinical trials.¹ Although there are several different staging systems for prostate cancer, the tumor, nodes, and metastases (TNM) staging system is the most widely used of such systems. The TNM staging system was developed and is maintained by the American Joint Committee on Cancer (AJCC) and the Union for International Cancer Control (UICC). The TNM staging system for prostate cancer was first introduced in 1992.² The current version of the AJCC TNM staging system for prostate cancer (2010) is presented in ► Table 7.1.³

Pelvic lymph node metastases have a significant impact on the prognosis of patients with malignancies. For example, even micrometastases in a single node are generally considered to rule out surgical cure by the available treatment protocols in prostate cancer patients.⁴ The status of the lymph nodes largely dictates the management of the primary tumor. In patients with low-risk prostate cancer, the rate of lymph node involvement is low, ranging between 0.5 and 0.7%.^{5,6} In patients with stage T2 disease, lymph node dissection reveals lymph node metastasis in 10 to 25% of cases. Recent data suggest that prostate cancer patients with minimal lymph node involvement can be cured by extended pelvic lymph node dissection when radical prostatectomy is performed as initial therapy.⁷

Imaging has become an indispensable tool in cancer research, clinical trials, and medical practice. Magnetic resonance (MR) imaging (MRI) is the most widely used cross-sectional imaging technique for prostate cancer. While ultrasound provides real-time data, it is also highly operator dependent and experience is needed in order to perform it well. Magnetic resonance (MR) imaging allows for a more standardized examination of the prostate and with the addition of functional imaging techniques such as diffusion-weighted MR imaging, proton MR spectroscopic imaging, and dynamic contrast-enhanced MR imaging, a unique insight can be obtained into the cancer characteristics.

This chapter focuses on the role of MR imaging in the assessment of extraprostatic extension, seminal vesicle invasion, and lymph node metastases, as well as in surgical planning for nerve-sparing procedures.

7.2 Staging of Prostate Cancer

Clinical staging of prostate cancer currently entails the use of digital rectal examination, prostate-specific antigen (PSA) measurement, as well as transrectal ultrasound. The clinical stage is identified using these variables and expressed using the TNM staging classification (► Table 7.1).

Stage T1a and T1b tumors cannot be identified by digital rectal examination of the prostate. They are found incidentally in prostatic tissue removed during transurethral resection or during prostatectomy performed for benign prostatic hypertrophy.

Table 7.1 American Joint Committee on Cancer (AJCC) clinical TNM staging classification of prostate cancer.

Stage definition
<i>Primary tumor (T) clinical</i>
Tx Primary tumor cannot be assessed
T0 No evidence of primary tumor
T1 Clinically inapparent tumor neither palpable nor visible by imaging
T1a Tumor incidental histologic finding in 5% or less of tissue resected
T1b Tumor incidental histologic finding in more than 5% of tissue resected
T1c Tumor identified by needle biopsy (for example, because of elevated PSA)
T2 Tumor confined within prostate ^a
T2a Tumor involves one-half of one lobe or less
T2b Tumor involves more than one-half of one lobe but not both lobes
T2c Tumor involves both lobes
T3 Tumor extends through the prostate capsule ^b
T3a Extraprostatic extension (unilateral or bilateral)
T3b Tumor invades seminal vesicle(s)
T4 Tumor is fixed or invades adjacent structures other than seminal vesicles, such as external sphincter, rectum, bladder, levator muscles, and/or pelvic wall
<i>Regional lymph nodes (N) clinical</i>
NX Regional lymph nodes were not assessed
N0 No regional lymph node metastasis
N1 Metastasis in regional lymph node(s)
<i>Distant metastasis (M)^c clinical</i>
M0 No distant metastasis
M1 Distant metastasis
M1a Nonregional lymph node(s)
M1b Bone(s)
M1c Other site(s) with or without bone disease

^a Tumor found in one or both lobes by needle biopsy but not palpable or reliably visible by imaging is classified as T1c.

^b Invasion into the prostatic apex or into (but not beyond) the prostatic capsule is classified not as T3 but as T2.

^c When more than one site of metastasis is present, the most advanced category is used. pM1c is most advanced, where "p" stands for "prostate".
Abbreviation: PSA, prostate-specific antigen.

Source: Adapted from the AJCC Cancer Staging Manual, 7th edition, 2010.³

Tumors of these stages are generally referred to as “incidental carcinomas.” These tumors are found in 8 to 12% of patients undergoing surgery for benign disease.^{8,9} Patients rarely die from T1a or T1b disease but rather from other age-related causes. Prostate cancer diagnosed by needle biopsy after an elevated PSA is termed stage T1c disease if both the digital rectal examination is normal and no lesions are visible on the transrectal ultrasound.

In disease stages T2a through T2c, there is either an organ-confined palpable nodule on digital rectal examination or evidence of one or multiple tumors on imaging. This category of prostate cancers is potentially curable. In patients with stage T2 disease, lymph node dissection reveals lymph node metastasis in 10 to 25% of cases.¹⁰ The natural history of T2 prostate cancer has been shown to be associated with a 10-year rate of local progression in 66% of patients diagnosed and progression to metastatic disease in 33% of patients diagnosed.¹¹

Stage T3 prostate cancers have extraprostatic extension and a much poorer prognosis compared to organ-confined disease. However, since radical prostatectomy offers promising oncologic outcomes in patients with pathologic T3 disease, preoperative MRI could be of help in both predicting the presence of extraprostatic extension and in providing information about the location of extraprostatic extension for surgical planning. Depending on the depth of extraprostatic involvement, lymph node metastases occur in up to 50% of these cases.

Because digital rectal examination and PSA have been shown to be of limited value in the prediction of stage T3 tumors, numerous imaging modalities have been applied to improve local staging accuracy. Computed tomography (CT), positron emission tomography (PET), as well as MR imaging, have been used to improve the prediction of stage T3 disease.

In the event of lymph node involvement, prognosis is determined by the N status rather than by the T category. It has been shown that cure rates with surgery alone are not to be expected to exceed 30%.¹² During pelvic lymphadenectomy, metastatic lymph nodes are identified to various degrees. Median time to progression in this group is on the order of 11 to 24 months. In terms of survival, it seems to be of little importance whether hormonal treatment is deferred or started immediately. The reported median time to progression can be prolonged up to 5 years with early hormonal treatment, although this is achieved at the cost of side effects.

7.3 Local Staging

Local staging is accomplished by examining the prostatic capsule and seminal vesicles. Multiparametric prostate MR imaging is currently the most accurate imaging modality to preoperatively stage prostate cancer.¹³ Magnetic resonance imaging has a higher accuracy in the assessment of intraprostatic disease (stage T2; ▶ Fig. 7.1), extraprostatic extension (▶ Fig. 7.2), and seminal vesicle invasion (stage T3; ▶ Fig. 7.3) as well as invasion of peri-prostatic structures (stage T4; ▶ Fig. 7.4), compared to other imaging techniques. In patients in whom the diagnosis of cancer has been established, reliably determining its local stage, along with localization of tumor within the gland, is an important element of prostate MR imaging.¹⁴ In the decade prior to this writing, the focus of MR imaging in prostate cancer moved from staging to localization of the disease. Information

regarding location of the tumor, capsule involvement, tumor volume, and neurovascular bundle integrity are becoming more important than “simple” stage information. With improvements in surgical techniques, it is now possible to combine all of this information in the surgical planning.

To justify the use of an expensive imaging modality such as MR imaging, patients’ outcome should be improved by preoperative staging.¹³ To achieve this goal, staging accuracy should be high, the results should affect diagnostic and especially therapeutic thinking, and the alternative therapy should increase life expectancy and quality of life.

In local staging, T2-weighted MR imaging (▶ Fig. 7.5) is the most important sequence. T2-weighted MR imaging has the highest in-plane spatial resolution compared to the other imaging sequences included in prostate MR imaging (i.e., DWI, MRSI, and DCE-MRI), and is therefore crucial in capsular and neurovascular bundle involvement assessment. However, it is not possible to state a single overall accuracy of MR imaging for staging prostate cancer because of a very wide divergence across published studies.¹⁵ In a meta-analysis, the reported summary receiver operating characteristic curve for MR imaging in prostate cancer local staging (T2 vs. T3) had a joint maximum sensitivity and specificity of 71 to 74%.^{15,16} However, this summary estimate is limited given the heterogeneity in staging performance across centers, such that the staging performance of MR imaging in one’s local practice is likely to differ. Furthermore, due to incomplete reporting within individual studies, it is not possible to fully explain the basis of this heterogeneity of staging performance in the literature. Nonetheless, it was suggested that use of turbo spin-echo imaging using an endorectal coil and multiple imaging planes improved staging performance.¹⁵

Magnetic resonance (MR) imaging sequences performed at low field strengths with the conventional body coil or phased-array surface coils lack sufficient resolution and signal-to-noise ratio to identify fine anatomical details of the prostate gland and periprostatic tissues necessary for accurate staging.¹⁷ However, improvements in coil technologies, higher field strength, and sequence development have led to higher staging

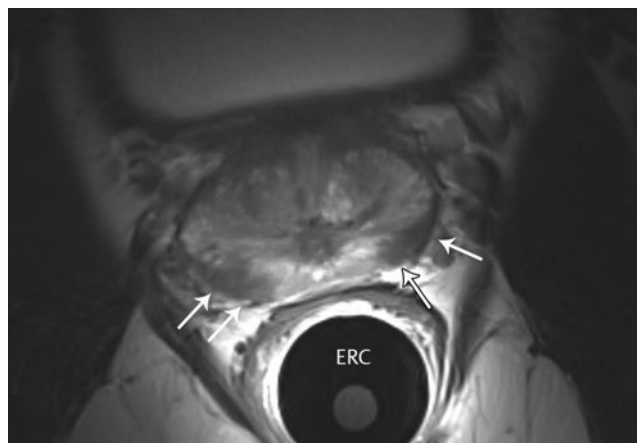


Fig. 7.1 A 63-year-old man with biopsy-proven bilateral prostate cancer (Gleason score 3 + 4 = 7) in peripheral zone of the midprostate and a prostate-specific antigen level of 6.8 ng/mL. The axial T2-weighted endorectal-coil MRI shows bilateral well-circumscribed low-signal-intensity areas (white arrows) confined to the prostate (stage T2 prostate cancer).

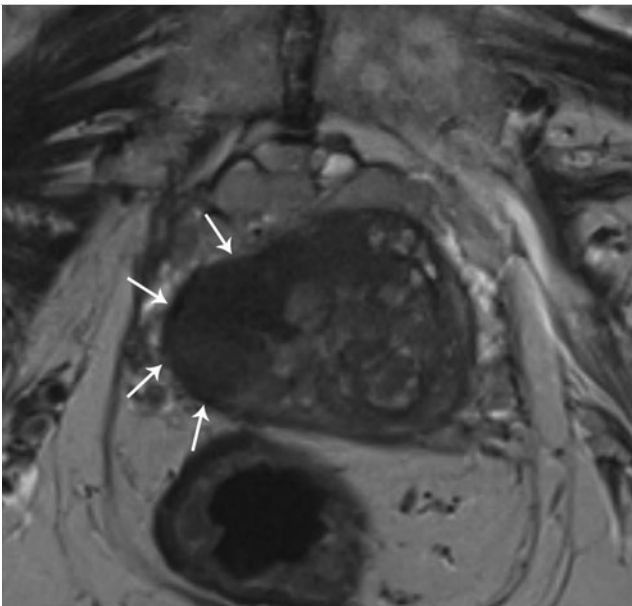


Fig. 7.2 A 74-year-old man with biopsy-proven prostate cancer (Gleason score 3+4 tumor in 6 out of 6 biopsy cores from the right lobe; benign in 6 out of 6 cores from the left lobe.) and a prostate-specific antigen level of 28 ng/mL. Digital rectal examination showed stage T2 prostate cancer. The patient underwent staging T2-weighted MRI without an endorectal coil, which revealed a large mass in the right half of the prostate with clear evidence of extraprostatic extension (*white arrows*) (stage T3a prostate cancer).

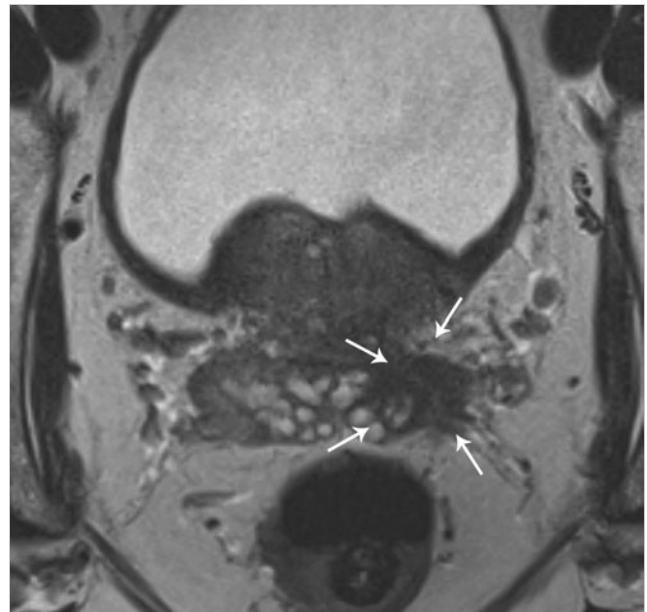


Fig. 7.3 A 3-T T2-weighted MRI of the prostate in a 66-year-old man with a prostate-specific antigen level of 9.5 ng/mL and biopsy-proven prostate cancer with a Gleason score of 4+3 in the left prostate. A low-signal-intensity lesion (*white arrows*) is visualized in the left seminal vesicle consistent with seminal vesicle invasion (stage T3b prostate cancer).

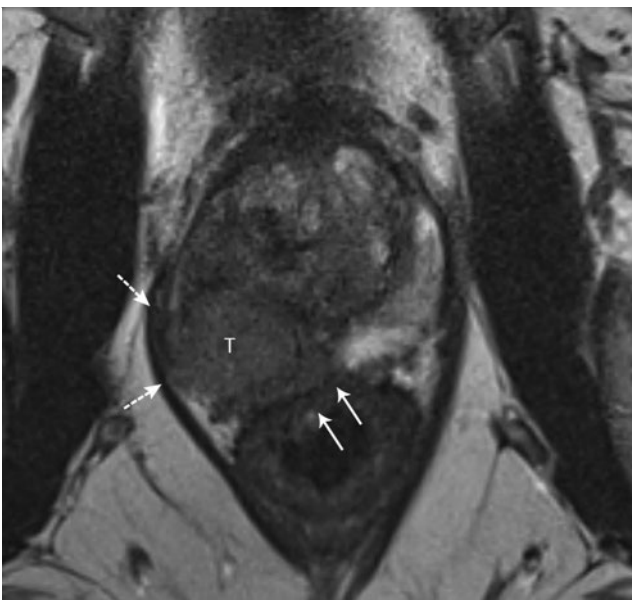


Fig. 7.4 A 71-year-old man with a prostate specific antigen level of 9.3 ng/mL and Gleason score 4 + 4 = 8 prostate cancer underwent staging MRI. The T2-weighted axial image shows a large bulky tumor (T) in the right prostate gland with evidence of invasion into the right puborectal sling (*dashed arrows*) and possible invasion into the rectal wall (*white arrows*) (stage 4 prostate cancer; invasion of periprostatic structures).

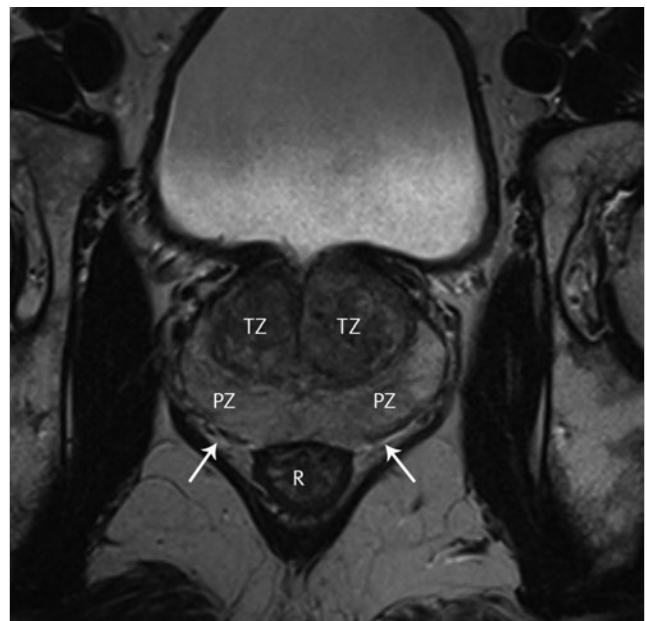


Fig. 7.5 An axial T2-weighted MRI of the prostate in a healthy man. The peripheral zone (PZ) has a higher signal intensity than the transition zone (TZ). The rectum (R) is located posterior to the prostate. The capsule is annotated with *white arrows*.

accuracies. Currently, endorectal 3-T MRI can be considered the most reliable noninvasive technique for the local staging of prostate cancer.^{13,18,19,20,21}

The most cost-effective group of patients to undergo local staging with endorectal MR imaging are those considered to have an intermediate risk of T3 prostate cancer, based on a PSA

level between 4 and 20 ng/mL and a Gleason score between 5 and 7.²² In this group of patients, endorectal MR imaging is useful because the decision on selection of treatment (prostatectomy or a form of radiation therapy and/or hormonal deprivation) is most likely to depend on the imaging results. Inclusion of MR imaging results in clinical nomograms that help improve the prediction of cancer extent, thereby improving patient selection for local therapy.²³ Ideally, prostate MR imaging should have a low percentage of false-positives for extraprostatic extension to ensure that few, if any, patients will be deprived of potentially curative treatment options. Historically, it has been suggested that all patients who are considered candidates for a radical treatment should undergo MR imaging with a high specificity interpretation in order to guide the final treatment selection.¹⁹ However, this conventional thinking is changing due to a combination of factors. First, nerve-sparing radical prostatectomy is now commonly applied as the routine surgical approach to localized prostate cancer. In addition, urologists now more commonly will consider performing radical prostatectomy in patients with suspected extraprostatic extension of prostate carcinoma (EPE), albeit with a wider surgical margin than in other patients. Thus, higher sensitivity for EPE on MRI in such contexts may be appropriate, given that an overcall of EPE would not preclude surgery in such centers and in order to reduce the risk of positive margins in those patients with EPE who do proceed to surgery.

7.3.1 Acquisition Protocol

Prostate MR imaging should be obtained at least 4 to 6 weeks after image-guided biopsy, given that postbiopsy hemorrhage (► Fig. 7.6) decreases not only the localization accuracy but also

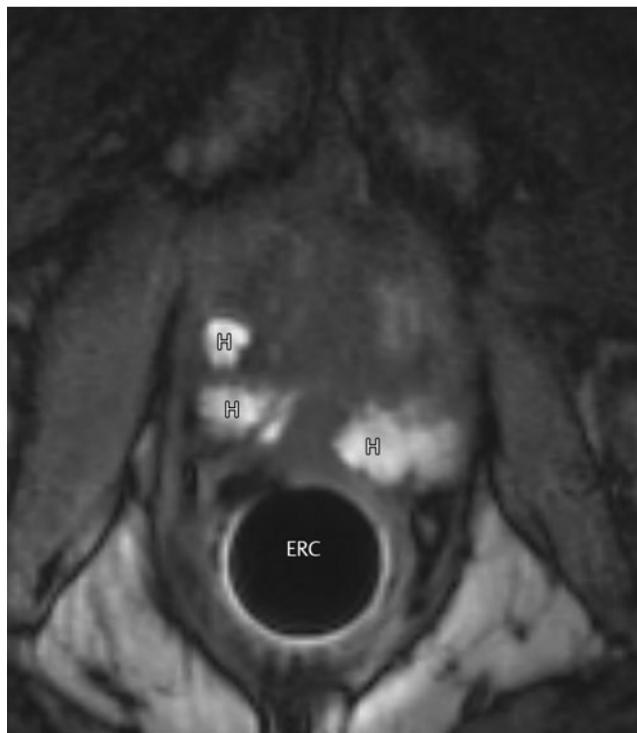


Fig. 7.6 Areas of high signal intensity (white Hs) representing biopsy hematoma on a T1-weighted MRI in the right and left peripheral zone.

the staging accuracy as well.^{24,25,26} Nonetheless when extensive postbiopsy change is present, the distribution of hemorrhage can be used to assist tumor detection. Namely, areas that are excluded from the otherwise extensive hemorrhage, when also showing a corresponding area of homogeneous low signal intensity at T2-weighted MR imaging, are likely to represent cancer.²⁷

In general, a combination of a pelvic phased-array coil and endorectal coil are used at a field strength of 1.5 T, while either the pelvic phased-array, endorectal coil, or a combination are used at 3 T. At both 1.5 T and 3 T, endorectal coils (► Fig. 7.7; ► Fig. 7.8) have been shown to improve prostate MR image quality and staging performance compared with those of pelvic phased-array coils, although the necessity of an endorectal coil at 3 T is debatable.²⁸ Patients tolerate the endorectal coil well, although the insertion remains uncomfortable.²⁹ For the endorectal coil, the primary potential adverse effect on imaging is an increase in the incidence of bowel motion artifacts, which deteriorate image quality.²¹ In the European Society of Urogenital Radiology prostate MRI guidelines, the combination of endorectal coil and pelvic phased-array coil are recognized to provide excellent signal-to-noise ratio and to be considered state-of-the-art imaging.³⁰

The imaging protocol consists of high in-plane resolution T2-weighted sequences in at least 2 planes, as well as DWI and DCE-MR imaging in the axial plane with preferably the same slice thickness and slice gap as the T2-weighted anatomical imaging sequence.

7.3.2 T2-Weighted MR Imaging

T2-weighted imaging provides the best depiction of the prostate's zonal anatomy and capsule³¹ (► Fig. 7.5; ► Fig. 7.9). Anatomical T2-weighted MR imaging is obtained with a small field of view covering the entire prostate and seminal vesicles. There is no evidence to support the usefulness of fat suppression for T2-weighted sequences. Indeed, use of frequency-selective fat

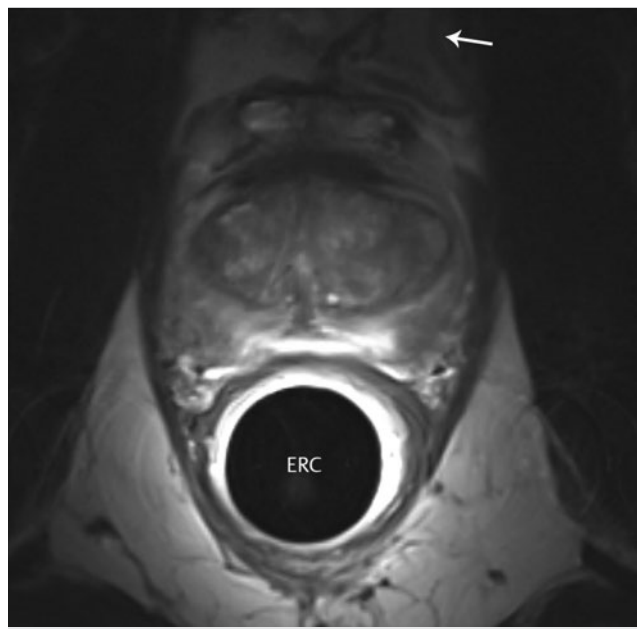


Fig. 7.7 An axial T2-weighted endorectal-coil MRI. Note the signal drop at the anterior part of the prostate and pubic bone (arrow).

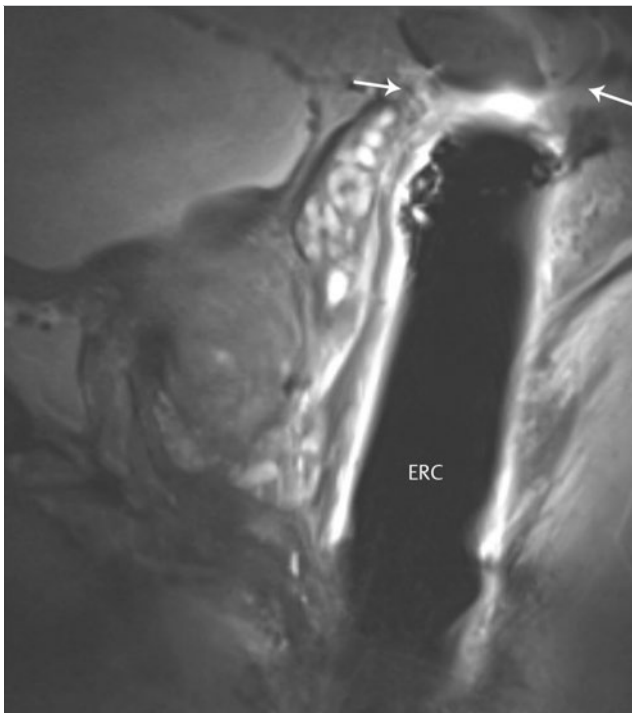


Fig. 7.8 A sagittal T2-weighted endorectal-coil (ERC) MRI. Artifacts are present related to the coil and bowel motion (arrows). However, these artifacts do not decrease the image quality of the prostate itself due to the head-to-feet readout of MRI acquisition.

suppression does not significantly improve the diagnosis of extraprostatic disease and decreases the signal-to-noise ratio, which may limit visualization of anatomical details and reduce the definition of the prostatic capsule. Moreover, suppression of fat signal intensity leads to the reduced definition of periprostatic anatomical planes and degrades the visualization of structures within the prostatic fat, such as the neurovascular bundles. Contrast between extraprostatic tumor and periprostatic fat may also be reduced.³²

Among locally invasive tumors, the distinction between those penetrating the prostate capsule but sparing the seminal vesicles (stage T3a) and those invading the seminal vesicles (stage T3b) is important in patient prognosis and therapeutic planning.³³ In addition, according to the TNM staging system, tumors invading but not penetrating the capsule are classified as T2 and not as T3 disease.³⁴

On T2-weighted images, extraprostatic extension can be detected by visualizing the direct extension of the tumor into the periprostatic fat. Indirect imaging criteria for the detection of EPE include asymmetry of the neurovascular bundle (► Fig. 7.10; ► Fig. 7.11), obliteration of the rectoprostatic angle, tumor bulge into the periprostatic fat (► Fig. 7.12), broad tumor contact with the surface of the capsule (> 1.5 cm) (► Fig. 7.13), and capsular retraction^{35,36,37,38} (► Table 7.2). Despite the development of these indirect criteria, the sensitivity and specificity for local staging with MRI vary considerably with technique and population: 14.4 to 100% and 67 to 100%, respectively.³⁶ This heterogeneity may also reflect that the accuracy for local staging can be influenced by the extent of EPE that is present, with MR imaging having high accuracy for established EPE, although

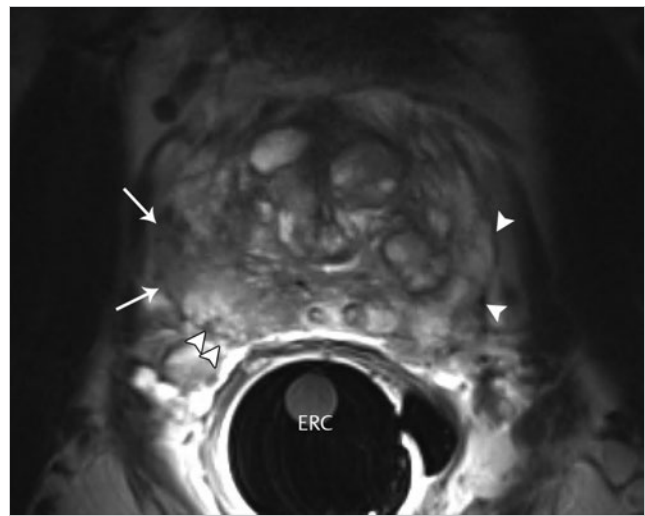


Fig. 7.9 An axial T2-weighted MRI of a 75-year-old man with histopathologically proven prostate cancer (Gleason score 4 + 3 = 7) in the right peripheral zone (arrows). The prostate capsule is a thin layer on T2-weighted imaging (arrowheads).

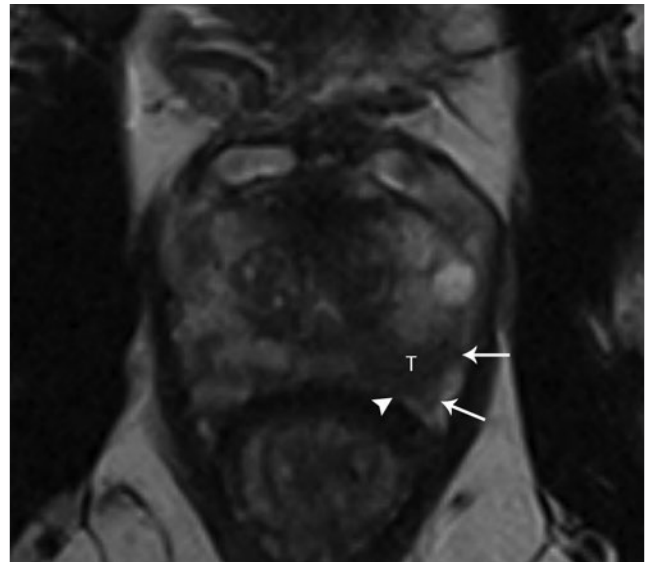


Fig. 7.10 A 64-year-old man with stage T3a prostate cancer in the left peripheral zone (PZ) though with minimal extraprostatic extension. T2-weighted MRI shows that the tumor (T) has lower signal intensity than the PZ. It also shows the asymmetry of the left rectoprostatic angle (arrowhead) and some capsular bulging (arrows).

more limited accuracy for focal or localized EPE. False-negative interpretations for EPE may occur in the presence of microscopic EPE, and false-positive interpretations for EPE may occur due to normal variation and heterogeneity in the appearance and degree of visualization of the capsule between patients (► Fig. 7.14; ► Fig. 7.15). Given these considerations, the definitive diagnosis of EPE on MRI should only be made when direct and/or gross EPE is visualized. In comparison, the diagnosis of EPE should only be suggested when just the previously noted secondary and/or indirect findings are present.

In patients with a diagnosis of prostate cancer, the presence of seminal vesicle invasion is associated with high rates of tumor

recurrence and therapy failure. Reported progression rates in these patients range from 40 to 95%.³⁹ The features of seminal vesicle invasion (SVI) that have high sensitivity and specificity on MR imaging include low signal intensity within the seminal vesicle (▶ Fig. 7.3) and/or lack of preservation of the normal architecture of the seminal vesicle (▶ Fig. 7.16)^{40,41} (▶ Table 7.3). The presence of tumor at the prostate base (▶ Fig. 7.17) is also associated with an increased incidence of SVI.⁴² In addition, expansion of the ejaculatory ducts and obliteration of the angle between the prostate gland and the seminal vesicle, although not sensitive, are highly specific for SVI, highly suggesting this diagnosis when the features are confidently detected at MR imaging.⁴¹ Furthermore, it has been suggested that the combination of tumor at the base of the prostate gland, associated extraprostatic extension, and features of seminal vesicle invasion

is more helpful than any imaging feature alone in predicting seminal vesicle invasion. The combinations of features that are most predictive of seminal vesicle invasion, however, will vary for different readers. Overall, the sensitivity and specificity for the detection of SVI are 23 to 80% and 81 to 99%, respectively. False-negative findings may occur due to microscopic tumor extension along the ducts, amyloidosis deposition, or fibrosis or scarring in the seminal vesicles.

The accuracy of endorectal MR imaging findings and of MR image interpretation is related to radiologists' experience and subspecialty training.³⁴ Several studies have suggested that radiologists who have completed a dedicated training program in prostate MRI interpretation tend to have better accuracy of

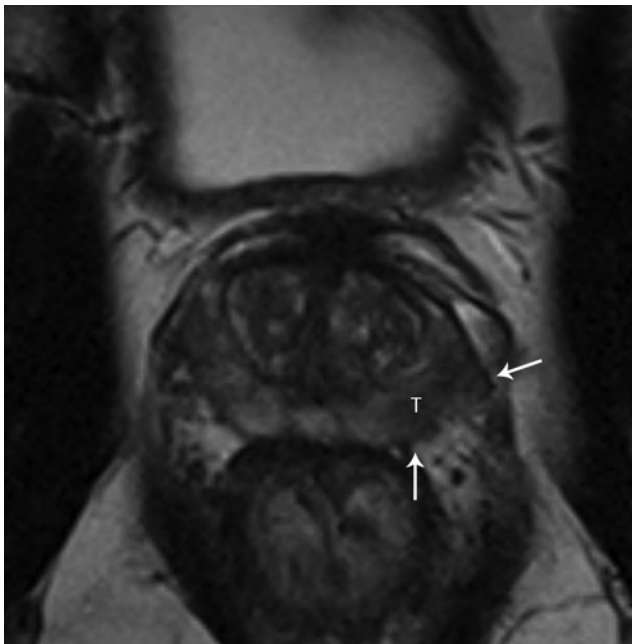


Fig. 7.11 A 71-year-old man with stage T3a disease in the left peripheral zone (PZ) (Gleason score 5 + 3 = 8). The T2-weighted MRI shows that the tumor (T) has lower signal intensity than the PZ and that there is bulging of the capsule (arrows).



Fig. 7.12 A 56-year-old man with stage T3a disease in the right peripheral zone (PZ) (Gleason score 7; PSA = 5.7 ng/mL). The T2-weighted MRI shows the bulky tumor (T) in the right PZ with obliteration of the rectoprostatic angle (arrow head) and the normal neurovascular bundle on the left side (NVB, white circle). The lesion shows clear extraprostatic extension (arrows).



Fig. 7.13 (a) Axial T2-weighted MRI of a 71-year-old man with histopathologically proven prostate cancer (Gleason score 3 + 4 = 7) in the right peripheral zone (arrows). The tumor (T) shows broad tumor contact. Whole-mount-section histopathology revealed microscopic capsular penetration at this site. (b) Axial apparent diffusion coefficient (ADC) map shows (arrows) restricted diffusion at the same location as the low-signal-intensity lesion on T2-weighted imaging. (c) Axial T1-weighted postcontrast MRI also shows early enhancement at the same location (arrow).

Table 7.2 Criteria for predicting extraprostatic extension.

- Asymmetry or involvement of the neurovascular bundle
- Obliteration of the rectoprostatic angle
- Capsular bulging
- Overt extraprostatic tumor
- Disruption of the prostatic capsule
- Broad contact of tumor with the capsule (>15 mm)

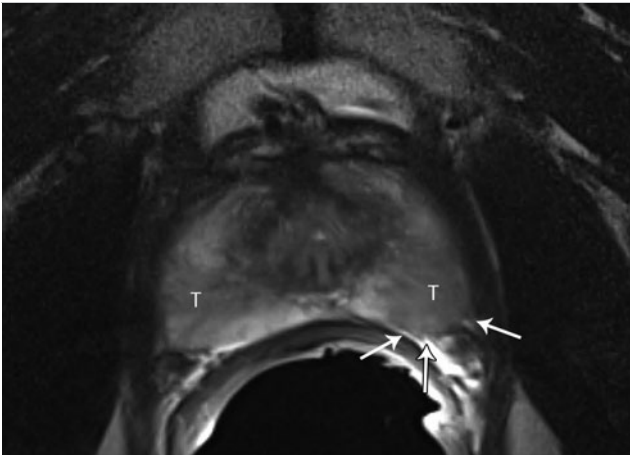


Fig. 7.14 A 54-year-old man with bilateral biopsy-proven prostate cancer (Gleason scores 3 + 4 [left] and 3 + 3 [right]). The T2-weighted MRI demonstrates broad tumor contact as well as bulging of the capsule on the left (*arrows*); minimal T3a was suggested in the report. Histopathology revealed stage pT2c tumors. The tumors were correctly localized on MR imaging. However, the tumor in the left peripheral zone was not invading the prostate capsule, despite the presence of indirect signs for extraprostatic extension on the MRI.

tumor localization than general body radiologists.^{13,43,44} Thus, although MRI has added value to the decision-making process in prostate cancer patients, it is equally important to have imaging reviewed by experienced, subspecialty trained radiologists with expertise in prostate MR interpretation, who function as part of a prostate imaging team.⁴⁵ One study showed that radiologists' accuracy in interpreting prostate MR imaging can be improved by the use of an interactive dedicated training curriculum.⁴³ In that study, radiology fellows' performance in local staging improved significantly after a training program incorporating individualized feedback and didactic lectures. Also, since the early reports of interobserver variability in prostate MR interpretation, both MR imaging technology and radiologists' skills have improved substantially.¹⁷ Yu et al reported that the combined use of endorectal MR imaging and MR spectroscopic imaging decreased interobserver variability and, for less experienced radiologists, significantly improved the detection of EPE in patients with prostate cancer.⁴⁶ Finally, the *reinterpretation* of prostate MRI examinations by subspecialized genitourinary oncologic radiologists, when available, also improves the detection of EPE of prostate cancer.⁴⁷

Table 7.3 Criteria for predicting seminal vesicle invasion.

- Lack of normal seminal vesicle architecture
- Focal or diffuse areas of low signal intensity within the seminal vesicle
- Low signal intensity within the seminal vesicle causing mass effect
- Enlarged ejaculatory ducts with low signal intensity
- Obliteration of the angle between the prostate and seminal vesicle on sagittal images
- Extension of the low signal intensity of tumor from the base of the prostate to the seminal vesicle

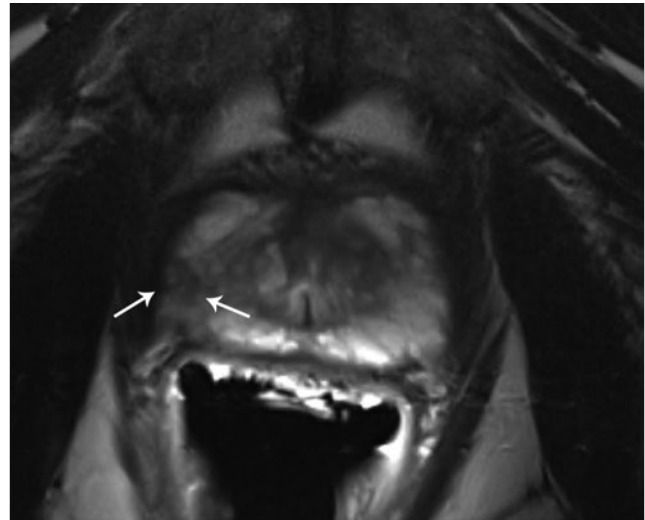


Fig. 7.15 A 63-year-old man with biopsy-proven prostate cancer (Gleason score 4 + 3) underwent MR imaging prior to radical prostatectomy. The T2-weighted MRI demonstrates a lesion in the right apex (*arrows*) with minimal capsular contact and no signs of extraprostatic extension (EPE). However, histopathology revealed a stage pT3a tumor in the right apex. The presence of only microscopic EPE (0.5 mm) may account for the false-negative interpretation on MR imaging.

7.3.3 Functional MR Imaging

Though the literature is still sparse on the added value of DCE-MRI to improve staging performance, it does appear to improve local staging performance when used in combination with T2-weighted imaging in patients with equivocal capsular penetration, seminal vesicle invasion, and neurovascular bundle involvement (► Fig. 7.18). Moreover, DCE-MRI may improve local prostate cancer staging for less experienced radiologists.⁴⁸ Dynamic subtraction contrast-enhanced endorectal MRI improves staging accuracy for both EPE and SVI (84 and 97%, respectively), with a 97% accuracy obtained for the assessment of neurovascular bundle involvement.⁴⁹

Diffusion-weighted MR imaging in addition to T2-weighted images may help to improve specificity and positive-predictive value for the diagnosis of SVI⁴⁰ (► Fig. 7.19). The addition of diffusion-weighted imaging (DWI) and apparent diffusion

coefficient (ADC) mapping to T2-weighted MRI improves the accuracy of preoperative detection of EPE. Furthermore, tumor ADC values in patients with and without EPE are significantly different.⁵⁰ Median and 10th and 25th percentile ADC values

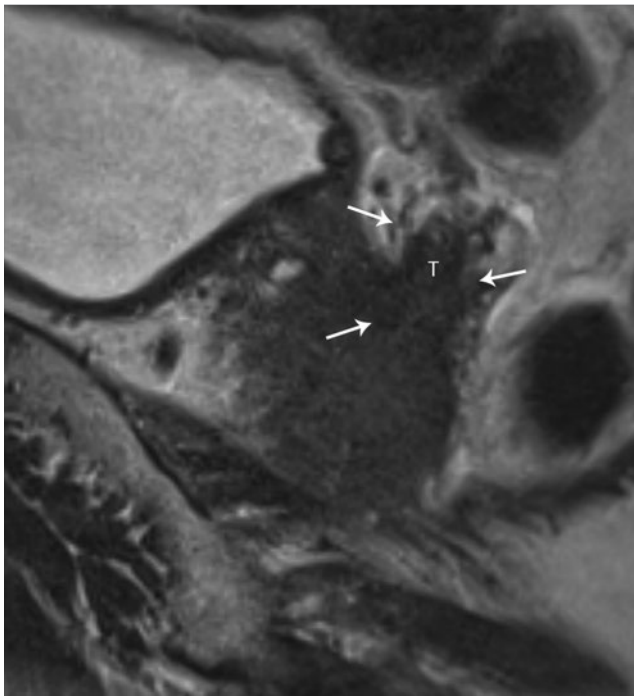


Fig. 7.16 A 3-T T2-weighted MRI of the prostate in a 66-year-old man with a prostate-specific antigen level of 9.5 ng/mL and biopsy-proven prostate cancer with Gleason score 4+3 in the left prostate. On the sagittal T2-weighted MRI, a low-signal-intensity lesion (*white arrows*) is seen in the left seminal vesicle, consistent with tumor invasion (stage T3b prostate cancer).

are significantly associated with the presence of EPE and may be useful in the pretreatment assessment of patients with prostate cancer.⁵¹ In one study, DWI showed comparable accuracy as T2-weighted MR imaging for side-specific assessment of EPE and had a greater sensitivity for EPE <2 mm for the less-experienced radiologist.⁵² The combination of DWI and T2-weighted MR imaging also improve the detection of SVI.⁵³

The addition of three-dimensional MR spectroscopic imaging to T2-weighted MR imaging improves accuracy for predicting EPE for both experienced and less-experienced readers (A_z increase from 0.78 to 0.86 and from 0.62 to 0.75, respectively, for T2-weighted imaging alone vs. combined imaging).⁴⁶

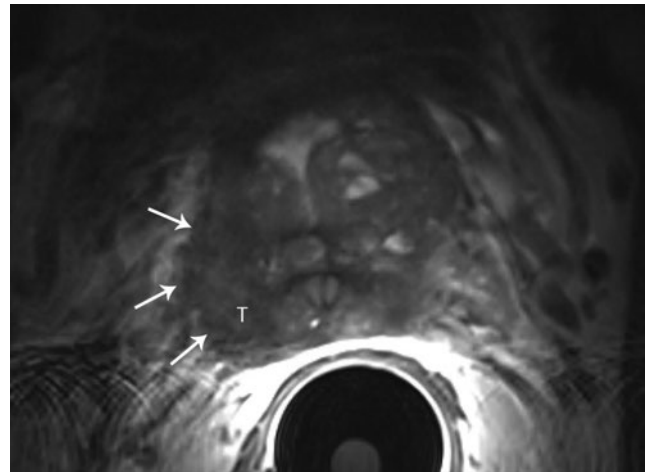


Fig. 7.17 A 53-year-old man with stage T3b disease in the right seminal vesicle (Gleason score 8; prostate-specific antigen = 15.7 ng/mL). The T2-weighted MRI shows the presence of a large tumor (T; *arrows*) at the base of the right half of the prostate. This feature is highly predictive of seminal vesicle invasion.

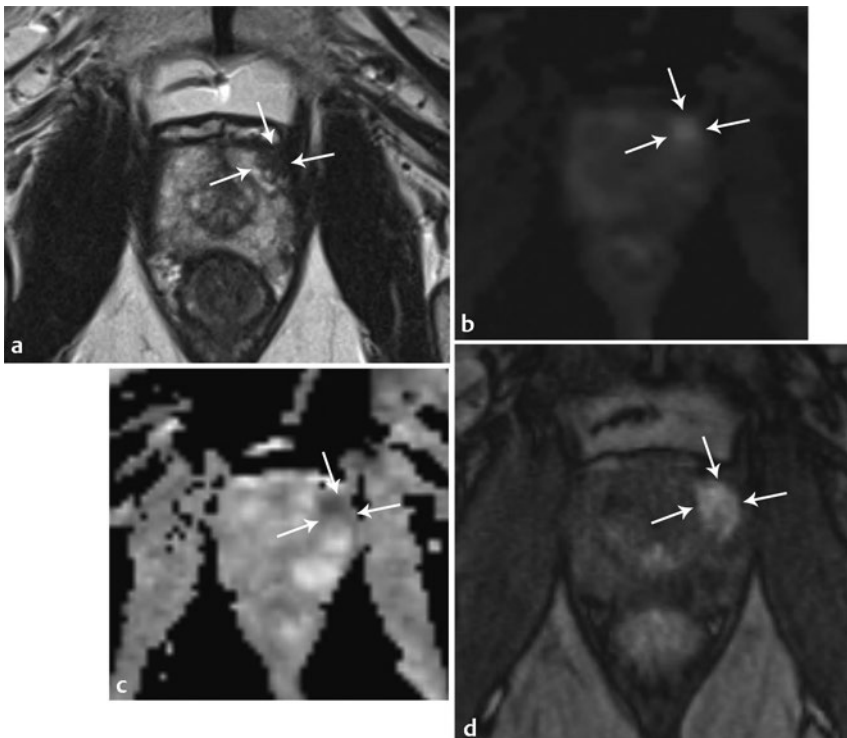


Fig. 7.18 A 62-year-old man with biopsy-proven prostate cancer underwent staging MRI of the prostate. (a) A tiny lesion in the left anterior horn can be appreciated (*arrows*) on the T2-weighted MRI. (b) The axial high b-value ($b = 1400 \text{ s/mm}^2$) diffusion-weighted image at the same level shows high signal intensity in the area (*arrow*), and (c) the axial apparent diffusion coefficient map shows restricted diffusion. (d) On the axial T1-weighted postcontrast MR image, the tumor (*arrows*) demonstrates early enhancement at the same location as the low signal intensity lesion on T2-weighted imaging. The functional techniques may help draw the attention of the radiologist to inspect this area on the T2-weighted images. Thus, by helping to localize the tumor, the functional techniques may also prompt the radiologist to more closely inspect the capsule at this particular location, which in this case shows no evidence for extraprostatic extension.

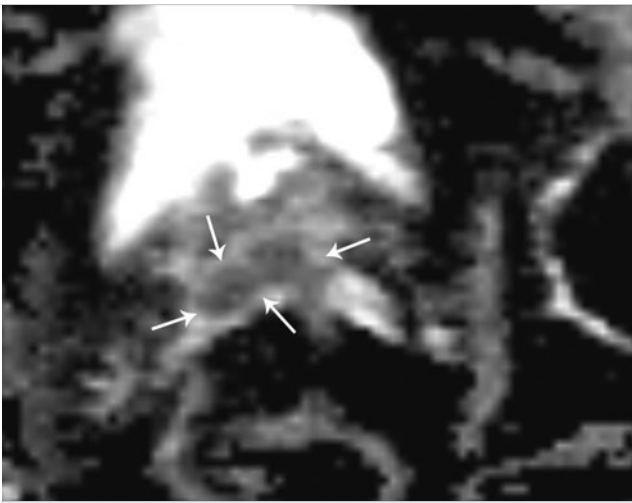


Fig. 7.19 A 75-year-old man with stage T3b disease in the right seminal vesicle. The apparent diffusion coefficient map demonstrates restricted diffusion in the right seminal vesicle (arrow). This may help to improve specificity and positive predictive value for the diagnosis of seminal vesicle invasion.

While these functional sequences may not directly show the EPE and/or neurovascular bundle involvement, these sequences all tend to improve staging performance by helping to localize the dominant tumor, which represents the likely site of any EPE that may be present. Furthermore, the acquired functional information may be used to guide and draw the attention of the less experienced radiologist to a particular area for closer scrutiny. Given these considerations, prostate cancer staging in routine practice has likely improved since the widespread adoption of DCE-MRI and DWI into standard protocols.

7.3.4 Field Strength

At 3 T, the increased signal-to-noise ratio (SNR) compared to 1.5 T offers options for clinical MR imaging such as faster imaging, increased spatial resolution, or a combination of these. Subsequently, the introduction of 3-T MRI scanners has promoted the implementation of prostate MR imaging in clinical practice. Moreover, the use of an external phased-array coil at 3 T yields an image quality that may be equivalent to that of an endorectal coil image at 1.5 T.⁵⁴ Indeed, the increased SNR that has been achieved through a combined endorectal and pelvic phased-array coil at 1.5 T has facilitated the role of MR imaging in the detection and staging of prostate cancer.¹⁵

It is a natural conclusion that the combined use of endorectal with external phased-array coils at 3 T can further improve spatial resolution and will likely yield superior image quality compared with either an external phased-array coil alone at 3 T or the combined phased-array coil and endorectal coil at 1.5 T. The value of T2-weighted MR imaging of the prostate depends on the visualization of the tumor and prostate capsule and the ability to assess their spatial relationships. This in turn is greatly influenced by the achievable spatial resolution and tissue contrast, leading some investigators to believe that a higher spatial resolution facilitates better clinical performance of MR imaging of the prostate.⁵⁵

The increased SNR resulting from an endorectal coil at 3 T has shown great potential to improve the spatial resolution of T2-weighted and spectroscopic images as well as either the spatial or temporal resolution of dynamic T1-weighted sequences for contrast-enhanced imaging.⁵⁶ For experienced radiologists, accuracies of 94% in the localization of prostate cancer have been achieved, which are higher than those reported at 1.5 T. Likewise, the high spatial resolution T2-weighted MR images also provide highly detailed information regarding the capsule and possible capsular penetration. Indeed, staging performance at 3 T using an endorectal coil alone is superior compared to pelvic-phased array imaging.

The need for an endorectal coil at higher field strengths has been investigated, as motion-related artifacts, as well as nearfield artifacts, both associated with the endorectal coil, can impair image quality. Heijmink et al compared image quality and the accuracy of prostate cancer localization and staging between body array coil and endorectal coil T2-weighted MR imaging at 3 T.⁵⁷ Significantly more motion artifacts were present when the endorectal coil was used. However, all other image quality characteristics improved significantly ($P < .001$) with endorectal coil imaging. Endorectal MR imaging significantly increased the area-under-the-ROC-curve for staging as well as the sensitivity for locally advanced disease in experienced readers from 7% to 73 to 80%, while maintaining a high specificity of 97 to 100%. In addition, EPE as small as 0.5 mm at histopathology could be accurately detected only with endorectal MR imaging. The significant increase in capsular delineation, visualization of the neurovascular bundle and rectoprostatic angle, and lesion visibility with endorectal MR imaging, improved the staging performance. These differences explain the increased sensitivity for locally advanced disease that was observed for all readers. Their study indicated that endorectal coil MR imaging at 3 T significantly improved image quality, which in combination with the higher spatial resolution also significantly increased the localization and staging performance for both experienced and less experienced radiologists.

7.4 Surgical Planning and Nerve-Sparing Surgery

There are several therapeutic options available for prostate cancer, including definitive radiation therapy, radical prostatectomy, thermal therapies, and focal therapy. The accurate definition of prostate cancer location influences the adjustments made in surgical techniques for reduction of positive margins and the improvement of overall oncologic outcomes. Radical prostatectomy is an established definitive treatment option in the management of organ-confined or minimal T3 disease. The goal of this procedure is to achieve excellent oncologic control with negative surgical margins while preserving urinary continence and erectile function.

A nerve-sparing radical prostatectomy preserves the neurovascular bundle running along the posterior-lateral aspect of the prostate. This procedure is the standard of care for men with a low preoperative risk of extraprostatic disease who wish to retain erectile function, and is also associated with improved urinary continence.^{58,59,60} The primary risk of a nerve-sparing approach is that it may lead to higher rates of surgical margins

that are positive for cancer^{61,62} given that prostate cancer most commonly arises in the peripheral zone (PZ) of the prostate, often posteriorly, just beneath the capsule.⁶³ Magnetic resonance (MR) imaging of the prostate can help guide decisions regarding the use of a nerve-sparing approach. One study reported that a significantly lower rate of positive surgical margins was observed in patients who underwent multiparametric MR imaging–directed intraoperative frozen-section analysis.⁶⁴ In addition, McClure et al reported that no ipsilateral positive margins were present in any patients switched from a non-nerve sparing to a nerve sparing approach based on MRI findings.⁶⁵ It is important to recognize that the surgeon is able to make a separate decision for each lobe regarding whether to spare or resect the ipsilateral nerve, or whether to perform an interfascial dissection with only a partial nerve resection, thereby indicating the value of MR imaging in assisting side-specific surgical planning. As an example of this nuanced approach based on imaging, the surgeon may choose to perform a slightly wider resection, inducing only partial resection of the nerve, on just one side if MR imaging shows bulky tumor or broad capsular contact of tumor in that lobe, even if not directly showing gross EPE.

Patients with larger prostates and with narrow, deep pelvises are predicted to have a more difficult robot-assisted laparoscopic prostatectomy. By depicting the pelvic anatomy, MRI can help predict the level of surgical difficulty and serve as a valuable adjunctive study prior to robot-assisted laparoscopic prostatectomy.⁶⁶ Furthermore, in open radical prostatectomy, surgeons typically use tactile feedback from manually identifying the neurovascular bundles to guide decisions regarding the extent of resection and whether to spare the bundles in order to preserve patient potency.⁶⁷ In comparison, during robot-assisted laparoscopic prostatectomy, surgeons lack such tactile feedback that is obtained during open surgery. Thus, while surgeons performing robot-assisted laparoscopic prostatectomy may also prefer to routinely dissect the neurovascular bundles from the capsule in order to achieve a nerve-sparing procedure in appropriate patients, the lack of tactile feedback may potentially affect surgical outcomes.⁶⁵ However, in comparison with traditional predictors such as serum PSA and digital rectal examination findings, prostate MR findings provide detailed spatial localization that may assist the robotic surgeon in individually tailoring the extent of resection.⁶³

7.5 Lymph Node Staging

The presence of lymph node metastases is a strong predictor of disease recurrence and progression and also directly affects treatment selection.⁶⁸ Imaging for lymph node metastases is necessary for men who are at higher risk of metastases, particularly those with a PSA level greater than 20 ng/mL, a Gleason score greater than 7, and/or clinical tumor stage T3 or higher (high-risk group).

Surgical pelvic lymph node dissection with histopathologic examination is currently the most reliable method of assessing lymph node status. A noninvasive, reliable method for detecting and staging nodal metastasis in the preoperative assessment may redirect clinicians towards less invasive treatment strategies. However, because normal and abnormal lymph nodes

have similar signal intensities on MRI and densities on CT, metastatic lymph nodes are currently identified largely based on size and to a lesser extent on shape criteria⁶⁹ (► Fig. 7.20). Size-based criteria commonly result in missing small metastases in normal-sized nodes,⁷⁰ as well as in overcalling metastases in enlarged benign reactive nodes (► Fig. 7.21). Additional morphological features that may help raise suspicion for a metastatic node include a round rather than elliptical shape, absence of a fatty hilum, and an ill-defined nodal margin.

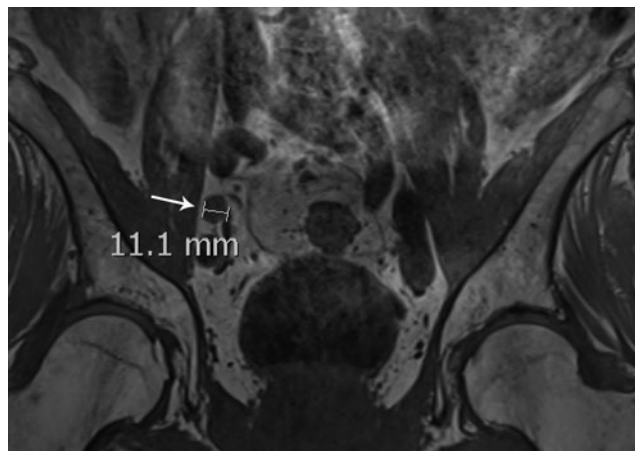


Fig. 7.20 A 78-year-old man with an elevated prostate-specific antigen level of 3.9 ng/mL 5 years after external-beam radiation therapy for prostate cancer. The T1-weighted MRI demonstrates an enlarged lymph node measuring 11 mm (short axis), which was biopsied and revealed metastatic adenocarcinoma.

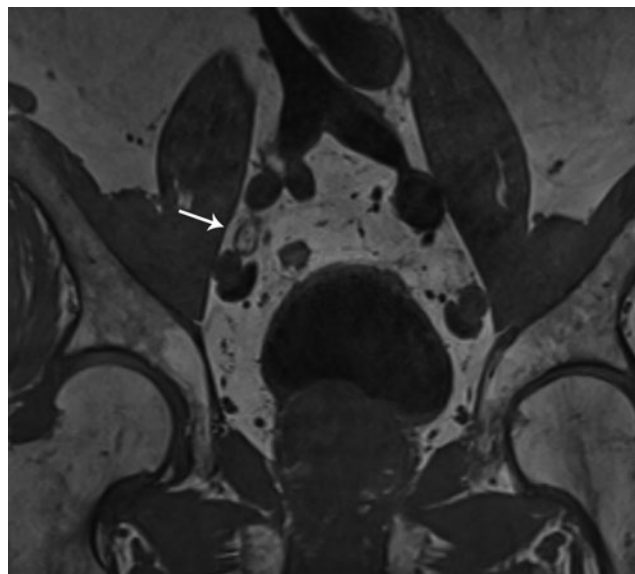


Fig. 7.21 An 81-year-old man with biopsy-proven prostate cancer (Gleason score 5 + 4 = 9) and a prostate-specific antigen level of 32 ng/mL underwent staging MR imaging. The coronal T1-weighted MRI demonstrates an enlarged lymph node next to the right common iliac artery (11 mm). The node had a preserved prominent fatty hilum, a benign morphological feature. CT-guided biopsy was performed and revealed a reactive lymph node without evidence for metastasis.

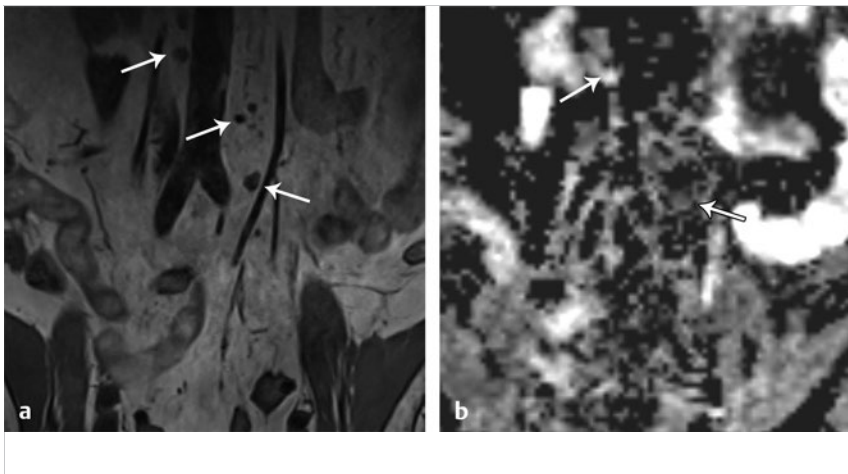


Fig. 7.22 (a) A 68-year-old man who previously underwent radical prostatectomy and radiation therapy to the prostate bed presents with a rapidly rising prostate-specific antigen level of 8.2 ng/mL. The coronal T1-weighted MRI demonstrates non-enlarged nodes in the para-aortic region (the largest node has a short axis of 7 mm). These nodes would be considered benign based on traditional size and shape criteria. (b) The coronal apparent diffusion coefficient map at the same level demonstrates restricted diffusion in a lymph node in the left para-aortic region, although a right para-aortic node does not show restricted diffusion (arrows). The patient underwent local radiation therapy of the para-aortic region. The PSA subsequently responded, decreasing to 0.3 ng/mL.

The sensitivity of CT and MRI for the detection of lymph node metastases based on morphological criteria is low, for instance being about 36%⁶⁹ in one study. This low sensitivity may be partly attributed to the typical requirement of a size ≥ 1 cm in diameter for the identification of lymph node metastases. Nonetheless, the specificity based on morphological evaluation has been reported to be about 82%.⁷¹ When confirmation is required, CT and MRI can be used as guidance for fine-needle aspiration biopsy of a suspicious lymph node.

Diffusion-weighted imaging has also been investigated to help evaluate pelvic lymph nodes⁷² (► Fig. 7.22), for instance potentially helping to detect small nodal metastases not meeting traditional size criteria. In addition, it is possible that the ADC value within the lymph node may have superior performance than traditional size criteria in discriminating benign and malignant lymph nodes. However, there remains overlap in the features of benign and malignant nodes on DWI and the ADC map, and reliance on DWI for detecting nodal metastases may result in an increased rate of false-positive interpretations. Therefore, further validation of the role of DWI in nodal assessment is required.

The introduction of lymphotropic paramagnetic iron oxide nanoparticles contrast agent [MR lymphangiography (MRL)] has improved the detection of nodal disease.^{70,73} The latter contrast agent is a freeze-dried iron oxide agent reconstituted in normal saline and administered intravenously by a slow drip infusion, which can easily be performed on an outpatient basis. Magnetic Resonance lymphangiography is performed 24 hours after the injection of the contrast agent and serves to evaluate the contrast enhancement of the identified lymph nodes. After IV injection, the particles slowly extravasate from the vascular to the interstitial space, are then transported to lymph nodes via lymphatic vessels, and finally are internalized by macrophages. Thus, this contrast agent is cell specific for macrophages. Once within normally functioning nodes, the intracellular iron oxide nanoparticles within the macrophages reduce the signal intensity of normal node tissue, given the T2*-susceptibility effects induced by the iron oxide, thereby producing a signal drop or negative contrast enhancement. In areas of lymph nodes that are involved with malignant cells, macrophages are replaced by cancer cells. Therefore, in these areas, there is no uptake of the iron oxide nanoparticles. In addition, due to increased vascular permeability and increased diffusion

in cancer tissue, there is minimal leakage of iron oxide nanoparticles into the extracellular space of malignant metastatic areas, which produces a low local concentration and non-clustering of particles at these sites. Magnetic resonance lymphangiography has significantly higher sensitivity and negative predictive value in the detection of lymph node metastases compared to CT.⁷⁴ In one study, MRL correctly identified all patients with nodal metastases, and a node-by-node analysis had a significantly higher sensitivity than conventional MRI (90.5% vs. 35.4%).⁷⁵ In patients with intermediate and high clinical risk of having lymph node metastasis, the posttest probability of having lymph node metastases following a negative MRL is low enough (less than 4%) to omit a pelvic lymph node dissection.⁷⁴

Although discussed in greater detail in Chapter 11, PET is a promising tool for lymph node evaluation that may complement and address limitations of multiparametric MR imaging. For example, gallium (⁶⁸Ga)-labeled prostate-specific membrane antigen (PSMA) PET/CT, which uses the affinity of the ⁶⁸Ga-labeled PSMA ligand to PSMA expressing prostate cancer cells, is an emerging imaging modality to detect lymph node metastases.⁷⁶ The most significant advantage of ⁶⁸Ga-PSMA PET/CT may be its sensitivity at low PSA levels for even small lymph node metastases,⁷⁶ which was reported in patients with biochemical recurrence after primary therapy. While ⁶⁸Ga-PSMA PET/CT is a promising tool for nodal assessment, the size of the lymph node metastasis continues to have a substantial impact on its diagnostic accuracy.⁷⁷

References

- [1] Edge SB, Compton CC. The American Joint Committee on Cancer: the 7th edition of the AJCC cancer staging manual and the future of TNM. *Ann Surg Oncol* 2010; 17(6):1471–1474
- [2] Beahrs OH, Henson DE, Hutter RVP, Kennedy BJ eds. American Joint Committee on Cancer Staging Manual. 4th ed. Philadelphia, PA: Lippincott; 1992
- [3] Edge S, Byrd DR, Compton CC, Fritz AG, Greene FL, Trotti A. *AJCC Cancer Staging Manual*. 7th ed. New York, NY: Springer; 2010
- [4] Messing EM, Manola J, Sarosdy M, Wilding G, Crawford ED, Trump D. Immediate hormonal therapy compared with observation after radical prostatectomy and pelvic lymphadenectomy in men with node-positive prostate cancer. *N Engl J Med* 1999; 341(24):1781–1788
- [5] Berglund RK, Sadetsky N, DuChane J, Carroll PR, Klein EA. Limited pelvic lymph node dissection at the time of radical prostatectomy does not affect 5-year failure rates for low, intermediate and high risk prostate cancer: results from CaPSURE. *J Urol* 2007; 177(2):526–529, discussion 529–530

- [6] Makarov DV, Humphreys EB, Mangold LA et al. Pathological outcomes and biochemical progression in men with T1c prostate cancer undergoing radical prostatectomy with prostate specific antigen 2.6 to 4.0 vs 4.1 to 6.0 ng/ml. *J Urol* 2006; 176(2):554–558
- [7] Briganti A, Blute ML, Eastham JH et al. Pelvic lymph node dissection in prostate cancer. *Eur Urol* 2009; 55(6):1251–1265
- [8] Bhojani N, Boris RS, Monn MF, Mandeville JA, Lingeman JE. Coexisting prostate cancer found at the time of holmium laser enucleation of the prostate for benign prostatic hyperplasia: predicting its presence and grade in analyzed tissue. *J Endourol* 2015; 29(1):41–46
- [9] Nunez R, Hurd KJ, Noble BN, Castle EP, Andrews PE, Humphreys MR. Incidental prostate cancer revisited: early outcomes after holmium laser enucleation of the prostate. *Int J Urol* 2011; 18(7):543–547
- [10] Huang Y, Isharwal S, Haese A et al. Prediction of patient-specific risk and percentile cohort risk of pathological stage outcome using continuous prostate-specific antigen measurement, clinical stage and biopsy Gleason score. *BJU Int* 2011; 107(10):1562–1569
- [11] Whitmore WF Jr. Natural history of low-stage prostatic cancer and the impact of early detection. *Urol Clin North Am* 1990; 17(4):689–697
- [12] Fleischmann A, Schobinger S, Schumacher M, Thalmann GN, Studer UE. Survival in surgically treated, nodal positive prostate cancer patients is predicted by histopathological characteristics of the primary tumor and its lymph node metastases. *Prostate* 2009; 69(4):352–362
- [13] Fütterer JJ. MR imaging in local staging of prostate cancer. *Eur J Radiol* 2007; 63(3):328–334
- [14] Scheenen TW, Rosenkrantz AB, Haider MA, Fütterer JJ. Multiparametric Magnetic Resonance Imaging in Prostate Cancer Management: Current Status and Future Perspectives. *Invest Radiol* 2015; 50(9):594–600
- [15] Engelbrecht MR, Jager GJ, Laheij RJ, Verbeek AL, van Lier HJ, Barentsz JO. Local staging of prostate cancer using magnetic resonance imaging: a meta-analysis. *Eur Radiol* 2002; 12(9):2294–2302
- [16] Sonnad SS, Langlotz CP, Schwartz JS. Accuracy of MR imaging for staging prostate cancer: a meta-analysis to examine the effect of technologic change. *Acad Radiol* 2001; 8(2):149–157
- [17] Rifkin MD, Zerhouni EA, Gatsonis CA et al. Comparison of magnetic resonance imaging and ultrasonography in staging early prostate cancer. Results of a multi-institutional cooperative trial. *N Engl J Med* 1990; 323(10):621–626
- [18] Otto J, Thörmer G, Seiwerts M et al. Value of endorectal magnetic resonance imaging at 3 T for the local staging of prostate cancer. *Rofo* 2014; 186(8):795–802
- [19] Fütterer JJ, Engelbrecht MR, Jager GJ et al. Prostate cancer: comparison of local staging accuracy of pelvic phased-array coil alone versus integrated endorectal-pelvic phased-array coils. Local staging accuracy of prostate cancer using endorectal coil MR imaging. *Eur Radiol* 2007; 17(4):1055–1065
- [20] Fütterer JJ, Barentsz JO, Heijmink SW. Value of 3-T magnetic resonance imaging in local staging of prostate cancer. *Top Magn Reson Imaging* 2008; 19(6):285–289
- [21] Fütterer JJ, Heijmink SW, Scheenen TW et al. Prostate cancer: local staging at 3-T endorectal MR imaging—early experience. *Radiology* 2006; 238(1):184–191
- [22] Engelbrecht MR, Jager GJ, Severens JL. Patient selection for magnetic resonance imaging of prostate cancer. *Eur Urol* 2001; 40(3):300–307
- [23] Wang L, Hricak H, Kattan MW, Chen HN, Scardino PT, Kuroiwa K. Prediction of organ-confined prostate cancer: incremental value of MR imaging and MR spectroscopic imaging to staging nomograms. *Radiology* 2006; 238(2):597–603
- [24] Ikonen S, Kivisaari L, Vehmas T et al. Optimal timing of post-biopsy MR imaging of the prostate. *Acta Radiol* 2001; 42(1):70–73
- [25] Kaji Y, Kurhanewicz J, Hricak H et al. Localizing prostate cancer in the presence of postbiopsy changes on MR images: role of proton MR spectroscopic imaging. *Radiology* 1998; 206(3):785–790
- [26] White S, Hricak H, Forstner R et al. Prostate cancer: effect of postbiopsy hemorrhage on interpretation of MR images. *Radiology* 1995; 195(2):385–390
- [27] Barrett T, Vargas HA, Akin O, Goldman DA, Hricak H. Value of the hemorrhage exclusion sign on T1-weighted prostate MR images for the detection of prostate cancer. *Radiology* 2012; 263(3):751–757
- [28] Haider MA, Krieger A, Elliott C, Da Rosa MR, Milot L. Prostate imaging: evaluation of a reusable two-channel endorectal receiver coil for MR imaging at 1.5 T. *Radiology* 2014; 270(2):556–565
- [29] Engelbrecht MR, Barentsz JO, Jager GJ et al. Prostate cancer staging using imaging. *BJU Int* 2000; 86 Suppl 1:123–134
- [30] Barentsz JO, Richenberg J, Clements R et al. European Society of Urogenital Radiology. ESUR prostate MR guidelines 2012. *Eur Radiol* 2012; 22(4):746–757
- [31] Sakai I, Harada K, Hara I, Eto H, Miyake H. A comparison of the biological features between prostate cancers arising in the transition and peripheral zones. *BJU Int* 2005; 96(4):528–532
- [32] Tsuda K, Yu KK, Coakley FV, Srivastav SK, Scheidler JE, Hricak H. Detection of extracapsular extension of prostate cancer: role of fat suppression endorectal MRI. *J Comput Assist Tomogr* 1999; 23(1):74–78
- [33] D'Amico AV, Whittington R, Malkowicz SB et al. Combination of the preoperative PSA level, biopsy gleason score, percentage of positive biopsies, and MRI T-stage to predict early PSA failure in men with clinically localized prostate cancer. *Urology* 2000; 55(4):572–577
- [34] Schiebler ML, Yankaskas BC, Tempny C et al. MR imaging in adenocarcinoma of the prostate: interobserver variation and efficacy for determining stage C disease. *AJR Am J Roentgenol* 1992; 158(3):559–562, discussion 563–564
- [35] Tempny CM, Rahmouni AD, Epstein JI, Walsh PC, Zerhouni EA. Invasion of the neurovascular bundle by prostate cancer: evaluation with MR imaging. *Radiology* 1991; 181(1):107–112
- [36] Turkbey B, Albert PS, Kurdziel K, Choyke PL. Imaging localized prostate cancer: current approaches and new developments. *AJR Am J Roentgenol* 2009; 192(6):1471–1480
- [37] Yu KK, Hricak H, Alagappan R, Chernoff DM, Bacchetti P, Zaloudek CJ. Detection of extracapsular extension of prostate carcinoma with endorectal and phased-array coil MR imaging: multivariate feature analysis. *Radiology* 1997; 202(3):697–702
- [38] Outwater EK, Petersen RO, Siegelman ES, Gomella LG, Chernesky CE, Mitchell DG. Prostate carcinoma: assessment of diagnostic criteria for capsular penetration on endorectal coil MR images. *Radiology* 1994; 193(2):333–339
- [39] Debras B, Guillonnet B, Bougaran J, Chambon E, Vallancien G. Prognostic significance of seminal vesicle invasion on the radical prostatectomy specimen. Rationale for seminal vesicle biopsies. *Eur Urol* 1998; 33(3):271–277
- [40] Soylu FN, Peng Y, Jiang Y et al. Seminal vesicle invasion in prostate cancer: evaluation by using multiparametric endorectal MR imaging. *Radiology* 2013; 267(3):797–806
- [41] Sala E, Akin O, Moskowitz CS et al. Endorectal MR imaging in the evaluation of seminal vesicle invasion: diagnostic accuracy and multivariate feature analysis. *Radiology* 2006; 238(3):929–937
- [42] Guillonnet B, Debras B, Veillon B, Bougaran J, Chambon E, Vallancien G. Indications for preoperative seminal vesicle biopsies in staging of clinically localized prostate cancer. *Eur Urol* 1997; 32(2):160–165
- [43] Akin O, Riedl CC, Ishill NM, Moskowitz CS, Zhang J, Hricak H. Interactive dedicated training curriculum improves accuracy in the interpretation of MR imaging of prostate cancer. *Eur Radiol* 2010; 20(4):995–1002
- [44] Mullerad M, Hricak H, Wang L, Chen HN, Kattan MW, Scardino PT. Prostate cancer: detection of extracapsular extension by genitourinary and general body radiologists at MR imaging. *Radiology* 2004; 232(1):140–146
- [45] Tan N, Margolis DJ, McClure TD et al. Radical prostatectomy: value of prostate MRI in surgical planning. *Abdom Imaging* 2012; 37(4):664–674
- [46] Yu KK, Scheidler J, Hricak H et al. Prostate cancer: prediction of extracapsular extension with endorectal MR imaging and three-dimensional proton MR spectroscopic imaging. *Radiology* 1999; 213(2):481–488
- [47] Wibmer A, Vargas HA, Donahue TF et al. Diagnosis of Extracapsular Extension of Prostate Cancer on Prostate MRI: Impact of Second-Opinion Readings by Subspecialized Genitourinary Oncologic Radiologists. *AJR Am J Roentgenol* 2015; 205(1):W73–8
- [48] Fütterer JJ, Engelbrecht MR, Huisman HJ et al. Staging prostate cancer with dynamic contrast-enhanced endorectal MR imaging prior to radical prostatectomy: experienced versus less experienced readers. *Radiology* 2005; 237(2):541–549
- [49] Ogura K, Maekawa S, Okubo K et al. Dynamic endorectal magnetic resonance imaging for local staging and detection of neurovascular bundle involvement of prostate cancer: correlation with histopathologic results. *Urology* 2001; 57(4):721–726
- [50] Chong Y, Kim CK, Park SY, Park BK, Kwon GY, Park JJ. Value of diffusion-weighted imaging at 3 T for prediction of extracapsular extension in patients with prostate cancer: a preliminary study. *AJR Am J Roentgenol* 2014; 202(4):772–777
- [51] Lawrence EM, Gallagher FA, Barrett T et al. Preoperative 3-T diffusion-weighted MRI for the qualitative and quantitative assessment of extracapsular extension in patients with intermediate- or high-risk prostate cancer. *AJR Am J Roentgenol* 2014; 203(3):W280–6

- [52] Rosenkrantz AB, Chandarana H, Gilet A et al. Prostate cancer: utility of diffusion-weighted imaging as a marker of side-specific risk of extracapsular extension. *J Magn Reson Imaging* 2013; 38(2):312–319
- [53] Ren J, Huan Y, Wang H et al. Seminal vesicle invasion in prostate cancer: prediction with combined T2-weighted and diffusion-weighted MR imaging. *Eur Radiol* 2009; 19(10):2481–2486
- [54] Sosna J, Rofsky NM, Gaston SM, DeWolf WC, Lenkinski RE. Determinations of prostate volume at 3-Tesla using an external phased array coil: comparison to pathologic specimens. *Acad Radiol* 2003; 10(8):846–853
- [55] Bloch BN, Rofsky NM, Baroni RH, Marquis RP, Pedrosa I, Lenkinski RE. 3 Tesla magnetic resonance imaging of the prostate with combined pelvic phased-array and endorectal coils; Initial experience(1). *Acad Radiol* 2004; 11(8):863–867
- [56] Fütterer JJ, Scheenen TW, Huisman HJ et al. Initial experience of 3 tesla endorectal coil magnetic resonance imaging and 1H-spectroscopic imaging of the prostate. *Invest Radiol* 2004; 39(11):671–680
- [57] Heijmink SW, Fütterer JJ, Hambrock T et al. Prostate cancer: body-array versus endorectal coil MR imaging at 3 T—comparison of image quality, localization, and staging performance. *Radiology* 2007; 244(1):184–195
- [58] Walz J, Burnett AL, Costello AJ et al. A critical analysis of the current knowledge of surgical anatomy related to optimization of cancer control and preservation of continence and erection in candidates for radical prostatectomy. *Eur Urol* 2010; 57(2):179–192
- [59] Kessler TM, Burkhard FC, Studer UE. Nerve-sparing open radical retropubic prostatectomy. *Eur Urol* 2007; 51(1):90–97
- [60] Burkhard FC, Kessler TM, Fleischmann A, Thalmann GN, Schumacher M, Studer UE. Nerve sparing open radical retropubic prostatectomy—does it have an impact on urinary continence? *J Urol* 2006; 176(1):189–195
- [61] Steineck G, Bjartell A, Hugosson J et al. LAPPRO steering committee. Degree of preservation of the neurovascular bundles during radical prostatectomy and urinary continence 1 year after surgery. *Eur Urol* 2015; 67(3):559–568
- [62] Miller J, Smith A, Kouba E, Wallen E, Pruthi RS. Prospective evaluation of short-term impact and recovery of health related quality of life in men undergoing robotic assisted laparoscopic radical prostatectomy versus open radical prostatectomy. *J Urol* 2007; 178(3 Pt 1):854–858, discussion 859
- [63] Hricak H, Wang L, Wei DC et al. The role of preoperative endorectal magnetic resonance imaging in the decision regarding whether to preserve or resect neurovascular bundles during radical retropubic prostatectomy. *Cancer* 2004; 100(12):2655–2663
- [64] Petralia G, Musi G, Padhani AR et al. Robot-assisted radical prostatectomy: Multiparametric MR imaging-directed intraoperative frozen-section analysis to reduce the rate of positive surgical margins. *Radiology* 2015; 274(2):434–444
- [65] McClure TD, Margolis DJ, Reiter RE et al. Use of MR imaging to determine preservation of the neurovascular bundles at robotic-assisted laparoscopic prostatectomy. *Radiology* 2012; 262(3):874–883
- [66] Mason BM, Hakimi AA, Faleck D, Chernyak V, Rozenblitt A, Ghavamian R. The role of preoperative endo-rectal coil magnetic resonance imaging in predicting surgical difficulty for robotic prostatectomy. *Urology* 2010; 76(5):1130–1135
- [67] Gralnek D, Wessells H, Cui H, Dalkin BL. Differences in sexual function and quality of life after nerve sparing and nonnerve sparing radical retropubic prostatectomy. *J Urol* 2000; 163(4):1166–1169, discussion 1169–1170
- [68] O'Dowd GJ, Veltri RW, Orozco R, Miller MC, Oesterling JE. Update on the appropriate staging evaluation for newly diagnosed prostate cancer. *J Urol* 1997; 158(3 Pt 1):687–698
- [69] Wolf JS Jr, Cher M, Dall'era M, Presti JC Jr, Hricak H, Carroll PR. The use and accuracy of cross-sectional imaging and fine needle aspiration cytology for detection of pelvic lymph node metastases before radical prostatectomy. *J Urol* 1995; 153(3 Pt 2):993–999
- [70] Harisinghani MG, Barentsz J, Hahn PF et al. Noninvasive detection of clinically occult lymph-node metastases in prostate cancer. *N Engl J Med* 2003; 348(25):2491–2499
- [71] Hövels AM, Heesakkers RA, Adang EM et al. The diagnostic accuracy of CT and MRI in the staging of pelvic lymph nodes in patients with prostate cancer: a meta-analysis. *Clin Radiol* 2008; 63(4):387–395
- [72] Eiber M, Beer AJ, Holzapfel K et al. Preliminary results for characterization of pelvic lymph nodes in patients with prostate cancer by diffusion-weighted MR-imaging. *Invest Radiol* 2010; 45(1):15–23
- [73] Bellin MF, Roy C, Kinkel K et al. Lymph node metastases: safety and effectiveness of MR imaging with ultrasmall superparamagnetic iron oxide particles—initial clinical experience. *Radiology* 1998; 207(3):799–808
- [74] Heesakkers RA, Hövels AM, Jäger GJ et al. MRI with a lymph-node-specific contrast agent as an alternative to CT scan and lymph-node dissection in patients with prostate cancer: a prospective multicohort study. *Lancet Oncol* 2008; 9(9):850–856
- [75] Harisinghani MG, Barentsz JO, Hahn PF et al. MR lymphangiography for detection of minimal nodal disease in patients with prostate cancer. *Acad Radiol* 2002; 9 Suppl 2:S312–S313
- [76] Afshar-Oromieh A, Zechmann CM, Malcher A et al. Comparison of PET imaging with a (68)Ga-labelled PSMA ligand and (18)F-choline-based PET/CT for the diagnosis of recurrent prostate cancer. *Eur J Nucl Med Mol Imaging* 2014; 41(1):11–20
- [77] Budaus L, Leyh-Bannurah SR, Salomon G et al. Initial Experience of (68) Ga-PSMA PET/CT Imaging in High-risk Prostate Cancer Patients Prior to Radical Prostatectomy. *Eur Urol* 2016; 69(3):393–396

8 Post-Treatment Follow-Up and Assessments for Recurrence

Adam T. Froemming, Lyndsay Viers, Eric May, and Akira Kawashima

8.1 Introduction

Understanding the clinical aspects of prostate cancer recurrence is critical to understanding the role of diagnostic imaging and intervention, as well as the evolution toward imaging-based patient specific management in this population. This chapter focuses on the imaging of prostate cancer recurrence with an emphasis on MRI. Indications for such imaging are reviewed, and emerging image-guided focal therapies for recurrent cancer are also highlighted.

8.2 Clinical Background on Prostate Cancer Recurrence

Radical prostatectomy (RP) remains the most common primary treatment for primary localized prostate cancer (PCa) and offers definitive cure in most patients. Primary whole gland radiation and ablative therapies also can achieve high success rates in appropriate patient populations. However, the incidence of biochemical recurrence (BCR) ranges from 19 to 35% at 10 years following radical prostatectomy and around 30% following primary radiation therapy,¹ posing a challenge in terms of further diagnosis and treatment. Biochemical recurrence, also variously called prostate specific antigen (PSA) failure or biochemical failure, is defined most commonly as two consecutive elevated serum PSA values above 0.2 ng/mL following RP. This definition is not universal, as Cookson et al identified 53 different definitions of BCR in a sampling of 145 papers.² The initial rise in serum PSA marks a crucial point in disease management as it can be the initial indicator of subsequent disease progression or eventual PCa related mortality.³ Importantly, BCR can precede clinically evident disease recurrence by 7 to 10 years (mean, 8 years).⁴ Detection of BCR serves as a trigger for further imaging-based evaluation to localize the site of any clinically evident recurrence (whether local or distant) so that targeted salvage therapy may be initiated to interrupt progression to PCa-related mortality.

Following RP, serum PSA is expected to rapidly fall to undetectable levels and is then routinely followed post-treatment at periodic intervals, typically every 6 to 12 months for 5 years and yearly thereafter.⁵ Presence of any detectable serum PSA provides as an exquisitely sensitive marker for recurrence and thus serves as a simple and robust follow-up test. Although, as stated above, the traditional definition of BCR is two consecutive serum PSA values >0.2 ng/mL, some have argued that an alternate criterion PSA value of 0.4 ng/mL with a subsequent rising level should be used. This alternative criterion may increase the specificity for *clinically relevant* recurrence as it has been shown to be more predictive of metastatic progression.^{3,6} Infrequently, the PSA level can remain persistently detectable postoperatively without ever reaching a zero nadir, which is typically due to residual noncancerous prostate tissue, subtotal carcinoma resection, or undetected distant metastasis

at the time of surgery. In this situation, imaging may be obtained, and if negative, PSA may then be followed more closely (every 3 to 6 months)⁵ than in patients achieving an undetectable PSA.

Although BCR is used as an early marker of primary treatment success, the natural history in patients with BCR is highly variable, ranging from an indolent nonprogressing pattern to rapid progression to end-stage disease. As such, it may be useful to additionally define the PSA doubling time (PSAdt) or PSA velocity (PSA_{vel}), which have additional implications for predicted rates of progression. A short PSAdt of <6 months and high PSA velocity > 0.5 ng/mL/month are associated with an increased risk of progression, distant metastasis, and PCa-related mortality.^{1,7} A relatively indolent disease course is often seen with a long PSAdt >6 months and low PSA_{vel}. Other predictors of an increased risk of progression, metastasis, and PCa-related mortality include a Gleason score >8 and early BCR occurring less than 24 months following primary treatment.¹

In general, patterns of PCa recurrence include (1) localized recurrent disease only; (2) distant metastatic disease only (typically nodal, less commonly osseous); and (3) a combination of these. Nomograms have been developed to predict the site of recurrence, which can be useful to guide decisions regarding imaging examinations performed and treatment selection. Overall, after RP, recurrent disease is most common in the prostate fossa (local recurrence), followed by pelvic and retroperitoneal lymph nodes, with skeletal metastases being much less common.^{8,9} Other distant sites of recurrence are even less common and include mediastinal and cervical lymph nodes as well as distant solid-organ metastases. A subset of patients with “oligometastatic” disease has recently been recognized, in part due to the use of specific PET imaging radiotracers such as C-11 choline, probably representing a state of lower progressive potential.¹⁰ Such patients were previously undiagnosed until developing more widespread end-stage disease. Both locally recurrent and distant metastases can be seen concurrently, most often in patients that are not imaged until their PSA is relatively high. Risk of progression to metastatic disease is higher when there is a short disease-free interval (<24 months), whereas local recurrence is more common with a late BCR.¹¹ Mild PSA elevations often represent local recurrence, while higher PSA values, short doubling times (<6 months), and high PSA velocities often represent distant metastasis.¹¹ Positive surgical margins increase the risk of both local recurrence and distant disease. Finally, patients with a Gleason score 8 to 10 or tumor stage pT3b (extraprostatic extension) or pTx pN1 at RP have an increased risk of systemic failure with distant metastasis and PCa-related mortality. In comparison, those with a Gleason score <7 or tumor stage pT3a (seminal vesical invasion) pN0 or pTx R1 (R1 = positive margin) more likely have a local recurrence.¹²

Traditionally, high-risk patients with recurrent disease (rapidly rising PSA, Gleason score 8 to 10, and early BCR—see above) are treated with nontargeted salvage radiation therapy (sRT), hormonal androgen deprivation therapy (ADT), systemic

chemotherapy, or a combination of these. These therapies may be considered blind treatment in that a specific site of recurrence has usually not been identified or, when it has, is not targeted specifically. This approach poses the potential for substantial treatment-related morbidity and may lack efficacy in halting the progression to advanced metastatic disease and PCa-related mortality. In particular, systemic ADT has demonstrated no proven mortality benefit in men with asymptomatic metastatic PCa¹⁰ despite a number of potential side effects, and the European Association of Urology guidelines suggest postponing palliative ADT due to the lack of a clear survival benefit.¹³ Additionally, salvage radiotherapy in patients with PSA > 2 ng/mL or with long PSA doubling times (> 6 months) had no proven benefit for PCa-specific survival when compared to active surveillance.¹⁴ Ureteral and urethral strictures, cystitis, urinary and rectal incontinence, and perineal pain are all common complications of nontargeted radiation therapy.^{15,16} In addition, systemic androgen deprivation therapy has lifestyle-limiting side effects and recently has been associated with severe cardiovascular risks.¹⁷ Given these considerations, surveillance may be deemed an appropriate alternative approach in select clinical settings.

As advanced imaging options improve and become more widely available, there is a movement towards targeted salvage treatment to specific sites of disease recurrence. Precise localization with imaging enables additional targeted treatment options that may achieve decreased patient morbidity in comparison with reliance on nontargeted systemic therapies. The current standard approach for salvage therapy following RP is nontargeted radiation to the pelvis. However this has reported failure rates as high as 42% in terms of providing adequate tumor control of local recurrences and is associated with many side effects as mentioned above.¹⁸ On the other hand, although technically challenging, salvage prostatectomy may be an option for treating local recurrence following primary radiation therapy.¹⁹ In addition, in patients with *oligometastatic disease*, which is a nonlocal recurrence identified at a single site, salvage surgical resection or image-guided ablation may be a viable option for curative intent, if not at least for delaying further progression.²⁰

Using the aforementioned nomograms, the most advantageous imaging modality can be chosen appropriately. Clinical symptoms such as bone pain also should be taken into consideration when imaging tests are ordered, (recognizing that bone metastases are very uncommon in patients that have a PSA under 10 ng/mL²¹). It is important to recognize that salvage treatment options are most efficacious when the tumor burden is the lowest, as is the case when the serum PSA first becomes detectable.¹⁴ Kitajima et al observed that 79 of 115 patients undergoing imaging at the time of BCR had only one site of recurrence, 70% of which were local, emphasizing the potential value of early imaging.⁹ When advanced imaging fails to identify the site of recurrence at low PSA values, other conventional nontargeted treatment options may be considered (versus serial PSA follow-up and later repeat imaging). Several of these salvage treatment options, including image-guided therapies, are discussed in 8.10 Image-Guided Focal Treatments.

There are multiple imaging modality choices for the evaluation of BCR. The chosen imaging modality should reflect the expected location of recurrence (local versus distant metastasis) based on the consideration of patient-specific factors described above (timing and rate of PSA recurrence as well as

symptoms). Nuclear medicine bone scintigraphy, computed tomography (CT), and fluorodeoxyglucose positron emission tomography—computed tomography (FDG PET/CT) have limited use for evaluation of new BCR. However, ¹¹C-choline PET/CT has shown great potential for evaluation of suspected distant metastatic disease, and pelvic MRI, potentially with targeted biopsy of any lesions in the prostate bed, may be useful for suspected local recurrence.

Magnetic resonance imaging is the primary imaging examination for evaluating the prostate bed in the setting of BCR, both for identifying local recurrence, and for enabling focal treatment options. Therefore MRI will be addressed in detail in the subsequent section. The remainder of this section describes alternative imaging modalities that may be complimentary to MRI, acknowledging key limitations of these options.

Transrectal ultrasound (TRUS) is of limited value in assessing the prostate bed for local recurrence, having a reported low sensitivity ranging from 25 to 54%.^{22,23} One study showed a higher sensitivity (80%) in patients with a higher PSA of over 2 ng/mL, although only moderate specificity (67%),²⁴ likely owing to overlap of imaging characteristics for normal postoperative changes, fibrotic tissue, and recurrent disease. Typically, local recurrence is characterized by a hypoechoic nodule, most likely near the vesicourethral anastomosis. However, in up to 30% of recurrences, the recurrent nodule may be isoechoic to the surrounding tissue, making lesion localization difficult (► Fig. 8.1). Transrectal ultrasound-guided biopsy is considered the gold standard for confirming local recurrence, although it has a low diagnostic yield especially at low PSA levels (< 1 ng/mL) and in the setting of small lesion size. Transrectal ultrasound-guided targeted biopsy of a suspected recurrent lesion in the prostatectomy bed that is initially detected using MRI achieves a greater diagnostic yield.²⁵

Computed tomography is widely available although it lacks sensitivity for evaluation of early BCR (► Fig. 8.2).^{21,22} In particular, CT has a minimal role in detecting local recurrence, only reliably identifying very large lesions measuring > 2 cm.²⁶ Computed tomography also has limited accuracy for diagnosing metastatic lymph nodes given its general reliance on nodal size, achieving a sensitivity of 27 to 75%, depending on the diagnostic criteria applied. For instance, if evaluating for metastatic lymph nodes based on a nodal diameter of over 1 cm, both poor sensitivity and specificity are achieved. Computed tomography is also suboptimal for skeletal metastases given low sensitivity for nonsclerotic lesions. In addition, CT is unreliable at assessing the response of sclerotic metastases to treatment given that such metastases often remain sclerotic despite adequate treatment response. Currently, the National Comprehensive Cancer Network guidelines suggest CT “may be considered” after RP when either the PSA fails to fall to an undetectable level (potentially representing undiagnosed presurgical metastatic disease) or, despite the above limitations, in the setting of BCR. Computed tomography may be most appropriate in the setting of advanced recurrent PCa, for instance, to monitor response of known metastatic lymphadenopathy or solid-organ metastases to androgen-deprivation therapy and/or chemotherapy (► Fig. 8.3).

Bone scintigraphy also has low positive predictive value and sensitivity, especially in patients with PSA < 10 ng/mL. While Kane et al suggested a threshold PSA value of 10 ng/mL before bone metastases may be detected on a bone scan,²¹ others have

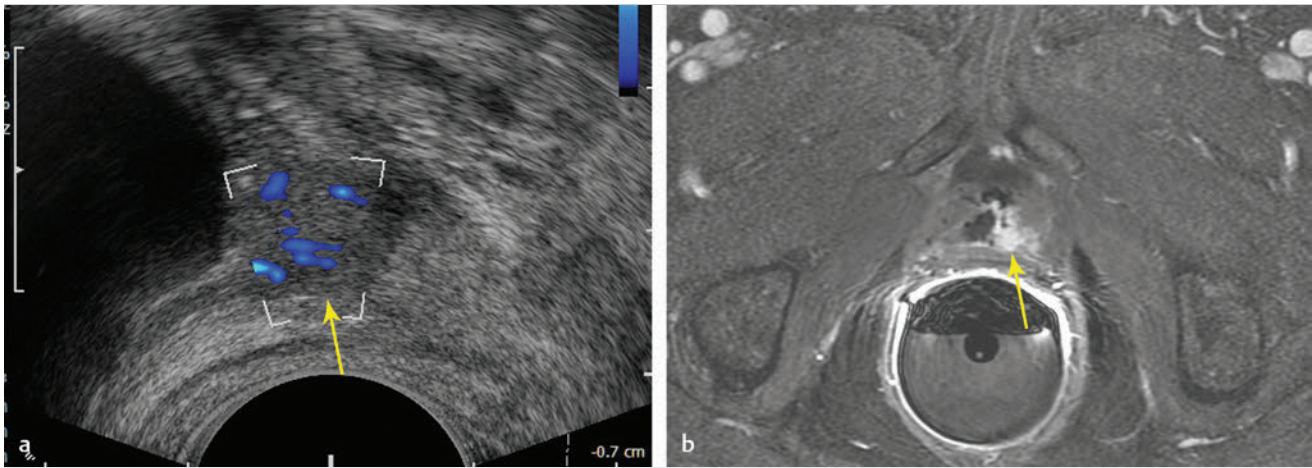


Fig. 8.1 Imaging of recurrent prostate carcinoma in a 70-year-old man with a history of robot-assisted prostatectomy and biochemical recurrence (prostate-specific antigen = 1.2 ng/mL). (a) Transrectal ultrasound with Doppler demonstrates a 1.2-cm rounded hypoechoic nodule with hypervascularity near the bladder neck (arrow). Transrectal ultrasound has low tissue and spatial resolution, making recurrence difficult to differentiate from normal postoperative changes. (b) At subsequent MRI, dynamic contrast-enhanced images confirm an abnormal focal hyperenhancing nodule (arrow), consistent with local recurrence along the left side of the vesicourethral anastomosis. The patient subsequently underwent salvage radiation resulting in an undetectable PSA.

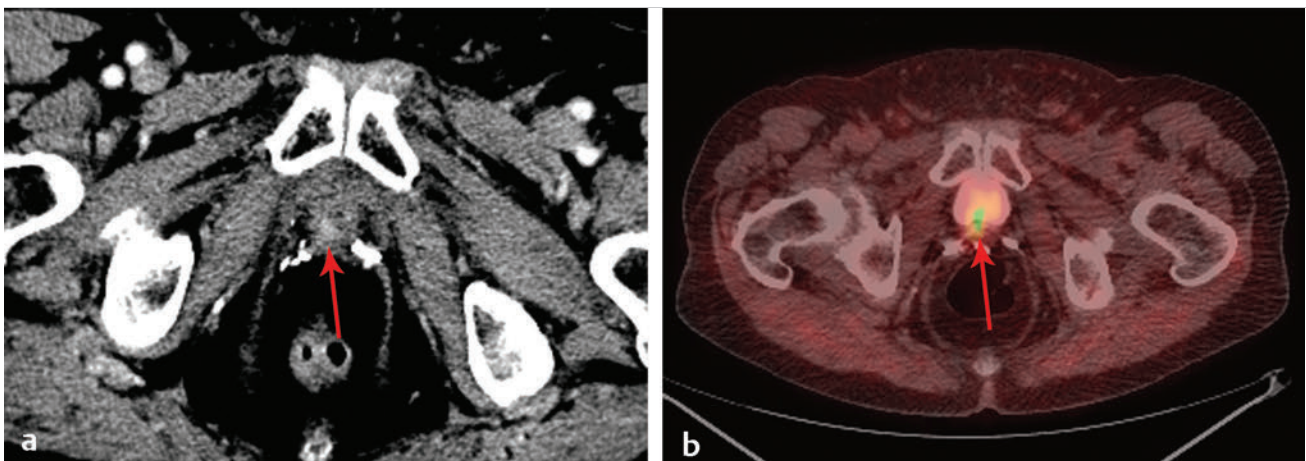


Fig. 8.2 An 86-year-old man with a history of Gleason score 3 + 4 stage pT3b, N0, M0 prostate cancer with a remote history of radical prostatectomy and salvage radiation therapy for a previous recurrence. His prostate-specific antigen has recently risen from an undetectable level to 2.0 ng/mL. (a) Contrast-enhanced CT images at narrow window settings shows a focus of enhancement at the right posterolateral vesicourethral anastomosis (arrow), considered highly suspicious for recurrence. No metastatic disease was identified. (b) Fused ¹¹C-choline PET/CT image confirms a choline-avid focus corresponding to the CT finding (arrow).

found that up to 34% of patients can have a positive bone scan with PSA values less than 10 ng/mL.¹¹ It should be noted, however, that average PSA values at the time of positive bone scans in these studies were 63 ng/mL and 123 ng/mL, respectively.^{11,21} For that reason American Urological Association (AUA) and NCCN guidelines suggest that the routine use of bone scintigraphy in the evaluation of BCR is not justified, but rather it should be reserved for follow-up of known skeletal metastases or in a patient with new bone pain and greatly elevated PSA (at least > 10 ng/mL).²⁷ While limited data suggests that ¹⁸F-NaF PET/CT may be able to detect otherwise occult osseous metastases including at lower PSA levels than typically diagnosed, the role of this examination in standardized diagnostic algorithms for BCR remains to be defined.²⁸

¹⁸F-FDG PET/CT is the mainstay of PET imaging for many other cancers, although it has limited value in evaluation of BCR likely owing to the low cellular proliferation and glucose metabolism of PCa cells. ¹⁸F-FDG PET/CT has particularly low sensitivity for evaluation of local recurrence in the prostate bed given urinary excretion and physiologic concentration of the radiotracer in the urinary bladder. Therefore, PET/CT is not recommended and has no significant clinical application in this setting (ACR appropriateness rating of 3).²⁹ ¹⁸F-NaF PET/CT has been shown to be more sensitive than a conventional bone scan in depicting osseous metastases in PCa.

¹¹C-choline is the only FDA approved PET/CT radiotracer for evaluation of BCR in the United States and has shown overall excellent performance in this application when considering

detection of both local and distant metastases using a single imaging examination. ^{11}C -choline has minimal background localization in the pelvis, thereby achieving very high specificity for PCa recurrence nearing 100%.⁹ Nonetheless, ^{11}C -choline PET/CT has limited spatial resolution, and urinary excretion may occasionally confound interpretation along the bladder neck. These factors diminish sensitivity for local recurrence. Thus, although potentially considered adequate for local recurrence, ^{11}C -choline PET/CT is inferior to MRI for this purpose. On the other hand, ^{11}C -choline shows the best performance among FDA-approved tests for detecting metastatic lymph nodes, including nodes as small as 5 mm, with an overall sensitivity of 83 to 100%⁹ (► Fig. 8.4). As expected, lesion detection improves with increasing PSA and with increasing primary tumor Gleason score.⁹ Also, given its whole body assessment, ^{11}C -choline

PET/CT can detect metastatic lesions above the pelvis, which are not routinely imaged using MRI. Some studies have shown an optimal threshold PSA level of 2 ng/mL for lesion detection. For example, Krause et al observed a diagnostic accuracy of 36% at PSA levels < 1 ng/mL, compared with 73% at PSA > 3 ng/mL.²² Also as previously mentioned, ^{11}C -choline PET/CT is helping to define a previously unrecognized population of patients with only a distant solitary focus of metastatic disease, termed oligometastatic. Logistically, use of ^{11}C -choline is limited by its short half-life (20.4 min), thus necessitating a local cyclotron for production of the radiotracer.

Radiographic bone surveys and Indium-111 capromab pentetide (ProstaScint) scans have very poor performance in the setting of BCR, and their use is generally not warranted, receiving ACR appropriateness ratings of 1 and 3, respectively.²⁹

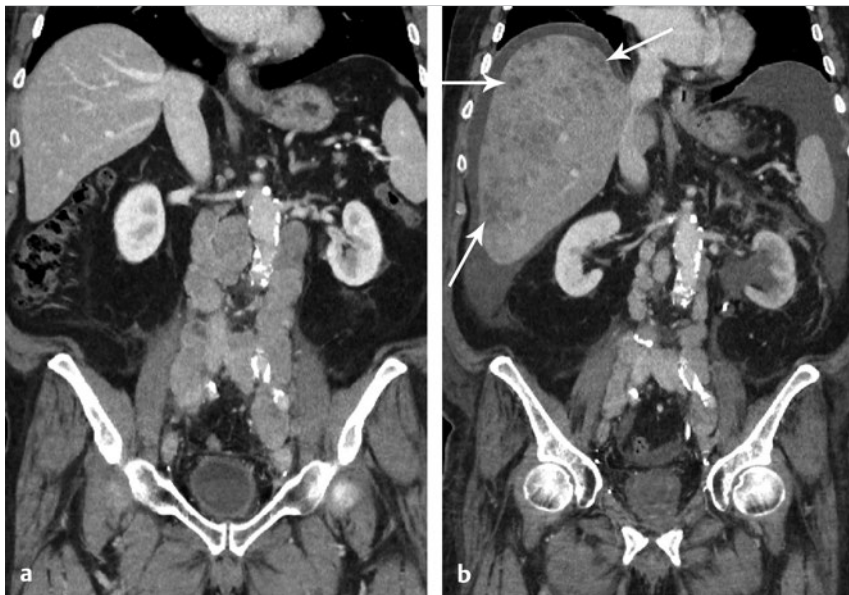


Fig. 8.3 A 78-year-old man who underwent radical prostatectomy 10 years previously, with subsequent salvage radiation for biochemical recurrence and more recent repeat relapse (prostate-specific antigen increasing rapidly to 42 ng/mL while on androgen-deprivation therapy). (a) Coronal CT image obtained at baseline prior to chemotherapy shows extensive metastatic retroperitoneal lymphadenopathy. (b) Coronal CT image obtained at follow-up shows partial response of the lymphadenopathy, although overall it shows progressive disease with extensive new hepatic metastases (arrows). Patient expired 1 week following the CT.

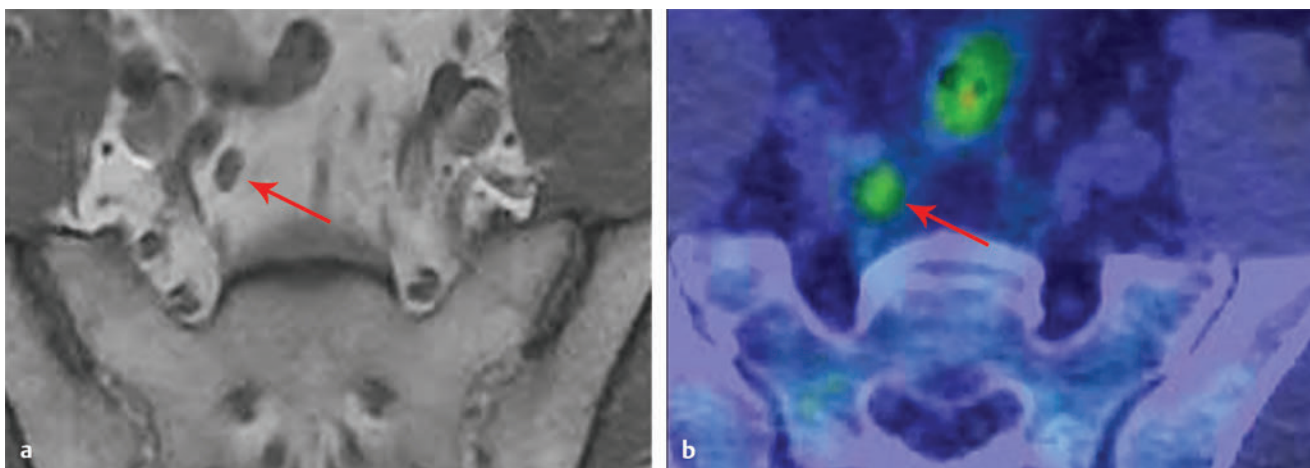


Fig. 8.4 Comparison of imaging modalities for pelvic lymph node recurrence. A 54-year-old man presented with a prostate-specific antigen level of 2.7 ng/mL 2.5 years after radical prostatectomy for prostate carcinoma with salvage external-beam radiation therapy to the surgical bed. (a) Axial T1-weighted MR image demonstrates a 0.5 cm x 0.7 cm lymph node in the right internal iliac chain (arrow), which was considered normal by size criteria. (b) ^{11}C -choline PET/CT image demonstrates corresponding significant choline avidity of this small node (arrow) with the maximum standardized uptake value of 3.8. This node was confirmed to be a metastasis by extended bilateral pelvic node dissection.

8.3 MRI for Evaluation of Biochemical Recurrence

The primary focus of this chapter is the imaging characteristics of recurrent PCa using MRI after failed primary treatment, including RP and radiation therapy. Multiparametric MRI (mpMRI) at 3 T using an endorectal coil may arguably be considered the gold standard for detection and delineation of local recurrence in the prostate fossa. MRI's role in detecting local recurrence is important given that most recurrences occur locally in the prostate bed, especially with lower PSA levels and a relatively late time to recurrence. For detecting local recurrences, MRI is superior to TRUS as well as to all other imaging modalities including ¹¹C-choline PET/CT, achieving a sensitivity of 83 to 95% (versus 45 to 75% for ¹¹C-choline PET/CT) at PSA levels greater than 0.6 ng/mL.²⁵ In addition to detecting recurrent lesions, MRI is able to define the postsurgical pelvic anatomy and the overall extent of a recurrent lesion, which are important factors for focal treatment planning.

MRI has shown overall similar performance for detecting pelvic osseous metastases as ¹¹C-choline PET/CT (sensitivity 87% vs. 81%, respectively).⁹ Nonetheless, MRI and ¹¹C-choline PET/CT could potentially play complimentary roles for this purpose, with each potentially detecting osseous metastases missed by the other test. The relative performance of the two examinations for osseous metastases may be influenced by treatment history, such as concurrent ADT or recent radiation therapy (RT).

The accuracy of MRI for nodal metastases (sensitivity 64%, accuracy 70%)⁹ is mildly improved compared with CT, although still largely limited by reliance on conventional size criteria. This limited accuracy in diagnosing nodal metastases remains a primary weakness of MRI in the setting of PCa recurrence.⁹ As previously noted, choline >PET/CT has shown significantly improved performance for evaluation of small lymph nodes (see ► Fig. 8.4). MR lymphography is a highly promising investigational technique with the potential for markedly improved performance in lymph node staging accuracy, including for very small nodes. Indeed, MR lymphography may outperform specific PET radiotracers due to improved spatial resolution.³⁰ While further investigation is required, the agent providing the best performance for MR lymphography in initial studies is not currently FDA approved for use in the United States.

In summary, MRI is the primary examination for evaluation of local tumor recurrence, and has reasonable performance for detecting osseous metastases (although these are relatively uncommon as an initial site of BCR). The main weakness of MRI is poor accuracy for lymph node metastases. ¹¹C-choline PET shows the best performance for lymph node staging among currently available FDA-approved imaging approaches, although its weakness is local recurrence evaluation. In combination, these two examinations offer excellent synergy in the work-up of BCR (► Table 8.1; ► Fig. 8.5). However, the most cost-effective sequence for performing these two examinations is yet to be determined.

Table 8.1 Complimentary performance characteristics of MRI and ¹¹C-choline PET/CT for initial evaluation of biochemical recurrence. Magnetic resonance imaging is superior for local recurrence detection, ¹¹C-choline PET/CT is superior for lymph node metastasis detection, and the performance of both is equivalent for bone metastases.

		Sensitivity	Specificity	Accuracy	AUC
		(95% CI)	(95% CI)	(95% CI)	(95% CI)
Local recurrence					
	MRI	88.5% ^a	84.6%	87.4% ^a	0.91 ^a
		(78.2%, 94.3%)	(66.5%, 93.8%)	(78.8%, 92.8%)	(0.85, 0.97)
	¹¹ C-choline PET/CT	54.1%	92.3%	65.5%	0.76
		(41.7%, 66.0%)	(75.9%, 97.9%)	(55.1%, 74.7%)	(0.67, 0.85)
Pelvic lymph node metastasis (n = 70)					
	MRI	64.0%	85.0%	70.0%	0.81
		(50.1%, 75.9%)	(64.0%, 94.8%)	(58.5%, 79.5%)	(0.71, 0.91)
	¹¹ C-choline PET/CT	90.0% ^a	100.0%	92.9% ^a	0.95 ^a
		(78.6%, 95.7%)	(83.9%, 100%)	(84.3%, 96.9%)	(0.91, 1.00)
Pelvic bone metastasis (n = 95)					
	MRI	87.5%	96.2%	94.7%	0.93
		(64.0%, 96.5%)	(89.4%, 98.7%)	(88.3%, 97.7%)	(0.84, 1.00)
	¹¹ C-choline PET/CT	81.3%	98.7%	95.8%	0.90
		(57.0%, 93.4%)	(93.2%, 99.8%)	(89.7%, 98.4%)	(0.80, 1.00)

Abbreviations: AUC, area under receiver operating characteristic curve; CI, confidence interval; n, number.

Source: Data from Kitajama et al 2015⁹.

^a A statistically significant difference between MRI and ¹¹C-choline PET/CT (p < 0.05).

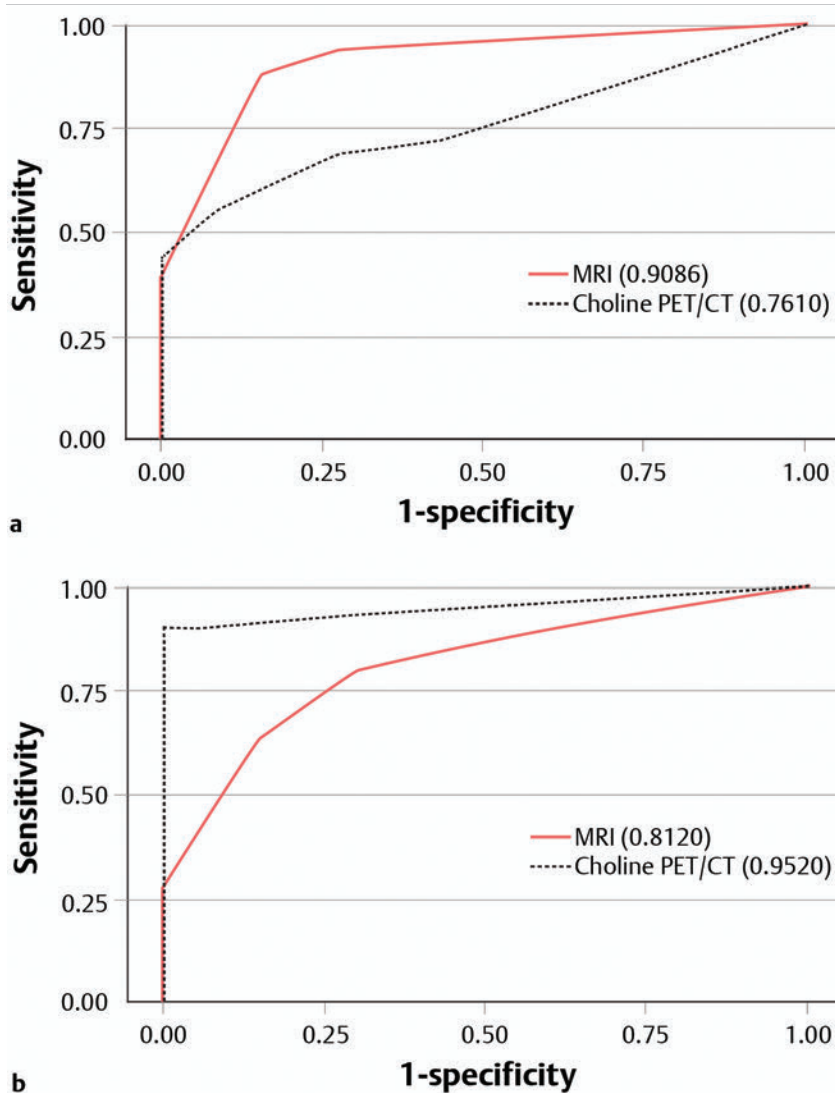


Fig. 8.5 Receiver operating characteristic (ROC) curves for MRI (solid red line) and ^{11}C -choline PET/CT (dashed black line) in (a) evaluation for local recurrence (area under curve [AUC] of 0.91 for MRI and 0.76 for PET/CT [$p < 0.05$]) and in (b) evaluation for pelvic lymph node metastases (AUC of 0.81 for MRI and 0.95 for PET/CT [$p < 0.05$]).

8.4 Post-Radical Prostatectomy Anatomy

Understanding the postoperative appearance of the pelvis is critical for the evaluation of BCR. Following RP, the bladder base descends inferiorly and the levator ani muscle complex shifts anteriorly and inferiorly, partially occupying the prostatectomy bed, while the bladder takes on an inverted pear shape. These findings are best visualized in the coronal and sagittal imaging planes (► Fig. 8.6). The location of the urogenital diaphragm is typically unaffected. In the absence of recurrent disease, the prostatectomy bed typically contains only fat, minimal scar tissue, and vasculature. There may be linear low T1 and T2 signal in the anterior rectal wall related to postoperative fibrosis as well as linear fibrosis of Denonvilliers' (rectoprostatic) fascia. A small-to-moderate amount of non-masslike low signal may occur at the site of the anastomosis of the urethra and bladder (vesicourethral anastomosis) due to normal postsurgical fibrosis. This finding is typically most prominent along the anterior aspect of the anastomosis and may result in indentation of the

bladder wall.³¹ Partial dehiscence of the vesicourethral anastomosis may be clinically inapparent and appears as a focal irregularly widened space or a focal outpouching (or pseudodiverticulum) between the bladder neck and membranous urethra, which in the chronic setting is very rarely of any clinical consequence.

The residual vas deferens terminate at the cranial aspect of the seminal vesicle resection (or vesiculectomy) beds, typically visualized as a linear or tubular low-to-intermediate signal structures on both T1- and T2-weighted imaging that follow the expected anatomical course.³² No residual seminal vesicle tissue should be present, with surgical clips and minimal scarring present in the seminal vesicle beds. In patients with persistently detectable PSA following RP, residual seminal vesicle tissue may occasionally be identified as the source. In these patients, the PSA level is typically low and relatively stable over time (► Fig. 8.7).

Rarely, portions of the prostate gland itself may unintentionally be retained (► Fig. 8.8). In our experience, this usually occurs following robot-assisted rather than open prostatectomy. The remaining gland may be entirely benign or still contain large areas of unresected tumor. Given that the typical

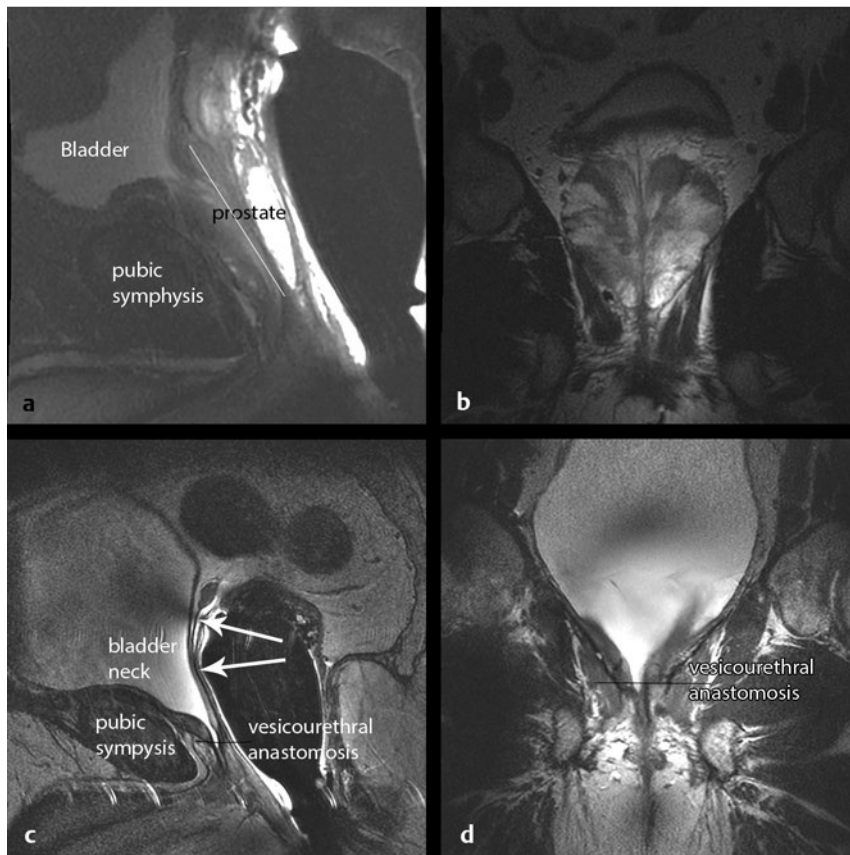


Fig. 8.6 (a) Sagittal and (b) coronal T2-weighted MRI of the prostate in a patient with biopsy-proven prostate carcinoma. (c) Sagittal and (d) coronal T2-weighted images of the pelvis in the same patient following radical prostatectomy, showing alterations in the anatomy. The bladder neck becomes elongated and tapered with the vesicourethral anastomosis near the level of the low pubic symphysis (noted on d). There is a fine linear scar typically visualized along the resection plane (c, arrows), with a small amount of scarring in the seminal vesicle beds at the superior aspect. The anus and rectum are shifted more anteriorly. (An endorectal coil is in place at both time points.)

management for persistently detectable PSA after RP is salvage radiation and/or systemic therapy, recognizing the presence of retained prostate tissue as a source of persistently detectable PSA is vital to directing these patients to appropriate management.

Metallic clips and a suture line in the operative bed may result in susceptibility artifact. Such artifacts can severely degrade the image quality and limit evaluation depending on the number, size, composition, and location of the clips. Metallic susceptibility artifact from a large number of clips is more pronounced on diffusion-weighted images (DWI) and on fat-suppressed T1-weighted spoiled gradient-echo dynamic contrast-enhanced (DCE) images than on fast spin-echo T2-weighted images. Fortunately, the surgical materials most commonly used in recent years cause relatively mild artifact that does not greatly hinder evaluation. When metallic susceptibility artifact is significant (e.g., in patients with a hip prosthesis), further targeted protocol optimization is necessary, including for instance, increasing the receiving bandwidth and not using frequency-selective fat saturation.

In cases without recurrent tumor, there is usually no early post-gadolinium enhancement of the anastomosis or the prostatic bed, and there is typically no enhancement or only minimal homogenous enhancement during later phases. It is critical to recognize the appearance of focal vascular enhancement near the surgical bed, which can often be asymmetric and mimic the focal early enhancement that is characteristic of early tumor. Such vascular enhancement is a common cause of a false-positive diagnosis of local recurrence (► Fig. 8.9).

8.5 Local Tumor Recurrence after Radical Prostatectomy

The most common site of local tumor recurrence following RP is around the vesicourethral anastomosis (► Fig. 8.12), most frequently around the posterior and lateral aspects of the vesicourethral anastomosis and less commonly along the anterior margin. Other common sites of local recurrence include the bladder neck (► Fig. 8.11) along the posterior bladder wall and in the seminal vesicle bed (► Fig. 8.10). Less common sites of recurrence include the perivesical tissues bilaterally, the pre-vesical space, inside the bladder wall, and the periureteral space, the presacral space, and the anterior rectal wall.

8.6 MRI Technique for Evaluation of Biochemical Recurrence

With increasing availability of 3-T MR scanners, the preferred imaging modality for evaluation of prostate cancer has become multiparametric MRI (mpMRI). At our institution, 3-T prostate MRI is routinely performed with integration of an anterior 8-channel phased-array surface coil and an endorectal coil to increase signal-to-noise ratio (SNR). If the patient cannot tolerate an endorectal coil, 3-T MRI is performed using only the surface coil. At our institution 1.5-T MRI using an integrated pelvic surface coil and an endorectal coil is reserved for patients who have a contraindication to 3-T MRI, such as an implantable device that has been documented to be MRI conditional at 1.5 T but not at 3 T.

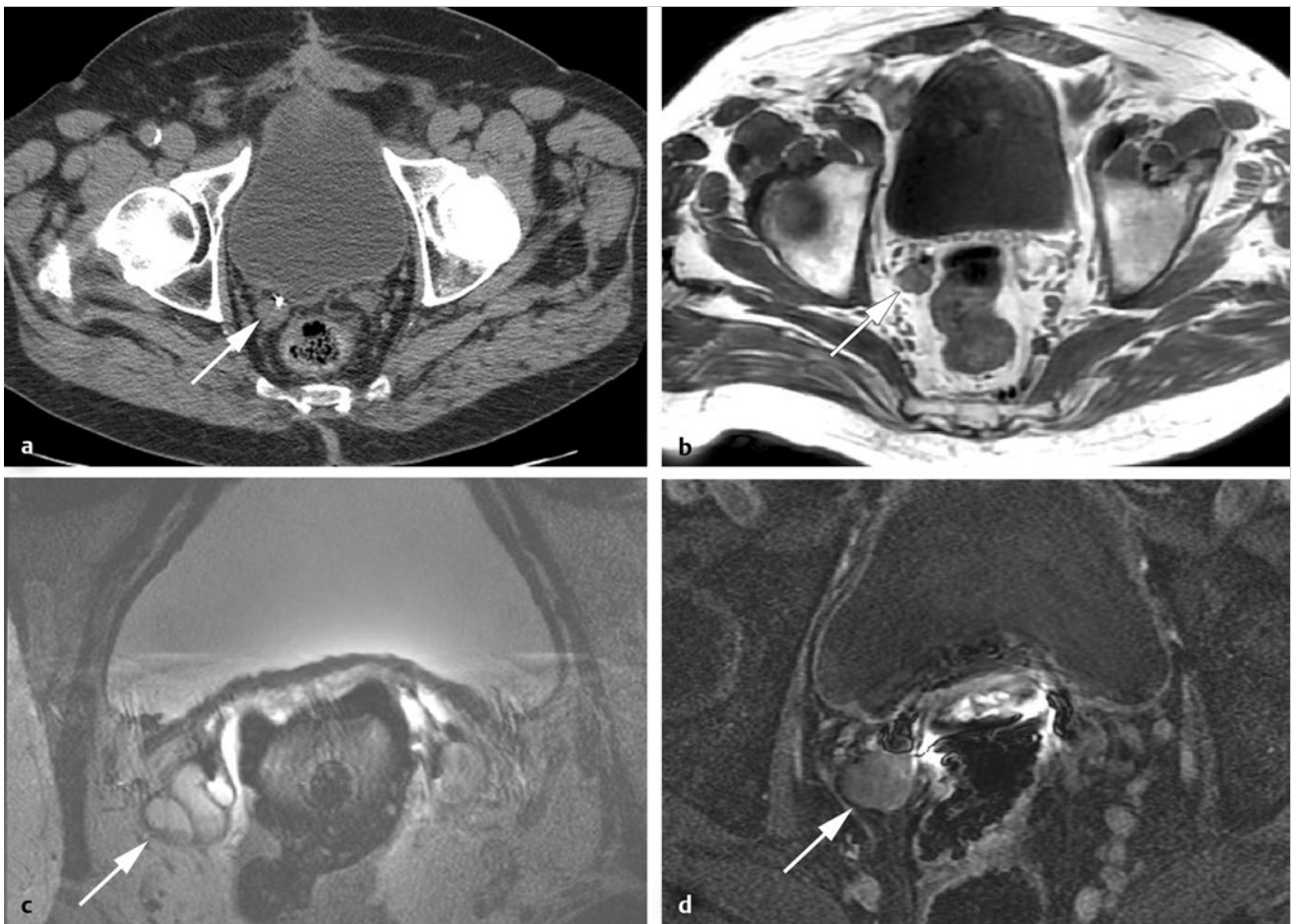


Fig. 8.7 A 77-year-old male who had a low, but detectable, and slowly rising prostate-specific antigen level following radical prostatectomy. (a) A computed tomogram performed at an outside institution was considered suspicious for recurrence due to a perceived “nodule” in the right pelvis. (b) Axial T1- and (c) T2-weighted images demonstrate a tubular fluid-filled structure lateral to the rectum, leading up to surgical clips (*arrows*). (d) DCE image demonstrates no suspicious internal enhancement to suggest tumor. The finding represents a benign seminal vesicle remnant (*arrow*). Note the surgical clip across the anteromedial aspect of the seminal vesicle remnant, with the remaining obstructed remnant distal to the clip. Artifact was minimal on T2-weighted and T1-weighted imaging, although it was more severe on diffusion-weighted imaging (not shown).

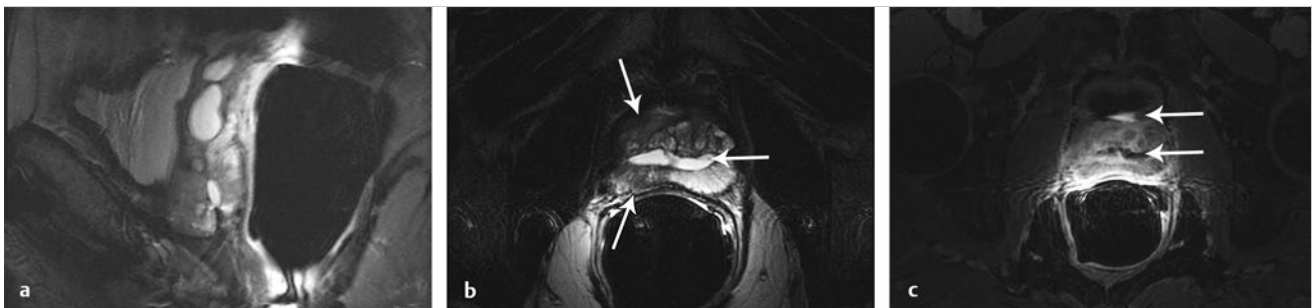


Fig. 8.8 Incomplete prostatectomy (unintentional) with a large amount of residual prostate gland and seminal vesicles. (a) Sagittal and (b) axial T2-weighted images demonstrate a large volume of unresected prostate, with an area of abnormal hypointense T2 signal in the residual right side of the gland that also demonstrates early hyperenhancement on the postcontrast image (c). Subsequent salvage radical prostatectomy confirmed the presence of residual tumor in the residual gland. Note on the sagittal image that the bladder neck and vesicourethral anastomosis are abnormally displaced anterior to the gland, an indication of an unsuccessful attempted prostatectomy. The bladder neck, which contains a small amount of excreted contrast in urine, is displaced anterior to the gland (c, *arrow*). A central cystic defect in the gland represents a disconnected urethra following transurethral resection of the prostate (*arrow* in b and c).

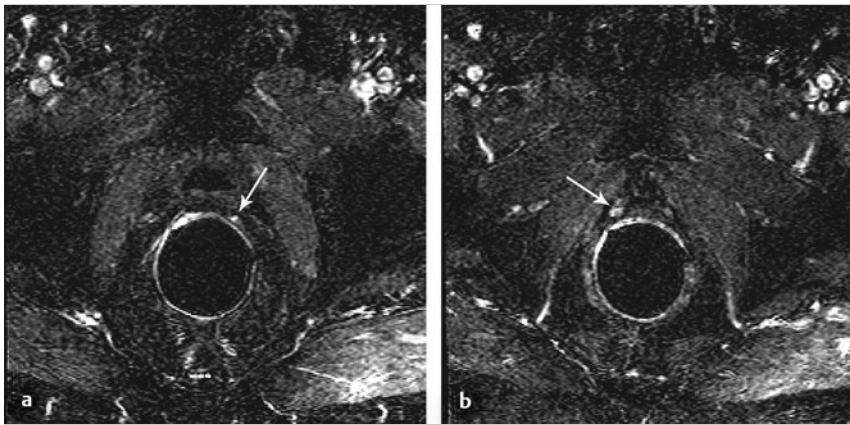


Fig. 8.9 Subtracted early-phase dynamic-contrast enhanced images (6 s/phase) demonstrate small foci of enhancement anterior to the rectum on the left (a, arrow) and posterolateral to the vesicourethral anastomosis on the right (b, arrow) that are potential tumor mimics due to benign vasculature. ▶ Fig. 8.19 also shows examples of benign enhancing vasculature along the margins of the vesicourethral anastomosis that are potential pitfalls.

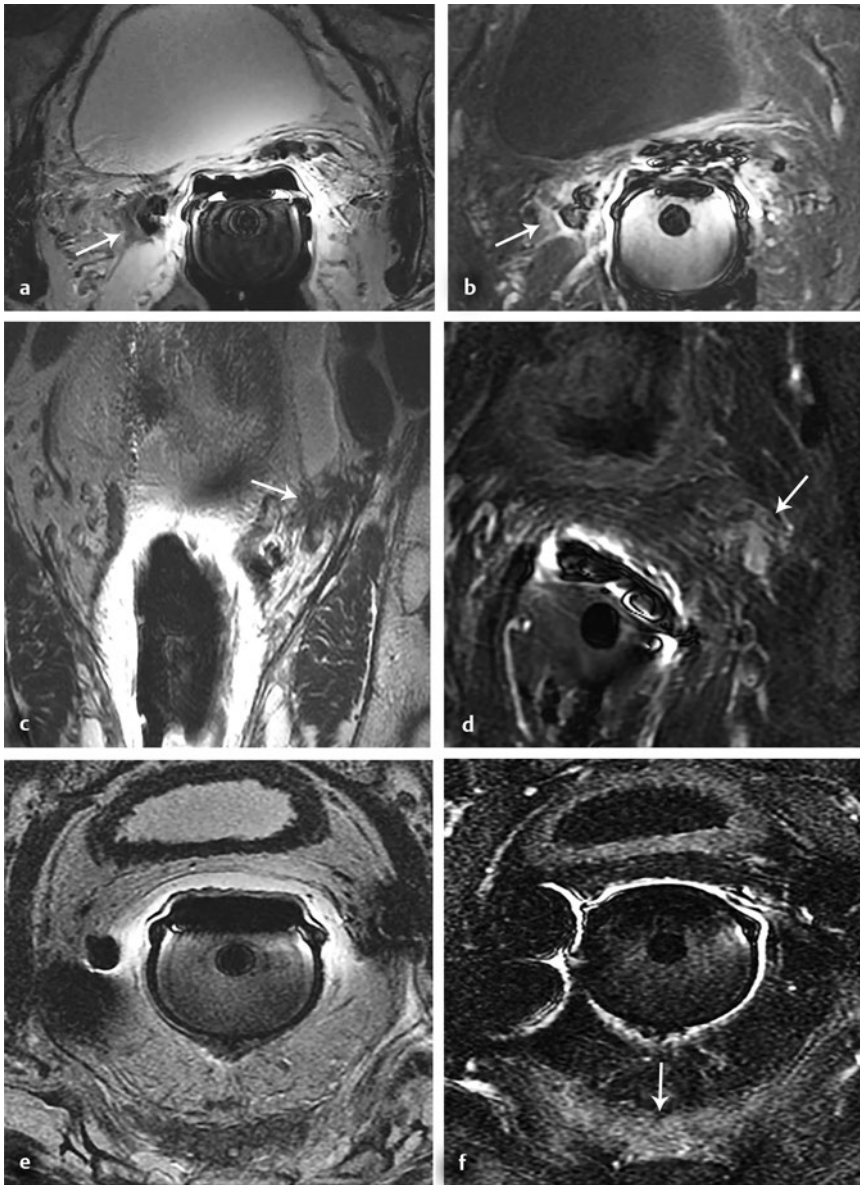


Fig. 8.10 Panel of T2-weighted (T2W) and dynamic contrast-enhanced (DCE) images of sites of locoregional recurrence in different patients. These include: (a) T2W and (b) DCE images of recurrence in the right seminal vesicle bed, appearing as decreased T2 signal and focal increased enhancement (arrow) adjacent to the clips; (c) coronal T2W and (d) axial DCE images of left periureteral recurrence (arrows); (e) axial T2W and (f) axial DCE images of sheet-like pre-sacral recurrence (arrow) (continued on top of p. 103)

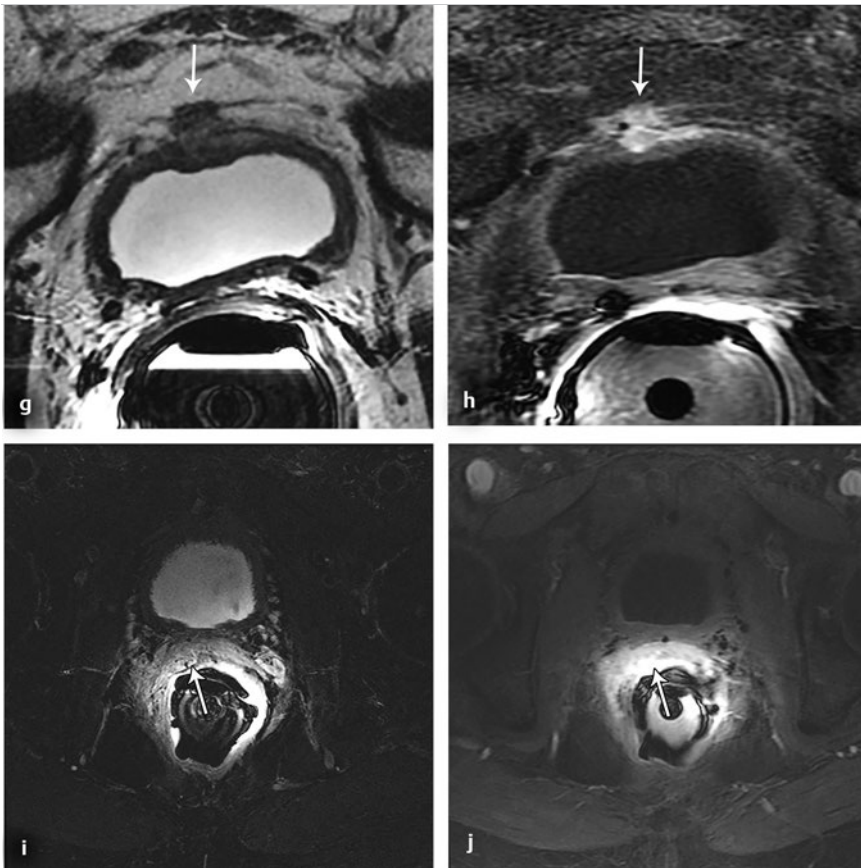


Fig. 8.10 (continued) (g) axial T2W and (h) axial DCE images of prevesical recurrence (arrows); (i) axial fat-saturated T2W and (j) axial DCE images of infiltrative recurrence in the anterior rectal wall (arrows). See ▶ Fig. 8.11 and ▶ Fig. 8.12 for additional demonstrations of common sites of recurrence.

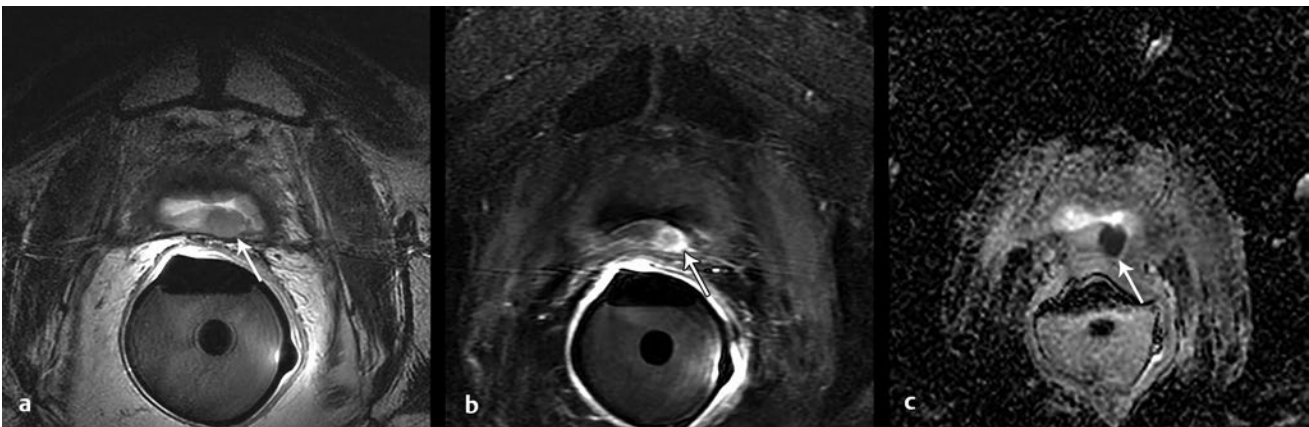


Fig. 8.11 Three axial MR images following radical prostatectomy demonstrate a well-defined local tumor recurrence in the posterior bladder neck to the left of midline (arrows) just above the vesicourethral anastomosis. The lesion is hypointense to muscle and scar tissue on the T2-weighted image (a) and hypointense relative to the adjacent heaped urothelium and shows intense arterial enhancement (b) and low apparent diffusion coefficient (ADC) on the ADC map (c).

As in assessment for primary disease, mpMRI of the prostate in the setting of BCR comprises multiplanar T2-weighted imaging (T2WI), axial diffusion-weighted imaging (DWI) (including b values in the range of 1400–2000 s/mm²), and axial three-dimensional (3D) T1-weighted DCE imaging. High-resolution mpMRI should cover the prostate and seminal vesicle beds. In patients with persistent or rising PSA after failed primary therapy, additional combinations of axial T1WI, DWI, T2WI, and

post-gadolinium fast spoiled gradient-echo MRI of the whole pelvis are helpful to assess pelvic lymph nodes and bones. ▶ Table 8.2 provides a suggested protocol for BCR evaluation, which at our institution differs from the protocols used in the primary preoperative setting.

Several studies show a limited value of T2WI alone for detection of local recurrence following RP.^{33,34,35,36} For example, Roy et al reported a sensitivity of 55% using T2WI alone for

Table 8.2 3-T MRI sequences and parameters with or without the use of an endorectal coil.

Sequence	Anatomical coverage	TR (ms)	TE (ms)	Slice thickness/gap (mm)	Field of view (cm)	Matrix	Additional information	
3.0 T with integration of pelvic phased-array and endorectal coils								
T1WI axial	Whole pelvis	< 500	9	6/1	36	416/192		
DWI axial (optional)	Whole pelvis	4000	65	7/1	36	200/192	b value of 600 ms/mm ²	
T2WI axial (optional)	Whole pelvis	4000	85	6/1	36	320/320		
T2WI axial	High resolution ^a	4500	105	2.5/0.5	18	416/224		
T2WI sagittal	High resolution ^a	7500	105	2.5/0.3	18	416/224		
T2WI coronal	High resolution ^a	4400	105	2.5/0.5	18	416/224		
DWI axial	High resolution ^a	≥ 3000	82	≤ 4/no gap	22	200/192	High b values of 1,400–2,000 ms/mm ²	
DCE axial	High resolution ^a						1. IV bolus injection of gadolinium-based MR contrast agent (0.1 mmol/kg) at 3 mL/s 2. Total observation after contrast administration ≥ 2 min	
	High-temporal-resolution approach	Prostate and seminal vesicles		MF	3/0	22	256/192	Temporal resolution at 6.5 s/phase
	High-spatial-resolution approach	Prostatectomy and seminal vesicectomy bed	5.2	MF	2.6/-1.3	14–18	256/192	1. Temporal resolution at 15–30 s/phase 2. Chemical shift with fat saturation or subtraction
Post-Gd 3D fast SPGR	Pelvis		MF	4/0	36	256/224		
3.0 T with pelvic phased-array coil only								
T1WI axial	Whole pelvis	< 500	MF	6/1	36	416/192		
DWI axial (option)	Whole pelvis	3100	65	7/1	36	200/192	b value of 600 s/mm ²	
T2WI axial (optional)	Whole pelvis	4000	85	6/1	36	320/320		
T2WI axial	High resolution ^a	6000	125	3/0	22	320/320		
T2WI sagittal	High resolution ^a	4000	125	3/1	22	288/224		
T2WI coronal	High resolution ^a	6000	125	3/0.3	22	320/320		
DWI axial	High resolution ^a	4000	85	3/0	30	128/160	High b values of 1,400–2,000 s/mm ²	
DCE 3D fast SPGR	High resolution ^a						1. IV bolus injection of gadolinium-based MR contrast agent at 3 mL/s 2. Total observation after contrast administration ≥ 2 min	
	High-temporal-resolution approach	Prostate and seminal vesicles	4.8	2.4	3/-1.5	22	256/192	Temporal resolution at 6.5 s/phase

Table 8.2 continued

Sequence		Anatomical coverage	TR (ms)	TE (ms)	Slice thickness/gap (mm)	Field of view (cm)	Matrix	Additional information
	High-spatial-resolution approach	Prostatectomy and seminal vesiculectomy bed	5.2	3	3/-1.5	14-18		1. Temporal resolution at 15-30 s/phase 2. Chemical shift with fat saturation or subtraction
Post-Gd 3D fast SPGR		Whole pelvis	5.2	2	4/0	36	256/224	

Abbreviations: T1WI, T1-weighted imaging; T2WI, T2-weighted imaging; DWI, diffusion-weighted imaging; DCE, dynamic contrast-enhanced imaging; 3D fast SPGR, 3-dimensional fast spoiled gradient-echo.

Source: Adapted from American College of Radiology (ACR) Prostate Imaging-Recording and Data System, version 2, (available at www.acr.org) and authors' institutional protocols.

^a High-resolution imaging should cover the prostate and seminal vesicles or the prostatectomy and seminal vesiculectomy bed after surgery.

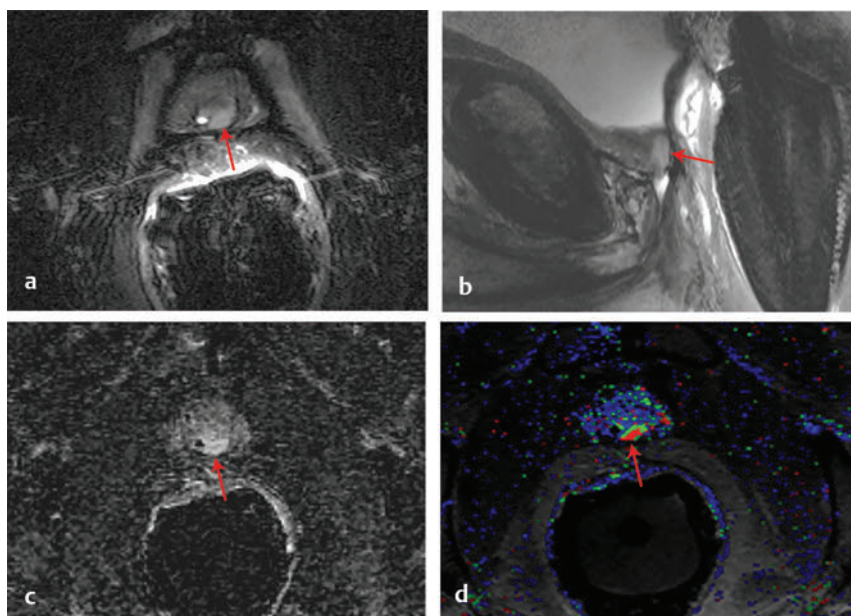


Fig. 8.12 Tiny local recurrence of prostate cancer at the vesicourethral anastomosis (arrows). (a) Sagittal and (b) axial fat-saturated T2-weighted images demonstrate a small mildly T2 hyperintense lesion along the posterior left side of the vesicourethral anastomosis. This demonstrates arterial hyperenhancement on an early subtraction image (c) and markedly abnormal washout kinetics with high conspicuity on a colorized parametric perfusion map (d) despite its tiny size. This lesion was not identifiable by diffusion-weighted imaging or the apparent diffusion coefficient map (not shown).

detection of recurrent tumors.³⁶ However, despite limited sensitivity for tumor detection, T2WI provides critical anatomical detail that supports findings on DWI and DCE-MRI, in localizing recurrences and identifying their relationship to neighboring structures and in identifying any residual benign prostate or seminal vesical tissue that may account for the patient's elevated PSA. A recurrent tumor usually appears as a mildly T2-hyperintense area relative to the surgical scar in the prostatectomy bed or in the muscle of the bladder neck and/or wall (although hypointense relative to the urothelium) (► Fig. 8.11a; ► Fig. 8.12a; ► Fig. 8.12b). In addition, recurrent tumors may appear as asymmetric nodular thickening of the peri-anastomotic soft tissue or loss of the integrity of the retro-anastomotic fat plane. Small recurrent tumors tend to demonstrate less intense T2 signal (relative to skeletal muscle) compared to large masses, in some instances due to partial volume averaging, and consequently they may be very difficult to differentiate from fibrous scar tissue in the prostate fossa using T2WI. Use of fat saturation may increase conspicuity of local recurrences on T2WI (► Fig. 8.12 a).

Early postcontrast MRI images are by far the most useful sequence for local recurrence evaluation. Roy et al published a

sensitivity of 100% for DCE-MRI alone in detection of recurrent disease following RP.²⁶ Recurrent lesions usually demonstrate heterogeneous arterial hyperenhancement that is greater and occurs earlier compared to benign fibrous tissue or any residual prostate tissue. Tumor recurrences may inconsistently show washout kinetics, which is a less important and less reliable feature for diagnosis. Subtraction of DCE T1-weighted SPGR images obtained without fat saturation may be helpful in determining the presence of enhancement in challenging cases. The optimal acquisition parameters for DCE-MRI in detecting recurrence are unclear given the trade-off between spatial and temporal resolution. In our experience, following RP, high-spatial-resolution DCE-MRI, albeit with slower temporal resolution, may increase sensitivity for detecting tiny early recurrences and can provide detailed anatomical information in localizing recurrent viable tumor in the surgical bed, which is invaluable for salvage focal ablative therapy planning (► Fig. 8.11). However, high-temporal-resolution DCE-MRI is typically preferred in detecting locally recurrent or residual viable tumor within a treated but intact prostate gland.¹⁸ The color maps depicting computed perfusion parameters that can be derived from pharmacokinetic analysis

may also increase conspicuity of local recurrences for some readers (► Fig. 8.12).

Diffusion-weighted imaging, including the apparent diffusion coefficient (ADC) map, has a complementary role in detecting locally recurrent tumor. Recurrent tumors following RP demonstrate focal increased DWI signal with a corresponding hypointense lesion on the ADC map (► Fig. 8.11c). The ability of DWI to detect recurrent PCa following RP is superior to T2WI, although DWI has technical limitations and is less sensitive than DCE-MRI alone.³⁶ For instance, DWI is not sensitive in detecting small (< 1 cm) lesions in the prostatectomy bed because of susceptibility artifact from metallic surgical clips, gas in the rectum, and the endorectal coil (Kitajima, *American Journal of Roentgenology*, 2016, in press). For example, ► Fig. 8.12 shows a small recurrence identified by DCE-MRI that is also visible on T2WI, although not identified on DWI/ADC. DWI is most useful after RP when findings are integrated with those from DCE-MRI and T2WI. It is possible that the detectability of small local recurrences after RP using DWI may be improved through use of a newer reduced field-of-view single-shot echo-planar imaging technique, but this is not yet proven.

One common pitfall for false-positive identification of local recurrence by MRI includes normal physiologic contrast enhancement along the midline anterior aspect of the proximal membranous urethra, immediately inferior to the level of the vesicourethral anastomosis at the urogenital diaphragm. Periurethral enhancement occurs normally, as it can be seen similarly in patients with no prior surgery. This finding usually has a morphology that can be confidently recognized as benign by experienced radiologists.³⁷ An additional previously mentioned common pitfall is residual periprostatic vasculature that may remain after RP and can mimic recurrence (► Fig. 8.9). Typically, these vessels appear as linear enhancing structures but that can be difficult to appreciate in the axial plane. The lack of any focal nodule on T2WI as well as the lack of any corresponding abnormality on DWI or the ADC map should increase the confidence that focal enhancement in the fat adjacent to the anastomosis is benign.

8.7 Post-Radiation Therapy

In patients who have undergone primary treatment with external-beam radiation therapy (RT), the prostate gland becomes

atrophic and has a diffusely changed internal makeup, with glandular tissue replaced by fibrotic and/or stromal tissue. Recurrences in this setting are usually intraprostatic, located most often in the peripheral zone (PZ), similar to the pretreatment population. The treated gland has a diffusely altered appearance (► Fig. 8.13). The PZ, which should normally be T2 hyperintense, shows diffuse intermediate T2 signal intensity, and the zonal anatomical distinctions often become obscured. A low-signal-intensity rim around the gland is frequently observed, and the capsule boundaries often become indistinct, making the evaluation of minimal T3 disease even more difficult. Thus, using T2WI, the tissue contrast between recurrent cancer and benign irradiated tissue is significantly decreased. Accordingly, T2WI demonstrates poor diagnostic performance in predicting recurrent cancer in patients with biochemical recurrence after radiation therapy.³⁸ For the prediction of locally recurrent cancer after radiation therapy (RT), both DCE-MRI alone as well as combined DCE-MRI and DWI have much greater sensitivity, specificity, and accuracy than T2WI alone.³⁶

Similar to post-RP, DCE-MRI is the most reliable sequence in depicting recurrence following radiation therapy (RT), with a reported sensitivity of 96%.³⁶ Acute or chronic inflammation may also occur as a result of the treatment, manifesting as a DCE-MRI appearance suggesting prostatitis (i.e., patchy or diffuse, nonfocal enhancement). The optimal DCE-MRI acquisition strategy (in terms of the trade-off between maximum spatial and temporal resolution) is again not clearly established in this setting and has varied in the literature. At our institution, we typically use a high-temporal-resolution DCE-MRI sequence (5–7 s/phase) and pharmacokinetic modelling analysis in this setting, as opposed to the lower-temporal-resolution and higher-spatial-resolution DCE-MRI sequence we use in patients with a low PSA after RP. Our rationale is that in an irradiated gland, the frequently present background fibrosis and inflammation may be easier to differentiate from recurrent intraprostatic tumor when considering enhancement kinetics as best appreciated from high-temporal-resolution DCE-MRI. (► Fig. 8.14).

Unlike in the post-RP setting, DWI and the ADC map have greater utility after radiation therapy (RT). One study suggests that the utility of DWI after RT approaches that of DCE-MRI.³⁶ This observation is likely at least partially explained by the limitation of DWI following RP due to artifacts from surgical clips. In comparison, far less susceptibility artifact is encountered following primary RT. After RT, three to four intraprostatic

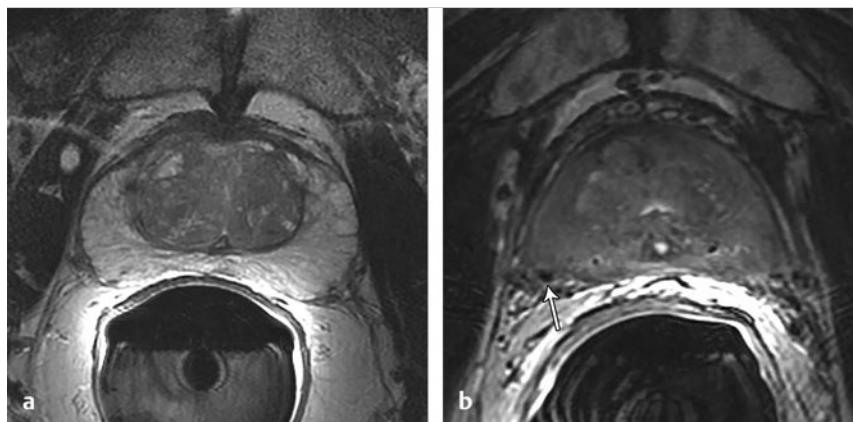


Fig. 8.13 (a) Axial T2-weighted image (T2WI) demonstrates the normal appearance of a benign, untreated prostate gland. In comparison, (b) axial T2WI of the prostate after radiation therapy shows a diffusely heterogeneous, decreased T2-signal gland with distortion of the normal zonal anatomy. Radiation targeting markers typically create very little imaging artifact (arrow).

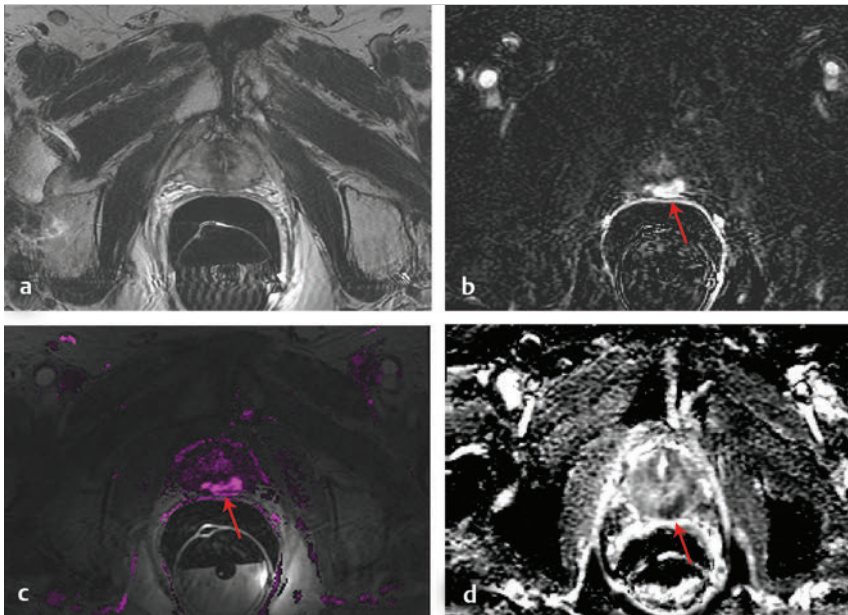


Fig. 8.14 An 85-year-old man treated with primary radiation therapy for Gleason score 4 + 4 tumor 10 years previously. His prostate-specific antigen level has recently increased to 3.4 ng/mL. (a) T2-weighted image does not clearly delineate a lesion. (b) Axial early postcontrast dynamic contrast-enhanced image and (c) K^{trans} overlay color map show a discrete focus of early arterial enhancement in the left posterior peripheral zone (arrow) consistent with recurrent viable tumor. (d) The apparent diffusion coefficient map shows corresponding low signal (arrow).

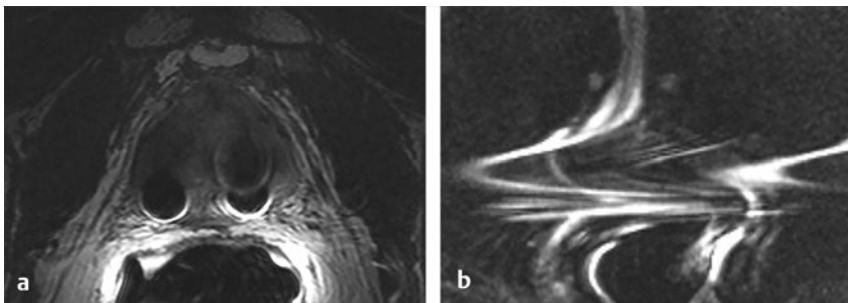


Fig. 8.15 (a) Axial T2-weighted image and (b) diffusion-weighted image show significant artifact from large radiation therapy targeting markers. These were placed over 10 years ago and create much more severe artifact than typical of the inert gold markers that are now commonly used (see ▶ Fig. 8.13 and ▶ Fig. 8.14 for example).

radiation therapy–targeting fiducial markers are often present. These typically comprise MRI-inert gold and usually create very little MRI artifact. However, occasionally these may be large, in which case greater artifact results (▶ Fig. 8.15). Recurrent cancer following RT typically demonstrates increased signal intensity on high b-value DWI with corresponding focal low signal on the ADC map, (▶ Fig. 8.14 d), which is likely related to the relative hypercellularity of the recurrence compared with that of the surrounding benign irradiated prostate tissue. Of note, the association between ADC values and Gleason score that has been established for the primary untreated prostate gland does not hold up in the post-treatment prostate. ADC values may be higher than would be expected for a given Gleason score when compared to those for an untreated prostate³⁹ and thresholds that practices may have defined for determining “significant” cancer in untreated PCa may not necessarily hold true following RT. This distinction is critical to recognize, given that any focus in the peripheral zone showing relative diffusion restriction with associated hyperenhancement should be considered highly suspicious for cancer following RT, irrespective of whether the quantitative ADC value falls below a threshold that may be used in other clinical settings. Likewise, tumors in an irradiated prostate are often not gradable by pathologists using the Gleason system due to post-treatment changes. This alteration of the tumor histology observed may contribute to the variance in ADC values in this setting as well.

8.8 Post-Interstitial Brachytherapy of the Prostate

Similar changes occur to the prostate following interstitial brachytherapy as following external-beam radiation therapy (e.g., atrophy, alterations in T2WI signal intensity of the peripheral zone, and distortion of zonal anatomy). However, following brachytherapy, numerous radioactive seed implants are also observed. These metallic seeds have minor image consequences on T2WI and DCE-MRI, although they may significantly degrade DWI (▶ Fig. 8.16). DCE-MRI is again the most important sequence in detecting local recurrent tumor, with T2WI playing an important complimentary role by assisting in anatomical delineation. In our experience, residual or recurrent tumor after brachytherapy is most often observed adjacent to the intraprostatic urethra, possibly relating to undertreatment in this region, or in the seminal vesicles, which are not directly treated by brachytherapy and may harbor occult tumor extension.

8.9 Salvage Pelvic Radiation Therapy

Salvage radiation therapy to the prostatectomy bed and potentially the entire pelvis is commonly performed in the setting of

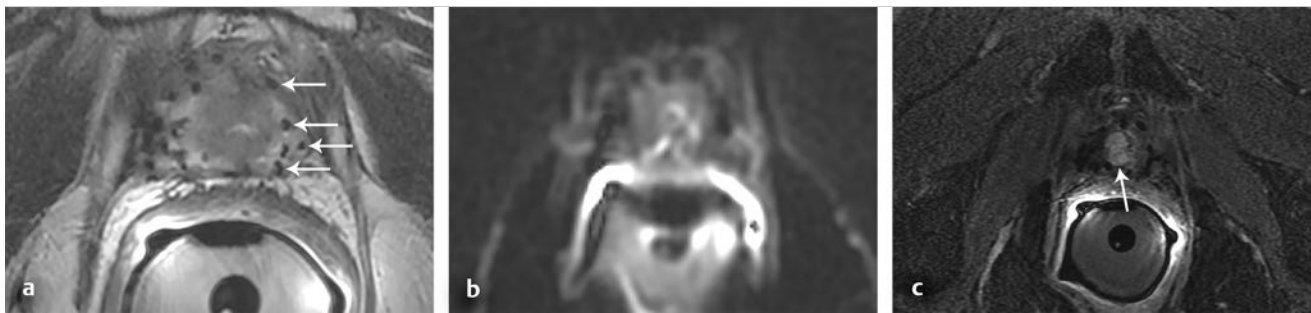


Fig. 8.16 A 62-year-old man with biochemical recurrence following primary brachytherapy treatment. (a) Axial T2-weighted image shows multiple small hypointense foci in the gland corresponding to the interstitial seeds (for example, *arrowheads* on left side of gland), although it has poor sensitivity for tumor. (b) Diffusion-weighted image exhibits much more significant susceptibility artifact from the seeds and is rendered nondiagnostic. However, an intraprostatic periurethral tumor recurrence is discretely identified only on the dynamic contrast-enhanced image (c, *arrow*), which shows only minor image degradation by the seeds, as seen as tiny foci of null signal.



Fig. 8.17 Perirectal recurrence following salvage radiation therapy. (a) Axial T2-weighted image demonstrates a small round mildly hyperintense lesion in the left perirectal space (*arrow*), which (b) shows hyperenhancement (*arrow*) on postcontrast T1-weighted image. (c) ^{11}C -choline PET/CT shows a corresponding avid focus of activity (*arrow*).

BCR after RP. This therapy is most often performed in a nontargeted manner when there has been an absence of identified distant or osseous metastases on imaging work-up to account for the BCR. This approach presumes that the recurrence is likely local (given the negative imaging evaluation for distant metastases) without in fact identifying a specific site of local disease. A fall in the elevated PSA levels following the initiation of salvage radiation therapy provides presumptive evidence that a local recurrence had indeed been present and then treated. This therapy generally involves radiating the prostatectomy bed as a whole and is variably extended to cover the low pelvic nodal stations to which PCa most commonly spreads depending on patient factors (i.e., history of lymphadenectomy) as well as the practice pattern of the radiation oncologist. The radiation fields in this application are often designed such that the radiation dose delivery spares the rectum, bladder, and femoral heads, which are the more common areas of potential radiation toxicity (anal bleeding or stenosis, cystitis, and avascular necrosis of the femoral heads). This dose distribution has specific implications for the common sites of recurrence after salvage radiation therapy.

In patients with a persistently elevated PSA following salvage RT, untreated or progressive PCa recurrences are frequently

located outside of the treatment field. Fortuin reported that up to 61% of metastatic lymph nodes are outside of the radiation target volume.³⁰ Nodular tumor recurrences in the perirectal space are particularly common after salvage pelvic radiation, as this area is relatively spared from treatment to avoid rectal complications. Similarly, lymph node recurrences after salvage pelvic radiation commonly involve high iliac node stations that are immediately above the cranial boundary of the treated field (► Fig. 8.17).

Following pelvic radiation therapy, the extent of bone marrow changes may provide a useful indication of the extent of anatomical coverage of the treatment field, which is rarely directly known (► Fig. 8.18).

MRI may help identify the precise location of a recurrent tumor after RT and thereby avoid nontargeted salvage radiation for a presumptive recurrence. Accurate identification of the recurrence site and size allows better selection of patients for a higher dose of intensity-modulated radiation therapy (IMRT) targeted at the recurrence site rather than a general templated treatment plan, potentially improving the chance of curing the patient or providing longer term durability of response. In patients in whom the recurrence had been identified by MRI before salvage radiation therapy, a follow-up MRI typically

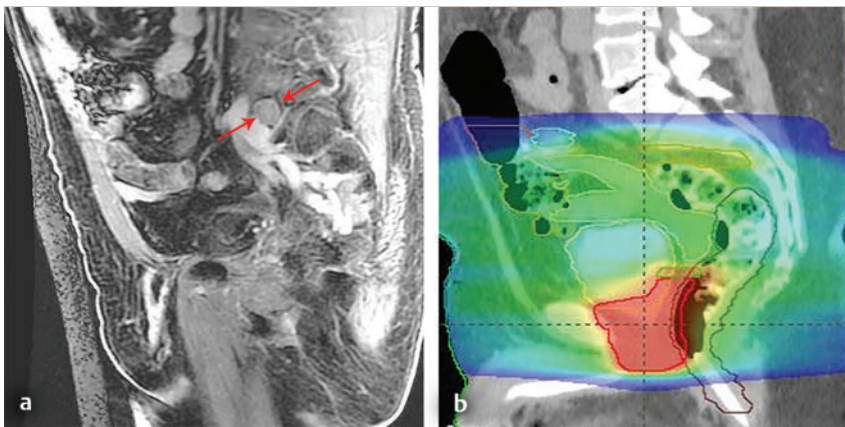


Fig. 8.18 A 64-year-old male with Gleason score 3 + 4 = 7 tumor following radical prostatectomy and subsequent salvage radiation therapy for biochemical recurrence. His prostate-specific antigen again recurred, measuring 1.9 ng/mL at the time of MRI. (a) The paramedian sagittal post-contrast T1-weighted image shows an enlarged left common iliac lymph node (arrows) as the site of recurrence, which is just above the top edge of the salvage radiation therapy dosimetry map (b). Note the region marked in red indicates the site of a boosted radiation dose delivered to the prostatectomy bed as a whole.

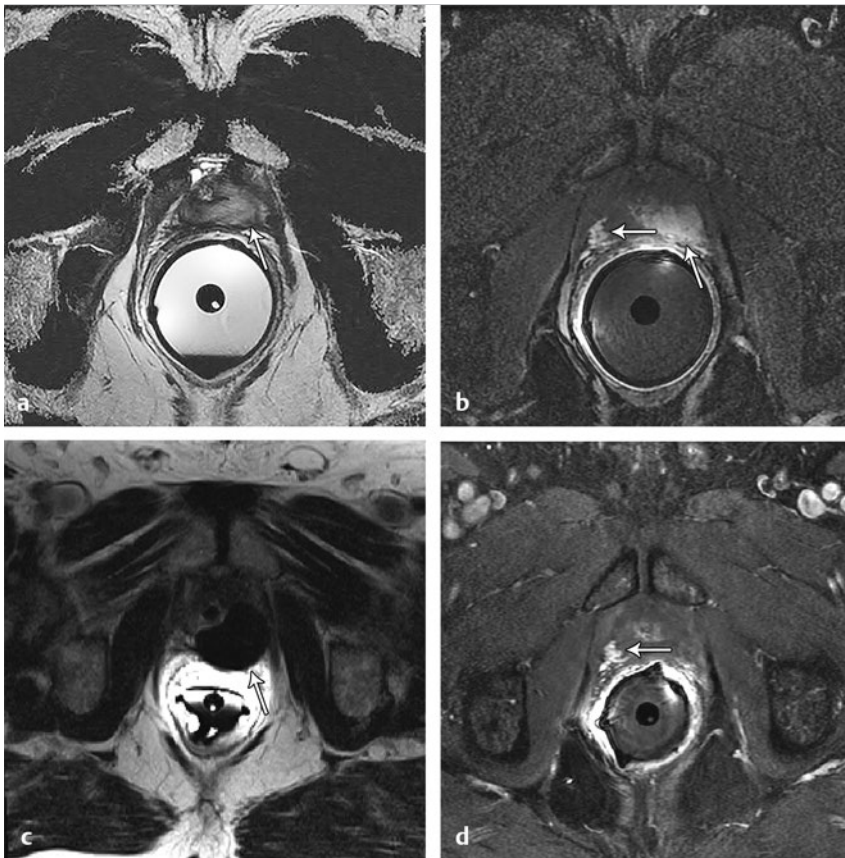


Fig. 8.19 A 63-year-old man presented with an elevated prostate-specific antigen (PSA) level of 1.9 ng/mL 7 years after radical prostatectomy for prostate carcinoma, Gleason score 3 + 4 = 7, pT3a, N0. (a) Axial T2-weighted and (b) dynamic contrast-enhanced (DCE) images show a hyper-enhancing mass at the left posterolateral bladder neck and vesicourethral anastomosis (arrows). Targeted biopsy confirmed adenocarcinoma, Gleason score 4 + 4 = 8. The patient underwent direct in-bore MR-guided transperineal cryoablation with a total of three cycles of 10-minute freeze and thaw. (c) Axial three-dimensional spin-gradient T1-weighted imaging with fat saturation during the procedure shows the hypointense reniform shaped iceball (arrow), partially wrapping around the urethra that has a warmer in place, with the iceball encompassing the biopsy-proven tumor. (d) DCE images 6 months following the procedure demonstrate no residual enhancing tumor. The patient's PSA remains undetectable over 4 years later. Note the stable benign enhancing vasculature in the tissues peripheral to the vesicourethral anastomosis on the right side (small arrow, also shown in b).

demonstrates interval decrease in enhancement as well as decrease in the size of the local recurrent tumor, indicative of positive treatment response.

8.10 Image-Guided Focal Treatments

The traditional therapy options for recurrent PCa are salvage radiation, androgen-deprivation therapy, and salvage surgery. However, precise visualization of recurrent tumors using MRI facilitates new treatment approaches using targeted ablative technologies. Multiple image-guided targeted treatment options are under investigation for treatment of locoregional

recurrence following RP. Focal ablative therapies used for local recurrence in the pelvis and prostate bed include cryoablation, laser ablation, high-intensity focused ultrasound (HIFU), and vascular-targeted photodynamic therapy (VTP).

Cryoablation to achieve whole-gland or hemigland ablation is most commonly performed under ultrasound guidance. However, cryoablation can also be performed under direct in-bore MRI guidance, in which case, MRI may assist differentiation of normal structures, including rectal and bladder wall and ureters, from tumor and frozen tissue (► Fig. 8.19). Magnetic resonance imaging also aids in monitoring of the iceball that forms during treatment. Preprocedure localizing T2-weighted images are obtained for fusion of the guidance grid. Following probe placement, intermittent gradient echo images are obtained for

iceball visualization in order to assure complete lesion coverage and proximity to adjacent structures including the urethra. The iceball is visualized as a well-defined hypointense mass on these sequences. Postprocedure imaging should include multiplanar T1WI and T2WI as well as DCE-MRI. Adequately ablated tissue demonstrates an irregular area of T2-hypointensity and nonenhancement. However, a thin rim of hyperenhancement may be present at the periphery of the ablation defect and is considered a normal finding, potentially persisting for several months after treatment. Typically, a follow-up prostate MRI is obtained at 6 months after therapy, at which time there should be no residual enhancing tissue if the procedure was technically successful. At this time, any persistent or new nodular enhancement is suspicious for residual or recurrent tumor. Although a relatively new procedure, MRI-guided cryoablation has shown adequate efficacy in halting disease progression with overall minimal side effects.¹⁸ A potential risk includes injury to the urethra resulting in urethral strictures or potentially acute urinary retention. Such risk can be minimized through use of a urethral warmer during the procedure, thus protecting the urethra from cryoablation-related injury.¹⁸

MR-guided laser ablation, or laser-induced interstitial thermal therapy (LITT), has shown promising results in early clinical trials, although long-term outcome data is still needed.⁴⁰ In this technique, locally placed laser fibers deliver thermal ablation to

targeted tissue. Laser-induced interstitial thermal therapy has been commonly performed within the bore of the MRI scanner. In addition, an MR thermometry sequence can be used to achieve real-time temperature monitoring and intraprocedural assessment of tissue destruction. Magnetic resonance-guided laser ablation aims to provide a more precise treatment margin than other ablative technologies. Imaging immediately after LITT may be difficult to interpret given heat fixation artifacts. Rather, follow-up MRI is typically obtained at 6 months after the procedure. T1 hyperintensity without associated enhancement may be a normal finding after thermal ablation, as is also observed in other organs such as the liver and kidney after such a treatment.

High-intensity focused ultrasound is an alternative salvage treatment option for intraprostatic recurrence following primary external-beam radiation therapy and has demonstrated successful cancer control in the short term, with reported progression-free survival of 66% at 1 year and 48% at 2 years.¹⁶ During the procedure, a focus of high energy density (in W/cc^2) propagates through the prostate causing tissue damage due to thermal necrosis or acoustic cavitation. High-intensity focused ultrasound is performed under ultrasound guidance, largely using a whole-gland or hemigland approach. However, recent studies describe truly focal ablation using HIFU to treat an MRI-visible tumor, albeit still under ultrasound guidance.^{41,42} During

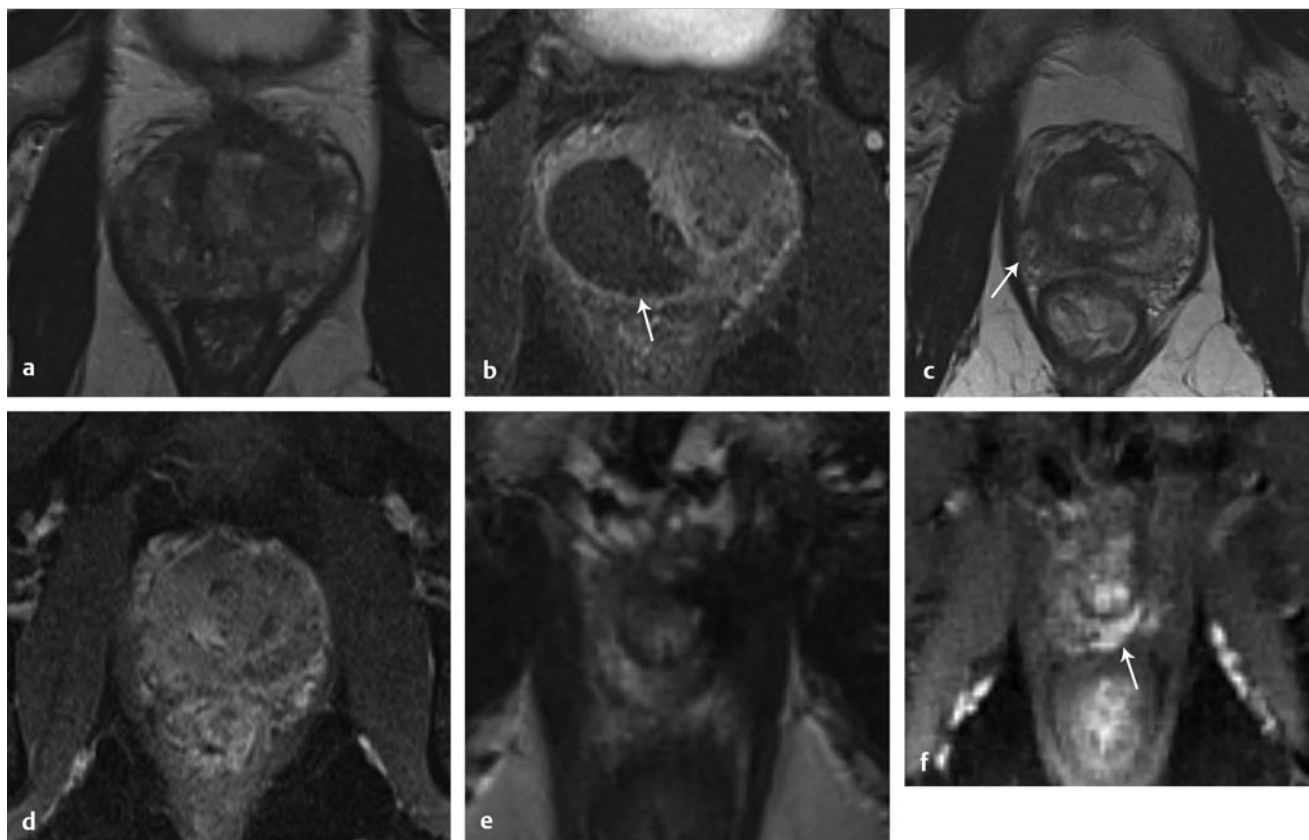


Fig. 8.20 A man following hemi-ablation with vascular-targeted photodynamic therapy (VTP). (a) Axial T2-weighted (T2W) image 1 week after treatment shows heterogeneous decreased T2 signal in right peripheral zone. (b) Corresponding dynamic contrast-enhanced (DCE) image shows a large nonenhancing cavity in right lobe (*arrow*). (c) T2W and (d) DCE images obtained 1 year later show resorption of the cavity and atrophy of the right lobe (c, *arrow*). His prostate-specific antigen (PSA) exhibited a subsequent rise at follow-up 3 years later. (e) T2W and (f) DCE images at time of PSA elevation show a new focal enhancing T2-hypointense lesion at the left apex (*arrow*). Targeted biopsy confirmed recurrent high-grade tumor.

treatment, a tumor that is initially hypoechoic on ultrasound exhibits hyperechoic changes, representing development of necrosed or nonviable tissue. Complications are similar to cryoablation and include incontinence, bladder outlet obstruction, erectile dysfunction, and rectourethral fistulas. However, HIFU has a relatively greater risk of significant urinary tract and rectal toxicities.⁴³

Vascular-targeted photodynamic therapy (VTP) is an ablative technique that has been most widely used for performing total-gland or hemigland ablation to treat primary localized PCa⁴⁴ (► Fig. 8.20), although more recently it has been used for treatment of localized recurrence as well. By using photosensitizers that are retained within the vascular system, selective ablation of neoplastic tissue can be achieved with minimal damage to other structures. Using image guidance, typically ultrasound, and placement grids similar to brachytherapy, energy-delivery probes can be inserted into the targeted tissue. Because the photosensitizer is confined to the vascular system, the mechanism of cell death is related to vascular occlusion and vascular oxidative stress.⁴⁴ Generally, with increased doses, a complete response can be obtained as indicated by undetectable PSA levels and negative biopsy at 6 months.⁴⁵ Contrast-enhanced prostate MRI at 7 days post-treatment can be used to assess for treatment response, with absence of enhancement predicting adequate therapy. As with all focal ablative techniques, injury to adjacent structures is a risk and includes urethral and ureteral strictures, rectal wall injury, and rectal fistulas.⁴⁵ At longer term follow-up, the ablated region typically atrophies, with no residual focal enhancement.

8.11 Summary

While PCa is exceedingly common, recurrence of disease after primary treatment is also common, thereby resulting in a large population of men with BCR. Conventional management of recurrent disease includes generalized or systemic therapies, usually for patients with uncertain disease status. Substantial advances in imaging over the last decade have enabled a paradigm shift in the management of men with BCR, paralleling ongoing shifts in the diagnosis and management of primary PCa because of MRI. Magnetic resonance imaging detects and defines locoregional recurrence early in the course of BCR and enables new targeted treatment options. Positron emission tomography with tracers having high specificity for PCa (including ¹¹C-choline and ¹⁸F-NaF) also improves staging and enables more accurate monitoring of disease status and treatment response. The advances in imaging of both local and distant tumor recurrence have improved tailored treatment selection and also facilitated MRI-targeted focally ablative therapies.

References

- [1] Freedland SJ, Humphreys EB, Mangold LA et al. Risk of prostate cancer-specific mortality following biochemical recurrence after radical prostatectomy. *JAMA* 2005; 294(4):433–439
- [2] Cookson MS, Aus G, Burnett AL et al. Variation in the definition of biochemical recurrence in patients treated for localized prostate cancer: the American Urological Association Prostate Guidelines for Localized Prostate Cancer Update Panel report and recommendations for a standard in the reporting of surgical outcomes. *J Urol* 2007; 177(2):540–545
- [3] Stephenson AJ, Kattan MW, Eastham JA et al. Defining biochemical recurrence of prostate cancer after radical prostatectomy: a proposal for a standardized definition. *J Clin Oncol* 2006; 24(24):3973–3978
- [4] Pound CR, Partin AW, Eisenberger MA, Chan DW, Pearson JD, Walsh PC. Natural history of progression after PSA elevation following radical prostatectomy. *JAMA* 1999; 281(17):1591–1597
- [5] Mohler JL, Kantoff PW, Armstrong AJ et al. National Comprehensive Cancer Network. Prostate cancer, version 2.2014. *J Natl Compr Canc Netw* 2014; 12(5):686–718
- [6] Amling CL, Bergstralh EJ, Blute ML, Slezak JM, Zincke H. Defining prostate specific antigen progression after radical prostatectomy: what is the most appropriate cut point? *J Urol* 2001; 165(4):1146–1151
- [7] Kim MB, Chen MH, de Castro M, Loffredo M, Kantoff PW, D'Amico AV. Defining the optimal approach to the patient with postradiation prostate-specific antigen recurrence using outcome data from a prospective randomized trial. *Cancer* 2013; 119(18):3280–3286
- [8] Mitchell CR, Lowe VJ, Rangel LJ, Hung JC, Kwon ED, Karnes RJ. Operational characteristics of (11)c-choline positron emission tomography/computerized tomography for prostate cancer with biochemical recurrence after initial treatment. *J Urol* 2013; 189(4):1308–1313
- [9] Kitajima K, Murphy RC, Nathan MA et al. Detection of recurrent prostate cancer after radical prostatectomy: comparison of ¹¹C-choline PET/CT with pelvic multiparametric MR imaging with endorectal coil. *J Nucl Med* 2014; 55(2):223–232
- [10] Ost P, Bossi A, Decaestecker K et al. Metastasis-directed therapy of regional and distant recurrences after curative treatment of prostate cancer: a systematic review of the literature. *Eur Urol* 2015; 67(5):852–863
- [11] Partin AW, Pearson JD, Landis PK et al. Evaluation of serum prostate-specific antigen velocity after radical prostatectomy to distinguish local recurrence from distant metastases. *Urology* 1994; 43(5):649–659
- [12] Novara G, Ficarra V, Mocellin S et al. Systematic review and meta-analysis of studies reporting oncologic outcome after robot-assisted radical prostatectomy. *Eur Urol* 2012; 62(3):382–404
- [13] Heidenreich A, Bastian PJ, Bellmunt J et al. European Association of Urology. EAU guidelines on prostate cancer. Part II: Treatment of advanced, relapsing, and castration-resistant prostate cancer. *Eur Urol* 2014; 65(2):467–479
- [14] Trock BJ, Han M, Freedland SJ et al. Prostate cancer-specific survival following salvage radiotherapy vs observation in men with biochemical recurrence after radical prostatectomy. *JAMA* 2008; 299(23):2760–2769
- [15] Stephenson AJ, Scardino PT, Kattan MW et al. Predicting the outcome of salvage radiation therapy for recurrent prostate cancer after radical prostatectomy. *J Clin Oncol* 2007; 25(15):2035–2041
- [16] Uddin Ahmed H, Cathcart P, Chalasani V et al. Whole-gland salvage high-intensity focused ultrasound therapy for localized prostate cancer recurrence after external beam radiation therapy. *Cancer* 2012; 118(12):3071–3078
- [17] Saylor PJ, Smith MR. Metabolic complications of androgen deprivation therapy for prostate cancer. *J Urol* 2013; 189(1) Suppl:S34–S42, discussion S43–S44
- [18] Woodrum DA, Kawashima A, Karnes RJ et al. Magnetic resonance imaging-guided cryoablation of recurrent prostate cancer after radical prostatectomy: initial single institution experience. *Urology* 2013; 82(4):870–875
- [19] Thompson IM, Valicenti RK, Albertsen P et al. Adjuvant and salvage radiotherapy after prostatectomy: AUA/ASTRO Guideline. *J Urol* 2013; 190(2):441–449
- [20] Karnes RJ, Murphy CR, Bergstralh EJ et al. Salvage lymph node dissection for prostate cancer nodal recurrence detected by ¹¹C-choline positron emission tomography/computerized tomography. *J Urol* 2015; 193(1):111–116
- [21] Kane CJ, Amling CL, Johnstone PA et al. Limited value of bone scintigraphy and computed tomography in assessing biochemical failure after radical prostatectomy. *Urology* 2003; 61(3):607–611
- [22] Krause BJ, Souvatzoglou M, Tuncel M et al. The detection rate of [¹¹C]choline-PET/CT depends on the serum PSA-value in patients with biochemical recurrence of prostate cancer. *Eur J Nucl Med Mol Imaging* 2008; 35(1):18–23
- [23] Connolly JA, Shinohara K, Presti JC Jr Carroll PR. Local recurrence after radical prostatectomy: characteristics in size, location, and relationship to prostate-specific antigen and surgical margins. *Urology* 1996; 47(2):225–231
- [24] Leventis AK, Shariat SF, Slawin KM. Local recurrence after radical prostatectomy: correlation of US features with prostatic fossa biopsy findings. *Radiology* 2001; 219(2):432–439
- [25] Linder BJ, Kawashima A, Woodrum DA et al. Early localization of recurrent prostate cancer after prostatectomy by endorectal coil magnetic resonance imaging. *Can J Urol* 2014; 21(3):7283–7289

- [26] Krämer S, Görlich J, Gottfried HW et al. Sensitivity of computed tomography in detecting local recurrence of prostatic carcinoma following radical prostatectomy. *Br J Radiol* 1997; 70(838):995–999
- [27] National Comprehensive Cancer Network NCCN Clinical Practice Guidelines in Oncology (NCCN Guideline): Prostate Cancer. Version 2.2014 ed. <https://www.tri-kobe.org/nccn/guideline/urological/english/prostate.pdf> Published April 1, 2014.
- [28] Jadvar H, Desai B, Ji L et al. Prospective evaluation of 18F-NaF and 18F-FDG PET/CT in detection of occult metastatic disease in biochemical recurrence of prostate cancer. *Clin Nucl Med* 2012; 37(7):637–643
- [29] American College of Radiology. ACR Appropriateness Criteria: Post-treatment Follow-up of Prostate Cancer. <https://acsearch.acr.org/docs/69369/Narrative/Updated2011>.
- [30] Fortuin AS, Deserno WM, Meijer HJ et al. Value of PET/CT and MR lymphography in treatment of prostate cancer patients with lymph node metastases. *Int J Radiat Oncol Biol Phys* 2012; 84(3):712–718
- [31] Wasserman NF, Kapoor DA, Hildebrandt WC et al. Transrectal US in evaluation of patients after radical prostatectomy. Part I. Normal postoperative anatomy. *Radiology* 1992; 185(2):361–366
- [32] Allen SD, Thompson A, Sohaib SA. The normal post-surgical anatomy of the male pelvis following radical prostatectomy as assessed by magnetic resonance imaging. *Eur Radiol* 2008; 18(6):1281–1291
- [33] Casciani E, Polettini E, Carmenini E et al. Endorectal and dynamic contrast-enhanced MRI for detection of local recurrence after radical prostatectomy. *AJR Am J Roentgenol* 2008; 190(5):1187–1192
- [34] Wassberg C, Akin O, Vargas HA, Shukla-Dave A, Zhang J, Hricak H. The incremental value of contrast-enhanced MRI in the detection of biopsy-proven local recurrence of prostate cancer after radical prostatectomy: effect of reader experience. *AJR Am J Roentgenol* 2012; 199(2):360–366
- [35] Cirillo S, Petracchini M, Scotti L et al. Endorectal magnetic resonance imaging at 1.5 Tesla to assess local recurrence following radical prostatectomy using T2-weighted and contrast-enhanced imaging. *Eur Radiol* 2009; 19(3):761–769
- [36] Roy C, Foudi F, Charton J et al. Comparative sensitivities of functional MRI sequences in detection of local recurrence of prostate carcinoma after radical prostatectomy or external-beam radiotherapy. *AJR Am J Roentgenol* 2013; 200(4):W361–8
- [37] Rischke HC, Schäfer AO, Nestle U et al. Detection of local recurrent prostate cancer after radical prostatectomy in terms of salvage radiotherapy using dynamic contrast enhanced-MRI without endorectal coil. *Radiat Oncol* 2012; 7:185
- [38] Haider MA, Chung P, Sweet J et al. Dynamic contrast-enhanced magnetic resonance imaging for localization of recurrent prostate cancer after external beam radiotherapy. *Int J Radiat Oncol Biol Phys* 2008; 70(2):425–430
- [39] Morgan VA, Riches SF, Giles S, Dearnaley D, deSouza NM. Diffusion-weighted MRI for locally recurrent prostate cancer after external beam radiotherapy. *AJR Am J Roentgenol* 2012; 198(3):596–602
- [40] Lee T, Mendhiratta N, Sperling D, Lepor H. Focal laser ablation for localized prostate cancer: principles, clinical trials, and our initial experience. *Rev Urol* 2014; 16(2):55–66
- [41] Ahmed HU, Dickinson L, Charman S et al. Focal Ablation Targeted to the Index Lesion in Multifocal Localised Prostate Cancer: a Prospective Development Study. *Eur Urol* 2015; 68(6):927–936
- [42] Alkhorayef M, Mahmoud MZ, Alzimami KS, Sulieman A, Fagiri MA. High-Intensity Focused Ultrasound (HIFU) in Localized Prostate Cancer Treatment. *Pol J Radiol* 2015; 80:131–141
- [43] Illing RO, Leslie TA, Kennedy JE, Calleary JG, Ogden CW, Emberton M. Visually directed high-intensity focused ultrasound for organ-confined prostate cancer: A proposed standard for the conduct of therapy. *BJU Int* 2006; 98(6):1187–1192
- [44] Lepor H. Vascular targeted photodynamic therapy for localized prostate cancer. *Rev Urol* 2008; 10(4):254–261
- [45] Trachtenberg J, Weersink RA, Davidson SR et al. Vascular-targeted photodynamic therapy (padoporfin, WST09) for recurrent prostate cancer after failure of external beam radiotherapy: a study of escalating light doses. *BJU Int* 2008; 102(5):556–562

9 Prebiopsy MRI and MRI-Targeted Biopsy

Karoly Viragh and Daniel J. A. Margolis

9.1 Introduction

This chapter discusses the role of magnetic resonance imaging (MRI) in the planning and execution of targeted prostate biopsies. Relevant clinical aspects of prostate cancer will be summarized very briefly in the introduction, followed by a detailed discussion of the use of MRI in the targeted biopsy setting.

Prostate cancer is the second most common cancer in men after skin cancer, with a lifetime prevalence of 1 in 6 males.^{1,2} Pathologically, prostate cancer is a heterogeneous disease exhibiting highly variable biological behavior, ranging from well-differentiated, slow-growing, locally-confined neoplasms that are frequently clinically innocuous to poorly-differentiated, aggressive, carcinomas with a high risk of metastasis and a very poor prognosis. Because only a small percentage of prostate cancers is aggressive, the overall death rate from prostate cancer is relatively low (approximately 1 in 6 affected males), and there is significant morbidity from overtreatment of clinically insignificant lesions.^{2,3,4} Most patients with prostate cancer die *with* the disease and not *from* the disease. Therefore, a clinical tool is needed to detect and risk-stratify prostate cancer in order to guide subsequent management.

MRI has strong potential to fill this gap, as multiparametric MRI (mpMRI) has been shown to have high specificity and high negative predictive value (NPV) for clinically significant cancer. As of 2016, mpMRI is the most accurate imaging technique for prostate cancer detection and staging.^{5,6,7} Disadvantages include its cost and availability. As discussed in earlier chapters, MRI plays a role in:

- Detection of prostate cancer as a secondary screening test for patients with a high suspicion for prostate cancer based on clinical, laboratory, or other imaging findings.
- Risk stratification and staging (cTNM) of prostate cancer.
- Surveillance of prostate cancer.
- Preprocedural prostate cancer localization and characterization (prebiopsy, as well as presurgery or preradiation).
- Procedural guidance (targeted biopsy guidance, focal therapeutic intervention).

This chapter focuses on the last two roles, specifically prebiopsy MRI and MRI-targeted biopsy guidance.

9.2 Prebiopsy Planning

The large majority of prostate cancer cases are multifocal, comprising numerous tumor foci within the gland. Nevertheless, prostate cancer may be regarded as a biologically unifocal disease, in which a single most aggressive tumor focus, termed the *index lesion*, drives the natural course of the disease and any adverse oncologic outcome by being the origin of any distant metastases.^{8,9,10} Therefore, a key goal of prostate MRI in the prebiopsy setting is to define and localize an index lesion, which can then be biopsied in order to best characterize the lesion and guide subsequent management.

9.2.1 Target Population: Who Needs a Prebiopsy MRI?

Prebiopsy MRI is generally performed in three clinical contexts.^{11,12,13,14,15}

Biopsy-Negative Patients

These are patients with clinically suspected prostate cancer, usually based on an elevated or increasing serum prostate specific antigen (PSA) level (PSA > 4.0 ng/mL), an increasing PSA velocity, or an abnormal digital rectal examination, who only have a prior negative biopsy, typically performed as a non targeted transrectal ultrasound-guided (TRUS-guided) biopsy using standard systematic sampling. MRI can detect prostate cancer in over 50% of men who have undergone a prior negative biopsy.^{6,16,17,18}

Biopsy-Naïve Patients

These are patients with clinically suspected prostate cancer who have not undergone a prior biopsy. This represents a growing group of patients and would represent the majority of patients undergoing MRI in the future if performing MRI in biopsy-naïve patients were to become the clinical standard of care. An advantage of performing MRI before any biopsy is performed is avoidance of any negative impact on interpretation from postbiopsy hemorrhage. An additional potential advantage, although controversial, is that if the MRI shows no suspicious lesion, then biopsy may potentially be avoided altogether.¹⁹ Prostate MRI in biopsy-naïve patients may be covered by some insurance carriers, given that an elevated PSA may be viewed as a presumptive diagnosis of prostate cancer.

Active Surveillance Patients

These are patients with biopsy-proven low-grade cancer who elect to defer immediate definitive treatment after careful consultation with prostate specialists. Although variable criteria are applied clinically for considering a patient with prostate cancer to be a candidate for active surveillance, traditional strict criteria require low-risk of disease as defined by the Epstein criteria (Gleason Score (GS) < 7 at biopsy, < 3 positive biopsy cores, < 50% of all biopsy cores positive, and a serum PSA < 10 ng/mL).²⁰ Active surveillance patients require close follow-up and potential intervention at a future time in the event of any evidence of disease progression. Traditionally, active surveillance regimens incorporate an early repeat biopsy to confirm the presence of low-risk disease, followed by additional repeat biopsies every 1 to 3 years for at least 10 years or until life expectancy is less than 10 years. However, prebiopsy and MRI-targeted biopsy has great potential to reduce the frequency of repeat biopsies for men being managed by active surveillance.

9.2.2 Prebiopsy MRI Technique

State-of-the-art prostate MRI technique has been discussed extensively in prior chapters. Given potentially large volumes of patients undergoing prostate MRI in the prebiopsy setting, protocols need to be efficient and provide the necessary information for biopsy planning without extraneous imaging that would decrease patient throughput. Thus, the technique is optimized for cancer detection and localization, not for locoregional staging.²¹

Patient Screening and Preparation

To screen patients for prostate MRI, practitioners should:

- Screen patients for MR eligibility (for example, MR-incompatible hardware is a contraindication).
- Screen patients for recent prostate therapy. MRI should be performed at least 3 weeks, ideally 6 to 8 weeks, after a prior prostate biopsy or treatment (surgery, radiation, chemotherapy).

Ideal patient preparation is simple and cost effective.

- Ensure complete evacuation of the rectum prior to scanning via use of an enema or suppository- and even rectal gas aspiration using a flexible tube.
- Some practices also administer an antiperistaltic agent (i.e., glucagon [unless there is a history of poorly controlled diabetes mellitus], scopolamine butylbromide, or hyoscine butylbromine), although there is a paucity of supporting data for use of such an agent.

Equipment

Technical parameters and recommendations for acquiring multiparametric MRI of the prostate are described in detail in Prostate Imaging-Reporting and Data System version 2 (PI-RADS v2).²²

Field Strength

While a 1.5-T system may be used, a 3-T MR system is optimal. Nonetheless, while the signal-to-noise ratio (SNR) is better at the higher magnetic field strength, some artifacts may also be worse, thus one must be familiar with one's system and technical optimization regardless of field strength.

Coils

A multichannel (at least 8 channels) external phased-array pelvic coil is suggested for use in the prebiopsy setting, in which MRI is being performed to detect and localize dominant lesions for targeted biopsy. The reduced cost and examination time of this approach, in comparison with use of an endorectal coil (ERC), is an important consideration when applying prostate MRI in large patient populations in prebiopsy settings. In addition, this approach avoids the potential susceptibility artifact and geometrical distortion that may result from use of an ERC. Furthermore, use of an external coil may increase the willingness of patients not facing imminent therapy for prostate cancer to undergo an MRI examination. Nonetheless, an ERC may be considered in patients with a large body habitus, in which

case SNR at the prostate is relatively limited, or in patients for whom surgery is considered likely and a more detailed characterization of the posterior prostate capsule and neurovascular bundles is desired.

Image Sequences

The image sequences performed^{23,24,25} must be reliable yet efficient in detecting suspicious lesions for targeted biopsy. Detailed characterization and staging, if necessary, may be performed at the time of a later examination. High matrix, small field-of-view acquisitions are preferred.

T2-Weighted Imaging

Axial T2-weighted images (T2WI) are the workhorse of anatomical prostate assessment, providing high spatial resolution and delineating zonal anatomy, as well as locating of various benign conditions such as prostatic hyperplasia and prostate cysts. Prostate cancer is generally T2 hypointense, although the specificity of T2WI for cancer is usually limited given the overlapping appearance on T2WI of various benign and malignant conditions. The differential diagnosis of a T2-hypointense lesion includes: cancer, hemorrhage (e.g. postbiopsy or trauma), benign prostatic hyperplasia, post-radiation therapy changes, post-hormonal therapy changes, and postinfectious or postinflammatory fibrosis. Furthermore, T2WI does not predict tumor aggressiveness.

Diffusion-Weighted Imaging

Diffusion-weighted imaging (DWI) provides physiologic information. As described in prior chapters, it offers microarchitectural tissue characterization based on the brownian motion of water molecules. Prostate cancer cells are more densely packed than healthy cells, leading to increased restriction of water movement. Therefore, DWI can distinguish malignant from benign lesions as well as low-grade from high-grade tumors, thereby providing increased specificity in cancer detection.²⁶

Dynamic Contrast-Enhanced Imaging

T1-weighted dynamic contrast enhanced (DCE) imaging provides further physiologic information through micro vascular tissue characterization based on the distribution of an intravenously administered gadolinium-containing contrast agent. Due to neovascularization, malignant lesions are frequently hypervascular. The precontrast images from the DCE acquisition can be used for the detection and localization of hemorrhage without requiring a separate dedicated T1-weighted acquisition for this purpose.

MR Spectroscopic Imaging and Large Field-of-View Images

Magnetic resonance spectroscopic imaging (MRSI) is usually deferred, given practical considerations of availability, variable technical expertise, general requirement for an endorectal coil, and the at least 10 minutes additional scanner time needed for acquisition.

Large field-of-view images for locoregional evaluation may also be deferred in the prebiopsy setting.

9.2.3 MRI Results and Reporting

Though multiple systems have been suggested, standardized reporting is recommended using PI-RADS v2, which facilitates communication between radiologists as well as with referring physicians, including both urologists and primary care physicians.²²

PI-RADS v2 was developed as a joint effort of the American College of Radiology (ACR), the European Society of Urogenital Radiology (ESUR), and AdMeTech Corporation. PI-RADS v2 employs standardized language based on RadLex, which is a comprehensive lexicon of well-defined radiology terms developed by the Radiologic Society of North America (RSNA). As discussed in Chapter 6, PI-RADS v2 not only defines the vocabulary but also the technical parameters required for prostate MRI and enhances research and quality assurance.

A critical advantage of using PI-RADS v2 is the assignment of discrete assessment categories to lesions to summarize the level of suspicion for aggressive prostate cancer. Though these assessment categories do not specify management, general guidelines for management (following the arrows in the list below) can be associated with them:

- Very low to low suspicion (PI-RADS v2 categories 1 and 2) → defer targeted biopsy given the low likelihood of the target representing significant cancer; although further data remains required, deferral of standard systematic biopsy may be considered as well; continue monitoring as clinically warranted
- Moderate suspicion (PI-RADS v2 category 3) → consider biopsy versus follow-up; further data regarding outcomes of PI-RADS category 3 lesions remains required, and there is currently a lack of consensus regarding management of such lesions
- High suspicion (PI-RADS v2 category 4) → targeted biopsy
- Very high suspicion (PI-RADS v2 category 5) → targeted biopsy; consider repeat targeted biopsy if the initial targeted biopsy is pathologically negative

An additional aspect of interpreting prostate MRI for targeted biopsy planning is three-dimensional (3D) segmentation of the prostate gland and any identified biopsy targets. Although unnecessary prior to in-bore biopsy, the segmentation is crucial in advance of image-fusion-targeted biopsy. The segmentation may be deferred at the time of initial MRI reporting, and then performed at a later date once the targeted biopsy is scheduled. Software packages used for segmentation may also be used to generate components of the report, including automatic capture of salient images.

9.3 Biopsy Guidance

The goal of prostate biopsy is essentially twofold²⁷: (1) to establish the presence or absence of cancer and (2) to determine the tumor grade as defined by the Gleason score (GS).

9.3.1 Biopsy Options

A variety of methods to perform a prostate biopsy are available (► Table 9.1), which in this section are categorized by modality, approach, and strategy.²⁸

Modality

The imaging modalities that can be used in targeted prostate biopsy are MRI, ultrasound (US), and computed tomography (CT). MRI and ultrasound are most common and can be used alone or in MRI-US fusion techniques. CT is used in the rare cases in which MRI and ultrasound are not feasible.

Approach

The transrectal approach is generally considered the standard of care as of 2016. This is typically performed using local anesthesia delivered to the periprostatic nerve plexus. The transperineal or transgluteal approaches are acceptable if the transrectal approach is not feasible (e.g., due to prior anorectal resection). Although controversial, such approaches are preferred by some practitioners due to a potential decreased risk of sepsis. A relative disadvantage of this approach is the requirement for conscious sedation.

Systematic Biopsy

Technique

Systematic biopsy entails methodically sampling the entire prostate according to a grid like map in order to maximize the chance of detecting significant prostate cancer. No single area of the prostate is specifically targeted. In routine clinical practice, 12 cores are obtained (medial and lateral cores from each of six sextants: right and left lobes at the levels of the base, midgland, and apex). However, a saturation biopsy comprising a larger number of cores (i.e., 30, if not more, cores) may be performed in an effort to further increase the cancer detection rate (► Fig. 9.1a).

Advantages

The advantages include that systematic biopsy is simple, is widely available, urologists are familiar with it and are trained in the procedure, and it does not require the additional expense of advanced technology for performing targeted biopsy. Systematic biopsy is supported by current American Urological Association (AUA) guidelines and represents the standard of care in most communities.

Disadvantages

The disadvantages of systematic biopsy include overdetection of insignificant lesions and underdetection or undergrading of significant lesions due to undersampling (particularly of the anterior and paramedian aspects of the prostate), all of which result in incorrect risk stratification and possible need for repeat biopsies due to uncertainty with a false-negative rate up to 47%.²⁹ In addition a greater number of cores are obtained in a single biopsy session in comparison with an approach in which only targeted cores are obtained.

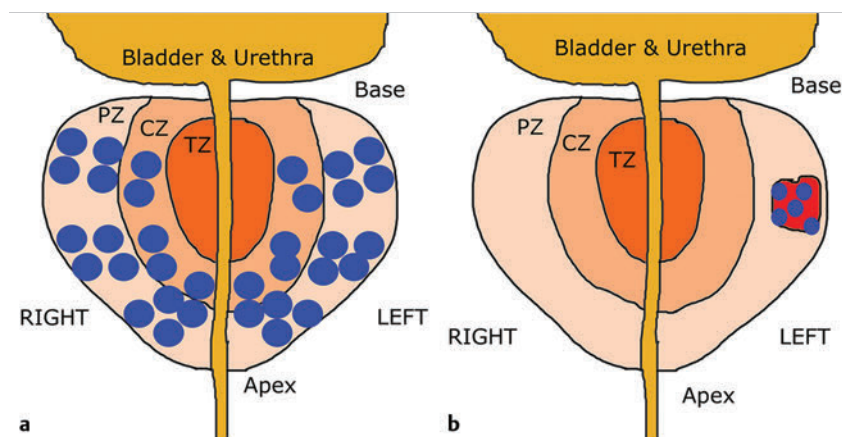


Fig. 9.1 Coronal views of the prostate comparing systematic and targeted biopsy approaches. (a) Anatomical distribution of cores for conventional systematic biopsy. Although typically entailing 12 cores, saturation biopsies may be performed, entailing a much larger number of cores (i.e., 36 cores in this illustration). (b) In comparison, targeted biopsies may obtain as few as 3 to 4 samples from a single imaging-identified target that is considered to be the most likely site of any clinically significant tumor that may be present. (CZ, central zone; PZ, peripheral zone; TZ, transition zone.)

Targeted Biopsy

Technique

Targeted biopsy entails directed sampling of lesions detected by mpMRI (► Fig. 9.1b).³⁰ Typically, the patient first undergoes mpMRI to identify the index lesion and any secondary targets. Then, during a subsequent session, targeted biopsy is accomplished in one of two ways:

- Direct (in-bore) biopsy, in which limited MRI sequences are performed to localize the previously identified abnormalities and provide needle guidance
- Indirect (fusion) biopsy, in which the MR images are fused to ultrasound images to be used for biopsy guidance. Fusion can be performed with or without software, as will be discussed in 9.3.4 MRI-Transrectal Ultrasound–Fusion Biopsy.

Advantages

In comparison with systematic biopsy, targeted biopsy improves detection of significant cancers (30% more high-risk cancers detected), reduces overdiagnosis of insignificant cancers (17% fewer low-risk cancers detected),^{31,32} and better predicts the GS from radical prostatectomy (GS concordance of 81% for MRI/US fusion biopsy vs. 40–65% for conventional systematic TRUS biopsy).³³ Furthermore, repeat biopsy of an imaging-defined target may allow for more reliable follow-up of prostate cancer patients undergoing active surveillance than is achieved by serial systematic biopsy. One European study suggested that over a 10-year period following initial clinical suspicion for prostate cancer, targeted biopsy achieves similar costs but improved quality of life compared with systematic biopsy, given the reduction in overdiagnosis and overtreatment from improved risk stratification.³⁴

Disadvantages

The disadvantages of targeted biopsy are: it is more complex and resource intensive; urologists have less experience doing it than systematic biopsy; it has a potentially longer procedural time than systematic biopsy; it is offered by a limited number of centers at present; there are high costs for purchasing technology for targeting; there is a lack of available data on targeted biopsy in comparison with systematic biopsy at present; and the time needed for utilization of MRI gantry (for the in-bore approach only).

Summary

Given the diversity of modalities, approaches, and strategies, there are many different scenarios available for performing prostate biopsy. However, existing data suggests that targeted biopsy provides overall optimal results when considering both detection of significant prostate cancer and reducing overdiagnosis of insignificant cancer. For example, one prospective study of 1,003 men undergoing both MRI-US fusion–targeted biopsy and systematic biopsy during the same biopsy session concluded that systematic biopsy would need to be performed in addition to targeted biopsy in 200 men in order to diagnose 1 additional high-risk cancer, and for each such additional high-risk cancer identified, 17 additional low-risk cancers would be diagnosed.³¹ In addition, a meta-analysis of 14 studies of indirect MRI-US targeted biopsy (with or without software-based image fusion) concluded that targeted biopsy detects more significant cancers using substantially fewer biopsy cores than does systematic biopsy alone.³⁵ Nonetheless, achieving optimal outcomes from targeted prostate biopsy requires high-quality MR image acquisition, image interpretation, and targeting technique. Errors in any of these aspects will diminish the performance of MRI-targeted biopsy in clinical practice in comparison with the high performance anticipated based upon the published literature.

9.3.2 Transrectal Ultrasound–Guided Biopsy

As of 2016, the most common approach to performing prostate biopsy is systematic TRUS-guided biopsy, which is considered the standard of care for most communities. However, multiple investigations have shown that it is a suboptimal technique on its own.^{32,35} Detection rates are at least 40% on first biopsy, 20% on second biopsy, and 10% on third biopsy.^{36,37} Sensitivity is limited, reported to be 62% in the base, 52% in the midgland, and 38% in the apex.³⁸ The poor sensitivity in part reflects the typically inconspicuous appearance of tumors within the prostate by ultrasound,³⁸ as tumors may be isoechoic or unable to be discriminated from benign nodules.¹² Because targeted biopsy based on ultrasound alone is generally not feasible, the systematic approach is overwhelmingly favored, despite incomplete sampling. The false-negative rate varies, although it is estimated to be up to 47%.^{39,40} Detection rates using ultrasound

alone are improved through the use of color power Doppler and intravenous ultrasound contrast.⁴¹ Although requiring further investigation, software systems for performing fusion-based targeted biopsy may also offer the ability to optimally space the nontargeted systematic cores across the prostate, thereby potentially improving the detection rate that is achieved by systematic biopsy.

9.3.3 Direct Transrectal MRI-Guided Biopsy (also known as In-Bore or MRI Fusion Biopsy)

Advantages

The advantages of direct transrectal MRI-guided biopsy include that there is visualization of the biopsy target using the same imaging modality as is used for lesion detection; direct confirmation of the needle position within the target, which may allow reducing the number of biopsy cores; and the potential for improved targeting of the lesion(s) in comparison with indirect approaches.

Disadvantages

The disadvantages of direct transrectal MRI-guided biopsy include: the cost; the availability of the procedure; that it is resource intensive, requiring MRI-compatible hardware; that it requires greater procedural time than US-guided biopsy schemes; that it may warrant moderate sedation thus requiring additional postprocedural patient observation; and that

systematic sampling (if desired) is less readily performed during the same biopsy session.

Technique

Transrectal MR-guided biopsy is performed in the MR imaging suite (► Fig. 9.2).⁴² It utilizes the prebiopsy MRI (► Fig. 9.3) as a guide for initial targeting for the biopsy.

Equipment

A normal or high-field-strength MRI system is preferred. While a higher field strength may lead to more artifact during the procedure, a lower field strength system may less clearly visualize the target. The MRI-compatible biopsy system includes the biopsy needle as well as the targeting and guidance system (► Fig. 9.2). As of 2015, the only FDA-approved device is DynaTRIM (Invivo Inc., Gainesville, FL), though others are in development.

Patient Preparation

Patient preparation includes:

- Nothing by mouth for 8 hours prior to the procedure and liquids only for 24 hours is recommended to minimize fecal material in the gastrointestinal system and to minimize the risk of aspiration during the procedure.
- A cleansing enema the night before and prior to the procedure, although no randomized controlled trial demonstrates its value.⁴³



Fig. 9.2 (a) Radiology suite with a 1.5-T MRI magnet used for direct in-bore targeted prostate biopsy. All objects inside the room during the procedure must be MRI compatible, including the biopsy instrument and potential surgical hardware inside the patient's body. (b) Invivo DynaTrim Automated Biopsy Gun (top; both 150-mm and 170-mm needle lengths available) and Needle Guide (bottom). The biopsy procedure is semi sterile. Peri-procedural antibiotic prophylaxis is provided to the patient. (c) Invivo DynaTrim Biopsy Device. The biopsy device provides needle control through three controllers. (d) The location of the needle-guide holder is described in a three-dimensional polar coordinate system. Controller #1 adjusts the horizontal angle (degrees). Controller #2 adjusts the vertical angle (degrees). Controller #3 adjusts the z-axis distance (mm) that the needle-guide holder is advanced along its track. (e) Invivo DynaTrim Computer Console. The polar coordinates to which the biopsy device shown in (e) is adjusted are derived by the computer through the calibration process and displayed on the computer screen. (f) Invivo DynaTrim Biopsy Device in place. With the patient positioned prone on the MRI gantry table, the biopsy device is placed in between the lower extremities and the needle guide is positioned in the rectum.

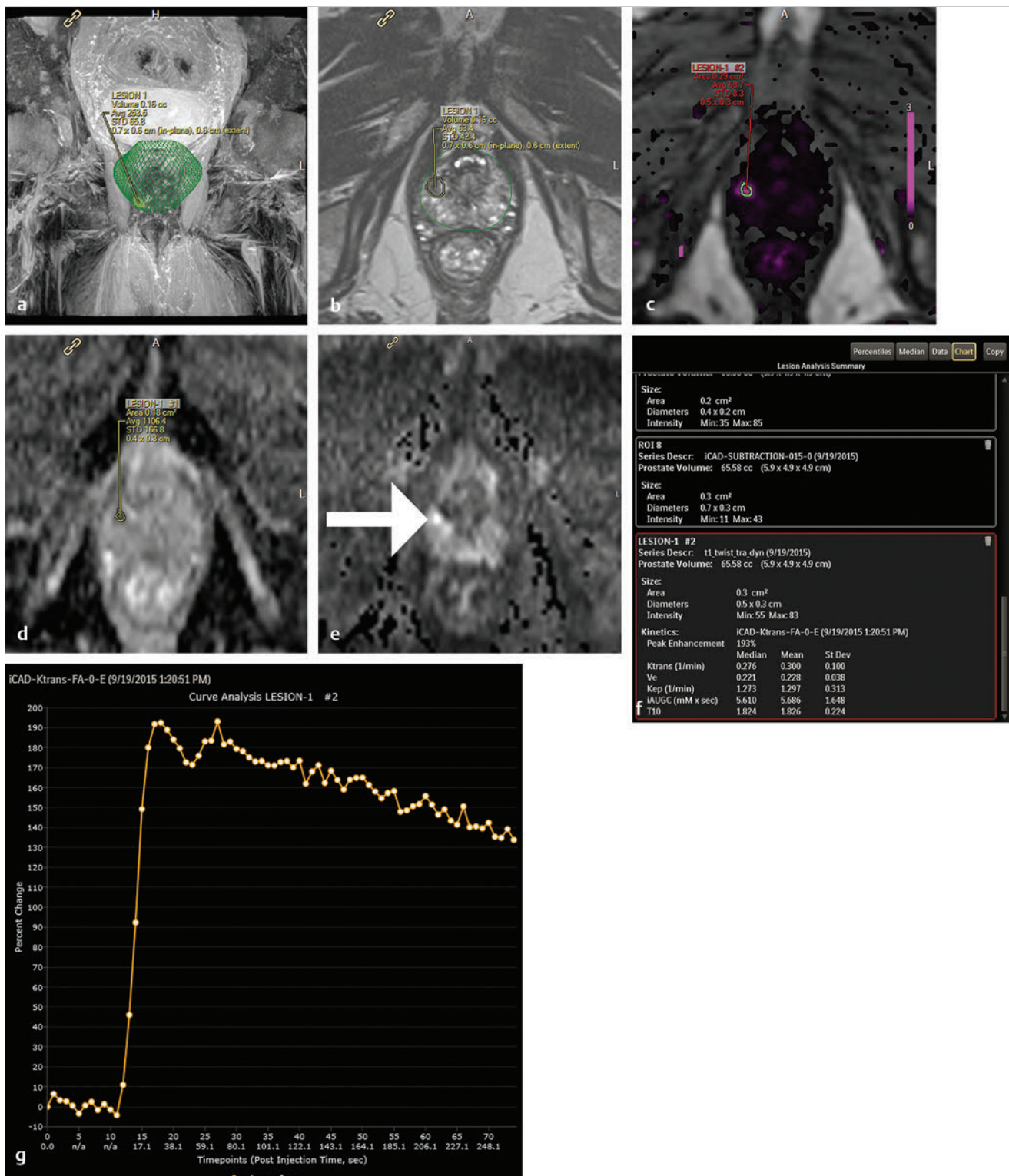


Fig. 9.3 Prebiopsy MRI for prostate cancer. A 73-year-old man presented with an increasing prostate-specific antigen level and three prior negative biopsies. Prebiopsy MRI was performed on a 3-T MRI scanner. There is a small right peripheral zone apex lesion located at the 9:00 o'clock position in the transverse plane at 60% of the prostate's craniocaudal distance from the apex, as indicated on the image in which both the prostate and the lesion are segmented (a). The lesion shows homogeneous hypointense T2 signal with irregular margins (b) and focal intense early enhancement on the K^{trans} map (c). The lesion also demonstrates restricted diffusion, with very low apparent diffusion coefficient (d) and focal markedly increased diffusion-weighted imaging signal (e). Quantitative perfusion kinetics are also summarized (f) with the associated time-intensity curve (g). Overall, the lesion was assigned a PI-RADS v2 assessment category 4 (high probability of clinically significant cancer).

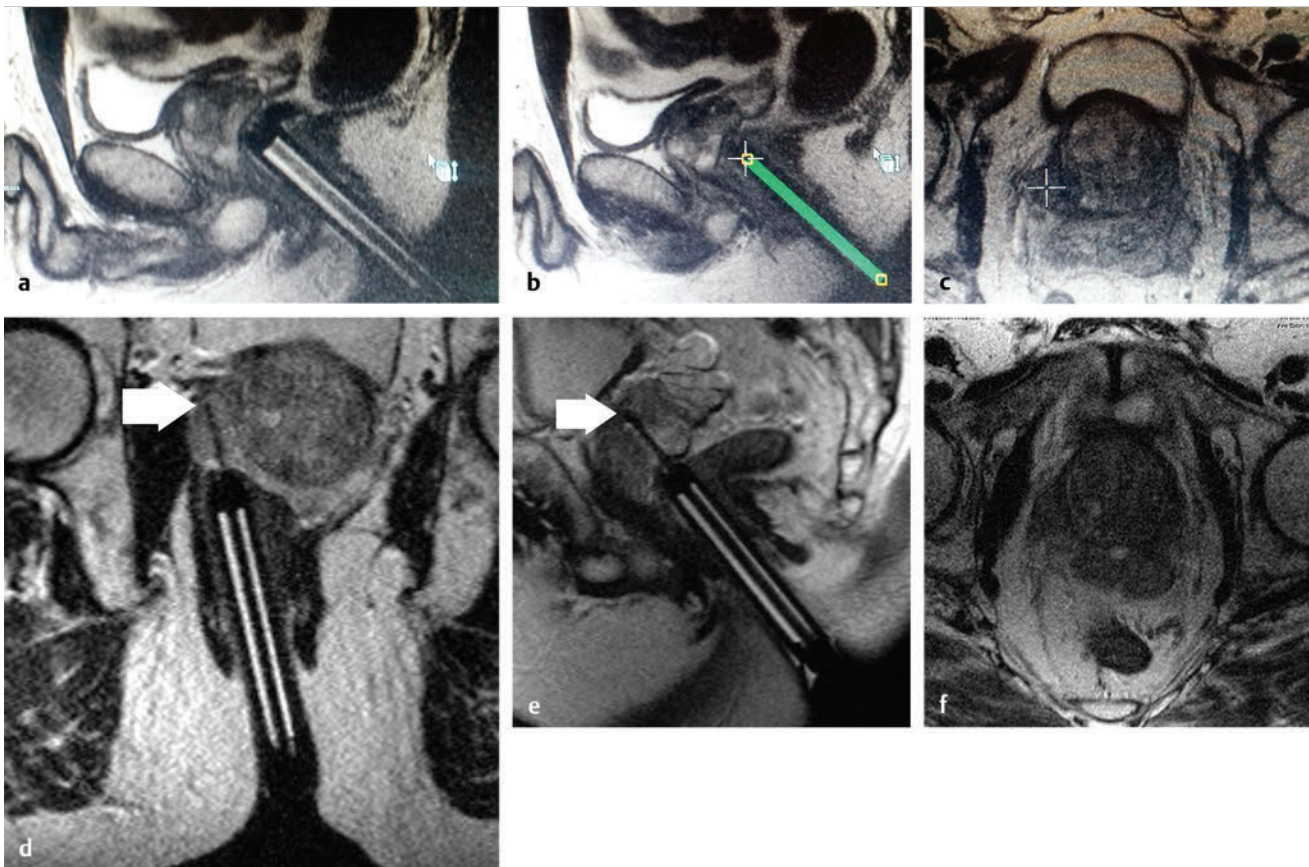


Fig. 9.4 MRI in-bore biopsy. (a) Placement of the biopsy-needle guide. T2-weighted sagittal image demonstrates proper transrectal positioning of the needle guide. (b) Calibration of the biopsy needle guide. T2-weighted sagittal image shows the calibration marker (x) as well as a green bar indicating proper alignment. The coordinates obtained from the calibration will be used as the origin of the polar coordinate system that is used for spatial localization during the biopsy. (c) Target localization. T2-weighted axial image shows placement of the calibration marker over the suspicious prostate lesion. The computer calculates the polar coordinates of the lesion with respect to the origin determined in the prior step. (d,e) Target sampling. T2-weighted axial and sagittal images confirm the position of the biopsy needle within the lesion (white arrows, needle tip). Multiple core biopsies are obtained from different parts of the lesion. In this case, 6 cores were obtained. (f) Postbiopsy appearance of the prostate. Gradient-echo (GRE) image demonstrates no significant hemorrhage.

- Prophylactic antibiotics for gram-negative bacilli (such as *E. coli*).⁴⁴
 - Ciprofloxacin 500 mg by mouth twice a day for 5 days prior to biopsy.
 - Ciprofloxacin 400 mg IV, Metronidazole 500 mg IV, and a 3rd generation cephalosporin (Ceftriaxone 1000 mg intramuscularly (IM) or IV) at the time of the procedure.
- Conscious (moderate) sedation, although not required, to increase patient comfort and decrease motion artifacts.
 - Midazolam 1 mg IV and fentanyl 50 mcg IV.
- Rectal gel and lidocaine
- Nerve-block may be performed, although it is usually not needed.

Procedure

1. Once appropriate staff is available and after an equipment check has been performed, informed consent is obtained from the patient, during which the benefits, risks, and alternatives are reviewed. An IV line is placed prior to the procedure. The patient is then brought into the MRI suite and positioned prone in the gantry with arms above his

head. A “time-out” is performed, during which the patient, the procedure, and the site of the procedure are confirmed.

2. Initial images are obtained with a transrectal biopsy guide in place (multiplanar T2WI; optional DWI) to re-identify the target (► Fig. 9.4).
3. Biopsy-guide calibration is then performed, using calculations based on the location of the needle guide (► Fig. 9.4b).
4. Target localization is next performed, which involves calculation of the coordinates for the areas of interest using dedicated planning computer software (► Fig. 9.4c).
5. The location and direction of the needle guide are adjusted according to the planning software, using the calculations from the guide and target locations. The guide is re-imaged using sagittal and oblique axial/coronal T2W images to confirm adjustment of the needle guide, and the correct core biopsy needle length and spacer are chosen.
6. The biopsy device is passed through the guide, and a core is obtained. The position is confirmed using a T2W image showing the biopsy needle in the target (► Fig. 9.4d; ► Fig. 9.4e). The midline urethra must be avoided.

Table 9.1 Pathology report from direct in-bore MRI-guided biopsy reveals high-grade adenocarcinoma in all 6 cores obtained from lesion. (PSA, prostate-specific antigen; yo M; year-old man.)

PATHOLOGY REPORT	
SPECIMEN(S): A. RIGHT BASE/MIDGLAND PERIPHERAL ZONE X 6	
CLINICAL INFORMATION:	
73 yo M with three negative prior biopsies. Elevated PSA.	
FINAL DIAGNOSIS:	
A1. PROSTATE, RIGHT BASE PERIPHERAL ZONE/MIDGLAND (BIOPSY):	
<ul style="list-style-type: none"> Prostatic adenocarcinoma, Gleason grade 4 + 4 = 8/10, involving multiple fragmented cores, measuring 8 mm, occupying 70% of biopsy tissue No perineural invasion 	
A2. PROSTATE, RIGHT BASE PERIPHERAL ZONE/MIDGLAND (BIOPSY):	
<ul style="list-style-type: none"> Prostatic adenocarcinoma, Gleason grade 4 + 4 = 8/10, involving fragmented cores, measuring 1 mm, occupying 20% of biopsy tissue No perineural invasion 	
A3. PROSTATE, RIGHT BASE PERIPHERAL ZONE/MIDGLAND (BIOPSY):	
<ul style="list-style-type: none"> Prostatic adenocarcinoma, Gleason grade 4 + 4 = 8/10, involving multiple fragmented cores, measuring 5 mm, occupying 60% of biopsy tissue No perineural invasion 	
A4. PROSTATE, RIGHT BASE PERIPHERAL ZONE/MIDGLAND (BIOPSY):	
<ul style="list-style-type: none"> Prostatic adenocarcinoma, Gleason grade 4 + 4 = 8/10, involving 2 of 2 cores, measuring 8 mm discontinuously, occupying 70% of biopsy tissue No perineural invasion 	
A5. PROSTATE, RIGHT BASE PERIPHERAL ZONE/MIDGLAND (BIOPSY):	
<ul style="list-style-type: none"> Prostatic adenocarcinoma, Gleason grade 4 + 4 = 8/10, involving fragmented cores, measuring 4 mm, occupying 50% of biopsy tissue No perineural invasion 	
A6. PROSTATE, RIGHT BASE PERIPHERAL ZONE/MIDGLAND (BIOPSY):	
<ul style="list-style-type: none"> Prostatic adenocarcinoma, Gleason grade 4 + 4 = 8/10, involving 1 of 2 cores, measuring 1.5 mm, occupying 15% of biopsy tissue No perineural invasion 	

- Additional samples are taken, as needed, following readjusting of the biopsy needle position.
- Postbiopsy T2W and gradient-echo images (GRE; ► Fig. 9.4f) are suggested to evaluate for complications (e.g., significant bleeding).
- A pathologist evaluates the biopsy cores and prepares a biopsy report (► Table 9.1).

Postbiopsy Patient Care

If conscious sedation is used, the patient is routinely observed for 3 hours, which also allows for immediate postprocedure monitoring for symptoms of complications (bleeding, pain, nausea and/or vomiting, oral-intake tolerance). The patient is then discharged home, usually with an accompanying person. Postprocedural prophylactic antibiotics are suggested (Ciprofloxacin 500 mg by mouth two times per day for 2–5 days after the biopsy).⁴⁴ Follow-up is usually scheduled with the referring physician.

Complications

Transrectal prostate biopsy is usually well tolerated. Minor complications occur in a minority of patients, and major com-

plications are rare.^{45,46} Complications include:

- pain,
- bleeding (hematuria, hemospermia, hematochezia),
- infection (urinary tract infection, prostatitis) (uncommon)
- urinary retention and/or bladder outlet obstruction (uncommon), and
- urethral fistula (very rare).

An insufficient or nondiagnostic biopsy sample is also a potential problem; in which case, a repeat biopsy is suggested.

9.3.4 Transrectal MRI-US Fusion Biopsy Advantages

The advantages of an MRI-US fusion biopsy are that it combines the superior sensitivity of MRI for detecting significant cancer with the widespread availability and ease of use of TRUS; it typically is quicker than direct in-bore MRI biopsy; it does not require utilization of MRI table time; and systematic sampling (if desired) can readily be performed during the same biopsy session.^{11,35,47}



Fig. 9.5 Artemis (Eigen), one of the 5 fusion devices that are currently approved by the U.S. Food and Drug Administration. The device has three major components: (1) a mechanical robotic arm, which provides localization tracking; (2) a computer screen to visualize the fused images; and (3) a computer to perform the calculations involved in coregistering the uploaded MR images with freshly obtained TRUS images.

Disadvantages

The disadvantages of an MRI-US fusion biopsy include that it is technically more complex; fusion accuracy may be compromised by prostate deformation from bladder or rectal filling, patient position, or the presence of US transducer, in turn leading to registration error and missing the suspected lesion; temporal separation between the diagnostic MRI and the biopsy session may allow for interval change; there is no direct visualization of the suspicious lesion or confirmation of needle placement within the lesion; and there is a high cost for the technologies used for software-based fusion (► Fig. 9.5).

Technique and Equipment

After the diagnostic MRI is performed, the patient presents to the outpatient practitioner's office, where the image fusion and the actual biopsy procedure are performed. If software-based fusion is performed, then both additional hardware and

software are required, and an additional planning step is required in advance of the procedure for segmentation of the prostate and the targets. ► Fig. 9.6 illustrates a MRI-US fusion biopsy using a mechanical robotic arm, targeting a PI-RADS v2 assessment category 5 lesion in the left peripheral zone.

Fusion can be achieved in one of two ways: either with or without the assistance of targeting software. In software-based fusion, navigation can be either sensor-based or organ-based.

Cognitive, or mental (without software), fusion

A planning MRI is obtained and suspicious lesions are identified. Then, the suspicious areas are targeted during a TRUS biopsy based on mental visualization by the operator of the lesion and of other anatomical landmarks identified on the planning MRI, in correlation with identification of these landmarks by ultrasound.^{12,17}

Advantages

The advantages of the cognitive approach for the MRI-TRUS fusion biopsy are that it is quick, straightforward, widely available, cheap, requires no additional purchase of technologies for in-bore or software-based targeting, and improves the cancer yield compared to systematic biopsy.

Disadvantages

The disadvantages of the cognitive approach to MRI-TRUS fusion biopsy are that it is unreliable due to potential human error in cognitive fusion, especially for small (< 1 cm) lesions⁴⁸; it requires understanding by the operator of prostate anatomy on both MRI and ultrasound; it requires familiarity by the operator with variable appearance of prostate cancer using mpMRI; and it can be confounded by differences in orientation of the prostate between MRI and ultrasound once the transducer is in place, without any software-based solution in place to correct for such differences.

Electronic fusion (with software)

After the targets are identified from the planning MRI, the stored images are delineated with contours of both the prostate gland and of the targets, using dedicated planning software. These segmented images are then transferred to, and stored on, the fusion system in advance of the biopsy procedure. At the start of the actual biopsy, a three-dimensional (3D) ultrasound acquisition of the prostate is performed, and the prostate is also contoured by the operator on these images (displayed as a stack of two-dimensional (2D) images). Then, the saved 3D contours from the MRI are superimposed (coregistered) to the 3D ultrasound images based on the respective contours from the two modalities. The aligned MRI and US data sets are then used for needle guidance at the time of obtaining the biopsy samples. Coregistration algorithms can be rigid or elastic. Rigid coregistration involves alignment of the MRI and US images by simple rotation and magnification. Elastic coregistration allows for prostate deformation during the procedure and thus is anticipated to provide better fusion reliability.^{12,35,49}

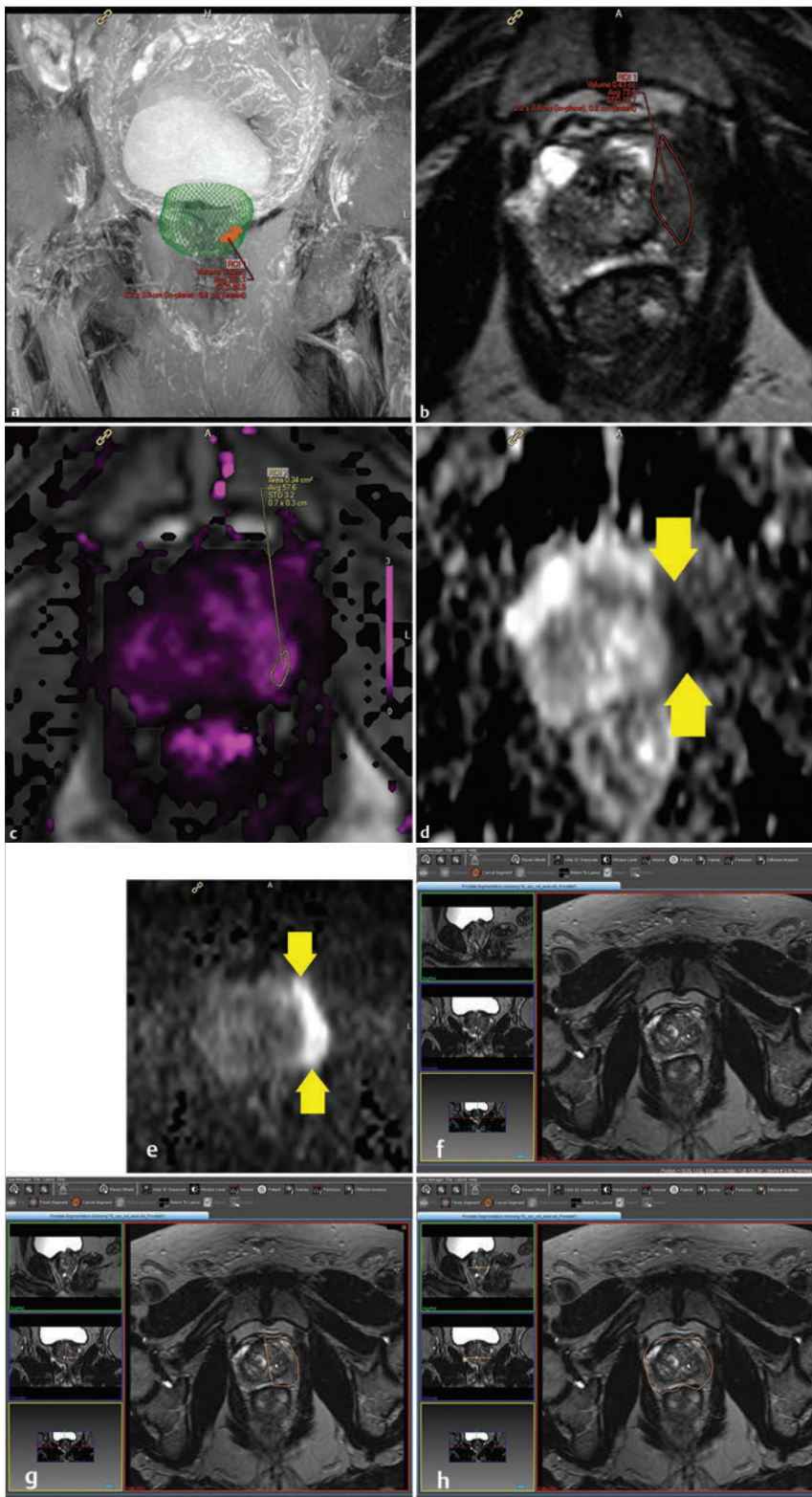


Fig. 9.6 (a) Prebiopsy segmented image of the prostate and the lesion. (b) T2-weighted image shows broad abutment of the lesion with the prostate capsule. (c) Parametric perfusion image generated from dynamic contrast-enhanced acquisition demonstrates intense focal enhancement. (d) The lesion is markedly hypointense on the apparent diffusion coefficient map. (e) The lesion is hyperintense on the high b-value diffusion-weighted image. (f) The MR images are transferred to the three-dimensional workstation. (g) The first prostate contour is drawn by dragging a circle around the prostate. (h) The mouse is released when the contour is complete. (continued on p. 123)

Advantages

The advantages of electronic fusion for MRI-TRUS fusion biopsy are that it is more reliable for targeting than cognitive fusion; contours saved by the fusion software facilitates tracking of biopsy sites across serial biopsies in a given patient.

Disadvantages

The disadvantages of electronic fusion for MRI-TRUS fusion biopsy are that it is more resource intensive than cognitive biopsy; it has a potential for registration error despite the use of software-based fusion; and its false reassurance of having

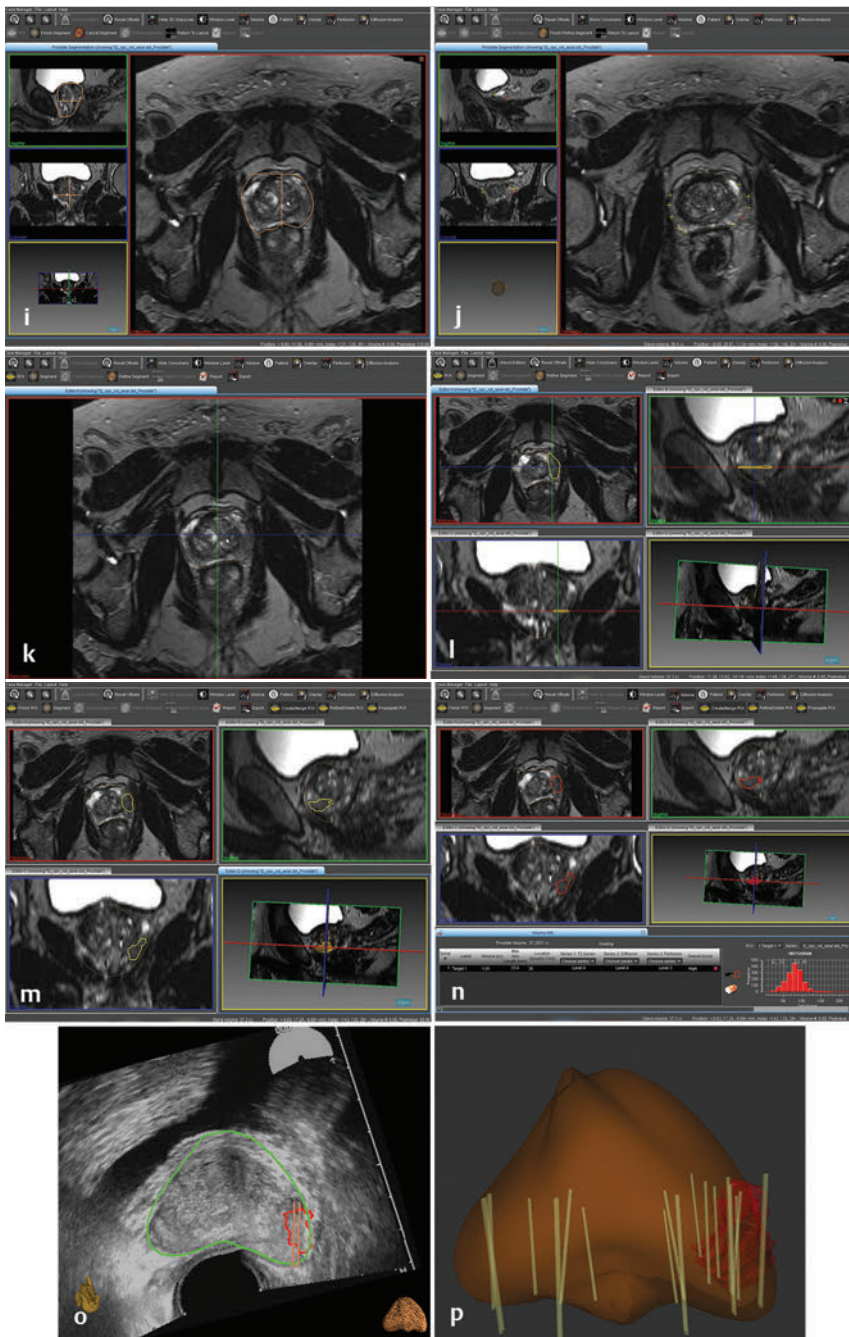


Fig. 9.6 (continued from p. 122) (i) One or more additional contours can be drawn, often in the coronal or sagittal plane. (j) After initial contouring by the operator is completed, the software propagates the contours across the prostate. Wherever the operator deems the contour to not conform to the prostate edge, “seeds” can be placed to refine the contour. (k) The three-dimensional segmentation of the prostate is now complete. (l) The target is contoured using the same method, except that each slice can be contoured for improved fidelity. (m) Upon completion, the ROI of the target (in yellow) can be projected on the contour of the entire prostate (orange). (n) The ROI can then be color-coded to indicate a level of suspicion. (o) Magnetic resonance imaging-transrectal ultrasound-guided fused image provides precise information about the location of the MRI-defined lesion relative to the boundaries of the prostate on US, thereby guiding the operator performing the biopsy. Several core biopsies were obtained from the suspicious area in addition to standard systematic cores obtained during the same biopsy session. (p) Reconstructed prostate image following the procedure depicts the exact location of the obtained biopsy cores (target in red; biopsy cores in yellow). Since the coordinates are saved in the computer, it is possible to re-sample the previously biopsied areas at the time of future biopsy sessions, if needed.

reliably sampled a lesion in situations when the coregistration has in fact failed.

Sensor-based navigation

Sensor-based navigation comprises GPS-like real-time tracking of the TRUS probe in order to provide real-time coordinates and image overlay using elastic fusion. Image registration relative to the tracked probe is then performed based on determination of matching landmark coordinates between the US and MR images.

Advantage

The advantage of sensor-based navigation for computer fusion in MRI-TRUS fusion biopsy is prospective real-time targeting of identified lesions.

Disadvantage

The disadvantage of sensor-based navigation in computer fusion for MRI-TRUS fusion biopsy is that it is sensitive to motion and consequently misregistration given that the patient as well as the prostate are not directly tracked.

Equipment

Two commonly used devices are the Artemis (Eigen, Grass Valley, CA) and the UroNav (Invivo, Inc., Gainesville, FL) systems, although these employ two distinct approaches for sensor-based navigation:

- Artemis uses mechanical tracking of an articulated robotic arm that contains sensors and also holds the TRUS probe throughout the procedure. One study estimated the targeting precision

to be 1.2 ± 1.1 mm.⁵⁰ A learning curve is generally required while gaining familiarity with use of the mechanical arm. In addition, while some operators may consider the mechanical arm to be logistically cumbersome, others may find the stabilization of the probe provided by the arm to be beneficial.

- UroNav uses electromagnetic tracking, in which sensors are embedded into the needle guide attached to the TRUS probe. The location of the sensors is followed in space using a small electromagnetic field source, which is placed in close proximity to the patient. The initial segmentation and coregistration are similar to the robotic arm method. In the guiding phase, the software provides small motion correction of the prostate. Although external electromagnetic tracking may be logistically simpler than incorporation of a mechanical arm and potentially allow for a shorter learning curve, the consequent free-hand nature of this approach may provide less stabilization of the probe in comparison with that achieved by the robotic arm. One study estimated the targeting precision to be 2.4 ± 1.2 mm.⁵¹

Organ-based navigation

Organ-based navigation, in comparison, does not track the TRUS probe, but rather tracks the prostate itself. The 3D shape of the prostate is determined from TRUS and then used as a basis for the MR image overlay.

Advantages

The advantage of organ-based navigation for computer fusion in MRI-TRUS fusion biopsy is that it is less sensitive to motion given direct tracking of the prostate.

Disadvantages

The disadvantages of organ-based navigation for computer fusion in MRI-TRUS fusion biopsy is the retrospective display of targets on the coregistered images and that there is no real-time tracking of targets.

Equipment

The most commonly used FDA-approved device is UroStation (Koelis; LaTronche, France). As in the previous schemes, the MRI segmentation is loaded into the workstation, and

coregistration of the 3D ultrasound and MRI is used in order to track the prostate. However, each time the operator wishes to identify the location of the target relative to the needle guide, a foot pedal is depressed, and the system acquires a new 3D ultrasound data set.

The software performs shape statistics-based semiautomatic prostate surface delineation incorporating elastic 3D organ-based registration, which can correct for prostate deformation from rectal probe insertion. The target is then identified on the images following both these rigid and elastic registration steps. The targeting precision is estimated to be 0.8 ± 0.5 mm.⁵²

The Biojet (Geoscan; Lakewood Ranch, FL) and HI-RVS (Hitachi; Reeuwijk, The Netherlands) systems have also been approved by the FDA. Additional systems are currently in development.

Procedure

1. A prebiopsy MRI is performed and interpreted to identify targets. The images are contoured by the radiologist and then loaded into the fusion device.
2. Transrectal US is performed, from which a 3D reconstruction of the prostate is generated by the fusion device. Software fusion of the MRI and TRUS images is performed.
3. The operator performs the transrectal biopsy, targeting the MRI-identified lesions, under the guidance of the fusion device.
4. Standard systematic cores (if desired) may also be obtained during the same biopsy session.

Postbiopsy Patient Care

The patient is discharged home at the end of the procedure, without further observation being necessary. Otherwise, care is similar to that described for the transrectal MR-guided biopsy approach.

Complications

The complications are similar to those described in 9.3.3 Direct Transrectal MR-Guided Biopsy.

Table 9.2 Summary of targeted biopsy approaches available as of 2015

Biopsy option	Technique	Comments
Direct in-bore MRI guidance	MRI is used to visualize the target and guide the biopsy needle.	Direct, good visualization of lesion, confirmation of needle within lesion. Lengthier procedure. Systematic biopsy less readily performed during same procedure.
MRI-TRUS cognitive fusion	Planning MRI reviewed, then TRUS biopsy obtained by imagining the target location.	Simple, quick, no additional technology investment. Not reliable in targeting the lesion.
MRI-TRUS software-based fusion: Eigen/Artemis Invivo (Phillips)/UroNav Koelis/UroStation Hitachi/Hi-RVS BioJet/Jetsoft	Planning MRI is obtained and uploaded onto a fusion device, which coregisters the images with real-time US of the prostate.	<i>Compared with direct in-bore targeting:</i> more efficient, although potentially greater misregistration. <i>Compared with cognitive fusion:</i> more complex, although more accurate registration.

Abbreviations: TRUS, transrectal ultrasound; US, ultrasound.

9.3.5 Postprocedure MRI Appearance of the Prostate

Biopsy causes bleeding, inflammation, infarction, and fibrosis in the prostate gland, which may persist for months or permanently and mimic prostate cancer on follow-up imaging.⁵³ The suggested interval for follow-up imaging, based on expert opinion, is 6 to 8 weeks. DCE imaging may help distinguish tumor from bleeding, as both the T2 and apparent diffusion coefficient (ADC) signal are decreased after therapy, mimicking cancer, whereas perfusion is often decreased, improving the conspicuity of hypervascular tumors. Post-treatment imaging and management of prostate cancer is discussed in more detail in Chapter 8.

9.4 Conclusion

Magnetic resonance imaging is an effective and powerful tool to detect and evaluate prostate cancer. While its role in image-guided biopsy is evolving, this approach has the potential to become the new standard of care for prostate biopsy as supporting data continues to emerge. Current areas of investigation include optimization of the precision of registration technologies as well as determination of the cost-effectiveness of targeted biopsy. Greater clinical availability of targeting systems, as well as familiarity and training in the use of such systems by practitioners, are required in order to achieve widespread implementation of MRI-targeted prostate biopsy.

Acknowledgement

The authors would like to thank Dr. Steven Raman and Dr. Leonard Marks for representative patient images from biopsies. Special thanks to Jeffrey Hughes for assistance with the MRI and DynaTrim hardware.

References

- [1] American Cancer Society – Prostate Cancer. <http://www.cancer.org/cancer/prostatecancer/>. Published 2015. Accessed May 28, 2015.
- [2] Eggener SE, Scardino PT, Walsh PC, et al. Predicting 15-year prostate cancer specific mortality after radical prostatectomy. *J Urol* 2011; 185(3):869–875
- [3] Andriole GL, Crawford ED, Grubb RL III, et al. PLCO Project Team. Mortality results from a randomized prostate-cancer screening trial. *N Engl J Med* 2009; 360(13):1310–1319
- [4] Schröder FH, Hugosson J, Roobol MJ, et al. ERSPC Investigators. Screening and prostate-cancer mortality in a randomized European study. *N Engl J Med* 2009; 360(13):1320–1328
- [5] Cornud F, Delongchamps NB, Mozer P, et al. Value of mpMRI in the work-up of prostate cancer. *Curr Urol Rep* 2012; 13(1):82–92
- [6] Sonn GA, Chang E, Natarajan S, et al. Value of targeted prostate biopsy using magnetic resonance-ultrasound fusion in men with prior negative biopsy and elevated prostate-specific antigen. *Eur Urol* 2014; 65(4):809–815
- [7] Presti JC. Prostate biopsy: current status and limitations. *Rev Urol* 2007; 9(3):93–98
- [8] Liu W, Laitinen S, Khan S, et al. Copy number analysis indicates monoclonal origin of lethal metastatic prostate cancer. *Nat Med* 2009; 15(5):559–565
- [9] Ahmed HU. The index lesion and the origin of prostate cancer. *N Engl J Med* 2009; 361(17):1704–1706
- [10] Mouraviev V, Villers A, Bostwick DG, Wheeler TM, Montironi R, Polascik TJ. Understanding the pathological features of focality, grade and tumour volume of early-stage prostate cancer as a foundation for parenchyma-sparing prostate cancer therapies: active surveillance and focal targeted therapy. *BJU Int* 2011; 108(7):1074–1085
- [11] Costa DN, Pedrosa I, Donato F Jr, Roehrborn CG, Rofsky NM. MR Imaging-Transrectal US Fusion for Targeted Prostate Biopsies: Implications for Diagnosis and Clinical Management. *Radiographics* 2015; 35(3):696–708
- [12] Cornud F, Brolis L, Delongchamps NB, et al. TRUS-MRI image registration: a paradigm shift in the diagnosis of significant prostate cancer. *Abdom Imaging* 2013; 38(6):1447–1463
- [13] Matlaga BR, Eskew LA, McCullough DL. Prostate biopsy: indications and technique. *J Urol* 2003; 169(1):12–19
- [14] Bjurlin MA, Meng X, Le Nobin J, et al. Optimization of prostate biopsy: the role of magnetic resonance imaging targeted biopsy in detection, localization and risk assessment. *J Urol* 2014; 192(3):648–658
- [15] Murphy G, Haider M, Ghai S, Sreeharsha B. The expanding role of MRI in prostate cancer. *AJR Am J Roentgenol* 2013; 201(6):1229–1238
- [16] Anastasiadis AG, Lichy MP, Nagele U, et al. MRI-guided biopsy of the prostate increases diagnostic performance in men with elevated or increasing PSA levels after previous negative TRUS biopsies. *Eur Urol* 2006; 50(4):738–748, discussion 748–749
- [17] Prando A, Kurhanewicz J, Borges AP, Oliveira EM Jr, Figueiredo E. Prostatic biopsy directed with endorectal MR spectroscopic imaging findings in patients with elevated prostate specific antigen levels and prior negative biopsy findings: early experience. *Radiology* 2005; 236(3):903–910
- [18] Hoeks CM, Schouten MG, Bomers JG, et al. Three-Tesla magnetic resonance-guided prostate biopsy in men with increased prostate-specific antigen and repeated, negative, random, systematic, transrectal ultrasound biopsies: detection of clinically significant prostate cancers. *Eur Urol* 2012; 62(5):902–909
- [19] El-Shater Bosaily A, Parker C, Brown LC, et al. PROMIS Group. PROMIS—Prostate MR imaging study: A paired validating cohort study evaluating the role of multi-parametric MRI in men with clinical suspicion of prostate cancer. *Contemp Clin Trials* 2015; 42:26–40
- [20] Epstein JI, Chan DW, Sokoll LJ, et al. Nonpalpable stage T1c prostate cancer: prediction of insignificant disease using free/total prostate specific antigen levels and needle biopsy findings. *J Urol* 1998; 160(6 Pt 2):2407–2411
- [21] Margolis DJA. mpMRI for Localized Prostate Cancer: Lesion Detection and Staging. *Biomed Res Int* 2014; 2014:684127
- [22] American College of Radiology (ACR) Prostate Imaging-Reporting and Data System version 2 (PIRADSv2). <http://www.acr.org/-/media/ACR/Documents/PDF/QualitySafety/Resources/PIRADS/PIRADS%20V2.pdf>. Published 2015. Accessed May 28, 2015.
- [23] Yacoub JH, Oto A, Miller FH. MR imaging of the prostate. *Radiol Clin North Am* 2014; 52(4):811–837
- [24] Bonekamp D, Jacobs MA, El-Khouli R, Stoianovici D, Macura KJ. Advancements in MRI imaging of the prostate: from diagnosis to interventions. *Radiographics* 2011; 31(3):677–703
- [25] Kirkham APS, Haslam P, Keanie JY, et al. Prostate MRI: who, when, and how? Report from a UK consensus meeting. *Clin Radiol* 2013; 68(10):1016–1023
- [26] Nagarajan R, Margolis D, Raman S, et al. MR spectroscopic imaging and diffusion-weighted imaging of prostate cancer with Gleason scores. *J Magn Reson Imaging* 2012; 36(3):697–703
- [27] Schwartz LH, Basch E. MR/ultrasound fusion-guided biopsy in prostate cancer: what is the evidentiary standard? *JAMA* 2015; 313(4):367–368
- [28] Robertson NL, Emberton M, Moore CM. MRI-targeted prostate biopsy: a review of technique and results. *Nat Rev Urol* 2013; 10(10):589–597
- [29] Kattan MW, Eastham JA, Stapleton AM, Wheeler TM, Scardino PT. A preoperative nomogram for disease recurrence following radical prostatectomy for prostate cancer. *J Natl Cancer Inst* 1998; 90(10):766–771
- [30] Logan JK, Rais-Bahrami S, Turkbey B, et al. Current status of magnetic resonance imaging (MRI) and ultrasonography fusion software platforms for guidance of prostate biopsies. *BJU Int* 2014; 114(5):641–652
- [31] Siddiqui MM, Rais-Bahrami S, Turkbey B, et al. Comparison of MR/ultrasound fusion-guided biopsy with ultrasound-guided biopsy for the diagnosis of prostate cancer. *JAMA* 2015; 313(4):390–397
- [32] Schoots IG, Roobol MJ, Nieboer D, et al. Magnetic Resonance Imaging-targeted Biopsy May Enhance the Diagnostic Accuracy of Significant Prostate Cancer Detection Compared to Standard Transrectal Ultrasound-guided Biopsy: A Systematic Review and Meta-analysis. *Eur Urol*. 2014 Dec 2. pii: S0302-2838(14)01220-2.
- [33] Le JD, Stephenson S, Bruggner M, et al. Magnetic resonance imaging-ultrasound fusion biopsy for prediction of final prostate pathology. *J Urol* 2014; 192(5):1367–1373

- [34] de Rooij M, Crienen S, Witjes JA, Barentsz JO, Rovers MM, Grutters JP. Cost-effectiveness of magnetic resonance (MR) imaging and MR-guided targeted biopsy versus systematic transrectal ultrasound-guided biopsy in diagnosing prostate cancer: a modelling study from a health care perspective. *Eur Urol* 2014; 66(3):430–436
- [35] Sonn GA, Margolis DJ, Marks LS. Target detection: magnetic resonance imaging-ultrasound fusion-guided prostate biopsy. *Urol Oncol* 2014; 32(6):903–911
- [36] Campodonico F, Casarico A, Gavazzi L et al. Cancer detection with TRUS-guided 10-core biopsy of the prostate. an institutional assessment at the first, repeated and surgical specimen biopsy. *Arch Ital Urol Androl* 2006; 78(2):39–43
- [37] Kravchick S, Cytron S, Stepnov E, Ben-Dor D, Kravchenko Y, Peled R. 7 to 10 years' follow-up of 573 patients with elevated prostate-specific antigen (> 4 ng/mL) or/and suspected rectal examination: biopsies protocol and follow-up guides. *J Endourol* 2009; 23(6):1007–1013
- [38] Wefer AE, Hricak H, Vigneron DB et al. Sextant localization of prostate cancer: comparison of sextant biopsy, magnetic resonance imaging and magnetic resonance spectroscopic imaging with step section histology. *J Urol* 2000; 164(2):400–404
- [39] Singh H, Canto EI, Shariat SF et al. Predictors of prostate cancer after initial negative systematic 12 core biopsy. *J Urol* 2004; 171(5):1850–1854
- [40] Rajinikanth A, Manoharan M, Soloway CT, Civantos FJ, Soloway MS. Trends in Gleason score: concordance between biopsy and prostatectomy over 15 years. *Urology* 2008; 72(1):177–182
- [41] Mitterberger M, Aigner F, Pinggera GM et al. Contrast-enhanced colour Doppler-targeted prostate biopsy: correlation of a subjective blood-flow rating scale with the histopathological outcome of the biopsy. *BJU Int* 2010; 106(9):1315–1318, discussion 1318
- [42] Blumenfeld P, Hata N, DiMaio S et al. Transperineal prostate biopsy under magnetic resonance image guidance: a needle placement accuracy study. *J Magn Reson Imaging* 2007; 26(3):688–694
- [43] Carey JM, Korman HJ. Transrectal ultrasound guided biopsy of the prostate. Do enemas decrease clinically significant complications? *J Urol* 2001; 166(1):82–85
- [44] Lee SJ. Infection after transrectal ultrasound-guided prostate biopsy. *Korean J Urol* 2015; 56(5):346–350
- [45] Egbers N, Schwenke C, Maxeiner A, Teichgräber U, Franiel T. MRI-guided core needle biopsy of the prostate: acceptance and side effects. *Diagn Interv Radiol* 2015; 21(3):215–221
- [46] Overduin CG, Fütterer JJ, Barentsz JO. MRI-guided biopsy for prostate cancer detection: a systematic review of current clinical results. *Curr Urol Rep* 2013; 14(3):209–213
- [47] Marks L, Young S, Natarajan S. MRI-ultrasound fusion for guidance of targeted prostate biopsy. *Curr Opin Urol* 2013; 23(1):43–50
- [48] Ukimura O, Desai MM, Palmer S et al. 3-Dimensional elastic registration system of prostate biopsy location by real-time 3-dimensional transrectal ultrasound guidance with magnetic resonance/transrectal ultrasound image fusion. *J Urol* 2012; 187(3):1080–1086
- [49] Valerio M, Donaldson I, Emberton M, et al. Detection of Clinically Significant Prostate Cancer Using Magnetic Resonance Imaging-Ultrasound Fusion Targeted Biopsy: A Systematic Review. *Eur Urol* 2014; 68(1):8–19
- [50] Natarajan S, Marks LS, Margolis DJ et al. Clinical application of a 3D ultrasound-guided prostate biopsy system. *Urol Oncol* 2011; 29(3):334–342
- [51] Xu S, Kruecker J, Turkbey B et al. Real-time MRI-TRUS fusion for guidance of targeted prostate biopsies. *Comput Aided Surg* 2008; 13(5):255–264
- [52] Baumann M, Mozer P, Daanen V, Troccaz J. Prostate biopsy tracking with deformation estimation. *Med Image Anal* 2012; 16(3):562–576
- [53] Thompson J, Lawrentschuk N, Frydenberg M, Thompson L, Stricker P USANZ. The role of magnetic resonance imaging in the diagnosis and management of prostate cancer. *BJU Int* 2013; 112 Suppl 2:6–20

10 MRI and Active Surveillance

Max Kates, H. Ballentine Carter, and Katarzyna J. Macura

10.1 Introduction

Prostate cancer remains the most common internal malignancy among men in the United States, with 241,740 new cases in 2012.¹ Over half of all U.S. men are screened for prostate cancer with prostate-specific antigen (PSA) testing, resulting in a dramatic increase in the incidence of low-risk, indolent cancers.^{2,3} Over 90% of these men are treated with active intervention in the form of radical prostatectomy or radiation therapy, despite the fact that the vast majority will not die of prostate cancer.⁴ The persistence of this overdiagnosis and overtreatment has led to a reexamination of strategies for the detection and treatment of lower-risk prostate cancer.⁵

In the last 20 years, active surveillance (AS) with curative intent has emerged as a safe alternative in carefully selected men with favorable-risk prostate cancer. While early adoption of AS was limited to major academic centers, recent analyses have demonstrated the diffusion of AS programs into the broader community.^{6,7} The primary goals of an AS program are to (1) minimize overtreatment and avoid unnecessary interventions, which negatively impact quality of life, and (2) identify patients originally diagnosed with low-risk cancer who may actually harbor higher-risk disease that was not detected initially or developed after AS was initiated. In successful AS programs, metastasis-free survival is above 99%.⁸

Yet, the vigilance necessary to maintain a rigorous AS program that prevents overtreatment while simultaneously avoiding cancer progression comes at a price. Annual transrectal ultrasound-guided (TRUS-guided) prostate biopsy has been the standard of care not only in diagnosing prostate cancer but also in monitoring patients with known prostate cancer who are on AS. However, annual TRUS-guided biopsies are expensive. In an economic analysis by Keegan et al, cost savings from AS were \$9,944 at 10 years compared with upfront intervention. However, these savings were erased if patients remained on the AS protocol beyond 10 years and TRUS-guided biopsies were performed annually for disease monitoring during this time.⁹ Additionally, 11 to 36% of patients on AS will undergo reclassification of their risk status and subsequent intervention while on AS, increasing the cost of their total prostate cancer treatment compared to upfront surgery or radiation alone.^{10,11,12,13}

Additionally, monitoring via serial prostate biopsy should not be considered a noninvasive management modality. Loeb et al have demonstrated that, following prostate biopsy, up to 25% of men have transient lower urinary tract symptoms and nearly 2% have urinary retention.¹⁴ The most feared complication, however, is febrile bacterial prostatitis, which leads to hospitalization and sepsis in 2 to 3% of patients and has been increasing in recent years due to increasing antimicrobial resistance.^{15,16} While the introduction of fluoroquinolone-resistance testing with rectal swab cultures has lessened postbiopsy-related infections, this testing is not yet routine.¹⁷ Alternative approaches to annual biopsy-based surveillance usually involve monitoring of PSA kinetics. However, such PSA-based schemes lack sufficient sensitivity and specificity to accurately follow these patients.^{15,16,18}

These considerations indicate that AS may serve as the key antidote in preventing the overtreatment of low-risk prostate cancer, although there is a need for strategies to reliably detect higher-risk disease in AS patients while avoiding overly frequent testing and biopsy. In other words, the morbidity and costs saved by avoiding potentially unnecessary surgery must be balanced with the morbidity and costs associated with frequent biopsy, noninvasive testing, and (sometimes) eventual surgery or radiation.

It is in this setting that MRI has gained momentum as a promising strategy to identify clinically significant prostate cancer, select patients who may benefit from AS, and monitor patients on AS protocols.¹⁹ Indeed, MRI is increasingly being employed to improve risk stratification at diagnosis and standardize AS protocols, both of which are crucial to broaden the utilization of AS for favorable risk disease.²⁰

10.2 Current Practices in Active Surveillance

Active surveillance is a management strategy designed to identify prostate cancer patients who are low risk of cancer progression and to intervene with active treatment only when disease progression is identified at follow-up.

Eligibility varies widely across different AS programs, incorporating criteria based on PSA level, PSA density, clinical T stage, Gleason score (GS), number of positive cores, and percentage of cancer involvement in each core.²¹ For example, in the Johns Hopkins cohort, eligibility is defined by the Epstein criteria: clinical stage T1c, PSA density ≤ 0.15 ng/mL/mL, GS ≤ 6 , ≤ 2 biopsy cores with cancer, and maximum of 50% involvement of any core with cancer. This definition is purposefully narrow in order to include only those patients who are least likely to undergo subsequent pathologic reclassification or, worse, tumor spread. However, many protocols, including those from the European Prostate Cancer Research International Active Surveillance (PRIAS) program, University of California San Francisco, and University of Toronto, include clinical stage T2 patients (i.e., patients with a positive digital rectal examination [DRE]).^{22,23,24} Moreover, other protocols include patients with GS = 7 and meeting National Comprehensive Cancer Network (NCCN) criteria for intermediate-risk disease.^{25,26}

Just as eligibility varies widely between AS protocols, so do monitoring strategies. Progression among men on AS is defined by reclassification into a higher-risk group. This reclassification is traditionally determined by progression based on any of a number of factors, including PSA kinetics (i.e., PSA velocity or doubling time beyond a certain threshold), Gleason grade reclassification, tumor volume reclassification (i.e., increased percentage of tumor involvement within positive cores or increased number of cores that are positive), and T stage progression (i.e., palpable abnormality on DRE). More recently, either an increasing tumor size or a more worrisome appearance of the tumor on MRI as well as worsening genetic features have been proposed as triggers for intervention.²⁷ Each

monitoring approach has its own risks and benefits. For example, while utilizing solely PSA kinetics avoids the costs and morbidity that are associated with annual prostate biopsy, such an approach would lead to misclassification in 12% of patients in the Johns Hopkins cohort.²⁸ Thus, PSA kinetics are currently being replaced with MRI as a way to monitor patients on AS and avoid annual biopsy.

Despite differences among protocols, long-term follow-up of AS cohorts has consistently demonstrated overall favorable outcomes. Nonetheless, different eligibility and monitoring strategies confer different risks of disease reclassification, progression to metastasis, and prostate cancer-related death. In a study from the University of Toronto by Klotz et al, patients with low-risk and favorable intermediate-risk (Gleason score 3+4 and/or PSA level of 10–20 ng/mL) disease were enrolled and monitored with a combination of PSA testing every 3 to 6 months and biopsies every 3 to 4 years. This enrollment and monitoring protocol resulted in 28 of 993 patients (2.8%) progressing to metastasis at a median time of 7.3 years after the initial biopsy.²⁹ While the majority of patients died of other causes (particularly cardiovascular disease), 15 patients (1.5%) died from prostate cancer. A disproportionate number of patients who were reclassified and progressed had Gleason score 3+4 disease at the time of enrollment. In comparison, in a Johns Hopkins cohort of 1298 men, enrollment was limited to patients with low-risk and very low-risk (i.e., all having Gleason score 6) disease, and men were monitored with annual biopsy.⁸ In that conservative protocol, metastasis-free survival was 99.4%, with just two deaths from prostate cancer (a 99.9% cancer-specific survival rate).

10.3 Multiparametric MRI of the Prostate: Technical Considerations

Multiparametric MRI (mpMRI) of the prostate combines morphological and functional assessments of intracellular and intercellular environments and tissue perfusion. In patients with small volume low-grade prostate cancer, cellular alterations and associated diffusion and perfusion abnormalities may be subtle and thus difficult to detect using mpMRI. On the other hand, in patients whose presumed low-risk disease was undersampled and in fact harbor intermediate- or high-risk cancer, mpMRI can reliably detect lesions that were not adequately sampled during systematic TRUS-guided biopsy, often in locations such as the anterior transition zone and the apex. These larger-volume, higher-grade cancers are typically visible on mpMRI and display characteristic features: (1) low signal intensity replacing the hyperintense background of normal prostate on T2-weighted imaging (T2WI); (2) restricted diffusion on diffusion-weighted imaging (DWI) due to the high cellular density and extracellular disorganization; (3) alterations in the tumor microvasculature leading to perfusion abnormalities on dynamic contrast-enhanced MRI (DCE-MRI) and (4) elevated choline levels on MR spectroscopic imaging (MRSI). Thus, mpMRI may improve the initial risk stratification of men with newly diagnosed prostate cancer by minimizing the overdiagnosis of insignificant disease and reliably detecting high-risk disease. In a similar fashion, mpMRI may facilitate more reliable monitoring of men enrolled in AS.

In one study, a combination of parameters derived from T2WI, DWI, and DCE-MRI was reported as comprising the optimal strategy for imaging low-risk prostate cancer in the peripheral zone, having a sensitivity and specificity of 85% and 83%, respectively.³⁰ For the detection of low-risk disease in the transition zone, the combination of T2WI and DWI, but without DCE-MRI (which exhibits highly overlapping features with benign prostatic hyperplasia in this zone), offered the highest sensitivity and specificity at 88% and 86%, respectively.³⁰ This combination of MR parameters was more beneficial for the detection of intermediate- and high-risk disease than for the detection of low-risk tumors in the transition zone.³¹ In addition, several studies assessed correlations between MR parameters and tumor grade. For example, Tamada et al evaluated the apparent diffusion coefficient (ADC) derived from DWI as a predictor of prostate cancer grade on histopathology.³² ADC values in peripheral zone tumors exhibited significant negative correlation with tumor Gleason score ($r=0.497$).³² Similarly, Doo et al reported that the mean ADC value of tumors with a Gleason score of 7 or higher ($<800 \times 10^6 \text{ mm}^2/\text{s}$) was significantly lower than that of tumors having a Gleason score of 6 ($>800 \times 10^6 \text{ mm}^2/\text{s}$).³¹ In comparison, quantitative parameters derived from DCE-MRI have not been shown to correlate with the grade or with vascular endothelial growth factor (VEGF) expression as a molecular marker of angiogenesis. However, one DCE-MRI parameter, the contrast agent backflow rate constant (k_{ep}) (washout), was positively correlated with the mean blood vessel count and the mean vessel area fraction estimated from prostate cancer ($r=0.440$ and 0.453 , respectively) in a study by Oto and colleagues.³³ Finally, the diagnostic performance of MRSI for tumor detection and grade prediction has been variable due to the complexity of scanning protocols and postprocessing of spectral data. MRSI tends to show improved performance for higher Gleason score tumors. In a study by Zakian et al, MRSI had higher sensitivity of 89.5% for detection of tumors with a Gleason score of 8 or above compared to a sensitivity of 44.4% for detection of low-grade tumors (Gleason score of 6).³⁴ A modest correlation between metabolite ratio and tumor grade was documented, with the mean choline and creatine-to-citrate ratio (CC/C ratio) discriminating low-grade tumors from higher-grade tumors that would not be eligible for AS.³⁴ There are several technical considerations when imaging men with small-volume prostate cancer. The 3-T whole-body MR scanners are increasing in availability and offer increased signal-to-noise ratio (SNR) and the potential for substantial improvements in spatial, spectral, and temporal resolution. The application of an endorectal coil (ERC) allows further increases in spatial resolution for morphological assessment, which may be especially useful for staging, in temporal resolution for DCE-MRI, as well as in spectral resolution for MRSI.³⁵ Although ERC is recommended at a standard clinical field strength of 1.5 T to obtain a sufficiently high SNR and adequate spatial resolution, the need for an ERC for the detection or localization of prostate cancer has not yet been resolved at the higher-field strength of 3 T. Advocates for imaging with an ERC argue that integrated dual-coil prostate MRI (using both ERC and pelvic coil) detects more cancer foci than nonendorectal-coil MRI, with reported sensitivities of 0.76 and 0.45 and positive predictive values of 0.80 and 0.64 for the dual-coil and nonendorectal-coil approaches, respectively.³⁶ The mean size of detected lesions

with nonendorectal-coil MRI was larger than that of lesions detected by dual-coil MRI (22 mm vs. 17.4 mm, respectively), suggesting more reliable detection of small lesions when using an endorectal coil.³⁶ On this basis, it has been suggested that adding MRI using an ERC to the initial clinical evaluation may be useful for achieving the most accurate assessment of eligibility for an AS program.³⁷ The arguments against the use of ERC include the increased susceptibility artifact and signal intensity inhomogeneity resulting from the nonuniform ERC-sensitivity profile, necessity for proper ERC positioning in order to optimize the anatomical coverage, additional time needed for placement and position verification, patient discomfort and motion artifact, gland deformation, and additional cost. For instance, one study showed that at 3 T, ERC was not necessary to achieve high accuracy for the detection of significant prostate cancer.³⁸ Given ongoing technological advancements along with standardization in prostate imaging reporting through the Prostate Imaging-Reporting and Data System (PI-RADS),³⁹ mpMRI, with its excellent soft-tissue contrast and ability to assess tissue diffusion and perfusion, offers a diagnostic tool to detect and characterize clinically significant prostate cancer in men

managed by AS, including in the anterior gland and apex that are traditionally undersampled on TRUS-guided biopsies. MRSI findings allow individual-based risk stratification that can be employed for better evaluation of candidates for AS, as well as for the triage of AS patients for curative treatment when intermediate- and high-risk tumors are detected.

10.4 MRI Detection of Clinically Significant Disease

Men on AS protocols are thought to harbor favorable-risk disease, such that the role of MRI in these patients is to expose a more worrisome lesion. As traditional TRUS-guided prostate biopsy inadequately samples the anterior portion of the prostate, a major concern in placing low-risk patients on AS is the presence of a missed high-grade anterior lesion.^{40,41}

The location of prostate cancer within the gland affects its detectability on standard biopsy. In this regard, mpMRI has the advantage over TRUS-guided biopsy by allowing a detailed assessment of the entire gland (► Fig. 10.1; ► Fig. 10.2). As

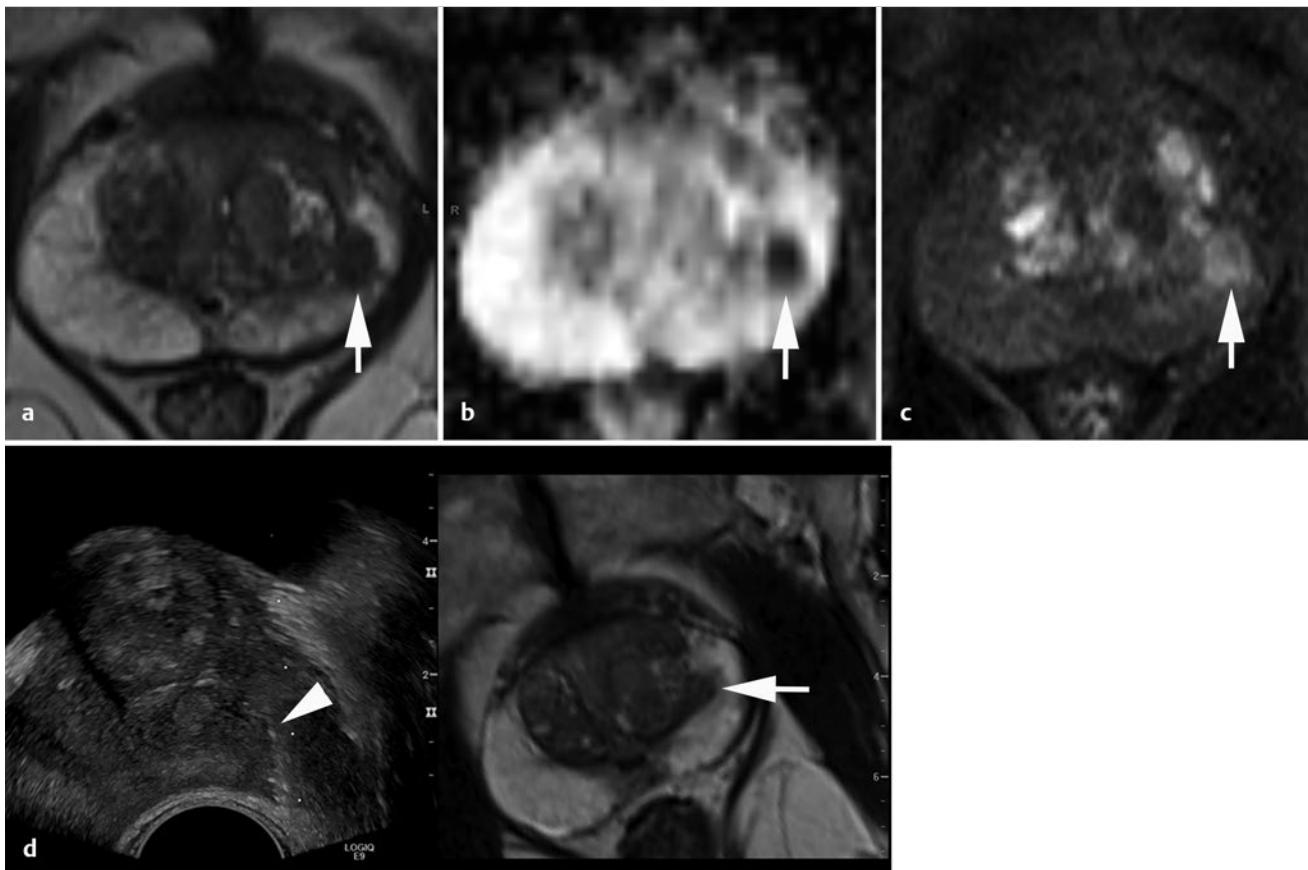


Fig. 10.1 A 71-year-old man with an elevated prostate-specific antigen (PSA) level of 4.83 ng/mL and multiple negative transrectal-ultrasound-guided (TRUS-guided) biopsies. Multiparametric MRI (mpMRI) at 3 T without an endorectal coil demonstrates on axial T2-weighted image (a) a circumscribed, homogeneously moderately hypointense 10-mm lesion (arrow) in the left mid-peripheral zone. On the apparent diffusion coefficient map (b), the lesion is markedly hypointense (arrow). On dynamic contrast-enhanced MRI (c), there is focal early enhancement (arrow) corresponding to (a) and (b). Based on mpMRI, this lesion is scored as PI-RADS 4 (clinically significant cancer is likely to be present). A targeted biopsy with MRI-TRUS fusion (arrow) was performed (d) on a GE Logiq E9 system (GE Healthcare, Milwaukee, WI), demonstrating the MRI lesion to harbor tumor with Gleason score 4 + 4 = 8 involving 2 cores (30%, 40%). Note axial TRUS (left) and MR (right) images displayed side by side following anatomical co-registration with the biopsy needle (arrowhead) in the target lesion on the TRUS image.

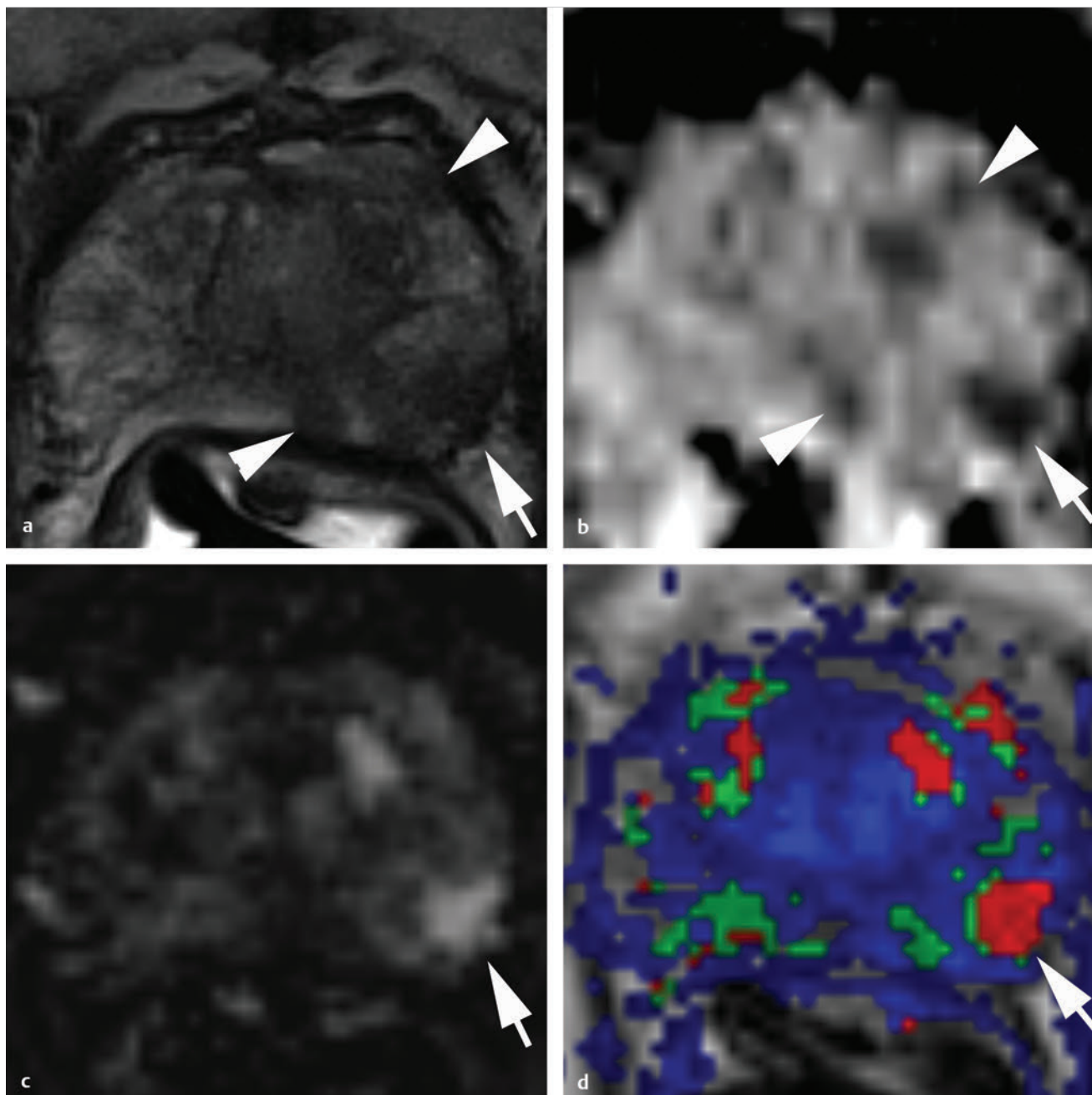


Fig. 10.2 A 72-year-old man with a prostate-specific-antigen (PSA) level increase from 3.0 to 4.5 ng/mL and standard 12-core transrectal ultrasound-guided (TRUS-guided) biopsy showing tumor with Gleason score 3 + 3 = 6 in 5% of 1 core from the right base, as well as high-grade prostatic intraepithelial neoplasia in 3 other cores and atypical glands in 1 core from the left apex. Based on the TRUS-guided biopsy results, the patient has very low-risk prostate cancer and was deemed a candidate for active surveillance. However, the patient was anxious and multiparametric MRI (mpMRI) was performed. mpMRI at 3 T with an endorectal coil shows on axial T2-weighted image (a) multiple hypointense foci (*arrowheads*) as well as a dominant 10-mm hypointense lesion (*arrow*) in the posterolateral left peripheral zone. The index lesion (*arrow*) abuts the capsule of the prostate with capsular irregularity and thus is at risk for extraprostatic tumor extension. On the apparent diffusion coefficient (ADC) map (b) all lesions are markedly hypointense (*arrowheads*), and the index lesion (*arrow*) exhibits an ADC value $< 800 \mu\text{m}^2/\text{s}$ while the neighboring peripheral zone exhibits ADC values above $1400 \mu\text{m}^2/\text{s}$. On dynamic contrast-enhanced MRI (DCE-MRI) (c), the index lesion shows early enhancement (*arrow*). The color-coded DCE-MRI (d) illustrates abnormal perfusion (red) in the dominant peripheral zone lesion (*arrow*) and within the additional lesions. Based on mpMRI, a multifocal prostate cancer was suspected with a score of PI-RADS 5 (clinically significant cancer is highly likely to be present). Patient underwent robot-assisted laparoscopic radical prostatectomy that showed a dominant Gleason score 4 + 3 = 7 tumor in the left lateral and posterolateral peripheral zone. There was nonfocal extraprostatic extension and microscopic left seminal vesicle invasion. Surgical margins were negative. The case illustrates the role of mpMRI in reclassifying patients who may be erroneously categorized as having low-risk disease due to undersampling of high-risk tumor on standard biopsy.

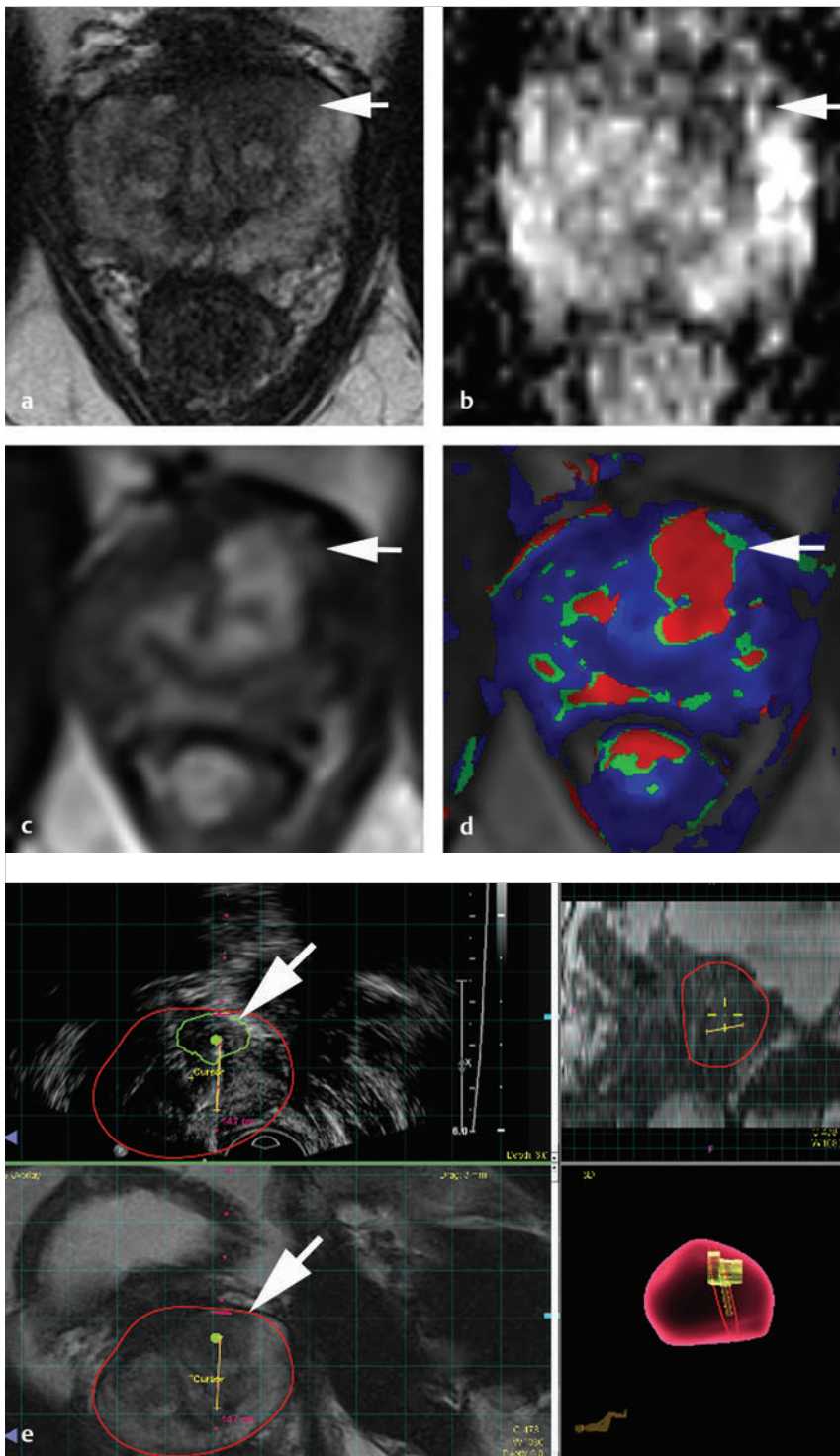


Fig. 10.3 A 65-year-old man with a slowly rising prostate-specific antigen level over 4 years from 2.98 to 6.95 ng/mL and with a negative transrectal ultrasound-guided (TRUS-guided) biopsy. Multiparametric MRI (mpMRI) at 3 T without an endorectal coil demonstrates on axial T2-weighted image (a) a noncircumscribed, moderately hypointense 16-mm lesion (arrow) in the left anterior transition zone. On the apparent diffusion coefficient map (b), the lesion is markedly hypointense (arrow). On dynamic contrast-enhanced MRI (DCE-MRI) (c), there is focal early enhancement (arrow) corresponding to (a) and (b). The color-coded DCE-MRI (d) shows abnormal perfusion (red) in the left anterior transition zone lesion (arrow) extending to the anterior prostate margin and appearing asymmetric when compared to the enhancement within the right transition zone. Based on mpMRI, this lesion is scored as PI-RADS 5 (clinically significant cancer is highly likely to be present). A targeted biopsy with MRI-TRUS fusion was performed (e) using the UroNav system (Invivo Inc. (Phillips), Gainesville, FL), in which the target lesion (arrow) demonstrated Gleason score 3 + 3 = 6 tumor involving 3 cores (100%, 40%, 5%). Note axial TRUS (top left) and MRI (bottom left) images displayed following three-dimensional volumetric coregistration of TRUS and MRI data-sets (red contours) with the biopsy needle trajectory marked (yellow) in the target lesion (green contour).

previously noted, intermediate-risk prostate cancer can be missed by TRUS-guided biopsy if located in the anterior transition zone (► Fig. 10.3) or at the apex (► Fig. 10.4). In a study by Komai and colleagues, 40% of patients (26 of 65) with a worrisome anterior lesion on MRI had negative prostate biopsies.⁴² These anterior tumors are more likely to be large (> 1 cm), and a subset of these tumors has high-risk features and an increased risk of extraprostatic extension.⁴³

One study evaluated 31 men with anterior predominant tumors on MRI, of whom 14 were on AS and 17 had previous

negative biopsies.⁴⁰ A substantial fraction of patients were reclassified using MRI.⁴⁰ The diagnostic yield of mpMRI for detection of anterior tumors was high, with a positive predictive value of 87%. Once anterior cancers are detected on mpMRI, targeted biopsy of the anterior prostate can be performed (► Fig. 10.3) with a high degree of accuracy, reaching these cancers that are frequently more aggressive than expected clinically.⁴⁰ In a study of MR-guided prostate biopsy in which sampling was directed to the area having the most restricted diffusion on DWI in an effort to detect the highest Gleason

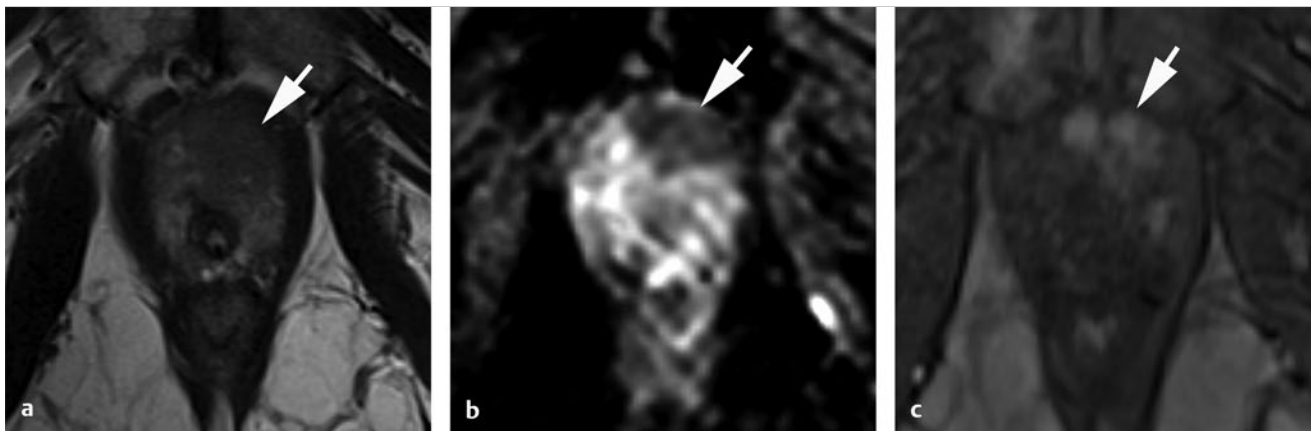


Fig. 10.4 A 71-year-old man with a prostate-specific antigen (PSA) level of 14.6 ng/mL (PSA density = 0.17) and with prior standard transrectal ultrasound-guided (TRUS-guided) biopsy showing Gleason score 3 + 3 = 6 prostate cancer in 20% of 1 core. Patient had urosepsis following the TRUS-guided biopsy. Multiparametric MRI (mpMRI) at 3 T without an endorectal coil demonstrates on axial T2-weighted image (a) a large homogeneously moderately hypointense 28-mm lesion (*arrow*) in the apex, located anterior to the urethra. On the apparent diffusion coefficient (ADC) map (b), the lesion is markedly hypointense (*arrow*), exhibiting an ADC value $< 800 \mu\text{m}^2/\text{s}$, which is suspicious for high-grade prostate cancer undersampled on the TRUS-guided biopsy. On dynamic contrast-enhanced MRI (c), there is focal early enhancement (*arrow*) corresponding to (a) and (b). Based on the mpMRI, this lesion is scored as PI-RADS 5 (clinically significant cancer is highly likely to be present). Given the results from mpMRI and PSA density, this patient was not a candidate for active surveillance and radiation therapy was recommended.

grade tumor, 18 of 22 (81.8%) of tumors contained Gleason grade 4 or 5.⁴⁴

Thompson et al systematically assessed the role of mpMRI in the detection of clinically significant prostate cancer among men with an elevated PSA or an abnormal DRE.⁴⁵ Men underwent saturation biopsy and, when appropriate, targeted biopsy of the prostate via a transperineal approach. MRI was suggestive of cancer (as indicated by a PI-RADS category of 3 through 5) in 66% of patients, and 61% of patients had prostate cancer on biopsy. In identifying clinically significant prostate cancer, the negative predictive value was 100% for high-risk patients and 96% for low-risk patients, while the positive predictive value was 71% for high-risk patients and 28% for low-risk patients. In their analysis, deferring prostate biopsy in men without a worrisome MRI lesion (namely, a lesion with a PI-RADS category of 3 through 5) would have avoided biopsies in 50% of patients. At the same time, only one Gleason score 3 + 4 cancer (and no tumors more aggressive than this) would have been missed.

10.4.1 Risk Stratification Using MRI

Efforts are underway to employ mpMRI to better risk stratify patients being evaluated for an elevated PSA as well as patients with clinically localized prostate cancer. Shukla-Dave et al developed a pre operative nomogram to predict the presence of significant prostate cancer, observing that the addition of mpMRI data increased the nomogram's area under the curve (AUC) from 0.558 to 0.741 in comparison to the use of clinical data alone.⁴⁶

Similarly, Stamatakis et al studied the MRI characteristics of 25 men (within an 85-patient cohort) who initially met Epstein criteria for entry into AS, but who were found to harbor more aggressive tumor on a confirmatory biopsy performed prior to enrollment in an AS program.⁴⁷ They found that three MRI-based factors (number of lesions, lesion suspicion, and lesion density) were associated with a confirmatory biopsy outcome and reclassification.⁴⁷

It should be noted the MRI is largely unable to predict extraprostatic extension with consistency, especially the presence of microscopic extraprostatic extension (EPE). In a study by Roskolnikov et al, 23% of 116 patients with MRIs that were negative for EPE were found to exhibit extraprostatic extension (EPE) on radical prostatectomy (RP).⁴⁸ On multivariate regression analysis, only patient age ($p = 0.002$) and MRI-TRUS fusion-targeted biopsy Gleason score ($p = 0.032$) were independent predictors of the presence of EPE on final RP pathology.

Thus, while MRI can be incorporated into many nomograms, it does not necessarily improve all predictive models, and its use within nomograms must be directed by the available data.

10.4.2 Role of MRI in Patient Selection for Active Surveillance

One area in which mpMRI is an adjunct tool to complement traditional clinical variables is the evaluation of men with low-volume, low-grade tumor who are in an AS program. Of men eligible for AS, a recent meta-analysis by Schoots et al estimated that 70% had positive findings on MRI.⁴⁹ This proportion is similar to the fraction of patients presenting for an initial prostate biopsy who have an abnormal MRI (62%).⁵⁰

Bonekamp et al examined the predictive value of mpMRI in comparison with clinical parameters for disease reclassification in a cohort of 50 men in AS.⁵¹ Morphological, spectroscopic, and perfusion MRI parameters were associated with disease reclassification in this study. mpMRI best predicted disease reclassification in patients who had a suspicious lesion that was 10 mm or greater, and it demonstrated incremental predictive value when used in combination with clinical AS enrollment criteria. A study by Margel et al also investigated the impact of mpMRI (T2WI, DWI, and DCE-MRI) on disease reclassification in AS patients.⁵² In this cohort, the reclassification rate was significantly higher among men with lesions larger than 10 mm

on MRI.⁵² In addition, more than half of the lesions larger than 10 mm (55%) were located in the anterior prostate.⁵²

Turkbey et al compared MRI to conventional scoring systems to identify the appropriate patients for AS and found that the Epstein criteria misclassified 12% of men, whereas MRI misclassified 8% of men.³⁶ The stratification of patients improved with the incorporation of mpMRI into the Epstein criteria. In a study by Borofsky et al, authors reported that among a group of 154 patients clinically eligible for AS, those with no suspicious lesions on MRI had an 8% likelihood of harboring Gleason score ≥ 7 tumor or stage \geq pT3 disease on subsequent RP, whereas patients with a suspicious lesion on MRI had a 48% chance of harboring either of these two.⁵³ In addition, Zakian et al observed that MRI had a far greater sensitivity for the detection of high-grade tumors (89.5%) compared with low-grade tumors (44.4%).³⁴ Indeed, the most important role of MRI at the time of initial AS enrollment is to detect any high-grade cancer that may be present.

Dianat et al assessed the association between mpMRI visibility of prostate cancer at baseline and biopsy outcome in 96 men in an AS program.⁵⁴ Adverse biopsy pathology, in terms of volume and/or Gleason grade, was present in 36.5% of patients. There were no significant differences in terms of the fulfillment of AS criteria at enrollment, PSA level or PSA density, prostate volume, or the number of biopsies between patients with MR-invisible tumor and patients with MR-visible prostate cancer. However, the MR-invisibility of tumor was associated with a lower risk of adverse biopsy pathology: 1 of 12 men (8.3%) with MR-invisible tumor had adverse biopsy pathology compared with 34 of 84 (40.5%) of men with MR-visible tumors. Despite these reassuring results, it must also be recognized that mpMRI may exhibit a false-negative result when histologically sparse higher-grade tumors infiltrate normal glandular tissue or when prostatitis or benign prostatic hyperplasia obscure cancer. In a recent meta-analysis, the pooled sensitivity and specificity of mpMRI for prostate cancer detection was 0.74 (95% confidence interval [CI], 0.66–0.81) and 0.88 (95% CI, 0.82–0.92), respectively.⁵⁵ The negative predictive values varied from 0.65 to 0.94, and positive predictive values ranged from 0.31 to 0.95.⁵⁵

10.4.3 MRI as a Marker of Active Surveillance Outcomes

MRI may have a role in predicting a patient's likelihood of successfully remaining on an AS protocol. Namely, existing data suggests that patients with suspicious lesions on MRI have an increased risk of subsequent disease reclassification compared with patients who have no visible MRI lesion. For instance, Margel et al reported positive and negative predictive values of 83% and 81% for MRI findings in predicting disease reclassification.⁵² Such findings have been confirmed in the Johns Hopkins cohort, in which MRI was found to have a specificity of 0.974 and a negative predictive value of 0.897 in detecting pathologic index lesions.⁵⁶

Lawrentshuk et al reviewed 14 patients on AS who had a predominant anterior tumor on MRI and a positive prostate biopsy while on AS.⁴⁰ In 12 of 14 patients, the MRI findings contributed to the subsequent decision for intervention (namely, surgery or radiation). Disease reclassification occurred in 7 of 14 patients: Gleason score 3 + 4 in 2 of 14 patients, Gleason score 4 + 3 in 3 of 14 patients, and Gleason score ≥ 8 in 2 of 14 patients.

Despite the increasing use of MRI in monitoring patients on AS, significant false-negative rates have also been reported by some investigators. For instance, in a study by Park et al, among 35 patients with no visible lesion on MRI, 14% had unfavorable pathology at the time of RP.⁵⁷ However, technical aspects of the MRI examination must be considered when evaluating such studies. While one study reported a reclassification rate in patients with a normal MRI of nearly 18%, this study employed only T2WI alone, without DWI or DCE-MRI.⁵⁸ In order for mpMRI to become established as the primary mode of monitoring while on AS, the false-negative rate must be reduced through utilization of a modern multiparametric protocol as well as standardization in acquisition parameters and interpretation, so as to optimize the detection of high-grade disease.

10.5 Targeted Prostate Biopsy in Surveillance Patients

Active surveillance protocols seek to delay or avoid overtreatment associated with surgery or radiation for low-risk prostate cancer, while at the same time uncovering any more aggressive tumor that does not warrant therapy. Although annual standard systematic biopsy may be better at detecting aggressive phenotypes compared with biochemical (i.e., PSA-based) data alone, the morbidity and costs associated with annual standard biopsies are substantial. MRI-guided biopsy has thus been proposed as a way to more accurately uncover higher-risk cancer while on AS and thereby potentially avoid routine systematic biopsies in many patients. While direct MRI-guided biopsies can be performed in the MR scanner, fusion of mpMRI with real-time ultrasound to allow for TRUS-guided MRI-targeted biopsy has become the approach having the largest footprint clinically.^{59,60}

Hu et al evaluated the role of mpMRI and MRI-TRUS fusion-targeted biopsies in selecting patients appropriate for AS.⁶¹ Among men meeting the Epstein criteria for clinically localized prostate cancer, combining targeted with non targeted biopsies resulted in reclassification above the Epstein criteria in 36 of 113 patients. However, 11% of high-grade tumors were diagnosed on systematic biopsy but not on targeted biopsy, while 3% of high-grade tumors were diagnosed on targeted biopsy but not on systematic biopsy. These findings suggest that targeted biopsies should be utilized in conjunction with systematic biopsies in order to optimize the identification of high-risk disease.

MRI-TRUS fusion-targeted biopsies have also been evaluated by Mouraviev et al, who reported that in men meeting low-risk criteria and pursuing AS, fusion-guided biopsies improved the detection of prostate cancer compared to TRUS-guided biopsies with only cognitive targeting of MRI lesions (46% vs. 33%, respectively). There were no clinically significant cancers missed by fusion-guided biopsy in this small cohort of men considered for AS.⁶²

Some MRI-TRUS fusion-targeted systems allow for electronic tracking of the spatial positioning of the MRI lesions between targeted biopsy sessions. This novel scheme may allow for more reliable monitoring of known MRI-visible tumor sites at the time of repeat biopsy. Sonn et al evaluated this approach in 53 men on AS undergoing rebiopsy of 74 positive biopsy sites.⁶³ Cancer was more commonly detected in MRI lesions that were resampled using electronic tracking between biopsy sessions

than in nontargeted systematic sites that were positive for cancer (61% vs. 29%, respectively).⁶³ The likelihood of finding cancer on repeat biopsy using the electronic tracking was associated with the length of tumor on the initial biopsy core.⁶³

10.6 Monitoring for Lesion Progression on Serial MRI Examinations in AS

Ultimately, the goal of an optimal AS program may be considered to be to avoid serial biopsies altogether while still reliably monitoring patients for the presence of higher-risk disease. One intriguing possibility would be to monitor patients via the appearance of their tumor on serial MRI examinations (► Fig. 10.5; ► Fig. 10.6; ► Fig. 10.7). This approach would require that stability in a lesion's appearance on MRI safely excludes the development of higher-risk disease, such that progression in a lesion's appearance on MRI can be used to select only a small subset of AS patients for subsequent targeted biopsy. A limited number of studies have explored this concept as of this writing. Walton Diaz et al evaluated 58 patients on AS with at least one follow-up MRI and subsequent biopsy including systematic and targeted cores (median follow-up of 16.1 months), in which 29% of patients exhibited Gleason grade progression. Progression on

serial MRI (considered as either an increase in suspicion level, largest lesion diameter, or the number of lesions) had a PPV and NPV for Gleason grade progression of 53% and 80%, respectively.⁶⁴ The authors suggest that stable findings on serial MRI examinations are associated with stability in Gleason score, and that serial MRI examinations may therefore help reduce the number of biopsies performed in AS patients.⁶⁴ In a study by Rosenkrantz et al of 55 patients undergoing serial MRI examinations at least 6 months apart, an increase in lesion size or suspicion score on MRI achieved higher accuracy than PSA velocity in predicting the presence of high-grade tumor on subsequent biopsy, although sensitivity remained suboptimal.⁶⁵ Given the preliminary nature of such studies, larger prospective investigations are needed to further evaluate the potential role of lesion progression on serial MRI examinations as a means of reducing the number of serial biopsies performed in AS patients.

10.7 Conclusions

Active surveillance has become an important strategy in the management of low-risk prostate cancer. With the goal of minimizing the invasiveness and costs associated with AS, AS protocols are increasingly incorporating MRI both in determining initial eligibility as well as in subsequent monitoring of patients while on AS. Currently, the most strongly established role of

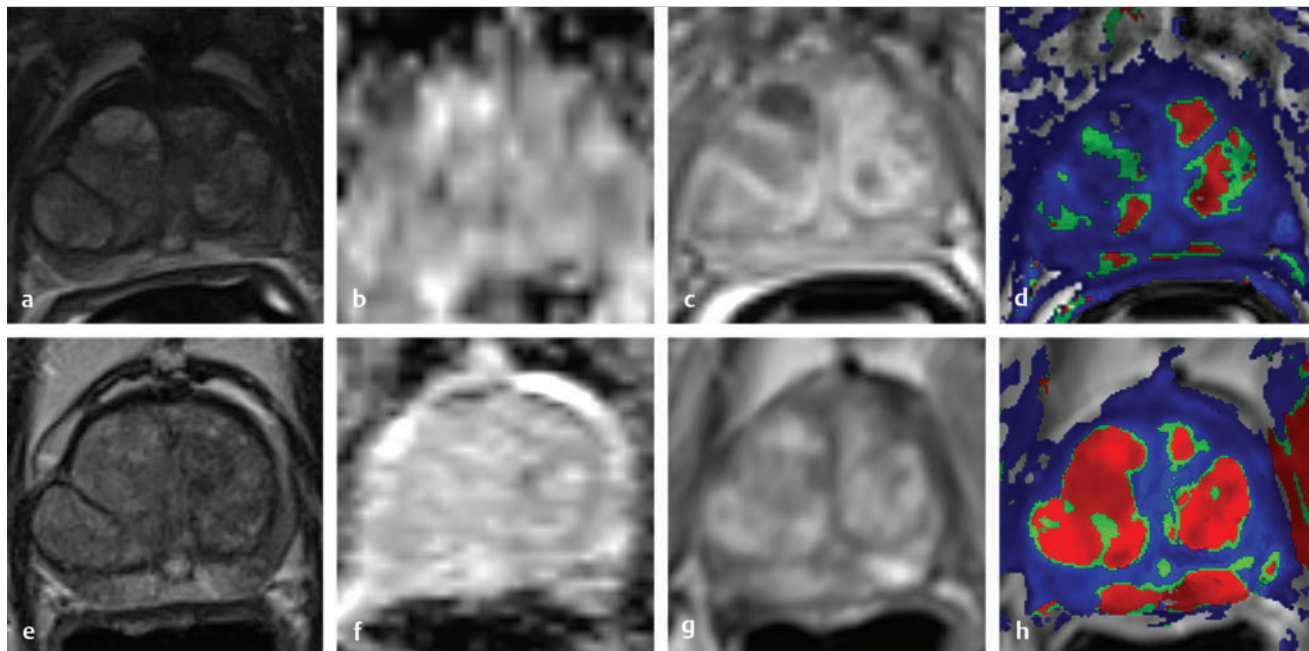


Fig. 10.5 A 75-year-old man with a prostate-specific antigen (PSA) level of 4.4 ng/mL and digital rectal examination revealing a firm nodule in the right apex to mid portion of the peripheral zone without evidence of extension or induration beyond the prostate, and standard transrectal ultrasound-guided (TRUS-guided) biopsy showing Gleason score 3 + 3 = 6 prostate cancer in 20% of 1 core. His initial multiparametric MRI (mpMRI) at 3 T was performed with an endorectal coil (ERC) and demonstrated on axial T2-weighted image (T2WI) (a) diffuse mildly hypointense signal in the peripheral zone without a focal abnormality and circumscribed benign prostatic hyperplasia (BPH) nodules in the transition zone. On the apparent diffusion coefficient (ADC) map (b), there is no focal lesion showing restricted diffusion. On dynamic contrast-enhanced MRI (DCE-MRI) (c,d), there is diffuse mild enhancement of the peripheral zone bilaterally as well as of the BPH nodules. Based on mpMRI, the overall assessment is PI-RADS 2 (clinically significant cancer is unlikely to be present). Given the results from mpMRI and the patient's low-volume, low-grade disease on TRUS-guided biopsy, he was offered active surveillance (AS) despite concern about the findings on the digital rectal examination. Repeat mpMRI was performed at 3 T without an ERC 2.5 years later. The follow-up examination showed no change in the benign appearance of the peripheral and transition zones on T2WI (e), ADC map (f), DCE-MRI (g,h). The stability of mpMRI findings were reassuring and patient remained in the AS program. A follow-up TRUS-guided biopsy after the second mpMRI did not detect any cancer in this patient.

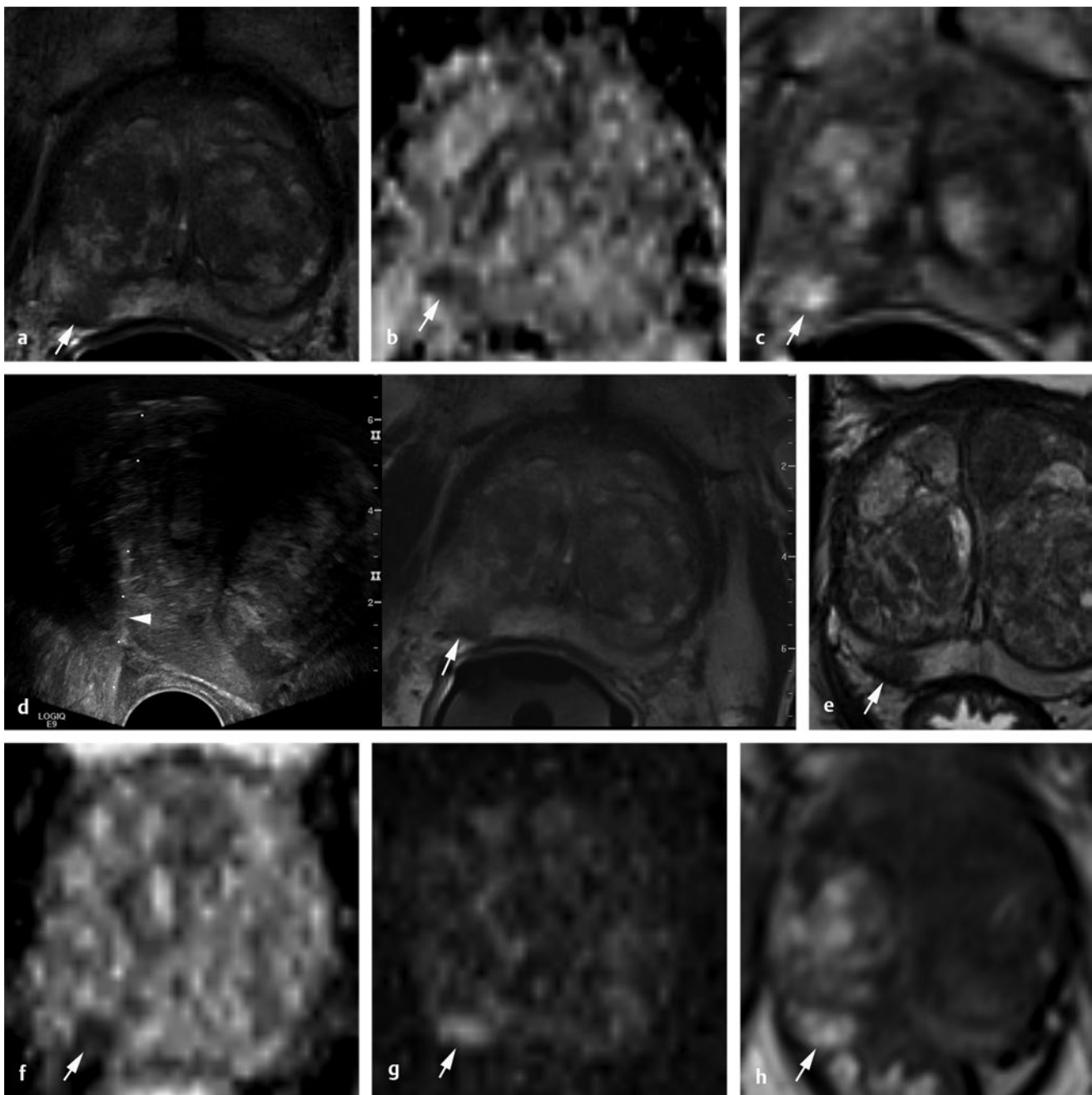


Fig. 10.6 A 75-year-old man with a prostate-specific antigen (PSA) level 11 ng/mL (PSA density = 0.11) and with prior standard transrectal ultrasound-guided (TRUS-guided) biopsy showing Gleason score 3 + 3 = 6 prostate cancer involving 2 cores from the right peripheral zone and 1 core from the left peripheral zone of the midgland. Digital rectal examination demonstrated clinically benign prostate without focal induration or nodularity. The patient was enrolled in an active surveillance (AS) program. His initial multiparametric MRI (mpMRI) at 3 T was performed with an endorectal coil (ERC) and demonstrates on axial T2-weighted image (T2WI) (a) a homogeneously moderately hypointense 10-mm lesion (*arrow*) in the right mid-peripheral zone. On the apparent diffusion coefficient (ADC) map (b), the lesion is markedly hypointense (*arrow*), exhibiting an ADC value $< 800 \mu\text{m}^2/\text{s}$. On dynamic contrast-enhanced MRI (DCE-MRI) (c), there is focal early enhancement (*arrow*) corresponding to (a) and (b). Based on mpMRI, this 10-mm lesion is scored as PI-RADS 4 (clinically significant cancer is likely to be present). Given the results from mpMRI, patient underwent MRI-TRUS fusion-targeted biopsy (d), on a GE Logiq E9 system (GE Healthcare, Milwaukee, WI) that showed Gleason score 3 + 3 = 6 prostate cancer (*arrow*) involving 60% of the core. The biopsy needle traversing the target nodule is seen on the left TRUS image (*arrowhead*) coregistered to the MRI image on the right. Although the Epstein criteria for low-volume, low-grade disease require that there is no more than 50% cancer in any core, this patient wished to remain in the AS program. A follow-up mpMRI was performed at 3 T without ERC two years later. The repeat mpMRI showed no change in the size or appearance of the right peripheral zone nodule on T2WI (e), ADC map and high b-value diffusion-weighted image (f,g), or DCE-MRI (h). The stability of mpMRI findings were reassuring and patient remained in active surveillance program.

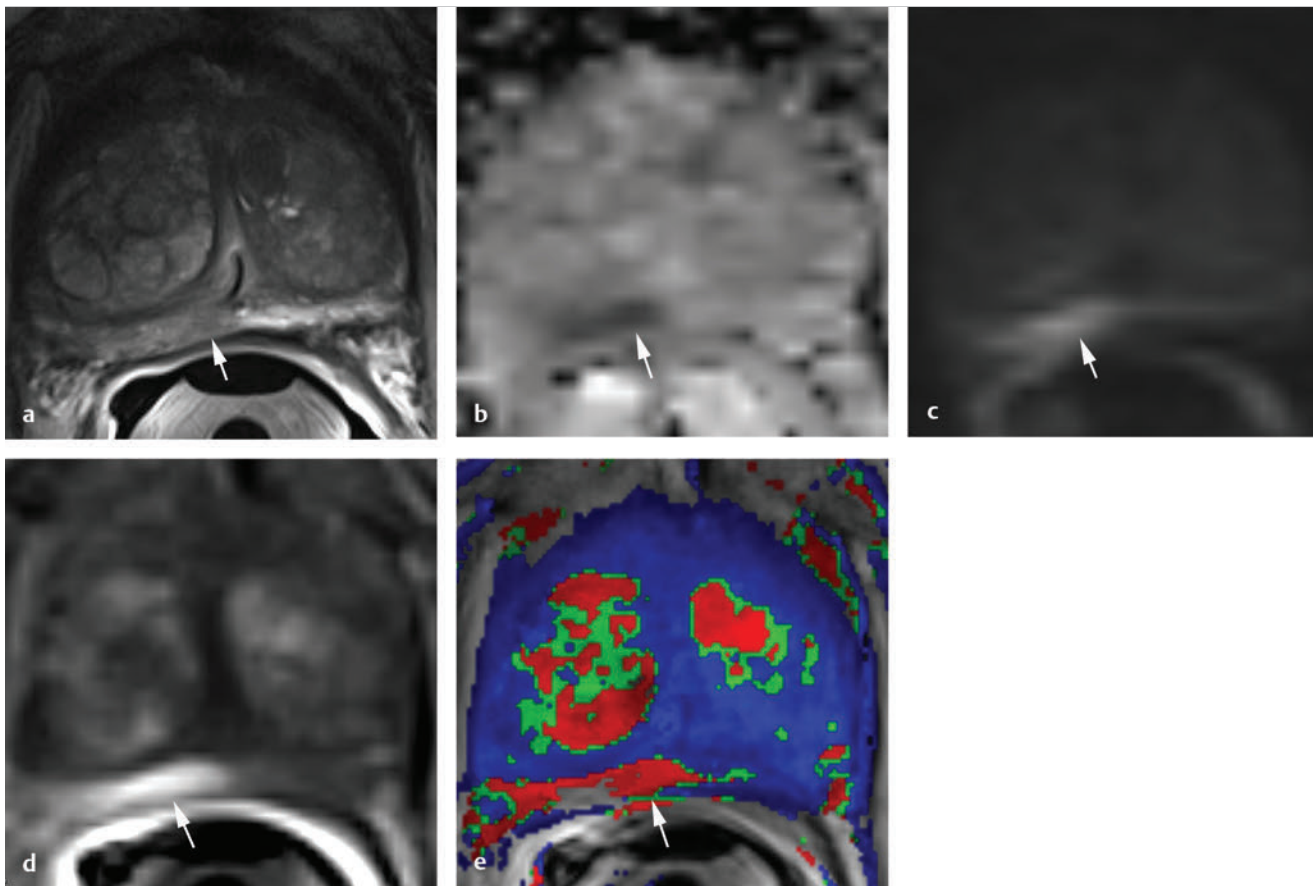


Fig. 10.7 A 70-year-old man with a prostate-specific antigen (PSA) level of 6.3 ng/mL (18% free) (PSA density = 0.05) and with prior standard transrectal-ultrasound-guided (TRUS-guided) biopsy showing Gleason score 3 + 3 = 6 prostate cancer involving 2 cores with up to 10% core involvement. The patient was followed in an active surveillance (AS) program for over 12 years. Digital rectal examination demonstrated a smooth, large prostate without focal nodularity. His initial multiparametric MRI (mpMRI) at 3 T was performed with an endorectal coil (ERC) at year 12 of his expectant management. It demonstrates on axial T2-weighted image (T2WI) (a) a heterogeneously moderately hypointense 9-mm lesion (*arrow*) in the right apex. On the apparent diffusion coefficient (ADC) map (b), the lesion is mildly hypointense (*arrow*), exhibiting an ADC value $< 1000 \mu\text{m}^2/\text{s}$. On high b-value diffusion-weighted image (c) there is mildly hyperintense signal in the lesion (*arrow*). On dynamic contrast-enhanced MRI (DCE-MRI) (d,e), there is focal early enhancement (*arrow*) corresponding to (a), (b), and (c). Based on mpMRI, this 9-mm lesion is scored as PI-RADS 4 (clinically significant cancer is likely to be present). The patient remained in the AS program and was followed with mpMRI 2.5 years later. On a repeat mpMRI performed at 3 T without an ERC, imaging showed on T2WI. (*continued on p. 137*)

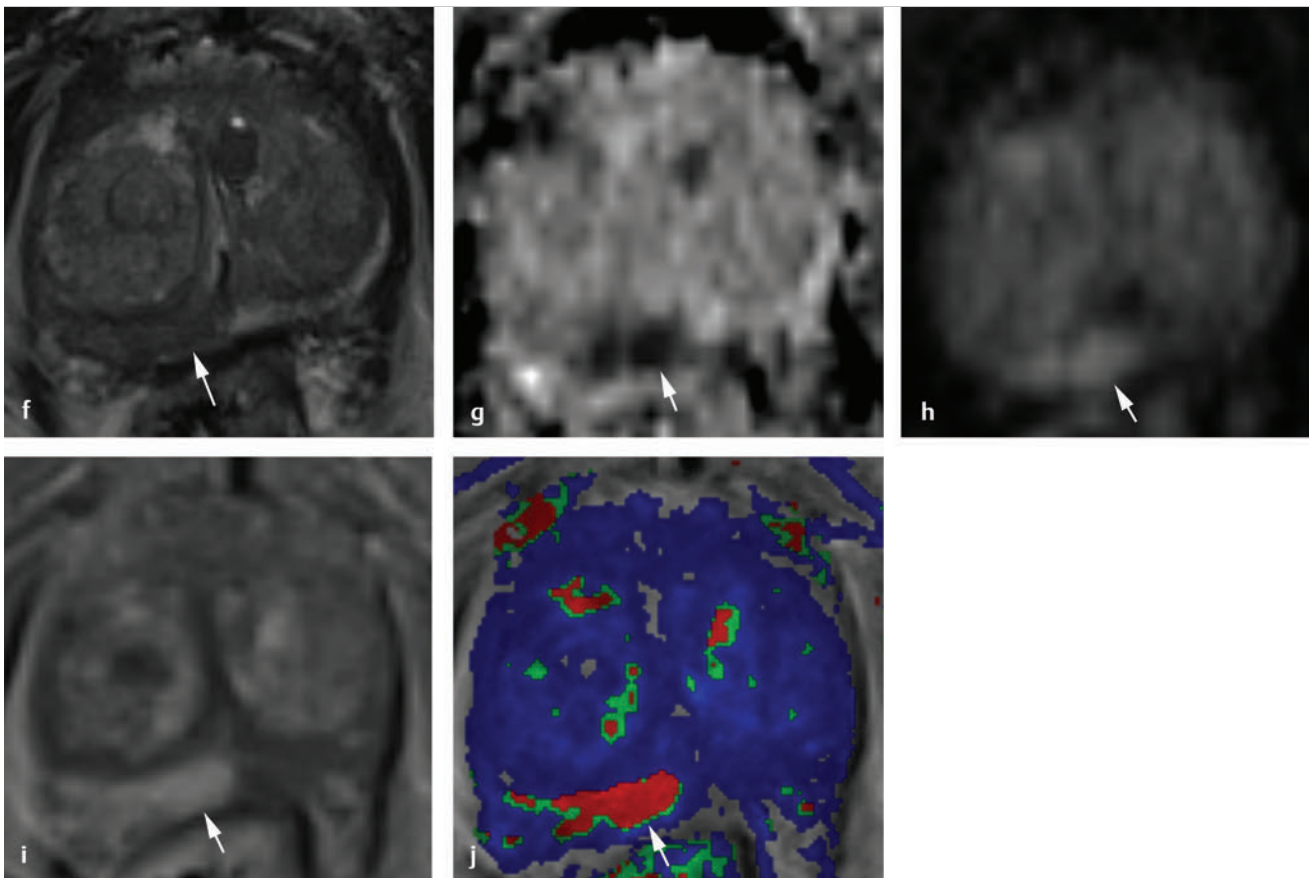


Fig. 10.7 (continued from p. 136) (f) 16-mm dominant nodule (arrow) in the right apex with homogeneous moderately hypointense signal on T2WI, focally markedly hypointense signal (arrow) on ADC map (g) exhibiting value $< 800 \mu\text{m}^2/\text{s}$ and markedly hyperintense signal on high b-value image (h; arrow). On DCE-MRI (i,j) there was focal early enhancement (arrow) corresponding to findings on (f–h). mpMRI was scored as PI-RADS 5 (clinically significant cancer is highly likely to be present) predominantly based on increase in size of the nodule on ADC $> 15 \text{ mm}$. Patient underwent radical prostatectomy, which revealed Gleason score $3 + 4 = 7$ prostate cancer in the dominant nodule in the right lateral apex. Disease was organ confined.

MRI in AS is to identify patients with higher-risk disease that is undersampled by standard biopsy. Future work may facilitate the use of MRI to reduce the number of biopsies performed while on AS. The use of MRI for such purposes requires optimization of the MRI examination to maximize the positive and negative predictive values for high-risk lesions. Rigorous comparative effectiveness studies are also needed to justify the costs associated with routinely performing MRI examinations as part of AS protocols.

References

- [1] Siegel R, Naishadham D, Jemal A. Cancer statistics, 2012. *CA Cancer J Clin* 2012; 62(1):10–29
- [2] Cooperberg MR, Lubeck DP, Meng MV, Mehta SS, Carroll PR. The changing face of low-risk prostate cancer: trends in clinical presentation and primary management. *J Clin Oncol* 2004; 22(11):2141–2149
- [3] Weir HK, Thun MJ, Hankey BF et al. Annual report to the nation on the status of cancer, 1975–2000, featuring the uses of surveillance data for cancer prevention and control. *J Natl Cancer Inst* 2003; 95(17):1276–1299
- [4] Rider JR, Sandin F, Andrén O, Wiklund P, Hugosson J, Stattin P. Long-term outcomes among noncuratively treated men according to prostate cancer risk category in a nationwide, population-based study. *Eur Urol* 2013; 63(1):88–96
- [5] Welch HG, Black WC. Overdiagnosis in cancer. *J Natl Cancer Inst* 2010; 102(9):605–613
- [6] Cooperberg MR, Carroll PR. Trends in management for patients with localized prostate cancer, 1990–2013. *JAMA* 2015; 314(1):80–82
- [7] Womble PR, Montie JE, Ye Z, Linsell SM, Lane BR, Miller DC Michigan Urological Surgery Improvement Collaborative. Contemporary use of initial active surveillance among men in Michigan with low-risk prostate cancer. *Eur Urol* 2015; 67(1):44–50
- [8] Tosoian J, Mamawala M, Epstein J et al. A prospective, longitudinal active surveillance program for favorable-risk prostate cancer: long term outcomes. *J Urol* 2015; 193(4, Suppl):e147
- [9] Keegan KA, Dall'Era MA, Durbin-Johnson B, Evans CP. Active surveillance for prostate cancer compared with immediate treatment: an economic analysis. *Cancer* 2012; 118(14):3512–3518
- [10] Cooperberg MR, Cowan JE, Hilton JF et al. Outcomes of active surveillance for men with intermediate-risk prostate cancer. *J Clin Oncol* 2011; 29(2):228–234
- [11] Klotz L, Zhang L, Lam A, Nam R, Mamedov A, Loblaw A. Clinical results of long-term follow-up of a large, active surveillance cohort with localized prostate cancer. *J Clin Oncol* 2010; 28(1):126–131
- [12] Tosoian JJ, Trock BJ, Landis P et al. Active surveillance program for prostate cancer: an update of the Johns Hopkins experience. *J Clin Oncol* 2011; 29(16):2185–2190

- [13] Soloway MS, Soloway CT, Eldefrawy A, Acosta K, Kava B, Manoharan M. Careful selection and close monitoring of low-risk prostate cancer patients on active surveillance minimizes the need for treatment. *Eur Urol* 2010; 58(6):831–835
- [14] Loeb S, Vellekoop A, Ahmed HU et al. Systematic review of complications of prostate biopsy. *Eur Urol* 2013; 64(6):876–892
- [15] Loeb S, Carter HB, Berndt SI, Ricker W, Schaeffer EM. Complications after prostate biopsy: data from SEER-Medicare. *J Urol* 2011; 186(5):1830–1834
- [16] Wagenlehner FM, van Oostrum E, Tenke P et al. GPIU investigators. Infective complications after prostate biopsy: outcome of the Global Prevalence Study of Infections in Urology (GPIU) 2010 and 2011, a prospective multinational multicentre prostate biopsy study. *Eur Urol* 2013; 63(3):521–527
- [17] Taylor AK, Zembower TR, Nadler RB et al. Targeted antimicrobial prophylaxis using rectal swab cultures in men undergoing transrectal ultrasound guided prostate biopsy is associated with reduced incidence of postoperative infectious complications and cost of care. *J Urol* 2012; 187(4):1275–1279
- [18] Ross AE, Loeb S, Landis P et al. Prostate-specific antigen kinetics during follow-up are an unreliable trigger for intervention in a prostate cancer surveillance program. *J Clin Oncol* 2010; 28(17):2810–2816
- [19] Tseng KS, Landis P, Epstein JI, Trock BJ, Carter HB. Risk stratification of men choosing surveillance for low risk prostate cancer. *J Urol* 2010; 183(5):1779–1785
- [20] Carter HB. Aligning evidence and practice: future research needs to increase utilization of active surveillance for favorable risk prostate cancer. *Curr Opin Urol* 2015; 25(3):277–282
- [21] Loeb S, Bruinsma SM, Nicholson J et al. Active surveillance for prostate cancer: a systematic review of clinicopathologic variables and biomarkers for risk stratification. *Eur Urol* 2015; 67(4):619–626
- [22] Bul M, Zhu X, Valdagni R et al. Active surveillance for low-risk prostate cancer worldwide: the PRIAS study. *Eur Urol* 2013; 63(4):597–603
- [23] Krakowsky Y, Loblaw A, Klotz L. Prostate cancer death of men treated with initial active surveillance: clinical and biochemical characteristics. *J Urol* 2010; 184(1):131–135
- [24] Whitson JM, Porten SP, Hilton JF et al. The relationship between prostate specific antigen change and biopsy progression in patients on active surveillance for prostate cancer. *J Urol* 2011; 185(5):1656–1660
- [25] Barayan GA, Brimo F, Bégin LR et al. Factors influencing disease progression of prostate cancer under active surveillance: a McGill University Health Center cohort. *BJU Int* 2014; 114(6):E99–E104
- [26] Loblaw A, Zhang L, Lam A et al. Comparing prostate specific antigen triggers for intervention in men with stable prostate cancer on active surveillance. *J Urol* 2010; 184(5):1942–1946
- [27] Klotz L. Defining 'progression' and triggers for curative intervention during active surveillance. *Curr Opin Urol* 2015; 25(3):258–266
- [28] Kates M, Tosoian JJ, Trock BJ, Feng Z, Carter HB, Partin AW. Indications for intervention during active surveillance of prostate cancer: a comparison of the Johns Hopkins and Prostate Cancer Research International Active Surveillance (PRIAS) protocols. *BJU Int* 2015; 115(2):216–222
- [29] Klotz L, Vesprini D, Sethukavalan P et al. Long-term follow-up of a large active surveillance cohort of patients with prostate cancer. *J Clin Oncol* 2015; 33(3):272–277
- [30] Delongchamps NB, Beuvon F, Eiss D et al. Multiparametric MRI is helpful to predict tumor focality, stage, and size in patients diagnosed with unilateral low-risk prostate cancer. *Prostate Cancer Prostatic Dis* 2011; 14(3):232–237
- [31] Doo KW, Sung DJ, Park BJ et al. Detectability of low and intermediate or high risk prostate cancer with combined T2-weighted and diffusion-weighted MRI. *Eur Radiol* 2012; 22(8):1812–1819
- [32] Tamada T, Sone T, Jo Y et al. Apparent diffusion coefficient values in peripheral and transition zones of the prostate: comparison between normal and malignant prostatic tissues and correlation with histologic grade. *J Magn Reson Imaging* 2008; 28(3):720–726
- [33] Oto A, Yang C, Kayhan A et al. Diffusion-weighted and dynamic contrast-enhanced MRI of prostate cancer: correlation of quantitative MR parameters with Gleason score and tumor angiogenesis. *AJR Am J Roentgenol* 2011; 197(6):1382–1390
- [34] Zakian KL, Sircar K, Hricak H et al. Correlation of proton MR spectroscopic imaging with gleason score based on step-section pathologic analysis after radical prostatectomy. *Radiology* 2005; 234(3):804–814
- [35] Fütterer JJ, Scheenen TW, Huisman HJ et al. Initial experience of 3 tesla endorectal coil magnetic resonance imaging and 1H-spectroscopic imaging of the prostate. *Invest Radiol* 2004; 39(11):671–680
- [36] Turkbey B, Mani H, Aras O et al. Prostate cancer: can multiparametric MR imaging help identify patients who are candidates for active surveillance? *Radiology* 2013; 268(1):144–152
- [37] Vargas HA, Akin O, Afaq A et al. Magnetic resonance imaging for predicting prostate biopsy findings in patients considered for active surveillance of clinically low risk prostate cancer. *J Urol* 2012; 188(5):1732–1738
- [38] Bains LJ, Studer UE, Froehlich JM et al. Diffusion-weighted magnetic resonance imaging detects significant prostate cancer with high probability. *J Urol* 2014; 192(3):737–742
- [39] American College of Radiology (ACR) Prostate Imaging–Reporting and Data System, versions 2.0. Accessed August 2015. <http://www.acr.org/Quality-Safety/Resources/PIRADS/>.
- [40] Lawrentschuk N, Haider MA, Daljeet N et al. 'Prostatic evasive anterior tumours': the role of magnetic resonance imaging. *BJU Int* 2010; 105(9):1231–1236
- [41] Haarer CF, Gopalan A, Tickoo SK et al. Prostatic transition zone directed needle biopsies uncommonly sample clinically relevant transition zone tumors. *J Urol* 2009; 182(4):1337–1341
- [42] Komai Y, Numao N, Yoshida S et al. High diagnostic ability of multiparametric magnetic resonance imaging to detect anterior prostate cancer missed by transrectal 12-core biopsy. *J Urol* 2013; 190(3):867–873
- [43] Duffield AS, Lee TK, Miyamoto H, Carter HB, Epstein JI. Radical prostatectomy findings in patients in whom active surveillance of prostate cancer fails. *J Urol* 2009; 182(5):2274–2278
- [44] Hambrook T, Hoeks C, Hulsbergen-van de Kaa C et al. Prospective assessment of prostate cancer aggressiveness using 3-T diffusion-weighted magnetic resonance imaging-guided biopsies versus a systematic 10-core transrectal ultrasound prostate biopsy cohort. *Eur Urol* 2012; 61(1):177–184
- [45] Thompson JE, Moses D, Shnier R et al. Multiparametric magnetic resonance imaging guided diagnostic biopsy detects significant prostate cancer and could reduce unnecessary biopsies and over detection: a prospective study. *J Urol* 2014; 192(1):67–74
- [46] Shukla-Dave A, Hricak H, Akin O et al. Preoperative nomograms incorporating magnetic resonance imaging and spectroscopy for prediction of insignificant prostate cancer. *BJU Int* 2012; 109(9):1315–1322
- [47] Stamatakis L, Siddiqui MM, Nix JW et al. Accuracy of multiparametric magnetic resonance imaging in confirming eligibility for active surveillance for men with prostate cancer. *Cancer* 2013; 119(18):3359–3366
- [48] Raskolnikov D, George AK, Rais-Bahrami S et al. The role of magnetic resonance image guided prostate biopsy in stratifying men for risk of extracapsular extension at radical prostatectomy. *J Urol* 2015; 194(1):105–111
- [49] Schoots IG, Petrides N, Giganti F et al. Magnetic resonance imaging in active surveillance of prostate cancer: a systematic review. *Eur Urol* 2015; 67(4):627–636
- [50] Moore CM, Robertson NL, Arsanian N et al. Image-guided prostate biopsy using magnetic resonance imaging-derived targets: a systematic review. *Eur Urol* 2013; 63(1):125–140
- [51] Bonekamp D, Bonekamp S, Mullins JK, Epstein JI, Carter HB, Macura KJ. Multiparametric magnetic resonance imaging characterization of prostate lesions in the active surveillance population: incremental value of magnetic resonance imaging for prediction of disease reclassification. *J Comput Assist Tomogr* 2013; 37(6):948–956
- [52] Margel D, Yap SA, Lawrentschuk N et al. Impact of multiparametric endorectal coil prostate magnetic resonance imaging on disease reclassification among active surveillance candidates: a prospective cohort study. *J Urol* 2012; 187(4):1247–1252
- [53] Borofsky MS, Rosenkrantz AB, Abraham N, Jain R, Taneja SS. Does suspicion of prostate cancer on integrated T2 and diffusion-weighted MRI predict more adverse pathology on radical prostatectomy? *Urology* 2013; 81(6):1279–1283
- [54] Dianat SS, Carter HB, Pienta KJ et al. Magnetic resonance-invisible versus magnetic resonance-visible prostate cancer in active surveillance: a preliminary report on disease outcomes. *Urology* 2015; 85(1):147–153
- [55] de Rooij M, Hamoen EH, Fütterer JJ, Barentsz JO, Rovers MM. Accuracy of multiparametric MRI for prostate cancer detection: a meta-analysis. *AJR Am J Roentgenol* 2014; 202(2):343–351

- [56] Mullins JK, Bonekamp D, Landis P et al. Multiparametric magnetic resonance imaging findings in men with low-risk prostate cancer followed using active surveillance. *BJU Int* 2013; 111(7):1037–1045
- [57] Park BH, Jeon HG, Choo SH et al. Role of multiparametric 3.0-Tesla magnetic resonance imaging in patients with prostate cancer eligible for active surveillance. *BJU Int* 2014; 113(6):864–870
- [58] Guzzo TJ, Resnick MJ, Canter DJ et al. Endorectal T2-weighted MRI does not differentiate between favorable and adverse pathologic features in men with prostate cancer who would qualify for active surveillance. *Urol Oncol* 2012; 30(3):301–305
- [59] Hadaschik BA, Kuru TH, Tulea C et al. A novel stereotactic prostate biopsy system integrating pre-interventional magnetic resonance imaging and live ultrasound fusion. *J Urol* 2011; 186(6):2214–2220
- [60] Muntener M, Patriciu A, Petrisor D et al. Transperineal prostate intervention: robot for fully automated MR imaging—system description and proof of principle in a canine model. *Radiology* 2008; 247(2):543–549
- [61] Hu JC, Chang E, Natarajan S et al. Targeted prostate biopsy in select men for active surveillance: do the Epstein criteria still apply? *J Urol* 2014; 192(2):385–390
- [62] Mouraviev V, Verma S, Kalyanaraman B et al. The feasibility of multiparametric magnetic resonance imaging for targeted biopsy using novel navigation systems to detect early stage prostate cancer: the preliminary experience. *J Endourol* 2013; 27(7):820–825
- [63] Sonn GA, Filson CP, Chang E et al. Initial experience with electronic tracking of specific tumor sites in men undergoing active surveillance of prostate cancer. *Urol Oncol* 2014; 32(7):952–957
- [64] Walton Diaz A, Shakir NA, George AK et al. Use of serial multiparametric magnetic resonance imaging in the management of patients with prostate cancer on active surveillance. *Urol Oncol* 2015; 33(5):202.e1–202.e7
- [65] Rosenkrantz AB, Rice SL, Wehrli NE, Deng FM, Taneja SS. Association between changes in suspicious prostate lesions on serial MRI examinations and follow-up biopsy results. *Clin Imaging* 2015; 39(2):264–269

11 PET/CT and PET/MR Imaging Evaluation of Prostate Cancer

Hossein Jadvar

11.1 Introduction

Imaging evaluation of prostate cancer remains challenging. This relates to the need for patient-specific and risk-adapted imaging strategies that optimize diagnostic yield. The conventional imaging modalities include transrectal ultrasonography (TRUS), computed tomography (CT), multiparametric magnetic resonance imaging (mpMRI), bone scintigraphy, and In-111 capromab pentetide scintigraphy. However, these imaging modalities do not fully meet the clinical needs of the remarkably heterogeneous biological behavior of prostate cancer. Positron emission tomography (PET) when used with various biologically relevant radiotracers is fundamentally suited to interrogate the underlying pathology in a quantitative manner. Over the past several years, there has been a plethora of research and development activity on the potential utility of PET in the imaging evaluation of prostate cancer. Stand-alone PET imaging systems have now largely been replaced by integrated PET/CT, with CT providing the capability for attenuation correction of PET data and hence allowing image quantitation (such as target to background ratio or, most often, mean or maximum standardized uptake value (SUV) in an image region of interest). Computed tomography also provides precise anatomical localization of PET data.

More recently, hybrid PET/MRI systems have become commercially available with the capability to perform mpMRI (including diffusion-weighted imaging [DWI] and dynamic contrast-enhanced imaging [DCE-MRI]), providing high soft-tissue

contrast and lower radiation dose compared to PET/CT.^{1,2} The physiologic information provided by PET (with a particular radiotracer) is coupled with the excellent morphological and, to some extent, functional information provided by MRI. However, this new technology is evolving significantly more slowly than PET/CT, which may be due to multiple factors including ongoing technological challenges with robust attenuation correction, clinical work flow, identification of unique clinical indications, and high acquisition and maintenance costs.³ The aim of this chapter is to review briefly the utility and limitations of PET/CT and the early experience with PET/MRI along the various clinical phases of the natural history of prostate cancer with emphasis on the most used PET radiotracers, including ¹⁸F-fluorodeoxyglucose (FDG), ¹⁸F-NaF, ¹¹C-acetate, and ¹⁸F- or ¹¹C-choline (► Table 11.1).

11.2 Primary Diagnosis and Staging

Prostate cancer is typically considered as a suspected diagnosis after an abnormal digital rectal examination and/or a high or rising serum prostate-specific antigen (PSA) level. The usual diagnostic approach includes standard 10- to 12-core TRUS-guided biopsy. However, the miss rate with TRUS-guided biopsy may be as high as 40% and even higher (up to 70%) in repeat biopsies.^{4,5} TRUS-guided biopsy generally lacks sufficient sensitivity and specificity to detect and localize prostate cancer,

Table 11.1 Summary of select PET radiotracers employed in prostate cancer

Radiotracer	Biological basis	Major potential utility in prostate cancer
¹⁸ F-fluorodeoxyglucose	Glucose metabolism	<ul style="list-style-type: none"> • Detection of aggressive primary tumor (Gleason score > 7) • Assessment of therapy response and prognostication in mCRPC
¹¹ C-acetate	Lipogenesis	• BCR
¹¹ C-choline	Lipogenesis	• BCR
¹⁸ F-fluorocholine	Lipogenesis	• BCR
¹⁸ F-NaF	Bone surface hydroxyapatite matrix	• Bone metastasis
¹⁸ F-FMAU	Cellular proliferation (thymidine analog)	• Primary tumor characterization (investigational)
anti- ¹⁸ F-FACBC	Amino acid metabolism	• BCR
Radiolabeled PSMA targeted agent (e.g. ⁶⁸ Ga-PSMA)	Prostate-specific membrane antigen (external moiety)	<ul style="list-style-type: none"> • Primary tumor detection/localization (investigational) • BCR (investigational)

Abbreviations: mCRPC, metastatic castration-resistant prostate cancer;

BCR, biochemical recurrence;

¹⁸F-FMAU, 2'-deoxy-2'-[¹⁸F]fluoro-5-methyl-1-β-D-arabinofuranosyluracil;

anti-¹⁸F-FACBC, anti-1-amino-3-¹⁸F-fluorocyclobutane-1-carboxylic acid;

PSMA, prostate specific membrane antigen;

⁶⁸Ga-PSMA, Glu-NH-CO-NHlys-(Ahx)-[⁶⁸Ga-HBED-CC] conjugate which binds the motif glutamate-urea-lysine with the chelator HBED-CC.

although ancillary techniques such as elastography and contrast enhancement may be potentially useful.⁶ Image-guided biopsy optimizes the probability of detection of clinically relevant tumors (e.g., aggressive tumors) and reduces the biopsy rate of clinically indolent tumors. Image-guided tumor localization and characterization allows for better informed treatment decision making, including selecting patients with low-grade tumors for active surveillance and selecting some patients with higher-grade tumors for focal therapy.

Multiparametric MRI including DWI and DCE-MRI at 3 T using pelvic phased-array and endorectal coils has offered improved diagnostic performance for the imaging evaluation of the prostate gland.^{7,8} Additionally, some investigators have included magnetic resonance spectroscopy imaging (MRSI) as a component of mpMRI, although this procedure is not routinely employed clinically in view of the need for specialized expertise in its execution and interpretation, longer imaging time, and, probably more importantly, the lack of definite evidence for significant incremental diagnostic contribution to those derived from the other methods in multiparametric MRI.⁹ Prostate cancer is typically characterized by low T2 signal intensity replacing the normally high T2 signal intensity in the peripheral zone. However, this feature has limited sensitivity since some tumors are isointense.⁷ Specificity is also limited since hemorrhage, scar, prostatitis, atrophy, and post-treatment changes may also result in low T2 signal intensity.

Diffusion-weighted imaging measures the brownian motion of free water molecules within the tissue. Prostate cancer generally demonstrates reduced diffusion of water, which has been attributed to the increased cellularity of malignant tissue and the reduction of the extracellular space.¹⁰ The measured parameter that reflects water diffusion is the apparent diffusion coefficient (ADC), which is typically 20 to 40% lower in malignant lesions than in benign lesions or normal prostatic tissue.⁷ DCE-MRI employs kinetic modeling typically with the external iliac artery serving as the arterial input function and a transfer constant K^{trans} that describes the microvascular permeability and blood flow.¹¹ Prostate cancer demonstrates increased tumor vascularity manifested as early, rapid, and intense hyperenhancement followed by rapid washout of contrast material from the tumor in comparison to normal prostate tissue.¹² DCE-MRI may be able to differentiate high-grade prostate cancer from chronic prostatitis, although low tumor volumes and infiltrative prostate cancer may be missed.¹³

A meta-analysis published in 2014 of the accuracy of mpMRI reported relatively high specificity but variable sensitivity for prostate cancer detection.¹⁴ While another systematic review and meta-analysis reported a similar finding, it interestingly also found that MRI-targeted biopsy and standard TRUS-guided biopsy did not differ significantly in overall prostate cancer detection.¹⁵ Nevertheless, MRI is particularly helpful for differentiating between organ-confined disease (stage T1 or T2) and early extraprostatic extension or seminal vesicle invasion (stage T3). The delineation of the extent of local disease can have important ramifications on treatment selection and patient management.

There is an increasing interest in the potential role of PET in prostate cancer imaging.¹⁶ Given the remarkable biological and clinical heterogeneity of prostate cancer, PET would be an ideal imaging tool for noninvasive interrogation of the underlying tumor biology in different phases of this prevalent disease. The

cumulative current experience with PET and the most studied radiotracers, namely ¹⁸F-FDG, ¹¹C-acetate and ¹⁸F- or ¹¹C-choline, suggests a generally limited role for these radiotracers in the imaging-based localization and characterization of primary prostate tumor due to the overlap of uptake among normal tissue, benign prostatic hyperplasia, and prostate cancer.¹⁷

The tumor uptake of FDG is based on the Warburg effect, a cancer-induced change in metabolism characterized by an increased rate of aerobic glycolysis rather than the typical mitochondrial oxidative phosphorylation, leads to complex biological mechanisms involved in malignancy-induced enhanced glucose metabolism.¹⁸ Shiiba et al correlated the FDG uptake level in primary prostate cancer with the biopsy specimen's Gleason score and found that at a cutoff SUV_{max} of 2.8, the sensitivity and specificity for differentiating between biopsy specimens with a summed Gleason score of 5 or less and specimens with a Gleason score of 6 or greater were 62%, and 80%, respectively.¹⁹ Minamimoto et al evaluated FDG PET/CT for detecting prostate cancer in 50 men with elevated serum PSA levels who underwent subsequent prostate biopsy.²⁰ The sensitivity and specificity were 51.9% and 75.7% for the entire prostate gland, 73% and 64% for the peripheral zone, and 22.7% and 85.9% for the transition zone, respectively. The conclusion was that FDG PET/CT might be useful for detection of peripheral zone prostate cancer in men at more than intermediate risk.

A systematic review and meta-analysis published in 2014 of 47,935 men reported a pooled prevalence of 1.8% for incidental high FDG uptake in the prostate gland.²¹ The pooled risk of malignancy with biopsy verification was 62% (95% confidence interval [CI]: 54–71%). In a similar investigation from South Korea that included 47,109 patients, the prevalence of incidental high FDG uptake in the prostate gland was 2.8% with the rate of observed malignancy being related to the serum PSA level (3.8% rate of cancer with PSA less than 2.5 ng/mL, but 60% rate of cancer with PSA greater than 2.5 ng/mL).²² These studies suggest that in some cases FDG PET may be able to characterize prostate tumors of sufficient size and malignancy grade (Gleason score of 7 or higher). In summary, FDG PET/CT is typically not useful for initial staging of disease, although in selected cases with high clinical suspicion for metastatic spread, it may be useful to delineate the extent of the metabolically active disease.

The results for the utility of lipogenesis radiotracers, ¹¹C-acetate and ¹⁸F- or ¹¹C-choline in the imaging evaluation of prostate cancer are generally similar.²³ Acetate is transported across the cellular membrane via monocarboxylate transporter and participates in production of phospholipids in the cellular membranes in a reaction catalyzed by the enzyme fatty acid synthase, which is upregulated in cancer.²⁴ Choline enters the cell via choline transporters and forms phosphorylcholine (in a reaction catalyzed by choline kinase, which is upregulated in cancer) which is then used to generate phosphatidylcholine in the tumor cell membrane.²⁵

A systematic review and meta-analysis of ¹¹C-acetate PET/CT reported a pooled sensitivity of 75.1% (95% CI: 69.8–79.8%) and pooled specificity of 75.8% (95% CI: 72.4–78.9%) for detection of primary prostate cancer.²⁶ Similar to the case with FDG, the uptake level of lipogenesis tracers in benign and neoplastic prostate tissues can overlap, which is fundamentally related to the nonspecificity of these tracers for cancer (► Fig. 11.1).²⁷

Both radiolabeled acetate and radiolabeled choline may be useful for initial staging in patients with intermediate to high risk for lymph node involvement. Haseebuddin et al performed ¹¹C-acetate PET/CT in 107 men with prostate cancer with intermediate to high risk for lymphadenopathy (either Gleason score of 7 and serum PSA level ≥ 10 ng/mL, or Gleason score ≥ 8, or serum PSA level ≥ 20 ng/mL) who were scheduled to undergo radical prostatectomy.²⁸ The sensitivity and specificity for detection of pelvic lymphadenopathy were 68% and 78%, respectively. Patients with positive PET scans had 3.3 times higher risk for therapy failure after surgery. Therefore, in selected intermediate- and high-risk cases, ¹¹C-acetate may provide useful information that

can lead to management change at the time of initial staging.²⁹

The detection of prostate tumor with ¹¹C-choline may depend on tumor configuration, with unifocal cancers detected more often than those that are multifocal or ringlike. Moreover, the extent of actual tumor may not completely overlap the area with abnormal uptake.^{30,31} Scher et al reported a sensitivity of 87% and a specificity of 62% for the detection of primary prostate cancer with histopathologic examination of the resection specimen or biopsy as reference standard.³² However, an Italian group of investigators reported a sensitivity of 66% and specificity of 81% for localization of primary prostate cancer on a sextant histopathologic analysis³³ (► Fig. 11.2). Martorana et al

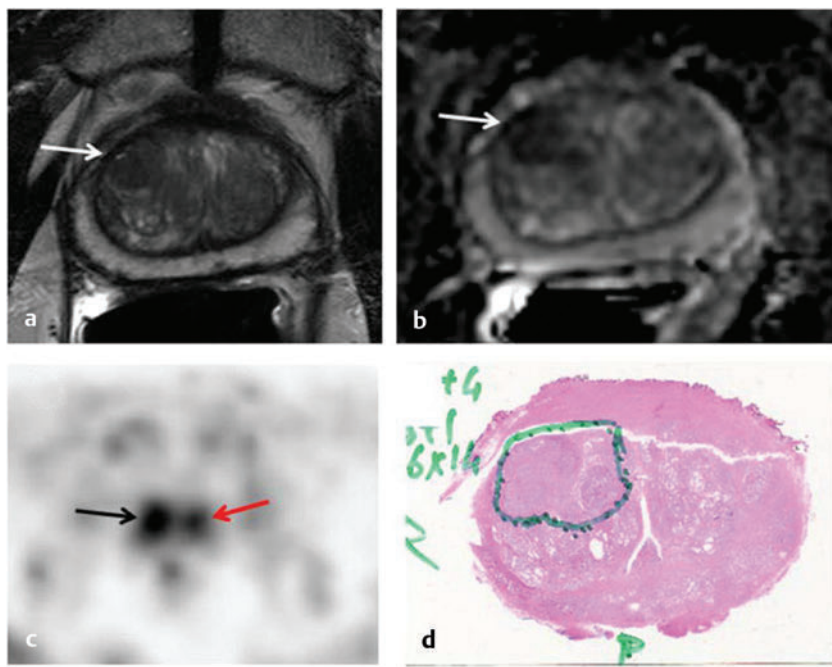


Fig. 11.1 A 69-year-old man with prostate cancer. Axial T2-weighted MRI (a) and apparent diffusion coefficient map (b) show focal low signal intensity in the right midanterior transition zone (white arrows), corresponding to increased ¹¹C-acetate uptake in positron emission tomography (PET) (black arrow) (c) and tumor (Gleason score 4 + 4) on histopathology (outlined in green; d) Focal ¹¹C-acetate uptake in the left transition zone corresponds to a benign prostatic hyperplasia nodule (red arrow) (c). (Reproduced with permission of Mena et al 2012,²⁷ Fig. 3.)

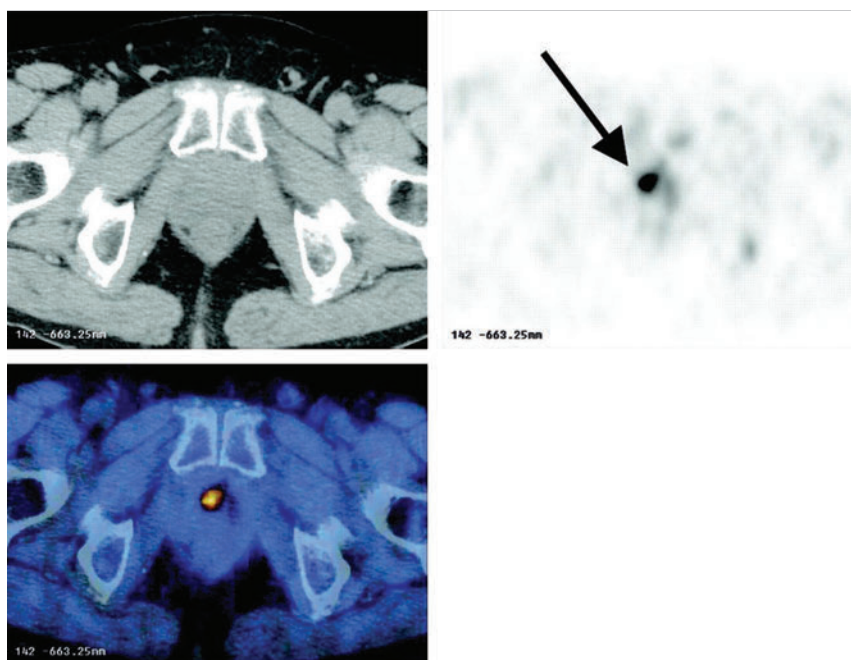


Fig. 11.2 Utility of ¹¹C-choline positron emission tomography-computed tomography-guided (PET/CT-guided) biopsy that confirmed tumor in the anterior transition zone of the prostate in a patient with a prior negative standard systematic 12-core biopsy. Axial CT (top left); ¹¹C-choline PET (top right); and fused ¹¹C-choline PET/CT (bottom left). (Reproduced with permission from Farsed et al 2005,³³ Fig. 4.)

reported a sensitivity of 83% in detection of primary tumor nodules of 5 mm and larger, although the sensitivity for assessment of extraprostatic extension was inferior to MRI (22% for ^{11}C -choline PET vs. 63% for MRI, $p < 0.001$).³⁴ Eschmann et al compared ^{11}C -choline PET/CT with whole-body MRI for staging of prostate cancer with histologic analysis and follow-up as validation criteria.³⁵ The sensitivity and specificity were 97% and 77%, respectively, for ^{11}C -choline PET and 79% and 94% for whole-body MRI. These results suggested that PET and MRI might provide complementary diagnostic information in the initial staging of prostate cancer. Overall, while ^{11}C -choline PET may be helpful in detecting primary prostate cancer, the diagnostic performance may depend on several important factors such as tumor grade, size, and location.³⁶

The potential use of other PET radiotracers in the setting of primary tumor detection and initial staging is unsettled in view of the paucity of published reports. There is one case report of the potential use of ^{68}Ga -labeled ligand of prostate-specific membrane antigen (PSMA) in the initial diagnostic setting.³⁷ However, another recent case report, also using this tracer, has indicated limitations, in particular, false-negative results in the poorly differentiated prostate cancer with neuroendocrine differentiation.³⁸ We recently reported a clinical case example of a patient with elevated serum PSA level of 10.5 ng/mL and a prior negative standard TRUS-guided biopsy who underwent a clinical 3-T multiparametric MRI and a research protocol PET/CT with the thymidine analog cellular proliferation radiotracer ^{18}F -FMAU (2'-deoxy-2'-[F]fluoro-5-methyl-1- β -D-arabinofuranosyluracil). The PET/CT and multiparametric MRI were fused with the TRUS for real-time combined image-based targeting of the biopsy needle to an area with abnormal tracer localization, which on histopathology revealed early malignancy.³⁹

It is anticipated that either through integrated PET/MRI or software-fused PET and MR images of the prostate, there will be clinical utility not only in detection and localization of prostate cancer (for targeted biopsy) but also in image characterization (indolent vs. aggressive) of tumor sites.^{40,41,42,43,44,45} Fusion of imaging data obtained from ^{11}C -acetate PET/CT and DCE-MRI at 1.5T has been shown to provide a competitive advantage over each separate imaging modality alone.⁴⁶ Park et al introduced a combined PET/MRI-derived parameter, the tumor-to-background ratio of each voxel's ^{11}C -choline SUV divided by its ADC, that was noted to be significantly different between prostate cancer with a Gleason score $\geq 3 + 4$ and prostate cancer with a Gleason score $\leq 3 + 3$. The authors suggested that this PET/MRI-derived parameter might be able to characterize prostate lesions.⁴⁷ Image-guided biopsy may be performed by either a direct MRI-guided approach or through dynamic fusion of MRI and TRUS images. Hartenbach et al reported that combined ^{18}F -fluoroethylcholine PET/MRI showed statistically significant higher accuracy in detection of the dominant malignant lesion in the prostate gland when compared to either PET or MRI alone.⁴⁸

Kim et al reported on the diagnostic performance of simultaneous PET/MRI with ^{18}F -fluorocholeline in 30 patients with localized prostate cancer prior to radical prostatectomy.⁴⁹ MRI, ^{18}C -fluorocholeline PET, and combined PET/MRI, all evaluated based on the single simultaneous PET/MRI acquisition, identified the sites of the prostate tumor in 83.3%, 80%, and 93.3% of cases, respectively. The authors concluded that combined

^{18}F -fluorocholeline PET/MRI demonstrated an improved diagnostic performance over either modality alone. Although this study was performed using a simultaneous PET/MRI system, the unique utility of simultaneity was not described. However, in this context, Rosenkrantz and colleagues showed that dynamic analysis of FDG PET data obtained during simultaneous PET/MRI data acquisition might be useful in localization of small prostate tumors.⁵⁰ Wetter et al showed that SUVs obtained from ^{18}F -fluorocholeline PET/MRI were significantly lower than those obtained with PET/CT, probably related to differing attenuation correction schemes.^{51,52,53}

11.3 Biochemical Recurrence and Restaging

Invasive treatment for localized disease (radical prostatectomy or radiation therapy) is done with the intent to cure. However, up to 35% of patients (or higher in select high-risk groups) may experience biochemical recurrence (PSA relapse) within a decade of primary definitive therapy.⁵⁴ Localization of disease in this group of patients is pivotal as it directs appropriate management, which may include salvage therapy (surgery or radiation) for local recurrence and systemic therapy for metastatic disease, or both. Biochemical failure is defined as an increase in serum PSA level with negative standard imaging studies after definitive therapy for primary prostate cancer. The American Urological Association (AUA) defines biochemical recurrence in post-prostatectomy patients as an initial serum PSA level of 0.2 ng/mL or higher, with a second confirmatory level higher than 0.2 ng/mL.⁵⁵ The American Society for Therapeutic Radiology and Oncology consensus definition for biochemical failure after primary external-beam radiation therapy is an increase of 2 ng/mL or more above the nadir PSA level, regardless of hormonal therapy.⁵⁶

In general, FDG PET appears to have a limited role in this clinical setting, although higher PSA levels may be associated with higher probability of detection of metabolically active disease. In one study, FDG PET demonstrated a sensitivity and specificity of 75% and 100%, respectively, for the detection of pelvic lymph node metastases, with validation based on histopathologic examination of the surgically harvested nodes.⁵⁷ We have reported our findings of a prospective investigation on the potential utility of FDG PET/CT and ^{18}F -NaF PET/CT in detection of occult metastases in 37 men with PSA relapse (range, 0.5–40.2 ng/mL) and strictly negative standard imaging studies.⁵⁸ ^{18}F -FDG PET/CT only was positive in 1 patient, ^{18}F -NaF PET/CT only was positive in 8 patients, and both were positive in another 2 patients. Overall, we found a detection rate of 8.1% for FDG PET/CT in the setting of biochemical recurrence. In another investigation, although not specific to prostate cancer, Eiber et al compared whole-body integrated PET/MRI with PET/CT for evaluation of bone lesions.⁵⁹ Given that most metastases from prostate cancer occur in the skeleton and that skeletal metastases are a major source of morbidity in this disease, the detection, localization, and evaluation of extent of osseous lesions by imaging are of prime importance. These investigators found that fully integrated whole-body FDG PET/MRI was superior to PET/CT for anatomical demarcation and localization of bone lesions. It remains to be seen if PET/MRI has a competitive

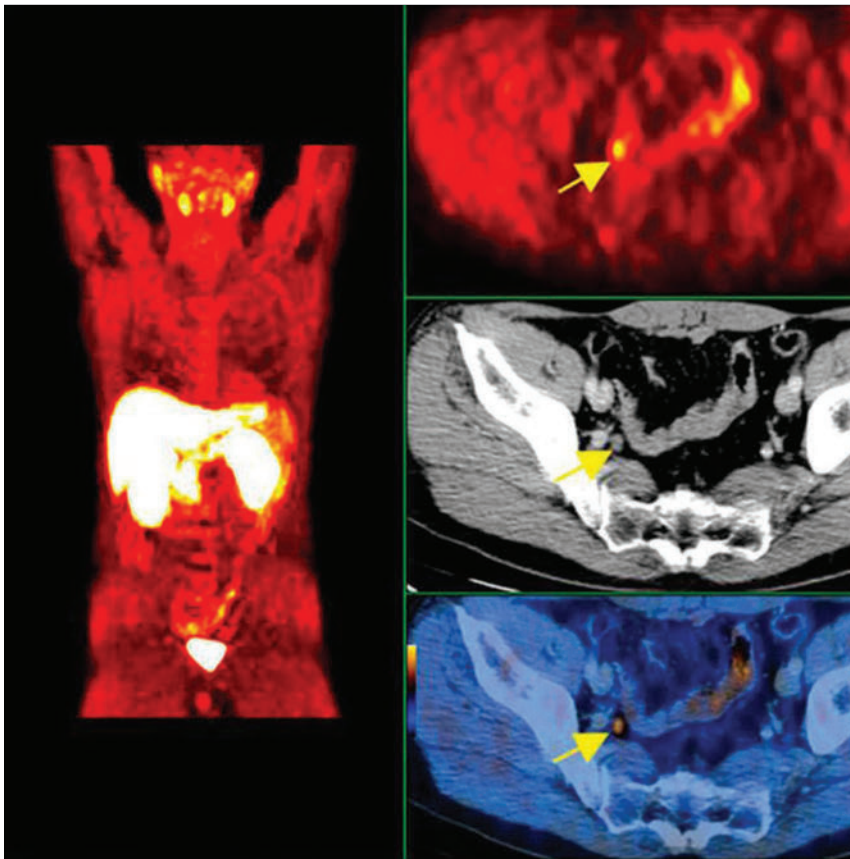


Fig. 11.3 A 60-year-old man with a history of prostate cancer who had undergone tumor resection and presented with a rising serum prostate-specific antigen level. Right column, from top to bottom, shows ^{18}F -fluorocholine positron emission tomography (PET), pelvic computed tomography (CT), and fused PET/CT images demonstrating abnormal accumulation of radiotracer in a normal-sized right internal iliac lymph node (arrows). Maximum-intensity-projection image on the left shows normal biodistribution of ^{18}F -fluorocholine and no other suspicious lesions. (Image courtesy of Dr. Mohsen Beheshti, St. Vincent's Hospital, Linz, Austria. Reproduced with permission of Jadvar et al 2011.¹⁷)

advantage over PET/CT in detection of disease sites in biochemical recurrence of prostate cancer.

Most studies with ^{11}C - and ^{18}F -choline in prostate cancer have been in the biochemical recurrence phase of the disease⁶⁰ (► Fig. 11.3). Umbehr et al provided a systematic review and meta-analysis of ^{11}C - and ^{18}F -choline in restaging patients with biochemical recurrence. They reported, on a per patient basis (12 studies, 1,055 patients), a pooled sensitivity and specificity of 85% (95% CI, 79–89%) and 88% (95% CI, 73–95%), respectively.⁶¹ A similar report by von Eyben et al examined 47 articles and data from 3,167 patients with regards to the diagnostic utility of choline PET/CT in staging and restaging of prostate cancer.⁶² They found that there was a statistically significant greater number of positive results in the prostate bed of biochemically relapsed patients who had previously undergone external-beam radiation therapy than in patients who had radical prostatectomy as the initial treatment. Moreover, choline PET/CT led to a change in treatment in 381 of 938 (41%) patients, leading to a complete response of PSA to treatment in 101 of 404 (25%) patients. Another systematic review and meta-analysis by Evangelista and colleagues (19 studies, including 12 studies for all sites of disease, 3 for lymph node metastases, and 4 for local recurrence; 1,555 patients) on the use of choline PET and PET/CT in biochemical relapse of prostate cancer reported a pooled sensitivity of 85.6% (95% CI: 82.9–88.1%) and pooled specificity of 92.6% (95% CI: 90.1–94.6%) for all sites of disease (prostatic fossa, lymph nodes, and bone), a pooled sensitivity of 75.4% (95% CI: 66.9–82.6%) and pooled specificity of 82% (95% CI: 68.6–91.4%) for prostatic fossa recurrence, and a pooled sensitivity of 100% (95% CI: 90.5–100%) and pooled specificity of 81.8% (95% CI:

48.2–97.7%) for lymph node metastases.⁶³ The reported 100% pooled sensitivity for detection of lymph node metastases may have been overestimated given the small number of publications that were included in the meta-analysis.

It has been noted that the diagnostic performance of choline PET/CT may depend on PSA level and kinetics. Treglia and coworkers performed a systematic review of 14 articles with the specific focus on the relationship between PSA level and kinetics (e.g., PSA doubling time [PSAdt] and PSA velocity [PSA_{vel}]) on the lesion detection rate in restaging prostate cancer.⁶⁴ The overall pooled detection rate of choline PET/CT in restaging prostate cancer was 58% (95% CI: 55–60%). The pooled detection rate increased to 65% (95% CI: 58–71%) when PSAdt was ≤ 6 months and to 71% (95% CI: 66–76%) and 77% (95% CI: 71–82%) when PSA_{vel} was > 1 or > 2 ng/mL-year, respectively. More recently, a retrospective multicenter study of 374 patients with biochemical relapse showed that a Gleason score < 5 or ≥ 8 could differentiate patients who had a positive and negative PET. In this regard, the optimal threshold values for PSA (checked on the day of the PET/CT examination) and PSAdt were 3 ng/mL and 6 months, respectively. Interestingly, in patients with a PSA less than 1.5 ng/mL, about 31% had evidence of disease on choline PET, with 7% demonstrating metastases.⁶⁵

Overall, there is relatively convincing evidence for the first-line use of choline PET/CT in restaging of patients with biochemical relapse of prostate cancer with a detection rate that is positively associated with increasing serum PSA level, increasing PSA_{vel} and decreasing PSAdt.⁶⁶

There is limited experience with other PET radiotracers in the clinical setting of biochemical recurrence. Recently, our group

at the University of Southern California reported on a comprehensive extraction and reanalysis of the PET detection data for FDG, ^{11}C -acetate, ^{11}C - or ^{18}F -choline, anti-1-amino-3- ^{18}F -fluorocyclobutane-1-carboxylic acid (anti- ^{18}F -FACBC), and radiolabeled ligand targeted to prostate-specific membrane antigen (PSMA), that have been explored for use in prostate cancer.⁶⁷ We found that FDG exhibited the lowest detection rate for any suspected disease. ^{11}C -acetate tended to have greater performance than radiolabeled choline in detecting local recurrence and lymph node lesions, although the difference was not statistically significant. Anti- ^{18}F -FACBC had greater likelihood of detecting local recurrence when compared to radiolabeled choline, although again this difference was not statistically significant. PSMA-based tracers tended to show a higher proportion of patients with suspected disease compared to the other four tracers.

Piccardo et al compared the accuracy of ^{18}F -fluorocholine PET/MRI with that of contrast-enhanced CT, ^{18}F -fluorocholine PET/CT, and multiparametric MRI in 21 patients with biochemical relapse of prostate cancer after definitive external-beam radiation therapy for primary tumor.⁶⁸ The authors reported a detection rate of 86% for ^{18}F -fluorocholine PET/MRI, 76% for ^{18}F -fluorocholine PET/CT, 43% for contrast-enhanced CT, and 81% for multiparametric MRI. A statistically significant inverse correlation was found between lesion SUV_{max} from PET and ADC from DWI. Souvatzoglou et al compared a single-injection dual-imaging protocol with PET/CT (with intravenous iodinated contrast) and subsequent PET/MRI using ^{11}C -choline in 32 patients with prostate cancer.⁶⁹ They found that the performance of simultaneous PET/MRI was overall comparable to that of PET/CT, although PET/MRI provided improved anatomical localization of lesions, especially in the bone and pelvis.

11.4 Treatment Response Evaluation

Literature on the potential utility of PET with various tracers in the imaging evaluation of treatment response in prostate cancer is relatively limited. Our preliminary results show that tumor FDG uptake decreases with successful treatment (using androgen deprivation or chemotherapy), although imaging findings may be discordant with those of other manifestations of disease including changes in the levels of serum PSA or circulating tumor cells. Also, there may be differences in imaging-based assessment based on the particular response criteria (i.e., Response Evaluation Criteria In Solid Tumors [RECIST 1.0 and RECIST 1.1] or PET Response Criteria in Solid Tumors [PERCIST 1.0]) that is used in the analysis.^{70,71} Another preliminary study from our group using ^{18}F -NaF PET-CT showed that semiquantitative ^{18}F -NaF PET-based analysis performs better than PSA-based response-assessment criteria.⁷² Clearly, additional studies are needed to decipher the optimal combination of relevant data that can most accurately reflect the effect of various current and novel therapies.

Yu et al reported in separate studies that ^{11}C -acetate and ^{18}F -NaF PET might be helpful in response assessment of bone metastases to therapy^{73,74} (► Fig. 11.4). Single case reports or small case series have been reported that suggest ^{18}F -NaF and

^{11}C -choline may be useful in the assessment response to ^{223}Ra dichloride therapy.^{75,76} Similar preliminary results have been reported for effects of neoadjuvant androgen deprivation and radical prostate radiation therapy with concurrent androgen-deprivation therapy on uptake level of ^{11}C -choline in tumors.^{77,78} There is currently very limited experience with other PET radiotracers in the clinical setting of treatment response assessment in patients with prostate cancer.

11.5 Prognostication

Until recently, most published articles have focused on the diagnostic rather than the prognostic utility of PET in prostate cancer. Oyama et al investigated the prognostic value of glucose metabolism of the primary tumors in 42 men with prostate cancer.⁷⁹ These authors showed that the FDG uptake level in primary tumors was positively correlated to relapse-free survival after radical prostatectomy. Patients with higher tumor uptake had a significantly poorer prognosis compared with those patients with tumors that showed lower FDG uptake. In another investigation of 43 patients with metastatic castration-resistant prostate cancer, the FDG uptake in the most active lesion was positively correlated with overall survival.⁸⁰ Jadvar and colleagues reported on a cohort of 87 patients with metastatic castration-resistant prostate cancer who underwent FDG PET/CT and were followed up prospectively for overall survival. In the multivariate analysis that adjusted for the potentially prognostic clinical parameters (age, serum PSA level, serum alkaline phosphatase level, use of pain medication, prior chemotherapy, and Gleason score at initial diagnosis), the sum of the SUV_{max} (sum of up to 25 active lesions including lymph nodes, bone, and soft tissue metastases) was significant with a hazard ratio of 1.01 (95% CI: 1.001–1.020; $p = 0.053$)⁸¹ (► Fig. 11.5).

In a study that reported on the comparative utility of ^{11}C -choline PET/CT over clinical staging nomograms for preoperative staging of lymph nodes in intermediate-risk and high-risk prostate cancer, ^{11}C -choline PET/CT performed better than clinical nomograms with equal sensitivity and better specificity.⁸² Gacci et al in a longitudinal study of 103 patients with biochemical recurrence, showed that an increase in serum PSA from baseline by greater than 5 ng/mL, a decrease in PSA doubling time to less than 6 months, and an increase in PSA velocity to greater than 6 ng/mL/month were highly associated with the outcome of progression on the follow-up PET/CT (6 months after baseline PET/CT).⁸³

Breeuwsma and colleagues associated the findings on ^{11}C -choline PET/CT with disease-specific survival in 64 men with biochemical recurrence after radical prostatectomy.⁸⁴ The investigators found that disease-specific survival was significantly higher in the group with negative PET/CT than in the group with positive PET/CT. In a similar study from Italy, the investigators evaluated retrospectively the potential utility of ^{11}C -choline PET/CT in prediction of prostate cancer-specific survival in 195 patients who presented with biochemical failure (PSA > 0.2 mg/mL during androgen-deprivation therapy) after radical prostatectomy. The median prostate cancer-specific survival in patients with positive and negative ^{11}C -choline PET/CT was 11.2 years and 16.4 years, respectively⁸⁵ (► Fig. 11.6). Kwee

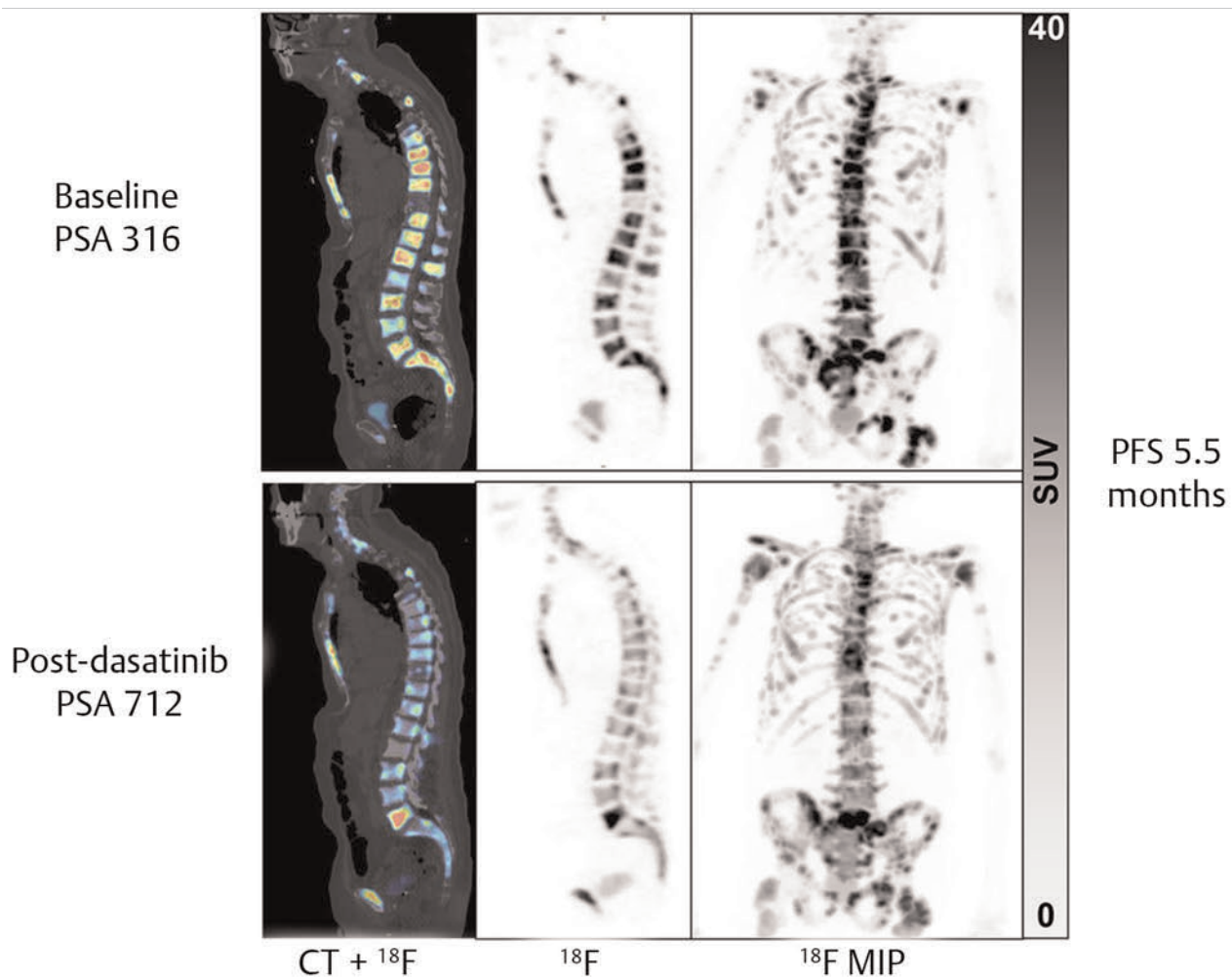


Fig. 11.4 A man with castration-resistant metastatic prostate cancer with stable disease on bone and computed tomography (CT) scans in response to treatment with dasatinib. Heterogeneous changes in ¹⁸F-NaF positron-emission tomography (PET) is noted in response to dasatinib, with a decrease in ¹⁸F-NaF uptake in most bone lesions except L5. MIP, maximum-intensity projection; PFS, progression-free survival; SUV, standardized uptake value. (Reproduced with permission of Yu et al 2015,⁶⁷ Fig. 4.)

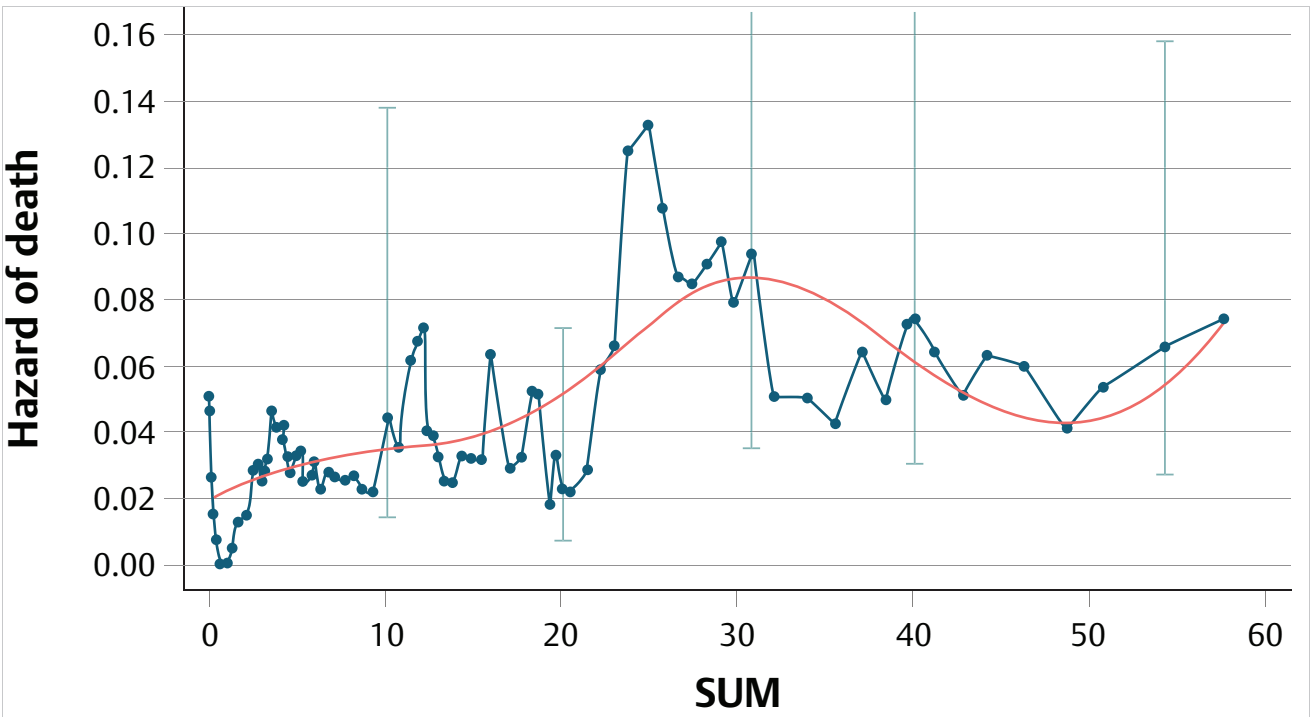


Fig. 11.5 Change in hazard of death (blue line) as a function of the sum of the maximum standardized uptake values (SUV_{max}) of metastatic lesions (SUM) interpreted as indicating the chance of death per person per month. A superimposed cubic spline-smoothed graph line (red) shows a marked upward shift indicating a greater risk of death for a sum of SUV_{max} greater than 20. (Reproduced with permission from Jadvar et al 2013.⁸¹)

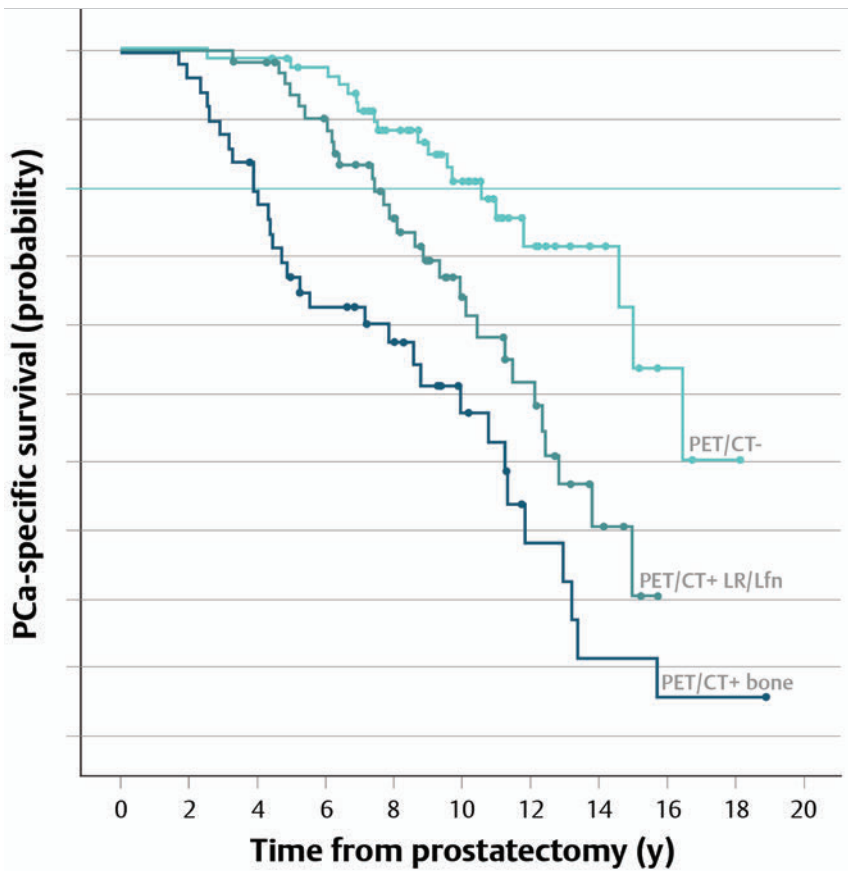


Fig. 11.6 Kaplan–Meier prostate cancer–specific survival probability curves in men with biochemical recurrence who had negative ¹¹C–choline positron emission tomography–computed tomography (PET/CT; light green line), positive ¹¹C–choline PET/CT suggestive of local recurrence or lymph node disease (PET/CT + LR/Lfn; medium green line), and positive ¹¹C–choline PET/CT suggestive of bone metastases (PET/CT + bone; dark green line). Note the longer prostate cancer–specific survival in patients with negative PET/CT compared to those with positive PET/CT, with the shorter survival in those patients with bone metastases compared to those with either local recurrence or lymph node disease. (Reproduced with permission of Giovacchini et al 2014.⁸⁵)

PET/CT-	No. at risk	83	83	82	77	55	38	18	9	4	1
	No. PCa-specific deaths	0	1	1	7	4	3	0	2	1	0
PET/CT+ LR/Lfn	No. at risk	63	63	61	53	39	22	15	5	0	0
	No. PCa-specific deaths	0	1	5	8	5	4	5	1	0	0
PET/CT+ bone	No. at risk	49	47	37	28	20	12	5	2	1	1
	No. PCa-specific deaths	2	9	7	2	3	4	3	1	0	0

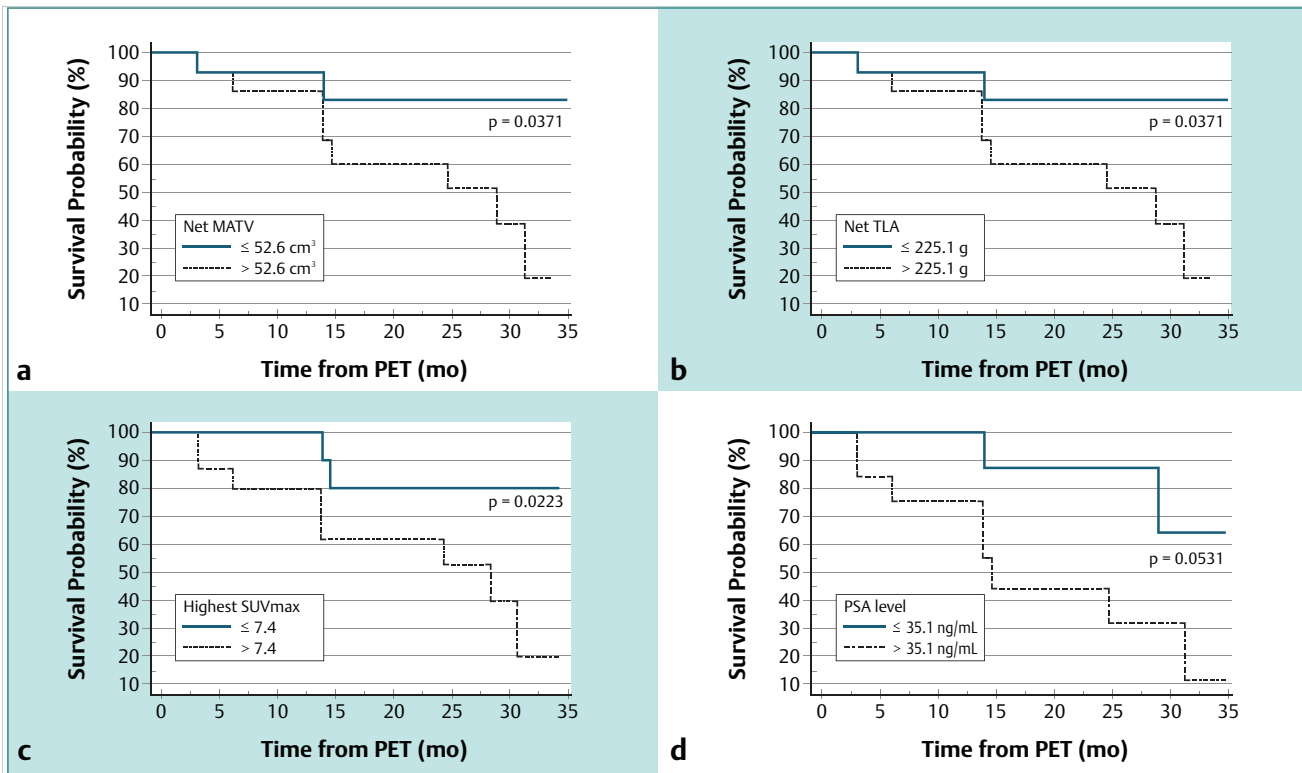


Fig. 11.7 Kaplan-Meier prostate cancer-specific survival probability curves based on ¹⁸F-fluorocholine positron emission tomography-computed tomography (PET/CT) performed in men with castration-resistant metastatic prostate cancer. Statistically significant differences are noted in survival among patients stratified by net metabolically active tumor volume (MATV) (a) net total lesion activity (TLA) (b) and maximum standardized uptake volume (SUV_{max}) of the most active tumor (c) with a borderline significant difference in survival in patients stratified by serum prostate-specific antigen (PSA) level (d). MATV, the metabolically active tumor volume, computed using an algorithm by which the voxel corresponding to the SUV_{max} of each lesion was identified, and a volume of interest was generated consisting of all spatially connected voxels within a fixed threshold of 40% of the SUV_{max} with the sum of all MATVs defined as the net MATV. TLA, the total lesion activity, calculated as the product of lesion mean SUV and MATV, with the sum of all TLAs defined as the net TLA. (Reproduced with permission of Kwee et al 2014.⁸⁶)

et al investigated the prognostic significance of metabolically active tumor volume (MATV) and of the activity distribution within the lesion volume, termed the total lesion activity (TLA) on ¹⁸F-fluorocholine PET/CT in 30 men with castration-resistant prostate cancer. The authors found that both net MATV and net TLA were significantly associated with overall survival⁸⁶ (► Fig. 11.7).

11.6 Conclusion

PET/CT and PET/MRI will play a major role in the imaging evaluation of patients with prostate cancer. The current published evidence is mostly on the diagnostic utility of PET/CT with radiolabeled choline in men with biochemical recurrence. In this clinical setting, PET with radiolabeled choline can be useful to detect and localize local recurrence and distant disease sites with an accuracy that is positively associated with the serum PSA level. There is, however, much room for additional studies with well-defined patient cohorts and select outcomes to decipher the exact role of PET with different radiotracers, and in combination with either CT or MRI, in the various phases in the natural history of this prevalent disease.

Acknowledgement

The preparation of this chapter was supported by the National Institutes of Health, National Cancer Institute grants R01-CA111613, R21-CA142426, P30-CA014089, and R21-EB017568.

References

- [1] Nensa F, Beiderwellen K, Heusch P, Wetter A. Clinical applications of PET/MRI: current status and future perspectives. *Diagn Interv Radiol* 2014; 20(5):438–447
- [2] Quick HH. Integrated PET/MR. *J Magn Reson Imaging* 2014; 39(2):243–258
- [3] Jadvar H, Colletti PM. Competitive advantage of PET/MRI. *Eur J Radiol* 2014; 83(1):84–94
- [4] Presti J Jr. Does the yield of prostate cancer biopsy and repeat biopsy justify the frequency of their use? *Nat Clin Pract Urol* 2008; 5(5):246–247
- [5] Keetch DW, Catalona WJ, Smith DS. Serial prostatic biopsies in men with persistently elevated serum prostate specific antigen values. *J Urol* 1994; 151(6):1571–1574
- [6] Pallwein L, Mitterberger M, Pelzer A et al. Ultrasound of prostate cancer: recent advances. *Eur Radiol* 2008; 18(4):707–715
- [7] Bonekamp D, Jacobs MA, El-Khouli R, Stojanovici D, Macura KJ. Advancements in MR imaging of the prostate: from diagnosis to interventions. *Radiographics* 2011; 31(3):677–703
- [8] Hoeks CMA, Barentsz JO, Hambrock T et al. Prostate cancer: multiparametric MR imaging for detection, localization, and staging. *Radiology* 2011; 261(1):46–66

- [9] Costa DN, Pedrosa I, Roehrborn C, Rofsky NM. Multiparametric magnetic resonance imaging of the prostate: technical aspects and role in clinical management. *Top Magn Reson Imaging* 2014; 23(4):243–257
- [10] Hosseinzadeh K, Schwarz SD. Endorectal diffusion-weighted imaging in prostate cancer to differentiate malignant and benign peripheral zone tissue. *J Magn Reson Imaging* 2004; 20(4):654–661
- [11] Tofts PS. Modeling tracer kinetics in dynamic Gd-DTPA MR imaging. *J Magn Reson Imaging* 1997; 7(1):91–101
- [12] Sciarra A, Panebianco V, Ciccariello M et al. Value of magnetic resonance spectroscopy imaging and dynamic contrast-enhanced imaging for detecting prostate cancer foci in men with prior negative biopsy. *Clin Cancer Res* 2010; 16(6):1875–1883
- [13] Franiel T, Stephan C, Erbersdobler A et al. Areas suspicious for prostate cancer: MR-guided biopsy in patients with at least one transrectal US-guided biopsy with a negative finding—multiparametric MR imaging for detection and biopsy planning. *Radiology* 2011; 259(1):162–172
- [14] de Rooij M, Hamoen EH, Fütterer JJ, Barentsz JO, Rovers MM. Accuracy of multiparametric MRI for prostate cancer detection: a meta-analysis. *AJR Am J Roentgenol* 2014; 202(2):343–351
- [15] Schoots IG, Roobol MJ, Nieboer D, Bangma CH, Steyerberg EW, Hunink MG. Magnetic resonance imaging-targeted biopsy may enhance the diagnostic accuracy of significant prostate cancer detection compared to standard transrectal ultrasound-guided biopsy: a systematic review and meta-analysis. *Eur Urol* 2015; 68(3):438–450
- [16] Jadvar H. Molecular imaging of prostate cancer: PET radiotracers. *AJR Am J Roentgenol* 2012; 199(2):278–291
- [17] Jadvar H. Prostate cancer: PET with 18F-FDG, 18F- or 11C-acetate, and 18F- or 11C-choline. *J Nucl Med* 2011; 52(1):81–89
- [18] Hanahan D, Weinberg RA. Hallmarks of cancer: the next generation. *Cell* 2011; 144(5):646–674
- [19] Shiiba M, Ishihara K, Kimura G et al. Evaluation of primary prostate cancer using 11C-methionine-PET/CT and 18F-FDG-PET/CT. *Ann Nucl Med* 2012; 26(2):138–145
- [20] Minamimoto U, Uemura H, Sano F et al. The potential of FDG-PET/CT for detecting prostate cancer in patients with an elevated serum PSA level. *Ann Nucl Med* 2011; 25(1):21–27
- [21] Bertagna F, Sadeghi R, Giovannella L, Treglia G. Incidental uptake of 18F-fluorodeoxyglucose in the prostate gland. Systematic review and meta-analysis on prevalence and risk of malignancy. *Nucl Med (Stuttg)* 2014; 53(6):249–258
- [22] Kwon T, Jeong JG, You D, Hong JH, Ahn H, Kim CS. Prevalence and clinical significance of incidental (18F)-fluoro-2-deoxyglucose uptake in prostate. *Korean J Urol* 2015; 56(4):288–294
- [23] Buchegger F, Garibotto V, Zilli T et al. First imaging results of an intraindividual comparison of (11C)-acetate and (18F)-fluorocholine PET/CT in patients with prostate cancer at early biochemical first or second relapse after prostatectomy or radiotherapy. *Eur J Nucl Med Mol Imaging* 2014; 41(1):68–78
- [24] Yoshimoto M, Waki A, Yonekura Y et al. Characterization of acetate metabolism in tumor cells in relation to cell proliferation: acetate metabolism in tumor cells. *Nucl Med Biol* 2001; 28(2):117–122
- [25] Janardhan S, Srivani P, Sastry GN. Choline kinase: an important target for cancer. *Curr Med Chem* 2006; 13(10):1169–1186
- [26] Mohsen B, Giorgio T, Rasoul ZS et al. Application of C-11-acetate positron emission tomography (PET) imaging in prostate cancer: systematic review and meta-analysis of the literature. *BJU Int* 2013; 112(8):1062–1072
- [27] Mena E, Turkbey B, Mani H et al. 11C-Acetate PET/CT in localized prostate cancer: a study with MRI and histopathologic correlation. *J Nucl Med* 2012; 53(4):538–545
- [28] Haseebuddin M, Dehdashti F, Siegel BA et al. 11C-acetate PET/CT before radical prostatectomy: nodal staging and treatment failure prediction. *J Nucl Med* 2013; 54(5):699–706
- [29] Strandberg S, Karlsson CT, Sundström T et al. (11C)-acetate PET/CT in pretherapeutic lymph node staging in high-risk prostate cancer patients and its influence on disease management - a retrospective study. *EJNMMI Res* 2014; 4(1):55
- [30] Souvatzoglou M, Weirich G, Schwarzenboeck S et al. The sensitivity of [11C] choline PET/CT to localize prostate cancer depends on the tumor configuration. *Clin Cancer Res* 2011; 17(11):3751–3759
- [31] Grosu AL, Weirich G, Wendl C et al. 11C-Choline PET/pathology image coregistration in primary localized prostate cancer. *Eur J Nucl Med Mol Imaging* 2014; 41(12):2242–2248
- [32] Scher B, Seitz M, Albinger W et al. Value of 11C-choline PET and PET/CT in patients with suspected prostate cancer. *Eur J Nucl Med Mol Imaging* 2007; 34(1):45–53
- [33] Farsad M, Schiavina R, Castellucci P et al. Detection and localization of prostate cancer: correlation of (11C)-choline PET/CT with histopathologic step-section analysis. *J Nucl Med* 2005; 46(10):1642–1649
- [34] Martorana G, Schiavina R, Corti B et al. 11C-choline positron emission tomography/computerized tomography for tumor localization of primary prostate cancer in comparison with 12-core biopsy. *J Urol* 2006; 176(3):954–960, discussion 960
- [35] Eschmann SM, Pfannenbergl AC, Rieger A et al. Comparison of 11C-choline-PET/CT and whole body-MRI for staging of prostate cancer. *Nucl Med (Stuttg)* 2007; 46(5):161–168, quiz N47–N48
- [36] Takei T, Souvatzoglou M, Beer AJ et al. A case of multimodality multiparametric 11C-choline PET/MR for biopsy targeting in prior biopsy-negative primary prostate cancer. *Clin Nucl Med* 2012; 37(9):918–919
- [37] Eiber M, Nekolla SG, Maurer T, Weirich G, Wester HJ, Schwaiger M. (68)Ga-PSMA PET/MR with multimodality image analysis for primary prostate cancer. *Abdom Imaging* 2015; 40(6):1769–1771
- [38] Chakraborty PS, Tripathi M, Agarwal KK, Kumar R, Vijay MK, Bal C. Metastatic poorly differentiated prostatic carcinoma with neuroendocrine differentiation: negative on 68Ga-PSMA PET/CT. *Clin Nucl Med* 2015; 40(2):e163–e166
- [39] Jadvar H, Chen K, Ukimura O. Targeted Prostate Gland Biopsy With Combined Transrectal Ultrasound, mpMRI, and 18F-FMAU PET/CT. *Clin Nucl Med* 2015; 40(8):e426–e428
- [40] Wetter A. Molecular research in urology 2014: update on PET/MR imaging of the prostate. *Int J Mol Sci* 2014; 15(8):13401–13405
- [41] Zetting O, Shah A, Hennesperger C et al. Multimodal image-guided prostate fusion biopsy based on automatic deformable registration. *Int J Comp Assist Radiol Surg* 2015; 10(12):1997–2007
- [42] Gatidis S, Scharpf M, Martirosian P et al. Combined unsupervised-supervised classification of multiparametric PET/MRI data: application to prostate cancer. *NMR Biomed* 2015; 28(7):914–922
- [43] Bagade S, Fowler KJ, Schwarz JK, Grigsby PW, Dehdashti F. PET/MRI evaluation of gynecologic malignancies and prostate cancer. *Semin Nucl Med* 2015; 45(4):293–303
- [44] de Perrot T, Rager O, Scheffler M et al. Potential of hybrid 18F-fluorocholine PET/MRI for prostate cancer imaging. *Eur J Nucl Med Mol Imaging* 2014; 41(9):1744–1755
- [45] Souvatzoglou M, Eiber M, Martinez-Moeller A et al. PET/MR in prostate cancer: technical aspects and potential diagnostic value. *Eur J Nucl Med Mol Imaging* 2013; 40 Suppl 1:S79–S88
- [46] Jambor I, Borra R, Kempainen J et al. Improved detection of localized prostate cancer using co-registered MRI and 11C-acetate PET/CT. *Eur J Radiol* 2012; 81(11):2966–2972
- [47] Park H, Wood D, Hussain H et al. Introducing parametric fusion PET/MRI of primary prostate cancer. *J Nucl Med* 2012; 53(4):546–551
- [48] Hartenbach M, Hartenbach S, Bechtloff W et al. Combined PET/MRI improves diagnostic accuracy in patients with prostate cancer: a prospective diagnostic trial. *Clin Cancer Res* 2014; 20(12):3244–3253
- [49] Kim YI, Cheon GJ, Paeng JC et al. Usefulness of MRI-assisted metabolic volumetric parameters provided by simultaneous (18F)-fluorocholine PET/MRI for primary prostate cancer characterization. *Eur J Nucl Med Mol Imaging* 2015; 42(8):1247–1256
- [50] Rosenkrantz AB, Koesters T, Vahle AK et al. Quantitative graphical analysis of simultaneous dynamic PET/MRI for assessment of prostate cancer. *Clin Nucl Med* 2015; 40(4):e236–e240
- [51] Wetter A, Lipponer C, Nensa F et al. Quantitative evaluation of bone metastases from prostate cancer with simultaneous [18F] choline PET/MRI: combined SUV and ADC analysis. *Ann Nucl Med* 2014; 28(5):405–410
- [52] Wetter A, Lipponer C, Nensa F et al. Evaluation of the PET component of simultaneous [(18)F]choline PET/MRI in prostate cancer: comparison with [(18)F]choline PET/CT. *Eur J Nucl Med Mol Imaging* 2014; 41(1):79–88
- [53] Wetter A, Lipponer C, Nensa F et al. Simultaneous 18F choline positron emission tomography/magnetic resonance imaging of the prostate: initial results. *Invest Radiol* 2013; 48(5):256–262
- [54] Bruce JY, Lang JM, McNeel DG, Liu G. Current controversies in the management of biochemical failure in prostate cancer. *Clin Adv Hematol Oncol* 2012; 10(11):716–722
- [55] Cookson MS, Aus G, Burnett AL et al. Variation in the definition of biochemical recurrence in patients treated for localized prostate cancer: the American Urological Association Prostate Guidelines for Localized Prostate Cancer Update Panel report and recommendations for a standard in the reporting of surgical outcomes. *J Urol* 2007; 177(2):540–545
- [56] Roach M III, Hanks G, Thames H Jr. et al. Defining biochemical failure following radiotherapy with or without hormonal therapy in men with

- clinically localized prostate cancer: recommendations of the RTOG-ASTRO Phoenix Consensus Conference. *Int J Radiat Oncol Biol Phys* 2006; 65(4):965-974
- [57] Chang CH, Wu HC, Tsai JJ, Shen YY, Changlai SP, Kao A. Detecting metastatic pelvic lymph nodes by 18F-2-deoxyglucose positron emission tomography in patients with prostate-specific antigen relapse after treatment for localized prostate cancer. *Urol Int* 2003; 70(4):311-315
- [58] Jadvar H, Desai B, Ji L et al. Prospective evaluation of 18F-NaF and 18F-FDG PET/CT in detection of occult metastatic disease in biochemical recurrence of prostate cancer. *Clin Nucl Med* 2012; 37(7):637-643
- [59] Eiber M, Takei T, Souvatzoglou M et al. Performance of whole-body integrated 18F-FDG PET/MR in comparison to PET/CT for evaluation of malignant bone lesions. *J Nucl Med* 2014; 55(2):191-197
- [60] Bauman G, Belhocine T, Kovacs M, Ward A, Beheshti M, Rachinsky I. 18F-fluorocholine for prostate cancer imaging: a systematic review of the literature. *Prostate Cancer Prostatic Dis* 2012; 15(1):45-55
- [61] Umbehr MH, Müntener M, Hany T, Sulser T, Bachmann LM. The role of 11C-choline and 18F-fluorocholine positron emission tomography (PET) and PET/CT in prostate cancer: a systematic review and meta-analysis. *Eur Urol* 2013; 64(1):106-117
- [62] von Eyben FE, Kairemo K. Meta-analysis of (11)C-choline and (18)F-choline PET/CT for management of patients with prostate cancer. *Nucl Med Commun* 2014; 35(3):221-230
- [63] Evangelista L, Zattoni F, Guttilla A et al. Choline PET or PET/CT and biochemical relapse of prostate cancer: a systematic review and meta-analysis. *Clin Nucl Med* 2013; 38(5):305-314
- [64] Treglia G, Ceriani L, Sadeghi R, Giovacchini G, Giovanella L. Relationship between prostate-specific antigen kinetics and detection rate of radiolabelled choline PET/CT in restaging prostate cancer patients: a meta-analysis. *Clin Chem Lab Med* 2014; 52(5):725-733
- [65] Rodado-Marina S, Coronado-Poggio M, García-Vicente AM et al. Clinical utility of (18)F-fluorocholine positron-emission tomography/computed tomography (PET/CT) in biochemical relapse of prostate cancer after radical treatment: results of a multicentre study. *BJU Int* 2015; 115(6):874-883
- [66] Castellucci P, Picchio M. 11C-choline PET/CT and PSA kinetics. *Eur J Nucl Med Mol Imaging* 2013; 40 Suppl 1:S36-S40
- [67] Yu CY, Desai B, Ji L, Groshen S, Jadvar H. Comparative performance of PET tracers in biochemical recurrence of prostate cancer: a critical analysis of literature. *Am J Nucl Med Mol Imaging* 2014; 4(6):580-601
- [68] Piccardo A, Paparo F, Picazzo R et al. Value of fused 18F-Choline-PET/MRI to evaluate prostate cancer relapse in patients showing biochemical recurrence after EBRT: preliminary results. *Biomed Res Int* 2014; 2014:103718
- [69] Souvatzoglou M, Eiber M, Takei T et al. Comparison of integrated whole-body [11C]choline PET/MR with PET/CT in patients with prostate cancer. *Eur J Nucl Med Mol Imaging* 2013; 40(10):1486-1499
- [70] Jadvar H, Desai B, Ji L, et al. RECIST 1.0, PERCIST 1.0 and PSA treatment response criteria in metastatic castrate-resistant prostate cancer. Paper presented at the 99th Annual Meeting of the Radiological Society of North America (RSNA), December 1-6, 2013; Chicago, IL, 2013. [Abstract]
- [71] Jadvar H, Desai B, Ji L, et al. Comparison of RECIST 1.0, PERCIST 1.0 and PCWG2 treatment response criteria in metastatic castrate-sensitive prostate cancer. Paper presented at the Annual Meeting of the Society of Nuclear Medicine and Molecular Imaging (SNMMI); June 1 to 6, 2015; Baltimore, MD. [Abstract]
- [72] Doroudinia A, Desai B, Yoon J, et al. Treatment Response Assessment in Metastatic Prostate Cancer with 18F-NaF PET/CT. Paper presented at the Annual Meeting of the Society of Nuclear Medicine and Molecular Imaging (SNMMI); June 1 to 6, 2015; Baltimore, MD. [Abstract]
- [73] Yu EY, Muzi M, Hackenbrach JA et al. C11-acetate and F-18 FDG PET for men with prostate cancer bone metastases: relative findings and response to therapy. *Clin Nucl Med* 2011; 36(3):192-198
- [74] Yu EY, Duan F, Muzi M et al. Castration-resistant prostate cancer bone metastasis response measured by 18F-fluoride PET after treatment with dasatinib and correlation with progression-free survival: results from American College of Radiology Imaging Network 6687. *J Nucl Med* 2015; 56(3):354-360
- [75] Cook G Jr Parker C, Chua S, Johnson B, Aksnes AK, Lewington VJ. 18F-fluoride PET: changes in uptake as a method to assess response in bone metastases from castrate-resistant prostate cancer patients treated with 223Ra-chloride (Alpharadin). *EJNMMI Res* 2011; 1(1):4
- [76] Miyazaki KS, Kuang Y, Kwee SA. Changes in skeletal tumor activity on (18)F-choline PET/CT in patients receiving (223)Radium radionuclide therapy for metastatic prostate cancer. *Nucl Med Mol Imaging* 2015; 49(2):160-164
- [77] Challapalli A, Barwick T, Tomasi G et al. Exploring the potential of [11C]choline-PET/CT as a novel imaging biomarker for predicting early treatment response in prostate cancer. *Nucl Med Commun* 2014; 35(1):20-29
- [78] Amanie J, Jans HS, Wuest M et al. Analysis of intraprostatic therapeutic effects in prostate cancer patients using [(11)C]-choline pet/ct after external-beam radiation therapy. *Curr Oncol* 2013; 20(2):104-110
- [79] Oyama N, Akino H, Suzuki Y et al. Prognostic value of 2-deoxy-2-[F-18]fluoro-D-glucose positron emission tomography imaging for patients with prostate cancer. *Mol Imaging Biol* 2002; 4(1):99-104
- [80] Meirelles GS, Schöder H, Ravizzini GC et al. Prognostic value of baseline [18F] fluorodeoxyglucose positron emission tomography and 99mTc-MDP bone scan in progressing metastatic prostate cancer. *Clin Cancer Res* 2010; 16(24):6093-6099
- [81] Jadvar H, Desai B, Ji L et al. Baseline 18F-FDG PET/CT parameters as imaging biomarkers of overall survival in castrate-resistant metastatic prostate cancer. *J Nucl Med* 2013; 54(8):1195-1201
- [82] Schiavina R, Scattoni V, Castellucci P et al. 11C-choline positron emission tomography/computerized tomography for preoperative lymph-node staging in intermediate-risk and high-risk prostate cancer: comparison with clinical staging nomograms. *Eur Urol* 2008; 54(2):392-401
- [83] Gacci M, Cai T, Siena G et al. Prostate-specific antigen kinetics parameters are predictive of positron emission tomography features worsening in patients with biochemical relapse after prostate cancer treatment with radical intent: Results from a longitudinal cohort study. *Scand J Urol* 2014; 48(3):259-267
- [84] Breeuwsma AJ, Rybalov M, Leliveld AM, Pruim J, de Jong IJ. Correlation of [11C]choline PET-CT with time to treatment and disease-specific survival in men with recurrent prostate cancer after radical prostatectomy. *Q J Nucl Med Mol Imaging* 2012; 56(5):440-446
- [85] Giovacchini G, Picchio M, Garcia-Parra R et al. 11C-choline PET/CT predicts prostate cancer-specific survival in patients with biochemical failure during androgen-deprivation therapy. *J Nucl Med* 2014; 55(2):233-241
- [86] Kwee SA, Lim J, Watanabe A, Kromer-Baker K, Coel MN. Prognosis Related to Metastatic Burden Measured by 18F-Fluorocholine PET/CT in Castration-Resistant Prostate Cancer. *J Nucl Med* 2014; 55(6):905-910

12 Teaching Atlas of Instructional and Interesting Cases

Ankur Doshi and Andrew Rosenkrantz

This chapter presents a broad range of prostate MRI cases, aiming to depict classic findings in addition to potential diagnostic pitfalls and challenges. Unless otherwise indicated, all examinations were performed using a 3-T system and a phased-array pelvic coil. High b-value diffusion-weighted images (DWI) using a b value of 1,500 s/mm² were computed from acquired DWI using b values of 50 and 1,000 s/mm². Lesions were evaluated using the Prostate Imaging-Reporting and Data System, version 2 (PI-RADS v2) scoring scheme.

Abbreviations used:

PSA: prostate-specific antigen

T2WI: T2-weighted imaging

DWI: diffusion-weighted imaging

ADC: apparent diffusion coefficient

DCE: dynamic contrast enhancement

MRI-TRUS: MRI- transrectal ultrasound

12.1 Case 1: PI-RADS 2 Lesion Corresponding to High-Grade Prostatic Intraepithelial Neoplasia

12.1.1 History

A 58-year-old man with a rising PSA level (4.1 ng/mL) and no prior prostate biopsy (► Fig. 12.1).

12.1.2 Prostate MRI Findings

- a) T2WI: Diffuse T2 hypointensity in the left base-to-midgland peripheral zone
- b) DWI (b = 1500 s/mm²): Indistinct mild hyperintensity
- c) ADC: Indistinct mild hypointensity
- d) DCE: Diffuse bilateral early enhancement (negative DCE)

PI-RADS v2 assessment category: 2

12.1.3 Diagnosis

High-grade prostatic intraepithelial neoplasia (HGPIN) in multiple bilateral cores.

Teaching points: HGPIN is considered a premalignant lesion and is a potential cause of false-positive MRI interpretations. Management entails a combination of repeat PSA measurements and prostate biopsies, although there is variation across protocols in the timing and number of follow-up biopsies.

12.1.4 Suggested Reading

- [1] Ramaswamy K, Lepor H, Taneja SS. Management of High-Grade Prostatic Intraepithelial Neoplasia (HGPIN). *Prostate Cancer Diagnosis*: Springer; 2013:241–254.
- [2] Rosenkrantz AB, Mussi TC, Borofsky MS, Scinti SS, Grasso M, Taneja SS. 3.0T multiparametric prostate MRI using pelvic phased-array coil: utility for tumor detection prior to biopsy. *Urol Oncol* 2013; 31(8):1430–1435

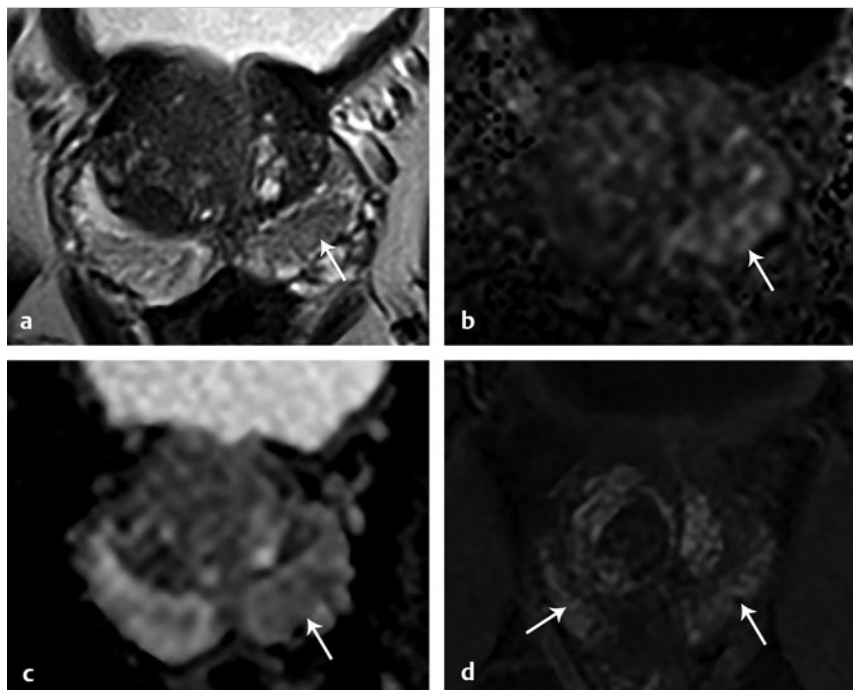


Fig. 12.1 PI-RADS v2 lesion corresponding to high-grade prostatic intraepithelial neoplasia.

12.2 Case 2: PI-RADS 3 Lesion Corresponding to Prostatitis

12.2.1 History

A 65-year-old man with an elevated PSA level of 7.5 ng/mL and prior negative prostate biopsy (► Fig. 12.2).

12.2.2 Prostate MRI Findings

- a) T2WI: Linear and wedge-shaped T2 hypointensity in bilateral midgland peripheral zones
- b) DWI ($b = 1500 \text{ s/mm}^2$): Mild hyperintensity bilaterally
- c) ADC: Mild low signal bilaterally
- d) DCE: Diffuse bilateral enhancement (negative DCE)

PI-RADS v2 assessment category: 3 for both lesions

12.2.3 Diagnosis

MRI-TRUS fusion biopsy revealed prostatitis.

Teaching Points: Prostatitis is often asymptomatic and can show decreased T2 signal, restricted diffusion, and early enhancement, which are also MRI features seen in cancer. However, the morphology of prostatitis is linear, wedge-shaped, or diffuse, and the degree of T2 hypointensity and diffusion signal abnormality is often mild.

12.2.4 Suggested Reading

- [1] American College of Radiology (ACR) Prostate Imaging-Reporting and Data System (PI-RADS), Version 2. <http://www.acr.org/~/media/ACR/Documents/PDF/QualitySafety/Resources/PIRADS/PIRADS%20V2.pdf>. Published 2015. Accessed on October 30, 2015.

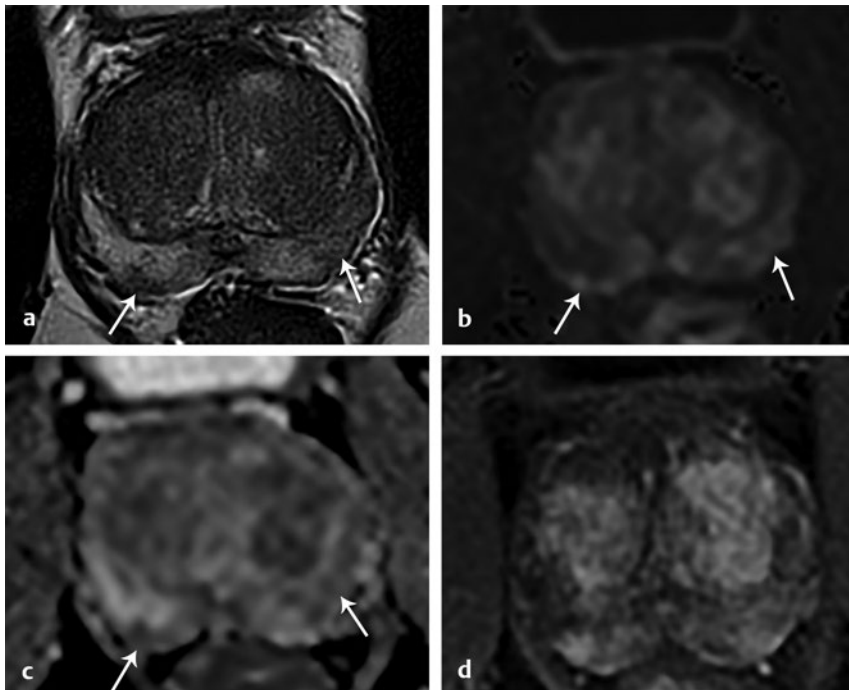


Fig. 12.2 PI-RADS 3 lesion corresponding to prostatitis.

12.3 Case 3: PI-RADS 3 Lesion Corresponding to Benign Prostate Tissue

12.3.1 History

A 62-year-old man with a PSA level of 5.2 ng/mL and no prior prostate biopsy (► Fig. 12.3).

12.3.2 Prostate MRI Findings

- a) T2WI: Wedge-shaped hypointensity in the right midgland peripheral zone
- b) DWI (b = 1500 s/mm²): Mild hyperintensity
- c) ADC: Mild low ADC
- d) DCE: No focal early enhancement matching the edges of the T2WI or DWI abnormality (negative DCE)

PI-RADS v2 assessment category: 3

12.3.3 Diagnosis

MRI-TRUS fusion biopsy revealed benign prostatic tissue.

Teaching point: Wedge-shaped lesion morphology on T2WI warrants a T2WI score of 2 and can be seen with prostatitis, atrophy, or fibrosis. However, this case was considered to show focal low ADC and DWI hyperintensity, thus warranting both a DWI score of 3 and overall PI-RADS assessment category of 3.

12.3.4 Suggested Reading

- [1] American College of Radiology (ACR) Prostate Imaging-Reporting and Data System (PI-RADS), Version 2. 2015. <http://www.acr.org/-/media/ACR/Documents/PDF/QualitySafety/Resources/PIRADS/PIRADS%20V2.pdf>. Published 2015. Accessed on October 30, 2015.

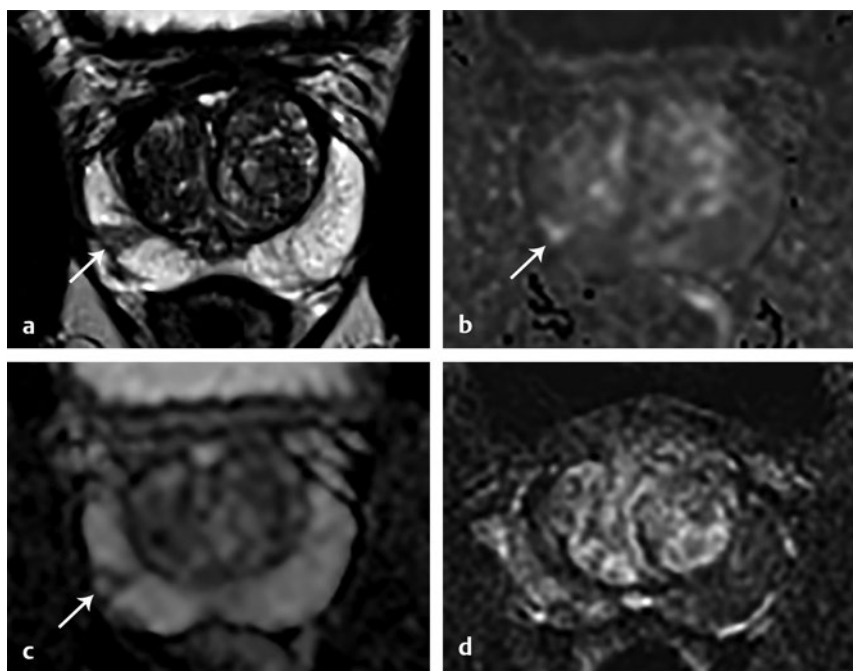


Fig. 12.3 PI-RADS 3 lesion corresponding to benign prostate tissue.

12.4 Case 4: PI-RADS 3 Lesion Corresponding to Low-Grade Prostate Cancer

12.4.1 History

A 56-year-old man with an elevated PSA level of 7.5 ng/mL and no prior prostate biopsy (► Fig. 12.4).

12.4.2 Prostate MRI Findings

- a) T2WI: Noncircumscribed moderate hypointensity in the right posterior base peripheral zone
- b) DWI ($b = 1500 \text{ s/mm}^2$): Focal mild hyperintensity
- c) ADC: Focal moderate low ADC
- d) DCE: Diffuse bilateral early enhancement (negative DCE)

PI-RADS v2 assessment category: 3

12.4.3 Diagnosis

MRI-TRUS fusion biopsy revealed Gleason score 3+3 prostate cancer.

Teaching points: The histologic diagnosis in this PI-RADS 3 lesion is consistent with published literature demonstrating the majority of PI-RADS 3 lesions to be benign or to harbor low-grade cancer.

12.4.4 Suggested Reading

- [1] Vargas HA, Hötter AM, Goldman DA et al. Updated prostate imaging reporting and data system (PI-RADS v2) recommendations for the detection of clinically significant prostate cancer using multiparametric MRI: critical evaluation using whole-mount pathology as standard of reference. *Eur Radiol* 2016; 26(6):1606–1612

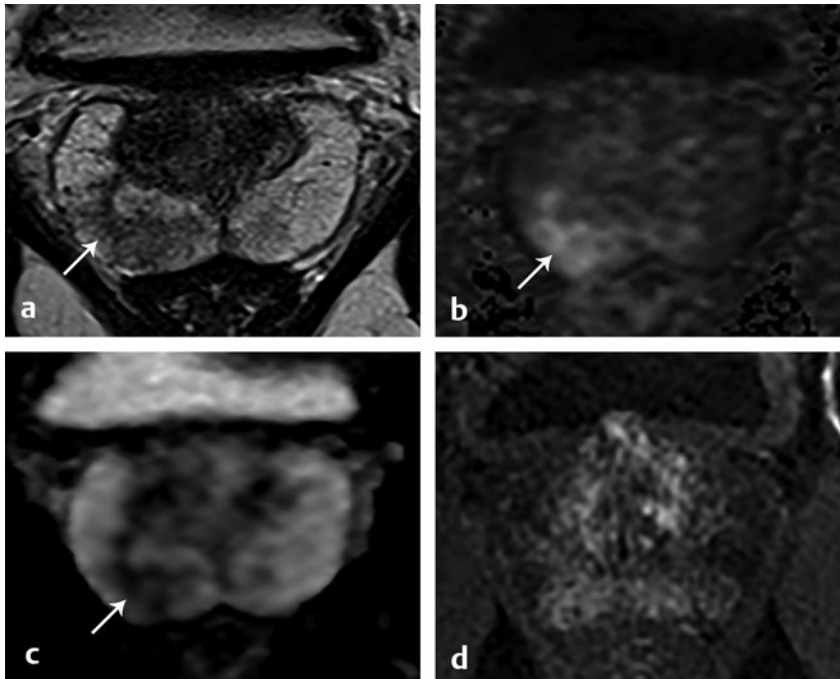


Fig. 12.4 PI-RADS 3 lesion corresponding to low-grade prostate cancer.

12.5 Case 5: PI-RADS 4 Lesion Corresponding to Intermediate-Grade Prostate Cancer

12.5.1 History

A 55-year-old man with a PSA level of 19 ng/mL and no prior prostate biopsy (► Fig. 12.5).

12.5.2 Prostate MRI Findings

- a) T2WI: 1-cm circumscribed, homogeneous, moderately hypointense mass in the left posteromedial midgland peripheral zone
- b) DWI (b = 1500 s/mm²): Focal marked hyperintensity measuring < 1.5 cm

- c) ADC: Focal marked hypointensity
- d) DCE: Focal early enhancement matching the edges of the lesion on other sequences (positive DCE)

PI-RADS v2 assessment category: 4

12.5.3 Diagnosis

Gleason score 3 + 4 prostate cancer.

Teaching points: A homogenous circumscribed mass in the peripheral zone with markedly abnormal DWI/ADC signal intensity likely represents clinically significant cancer.

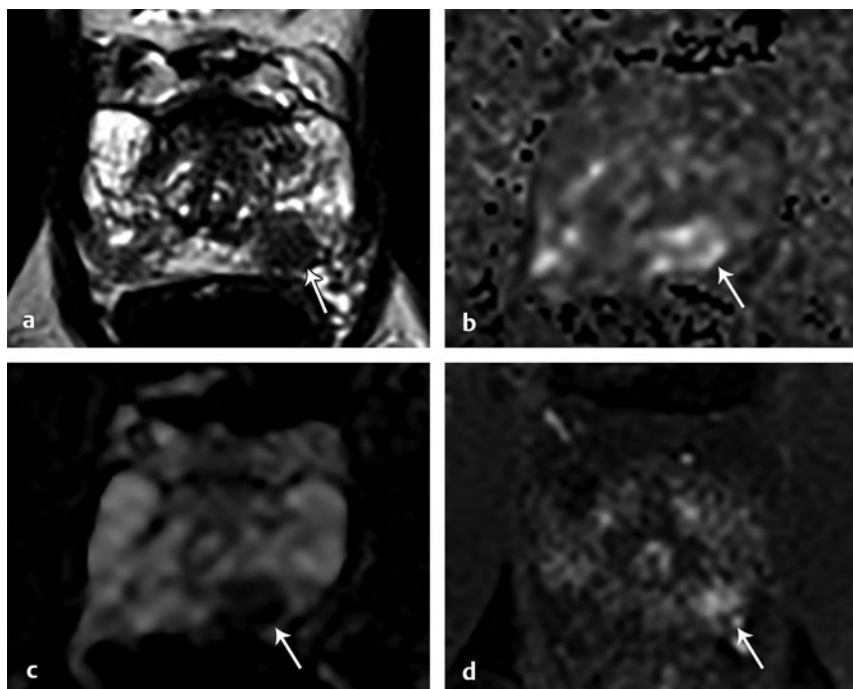


Fig. 12.5 PI-RADS 4 lesion corresponding to intermediate-grade prostate cancer.

12.6 Case 6: PI-RADS 5 Lesion Corresponding to High-Grade Prostate Cancer

12.6.1 History

A 63-year-old man with an elevated PSA level of 29.3 ng/mL and no prior prostate biopsy (► Fig. 12.6).

12.6.2 Prostate MRI Findings

- T2WI: 1.7-cm circumscribed, homogeneous, markedly hypointense mass in the right posteromedial midgland peripheral zone
- DWI (b = 1500 s/mm²): Focal marked hyperintensity measuring ≥ 1.5 cm
- ADC: Focal marked hypointensity. ADC value was 450 μm²/s
- DCE: Focal early enhancement matching the edges of the lesion on other sequences (positive DCE)

PI-RADS v2 assessment category: 5

12.6.3 Diagnosis

Gleason score 4 + 5 prostate cancer.

Teaching points: Assessment of lesion ADC is generally performed using qualitative visual inspection. While lower ADC values have been shown to be associated with higher-grade tumor, ADC values overlap between benign prostate tissue and low- and high-grade cancer. Additionally, quantitative ADC values vary based on scanner platform as well as acquisition and measurement technique. Allowing for these caveats, an ADC value below 750 to 900 μm²/s has been proposed as a threshold for clinically significant cancer.

12.6.4 Suggested Reading

- [1] American College of Radiology (ACR) Prostate Imaging-Reporting and Data System (PI-RADS), Version 2. 2015. <http://www.acr.org/-/media/ACR/Documents/PDF/QualitySafety/Resources/PIRADS/PIRADS%20V2.pdf>. Published 2015. Accessed on October 30, 2015.

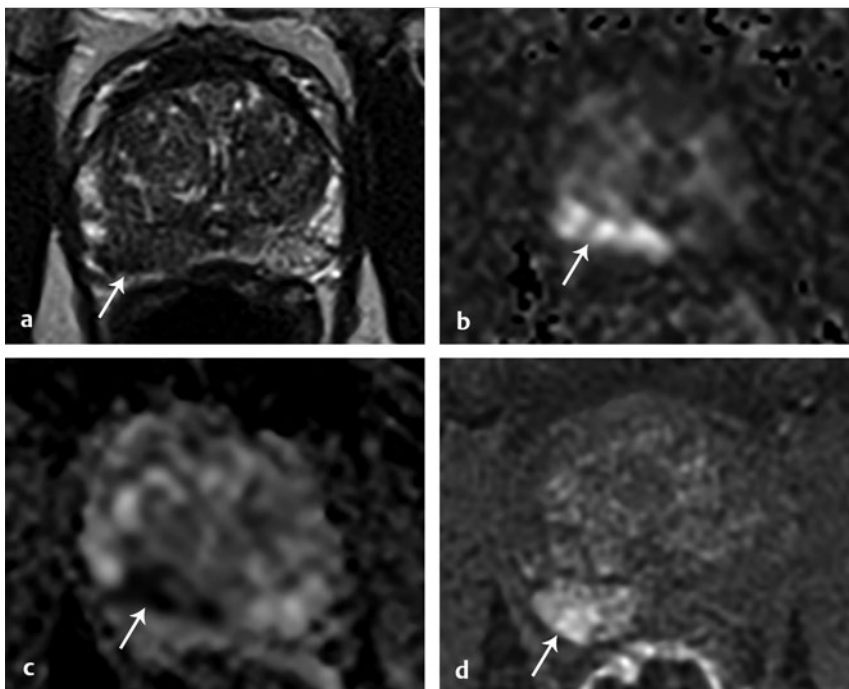


Fig. 12.6 PI-RADS 5 lesion corresponding to high-grade prostate cancer.

12.7 Case 7: PI-RADS 2 Lesion Corresponding to Atypical Benign Prostatic Hyperplasia Nodule

12.7.1 History

A 69-year-old man with an elevated PSA level of 6.9 ng/mL and no prior biopsy (► Fig. 12.7).

12.7.2 Prostate MRI Findings

- T2WI: 1.9-cm oval, well-circumscribed, homogeneously T2 hypointense nodule in the right posterior midgland transition zone
- DWI: Isointense to the remainder of the transition zone
- ADC: Mild focal hypointensity on ADC
- DCE: Focal early enhancement matching the edges of the T2WI and ADC abnormality (positive DCE)

PI-RADS v2 assessment category: 2

12.7.3 Diagnosis

MRI-TRUS fusion biopsy was benign. This is a minimally atypical, stromal benign prostatic hyperplasia (BPH) nodule.

Teaching points: In the transition zone, the T2WI appearance is the predominant driver of the overall PI-RADS category. Since the T2WI appearance of this lesion warranted a score of 2, the overall PI-RADS category was 2, regardless of the DWI and DCE findings. This scheme reflects the fact that BPH nodules commonly show restricted diffusion and positive DCE. BPH nodules that are mostly comprised of glandular components are T2 hyperintense, while those that are mostly stromal appear T2 hypointense. BPH nodules typically show a mixture of signal intensities, giving a heterogeneous appearance. A round or oval shape, well-circumscribed border, and capsule are features suggesting a BPH nodule rather than transition zone tumor.

12.7.4 Suggested Reading

- American College of Radiology (ACR) Prostate Imaging-Reporting and Data System (PI-RADS), Version 2. 2015. <http://www.acr.org/~media/ACR/Documents/PDF/QualitySafety/Resources/PIRADS/PIRADS%20V2.pdf>. Published 2015. Accessed on October 30, 2015.

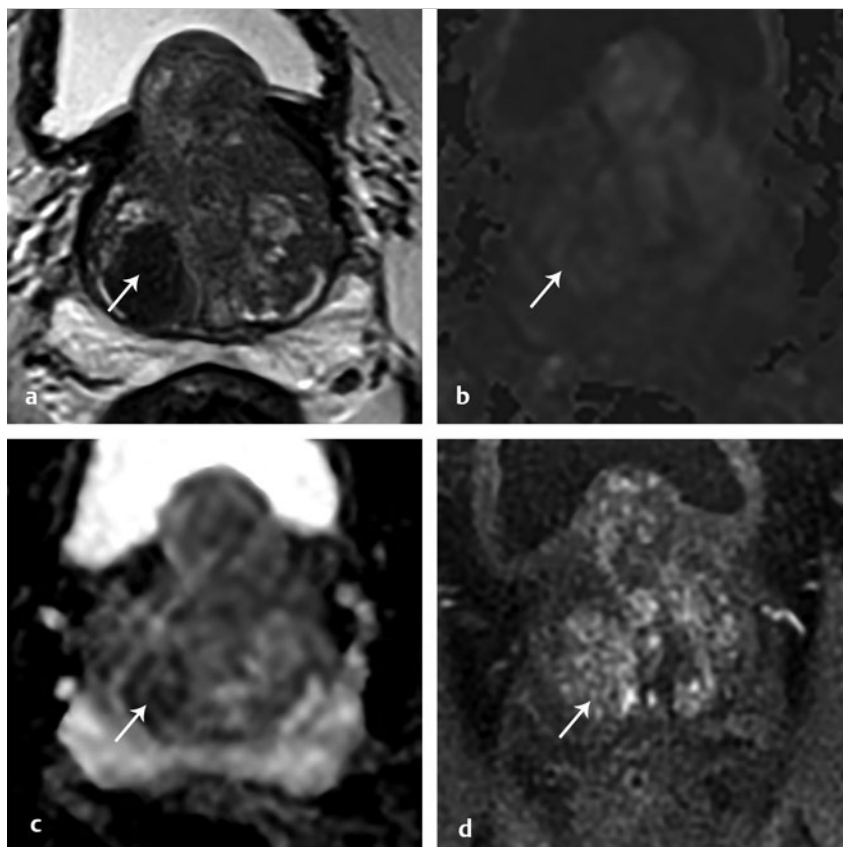


Fig. 12.7 PI-RADS 2 lesion corresponding to atypical benign prostatic hyperplasia nodule.

12.8 Case 8: PI-RADS 3 Lesion in the Transition Zone Corresponding to Low-Grade Prostate Cancer

12.8.1 History

A 77-year-old man with a PSA level of 2.4 ng/mL and high-grade prostatic intraepithelial hyperplasia (HGPIN) on prior prostate biopsy (► Fig. 12.8).

12.8.2 Prostate MRI Findings

a) T2WI: 1.1 cm T2 hypointense lesion in the right anterior transition zone that is slightly heterogeneous with obscured margins. Notice the irregular shape and absence of a complete, smooth, well-defined capsule.

- b) DWI ($b = 1500 \text{ s/mm}^2$): Marked hyperintensity
- c) ADC: Moderate hypointensity
- d) DCE: Focal early enhancement matching the edges of the lesion on the other sequences (positive DCE)

PI-RADS v2 assessment category: 3

12.8.3 Diagnosis

Gleason score 3 + 3 prostate cancer

Teaching points: Differentiation of atypical benign prostatic hyperplasia nodules and transition zone tumors is challenging. Signal abnormality on T2WI and DWI/ADC should be assessed relative to the remainder of the TZ in the same patient. Obscured margins raise suspicion for TZ tumor.

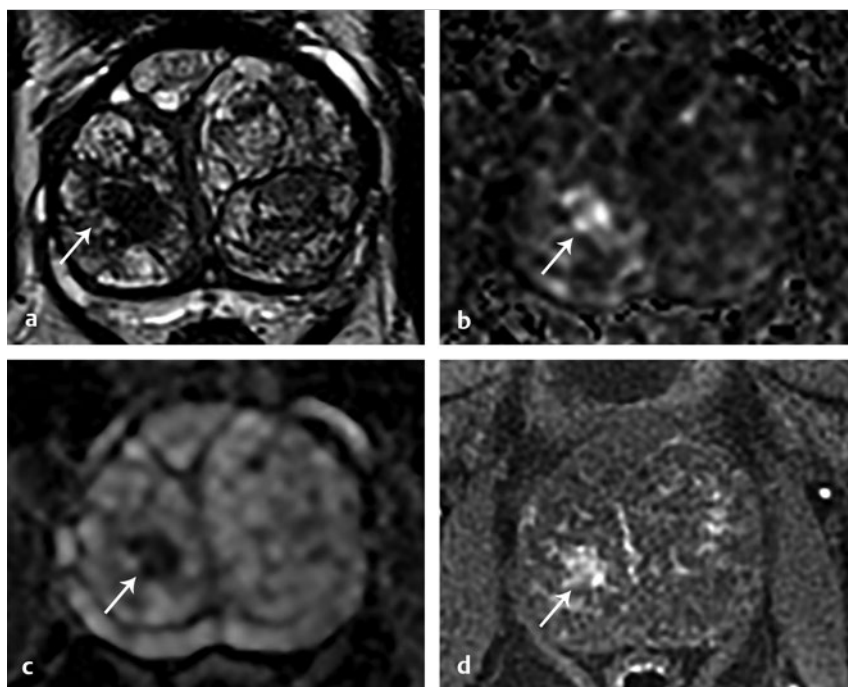


Fig. 12.8 PI-RADS 3 lesion in the transition zone corresponding to low-grade prostate cancer.

12.9 Case 9: PI-RADS 4 Lesion in the Transition Zone Corresponding to Intermediate-Grade Prostate Cancer

12.9.1 History

A 67-year-old man with a PSA level of 3.1 ng/mL and negative prior prostate biopsy (► Fig. 12.9).

12.9.2 Prostate MRI Findings

a) T2WI: 1.3-cm noncircumscribed, moderate T2 hypointense lesion in the right anterior transition zone measuring 1.3 cm

- b) DWI (b = 1500 s/mm²): Marked hyperintensity measuring < 1.5 cm
- c) ADC: Marked hypointensity measuring < 1.5 cm
- d) DCE: Focal early enhancement matching the edges of the lesion on the other sequences (positive DCE)

PI-RADS v2 assessment category: 4

12.9.3 Diagnosis

Gleason score 3 + 4 prostate cancer

Teaching points: This transition zone lesion is visually most striking on DWI/ADC. Although DWI is not the primary determinant of the PIRADS v2 assessment category for transition zone lesions, it can be helpful for initial identification of lesions and for calling the reader's attention to areas to scrutinize more closely on T2WI.

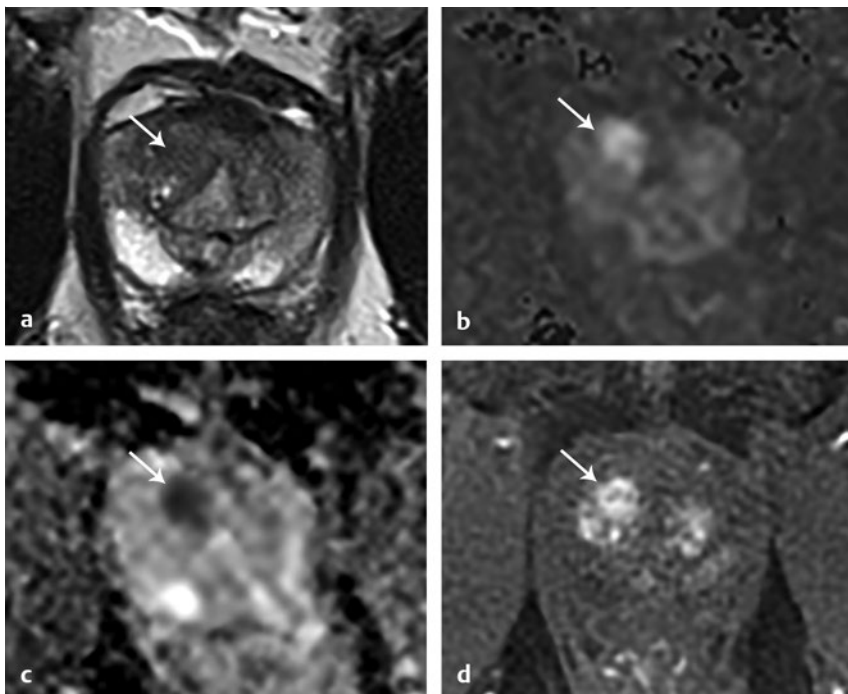


Fig. 12.9 PI-RADS 4 lesion in the transition zone corresponding to intermediate-grade prostate cancer.

12.10 Case 10: PI-RADS 5 Transition Zone Lesion Corresponding to High-Grade Prostate Cancer

12.10.1 History

A 65-year-old man with an elevated PSA level of 16 ng/mL and negative prior prostate biopsy (► Fig. 12.10).

12.10.2 Prostate MRI Findings

- T2WI: Homogenous, moderately hypointense lesion with noncircumscribed partially obscured margin measuring 1.7 cm
- DWI (b = 1500 s/mm²): Focal marked hyperintensity measuring > 1.5 cm
- ADC: Focal marked hypointensity measuring > 1.5 cm
- DCE: Focal early enhancement matching the edges of the lesion on the other sequences (positive DCE)

PI-RADS v2 assessment category: 5

12.10.3 Diagnosis

Gleason score 4 + 4 prostate cancer.

Teaching points: The “erased charcoal” sign on T2WI can help identify transition zone tumors. This sign refers to a lesion that is T2 hypointense with blurred, indistinct margins. This appearance has also been described as resembling a smudged fingerprint.

12.10.4 Suggested Reading

- [1] American College of Radiology (ACR) Prostate Imaging-Reporting and Data System (PI-RADS), Version 2. 2015. <http://www.acr.org/-/media/ACR/Documents/PDF/QualitySafety/Resources/PIRADS/PIRADS%20V2.pdf>. Published 2015. Accessed on October 30, 2015.

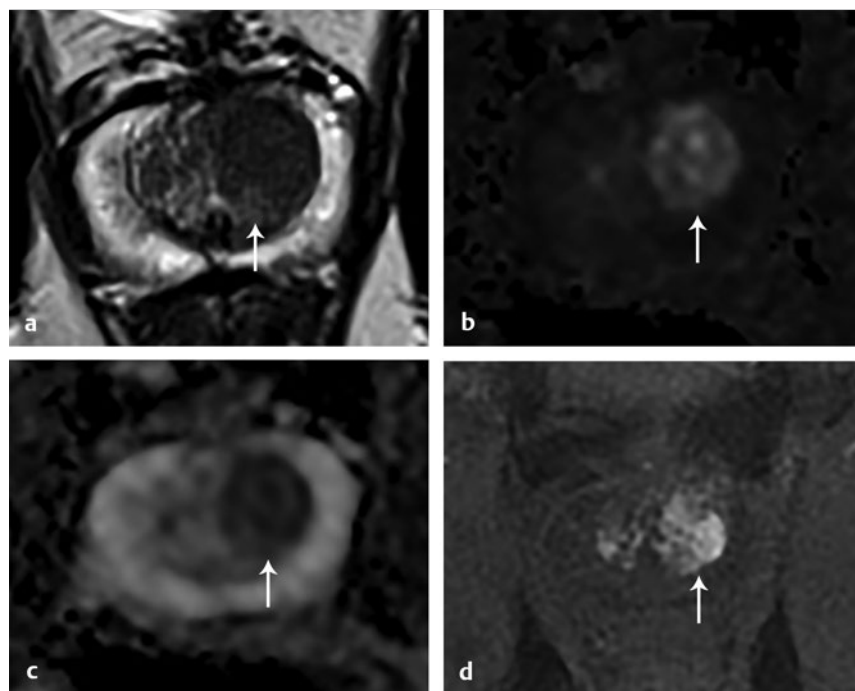


Fig. 12.10 PI-RADS 5 transition zone lesion corresponding to high-grade prostate cancer.

12.11 Case 11: PI-RADS 5 Lesion in the Transition Zone Corresponding to Low-Grade Prostate Cancer

12.11.1 History:

A 67-year-old man with an elevated PSA level of 5.1 ng/mL and negative prior prostate biopsy (► Fig. 12.11).

12.11.2 Prostate MRI Findings

- T2WI: 2.1-cm crescentic-shaped lesion in the right anterior midgland transition zone that is homogenous and moderately T2 hypointense
- DWI (b = 1500 s/mm²): Focal marked hyperintensity measuring ≥ 1.5 cm
- ADC: Focal marked hypointensity measuring ≥ 1.5 cm. The ADC value was 480 μm²/s

PI-RADS v2 assessment category: 5

12.11.3 Diagnosis

Gleason score 3 + 3 prostate cancer.

Teaching points: Although this lesion is markedly hypointense on ADC, the tumor was found to be low grade. The association between ADC values and Gleason score assessment category in the transition zone is not as strong as their association in the peripheral zone.

12.11.4 Suggested Reading

- [1] Hambrock T, Somford DM, Huisman HJ et al. Relationship between apparent diffusion coefficients at 3.0-T MR imaging and Gleason grade in peripheral zone prostate cancer. *Radiology* 2011; 259(2):453–461
- [2] Tamada T, Sone T, Jo Y et al. Apparent diffusion coefficient values in peripheral and transition zones of the prostate: comparison between normal and malignant prostatic tissues and correlation with histologic grade. *J Magn Reson Imaging* 2008; 28(3):720–726
- [3] Verma S, Rajesh A, Morales H et al. Assessment of aggressiveness of prostate cancer: correlation of apparent diffusion coefficient with histologic grade after radical prostatectomy. *AJR Am J Roentgenol* 2011; 196(2):374–381

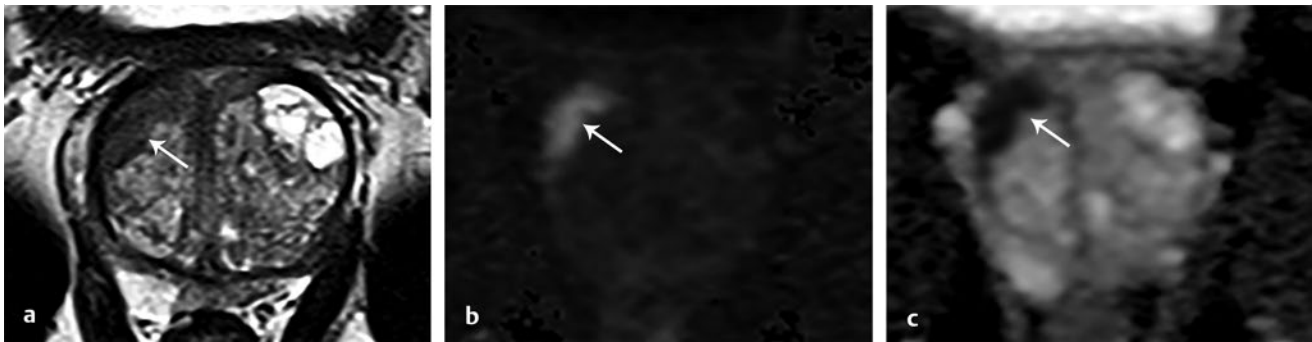


Fig. 12.11 PI-RADS 5 lesion in the transition zone corresponding to low-grade prostate cancer.

12.12 Case 12: Normal Central Zone

12.12.1 History

A 68-year-old man with an elevated PSA level of 5.5 ng/mL (► Fig. 12.12).

12.12.2 Prostate MRI Findings

- Axial T2WI: Symmetric, dumbbell-shaped, T2 hypointensity at the base of the prostate surrounding the ejaculatory ducts
- Coronal T2WI: Symmetric T2 hypointensity at the base of the prostate
- DWI (b = 1500 s/mm²): Minimal hyperintensity (*long arrow*). Note the increased signal within the ejaculatory ducts (*arrowheads*).
- ADC: Moderately hypointense
- DCE: Mild, delayed enhancement

12.12.3 Diagnosis

Characteristic symmetric appearance of the central zone (benign).

Teaching points: The central zone surrounds the ejaculatory ducts and is located predominantly at the base of the prostate and extends to the verumontanum. It can be distinctly visualized in the large majority of patients. The central zone typically appears as a symmetric band of T2 hypointensity at the base of the prostate that shows decreased ADC. One study reported that the normal CZ shows progressive (type 1) or plateau (type 2) enhancement on DCE. Coronal images can help show the symmetric, triangular appearance of the central zone.

12.12.4 Suggested Reading

- [1] Hansford BG, Karademir I, Peng Y et al. Dynamic contrast-enhanced MR imaging features of the normal central zone of the prostate. *Acad Radiol* 2014; 21(5):569–577
- [2] Vargas HA, Akin O, Franiel T et al. Normal central zone of the prostate and central zone involvement by prostate cancer: clinical and MR imaging implications. *Radiology* 2012; 262(3):894–902
- [3] Yu J, Fulcher AS, Turner MA, Cockrell CH, Cote EP, Wallace TJ. Prostate cancer and its mimics at multiparametric prostate MRI. *Br J Radiol* 2014; 87(1037):20130659

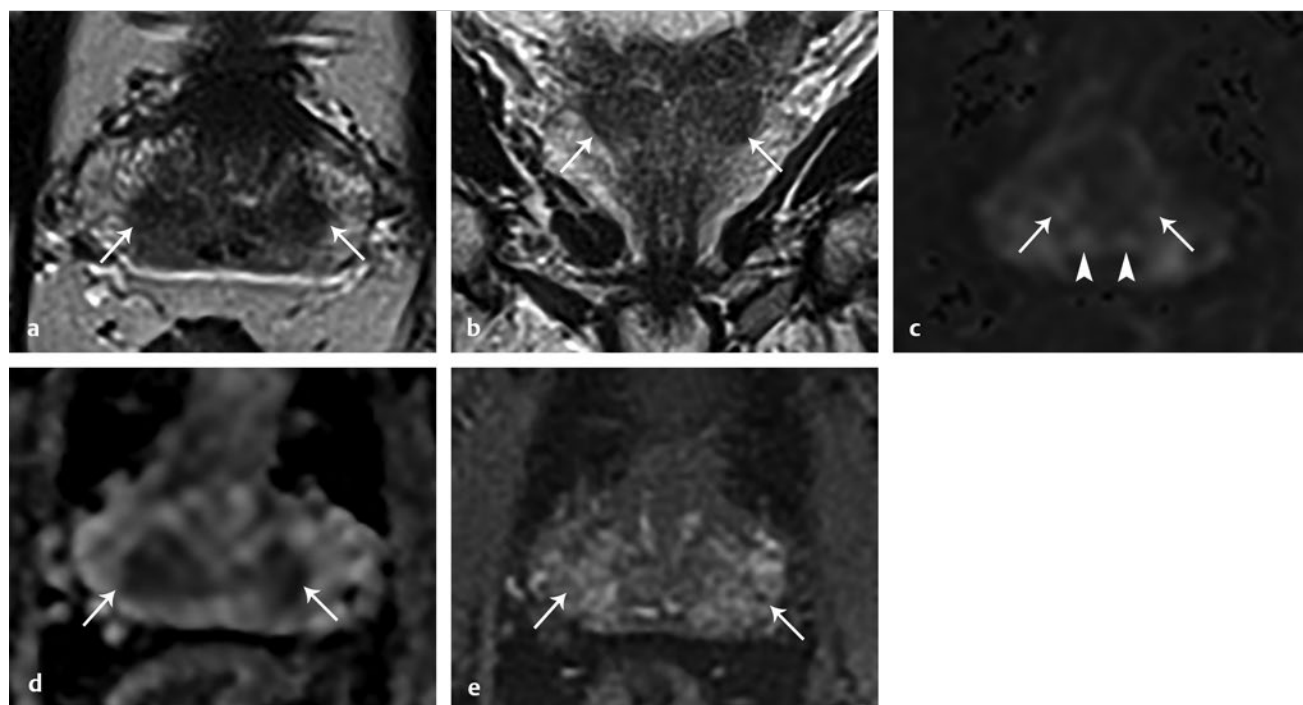


Fig. 12.12 Normal central zone.

12.13 Case 13: Central Zone Displaced Laterally

12.13.1 History

A 60-year-old man with a PSA level of 2.9 ng/mL and Gleason score 3+3 prostate cancer at the right apex on active surveillance (► Fig. 12.13).

12.13.2 Prostate MRI Findings

a) T2WI: Symmetric, bandlike, crescentic T2 hypointensity at the base of the prostate, positioned between the transition and peripheral zones bilaterally

b) DWI (b = 1500 s/mm²): No hyperintensity

c) ADC: Marked hypointensity

d) DCE: No early enhancement

12.13.3 Diagnosis

Benign central zone displaced laterally

Teaching points: The two lobes of the normal central zone can be displaced laterally. The symmetric appearance and lack of DWI hyperintensity helps establish the finding as the central zone.

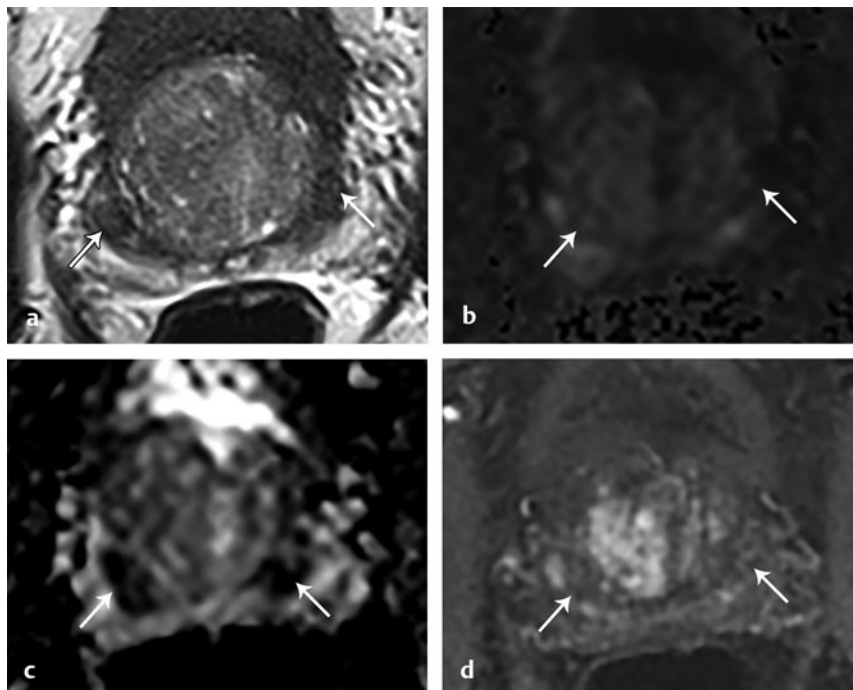


Fig. 12.13 Central zone displaced laterally.

12.14 Case 14: Central Zone Tumor

12.14.1 History

A 60-year-old man with an elevated PSA level of 6.1 ng/mL and no prior biopsy (► Fig. 12.14).

12.14.2 Prostate MRI Findings

- a) T2WI: Asymmetric prominence of the right central zone within the right posteromedial base
- b) DWI ($b = 1500 \text{ s/mm}^2$): Marked hyperintensity measuring $\geq 1.5 \text{ cm}$.
- c) ADC: Marked hypointensity measuring $\geq 1.5 \text{ cm}$
- d) DCE: Focal early enhancement with edges matching the T2 and DWI abnormality

PI-RADS v2 assessment category: 5

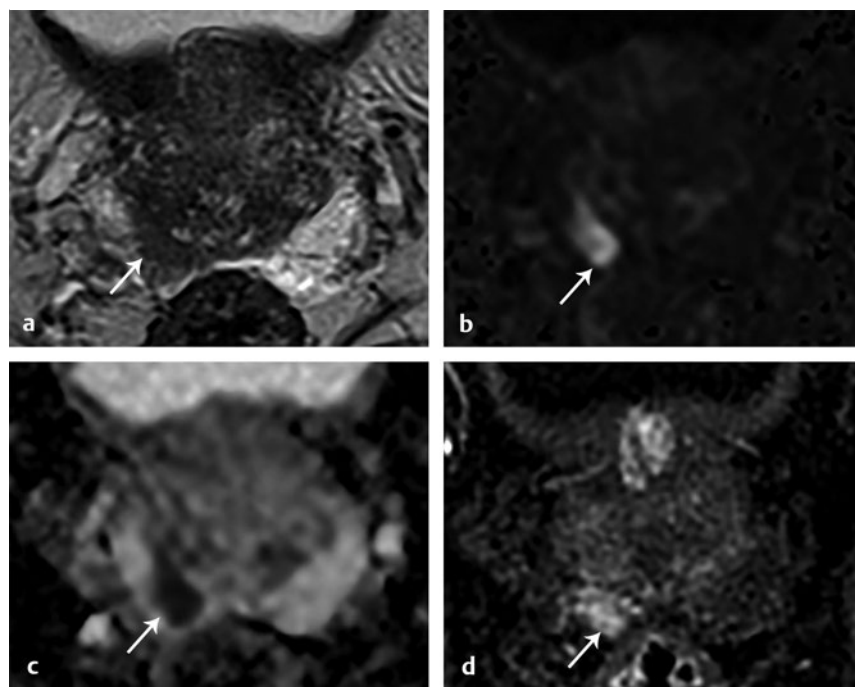


Fig. 12.14 Central zone tumor. (Reproduced with permission from the American Journal of Roentgenology. Rosenkrantz AB et al. Prostate Cancer: Top Places Where Tumors Hide on Multiparametric MRI. *Amer J Roentgenol* 2015;204:W449-W456.)

12.14.3 Diagnosis

MRI-TRUS fusion biopsy revealed Gleason score 3+4 prostate cancer. Concurrent standard 12-core biopsy was negative.

Teaching points: Although less than 5% of tumors occur in the central zone, they tend to be more aggressive. Normal central zone is hypointense on T2WI and ADC and typically has a symmetric appearance. A central zone tumor can be suspected in the presence of central zone asymmetry with greater T2WI and ADC hypointensity compared to the contralateral side and early enhancement with washout (type 3 enhancement).

12.14.4 Suggested Reading

- [1] Vargas HA, Akin O, Franiel T et al. Normal central zone of the prostate and central zone involvement by prostate cancer: clinical and MR imaging implications. *Radiology* 2012; 262(3):894–902

12.15 Case 15: Benign Thickening of the Anterior Fibromuscular Stroma.

12.15.1 History

A 74-year-old man undergoing work-up for hematuria found to have an abnormality of the prostatic urethra during cystoscopy. Biopsy revealed Gleason score 4+3 prostate cancer (► Fig. 12.15).

12.15.2 Prostate MRI Findings

- a) T2WI: Noncircumscribed, convex T2 hypointense lesion involving the anterior fibromuscular stroma (AFMS)
- b) DWI (b = 1500 s/mm²): No abnormality
- c) ADC: Mild hypointensity

- d) DCE: No focal early enhancement matching the T2 or ADC abnormality

12.15.3 Diagnosis

Benign thickening of the AFMS. The patient underwent radical prostatectomy for tumor elsewhere in the gland, and no tumor was found in the AFMS or elsewhere in the anterior prostate.

Teaching points: Although the appearance on T2WI is suspicious for tumor in this case, the lack of DWI hyperintensity or positive DCE indicate this is benign thickening of the anterior fibromuscular stroma.

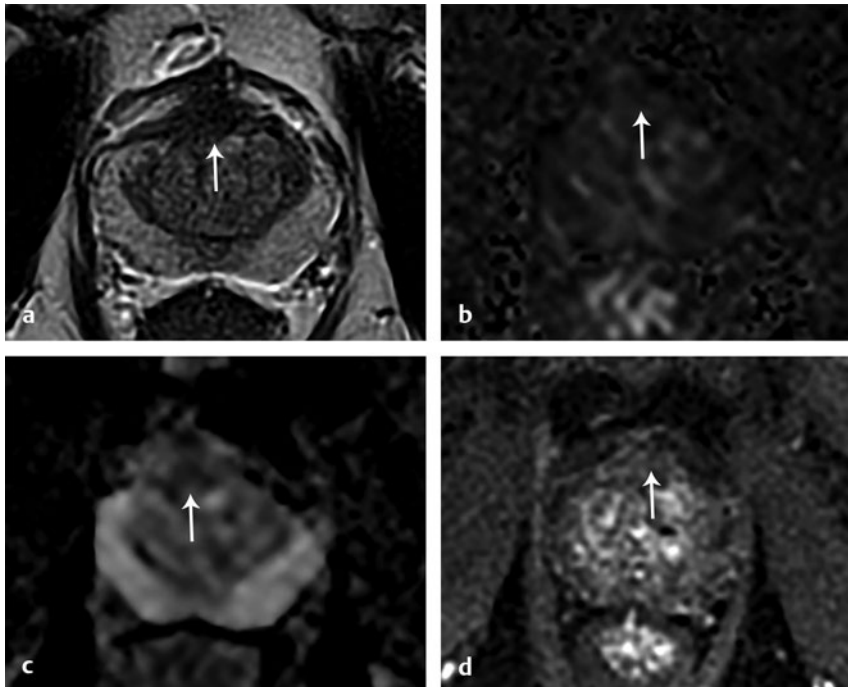


Fig. 12.15 Benign thickening of the anterior fibromuscular stroma.

12.16 Case 16: Tumor Involving the Anterior Fibromuscular Stroma

12.16.1 History

A 67-year-old with an elevated PSA level of 14.8 ng/mL and prior biopsy revealing high-grade prostatic intraepithelial neoplasia (HGPIN) (► Fig. 12.16).

12.16.2 Prostate MRI Findings

- a) T2WI: Homogenous, crescentic T2 hypointense mass involving the midline anterior transition zone and anterior fibromuscular stroma
- b) DWI ($b = 1500 \text{ s/mm}^2$): Marked hyperintensity measuring $\geq 1.5 \text{ cm}$
- c) ADC: Marked hypointensity measuring $\geq 1.5 \text{ cm}$
- d) DCE: Mild early enhancement

PI-RADS v2 assessment category: 5

12.16.3 Diagnosis

MRI-TRUS fusion biopsy revealed Gleason score 3+4 prostate cancer

Teaching points: The anterior fibromuscular stroma (AFMS) forms the anterior border of the prostate gland and is composed of T2 hypointense fibrous and smooth muscle tissue. Although the AFMS does not have glandular tissue, it has been recognized that tumors may grow predominantly within this region after arising from the margin of the transition zone. The tumors can expand the AFMS as they extend anteriorly and often have a lenticular shape. The presence of positive DCE can be helpful for tumor detection in this region, as the normal AFMS is hypovascular.

12.16.4 Suggested Reading

- [1] Rosenkrantz AB, Verma S, Turkbey B. Prostate cancer: top places where tumors hide on multiparametric MRI. *AJR Am J Roentgenol* 2015; 204(4): W449–W456

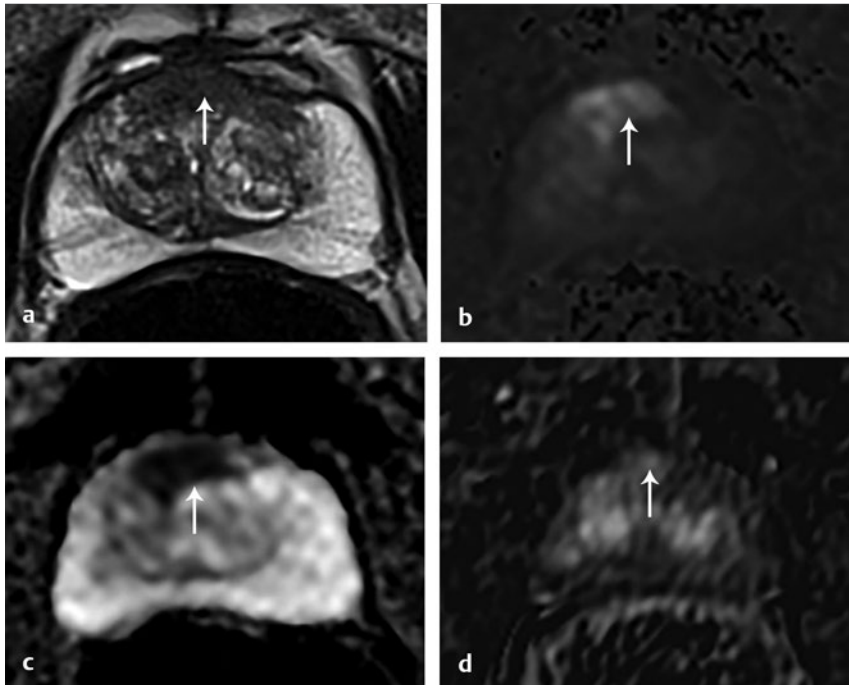


Fig. 12.16 Tumor involving the anterior fibromuscular stroma.

12.17 Case 17: Extruded Benign Prostatic Hyperplasia Nodule in the Peripheral Zone

12.17.1 History

A 66-year-old man with an elevated PSA level of 8 ng/mL (► Fig. 12.17).

12.17.2 Prostate MRI Findings

Axial T2WI: Round, heterogeneous, circumscribed, encapsulated lesion in the right posterolateral peripheral zone abutting the interface with the transition zone. The nodule contains

areas of internal T2 hyperintensity and a thin, peripheral hypointense capsule.

12.17.3 Diagnosis

Extruded benign prostatic hyperplasia (BPH) nodule.

Teaching points: Extruded BPH nodules may occur in the peripheral zone. A round, encapsulated nodule in the peripheral zone can be given an assessment category of 2 despite low ADC. Heterogeneous T2 signal resembling other typical BPH nodules in the transition zone, presence of a peripheral capsule, and location along the transition zone are reassuring features that support a diagnosis of an extruded BPH nodule.

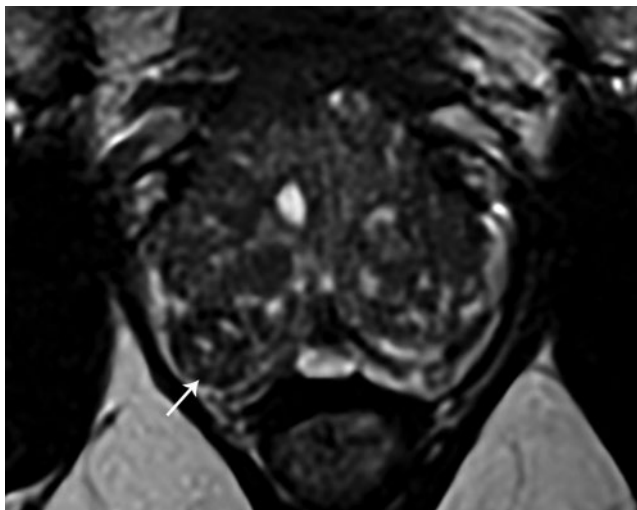


Fig. 12.17 Extruded benign prostatic hyperplasia (BPH) nodule in the peripheral zone.

12.18 Case 18: Extruded Benign Prostatic Hyperplasia Nodule in the Peripheral Zone

12.18.1 History

A 57-year-old man with an elevated PSA level of 5.9 ng/mL and negative prior prostate biopsy (► Fig. 12.18).

12.18.2 Prostate MRI Finding

- Axial T2WI: Round, circumscribed T2 hypointense lesion in the right anterolateral midgland peripheral zone abutting the interface with the transition zone
- DWI (b = 1500 s/mm²): Marked hyperintensity measuring < 1.5 cm
- ADC: Marked hypointensity measuring < 1.5 cm
- DCE: Focal early enhancement matching the edges of the T2WI and DWI abnormality

PI-RADS v2 assessment category: 2

12.18.3 Diagnosis

MRI-TRUS fusion biopsy revealed benign prostate tissue. This represents an extruded benign prostatic hyperplasia (BPH) nodule.

Teaching points: Extruded BPH nodules may be found in the peripheral zone. A round, encapsulated nodule in the peripheral zone can be assigned a PI-RADS assessment category of 2 despite low ADC. As with BPH nodules in the transition zone, these extruded nodules can show restricted diffusion and positive DCE.

12.18.4 Suggested Reading

- [1] American College of Radiology (ACR) Prostate Imaging-Reporting and Data System (PI-RADS), Version 2. 2015. <http://www.acr.org/-/media/ACR/Documents/PDF/QualitySafety/Resources/PIRADS/PIRADS%20V2.pdf>. Published 2015. Accessed on October 30, 2015.

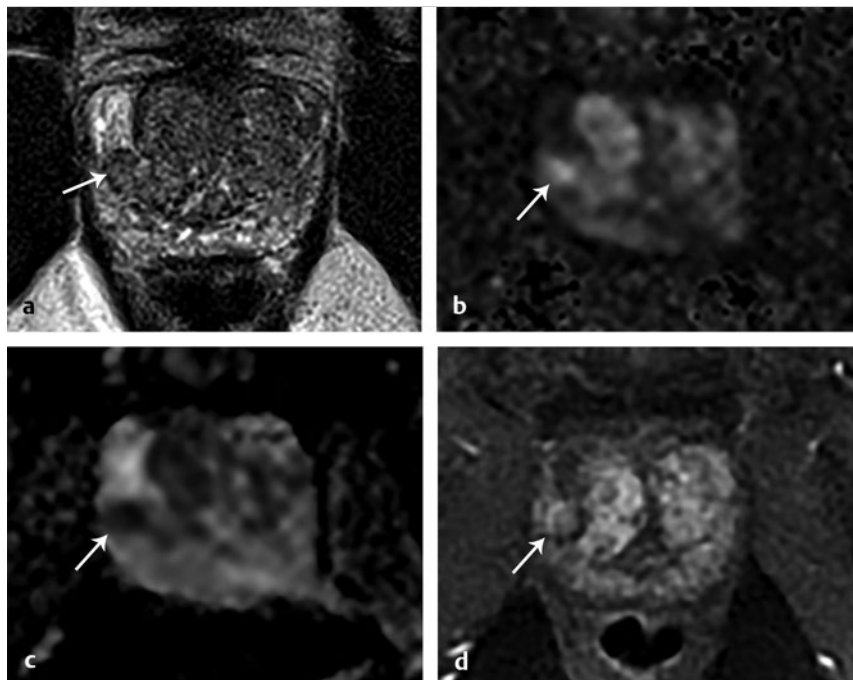


Fig. 12.18 Extruded benign prostatic hyperplasia (BPH) nodule in the peripheral zone.

12.19 Case 19: Midline Pseudolesion

12.19.1 History

A 66-year-old man with an elevated PSA level of 6.4 ng/mL and two negative prior prostate biopsies (► Fig. 12.19).

12.19.2 Prostate MRI Findings

- a) T2WI: Wedge shaped T2 hypointensity in the midline base-to-midgland peripheral zone
- b) DWI (b = 1500 s/mm²): Focal hyperintensity
- c) ADC: Focal hypointensity
- d) DCE: No associated early enhancement

12.19.3 Diagnosis

Midline pseudolesion

Teaching points: The so-called pseudolesion is a focal T2 hypointense, diffusion-restricting structure in the midline base-to-midgland peripheral zone. It is suggested that this may represent fibrous thickening in the region of fusion of the prostate capsule and overlying fascia at the junction of the two lobes. Features that support the diagnosis of a pseudolesion rather than a tumor include the typical base-to-midgland midline location, wedged shape, and lack of early enhancement. Tumor should be suspected if the lesion is rounded or masslike, extends more caudally towards the apex, or shows positive DCE findings.

12.19.4 Suggested Reading

- [1] Yu J, Fulcher AS, Turner MA, Cockrell CH, Cote EP, Wallace TJ. Prostate cancer and its mimics at multiparametric prostate MRI. *Br J Radiol* 2014; 87 (1037):20130659

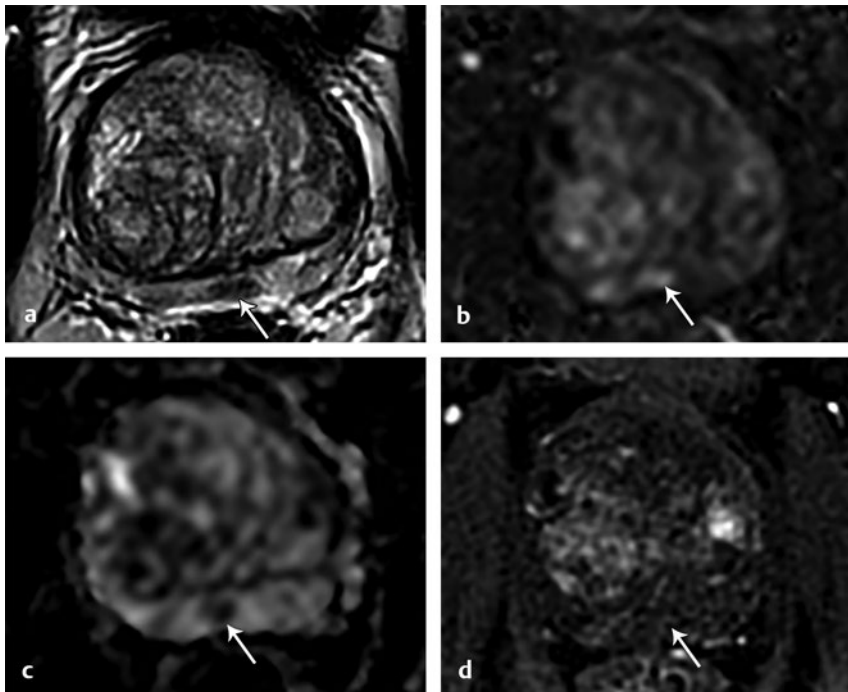


Fig. 12.19 Midline pseudolesion.

12.20 Case 20: Prostate Cancer Mimicking the Midline Pseudolesion

12.20.1 History

A 76-year-old man with an elevated PSA level of 5 ng/mL and no prior prostate biopsy (► Fig. 12.20).

12.20.2 Prostate MRI Findings

a) T2WI: Circumscribed, homogenous moderate T2 hypointense mass measuring 1.2 cm in the right paramedian midland-to-apex peripheral zone

- b) DWI ($b = 1500 \text{ s/mm}^2$): Marked hyperintensity measuring $< 1.5 \text{ cm}$
- c) ADC: Moderate hypointensity measuring $< 1.5 \text{ cm}$
- d) DCE: Focal early enhancement matching the edges the T2WI and DWI findings

PI-RADS v2 assessment category: 4

12.20.3 Diagnosis

Gleason score 4+5 prostate cancer

Teaching points: Features of this lesion that help differentiate it from the midline pseudolesion include its eccentric location to the right of midline, rounded margins, and focal early enhancement.

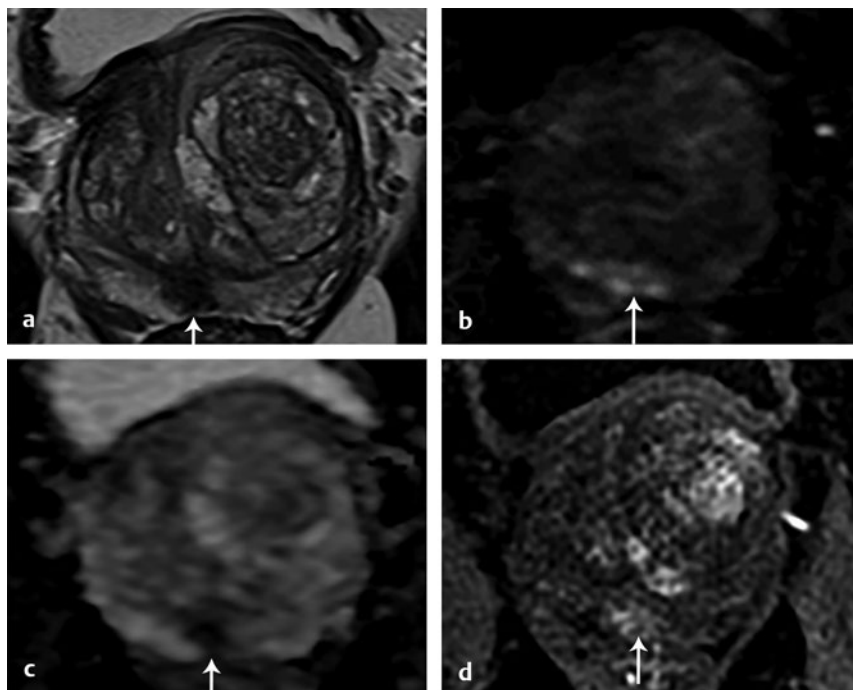


Fig. 12.20 Prostate cancer mimicking the midline pseudolesion.

12.21 Case 21: Distal Apex Tumor

12.21.1 History

A 62-year-old-man with an elevated PSA level of 6.5 ng/mL and negative prior prostate biopsy (► Fig. 12.21).

12.21.2 Prostate MRI Findings

- a) T2WI: Circumscribed, homogenous, T2 hypointense mass located within the right posteromedial distal apex peripheral zone
- b) DWI (b = 1500 s/mm²): Marked hyperintensity measuring < 1.5 cm
- c) ADC: Marked hypointensity measuring < 1.5 cm
- d) DCE: Focal early enhancement matching the edges of the T2WI and DWI findings

PI-RADS v2 assessment category: 4

12.21.3 Diagnosis

MRI-TRUS fusion biopsy revealed Gleason score 4+3 prostate cancer

Teaching points: Distal apical tumors are frequently not detected on systematic biopsy given challenges in adequately sampling this region using standard biopsy strategies. The region can more readily be sampled using MRI-targeted biopsy.

12.21.4 Suggested Reading

- [1] Nix JW, Turkbey B, Hoang A et al. Very distal apical prostate tumours: identification on multiparametric MRI at 3 Tesla. *BJU Int* 2012; 110(11 Pt B): E694–E700

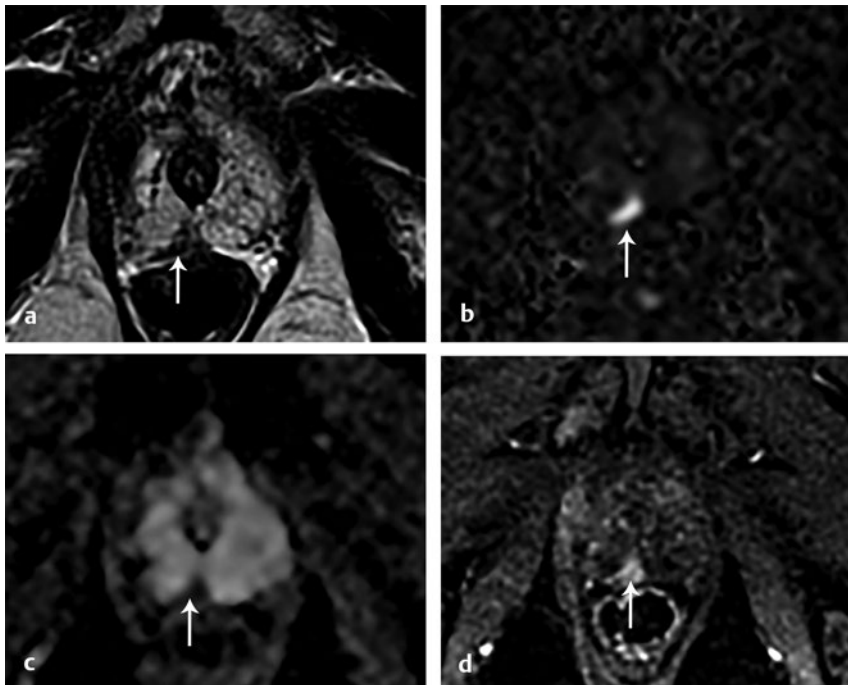


Fig. 12.21 Distal apex tumor.

12.22 Case 22: Distal Apex Tumor

12.22.1 History

A 67-year-old man with an elevated PSA level of 5.1 ng/mL and no prior prostate biopsy (► Fig. 12.22).

12.22.2 Prostate MRI Findings

- T2WI: Circumscribed, homogenous, T2 hypointense mass in the left anterior distal apex peripheral zone
- DWI (b = 1500 s/mm²): Marked hyperintensity measuring < 1.5 cm
- ADC: Marked hypointensity measuring < 1.5 cm
- DCE: Focal early enhancement matching the edges of the T2WI and DWI abnormalities

PI-RADS v2 assessment category: 4

12.22.3 Diagnosis

MRI-TRUS fusion biopsy revealed Gleason score 3+4 prostate cancer

Teaching points: Distal apical tumors are frequently not detected on standard biopsy due to their location and difficulty in sampling them.

12.22.4 Suggested Reading

- [1] Nix JW, Turkbey B, Hoang A et al. Very distal apical prostate tumours: identification on multiparametric MRI at 3 Tesla. *BJU Int* 2012; 110(11 Pt B):E694–E700

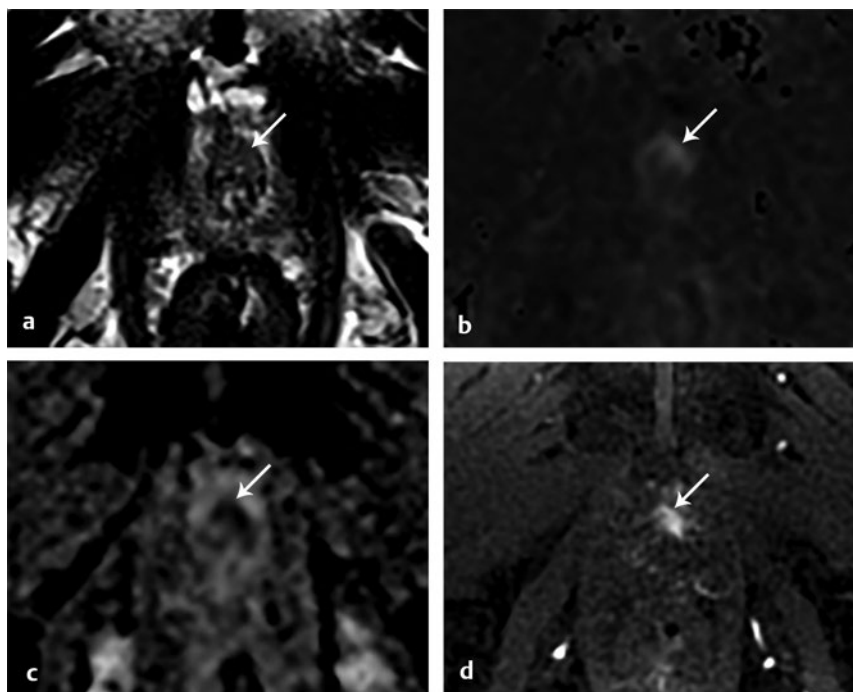


Fig. 12.22 Distal apex tumor.

12.23 Case 23: Prostate Cancer Contacting the Urethra

12.23.1 History

A 54-year-old man with an elevated PSA level of 13.5 ng/mL (► Fig. 12.23).

12.23.2 Prostate MRI Findings

- a) Axial T2WI: Circumscribed, homogenous, moderate T2 hypointense mass measuring ≥ 1.5 cm in the right posterior apex with gross extraprostatic extension (*long arrow*). The mass is inseparable from the urethra (*arrowhead*).
- b) Coronal T2WI: The mass (*long arrow*) shows a broad interface with the urethra (*arrowhead*).

- c) DWI ($b = 1500 \text{ s/mm}^2$): Marked hyperintensity measuring ≥ 1.5 cm
- d) ADC: Marked hypointensity measuring ≥ 1.5 cm

PI-RADS v2 assessment category: 5

12.23.3 Diagnosis

Biopsy showed multifocal, bilateral prostate cancer, including Gleason score 4 + 4 prostate cancer at the right apex.

Teaching points: The prostatic urethra can be visualized on T2WI as a round, hyperintense structure in the midline prostate. It is important to inspect midline tumors for urethral involvement.

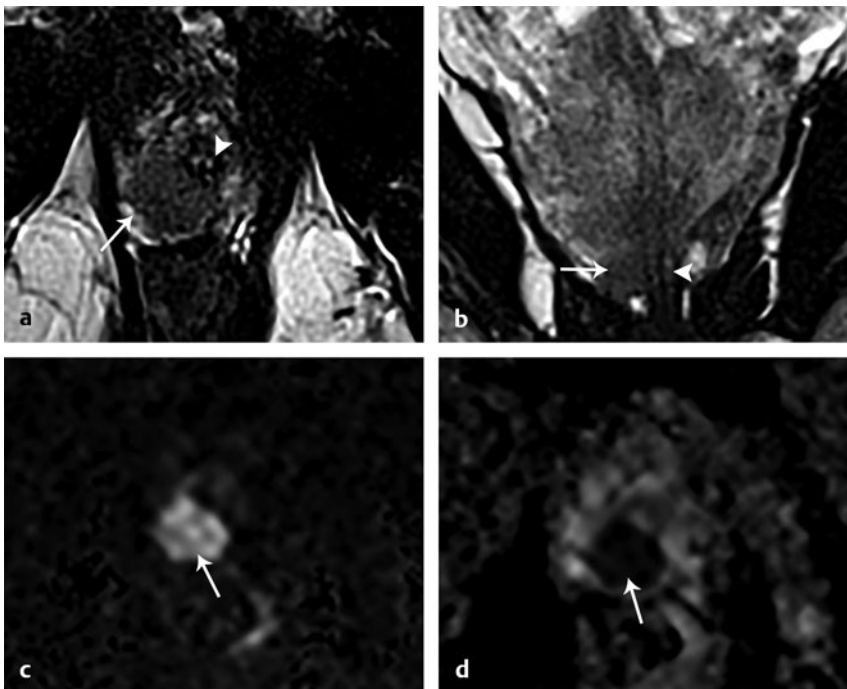


Fig. 12.23 Prostate cancer contacting the urethra.

12.24 Case 24: Lesion involving the External Urethral Sphincter

12.24.1 History

A 66-year-old man with an elevated PSA level of 14 ng/mL and prior negative biopsy (► Fig. 12.24).

12.24.2 Prostate MRI Finding

- a) Axial T2WI: Circumscribed, homogenous mass in the right anterior apex peripheral zone (*long arrow*) partially invading the prostatic urethra (*arrowhead*)
- b) Coronal T2WI: The mass (*long arrow*) involves the right external urethral sphincter. The normal left urethral sphincter is visualized (*arrowhead*) as a low-intensity structure surrounding the distal urethra.

- c) DWI ($b = 1500 \text{ s/mm}^2$): Marked hyperintensity measuring $\geq 1.5 \text{ cm}$
- d) ADC: Marked hypointensity measuring $\geq 1.5 \text{ cm}$

PI-RADS v2 assessment category: 5

12.24.3 Diagnosis

Teaching points: The external urethral sphincter normally appears as T2 hypointense tissue surrounding the distal urethra. It is important to scrutinize distal apical tumors for urethral sphincter involvement.

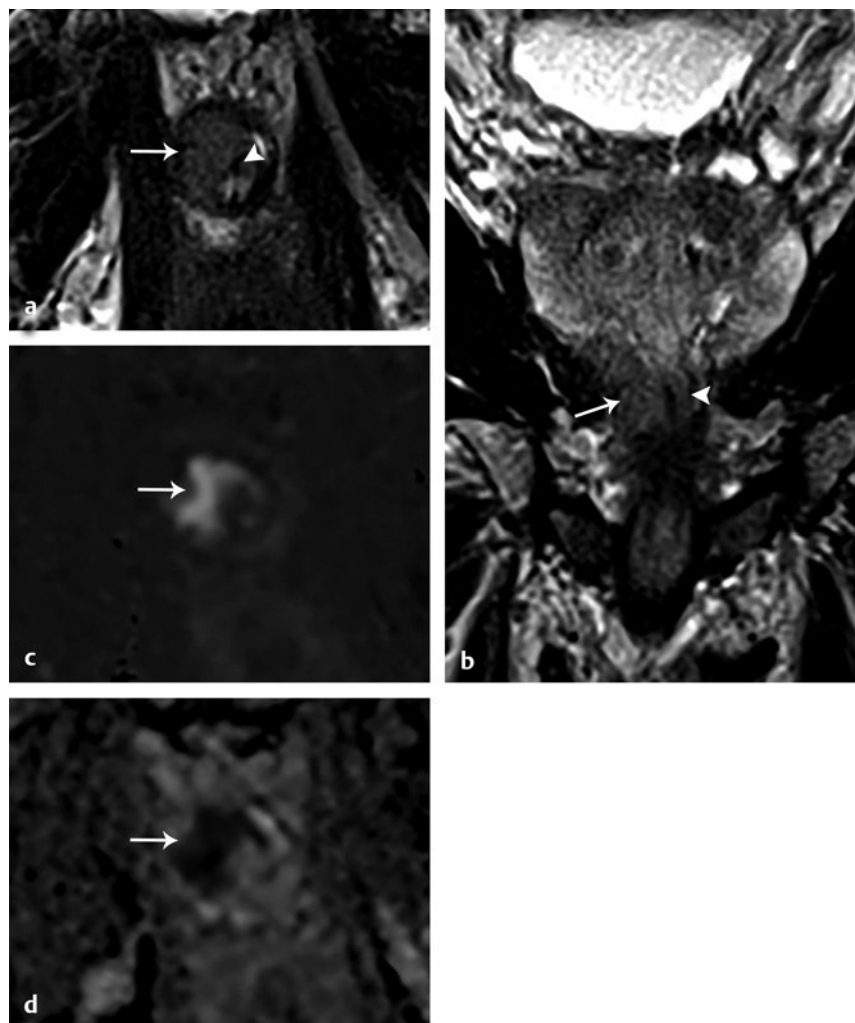


Fig. 12.24 Lesion involving the external urethral sphincter.

12.25 Case 25: Subcapsular Tumor

12.25.1 History

A 70-year-old man with elevated PSA of 11 ng/mL and prior prostate biopsy revealing Gleason score 3+4 prostate cancer in the left midgland (► Fig. 12.25).

12.25.2 Prostate MRI Findings

- a) T2WI: Crescentic, subcapsular T2 hypointense lesion
- b) DWI (b = 1500 s/mm²): Marked hyperintensity measuring ≥ 1.5 cm
- c) ADC: Marked hypointensity measuring ≥ 1.5 cm
- d) DCE: Focal early enhancement matching the edges of the T2WI and DWI abnormality

PI-RADS v2 assessment category: 5

12.25.3 Diagnosis

Prostatectomy revealed Gleason score 3+4 prostate cancer

Teaching points: DCE-MRI and DWI are helpful for the detection of subcapsular tumors, as they can often be difficult to identify on T2WI.

12.25.4 Suggested Reading

- [1] Rosenkrantz AB, Verma S, Turkbey B. Prostate cancer: top places where tumors hide on multiparametric MRI. *AJR Am J Roentgenol* 2015; 204(4): W449-W456

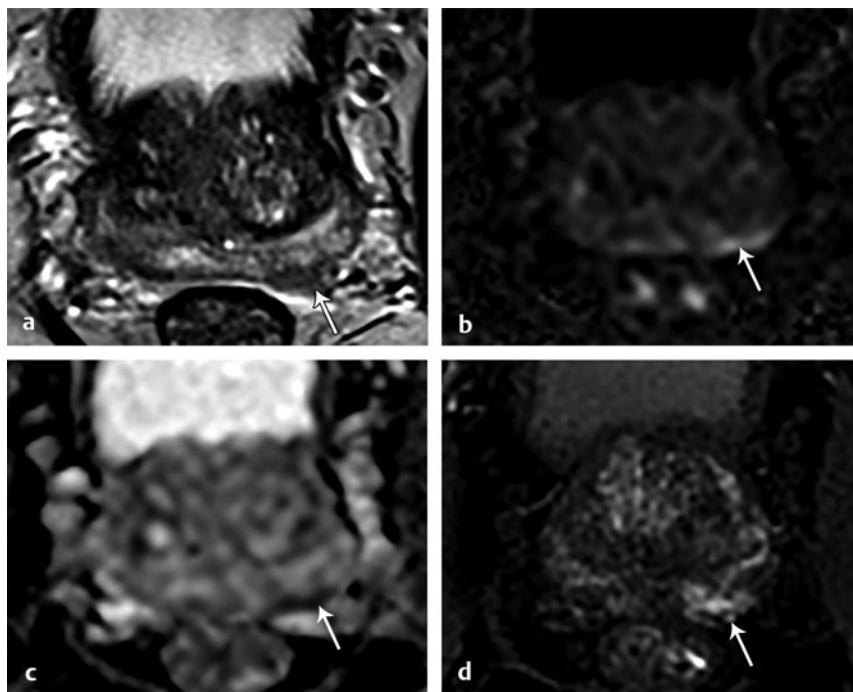


Fig. 12.25 Subcapsular tumor.

12.26 Case 26: Anterior Horn Peripheral Zone Tumor

12.26.1 History

A 63 year-old-man with an elevated PSA level of 5 ng/mL (► Fig. 12.26).

12.26.2 Prostate MRI Findings

- a) T2WI: Circumscribed T2 hypointense mass in the left antero-medial peripheral zone (anterior horn) measuring ≥ 1.5 cm.
- b) DWI ($b = 1500 \text{ s/mm}^2$): Marked hyperintensity measuring ≥ 1.5 cm.
- c) ADC: Marked hypointensity measuring ≥ 1.5 cm
- d) DCE: Focal early enhancement matching the edges of the T2WI and DWI abnormality

PI-RADS v2 assessment category: 5

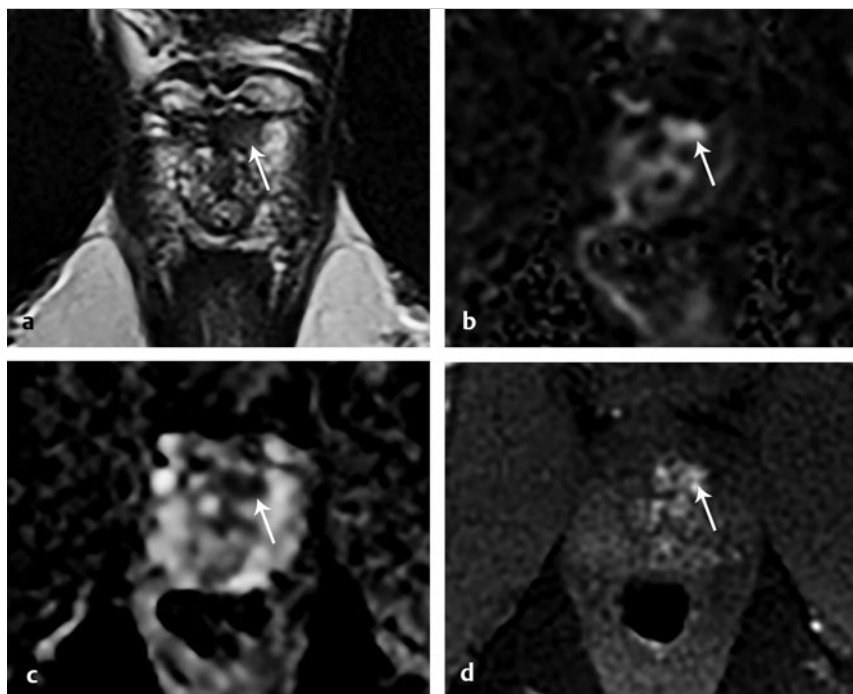


Fig. 12.26 Anterior horn peripheral zone tumor.

12.26.3 Diagnosis

MRI-TRUS fusion biopsy revealed Gleason score 3+3 prostate cancer. Standard 12-core biopsy was negative.

Teaching points: Identification of the zonal location of a lesion is crucial for determining the appropriate PI-RADS category, since the T2 signal is the determining factor of the assessment category in the transition zone, while the DWI signal is the primary determining factor of the assessment category for peripheral zone lesions. Confidant determination of the zonal location can be challenging for lesions in the anterior prostatic apex, where the anterior horn of the peripheral zone is typically very closely approximated to the transition zone and anterior fibromuscular stroma.

12.27 Case 27: Postbiopsy Hemorrhage Mimicking Tumor

12.27.1 History

A 71-year-old man with an elevated PSA level of 5.3 ng/mL and a biopsy performed 6 weeks prior revealing Gleason score 7 cancer on the right (► Fig. 12.27)

12.27.2 Prostate MRI Findings

- T2WI: Circumscribed T2 hypointense lesion in the right posterior midgland peripheral zone
- T1WI: Matching T1 hyperintensity on the precontrast image, representing postbiopsy hemorrhage
- DWI (b = 1500 s/mm²): No abnormality
- ADC: No abnormality
- DCE: Subtracted postcontrast image shows no early enhancement

PI-RADS v2 assessment category: 1

12.27.3 Diagnosis

Postbiopsy hemorrhage

Teaching points: The prostate gland produces citrate, which functions as a preservative in semen. In addition, citrate has anticoagulant properties, which may contribute to the prolonged presence of postbiopsy hemorrhage in the prostate. Although the hemorrhage may persist for months, PI-RADS v2 advises an interval of at least 6 weeks between biopsy and MRI to allow for the hemorrhage to mostly resolve. Hemorrhage exhibits T1 hyperintensity and is often T2 hypointense, potentially mimicking tumor on T2WI. However, hemorrhage typically shows relatively mild changes on DWI and DCE-MRI, which help differentiate postbiopsy hemorrhage from tumor.

12.27.4 Suggested Reading

- Radiology (ACR) Prostate Imaging-Reporting and Data System (PI-RADS). Version 2. 2015. <http://www.acr.org/-/media/ACR/Documents/PDF/QualitySafety/Resources/PIRADS/PIRADS%20V2.pdf>. Published 2015. Accessed on October 30, 2015.
- Rosenkrantz AB, Mussi TC, Hindman N et al. Impact of delay after biopsy and post-biopsy haemorrhage on prostate cancer tumour detection using multi-parametric MRI: a multi-reader study. *Clin Radiol* 2012; 67(12):e83–e90
- Tamada T, Sone T, Jo Y et al. Prostate cancer: relationships between post-biopsy hemorrhage and tumor detectability at MR diagnosis. *Radiology* 2008; 248(2):531–539

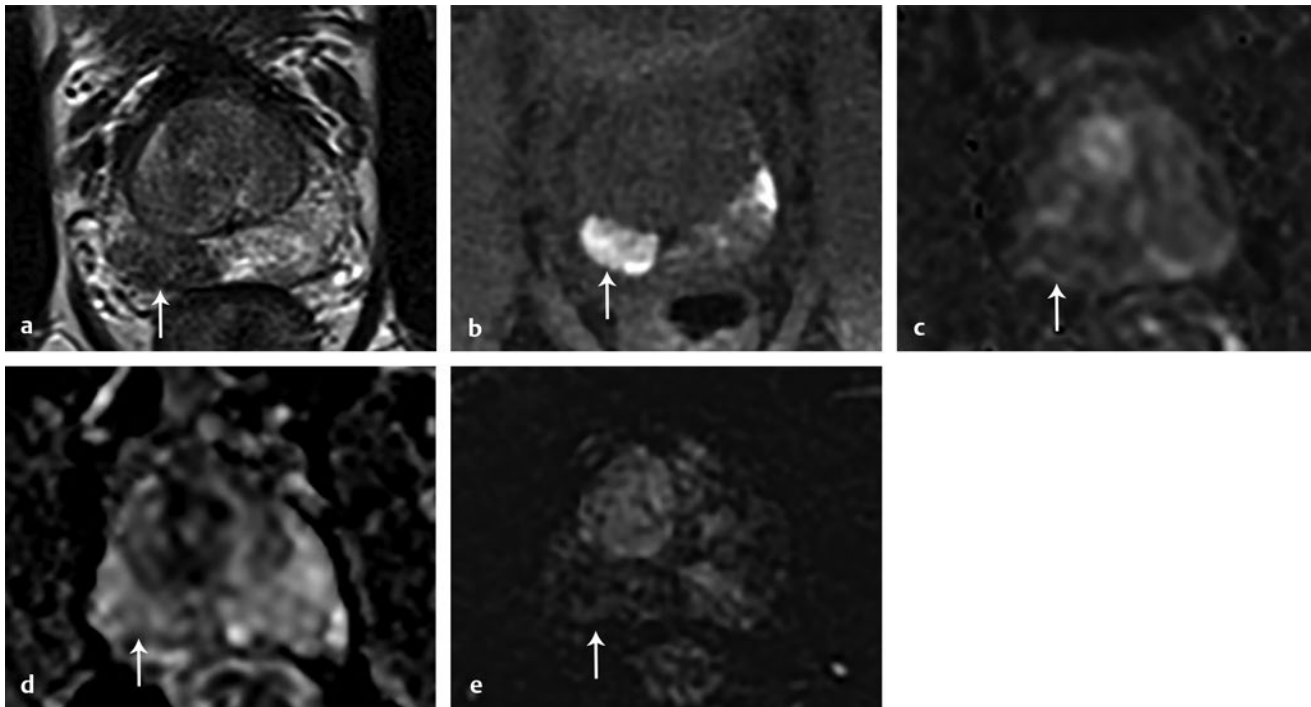


Fig. 12.27 Post biopsy hemorrhage mimicking tumor.

12.28 Case 28: Tumor Well Visualized Despite Hemorrhage, Exhibiting Hemorrhage Exclusion Sign

12.28.1 History

A 54-year-old man with prostate biopsy 4 weeks prior revealing cancer (► Fig. 12.28).

12.28.2 Prostate MRI Findings

- T2WI: Circumscribed T2 hypointense lesion in the right posterolateral midgland peripheral zone
- T1 WI: Precontrast T1WI shows diffuse hyperintensity throughout the peripheral zone with an area of sparing that matches the T2 abnormality
- DWI ($b = 1500 \text{ s/mm}^2$): Marked hyperintensity measuring $< 1.5 \text{ cm}$

- ADC: Marked hypointensity measuring $< 1.5 \text{ cm}$
- DCE: Subtracted postcontrast image shows focal early enhancement matching the edges of the T2WI and DWI abnormality

PI-RADS v2 assessment category: 4

12.28.3 Diagnosis

Prostate cancer outlined by extensive postbiopsy hemorrhage.

Teaching points: In the setting of extensive postbiopsy hemorrhage, dominant tumors may be spared and outlined by the hemorrhage. Therefore, thorough evaluation of T1-weighted images can help detect tumors in conjunction with assessment for corresponding abnormality on other sequences.

12.28.4 Suggested Reading

- [1] Barrett T, Vargas HA, Akin O, Goldman DA, Hricak H. Value of the hemorrhage exclusion sign on T1-weighted prostate MR images for the detection of prostate cancer. *Radiology* 2012; 263(3):751–757

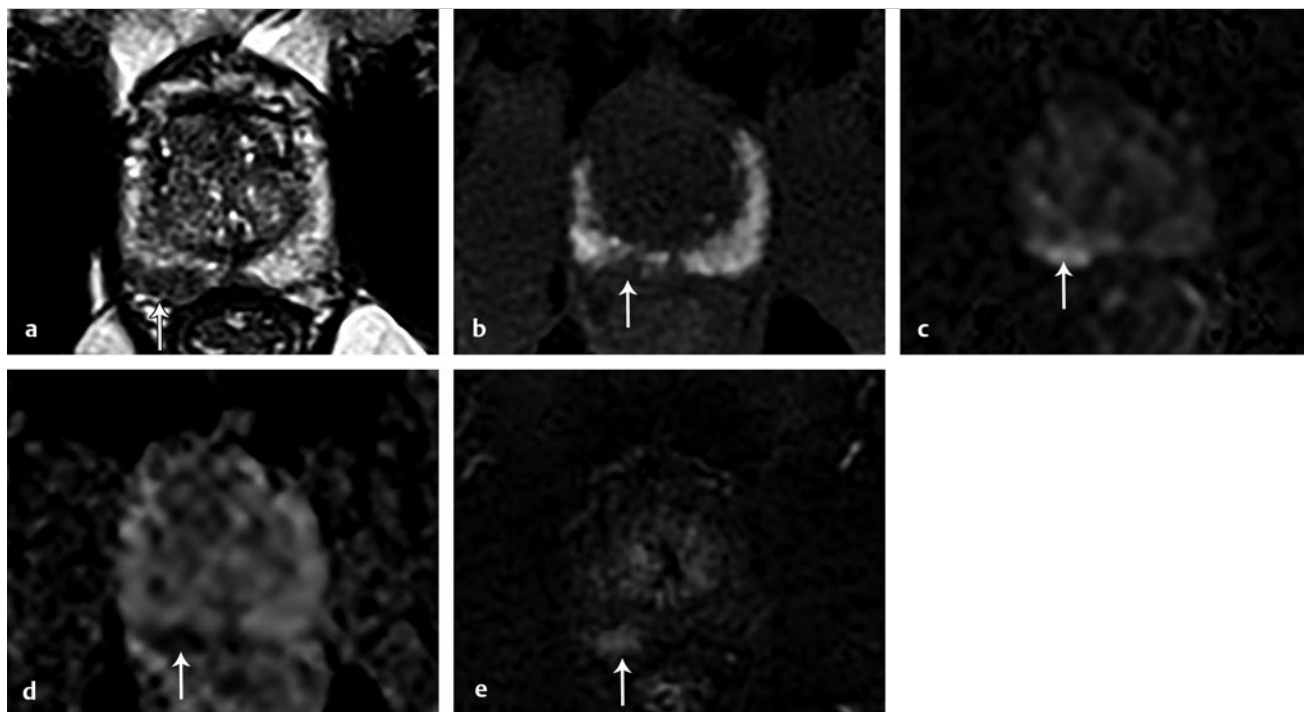


Fig. 12.28 Tumor well visualized despite hemorrhage, exhibiting hemorrhage exclusion sign.

12.29 Case 29: Benign Thickening of the Junction of the Peripheral Zone and the Transition Zone

12.29.1 History

A 61-year-old man with an elevated PSA level of 4.2 ng/mL with prior biopsy revealing Gleason score 3+3 prostate cancer (► Fig. 12.29).

12.29.2 Prostate MRI Findings

- a) T2WI: Crescentic, linear hypointensity in the left posterolateral midgland at the junction of the transition and peripheral zones that is asymmetrically thickened when compared to the right
- b) DWI ($b = 1500 \text{ s/mm}^2$): No abnormality
- c) ADC: Crescentic hypointensity, asymmetrically thickened when compared to the right

d) DCE: No associated abnormal enhancement

PI-RADS v2 assessment category: 1

12.29.3 Diagnosis

Asymmetric thickening of the junction between the peripheral and transition zones, a benign finding.

Teaching points: A pseudocapsule surrounds the transition zone and appears as a thin, linear, crescentic T2 hypointensity with low ADC. It may be more conspicuous or asymmetric in some patients. The typical location and shape and signal features can help differentiate an asymmetrically thickened capsule from tumor.

12.29.4 Suggested Reading

- [1] Rosenkrantz AB, Taneja SS. Radiologist, be aware: ten pitfalls that confound the interpretation of multiparametric prostate MRI. *AJR Am J Roentgenol* 2014; 202(1):109–120

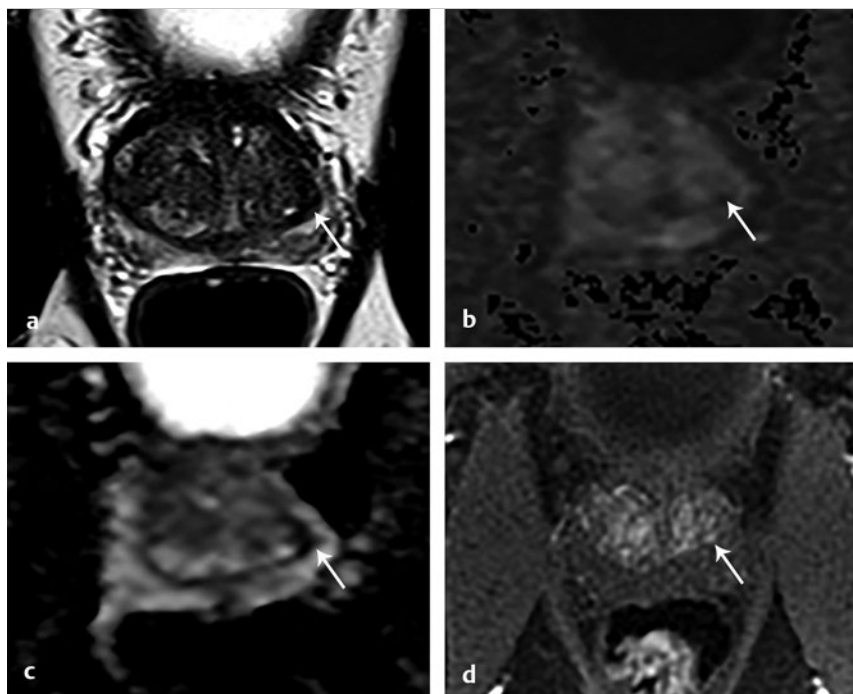


Fig. 12.29 Benign thickening of junction between the peripheral zone and the transition zone, called the pseudocapsule.

12.30 Case 30: Granulomatous Prostatitis Mimicking Tumor

12.30.1 History

A 68-year-old man with urothelial cancer of the urinary bladder, status post transurethral resection and intravesical infusion of bacillus Calmette-Guerin (BCG). Digital rectal examination revealed induration of the left prostate base. PSA was elevated to 8 ng/mL (► Fig. 12.30).

12.30.2 Prostate MRI Findings

- a) T2WI: Circumscribed, homogenous T2 hypointense mass in the left posterolateral base-to-midgland peripheral zone
- b) DWI ($b = 1500 \text{ s/mm}^2$): Marked hyperintensity measuring $\geq 1.5 \text{ cm}$.
- c) ADC: Marked hypointensity measuring $\geq 1.5 \text{ cm}$
- d) DCE: Focal enhancement matching the edges of the T2WI and DWI abnormality

PI-RADS v2 assessment category: 5

12.30.3 Diagnosis

MRI-TRUS fusion biopsy revealed granulomatous prostatitis.

Teaching points: Granulomatous prostatitis can appear as a highly suspicious lesion on MRI that mimics clinically significant cancer. It can present as a firm palpable nodule and with an elevated PSA level. Possible etiologies include intravesical BCG therapy, tuberculous prostatitis, and prior interventions, although most cases are idiopathic. Granulomatous prostatitis may exhibit areas of nonenhancement on DCE-MRI, representing necrosis. In addition, a history of BCG therapy or prior tubercular or fungal infection may suggest the diagnosis. However, in most cases, biopsy is needed to exclude tumor. If granulomatous prostatitis is suspected on clinical grounds, then a follow-up MRI may be obtained after antimicrobial therapy to assess for improvement.

12.30.4 Suggested Reading

- [1] Bour L, Schull A, Delongchamps N-B et al. Multiparametric MRI features of granulomatous prostatitis and tubercular prostate abscess. *Diagn Interv Imaging* 2013; 94(1):84-90
- [2] Logan JK, Walton-Diaz A, Rais-Bahrami S et al. Changes Observed in Multiparametric Prostate MRI Characteristics Correlate with Histopathological Development of Chronic Granulomatous Prostatitis Following Intravesical BCG Therapy. *J Comput Assist Tomogr* 2014; 38(2):274

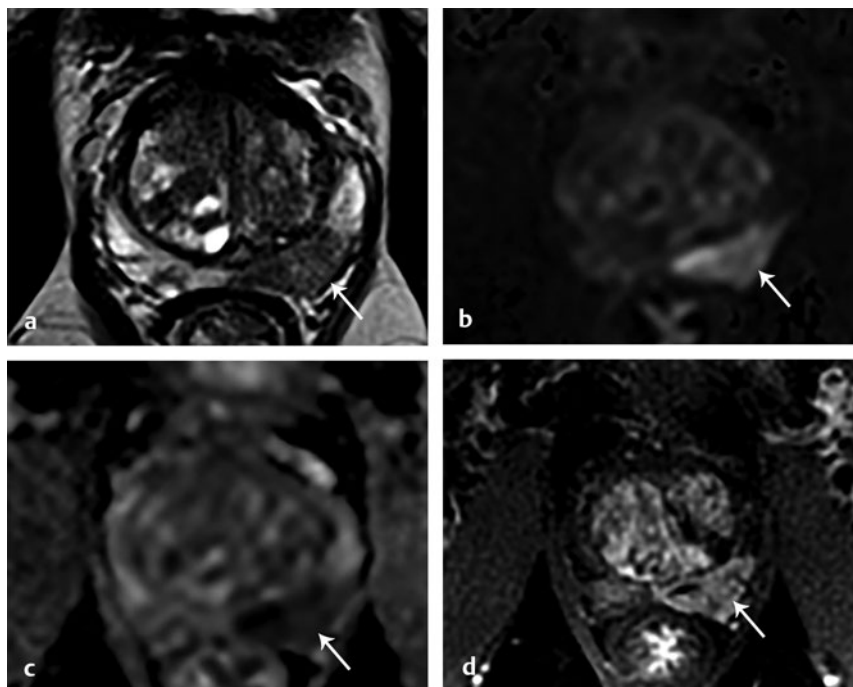


Fig. 12.30 Granulomatous prostatitis mimicking tumor.

12.31 Case 31: Tumor with Indirect Findings of Extraprostatic Extension

12.31.1 History

A 73-year-old man with a PSA level of 2.6 ng/mL and prior biopsy revealing Gleason score 3 + 4 prostate cancer (► Fig. 12.31)

12.31.2 Prostate MRI Findings

- a) T2WI: Circumscribed, homogenous, T2 hypointense mass with broad contact with the overlying capsule measuring 1.2 cm in length
- b) DWI (b = 1500 s/mm²): Marked hyperintensity measuring < 1.5 cm.
- c) ADC: Marked hypointensity measuring < 1.5 cm
- d) DCE: Focal early enhancement matching the T2WI and DWI abnormality

PI-RADS v2 assessment category: 4. Broad contact with the overlying capsule suspicious for extraprostatic extension.

12.31.3 Diagnosis

Prostatectomy revealed Gleason score 3+4 prostate cancer with extraprostatic extension.

Teaching points: Broad capsular contact is an indirect finding suspicious for extraprostatic extension. PI-RADS v2 suggests 1 cm of capsular contact as a potential threshold.

12.31.4 Suggested Reading

- [1] Radiology (ACR) Prostate Imaging-Reporting and Data System (PI-RADS), Version 2. 2015. <http://www.acr.org/-/media/ACR/Documents/PDF/QualitySafety/Resources/PIRADS/PIRADS%20V2.pdf>. Published 2015. Accessed on October 30, 2015.

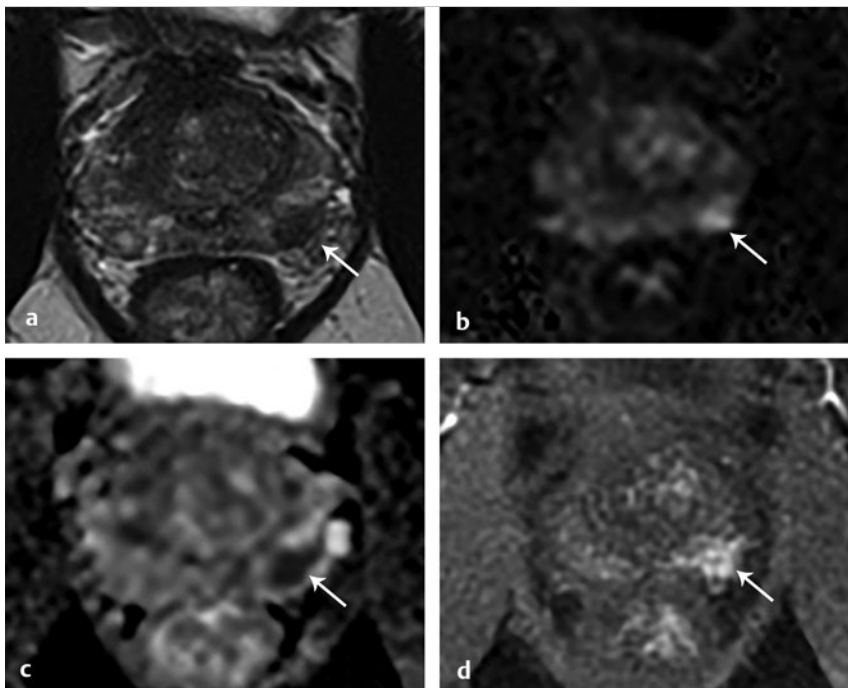


Fig. 12.31 Tumor with indirect findings of extraprostatic extension.

12.32 Case 32: Tumor with Extraprostatic Extension

12.32.1 History

A 50-year-old man with an elevated PSA level of 4.9 ng/mL and prostate biopsy revealing Gleason score 4+4 prostate cancer (► Fig. 12.32)

12.32.2 Prostate MRI Findings

T2WI: Circumscribed, homogenous, T2 hypointense mass in the right posterolateral base peripheral zone with associated capsular bulging

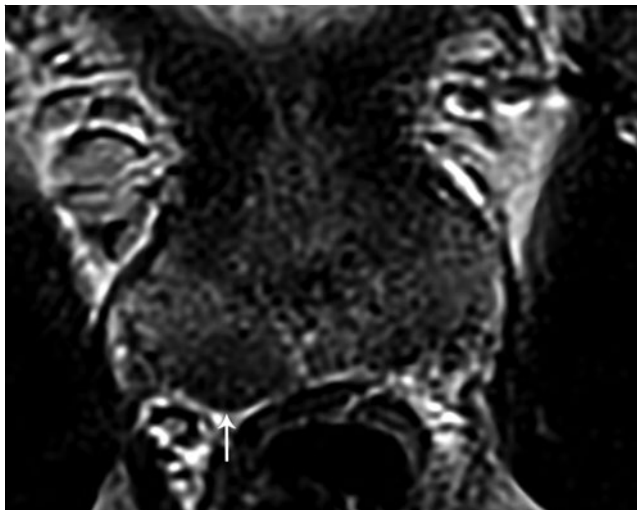


Fig. 12.32 Tumor with extraprostatic extension.

12.32.3 Diagnosis

Prostatectomy revealed Gleason score 4+3 prostate cancer with extraprostatic extension. Teaching points: Capsular bulging is an indirect finding suspicious for extraprostatic extension.

12.32.4 Suggested Reading

- [1] Radiology (ACR) Prostate Imaging–Reporting and Data System (PI-RADS), Version 2. 2015. <http://www.acr.org/~media/ACR/Documents/PDF/QualitySafety/Resources/PIRADS/PIRADS%20V2.pdf>. Published 2015. Accessed on October 30, 2015.

12.33 Case 33: Tumor with Gross Extraprostatic Extension

12.33.1 History

A 70-year-old man with an elevated PSA level of 38 ng/mL and three negative prior biopsies (► Fig. 12.33).

12.33.2 Prostate MRI Findings

T2WI shows large tumor (*long arrow*) involving both the peripheral and transition zones anteriorly with gross extension of tumor beyond the anterior fibromuscular stroma. Small T2 hypointense foci encased by the tumor represent flow voids from the dorsal venous complex, involved by tumor

(*arrowheads*). The tumor also intimately abuts the endopelvic fascia (*dashed arrow*).

12.33.3 Diagnosis

MRI-TRUS fusion biopsy revealed Gleason score 4+5 prostate cancer.

Teaching points: The prostate lacks a true capsule anteriorly, and anterior fibromuscular tumors may extend anteriorly to involve soft-tissue structures located anterior to the prostate. Thus, T2WI need to be scrutinized for evidence of such anterior extraprostatic extension by AFMS tumors.

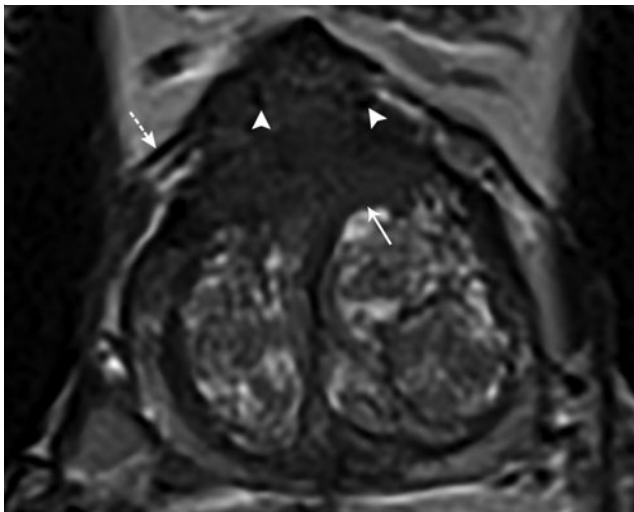


Fig. 12.33 Tumor with gross extraprostatic extension.

12.34 Case 34: Tumor with Seminal Vesicle Invasion

12.34.1 History

A 61-year-old man with an elevated PSA level of 10.4 ng/mL and biopsy revealing Gleason score 4+4 prostate cancer (► Fig. 12.34).

12.34.2 Prostate MRI Findings

- a) T2WI: Subtle focus of T2 hypointensity within the right seminal vesicle. Tumor at the right posterior base abuts the right seminal vesicle (not shown).
- b) DWI ($b = 1500 \text{ s/mm}^2$): Focal hyperintensity in the right seminal vesicle matching the T2WI abnormality

- c) ADC: Focal hypointensity in the right seminal vesicle matching the T2WI abnormality
- d) DCE: Focal early enhancement matching the edges of the T2WI and DWI abnormality

12.34.3 Diagnosis

Prostatectomy revealed Gleason score 4+5 prostate cancer with invasion of the right seminal vesicle

Teaching points: DWI can help to detect seminal vesicle invasion that otherwise may be subtle on T2WI alone.

12.34.4 Suggested Reading

- [1] Soylu FN, Peng Y, Jiang Y et al. Seminal vesicle invasion in prostate cancer: evaluation by using multiparametric endorectal MR imaging. *Radiology* 2013; 267(3):797–806

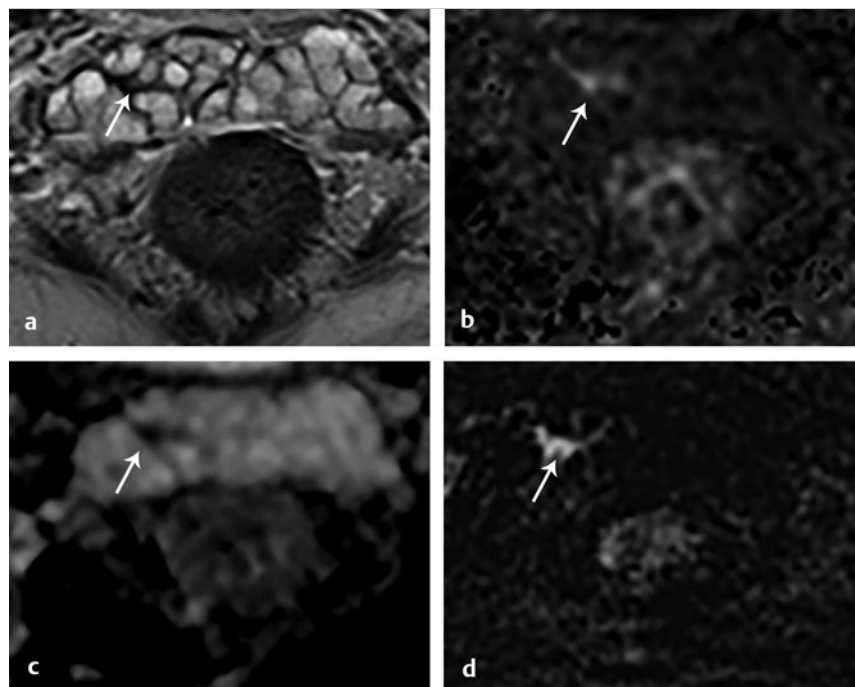


Fig. 12.34 Tumor with seminal vesicle invasion.

12.35 Case 35: Spectrum of Retained Seminal Vesicles in Different Patients Following Prostatectomy

- a) Axial T2WI: Completely retained seminal vesicles (SVs) are present bilaterally in their normal expected anatomical location.
- b) Axial T2WI: The distal tips of both SVs are retained
- c) Axial T2WI: Bilateral collapsed SV remnants are noted
- d) Axial T2WI: A T2 hypointense right seminal vesicle remnant is present

Teaching points: It is important to be aware of the spectrum of appearances of retained seminal vesicles after prostatectomy to

avoid misinterpreting the finding as recurrent tumor. One study observed SV remnants in 20% of patients following prostatectomy, most commonly bilateral. Completely retained SVs were present in 29% of patients, partial SV remnants in 52%, and only distal lateral retained portions in 19%. The T2 signal intensity will vary based on the degree of fluid and fibrosis present. The typical location, symmetry, and lobulated morphology are features to help correctly identify a retained SV (► Fig. 12.35).

12.35.1 Suggested Reading

- [1] Sella T, Schwartz LH, Hricak H. Retained seminal vesicles after radical prostatectomy: frequency, MRI characteristics, and clinical relevance. *AJR Am J Roentgenol* 2006; 186(2):539–546

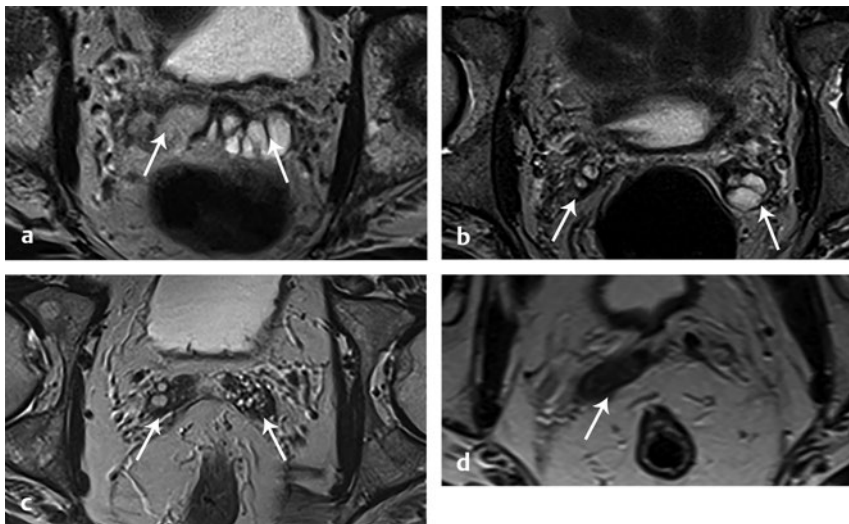


Fig. 12.35 Spectrum of retained seminal vesicles (SVs) in different patients following prostatectomy.

12.36 Case 36: Recurrent Tumor Following Prostatectomy

12.36.1 History

A 72-year-old man with history of Gleason score 7 pT3a prostate cancer treated by radical prostatectomy 15 years prior, presents with a rising PSA level (initially undetectable with progressive increase to 1.4 ng/mL) (► Fig. 12.36).

12.36.2 Prostate MRI Findings

- a) T2WI: 1.4-cm T2 intermediate mass within the right prostatectomy bed interposed between the rectum and bladder
- b) DWI ($b = 1500 \text{ s/mm}^2$): Focal marked hyperintensity matching the T2WI abnormality

- c) ADC: Focal marked hypointensity matching the T2WI abnormality
- d) DCE: Focal early enhancement matching the edges of the T2WI and DWI abnormality

12.36.3 Diagnosis

Prostate cancer recurrence.

Teaching points: DWI and DCE images can be helpful to detect local recurrences that otherwise may be less conspicuous using T2WI alone. Recurrent tumor usually demonstrates mild to marked T2 hyperintensity, while scar tissue is T2 hypointense.

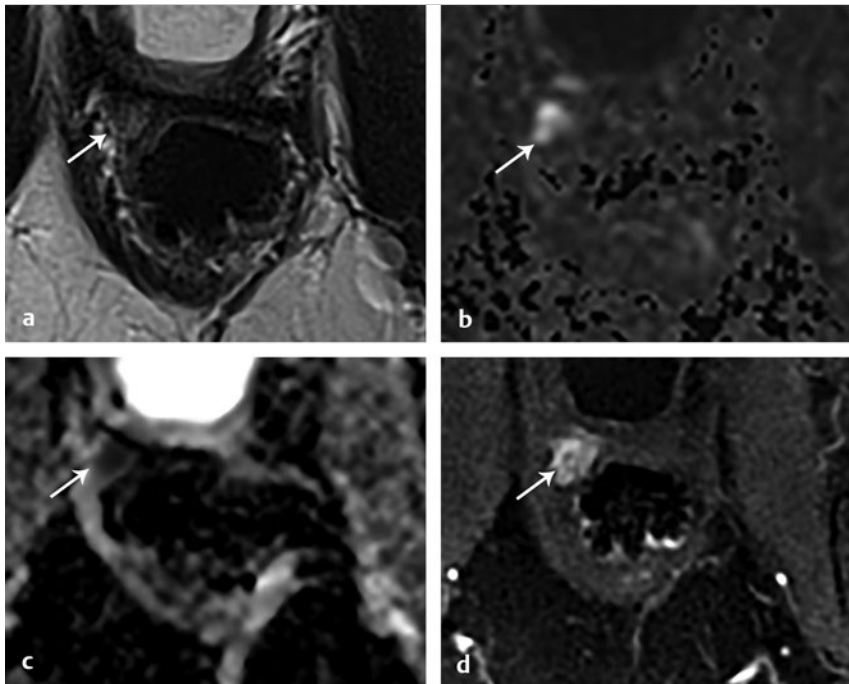


Fig. 12.36 Recurrent tumor following prostatectomy.

12.37 Case 37: Appearance of the Prostate after Total Gland Ablation

12.37.1 History

A 58-year-old man with Gleason score 3+4 prostate cancer treated with whole-gland high-intensity focused ultrasound (HIFU) 4 years prior (► Fig. 12.37).

12.37.2 Prostate MRI Findings

- a) T2WI: The prostate gland is small in size with loss of normal zonal anatomy and diffuse decreased T2 signal. There is a central T2 hyperintense cavity (*arrowhead*) that is contiguous with the urethra.
- b) DWI (b = 1500 s/mm²): No abnormality
- c) ADC: No abnormality
- d) DCE: No abnormality

12.37.3 Diagnosis

Atrophic prostate gland following whole-gland HIFU

Teaching points: Total-gland ablation can lead to marked atrophy of the prostate, which may lose its normal zonal anatomy. One group observed that the volume of the prostate decreased by more than 45% at 6 months following whole-gland HIFU. A central periurethral cystic cavity surrounded by the atrophic prostate tissue may form, as depicted in this case.

12.37.4 Suggested Reading

- [1] Kirkham AP, Emberton M, Hoh IM, Illing RO, Freeman AA, Allen C. MR imaging of prostate after treatment with high-intensity focused ultrasound. *Radiology* 2008; 246(3):833–844

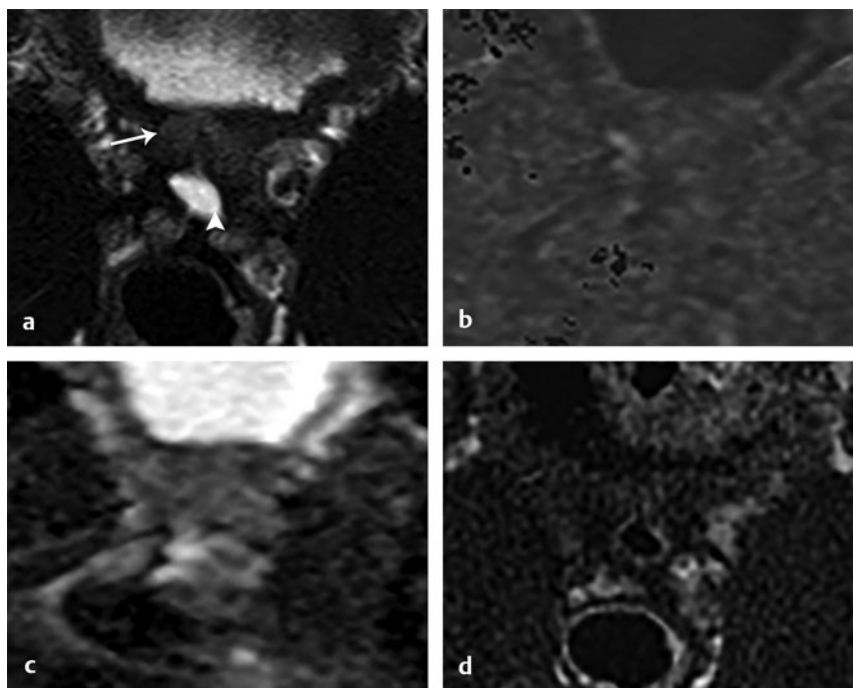


Fig. 12.37 Appearance of the prostate after total gland ablation.

12.38 Case 38: Benign Ablation Cavity Following Focal Cryoablation

12.38.1 History

A 77-year-old man with Gleason score 4+3 prostate cancer, following focal cryoablation (► Fig. 12.38).

12.38.2 Prostate MRI Findings

- a) T2WI (pretreatment): Circumscribed homogenous T2 hypointense mass in the right posteromedial midgland peripheral zone, which was found to represent Gleason score 4+3 prostate cancer on biopsy
- b) DWI (b = 1500 s/mm²; pretreatment): Marked hyperintensity measuring < 1.5 cm
- c) ADC (pretreatment): Marked hypointensity measuring < 1.5 cm
- d) DCE (pretreatment): Focal early enhancement matching the edges of the T2WI and DWI abnormality
- e) T2WI (1 month post-treatment): Crescentic T2 hypointensity in the area of treatment

- f) DWI (b = 1500 s/mm²; 1 month post-treatment): No diffusion abnormality
- g) ADC (1 month post-treatment): No ADC abnormality
- h) DCE (1 month post-treatment): A circumscribed nonenhancing region consistent with a treatment cavity at the treatment site. Smooth, linear enhancement along the periphery of the cavity is likely reactive.

12.38.3 Diagnosis

Benign treatment cavity following focal cryoablation.

Teaching points: DCE is helpful for detecting a nonenhancing treatment cavity in the initial postablation period, which has been described as an indicator of treatment efficacy. Treatment cavities after ablation have been described to be most conspicuous on postcontrast images, potentially being undetectable on other sequences.

12.38.4 Suggested Reading

- [1] De Visschere PJ, De Meerleer GO, Fütterer JJ, Villeirs GM. Role of MRI in follow-up after focal therapy for prostate carcinoma. *AJR Am J Roentgenol* 2010; 194(6):1427–1433

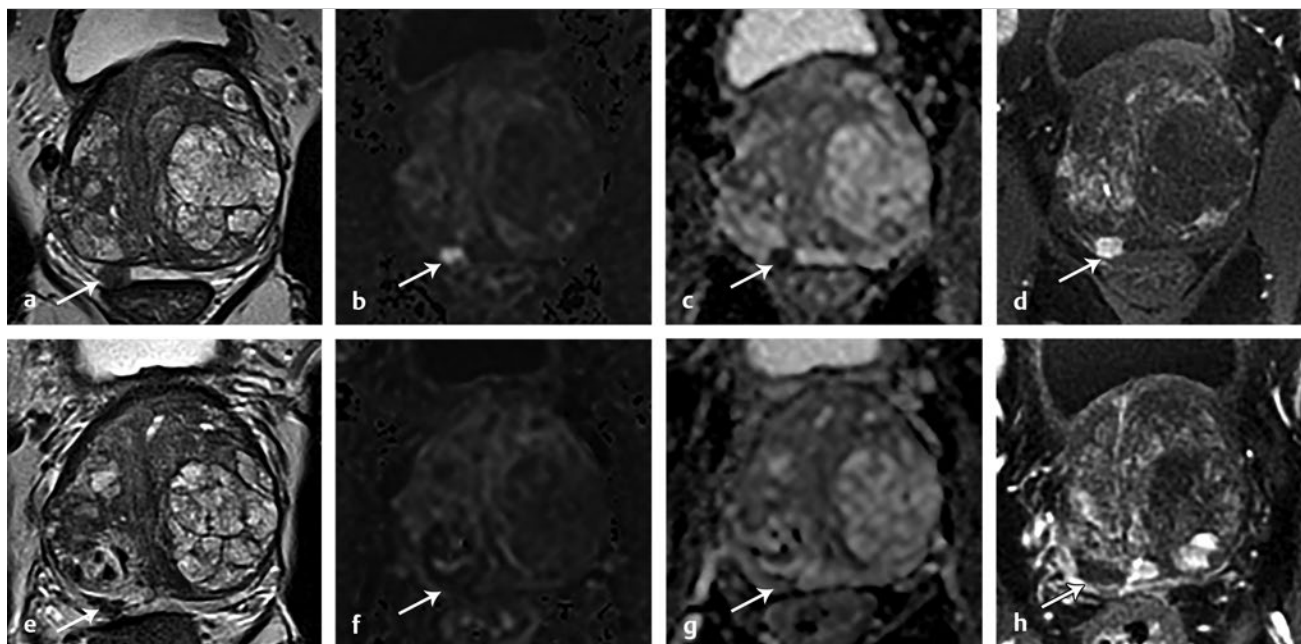


Fig. 12.38 Benign ablation cavity following focal cryoablation.

12.39 Case 39: Recurrent Tumor Following Focal Ablation

12.39.1 History

A 79-year-old man with Gleason score 3+4 prostate cancer at the right apex following focal laser ablation (► Fig. 12.39).

12.39.2 Prostate MRI Findings

- T2WI (pretreatment): Circumscribed homogenous T2 hypointense mass in the right posterolateral midgland-to-apex peripheral zone, which was shown to represent Gleason score 3+4 prostate cancer on biopsy
- DWI (b = 1500 s/mm²; pretreatment): Marked hyperintensity measuring ≥ 1.5 cm
- ADC (pretreatment): Marked hypointensity measuring ≥ 1.5 cm
- T2WI (post-treatment, 1 year post treatment): Distortion and marked T2 hypointensity of the right anterior peripheral gland, compatible with post-treatment change (*arrowhead*). An additional circumscribed lesion in the right posteromedial peripheral zone is mildly T2 hypointense (*long arrow*).

e) DWI (b = 1500 s/mm²; post-treatment, 1 year after): The anterior peripheral zone shows no diffusion abnormality (*arrowhead*); the posteromedial peripheral zone lesion is associated with marked increased diffusion signal (*long arrow*).

f) ADC (post-treatment, 1 year after): The anterior peripheral zone shows no ADC abnormality (*arrowhead*); the posteromedial peripheral zone lesion is associated with marked low ADC (*long arrow*).

12.39.3 Diagnosis

MRI-TRUS fusion biopsy of the right posteromedial lesion revealed recurrent Gleason score 3+4 prostate cancer. The anterior region findings were attributed to post-treatment change.

Teaching points: Decreased T2 signal is nonspecific after focal ablative therapy, possibly representing post-treatment change. Corresponding abnormalities on DWI and DCE-MRI are helpful for raising suspicion for recurrent tumor.

12.39.4 Suggested Reading

- [1] De Visschere PJ, De Meerleer GO, Fütterer JJ, Villeirs GM. Role of MRI in follow-up after focal therapy for prostate carcinoma. *AJR Am J Roentgenol* 2010; 194(6):1427–1433

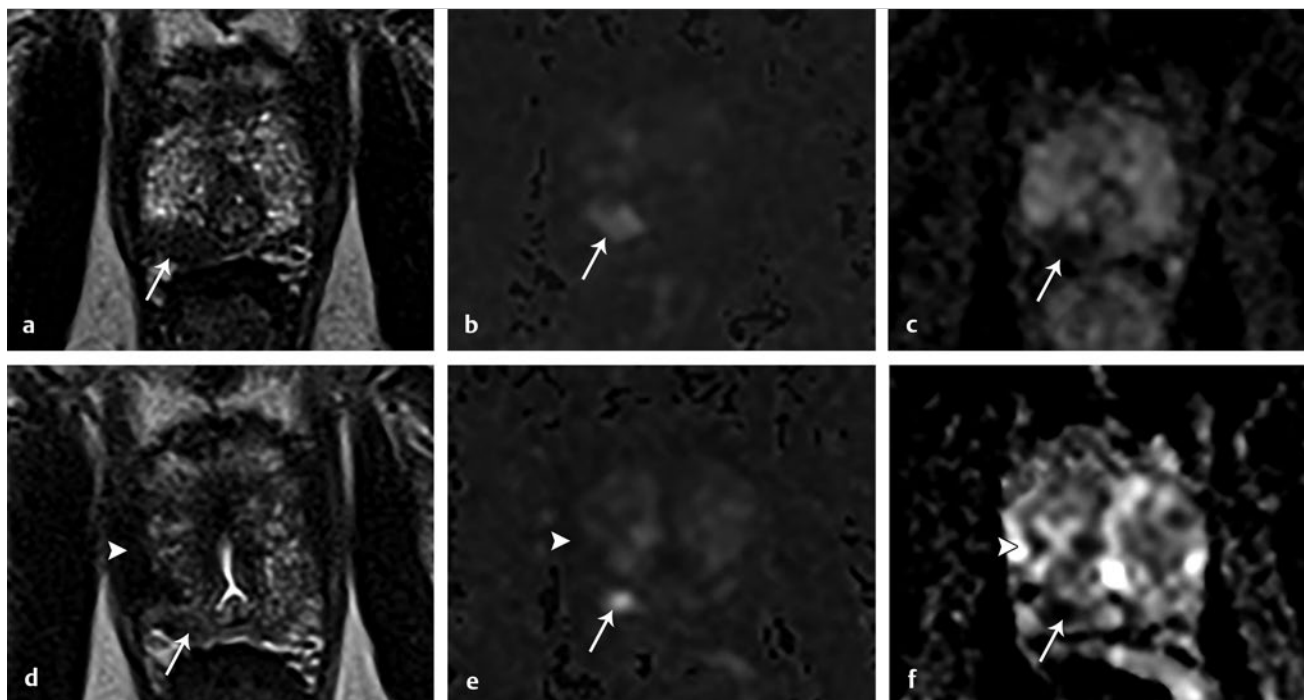


Fig. 12.39 Recurrent tumor following focal ablation.

12.40 Case 40: Recurrent Tumor Following Brachytherapy

12.40.1 History

A 72-year-old man with history of prostate cancer treated with brachytherapy 8 year prior, presenting with a rising PSA level (► Fig. 12.40).

12.40.2 Prostate MRI Findings

- a) T2WI: Numerous small round foci of marked T2 hypointensity throughout the peripheral zone compatible with radiation therapy seeds (*arrowhead*). There is diffuse mild reduction in T2 signal of the peripheral zone, related to prior treatment. However, there is also a faint small focus of moderate T2 hypointensity in the left posteromedial midgland peripheral zone (*long arrow*).
- b) DWI ($b = 1500 \text{ s/mm}^2$): Marked hyperintensity measuring $< 1.5 \text{ cm}$.
- c) ADC: Marked hypointensity measuring $< 1.5 \text{ cm}$

- d) DCE: Focal early enhancement matching the T2WI and DWI abnormality

PI-RADS v2 assessment category: 4

12.40.3 Diagnosis

MRI-TRUS fusion biopsy revealed Gleason score 3+4 prostate cancer

Teaching points: DWI and DCE-MRI can help detect recurrent tumor after treatment that otherwise may be less conspicuous on T2WI alone.

12.40.4 Suggested Reading

- [1] De Visschere PJ, De Meerleer GO, Fütterer JJ, Villeirs GM. Role of MRI in follow-up after focal therapy for prostate carcinoma. *AJR Am J Roentgenol* 2010; 194(6):1427-1433

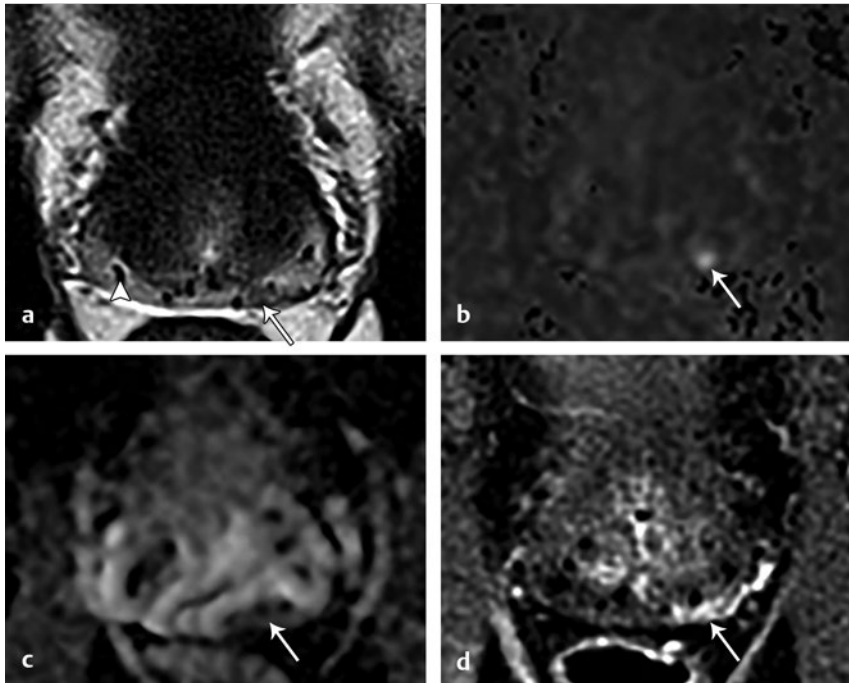


Fig. 12.40 Recurrent tumor following brachytherapy.

12.41 Case 41: Serial MRI for Monitoring of Low-Grade Tumor on Active Surveillance

12.41.1 History

A 66-year-old man on active surveillance for Gleason score 3 + 3 prostate cancer (► Fig. 12.41).

12.41.2 Prostate MRI Findings

T2WI: 9-mm circumscribed, T2 hypointense mass in the left posterolateral midgland peripheral zone that demonstrated Gleason score 3+3 prostate cancer on biopsy (a). That patient

elected to undergo active surveillance. Subsequent MRI 1 year later (b) and 2 years later (c) showed stable tumor size.

Teaching points: Active surveillance may be an appropriate management approach for patients with low-grade tumor on biopsy. This approach involves periodic digital rectal examination, PSA level measurement, and prostate biopsy. However, MRI may also have a role in the noninvasive monitoring of such lesions.

12.41.3 Suggested Reading

- [1] Fascelli M, George AK, Frye T, Turkbey B, Choyke PL, Pinto PA. The role of MRI in active surveillance for prostate cancer. *Curr Urol Rep* 2015; 16(6):42

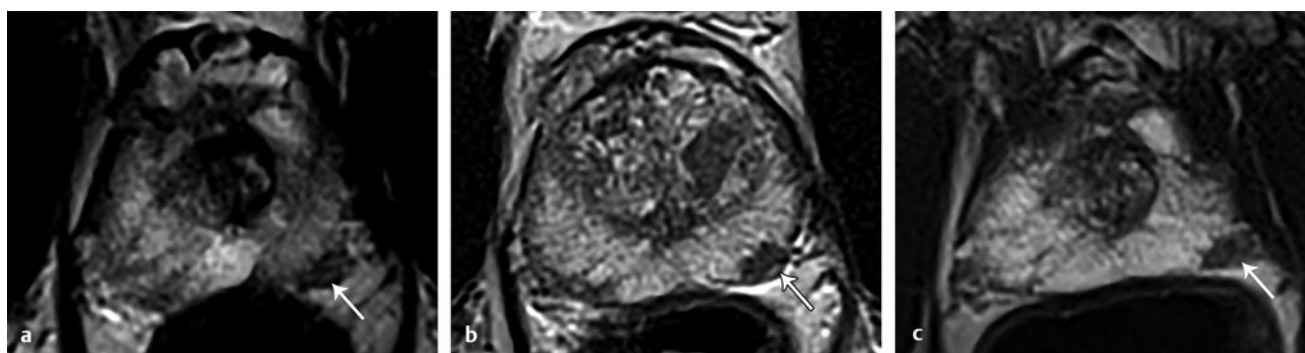


Fig. 12.41 Serial MRI for monitoring of low-grade tumor on active surveillance.

12.42 Case 42: Enlarging Lesion on MRI in a Patient on Active Surveillance

12.42.1 History

A 67-year-old man on active surveillance for Gleason score 3+3 prostate cancer at initial diagnosis (► Fig. 12.42).

12.42.2 Prostate MRI Findings

- T2WI (initial study): There is a 7-mm circumscribed, homogeneous hypointense mass in the left anteromedial apex peripheral zone.
- T2WI (1 year later): The left anteromedial apex peripheral zone mass has increased in size to 10 mm.
- T2WI (3 years after initial study): The left anteromedial apex peripheral zone mass has increased in size to 13 mm.

12.42.3 Diagnosis

Initial biopsy revealed Gleason score 3+3 prostate cancer and the patient opted for active surveillance. Although the lesion slightly increased in size the subsequent year, PSA and repeat biopsy showed stable findings, and the patient remained on active surveillance. On continued follow-up, the lesion progressively increased in size, and the PSA also increased. The patient underwent radical prostatectomy, which showed Gleason score 3+4 prostate cancer anteriorly.

Teaching points: Serial MRI examinations may have a role in active surveillance. The identification of an enlarging lesion can prompt repeat biopsy to identify clinically significant disease.

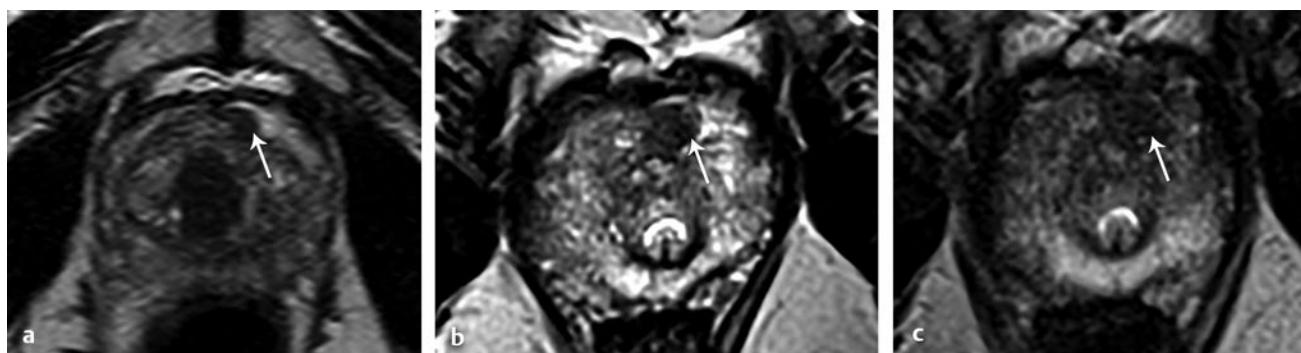


Fig. 12.42 Enlarging lesion on MRI in a patient on active surveillance.

12.43 Case 43: Pitfall: T2 Blackout Effect

12.43.1 History

A 79-year-old man with an elevated PSA level of 13.7 ng/mL and prior negative prostate biopsy (► Fig. 12.43).

12.43.2 Prostate MRI Findings

- T2WI: Circumscribed, T2 hypointensity measuring < 1.5 cm in the right posterolateral midgland peripheral zone
- DWI (b = 50 s/mm²): Hypointense signal matching the T2WI abnormality
- DWI (b = 1500 s/mm²): Central region of hypointense signal
- ADC: Moderate hypointensity matching the T2W abnormality

PI-RADS v2 assessment category: 1

12.43.3 Diagnosis

T2 blackout effect mimicking a suspicious lesion on the ADC map

Teaching points: Lesions that are markedly T2 hypointense may also exhibit reduced signal intensity on low b-value DWI, which reduces the reliability of high b-value DWI and ADC map assessment. This finding may erroneously be interpreted as representing a suspicious lesion based on its decreased ADC. However, the lesion is not hyperintense on the b = 1500 s/mm² image. Further assessment of the b = 50 s/mm² image demonstrates diffuse hypointensity, which may account for the reduced ADC. Possible causes of this T2 blackout effect include hemorrhage, fibrosis, and calcification.

12.43.4 Suggested Reading

- Hiwatashi A, Kinoshita T, Moritani T et al. Hypointensity on diffusion-weighted MRI of the brain related to T2 shortening and susceptibility effects. *AJR Am J Roentgenol* 2003; 181(6):1705–1709

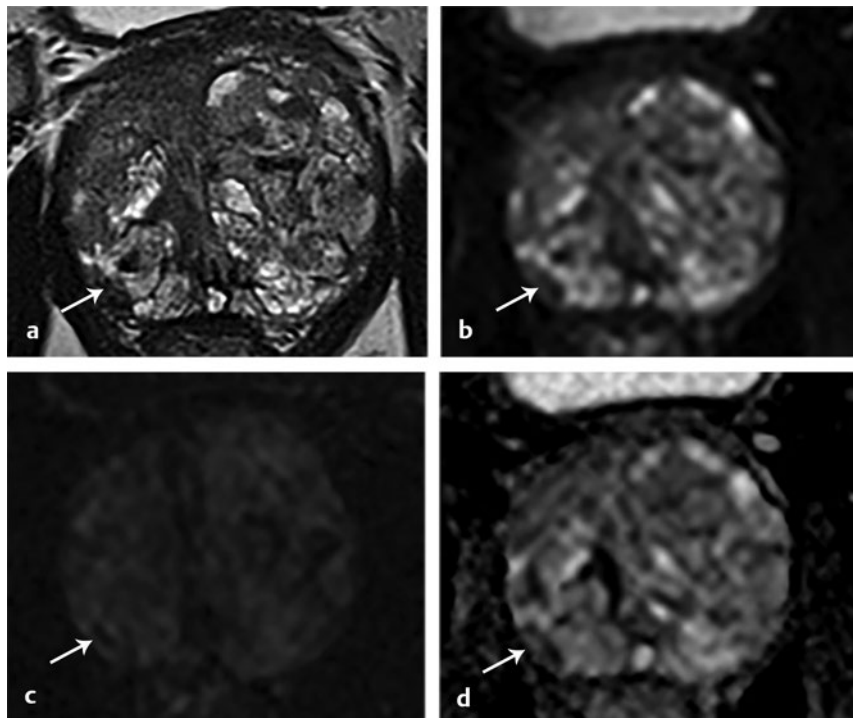


Fig. 12.43 Pitfall: T2 blackout effect.

12.44 Case 44: Pitfall: Vessel Mimicking Tumor

12.44.1 History

A 60-year-old man with an elevated PSA level of 9.3 ng/mL (► Fig. 12.44).

12.44.2 Prostate MRI Findings

- a) T2WI: Thin, serpentine T2 hypointensity in the base-to-midgland of the left peripheral zone
- b) DWI ($b = 1500 \text{ s/mm}^2$): Serpentine hyperintensity
- c) ADC: Serpentine hypointensity
- d) DCE: Serpentine enhancement matching the T2WI and DWI findings. This enhancement has the configuration of a vessel and was able to be traced back to the periprostatic venous plexus.

PI-RADS v2 assessment category: 1

12.44.3 Diagnosis

A vessel traversing the peripheral zone mimicking a tumor. Standard systematic prostate biopsy was negative.

Teaching points: Vessels associated with the prostate may mimic tumor. Careful assessment of the course and morphology of the enhancement on DCE-MRI is useful in determining the presence of a vessel.

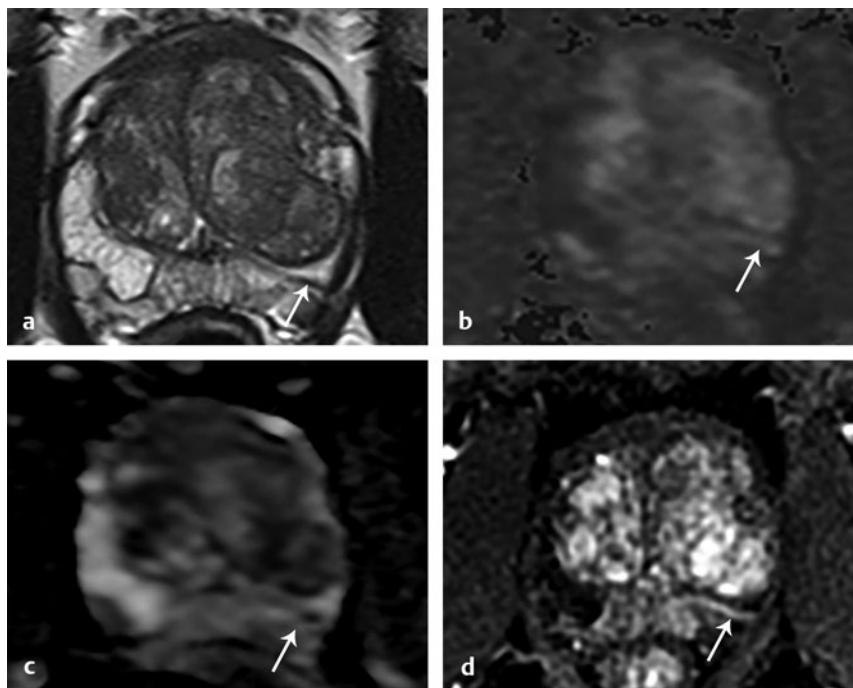


Fig. 12.44 Pitfall: Vessel mimicking tumor.

12.45 Case 45: Utility of Coronal T2-Weighted Images for Tumor Detection

12.45.1 History

A 54-year-old man with a rising PSA level, most recently 3.6 ng/mL (► Fig. 12.45).

12.45.2 Prostate MRI Findings

- a) Axial T2WI: No discrete abnormality
- b) Coronal T2WI: Noncircumscribed moderate hypointensity in the right peripheral zone apex
- c) DWI (b = 1500 s/mm²): Marked hyperintensity < 1.5 cm

- d) ADC: Marked hypointensity < 1.5 cm
- e) DCE: Focal early enhancement matching the DWI abnormality

PI-RADS v2 assessment category: 4

12.45.3 Diagnosis

MRI-TRUS fusion biopsy revealed Gleason score 4+3 prostate cancer.

Teaching points: Coronal T2W images can assist in tumor detection. In addition, multiplanar imaging can help confirm the presence of a lesion detected on DWI or DCE-MRI when no clear abnormality is identified on the axial T2W images.

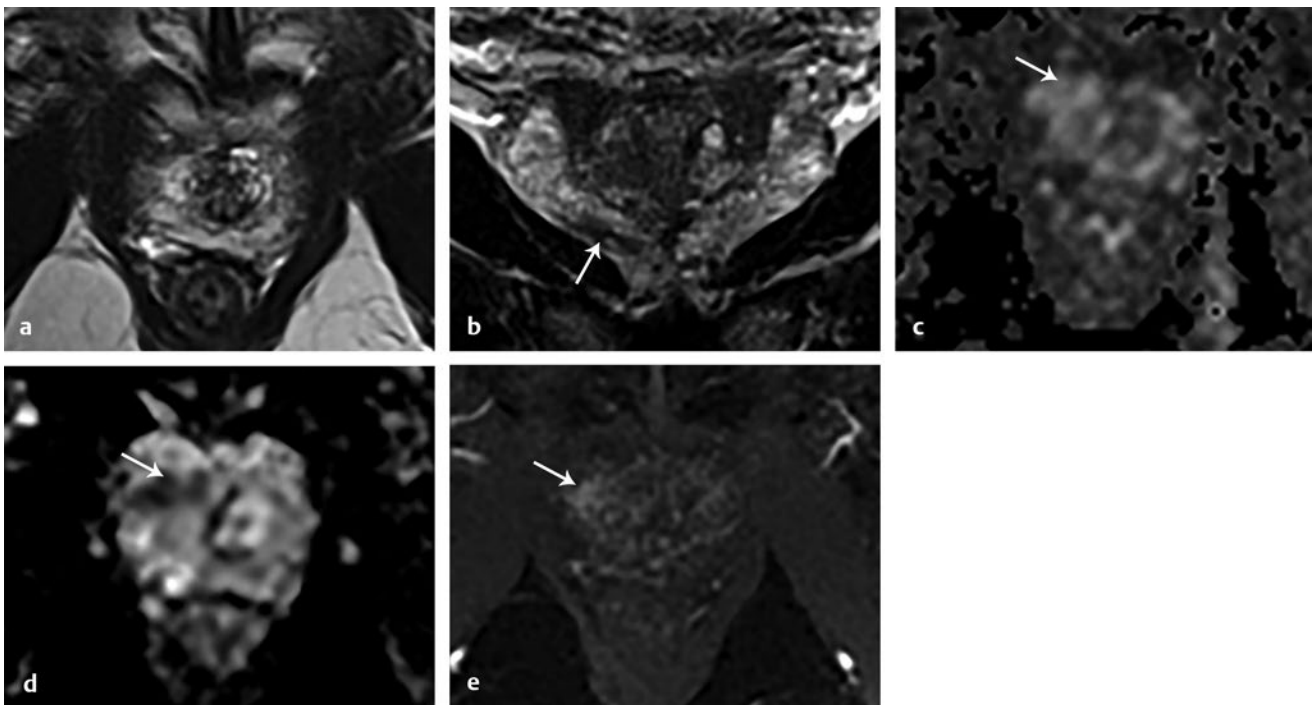


Fig. 12.45 Utility of coronal T2-weighted images for tumor detection.

12.46 Case 46: Utility of DWI for Tumor Detection Compared with T2WI Alone

12.46.1 History

A 70-year-old man with an elevated PSA level of 3.5 ng/mL and negative prostate biopsy (► Fig. 12.46).

12.46.2 Prostate MRI Findings

- a) T2WI: No discrete abnormality is apparent within the peripheral zone
- b) DWI ($b = 1500 \text{ s/mm}^2$): Focal marked hyperintensity measuring $< 1.5 \text{ cm}$ in the left posterolateral midgland-to-apex peripheral zone

- c) ADC: Focal marked hypointensity measuring $< 1.5 \text{ cm}$
- d) DCE: Focal early enhancement matching the DWI abnormality

PI-RADS v2 assessment category: 4

12.46.3 Diagnosis

MRI-TRUS fusion biopsy revealed Gleason score 3+3 prostate cancer

Teaching points: DWI and DCE-MRI can help to detect some tumors that may not be apparent using T2WI alone.

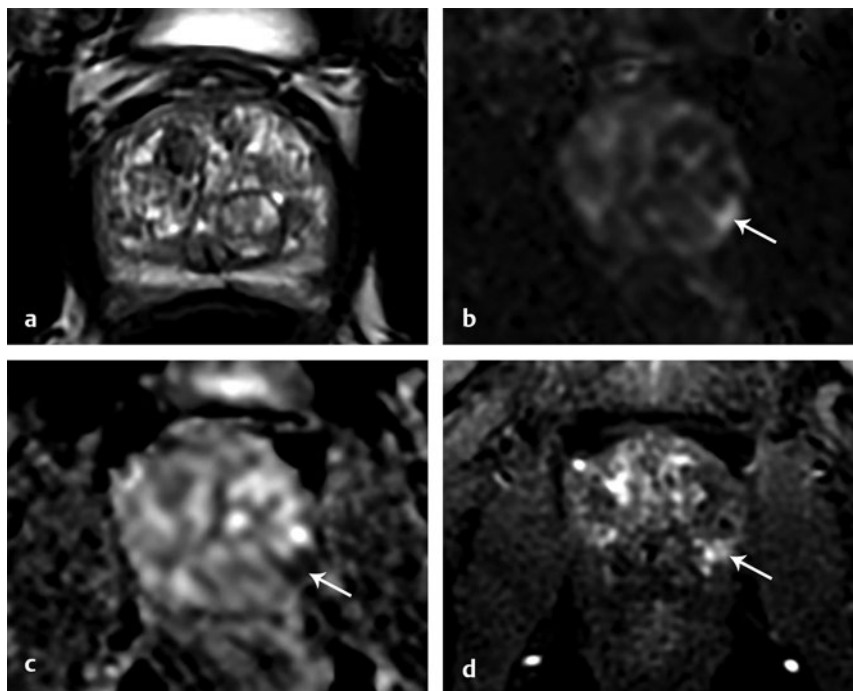


Fig. 12.46 Utility of DWI for tumor detection compared with T2WI alone.

12.47 Case 47: Utility of Dynamic Contrast-Enhanced Images for Assessment of Equivocal Peripheral Zone Lesions Having a Diffusion-Weighted Imaging Score of 3

12.47.1 History

A 64-year-old man with an elevated PSA level of 6.4 ng/mL and prior prostate biopsy revealing Gleason score 3+3 prostate cancer (► Fig. 12.47).

12.47.2 Prostate MRI Findings

a) T2WI: Linear, heterogeneous T2 hypointensity in the left posteromedial midgland peripheral zone (score 3)

- b) DWI ($b = 1500 \text{ s/mm}^2$): Mild hyperintensity (score 3)
- c) ADC: Moderate hypointensity (score 3)
- d) DCE: Focal early enhancement matching the edges of the T2WI and DWI abnormality (positive DCE)

PI-RADS v2 assessment category: 4

12.47.3 Diagnosis

MRI-TRUS fusion biopsy revealed Gleason score 4+4 prostate cancer

Teaching points: Peripheral zone lesions receiving a DWI score of 3 receive an overall PI-RADS v2 assessment category of 4 if DCE is positive.

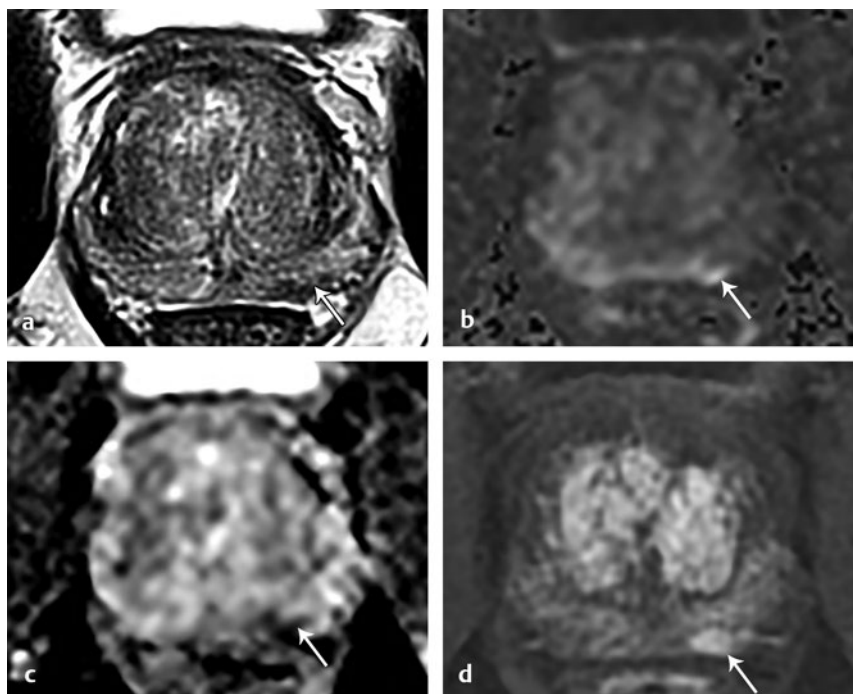


Fig. 12.47 Utility of dynamic contrast-enhanced images for assessment of equivocal peripheral zone lesions having a diffusion-weighted imaging score of 3.

12.48 Case 48: Comparison of Different b-Value Diffusion-Weighted Images

12.48.1 History

A 65-year-old man with an elevated PSA level of 11 ng/mL and prior prostate biopsy revealing high-grade prostatic intraepithelial neoplasia (HGPIN) (► Fig. 12.48).

12.48.2 Prostate MRI Findings

- a) T2WI: Circumscribed, moderate T2 hypointense lesion in the left posteromedial base peripheral zone
- b) DWI (b = 1000 s/mm²): Diffuse hyperintensity throughout the peripheral zone bilaterally

- c) DWI (b = 1500 s/mm²): More focal hyperintensity matching the T2WI abnormality measuring < 1.5 cm
- d) ADC: Moderate hypointensity measuring < 1.5 cm

PI-RADS v2 assessment category: 4

12.48.3 Diagnosis

MRI-TRUS fusion biopsy revealed Gleason score 4+3 prostate cancer

Teaching points: Higher b values for DWI are useful for suppressing signal within normal prostate tissue that may be present at lower b values, thereby improving conspicuity of tumor. PI-RADS v2 recommends incorporating DWI with a high b value of ≥ 1400 s/mm², which may be obtained by either direct acquisition or by extrapolation based on DWI acquired at lower b values.

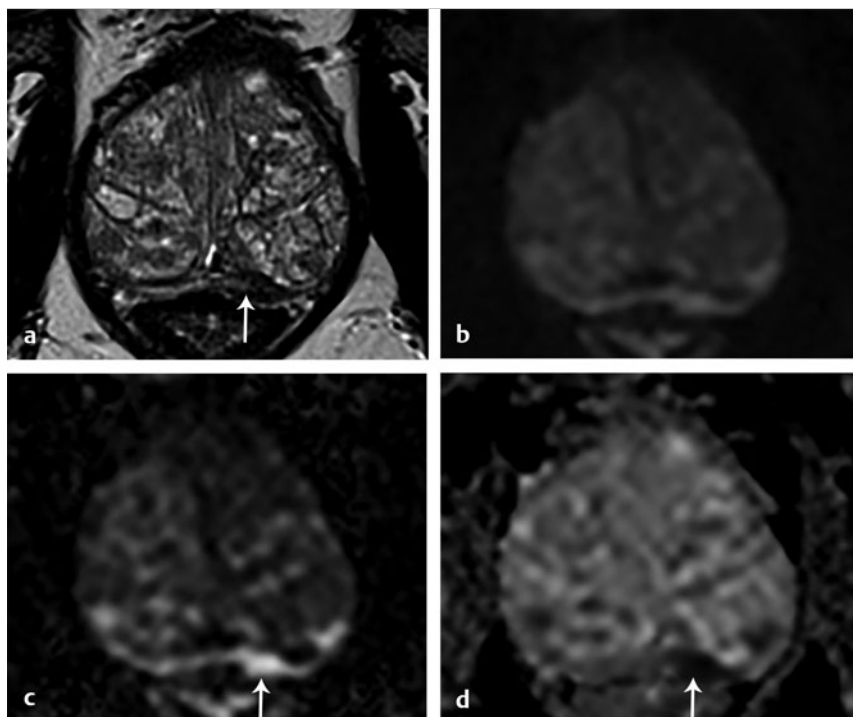


Fig. 12.48 Comparison of different b-value diffusion-weighted images.

12.49 Case 49: Value of Dynamic Contrast-Enhanced Images when Diffusion-Weighted Imaging is Suboptimal

12.49.1 History

A 57-year-old man with an elevated PSA level of 6.8 ng/mL and no prior prostate biopsy (► Fig. 12.49).

12.49.2 Prostate MRI Findings

- T2WI: Circumscribed T2 hypointense mass in the right anterior midgland peripheral zone
- DWI ($b = 1500 \text{ s/mm}^2$): Although the image is mildly distorted, there is focal hyperintensity measuring $< 1.5 \text{ cm}$.
- ADC: No abnormality. Mild image distortion is noted.
- DCE: Focal early enhancement matching the T2WI and DWI abnormality

PI-RADS v2 assessment category: 4

12.49.3 Diagnosis

MRI-TRUS fusion biopsy showed Gleason score 3+4 prostate cancer.

Teaching points: DCE-MRI can be helpful when DWI/ADC images are suboptimal. In this case, the $b = 1500 \text{ s/mm}^2$ DWI image shows focal hyperintensity, but there is no clear abnormality on the ADC map. When DWI/ADC is suboptimal, PI-RADS v2 gives greater importance to DCE-MRI for assessment of peripheral zone lesions.

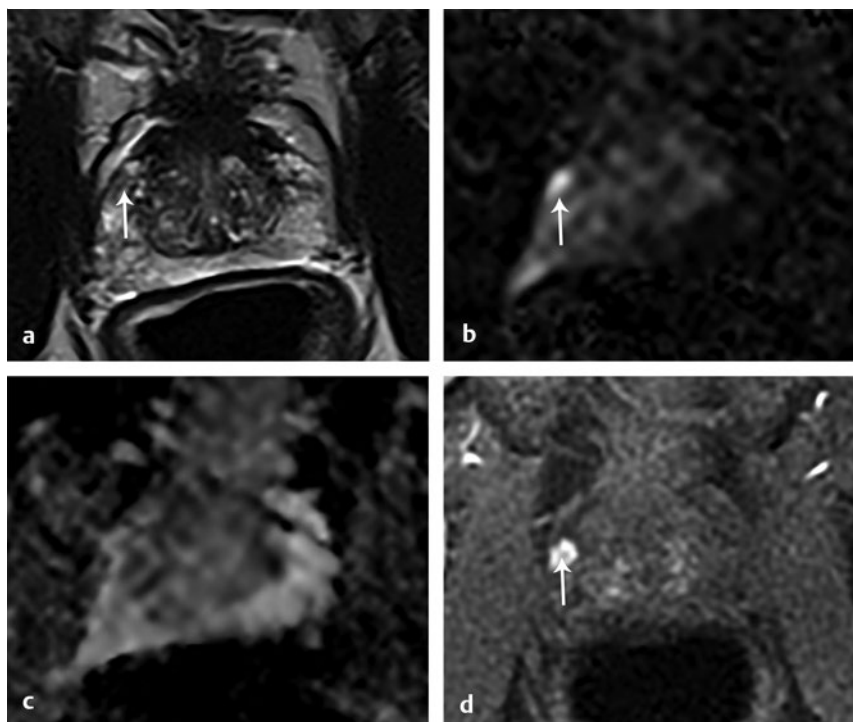


Fig. 12.49 Value of dynamic contrast-enhanced images when diffusion-weighted imaging is suboptimal.

12.50 Case 50: Metastatic Lymph Nodes

12.50.1 History

A 70-year-old man with an elevated PSA level of 36.5 ng/mL and no prior prostate biopsy (► Fig. 12.50).

12.50.2 Prostate MRI Findings

- T2WI: Circumscribed mass within the right anterolateral base-to-apex peripheral zone.
- DWI ($b = 1500 \text{ s/mm}^2$): Marked hyperintensity measuring $\geq 1.5 \text{ cm}$
- ADC: Marked hypointensity measuring $\geq 1.5 \text{ cm}$
- T2WI more cranially: Enlarged, $2.6 \times 1.6 \text{ cm}$ right external iliac lymph node with absence of fatty hilum
- DWI more cranially: The lymph node shows marked hyperintensity.
- ADC more cranially: The lymph node shows marked low ADC.

PI-RADS v2 assessment category: 5

12.50.3 Diagnosis

MRI-TRUS fusion biopsy revealed Gleason score 4+4 prostate cancer. CT of the abdomen and pelvis (not shown) showed bulky retroperitoneal and pelvic lymphadenopathy, consistent with nodal metastases.

Teaching points: Benign and metastatic lymph nodes overlap in terms of DWI/ADC signal characteristics. Thus, size and morphology remain as the primary imaging criteria for diagnosing nodal metastases. Nonetheless, DWI/ADC may be useful for initial detection of potentially subtle nodes for further scrutiny on T2WI or for raising the level of concern for nodes that are equivocal on conventional sequences.

12.50.4 Suggested Reading

- [1] Thoeny HC, Froehlich JM, Triantafyllou M et al. Metastases in normal-sized pelvic lymph nodes: detection with diffusion-weighted MR imaging. *Radiology* 2014; 273(1):125–135

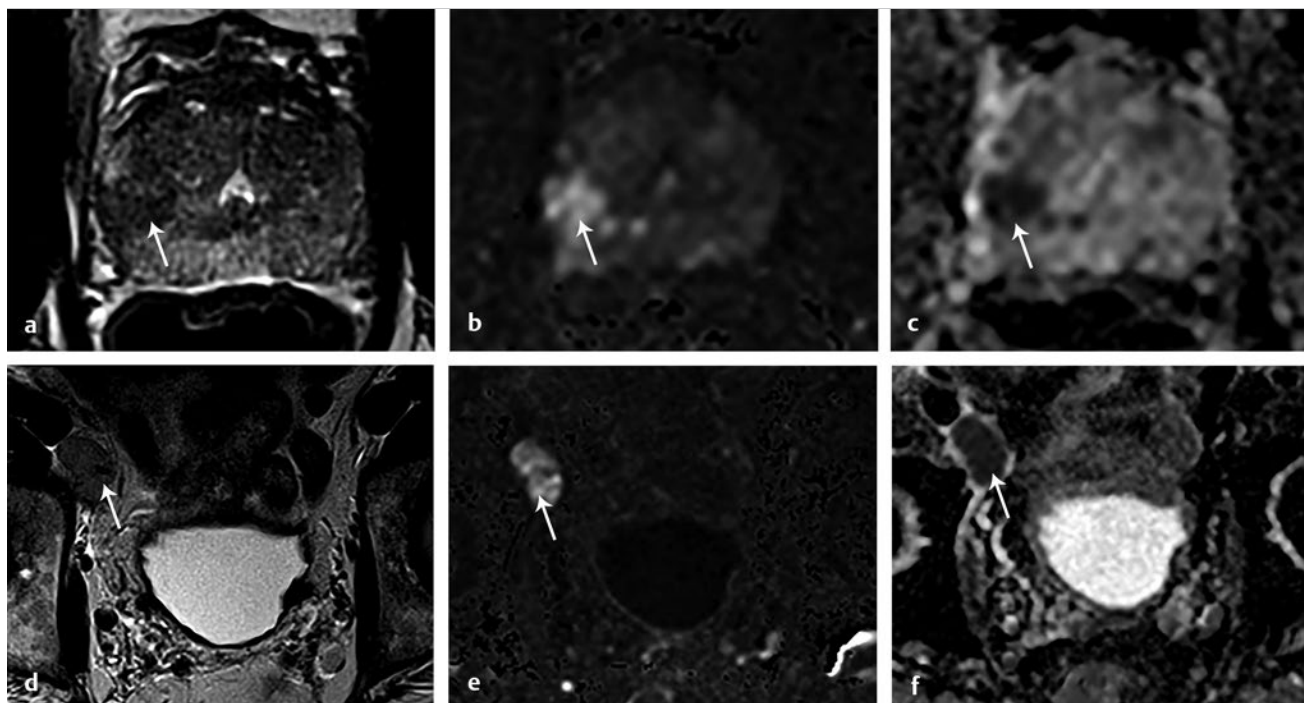


Fig. 12.50 Metastatic lymph nodes.

12.51 Case 51: MR Spectroscopy Showing Prostate Cancer

12.51.1 History

A 73-year-old man with an elevated PSA level of 41 ng/mL (► Fig. 12.51).

12.51.2 MRI Findings

- a) T2WI: Circumscribed, T2 hypointense mass in the right posterolateral midgland peripheral zone measuring > 1.5 cm.
- b) MR spectroscopy: The tumor shows abnormal increased choline-to-citrate ratio (*), while the normal left peripheral zone shows normal choline-to-citrate ratio (**).

Teaching point: MR spectroscopy depicts alterations in metabolite concentration within large voxels and has been applied for assisting tumor detection and localization, although is not formally incorporated within PI-RADS v2.

12.51.3 Suggested Reading

- [1] Scheidler J, Hricak H, Vigneron DB et al. Prostate cancer: localization with three-dimensional proton MR spectroscopic imaging—clinicopathologic study. *Radiology* 1999; 213(2):473–480

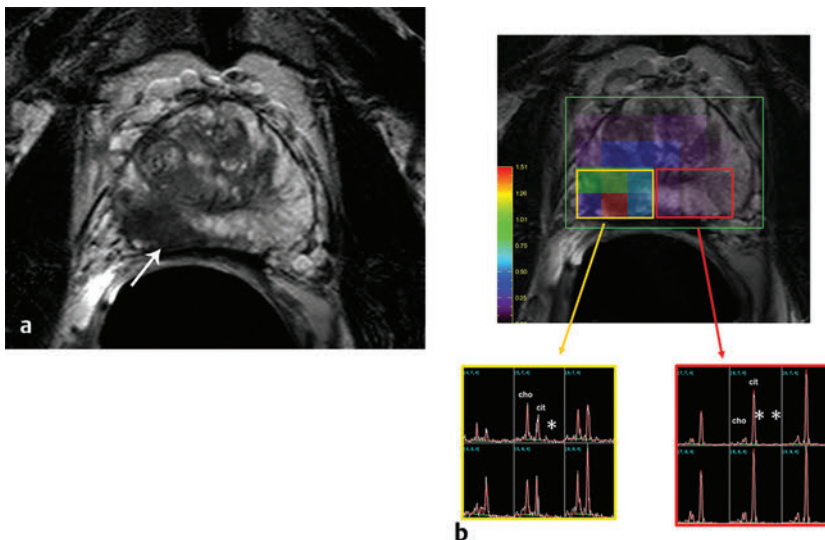


Fig. 12.51 MR spectroscopy showing prostate cancer. (Images courtesy of Dr. Baris Turkbey National Cancer Institute, National Institutes of Health, Bethesda, MD.)

12.52 Case 52: False Positive MR Spectroscopy

12.52.1 History

A 73-year-old man with an elevated PSA level of 41 ng/mL and tumor identified in the right peripheral zone (► Fig. 12.52).

12.52.2 MRI Findings

MR spectroscopy: Increased choline-to-citrate ratio is observed in the base of the left peripheral zone. However, the finding is artifactual and attributed to the region's close proximity to the

left seminal vesicle and the very high glycerophosphocholine level in seminal vesicle fluid.

12.52.3 Diagnosis

False positive finding of abnormal spectra in the left base peripheral zone.

Teaching point: MR spectroscopy is prone to a range of artifacts that can contribute to contaminated spectra and misinterpretations. When performing MR spectroscopy of the prostate, meticulous attention to detail and appropriate level of expertise are required in order to obtain reliable results.

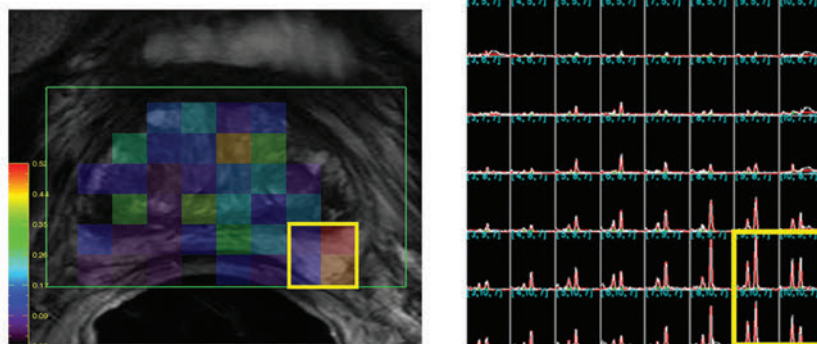


Fig. 12.52 False-positive MR spectroscopy. (Images courtesy of Dr. Baris Turkbey, National Cancer Institute, National Institutes of Health, Bethesda, MD.)

Index

A

Ablation, *see* Cryoablation, High-intensity focused ultrasound, Laser-induced interstitial thermal therapy (LITT)

Active surveillance (AS)

- apparent diffusion coefficient map in 128
- as treatment option 5
- cases 192, 192, 193, 193
- current practices in 127
- dynamic contrast-enhanced MRI in 128
- eligibility for 127
- monitoring strategies in 127
- MRI in 192, 192, 193, 193
- as outcome marker 133
- detection of clinically significant disease in 129, 129, 130–132
- in patient selection 132
- lesion-progression monitoring in 134, 134, 135–137
- risk stratification with 132
- technical considerations 128
- prebiopsy MRI in 113
- targeted biopsy in 133

ADC, *see* Apparent diffusion coefficient (ADC) map

African Americans 1

Age, as risk factor 1

Anisotropy, diffusion tensor imaging and 54, 55

Anterior fibromuscular stroma

- benign thickening case 166, 166
- in anatomy 11, 27, 28
- tumor involving case 167, 167

Apparent diffusion coefficient (ADC) map 46, 48

- and Gleason score of peripheral zone tumors 49
- and peripheral zone tumor aggressiveness 49
- and tumor volume 51
- fibrosis in 78
- in active surveillance 128
- ratio, and Gleason score 50, 50, 51

Artemis 123–124

Artifacts, in MRI 35, 36–38, 100

AS, *see* Active surveillance (AS)

Atrophy, in PI-RADS 78

ATYP, *see* Atypical glands suspicious for cancer (ATYP)

Atypical glands suspicious for cancer (ATYP) 20

B

BCR, *see* Biochemical recurrence (BCR)

Benign ablation cavity, following focal cryoablation 189, 189

Benign mimickers 20, 21, 181, 181, 192, 195

Benign prostatic hyperplasia (BPH) 11, 12

- as mimicker 21
- atypical nodule 158, 158
- case 158, 158
- extruded nodule in peripheral zone case 168, 168, 169, 169

- in PI-RADS 78
 - on T2-weighted MRI 30
 - transition zone in 73
- Benign thickening of junction of peripheral zone with transition zone, case 180, 180
- Benign tissue 154, 154
- Biexponential diffusion 51, 52–53
- Biochemical recurrence (BCR), *see* Recurrence
- and post-radical prostatectomy anatomy 99, 100
 - bone scintigraphy in 95
 - clinical background on 94, 95, 96–97
 - computed tomography in 95, 96
 - defined 94
 - detection, local, dynamic contrast-enhanced MRI in 66, 67
 - image-guided focal treatments for 109, 109, 110
 - magnetic resonance imaging in 95, 97–98, 98, 99, 100, 104
 - PET in 143, 144
 - positron emission tomography in 95–96, 98
 - salvage pelvic radiation therapy for 107, 108–109
 - transrectal ultrasound in 95, 96
- Biomarkers 3, 31

Biopsy

- complications 4, 4–5
 - Gleason score in, vs. radical prostatectomy Gleason score 17
 - guidance 115, 116–124
 - hemorrhage after 30, 35, 84, 84, 178, 178
 - in active surveillance patients 133
 - limitations 5, 5
 - planning 113
 - prostate appearance after 125
 - quantification of amount of cancer in 18
 - systematic 3, 3, 4, 115
 - targeted 116, 116, 133
 - timing of MRI in setting of 35
 - transrectal MRI-guided 117, 117, 118–120
 - transrectal MRI-US-fusion 120, 121–124
 - transrectal ultrasound-guided 3, 3, 4, 116, 117
- Blackout effect 194, 194
- Bone scintigraphy, in recurrence 95
- BPH, *see* Benign prostatic hyperplasia (BPH)
- Brachytherapy
- as treatment option 6
 - recurrence after 107, 108, 191, 191

C

Calcifications, in PI-RADS 78

Cases

- active surveillance 192, 192, 193, 193
- anterior fibromuscular stroma -- benign thickening of 166, 166
- tumor 167, 167
- benign ablation cavity following focal cryoablation 189, 189

- benign prostate tissue 154, 154
 - benign prostatic hyperplasia 158, 158
 - extruded nodule in peripheral zone 168, 168, 169, 169
 - benign thickening of junction of peripheral zone with transition zone, case 180, 180
 - central zone
 - lateral displacement 164, 164
 - normal 163, 163
 - tumor 165, 165
 - coronal images with T2-weighted images 196, 196
 - diffusion-weighted imaging
 - b-values comparison in 199, 199
 - vs. dynamic contrast-enhanced MRI 200, 200
 - vs. T2-weighted imaging 197
 - dynamic contrast-enhanced MRI in peripheral zone lesions 198, 198
 - extraprostatic extension 182, 182, 183, 183, 184, 184
 - hemorrhage exclusion sign 179, 179
 - high-grade prostatic intraepithelial neoplasia 152
 - lymph node metastasis 201, 201
 - magnetic resonance spectroscopy 202, 202, 203, 203
 - midline pseudolesion 170, 170
 - prostate cancer mimicking 171, 171
 - postbiopsy hemorrhage mimicking tumor 178, 178
 - prostate cancer
 - anterior fibromuscular stroma tumor 167, 167
 - anterior horn peripheral zone tumor 177, 177
 - central zone tumor 165, 165
 - contacting urethra 174, 174
 - distal apex tumor 172, 172, 173, 173
 - external urethral sphincter lesion 175, 175
 - high-grade 157, 157, 161, 161
 - intermediate-grade 156, 156, 160, 160
 - low-grade 155, 155, 159, 159, 162, 162
 - subcapsular tumor 176, 176
 - prostatitis 153, 153
 - recurrence of prostate cancer
 - after brachytherapy 191, 191
 - after laser ablation 190, 190
 - after radical prostatectomy 187, 187
 - seminal vesicle invasion 185, 185
 - seminal vesicle retention, after prostatectomy 186, 186
 - T2 blackout effect 194, 194
 - transition zone tumor 159, 159, 160, 160, 161, 161, 162, 162
- Central zone (CZ)
- in T2-weighted imaging 27
 - lateral displacement case 164, 164
 - normal, case 163, 163
 - tumor, case 165, 165
- Choline 31, 33
- Citrate 31, 33

Complications, in transrectal MRI-guided biopsy 120

Computed tomography (CT)

- in biochemical recurrence 95, 96
 - in lymph node metastases 91
- Costs, of prostate cancer, in public health 1

Creatine 31

Cryoablation

- benign ablation cavity following, case 189, 189

- for recurrence 109, 109

Cryosurgery 6

CT, *see* Computed tomography (CT)

Cysts, in PI-RADS 78

CZ, *see* Central zone (CZ)

D

DCE-MRI, *see* Dynamic contrast-enhanced MRI (DCE-MRI)

Diagnosis, *see* Biopsy

- in management pathway 7

- PET in 140, 142

- systematic transrectal ultrasound-guided prostate biopsy in 3, 3, 4

Diffusion kurtosis imaging 54, 54

Diffusion tensor imaging (DTI) 54, 55

Diffusion-weighted imaging (DWI) 35

- acquisition parameters in 42
- apparent diffusion coefficient map in 46, 48

- b-value comparison in 199, 199

- dynamic contrast-enhanced MRI vs. 200, 200

- high b-value images in 42, 43–47

- in biochemical recurrence evaluation 104, 106

- in lymph node staging 91, 91

- in peripheral zone 48, 50–51, 51, 52–55

- in prebiopsy MRI 114

- in transition zone 55, 56

- perfusion and diffusion effect separation in 51, 52–53

- scoring in PI-RADS 70, 70, 71–73

- seminal vesical invasion in 87, 89

- T2-weighted imaging vs. 197, 197

- technical aspects of 41, 41, 42

Distal apex tumor, case 172, 172, 173, 173

DN, *see* Dominant nodule (DN)

Dominant nodule (DN), in radical prostatectomy 12

DTI, *see* Diffusion tensor imaging (DTI)

DWI, *see* Diffusion-weighted imaging (DWI)

Dynamic contrast-enhanced MRI (DCE-MRI) 35

- benign prostatic hyperplasia in 78

- challenges of 68, 68, 69

- defined 60

- diffusion-weighted imaging vs. 200, 200

- evaluation of 60

- for tumor aggressiveness assessment 64

- in active surveillance 128

- in biochemical recurrence evaluation 104, 105–106, 107

- in local recurrence detection 66, 67
 - in localized prostate cancer detection 61, 62–66
 - in prebiopsy MRI 114
 - interpretation of 60
 - peripheral zone lesions in, case 198, 198
 - prostatitis in 78
 - scoring
 - criteria 61
 - in PI-RADS 75, 77
 - scoring criteria 61
 - sequence parameters 60
- ## E
- Ejaculation, before MRI 38
- Endorectal coils (ERC)
- in diffusion-weighted imaging 42
 - in MRI 23, 24–25
 - artifacts with 35, 36, 37, 38
 - in recurrence detection 98, 100
 - in staging 89
- EPE, *see* Extraprostatic extension (EPE)
- Epstein criteria 13
- Erased charcoal 27, 31
- ERC, *see* Endorectal coils (ERC)
- External-beam radiation therapy 6
- recurrence after 106, 106, 107
 - salvage pelvic 107, 108–109
- External urethral sphincter tumor, case 175, 175
- Extraprostatic extension (EPE) 18, 18
- cases 182, 182, 183, 183, 184, 184
 - gross 184, 184
 - in staging 55, 83, 85, 85–87
 - in T2-weighted imaging 29, 31, 85, 85–87
- ## F
- Family history, as risk factor in prostate cancer 1
- Fibrosis, in PI-RADS 78
- Field strength
- in MRI 23
 - in prebiopsy MRI 114
 - in staging 89
- fPSA, *see* Free PSA (fPSA)
- Free PSA (fPSA) 3
- Functional MRI, in staging 87, 88–89
- ## G
- Gleason score 15
- apparent diffusion coefficient map and, in peripheral zone tumors 49
 - apparent diffusion coefficient map ratio and 50, 50, 51
 - changes in 15
 - further modification of 17
 - implications of 16
 - in active surveillance 5
 - in biopsy vs. radical prostatectomy 17
 - in dominant nodule concept 13
 - in external-beam radiation therapy 6
 - in insignificant prostate cancer 13
 - in staging 7
 - in tumor grading 7
 - limitations of 17
- modified vs. original 16
 - of 6 16
 - patient management and 16
- Grading 7
- *See also* Gleason score, Staging
- ## H
- Hardware requirements, in MRI 23
- Hemorrhage
- in PI-RADS 78
 - mimicking tumor 178, 178
 - on T1-weighted imaging 30
 - on T2-weighted imaging 27, 30
 - postbiopsy 30, 35, 84, 84, 178, 178
- Hemorrhage exclusion sign 179, 179
- HGPIN, *see* High-grade prostatic intraepithelial neoplasia (HGPIN)
- High-grade prostatic intraepithelial neoplasia (HGPIN) 19, 152
- High-intensity focused ultrasound
- appearance of prostate after total ablation with 188, 188
 - for recurrence 110
- Histology
- benign prostatic hyperplasia 11, 12
 - prostate 1, 11
 - prostate cancer 11, 12
 - suggestive of benign diagnosis 21
- ## I
- In-bore biopsy 117, 117, 118–120, 124
- Inflammation, as risk factor 1
- Insignificant prostate cancer 13
- Interstitial prostate brachytherapy 6
- Intraductal carcinoma of the prostate 14, 14
- Intravoxel motion phenomenon 51, 52–53
- ## K
- Kurtosis, definition 54, 54
- ## L
- Laser-induced interstitial thermal therapy (LITT) 110, 190, 190
- LITT, *see* Laser-induced interstitial thermal therapy (LITT)
- Local staging 82, 82, 83–89
- *See also* Staging
- Lymph node involvement, staging and 81–82
- *See also* Metastases
- Lymph node staging 90, 90, 91
- Lymphangiography 91
- ## M
- Magnetic resonance imaging (MRI)
- artifacts in 35, 36–38, 100
 - diffusion-weighted 35
 - acquisition parameters in 42
 - apparent diffusion coefficient map in 46, 48
 - b-value comparison in 199, 199
 - dynamic contrast-enhanced MRI vs. 200, 200
 - high b-value images in 42, 43–47
 - in biochemical recurrence evaluation 104, 106
 - in lymph node staging 91, 91
 - in peripheral zone 48, 50–51, 51, 52–55
 - in prebiopsy MRI 114
 - in transition zone 55, 56
 - perfusion and diffusion effect separation in 51, 52–53
 - scoring in PI-RADS 70, 70, 71–73
 - seminal vesicle invasion in 87, 89
 - T2-weighted imaging vs. 197, 197
 - technical aspects of 41, 41, 42
 - dynamic contrast-enhanced 35
 - benign prostatic hyperplasia in 78
 - challenges of 68, 68, 69
 - defined 60
 - diffusion-weighted imaging vs. 200, 200
 - evaluation of 60
 - for tumor aggressiveness assessment 64
 - in active surveillance 128
 - in biochemical recurrence evaluation 104, 105–106, 107
 - in local recurrence detection 66, 67
 - in localized prostate cancer detection 61, 62–66
 - in prebiopsy MRI 114
 - interpretation of 60
 - peripheral zone lesions in 198, 198
 - prostatitis in 78
 - scoring
 - criteria 61
 - in PI-RADS 75, 77
 - sequence parameters 60
 - ejaculation before 38
 - endorectal coils in 23, 24–25
 - field strength 23
 - functional, staging in 87, 88–89
 - hardware requirements 23
 - in active surveillance 192, 192, 193, 193
 - as outcome marker 133
 - detection of clinically-significant disease in 129, 129, 130–132
 - in patient selection 132
 - lesion-progression monitoring 134, 134, 135–137
 - risk stratification with 132
 - technical considerations 128
 - in biochemical recurrence 95, 97–98, 98, 99
 - in transrectal MR-guided biopsy 117, 117, 118–120
 - patient preparation for 38
 - pelvic phased array in 24
 - prebiopsy 113
 - pulse sequences in 25, 26–34, 36
 - surface coils in 25, 26
 - T1-weighted 30
 - cysts in 78
 - in biochemical recurrence evaluation 104
 - T2-weighted 25, 27–32
 - anatomy in 27, 27, 28
 - atrophy in 78
 - benign prostatic hyperplasia in 78
 - blackout effect in 194, 194
 - coronal images in 196, 196
 - cysts in 78
 - diffusion-weighted imaging vs. 197, 197
 - extraprostatic extension in 85, 85–87
 - fibrosis in 78
 - in biochemical recurrence evaluation 103, 104, 106
 - in prebiopsy MRI 114
 - in staging 82, 83, 84, 85–88
 - pathology on 27, 29–32
 - scoring, in PI-RADS 73, 74–76
 - seminal vesicle invasion in 85, 88
 - technique 25, 26
 - timing of, in setting of recent biopsy 35
- Magnetic resonance lymphangiography (MRL) 91
- Magnetic resonance spectroscopy (MRSI) 31, 33–34, 114, 128, 202, 202, 203, 203
- Magnetic susceptibility 37, 37–38, 100
- Management pathway for prostate cancer 7
- Metastases, *see* Recurrence
- case 201, 201
 - in computed tomography 91
 - in T1-weighted imaging 30
 - perineural invasion and 18
 - recurrence and 94–96, 96–97, 98, 98
 - staging and 81, 81, 82, 90, 90, 91
- Mimickers, benign 20, 21, 181, 181, 195, 195
- Motion artifacts, in MRI 36
- MRI, *see* Magnetic resonance imaging (MRI)
- MRL, *see* Magnetic resonance lymphangiography (MRL)
- MRSI, *see* Magnetic resonance spectroscopy (MRSI)
- Multifocality, in radical prostatectomy 12
- ## N
- Nerve-sparing surgery 89
- Neuroendocrine differentiation in prostate cancer 14
- Neurovascular bundle invasion (NVBI), in T2-weighted imaging 27, 32
- NVBI, *see* Neurovascular bundle invasion (NVBI)
- ## O
- Obesity, as risk factor for prostate cancer 1
- Optical shimming, in magnetic resonance spectroscopy 33
- ## P
- Patient preparation
- for MRI 38
 - for prebiopsy MRI 114
 - for transrectal MR-guided biopsy 117
- Pelvic phased array (PPA), in MRI 24, 114
- Perineural invasion 18
- Peripheral zone (PZ)
- anterior horn tumor 177, 177
 - benign thickening of junction with transition zone, case 180, 180
 - bleeding in, after biopsy, in MRI 35

- diffusion-weighted imaging in 48, 50–51, 51, 52–55, 72
 - in PI-RADS 71, 73
 - extruded benign prostatic hyperplasia nodule, case 168, 168, 169, 169
 - in T2-weighted imaging 27, 27, 29, 73, 74
 - PET, *see* Positron emission tomography (PET)
 - PI-RADS, *see* Prostate Imaging and Reporting Data System (PI-RADS)
 - PIN, *see* Prostatic intraepithelial neoplasia (PIN)
 - Point-resolved spectroscopy (PRESS) box 33, 34
 - Positron emission tomography (PET)
 - in diagnosis
 - biochemical recurrence 143, 144
 - primary 140, 142
 - in lymph node staging 91
 - in prognostication 145, 147–149
 - in recurrence 95–96, 98
 - in staging 140, 142
 - in treatment response evaluation 145, 146
 - radiotracers in 140
 - PPA, *see* Pelvic phased array (PPA)
 - Prebiopsy MRI 113
 - Prognostication, PET in 145, 147–149
 - Prostate
 - anatomy 11
 - appearance after total ablation 188, 188
 - histology 1, 11
 - Prostate cancer 13
 - as public health burden 1
 - benign mimickers of 20, 21
 - biopsy 3, 3, 4–5
 - cases
 - anterior fibromuscular stroma tumor 167, 167
 - anterior horn peripheral zone tumor 177, 177
 - central zone tumor 165, 165
 - contacting urethra 174, 174
 - distal apex tumor 172, 172, 173, 173
 - external urethral sphincter tumor 175, 175
 - high-grade 157, 157, 161, 161
 - intermediate-grade 156, 156, 160, 160
 - low-grade 155, 155, 159, 159, 162, 162
 - subcapsular tumor 176, 176
 - clinically significant 15
 - demographics of 1
 - grading 7
 - hemorrhage mimicking 178, 178
 - histologic variants 13, 13, 14
 - histology 11, 12
 - incidence of 1
 - insignificant vs. significant 13
 - intraductal carcinoma 14, 14
 - management pathway 7
 - mimicking midline pseudolesion 171, 171
 - risk factors 1
 - screening 1, 2
 - staging 7, 18
 - acquisition protocol in 84, 84, 85
 - definitions in 81
 - endorectal coils in 89
 - field strength in 89
 - functional MRI in 87, 88–89
 - local 82, 82, 83–89
 - lymph node 90, 90, 91
 - metastases and 81
 - T1 stage 81–82
 - T2 stage 82
 - T2-weighted imaging in 82, 83, 84, 85–88
 - T3 stage 82–83
 - survival in 1
 - symptoms of 1
 - treatment options 5
 - with neuroendocrine differentiation 14
 - Prostate capsule, in T2-weighted imaging 27, 28
 - Prostate Imaging–Reporting and Data System (PI-RADS)
 - assessment 70
 - atrophy in 78
 - benign findings in 77
 - benign prostatic hyperplasia in 78
 - calcifications in 78
 - category X in 77, 77, 78
 - cysts in 78
 - diffusion-weighted imaging in 56
 - scoring 70, 70, 71–73
 - dynamic contrast-enhanced MRI in 60, 60, 61, 61, 64
 - scoring 75, 77
 - fibrosis in 78
 - hemorrhage in 78
 - high b-values images in 42
 - prostatitis in 78
 - reporting 79, 79
 - T2-weighted imaging in 26
 - scoring 73, 74–76
 - Prostate-specific antigen (PSA), *see also* Free PSA, PSA density, PSA doubling time, PSA slope, PSA velocity.
 - derivatives 3
 - in biochemical recurrence definition 94
 - in screening 1, 2
 - Prostatectomy 6, 12
 - anatomy post 99, 100–102
 - Gleason score in, vs. biopsy Gleason score 17
 - nerve-sparing 89
 - prostate retention after 99, 101
 - prostate tissue retention after 99, 101
 - quantification of amount of cancer in 18
 - recurrence after 100, 102–103, 105, 187, 187
 - seminal vesicle retention after 186, 186
 - Prostatic intraepithelial neoplasia (PIN) 19, 19
 - Prostatic utricle cyst 27
 - Prostatitis
 - apparent diffusion coefficient map and 50
 - case 153, 153
 - granulomatous 181, 181
 - in diffusion-weighted imaging 46, 46
 - in dynamic contrast-enhanced MRI 78
 - in PI-RADS 78
 - in T2-weighted imaging 30
 - mimicking tumor 181, 181
 - PSA, *see* Prostate-specific antigen (PSA)
 - PSA density (PSAD) 3, 127
 - PSA doubling time 3, 94
 - PSA slope 3
 - PSA velocity (PSAV) 3
 - Pseudolesion, midline case 170, 170
 - prostate cancer mimicking 171, 171
 - Public health, prostate cancer in 1
 - Pulse sequences, in MRI 25, 26–34, 36
 - PZ, *see* Peripheral zone (PZ)
- ## R
- Race, as risk factor for prostate cancer 1
 - Radiation therapy 6
 - recurrence after 106, 106, 107
 - salvage pelvic 107, 108–109
 - Radical prostatectomy 6, 12
 - anatomy following 99, 100–102
 - Gleason score in, vs. biopsy Gleason score 17
 - nerve-sparing 89
 - prostate retention after 99, 101
 - prostate tissue retention after 99, 101
 - quantification of amount of cancer in 18
 - recurrence after 100, 102–103, 105, 187, 187
 - seminal vesicle retention after 186, 186
 - Radiotracers, in PET 140
 - Recurrence, *see* Biochemical recurrence (BCR)
 - after brachytherapy 107, 108, 191, 191
 - after laser ablation 190, 190
 - after radical prostatectomy 100, 102–103, 105, 187, 187
 - after radiotherapy 106, 106, 107
 - case 187, 187
 - image-guided focal treatments for 109, 109, 110
 - patterns of 94
 - treatment of 94
 - Risk factors 1
 - Risk stratification, with MRI in active surveillance 132
- ## S
- Salvage pelvic radiation therapy 107, 108–109
 - Scintigraphy, in recurrence 95
 - Scoring, of diffusion-weighted imaging, in PI-RADS 70, 70, 71–73
 - Screening 1, 2
 - Seminal vesicle invasion (SVI) 18
 - case 185, 185
 - in diffusion-weighted imaging 87, 89
 - in staging 55, 83, 85, 88
 - in T2-weighted imaging 27, 32, 85, 88
 - Seminal vesicle retention, after prostatectomy 186, 186
 - Shimming, in magnetic resonance spectroscopy 33
 - Signal flare artifact 35, 36
 - Smoking, as risk factor for prostate cancer 1
 - Smudgy fingerprint 27, 31
 - Staging 7, 18
 - acquisition protocol in 84, 84, 85
 - definitions in 81
 - endorectal coils in 89
 - field strength in 89
 - functional MRI in 87, 88–89
 - local 82, 82, 83–89
 - lymph node 90, 90, 91
 - metastases and 81
 - PET in 140, 142
 - T1 stage 81–82
 - T2 stage 82
 - T2-weighted imaging in 82, 83, 84, 85–88
 - T3 stage 82–83
 - Subcapsular tumor, case 176, 176
 - Surface coils, in MRI 25, 26
 - Surgical planning 89
 - Susceptibility artifacts 37, 37–38, 100
 - SVI, *see* Seminal vesicle invasion (SVI)
 - Symptoms 1
 - Systematic biopsy 3, 3, 4–5, 115
- ## T
- T1 stage, prostate cancer 81–82
 - T1-weighted imaging 30
 - cysts in 78
 - in biochemical recurrence evaluation 104
 - T2 stage, prostate cancer 82
 - T2-weighted imaging 25, 27–32
 - anatomy in 27, 27, 28
 - atrophy in 78
 - benign prostatic hyperplasia in 78
 - blackout effect in 194, 194
 - coronal images in 196, 196
 - cysts in 78
 - diffusion-weighted imaging vs. 197, 197
 - extraprostatic extension in 85, 85–87
 - fibrosis in 78
 - in biochemical recurrence evaluation 103, 104, 106
 - in prebiopsy MRI 114
 - in staging 82, 83, 84, 85–88
 - pathology on 27, 29–32
 - scoring, in PI-RADS 73, 74–76
 - seminal vesicle invasion in 85, 88
 - technique 25, 26
 - T3 stage, prostate cancer 82–83
 - Transition zone (TZ)
 - benign thickening of junction with peripheral zone 180, 180
 - diffusion-weighted imaging in 55, 56, 72
 - in benign prostatic hyperplasia 73
 - in PI-RADS 72
 - in T2-weighted imaging 27, 31, 73, 75–76
 - lesion case 159, 159, 160, 160, 161, 161, 162, 162
 - Transrectal MRI-guided biopsy 117, 117, 118–120, 124
 - Transrectal MRI–US–fusion biopsy 120, 121–124
 - Transrectal ultrasound (TRUS)
 - in prostate biopsy 3, 3, 4–5, 116, 120, 121–124

- in recurrence 95, 96

Treatment

- of recurrence 109, 109, 110
- options, for prostate cancer 5
- PET in evaluation of response to 145, 146

TRUS, *see* Transrectal ultrasound (TRUS)

Tumor grading 7

TZ, *see* Transition zone (TZ)

U

Ultrasound, *see* High-intensity focused ultrasound, Transrectal ultrasound (TRUS)

Urethra, prostate cancer contacting 174, 174

UroNav 123–124

V

Vascular-targeted photodynamic therapy (VTP) 111

Vessel mimicking tumor 195

VTP, *see* Vascular-targeted photodynamic therapy (VTP)

